



Universiteit
Leiden
The Netherlands

Beyond the trenches: a landscape-oriented chronostratigraphic approach to MIS 5 Middle Paleolithic open-air sites on the European Plain : case studies from Lichtenberg and Khotylevo I

Hein, M.

Citation

Hein, M. (2023, June 6). *Beyond the trenches: a landscape-oriented chronostratigraphic approach to MIS 5 Middle Paleolithic open-air sites on the European Plain : case studies from Lichtenberg and Khotylevo I*. Retrieved from <https://hdl.handle.net/1887/3620064>

Version: Publisher's Version

License: [Licence agreement concerning inclusion of doctoral thesis in the Institutional Repository of the University of Leiden](#)

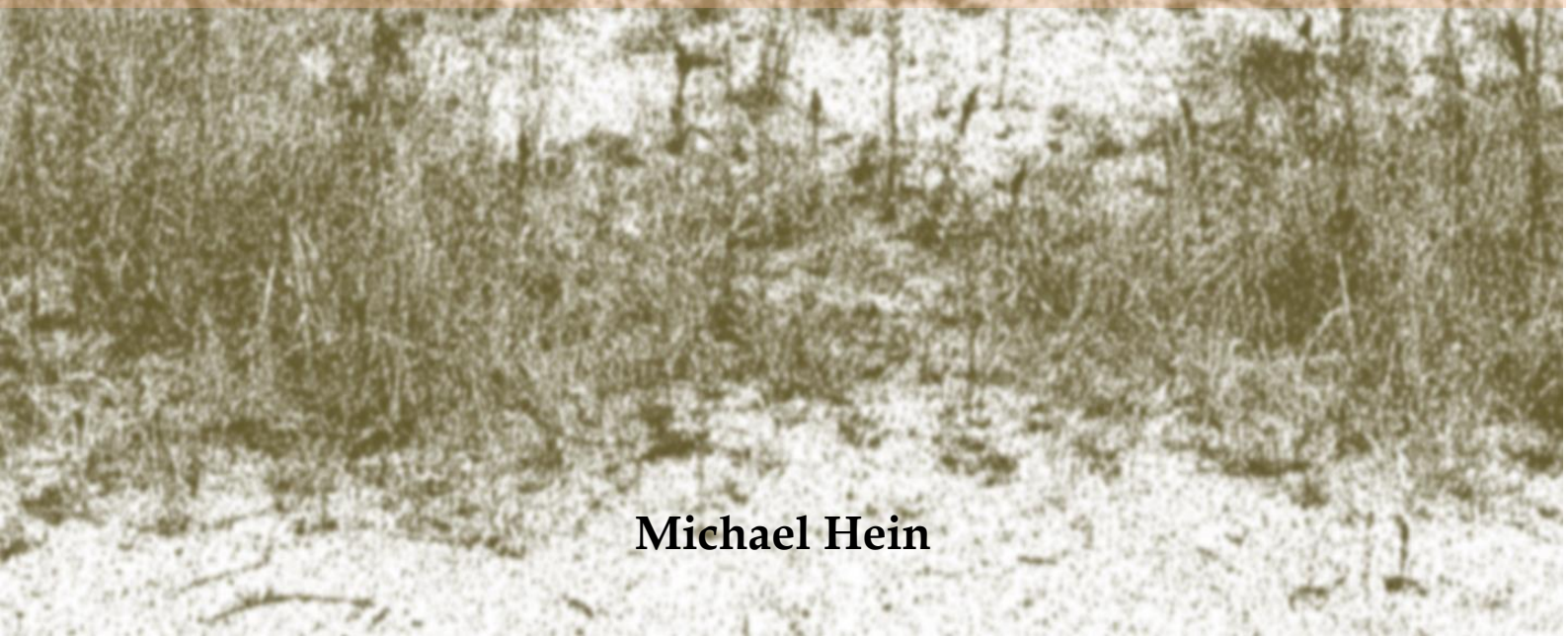
Downloaded from: <https://hdl.handle.net/1887/3620064>

Note: To cite this publication please use the final published version (if applicable).



Beyond the trenches –A landscape-oriented chronostratigraphic approach to MIS 5 Middle Paleolithic open-air sites on the European Plain

Case studies from Lichtenberg and Khotylevo I



Michael Hein

**Beyond the trenches – A landscape-oriented
chronostratigraphic approach to MIS 5 Middle Paleolithic
open-air sites on the European Plain
Case studies from Lichtenberg and Khotylevo I**

Proefschrift

ter verkrijging van
de graad van doctor aan de Universiteit Leiden
op gezag van rector magnificus prof. dr. ir. H. Bijl,
volgens besluit van het college voor promoties
te verdedigen op dinsdag 6 juni 2023
klokke 15:00 uur

door

Michael Hein
Geboren te Sebnitz, Duitsland
in 1982

Promotor: Prof. Jean-Jacques Hublin (Universiteit Leiden)

Co-promotor: Dr. Tobias Lauer (University of Tübingen)

Co-promotor: Dr. Hans von Suchodoletz (University of Leipzig)

Promotiecommissie:

Prof. dr. M.A. Soressi (Universiteit Leiden)

Prof. dr. J.W.M Roebroeks (Universiteit Leiden)

Prof. dr. JF Vandenberghe (Vrije Universiteit Amsterdam)

Prof. dr. M. van Kolfschoten (Universiteit Leiden)

Dr. A. Verpoorte (Universiteit Leiden)

This research was funded by the Max Planck Society.

CONTENTS

CHAPTER I: INTRODUCTION	1
1.1 CONTRIBUTION OF LANDSCAPE RESEARCH FOR UNDERSTANDING NEANDERTHAL BEHAVIOR	1
1.2 CHOICE OF STUDY SITES AND SPATIO-TEMPORAL SCOPE	6
1.3 NEANDERTHALS IN THEIR ENVIRONMENTS DURING THE LAST INTERGLACIAL/GLACIAL CYCLE	8
1.3.1 Climatic development inferred from global palaeoclimate archives	8
1.3.2 Terrestrial/continental evolution of palaeoenvironments on the European Plain	11
1.3.3 Neanderthal population dynamics	19
1.4 METHODS	26
1.4.1 Prospection and Fieldwork	26
1.4.2 Luminescence dating	27
1.4.3 Grain size analysis	29
1.4.4 Palynological analysis	30
1.5 RESEARCH OBJECTIVES	33
1.6 REFERENCES	38
CHAPTER II: LUMINESCENCE CHRONOLOGY OF THE KEY-MIDDLE PALEOLITHIC SITE OF KHOTYLEVO I (WESTERN RUSSIA) – IMPLICATIONS FOR THE TIMING OF OCCUPATION, SITE FORMATION AND LANDSCAPE EVOLUTION	56
CHAPTER III: EEMIAN LANDSCAPE RESPONSE TO CLIMATIC SHIFTS AND EVIDENCE FOR NORTHERLY NEANDERTHAL OCCUPATION AT A PALAEOLAKE MARGIN IN NORTHERN GERMANY.	75
CHAPTER IV: NEANDERTHALS IN CHANGING ENVIRONMENTS FROM MIS 5 TO EARLY MIS 4 IN NORTHERN CENTRAL EUROPE – INTEGRATING ARCHAEOLOGICAL, (CHRONO)STRATIGRAPHIC AND PALEOENVIRONMENTAL EVIDENCE AT THE SITE OF LICHTENBERG	94
CHAPTER V: CONCLUSION	120
5.1 OUTLINE OF THE THESIS CHAPTERS II TO IV	120
5.2 DISCUSSION	126
5.2.1 Evaluation of the chronological and biostratigraphic data	126
5.2.2 Stratigraphic implications of the results	135
5.2.3 Implications for late Pleistocene Neanderthal population dynamics	138
5.3 OUTLOOK	141
5.4 REFERENCES	144
Appendix I: Supplementary Information for Chapter 2	152
Appendix II: Supplementary Information for Chapter 3	155
Appendix III: Supplementary Information for Chapter 4	172

Summary.....	273
Samenvatting.....	275
Aknowledgments	277
Curriculum vitae	278

FIGURES

Figure 1: Map of the European Plain and the Middle Palaeolithic archaeological sites mentioned in the text, presumed to be Eemian and/or Early Weichselian.....	5
Figure 2: Climato-stratigraphic subdivision of the last interglacial/glacial cycle in Central and Western Europe (modified after Peeters et al., 2015)	9
Figure 3: Stepwise and iterative, landscape-oriented research approach to increase chronostratigraphic robustness at Middle Palaeolithic open-air sites.....	36
Figure 4: Abanico Plots of the D_e -distributions for the two samples each, taken from the find layers Li-I & Li-II in Lichtenberg	131

CHAPTER I: INTRODUCTION

1.1 CONTRIBUTION OF LANDSCAPE RESEARCH FOR UNDERSTANDING NEANDERTHAL BEHAVIOR

Gaining knowledge on past human behavior is arguably the essence of archaeological research (Rapoport, 2008; Reid et al., 1974). In the Middle Palaeolithic period – in Europe solely associated with Neanderthals (Conard, 2001) – behavioral mannerisms are mainly concluded from archaeological remains, particularly from lithic artifacts due to their good preservation. Even though huge progress has been made in the field of computational artifact analysis in recent years (Archer, 2016; Delpiano and Uthmeier, 2020; Presnyakova et al., 2015; Weiss, 2020), which furthered our understanding of their manufacture and usage, the explanatory power of stone tools is limited, eventually. Thus, they represent biased, i.e. not fully representative records for human behavior. Apart from lithics, human behavior can also be inferred from other objects of the material culture. Depending on the site preservation, there is evidence for wooden tools/weapons (Thieme, 2007), intentional bone cut marks and bone tools (Culotta, 1999; Gaudzinski, 1999; Van Kolfschoten et al., 2015) or hearth features (Goldberg et al., 2012; cf. Pop et al., 2016) from Lower and Middle Palaeolithic sites in Central Europe. Rare - and strongly debated - are hints that point towards symbolic or even ‘artistic’ behavior (Hoffmann et al., 2018; Leder et al., 2021). Possible funeral practices (Dibble et al., 2015) as well as aspects of mobility and sustenance can furthermore be inferred from occasional skeletal finds (Germonpré et al., 2013; Hublin, 1984) and the anatomic, isotopic or genetic analysis on those (Bocherens, 2011; Hublin and Roebroeks, 2009; Pereira-Pedro et al., 2020; Vernot et al., 2021; Weyrich et al., 2017). While these records can cover important facets of behavioral traits, they need to be put in context of their timing and contemporaneous natural environments in order to identify possible adaptations or socially induced decision-making (cf. Goldberg and Macphail, 2006; Locht et al., 2016; Pederzani et al., 2021). This shall be demonstrated by the definition of the term behavior as used in this thesis:

DEFINITION OF “behavior”: The term ‘behavior’ could be defined as a range of actions and habits displayed by individual organisms or groups in response to internal and

external stimuli, i.e. in conjunction with themselves and their **physical environments** (cf. Hull, 1951; Minton and Kahle, 2013).

This definition inevitably leads to the concept of landscapes as manifestations of these physical environments that are related to human behavior.

DEFINITION OF “landscapes”: Landscapes are the results and the expressions of the lithosphere, atmosphere, hydrosphere, biosphere, and **anthroposphere** mutually influencing and interpenetrating each other to form highly complex (semi-)open systems of these connected components (Fergusson and Bangerter, 2015; Neef, 1967; Simensen et al., 2018).

Firstly, that makes landscapes vaguely delimited entities of the physical environments within a certain area. Secondly, and most crucially, it represents the notion that landscapes do not exist independently of their observers and users, meaning that ‘**environments**’ become ‘**landscapes**’ in the human presence (Kühne et al., 2019; Richter, 2006). Because the two terms are so intimately linked, they will be used synonymously in this thesis. There are three conceivable dimensions to the human-landscape relationship in the Middle Palaeolithic period, as landscapes can (i) affect, (ii) be subject to, and (iii) archive human behavior:

(i) Landscapes provide the context and scenery for human occupation. They were used to procure food, water, raw material, and shelter. The availability and quality of these resources is influenced by complex and sometimes antithetic fluctuations, mainly governed by climate changes. Partly because of this complexity, the knowledge of Neanderthal habitat preference, i.e. the balance of push and pull factors for occupation and migration is still incomplete (Nielsen et al., 2019). For instance, the temperate and fully-forested landscapes of the Eemian Interglacial (~MIS 5e), and the cold tundra steppes of the Early Pleniglacial (~MIS 4) have both variously been regarded as too unfavorable for Neanderthal presence by different authors (cf. Defleur and Desclaux, 2019; Hublin and Roebroeks, 2009). In contrast, the longstanding Neanderthal colonization of the European Plain (>300 ka), indicates a high ecological tolerance and a wide range of exploited environments (Hérisson et al., 2016; Roebroeks et al., 1992) (see 1.3.3).

(ii) Human activities and the exploitation of their environments might have intentionally or incidentally changed landscape segments in terms of faunal or floral composition, which in turn, would have affected the sedimentary and hydrological regimes, as well (cf. Piacente, 1996). This concerns for instance the promotion or suppression of select plant and animal species that were part of the Neanderthal diet or not. As an example of how dramatically the introduction of such a top predator can alter ecosystems may serve the well-documented rewilding of the wolf in Yellowstone National Park, USA. Wolves created an “ecology of fear” that changed behavioral patterns among their prey and led to various ripple effects and feedback mechanisms. Thus, only a few years after the wolf resettled the park, a substantial raise in biodiversity and increased fluvial dynamics had taken place (Beschta and Ripple, 2016). Possible Neanderthal effects on landscapes also concern the obscure topic of Neanderthal fire use. It is still a matter of debate, whether Middle Palaeolithic people could start a fire, but they were surely capable of occasional and opportunistic wildfire management/scavenging (Allué et al., 2022; Pop et al., 2016; Roebroeks et al., 2015; Sandgathe et al., 2011). As ethnographic studies demonstrate, hunter-gatherers use fire not only for cooking and warmth, but also for protection, communication and as a means for hunting (Scherjon et al., 2015). This includes driving game with fire or attracting it by fire-stimulated plant growth. Moreover, the use as a kind of landscape engineering tool is often documented, e.g. to clear pathways or prepare the ground when re-visiting ephemeral sites (ibid.). Furthermore, Neanderthal birch-tar production as an adhesive for hafted tools is well-established and related to controlled fire use (Kozowyk et al., 2017). Although it is still challenging to distinguish natural from anthropogenic fires in the sedimentary records (e.g. Dibble et al., 2018), the mere notion of it is intriguing (cf. Bowman et al., 2013; Roos et al., 2014). Large-scale intentional burning of landscapes would have had significant repercussions on geo-ecological systems and would have turned landscape segments into artifacts, informative of human behavior. With the current state of knowledge, however, the general Neanderthal ecological footprint is hard to account for.

(iii) Because sediments in certain geomorphic positions store the occupational remains, landscapes serve as important repositories for human behavior. Widely acknowledged

for that are e.g. loess plains (Chu and Nett, 2021; Loch et al., 2016; Valde-Nowak and Łanczont, 2021), riverine landscapes (Antoine et al., 2007; Basell et al., 2011; Vandenberghe, 2015; Weber and Beye, 2015), but on the northern European Plain especially lakelands (Kindler et al., 2020; Thieme and Veil, 1985). Deciphering the (syn-/non-/post-) depositional developments on sites and their surroundings – including pedogenic, hydromorphic, cryogenic, and biogenic processes – is invaluable to assess the integrity of an artifact assemblage and the choice of ‘settlement’ location. And it is also an indispensable requirement for establishing a luminescence-based chronological framework. Comprehension of off-site processes is just as important because they can *inter alia* provide information on a potential occupational hiatus in the archaeological sequence due to extensive erosion or cryoturbation disturbances (Vandenberghe, 2013).

It has been shown here that palaeoenvironments have played an important role in Neanderthal behavioral patterns. However, the low resolution and paucity of ecological, chronological and archaeological data (Chapter 1.3) often still precludes well-founded conclusions on adaptations or cultural and biological evolution (e.g. Discamps et al., 2011). To unlock the full potential of Neanderthal records, an integrative combination of archaeological and geoscientific research and precise dating is needed (cf. Goldberg and Macphail, 2006). This is the intention of the present thesis, dedicated to the chronology of landscape conditions and processes at or around open-air sites, using case studies in Lichtenberg, N-Germany and Khotylevo I, W-Russia (cf. detailed research objectives in Chapter 1.5).

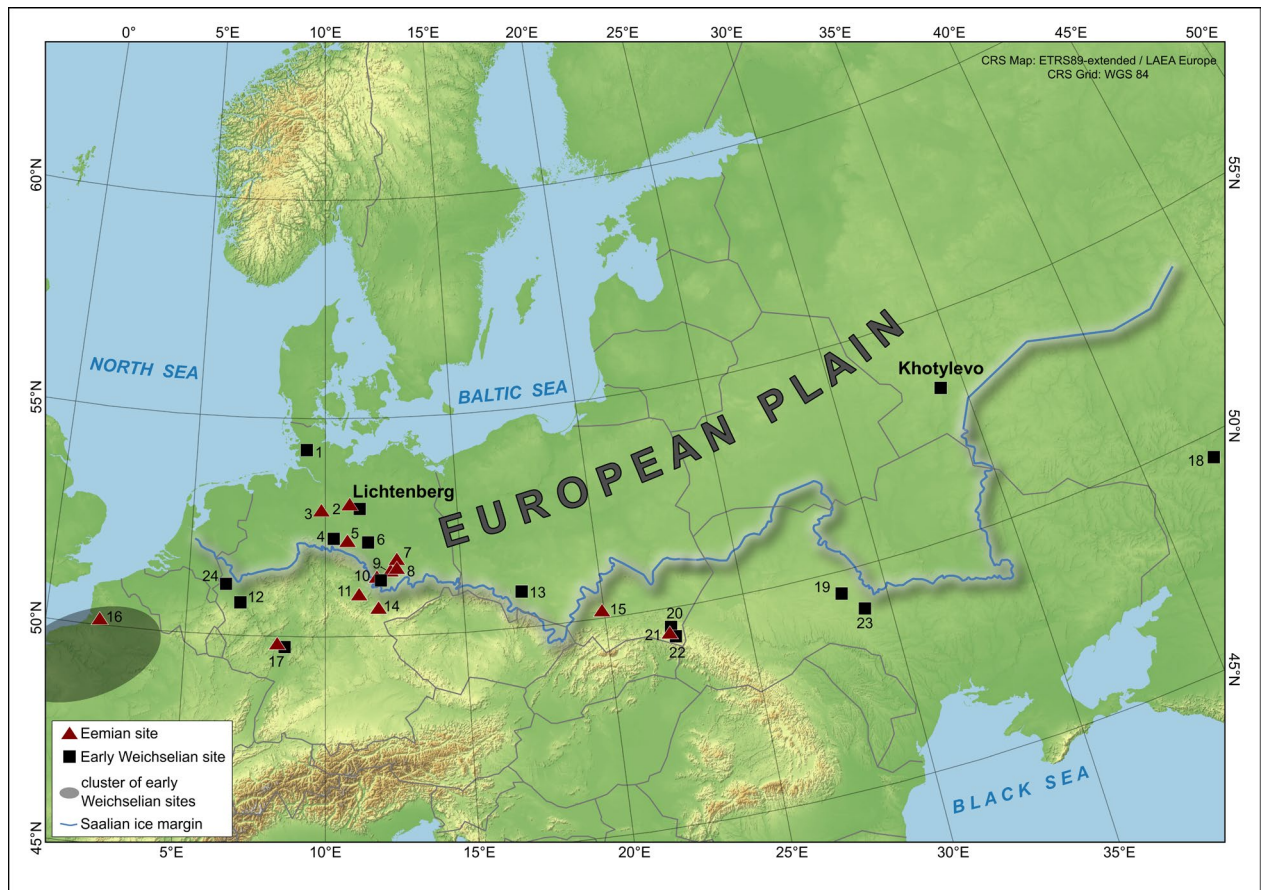


Figure 1: Map of the European Plain and the Middle Palaeolithic archaeological sites mentioned in the text, presumed to be Eemian and/or Early Weichselian. 1 – Schalkholz, 2 – Woltersdorf, 3 – Lehringen, 4 – Salzgitter Lebenstedt, 5 – Steinmühle/Veltheim, 6 – Königsau, 7 – Gröbern, 8 – Grabschütz, 9 – Rabutz, 10 – Neumark Nord, 11 – Burgtonna, 12 – Tönchesberg, 13 – Wrocław Hallera Av., 14 – Weimar Parktravertin and Taubach, 15 – Kraków-Zwierzyniec, 16 – Caours, 17 – Wallertheim, 18 – Sukhaya Mechetka, 19 – Moldova, 20 – Pikulice, 21 – Orzechowce, 22 – Nehrybka, 23 – Vykhvatinskiy naves, 24 – Rheindahlen Westwand (B1). Study sites Lichtenberg and Khotylevo I are labelled, instead of numbered. Digital Elevation model based on SRTM-data (downloaded from <https://earthexplorer.usgs.gov/>), national borders obtained from Eurostat (<https://ec.europa.eu/eurostat/de/web/gisco/geodata/reference-data>). Maximum Saalian glacier extent after Ehlers et al. (1984), Matoshko (2011) and Velichko et al. (2006) (see Chapter 3).

1.2 CHOICE OF STUDY SITES AND SPATIO-TEMPORAL SCOPE

The European Plain (henceforth: EP) is widely regarded as one of the Earth's largest expanses of uninterrupted lowlands, but there is no general agreement on its actual extent (cf. Encyclopædia Britannica). For the purposes of this study, the European Plain is determined as the area largely congruent with the Saalian ice-sheet cover in MIS 6, stretching from the lowlands of the Benelux in the west to the Ural Mountains in the east (Figure 1). From a pre-LGM Weichselian point of view, the EP with its rather homogeneous topographies and recent glacio-geological history, represented an uninterrupted biome, that facilitated lateral exchanges of the faunal and floral elements (see 1.3.2). This is also reflected in the Middle Palaeolithic archaeological remains of this area, which are very similar across the vast dimensions of the EP (Weiss, 2019). The choice of study areas takes this fact into account by selecting the open-air sites Khotylevo I-6-2 at the eastern and Lichtenberg at the western periphery of the EP (Figure 1). Contrasting with the distance that separates them (ca. 1,800 km), these two sites share an astonishing number of similarities (Otcherednoi et al., 2014; Veil et al., 1994):

(i) Both are located at approx. 53° N and are among the northernmost undisputed Middle Palaeolithic sites of their major regions and of the entire European Plain, respectively (see 1.3.3). This northerly latitudinal location was another key criterion for choosing these sites. Given the geographic distribution of known Neanderthal occupations, it seems to be the general consensus that the tentative northern margin of the Neanderthal habitat was at 55° N, even during times of ameliorating climates (Hublin and Roebroeks, 2009). In that regard, the present author fully agrees with Nielsen et al. (2017) about the potential of this extreme boundary to reveal crucial information on Neanderthal resilience or constraints towards changing environmental conditions. This kind of information is usually obtained from combining environmental, chronological, and archaeological findings, the latter mainly being based on lithic artifacts.

(ii) Both sites in question show a very consonant and distinctly rich Middle Palaeolithic stone tool assemblage, associated with the *Keilmessergruppen* (see 1.3.3).

(iii) Both occupational layers have been numerically dated to MIS 3; Khotylevo I-6-2 by means of radiocarbon (Otcherednoi et al., 2014) and Lichtenberg using thermoluminescence on sediments (Veil et al., 1994) (see the particular discussions in Chapters 2 and 4).

(iv) In both cases, there are thick and highly-resolved sediment sequences available, either directly on site or in the immediate vicinity. These are key-archives for the reconstruction of Early Weichselian environments.

(v) This supplemental stratigraphic and environmental data could at both sites justify to rather assign the occupations to MIS 5, which has indeed previously been suggested for both sites (Jöris, 2004; Velichko, 1988).

In concurrence with these plausible stratigraphic arguments, the MIS 5, i.e. the last interglacial and subsequent early glacial is the temporal scope of this thesis. For all those aforementioned similarities, it shall not be concealed that Khotylevo I-6-2 and Lichtenberg differ in two important respects, namely (1) the raw material procurement for lithic production and (2) bone preservation: (1) In Khotylevo, along the valley of the River Desna, Cretaceous chinks and marls crop out that hold primary, high-quality tabular flints (see Chapter 2). This ubiquity does not exist in Lichtenberg. Middle Palaeolithic people there had to rely on Baltic flint diluted within the containing Saalian glacial deposits. Thus, they were likely depending on sediment (re)depositions providing fresh material (see Chapter 4). (2) Whereas in Khotylevo, the occupation layer produced a decent faunal spectrum due to good bone preservation in the contact zone with Cretaceous chalk (Chubur, 2013), in Lichtenberg, evidence for animal remains is missing so far from the respective layers.

1.3 NEANDERTHALS IN THEIR ENVIRONMENTS DURING THE LAST INTERGLACIAL/GLACIAL CYCLE

1.3.1 Climatic development inferred from global palaeoclimate archives

Marine cores

Interpretations of North Atlantic marine palaeoclimate records have substantially furthered our understanding of how sensitive global climate responded to orbital changes with different cyclicities between ca. 1,000 and 100,000 years. Based on the oxygen isotope ratio ($\delta^{18}\text{O}$) of the calcite shells in benthic foraminifera, alternating warmer and colder intervals in Earth's palaeoclimate can be inferred from successive layers in marine sediment cores. Dating of these sequences is provided by radiocarbon in the upper section <40 ka, correlation with better-dated palaeoclimate archives (e.g., speleothems and ice cores), and tuning to global orbital changes (Lisiecki and Stern, 2016). The established Marine isotope stages (MIS) timescale assigns an odd number to warm and an even number to cold phases, starting with number 1 for the Holocene and covering >>100 stages (Emiliani, 1955). Within the Pleistocene, the cycles of this record were found to be linked with evidence for terrestrial glacials and interglacials (Shackleton, 1967), making the (globally stacked) benthic $\delta^{18}\text{O}$ records perhaps the most prominent chronological reference point in Quaternary research, *sensu lato*, over the last decades (esp. Lisiecki and Raymo, 2005). Stage 5 in the MIS record, dated to 130 ka - 71 ka (Lisiecki and Raymo, 2005), was divided into 5 substages by Shackleton (1969; Shackleton et al., 2002), realizing that only the first part of this marine interglacial corresponds to terrestrial ones on the continents. He assigned MIS 5e to the Eemian Interglacial, whereas MIS 5c and 5a represent subsequent warm intervals, and MIS 5d and 5b cooler intervals, respectively. For Substages 5e to 5a no clearly defined boundaries exist, but their maximum $\delta^{18}\text{O}$ -values are ascribed to ages of 123 ka (5e), 109 ka (5d), 96 ka (5c), 87 ka (5b), and 82 ka (5a) (Lisiecki and Raymo, 2005)(Figure 2). In the course of MIS 5, rather temperate conditions prevailed, with an overall and gradual cooling tendency. This trend was interrupted by brief colder spells that did not, however, regularly reach values indicative of glacial conditions, such as in the neighboring Stages MIS 4 and 6 (Lisiecki and Stern, 2016). The timing of MIS 5

is regarded as broadly equivalent to the cumulative Eemian and Early Weichselian, which is the period under consideration for this thesis.

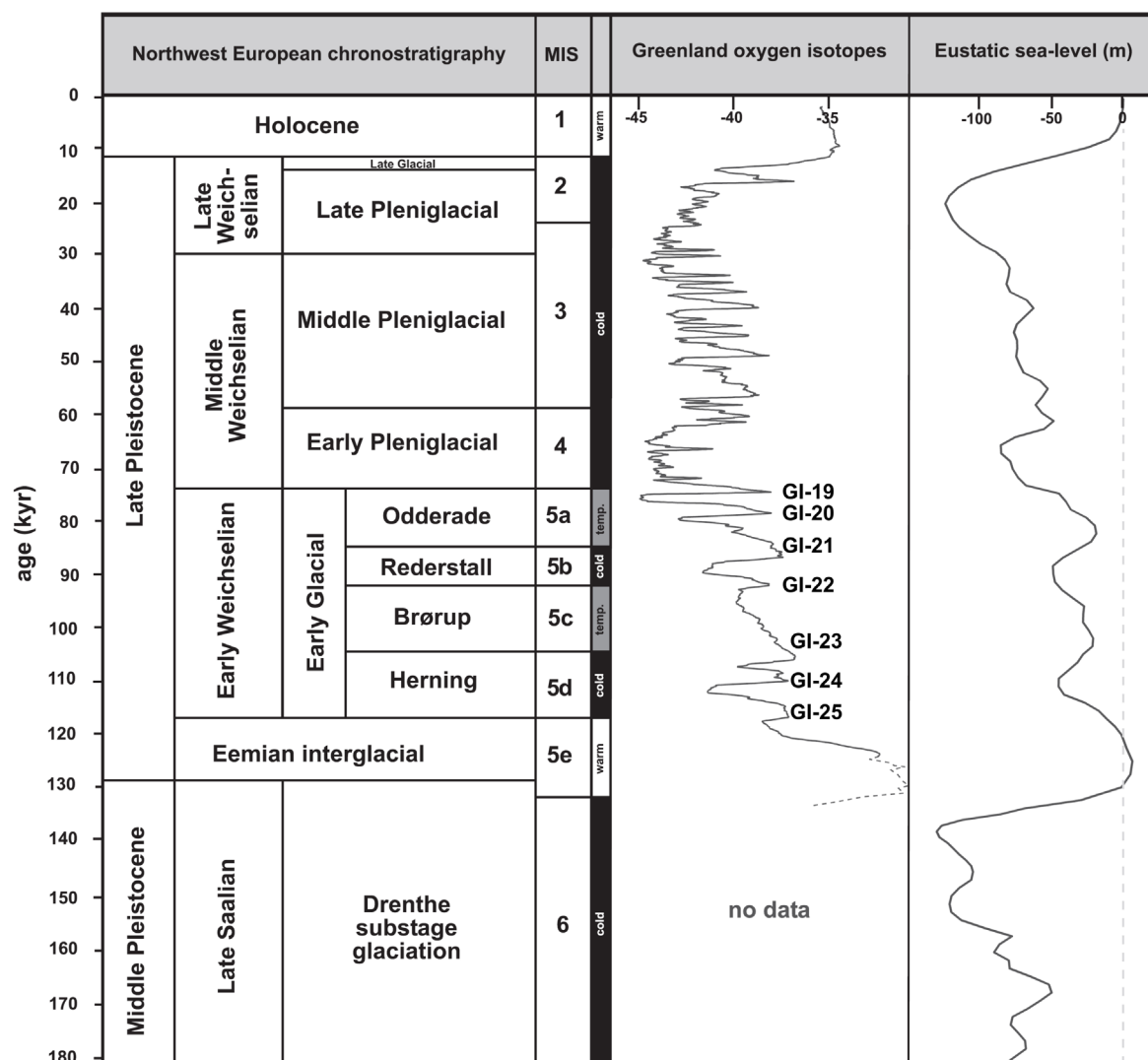


Figure 2: Climato-stratigraphic subdivision of the last interglacial/glacial cycle in Central and Western Europe (modified after Peeters et al., 2015).

Greenland ice cores

Another outstanding and extensive palaeoclimatic record is provided by several long cores, such as GISP, GISP2, GRIP, NEEM, and NGRIP, drilled at the polar ice-cap of Greenland to depths of up to 3 km and covering the last interglacial/glacial cycle (Rasmussen et al., 2014). The three ice cores GRIP, GISP2, and NGRIP were correlated by volcanic and chemo-stratigraphic matching, i.e., comparing tephra, peaks in the

sulfur concentrations (SO_4^{2-}), dust input (Ca^{2+}), and biomass burning events (NH_4^+). The chronology relies on known ages of the contained tephras and on annual layer countings for certain sections in the different cores (Seierstad et al., 2014). Temperature reconstructions are based on $\delta^{15}\text{N}$ measurements on air bubbles, entrapped within the glacier and on $\delta^{18}\text{O}$ -values of the ice (Kindler et al., 2014). Within this record, millennial-scale climatic fluctuations between stadial and interstadial conditions were detected, known as Dansgaard-Oeschger (D-O) events. Every such event cycle is asymmetric in nature and consists of abrupt warming followed by a gradual decrease in temperature (Dansgaard et al., 1982). Numbering starts with 1 for the last pre-Holocene cycle (Younger Dryas) and numbers increase consistently with growing age up to 26. Later, a revised scheme was proposed, maintaining the numeration but dividing each D-O cycle into the initial warm and the successive cold phase, i.e., into a Greenland Interstadial (GI) and a Greenland Stadial (GS) (Rasmussen et al., 2014). It remains unclear, how these events are triggered (Sánchez Goñi, 2020). However, they seem to be closely corresponding to changes in strength and a southward shift of the AMOC (Atlantic meridional overturning circulation, *vulgo*: Gulf Stream) and likely also the ITCZ (Intertropical Convergence Zone) (Kindler et al., 2014). The overall climatic trends for the northern hemisphere are similar to the MIS patterns (see above), but the ice core records exhibit a distinctly better resolution, because of higher accretion rates, negligible bioturbation, and a more precise dating (Aitken and Stokes, 1997). Therefore, they are much more sensitive to those short-term events (D-O/GI, GS). Relevant to the timescale in question for this thesis is the period from Greenland Stadial GS-26 (starting at 119 ka) to Greenland Interstadial GI-19 (ca. 71 ka), which altogether relates to the Early Weichselian, whereas for the last interglacial, no Greenland Interstadial is assigned (Rasmussen et al., 2014) (Figure 2).

These global or hemispherical palaeoclimate records provide an eminently valuable reference system for palaeoenvironmental and archaeological research in the Late Pleistocene. However, those macro-climatic findings cannot directly be transferred to terrestrial conditions because of complex ecological and meso-climatic responses at the continental scales (e.g. Shackleton et al., 2003). For that reason, it is inevitable to include terrestrial archives in order to examine the relationship of global climatic trends and

continental developments, and to provide local environmental context for archaeological sites.

1.3.2 Terrestrial/continental evolution of palaeoenvironments on the European Plain

Preliminary remarks

It is important to note that the functioning of these former, Late Pleistocene ecosystems is not easily compared to present-day equivalents. Their compartments had unusual (non-analog) associations and characteristics, resulting from individualistic and unexpected responses to repeatedly changing climates (cf. Guthrie, 2001). This has long been realized for the fauna (Bolland et al., 2021; Graham, 2005; Stewart, 2005), vegetation (Chytrý et al., 2019; Pross et al., 2000), and their mutual relationship. It led *inter alia* to the introduction of the “steppe-tundra” or “mammoth-steppe” concept for the Weichselian Pleniglacial (Guthrie, 1990; Zimov et al., 2012). But also soil formations differed from current counterparts in terms of thickness, typology and associated pedogenic processes (Meszner and Faust, 2018; Stremme et al., 1982; cf. Velichko and Morozova, 2010). While this was undoubtedly co-determined by climatic variations, palaeoclimate *itself* might be regarded as non-analog: Considerable fluctuations in sea levels, the AMOC, ice extents, and insulation affected the European Plain in various ways and combinations (e.g. Salonen et al., 2013). And lastly, CO₂ concentrations of c.280 ppm have been measured for the last interglacial, decreasing to <200 ppm in late MIS 5 (Fischer et al., 1999). Hence, CO₂ values for most of MIS 5 would have been significantly lower than the ditto 280 ppm in pre-industrial times of the Holocene (Monnin et al., 2001). Lower atmospheric CO₂ concentrations would have had negative physiological effects on plant growth due to reduced photosynthesis and increased transpiration. It would have also affected floristic compositions, as CO₂ depletion seems to constrain trees stronger than herbaceous plants (Harrison and Bartlein, 2012). This non-exhaustive compilation of non-analog conditions is not meant to overemphasize these factors, but nor should they be carelessly disregarded when investigating and interpreting palaeoenvironmental processes.

Overarching characteristics of the Eemian Interglacial and Early Weichselian Glacial

Information on the Eemian and Early Weichselian palaeoenvironments and -climates are to a large extent derived from abundant palaeolake basins whose formation is associated with the Saalian glaciation (Caspers et al., 2002; Helmens, 2014). Apart from these lacustrine archives, access to meaningful data is very much restricted to coastal areas (Höfle et al., 1985; Marks et al., 2014) and loess/riverine landscapes which tend to preserve respective palaeosols and deposits (Antoine et al., 2016; Fuchs et al., 2013; Turner, 2000; Vandenberghe, 2015). And additionally, deposits of that period can be found in zones of tectonic subsidence (Knipping, 2008; Schokker et al., 2004). From these archives it is known, that roughly in congruence with the North Atlantic data (see 1.3.1), the European Plain saw frequent and high-amplitude climatic changes during MIS 5. The terrestrial information, mainly based on palynology, reveals rapid warming in the Early Eemian Interglacial and then an overall deteriorating climate from the Mid-Eemian to the onset of the first glacial maximum in MIS 4. This is chiefly expressed by increasing continentality with strong shifts in winter temperatures and precipitation (Salonen et al., 2013). The general cooling trend in the period in question was superimposed all across the European Plain by three fully-forested intervals: the Eemian Interglacial, the Brörup Interstadial, and the Odderade Interstadial (~MIS 5e, 5c and 5a). These were separated by two cooler phases with more open vegetation: the Herning and Rederstall Stadials (~MIS 5d and 5b) (Behre, 1989; Caspers and Freund, 2001). This variation had significant and poorly understood geo-environmental effects. It necessitated repeated reconfigurations and redistributions of the vegetation and fauna but and also similar adjustments within the sedimentary and hydrographic systems (e.g. Pecl et al., 2017). However, such responses often lagged behind the climatic development and also differed spatially (cf. Brauer et al., 2007; Sier et al., 2015). Within the former vegetation, there is a general trend, that steppic floral elements increase toward the east, (sub-)arctic elements enlarge toward the north, and the continentality gradient was more enhanced in colder stages than in warmer intervals (Caspers and Freund, 2001; Emontspohl, 1995; Helmens, 2014; Velichko et al., 2005; Yelovicheva and Sanko, 1999, see also below).

Without much systematic research on landscape dynamics in this period (i.e. on geomorphic activity and stability phases) and a scarcity of numerical ages, our comprehension of how terrestrial sediment systems adjusted to these climatic changes remains vague. Usually, for the Eemian, stable surfaces are assumed, enabling soil formation on well-drained positions and humus accumulation in waterlogged basins (e.g. Menke, 1992). In one of the few studies that cover this topic, Schokker et al. (2004), confirm this notion for the Eemian optimum, but report increased clastic sediment redeposition in the early and late phases of the interglacial. This is in agreement with the ubiquitous occurrence of truncated (i.e. partially eroded) Eemian palaeosols in the loess belt (Antoine et al., 2016; Jary and Ciszek, 2013; Lehmkuhl et al., 2016). For the Early Weichselian in NW Germany, Lade and Hagedorn (1982) developed a depositional model that encompasses soil formation/humus accumulation in the warmer interstadials and slopewash/solifluction in the colder stadials. Although this model is not based on numerical dating, it seems to hold true for the loess areas, as well (e.g. Chu and Nett, 2021; Lehmkuhl et al., 2016). Likewise, the temporal and spatial coupling of landscape dynamics in the hinterlands and fluvial discharge/aggradation patterns in the river valleys remains vastly unexplored for MIS 5 (but see Panin et al., 2020; Winsemann et al., 2015). Even so, such knowledge could vastly enhance our understanding and interpretation of artifact scatters in secondary contexts of fluvial gravels (Bridgland et al., 2006).

Fluvial dynamics of this period are not easy to assess. Changes in the sedimentary budget of rivers (i.e. incision/aggradation) usually occur in transitional phases from warm to cold or *vice versa*, when the fluvial systems need to rearrange toward a new equilibrium (Bridgland and Westaway, 2008). However, the specific behavior of any given river in any given time is highly individual. Fluvial reactions are non-linear and governed by the interplay of a whole set of influencing factors, such as longitudinal gradient, sediment supply, and discharge. All of these influences are themselves depending on various aspects (climate, vegetation, sea level, tectonics) (Vandenbergh, 2015). During the Eemian, stable floodplains with meandering or anastomosing rivers are assumed, characterized by low overbank aggradation rates (Gao and Boreham, 2011). Subsequently, at the Eemian-Weichselian transition (~MIS

5e/5d), many European rivers in Germany, Belgium, Northern France, and Britain responded in the form of incision. This eradicated much of the previous Eemian floodplain along with potential Neanderthal occupation traces within the valley (Antoine et al., 2007; De Clercq et al., 2018; Gibbard and Lewin, 2002; Winsemann et al., 2015). For the Russian Plain, no numerical dates have been obtained yet, but a coincidental development could be assumed because Eemian deposits are extremely rare in the fluvial archives there (Panin et al., 2017). For the Early Weichselian, chronological information is on thin ground, but Winsemann et al. (2015) reconstructed incision events during MIS 5d and the MIS 5c for the German Weser-Leine catchment. In the paleo-Scheldt valley in N-Belgium and the Lower Rhine valley, stable conditions prevailed throughout the Early Weichselian (Busschers et al., 2007; De Clercq et al., 2018), but were likely influenced by near-coastal conditions. At the same time, incipient aggradation occurred in Russia (Panin et al., 2017). Lastly, the major climatic shift at the MIS 5a/4 transition was accompanied by roughly simultaneous incisions of the Lower Rhine (Peeters et al., 2015), many smaller rivers in the Netherlands and Poland (various authors cited in Mol et al., 2000), and the Weser river in Northern Germany (Winsemann et al., 2015). Again, this fluvial erosion likely compromised *in situ* archaeological records of the Early Weichselian in the valleys (cf. Bridgland et al., 2006).

Similarly, the reconstruction of specific faunal elements suffers from low spatio-temporal resolution and a shortage of reliable data (Finlayson and Carrión, 2007). In the Eemian, a warm-adapted forest fauna was present, including large species such as straight-tusked elephant (*Elephas antiquus*), the narrow-nosed rhinoceros (*Stephanorhinus hemitochus*), and the giant deer (*Megaloceros*), but also woodland ungulates, such as red and fallow deer (*Cervus elaphus* and *Dama dama*) and aurochs (*Bos primigenius*). The widest spectrum of this Eemian fauna was obtained at the archaeological sites of Neumark Nord (Kindler et al., 2020; Strahl et al., 2010), Gröbern (Litt and Weber, 1988), and Lehringen (Thieme and Veil, 1985). This warm fauna disappeared from the European Plain before the end of the Early Weichselian. As to when that happened there is no real consensus. This transition process might have started as early as the Mid-Eemian (Richter, 2016) and was definitely completed before

the onset of the Pleniglacial (~MIS 4) (Defleur and Desclaux, 2019; Finlayson and Carrión, 2007). In the cooler spells of the Early Weichselian, a less varied spectrum of cold-adapted open woodland and steppe fauna surfaced and later on dominated. It was characterized by reindeer (*Rangifer tarandus*), steppe bison (*Bison priscus*) and horse (*Equus*) (Finlayson and Carrión, 2007; Loch et al., 2014; Roebroeks et al., 1992). Finally, by no later than MIS 5a, the woolly mammoth (*Mammuthus primigenius*) and woolly rhinoceros (*Coelodonta antiquitatis*) appear in the sequences (Chubur, 2013; Richter, 2016). This cold-adapted faunal association prevailed through much of the later Weichselian as an inseparable part of the mammoth steppe biome (Guthrie, 2001).

Eemian Interglacial (~MIS 5e)

For the Eemian Interglacial a typical vegetation succession can be observed throughout the European Plain (Turner, 2002; Velichko et al., 2005) and in southern Scandinavia (Björck et al., 2000; Salonen et al., 2013). The uniformity of the diagnostic tree species development in the area allows for low-effort correlations between several archives. In Northern Germany, according to the dominant arboreal taxa, the Eemian is subdivided into seven pollen assemblage zones, PAZ E1 to E7 (Caspers et al., 2002; Menke and Tynni, 1984). The succession is as follows: birch → pine/birch → thermophilous mixed oak forests → admixture of hazel-yew-lime → hornbeam-spruce → boreal type forests with pine-spruce-fir → pine. For neighboring regions, such as France, the Netherlands, Poland, and Russia, very similar and correlatable classification schemes exist (de Beaulieu and Reille, 1992; Grichuk, 1961; Mamakowa, 1989; Zagwijn, 1961). This progression is descriptive of a rapid warming period followed by an extensive thermal optimum and finally a temperature deterioration towards the end of the interglacial.

The rather small longitudinal variation in the floral compositions of different regions was facilitated by a more oceanic climate even in Eastern Europe. This effect is connected to the generally higher eustatic sea levels in the Mid-Eemian, which surpassed the current stands by 5 to 9 meters (Dutton and Lambeck, 2012). More regionally, these raised levels caused the separation of the Jutland peninsula from the

Central European landmass and also formed a direct connection between the Baltic and the White Sea through Karelia (Miettinen et al., 2014).

Palaeoclimatic parameters, derived from pollen, botanical macro remains, but also from different faunal assemblages (Behre et al., 2005; Caspers et al., 2002; Köhl et al., 2007; Kupryjanowicz et al., 2018; Russell Coope, 2000; Zagwijn, 1996) indicate that the temperatures were similar or up to 2-3 degrees higher than today in the Eemian optimum all across the European Plain. Especially the winter temperatures exceeded present-day values by several degrees. Notably, in different studies, there are contradictory gradients of continentality towards south-eastern Europe (Brewer et al., 2008; Kaspar, 2005). Precipitation values are even more difficult to reconstruct but assumed to be comparable to, yet more variable than today, especially in the eastern region (Pidek et al., 2021).

Recently, there is a lot of debate on the duration and timing of the Eemian. Traditionally, the Eemian is correlated with MIS 5e and thought to have lasted from 128 to 117 ka (cf. Tzedakis, 2003). This was in good agreement with varve countings at the site of Bispingen (Northern Germany) that implied a duration of 10,000 to 11,000 years (Müller, 1974). However, marine cores off the coast of Iberia suggested a considerable time offset between MIS 5e and the terrestrial interstadial (Shackleton et al., 2003). For Central Europe, Sier et al. (2015, 2011) recognized a delayed onset of the Eemian with respect to MIS 5e by as much as 10,000 years. Conversely, Brauer et al. (2007) determined a simultaneous beginning with MIS 5e but a much longer duration of 17,000 years, based on varves in Southern Italy. This diachroneity indicates a time-transgressive onset of the Eemian throughout Europe with a noticeable delay in Central Europe. The discussion of possible reasons for that is not within the scope of this thesis. However, these seemingly contradicting estimates for the Eemian chronology point out, that caution should be exercised when interpreting MIS 5e-equivalent numerical ages in the absence of biostratigraphical control.

Early Weichselian (~MIS 5d – 5a)

Herning Stadial (WF I): Temperatures dropped after the Eemian (mean of 10°C and -15°C for July and January) and low sea levels (ca. 40m lower than today) caused a

higher continentality (Helmens, 2014; Zagwijn, 1983). Therefore, most tree taxa had retreated to the south, and open vegetation, comprised of heath (*Calluna vulgaris*) and grasses (Poaceae) dominated on the European Plain, with some admixture of juniper (*Juniperus*) (Behre, 1989; Helmens, 2014). Much of the European Plain was likely situated in the forest/tundra ecotone, a transitional zone between tundra and taiga, where boreal tree pollen amount to max. 50% (Emontspohl, 1995).

Brörup Interstadial (WF II): The Herning was followed by a climatic amelioration. Mean July and January temperatures increased to 15 to 19°C and -8 to -14°C, respectively (Caspers and Freund, 2001; cf. Köhl et al., 2007). Compared to the Eemian, this development shows the advancing degree of continentality, comprising low winter temperatures and low precipitation values, due to much lower sea levels. According to Behre (1989) and Caspers and Freund (2001), this distinct seasonality is the major reason, why temperate forests species did not fully re-immigrate during the Early Weichselian interstadials on the European Plain. Instead, this interval saw the dominance of birch and pine forests, with the admixture of spruce, larch, and alder. Birches were determining the first half (WF IIa) and pines were more abundant in the second half (WF IIb) of the Brörup Interstadial. To the north, the forest/tundra ecotone was situated approximately in central Jutland (Björck et al., 2000; Caspers and Freund, 2001; Emontspohl, 1995). To the east, tree species composition remained similar to Central Europe, only the abundance of moisture-loving taxa decreased (e.g. *Calluna vulgaris*, *Sphagnum*), while the percentage of steppe species was higher (e.g. *Artemisia*, *Chenopodiaceae*) (Helmens, 2014). Also, the values for the relatively thermophilous deciduous trees, such as alder (*Alnus*) seem to be even lower in Eastern Europe (Caspers and Freund, 2001; Yelovicheva and Sanko, 1999). By contrast, in the western part of the European Plain (e.g. Amersfoort, NL), oceanic conditions have fostered higher *Alnus*-, *Calluna*- and *Sphagnum*-percentages and even the more demanding oaks, that did not clearly colonize Central and Eastern Europe (Emontspohl, 1995; Zagwijn, 1989). Based on annual varves in the diatomite at the Rederstall site, a duration of 5,800 to 10,500 years was estimated for the Brörup Interstadial (Grüger, 1991). This appears too short in comparison with the North Atlantic palaeoclimate records, which seem to suggest a time interval closer to 15,000 years (see below).

Rederstall Stadial (WF III): Rederstall deposits only occur infrequently, especially pollen-bearing sequences. This is why, only the beginning and end of this stadial are usually documented, if at all (Caspers and Freund, 2001). The records indicate open heliophile vegetation, dominated by Poaceaea, steppe taxa and *Juniperus* (juniper) (Behre, 1989; Helmens, 2014). Thicker sediments and first evidence of (discontinuous) permafrost imply a stronger climatic deterioration than in the Herning (Caspers, 1997). Even so, fossil beetle evidence indicates comparable temperatures to the Herning Stadial (-9 to -12°C and 11°C for January and July) (Walkling, 1997). Furthermore, an increased seasonality compared to the Herning is inferred from the more western distribution pattern of *Artemisia* (Emontspohl, 1995; Helmens, 2014).

Odderade Interstadial (WF IV): The Odderade Interstadial is considered more or less analogous to the Brörup regarding vegetation patterns and their distribution (Behre, 1989; Zagwijn, 1989). As a slight difference to this previous interstadial, boreal pine-birch forests did not reach as far north and *Alnus* is generally less represented. Both indicates marginally cooler and more continental conditions (cf. Emontspohl, 1995; Zagwijn, 1989). Mean temperatures of 12 to 17°C and -11 to -22°C have been established for summer and winter in this period (Helmens, 2014; Kühl et al., 2007). Quick readvances of forests after the Rederstall suggest, that the boreal tree species survived the preceeding stadial phases in the wider region and/or in favorable topographic positions (Caspers and Freund, 2001). In the absence of varved sediments, the duration of the Odderade has been assessed to 5,000 and 10,000 years, leaning on the sediment thickness and the general comparability with the Brörup Interstadial (Behre and van der Plicht, 1992). After the Odderade and before the onset of the first glacial maximum, there are one or two short climatic amelioration phases, in which boreal forests briefly reappeared in France and the Alpine Foreland in Germany and Switzerland (de Beaulieu and Reille, 1992; Müller and Sánchez Goñi, 2007). For the European Plain, there is no palynological evidence for such fluctuations in this transitional period, so far (see Chapter 4).

The timing of the Early Weichselian Interstadials is not officially determined. Conventionally, Brörup and Odderade are correlated with MIS 5c and 5a, respectively (Behre and van der Plicht, 1992) and with GI-23/22 and 21 (Rasmussen et al., 2014;

Richter, 2016). Accordingly, the Herning and Rederstall Stadials are assigned to MIS 5d and 5b (Behre and van der Plicht, 1992). In the Alpine Foreland and the loess belt of central and western Europe, this congruence has been confirmed (Antoine et al., 2016; Boch et al., 2011, see also discussion in Chapter 4), whereas in the type region of these (inter)stadials – the NW European Plain – no conclusive chronology has been established, yet.

1.3.3 Neanderthal population dynamics

In the foregoing sections, palaeoclimatic and palaeoenvironmental background information was provided which may serve as a mental framework to assess Neanderthal occupation on the European Plain in the Late Pleistocene. In this section, the focus lies on the geographical distribution of archaeological remains in different temporal phases and some aspects of subsistence. It is not within the scope of this thesis to review and address specific tool production methods or nomenclatorial, typological, or even “cultural” issues. For an overview of these complex and in some cases ambiguous questions, see e.g., Rolland & Dibble (1990), Soressi (2005), Jöris (2006), and Richter (2016).

The geographic map of the Middle Palaeolithic ecumene in the Eemian and Early Weichselian is rather vague and low in content, and it suffers from **(1)** a research bias and **(2)** a geological or preservation bias (cf. Nielsen et al., 2017).

(1) Conceivably, just a very low percentage of human occupations through time has been discovered yet (cf. Roebroeks, 2014; Speleers, 2000). Sites seem to cluster in regions, where artificial exposures of the aggregate industry enabled regular surveys (Kels and Schirmer, 2011; Richter, 2016; Valde-Nowak and Łanczont, 2021) or where rescue excavations related to large-scale construction and infrastructure projects have been conducted, e.g. in northern France (Locht et al., 2016, 2014). Apart from that, systematic search for new sites has been rather patchy, and only recently, commendable endeavors to locate unknown occupations have started in the form of geodata-based predictive modeling (Nielsen et al., 2019, for SW-Scandinavia). Furthermore, the sites that exist mostly lack a precise dating (e.g. Wiśniewski et al.,

2019), so that their chronological allocation often remains disputable (Jöris, 2004; cf. Richter, 2016).

(2) Following the disintegration of the Saalian ice sheet, natural processes have been persistently working towards a leveling of the undulating late glacial landscape, employing erosion and deposition (e.g. Fränzle, 1988; Zagwijn and Paepe, 1968). These processes are bound to have jeopardized the archaeological record, especially in (but not restricted to) sloping positions. Since the geomorphological dynamics of the period in question are also largely unspecified (see 1.3.2), the extent of the occupational records being endangered or eradicated cannot even be estimated. To give an example, numerous sedimentary archives across the European Plain bear witness to an extensive and severe erosion event at the late Eemian/Early Weichselian transition (see 1.3.2). In loess-palaeosol sequences, the uppermost ~50 cm, i.e. the E-horizons of the Eemian luvisol soils are always missing (e.g. Antoine et al., 2016 see also above), so likewise is the entire Eemian occupation surface (cf. Uthmeier et al., 2011). As already mentioned, in river valleys, more often than not, fluvial downcutting at the Eemian-Weichselian transition has caused the predominant eviction of the previous Eemian sediment suites (Ehlers, 1990; Gibbard and Lewin, 2002; Vandenberghe, 2015; Winsemann et al., 2015). During the following stadials Herning and Rederstall (~MIS 5d and 5b), increased slope erosion has to be assumed on account of lighter vegetation cover (Lade and Hagedorn, 1982). Posterior cryoturbation mainly in MIS 4 and 2 would have had additional disturbing effects on the stratigraphic integrities in shallow sediment suites (e.g. Bertran et al., 2014). This leaves us with topographic depressions as reliable repositories for human occupation in that period (esp. palaeolake basins, see 1.3.2). These special geomorphological situations inhibit erosion and can preserve Eemian and Early Weichselian deposits, and – by extension – also the archaeological remains. So if a large share of the MIS 5 sites on the European Plain is associated with palaeolakes of various dimensions (see below), it is difficult to decide, whether this is due to the selective preservation of these (closed-depression) landforms or rather the attraction of the former watering places.

Eemian (~MIS 5e)

For the Eemian Interglacial, sites are overall very sparse on the European Plain, except for a cluster in Germany, which displays a considerable record compared to the neighboring regions (see Wenzel, 2007 for a compiled map). Among those sites are Lehringen (Thieme and Veil, 1985), Neumark-Nord 2/2 (Kindler et al., 2020), Gröbern (Mania et al., 1990), Grabschütz, and Rabutz (Weber, 1990) all discovered in open-cast mines for lignite or aggregates and preserved in palaeolake basins associated with the Saalian Glaciation (cf. Chapter 3). A rather unknown site in Woltersdorf (ca. 3 km from Lichtenberg) falls in the same category as the artifacts are contained in a mid/late Eemian peat of a small palaeolake (Breest, 1992). Furthermore, some sites are preserved in travertines, e.g. Steinmühle/Veltheim, Burgtonna, Weimar Parktravertin (Wenzel, 2007), and Taubach (Bratlund, 1999), or more rarely in fluvial sediments, e.g. Wallertheim (Adler et al., 2003). In adjacent Northern France, although many decades of intensive research in the loess area were carried out, only a handful of sites has been discovered from that time period (Locht et al., 2014). And in the loess belt of Southern Poland, just the two sites of Orzechowce and Kraków-Zwierzyniec are tentatively assigned to the Eemian for stratigraphical reasons (Valde-Nowak and Łanczont, 2021). In SW Scandinavia (Jutland) and on the British Isles, confirmed occupations lack altogether (Lewis et al., 2011; Nielsen et al., 2017), in spite of climatically favorable conditions (see 1.3.2). Similarly, from the vast Russian Plain, no Eemian sites have been reported so far (Velichko, 1988).

The low number of sites resulted in the assumption of particularly low population densities in the Eemian (e.g. Roebroeks et al., 1992). This decline is attributed to rather challenging environmental conditions in the densely-forested landscapes with a presumed lower carrying capacity (esp. abundance) for ungulate biomass compared to open landscapes (Hublin and Roebroeks, 2009). Coupled with the higher energetic costs of Neanderthals for sustenance and mobility (Roebroeks and Soressi, 2016) this could have led to dietary stress compromising human reproduction, and even to Neanderthals resorting to cannibalism in the interglacial (Defleur and Desclaux, 2019 present evidence from the Moula Guercy cave in S-France). However, it is highly probable that the number of currently known sites is far from representing a realistic

record for the actual Neanderthal occupation (cf. Locht et al., 2014), so that the causal reasoning of Defleur and Desclaux (2019) might be premature.

Alternatively, the geographic asymmetry and also the general scarcity of Eemian sites are possibly best explained by different research histories/intensities and geological or topographical factors (e.g. Speleers, 2000). Examples for the latter would be marine channels barring the dispersal to Britain and Scandinavia, or the large-scale erosion after the Eemian, or the scarcity of accommodating landforms outside of the Saalian Glaciation area (cf. Nielsen et al., 2019).

Eemian sites are commonly described as short-term but occasionally recurring occupations relating to lithic production, hunting, and butchering, indicating a highly mobile land use strategy (Wenzel, 2007). However, for Neumark-Nord 2/2 it could be shown that this high mobility is rather local compared to mobility in open landscapes, inferred from the more locally roaming prey. This led to frequent and repeated site occupations and intensive site use (Kindler et al., 2020). Humans exploited ungulates like aurochs (*Bos primigenius*) and cervids (*Cervus elaphus* and *Dama dama*) as well as big game, such as rhino (*Dicerorhinus kirchbergensis*) and elephant (*Palaeoloxodon antiquus*) (Kindler et al., 2020). Lithic assemblages are dominated by small-sized, discoid and levallois artifacts, produced on simple blanks, whereas bifacial technology is rare (Pop, 2014; Richter, 2016; Wenzel, 2007). Therefore, an opportunistic, rather unselective raw material procurement and exploitation from local sources were proposed, presumably constrained by the limited accessibility of flint on the densely-vegetated and stable surfaces (Locht et al., 2014; cf. Pop and Bakels, 2015; Richter, 2016).

Early Weichselian (~MIS 5d – 5a)

Just like for the Eemian, there is merely a very small number of open-air sites from the Early Weichselian on the European Plain (Figure 1). In Germany, only four sites seem to be uncontested: (1) Tönchesberg 2B, thought to correspond to MIS 5d or 5c (Conard, 1992; Roebroeks et al., 1992), (2) Wallertheim D, E, F, correlated with MIS 5c (Conard and Adler, 1997), (3) Rheindahlen-Westwand B1, stratigraphically related to the Early Weichselian (Bosinski, 2008; Schmitz and Thissen, 1998), and (4) Neumark Nord 2/0

(Laurat and Brühl, 2021; Richter and Krbetschek, 2014), dated to MIS 5c or 5a based on luminescence dating. Apart from that, Middle Palaeolithic artifacts at the site of Schalkholz on the Jutland peninsula are contained within a peat deposit from the Brörup Interstadial (~MIS 5c) (Arnold, 1978; Nielsen et al., 2017). In Southern Poland, the two sites of Pikulice (dated to MIS 5c) and Nehrybka (associated with Early Weichselian soil formation) fall in this time period (Valde-Nowak and Łanczont, 2021). On the Russian Plain, a couple of sites have the potential to be of Early Weichselian antiquity for their stratigraphic situation, such as Sukhaya Mechteka, Khotylevo I, Vykhvatinskiy naves, and Moldova I and V (Velichko, 1988) (Figure 1), but reliable numerical dates have not yet been obtained.

This shortage of sites is in stark contrast to the neighboring region of northern France where numerous occupations ($n > 40$) from the Early Weichselian have been discovered in recent decades in the course of targeted infrastructure activities (Locht et al., 2016). This contrast suggests, that just like for the Eemian, a pronounced research bias exists that strongly distorts the occupation geography (cf. Nielsen et al., 2017). Another important point is the vagueness of chronologies for the majority of Middle Palaeolithic sites: In contrast to the MIS 5 record, there is an unevenly larger share of Middle Palaeolithic occupations on the European Plain that is placed into MIS 3, but mainly due to typological considerations and not based on numerical dating. This is particularly true for assemblages of the *Keilmessergruppen* (Mania et al., 1990; Veil et al., 1994), also called MMO-assemblages (Mousterian with Micoquian Option) (Richter, 2016, 1997). However, at least for a couple of these sites, there are good (bio-)stratigraphic arguments to assign them to MIS 5a, instead of MIS 3 (e.g. Jöris, 2004; contra Richter, 2016). This applies, for instance, for the sites of Königsau (Mania, 2002), Lichtenberg (Veil et al., 1994) and Salzgitter Lebenstedt (Hublin, 1984; Pastoors, 2001; Tode, 1982). The present author fully endorses this alternative notion after reviewing the published environmental information (Mania and Toepfer, 1973; Pfaffenberg, 1991; Veil et al., 1994). Therefore, these three sites appear in Figure 1 tagged as “Early Weichselian”, acknowledging that the occupations of Salzgitter Lebenstedt and Lichtenberg might even have happened at the MIS 5a/4 transition (cf. Jöris, 2004). For the period of this MIS 5a/4 boundary, elsewhere also the site of

Wrocław Hallera Av., Complex B, Poland (Wiśniewski et al., 2013) and more than 10 sites in Northern France have been documented (Locht et al., 2016).

The artifacts of Early Weichselian sites are usually contained within shallow colluvial or solifluction sediments (Locht et al., 2016; Valde-Nowak and Łanczont, 2021), limnic/peaty deposits at palaeolake shores (Caspers and Freund, 2001; Laurat and Brühl, 2021), or fluvial deposits (Wiśniewski et al., 2013). In the Central European assemblages, a certain typological continuity from the Eemian is displayed (Laurat and Brühl, 2006; Loch et al., 2016; Richter, 2016), with “microlithic” tools made on Levallois or - less frequently - discoidal blanks. In some assemblages occur small blades with backed or retouched points (Hublin and Roebroeks, 2009). Especially sites west of the Rhine, like Tönchesberg 2B, Wallertheim D, and Rheindahlen B1 have a large blade component. Contemporaneous Early Weichselian blade assemblages are also known from sites in northwestern France and Belgium (Bosinski, 2008; Conard, 2012; Loch et al., 2016). As a tendency, more diversified reduction strategies with co-existing systems can be observed. Compared to the Eemian, this relative diversification implies a slightly improved, but still difficult raw material procurement, with less dense forests allowing some minor sediment redeposition and better access to lithic resources (Locht et al., 2014). If the mentioned *Keilmessergruppen* sites are considered to be (late) MIS 5a, then at the end of the Early Weichselian, a clear shift in the assemblages has to be noted towards larger, bifacial, and less variable tools made from large-sized, high-quality raw material (Keilmesser, handaxes, leaf-shaped scrapers) (Weiss, 2019; Weiss et al., 2018). Interestingly, this typological shift would have happened in parallel with the gradual disappearance of the woodland fauna and the emergence of the steppe species (cf. Loch et al., 2014; Richter, 2016).

Pleniglacial (~MIS 4 and early MIS 3)

During the first glacial maximum of the Weichselian (~MIS 4), Neanderthals seem to have avoided the European Plain, i.e., the “northern” realms of Europe, where periglacial conditions prevailed (Richter, 2016; Wiśniewski et al., 2013). Hublin and Roebroeks (2009) make a convincing point, that this apparent desertion might have been caused by regional extinction, rather than migrations to the south. Either way,

after this void, a recolonization can be observed, starting from the more southern parts of the European Plain and neighboring areas in late MIS 4 (Locht et al., 2014; Wiśniewski et al., 2019). Albeit, there are two notable exceptions to this pattern: (1) The Garzweiler open-cast mine in western Germany yielded numerous artifacts and as many as eight sites in the MIS 4 loess, thought to relate to gelic Gleysols (Kels and Schirmer, 2011; Uthmeier et al., 2011). (2) The site of Havrincourt in N-France features an occupation associated with an arctic brown soil that can credibly be correlated with GI-18 (ca. 64 ka) in mid-MIS 4 (Antoine et al., 2014; Guérin et al., 2017; Loch et al., 2016). This evidence sheds new light on the MIS 4 ‘settlement’ geography. At least in the western part of the European Plain and the adjoining northern France region, the more oceanic conditions seem to have allowed for ephemeral occupations. Hence, these landscapes were possibly “far away from being [...] hostile cold desert(s)” (Uthmeier et al., 2011). Further claims for MIS 4 occupations in northern France and thus a relative settlement continuity cannot be chronostratigraphically substantiated yet in the present author’s opinion (Banks et al., 2021; Loch et al., 2016).

The assemblages of early MIS 3 all across the European Plain constitute the richest Middle Palaeolithic ecumene and are mostly assigned to the *Keilmessergruppen*/MMO (Richter, 2016). Only recently, increased efforts have been made to gradually establish chronologies for these open-air records (Weiss, 2019, 2015; Winsemann et al., 2015; Wiśniewski et al., 2019). Yet, with many sites remaining undated and a large share of surface finds with ambiguous stratigraphic context, an uncertain portion of these occupations could likely have occurred in MIS 5a, as well (see Jöris, 2004; cf. Richter, 2016, for discussions on the “long” vs. “short” chronology of the *Keilmessergruppen*).

1.4 METHODS

In the following section, the main methods of palaeoecological and chronological analysis used for this work are described with respect to the gain of knowledge they can provide. More detailed technical aspects and also archaeological methods in a stricter sense can be found in the respective paragraphs of Chapters 2 to 4 and the related supplementary information.

Apart from the methods outlined below, the present author also actively took part in sampling and discussion of the results for micromorphology and phytolith analysis (Chapter 4). Sampling and interpretation of values for soil organic carbon and total nitrogen has been done by the author, and he was an integral part in the seismic measurements and their interpretation (Chapter 3). Furthermore, he jointly planned, organized and conducted the excavations in Lichtenberg with Dr. Marcel Weiss, i.a. operating the mechanical excavator (Chapter 4).

The only aspects, the present author did not directly contribute to, are the preliminary statistical analysis of the Lichtenberg lithic artefacts and the traceology on this material (Supplementary Information 1 for Chapter 4).

1.4.1 Prospection and Fieldwork

Particular emphasis was put on the geomorphological and stratigraphic settings of the two sites investigated. Prior to fieldwork, a simple GIS-based terrain analysis has been conducted, in order to preliminarily assess the temporal relationship of different depositional processes and to better locate positions for future fieldwork (cf. Cook et al., n.d.; Garrison, 2016). This analysis encompassed topographical, geological and historical maps, as well as aerial photographs and digital elevation models (DEMs) in horizontal resolutions between 25 and 1 m (cf. Otto et al., 2018) (see supplementary information for Chapter 3). For Khotylevo, this was only possible to a limited extent, unfortunately, as high-resolution data were more difficult to access. Building on this, artificial exposures of the study region were examined, and for Lichtenberg, an extensive coring campaign was planned and carried out. The latter started with dispersed probing in the wider area to gain a profound overview of the depositional variety and it led to the targeted coring transect across the excavation site as reported

in Chapters 3 and 4. Mechanical coring using a motor hammer and open gouges is a versatile and well-established prospection method, both in geomorphology and archaeology and it allows for quick and cost-effective stratigraphic assessment and correlation. Therefore, coring can serve to localize unknown occupations or give environmental context for find layers (Canti and Meddens, 1998; Frew, 2014). With that kind of stratigraphic knowledge, more costly coring activity with truck-mounted systems could be arranged in good conscience. The results of which have already been partly incorporated into this thesis (Chapter 3). Again, because of logistic reasons, in this case, retrieving cores was not feasible for Khotylevo - nor was it strictly necessary. Huge natural exposures and large-scale Paleolithic excavations on the raised bank of River Desna provided a satisfactory insight into the regional sediment suites even beyond the investigated site (Gavrilov et al., 2015; Otcherednoi et al., 2014). All available stratigraphies on- and off-site were described in the field according to German soil mapping standards (AG Boden, 2005), comprising texture, color, bedding, admixtures, as well as carbonate and organic matter contents. Special care was taken to identify disconformities, as well as pedogenic and cryogenic features (Vandenbergh, 2013a). Descriptions of lacustrine and organic sediments followed Meier Uhlherr et al. (2015). That way, the *qualitative* understanding of sedimentary processes and even a notion of their spatial distribution preceded any *quantitative* analysis. In fact, the present author considers this kind of comprehension a prerequisite for establishing the sampling design for any further palaeoenvironmental method.

1.4.2 Luminescence dating

Constraining the ages of deposits and identifying the sequence of events driving archaeological site formation and landscape development is essential for the study of palaeoenvironments and Palaeolithic occupations alike. Numerical dates are utilized to establish and to test theoretical models and concepts (cf. Garrison, 2016; Richter and Wagner, 2015). With the Middle Palaeolithic period being mostly outside of the radiocarbon range (< ca. 50 ka) (Wood, 2015), luminescence techniques are frequently chosen for chronological control. Luminescence dating can estimate the time that has elapsed since a burning event or the burial of sediment (Aitken, 1998). While the

application of luminescence on heated artifacts is constantly evolving and returns remarkable results (e.g. Richter et al., 2017), the scope for this thesis only comprises sedimentation events. The basic principle relies on the phenomenon that certain minerals (called “dosimeters”, esp. quartz and feldspar), due to defects in their crystal lattice, can store energy produced by omnipresent ionizing background radiation within the sediment and from cosmic rays (Aitken, 1998).

Upon stimulation of the mineral by light or heat, the accumulated energy therein is released as luminescence, i.e. visible light. In nature, this procedure of *resetting* the dosimeters (called “bleaching”) is activated by exposure to sunlight during sediment transport, whereby different transportation processes have disparate bleaching potentials (Murray et al., 2012; Wallinga, 2002). After deposition and burial of the mineral grains, energy accumulation starts again, only discontinued by the sampling and measuring activity. In the laboratory, resetting is achieved by stimulating the grains with artificial light at specific wavelengths under above-ambient temperature conditions. The resulting *natural luminescence* signal is detected and documented. In a following sequence of applying known radiation doses and measuring the respective luminescence intensities, the distinct radiation dose value is estimated, required to evoke a luminescence intensity, which is equivalent to the measured natural one (Murray and Wintle, 2003). Hence, this value is called *equivalent dose*, with the SI unit Gy. To calculate the burial age, the equivalent dose is divided by the energy deposited in the mineral per year owing to background radiation, expressed as the *dose rate* (Gy/a):

$$\text{Age (a)} = \frac{\text{Equivalent dose (Gy)}}{\text{Dose rate (Gy a}^{-1}\text{)}}$$

The amount of energy that can possibly be stored in the minerals is obviously not indefinite which sets the upper limit to the ages that can be obtained. The actual point of *saturation* is specific to the type of dosimeter. Quartz is reported to have average saturation values of ca. 150 Gy (Wallinga and Cunningham, 2014; Wintle, 1997), which depending on the dose rates usually correspond to ages of <150,000 years. Feldspar saturates at higher doses of up to 1,000 Gy and is therefore particularly attractive for older deposits of up to 600 ka (Buylaert et al., 2012). Additional benefits and drawbacks

of using quartz or feldspar are e.g. summarized in Preusser et al. (2008). Luminescence dating has been successfully applied to Neanderthal sites and a wide range of settings and palaeoenvironments, which are time-equivalent to the Middle Palaeolithic (Bateman and Van Huissteden, 1999; Fuchs et al., 2013; Guérin et al., 2015; Lauer et al., 2020; Mercier et al., 2003; Strahl et al., 2010; Thrasher et al., 2009; Wiśniewski et al., 2019).

For the research within this thesis, the luminescence signal of quartz could not be exploited. Pre-tests had shown that the quartz at both study sites either saturates too early to give a reliable account of the depositional ages (Khotylevo), or has unpredictable luminescence characteristics (Lichtenberg). Instead, dating was based on potassium feldspar, using state-of-the-art protocols and methods (Buylaert et al., 2012; Thiel et al., 2011). The present author conducted sampling, equivalent dose estimation, as well as calculation and interpretation of the ages at the Max Planck Institute for Evolutionary Anthropology. The dose rates were determined for all samples by D. Degering at the VTKA laboratory in Dresden. In cases of very thin sediment layers, additional in-situ measurements took place, using a portable high-resolution germanium gamma spectrometer (Arnold et al., 2012).

1.4.3 Grain size analysis

Sediments are traditionally regarded as the most integral and thus most informative element of landscapes. Their deposition and alteration processes are linked to climate, biological factors, as well as geological, hydrological, and geomorphological dynamics (Blott and Pye, 2001; Folk and Ward, 1957). During their entrainment, transport and aggradation, sediments are affected by the energy and the endurance of their transporting media – such as wind, water or glaciers – resulting in characteristic grain-size distributions. These distributions, in turn, can be used to infer transport processes (e.g. fluvial, aeolian, limnic, glacial) and distances, but also source areas and post-depositional modifications by pedogenic, cryogenic or biogenic factors (Cordier et al., 2012; Farrell et al., 2012; Flemming, 2007; King et al., 1998; Meszner et al., 2014; Vandenberghe, 2013b). Classically, three major grain size classes or fractions – sand, silt and clay – were distinguished, divided into ‘coarse’, ‘medium’ and ‘fine’

subfractions, respectively. They were formed through mechanical sieving and sedimentation from a suspension (Beuselinck et al., 1998). With the more recent advent of laser diffractometry, high-resolution (>100 fractions) measurements on large sample sets became possible. This enabled the enhanced identification of multiple, overlapping transportation processes and complex scenarios of redeposition (Dietze and Dietze, 2019; Vandenberghe et al., 2018), reinforcing and renewing the worth of the method. Thus, in their function as key properties of soils, deposits and entire environments, grain size distributions are among the standard analyzed parameters in various disciplines, studying the subsurface of the Earth (e.g. quaternary geology, geomorphology, sedimentology, pedology, and palaeoenvironmental research). But also in archaeology, grain size analysis is increasingly acknowledged as a valuable tool and applied in various contexts (Antoine et al., 2016; Garrison, 2016; Goldberg and Macphail, 2006). Lastly, pore water content and the depositional process are indispensable information for luminescence dating. Since these sediment properties can be derived from grain size distributions, their analysis also supports the correct interpretation of luminescence ages (Nelson and Rittenour, 2015).

The present author conducted sampling and is responsible for processing, interpretation and discussion of the results. Measurements were done by S. Riemenschneider at the Leibniz Institute for Applied Geophysics in Hannover.

1.4.4 Palynological analysis

The analysis of pollen and spores (palynomorphs) is one of the most widely-applied methods in quaternary science and palaeoecology (e.g. Beug, 2004). This is due to their abundance, explanatory power, and preservation (Behre, 1989; Faegri et al., 1989; Moore et al., 1991): Palynomorphs are the most frequent botanical remains in quaternary deposits. Grains differ in shape, size, surface features, and concerning the position and number of apertures (=germination openings, only in pollen grains). The different combinations of these main characteristics result in a large number of pollen and spore types. Up to which taxonomic rank the palynomorphs can be determined, varies substantially. For some types, only the identification of the family is possible (e.g. Chenopodiaceae, Poaceae), whereas the great majority of types allow the

determination of the genus (e.g. *Pinus*, *Corylus*). Only in exceptional cases, differentiation of single species is feasible (e.g. *Sanguisorba officinalis*, *Myriophyllum alterniflorum*). In spite of their minuscule sizes (ca. 2-100 μm), pollen and spore grains preserve exceptionally well over millions of years (e.g. Labandeira et al., 2007). This is because their cell walls contain sporopollenin, one of the most chemically inert biological substances on Earth (Brooks and Shaw, 1978). Preservation is particularly good under anoxic conditions (peat, lake deposits), while palynomorphs tend to decompose much quicker in better-aerated sediments and soils, except for very acidic members (Dimbleby, 1961; Havinga, 1968). Pollen and spores are used to draw conclusions about former vegetation conditions and -developments. Typical time sequences can be correlated between different archives to create supra-regional pollen zones (e.g. Zagwijn, 1989), making palynology a powerful biostratigraphic tool especially in periods of sparse numerical age information (Velichko et al., 2005). For that reason, the whole stratigraphic framework of the last interglacial and early glacial on the European Plain largely relies on pollen zones (Caspers and Freund, 2001; Helmens, 2013), whereby type localities of pollen archives lend their names to specific intervals. For example, the Eemian, the Brörup and the Odderade are named after locations in the Netherlands, Denmark and N-Germany, respectively (Menke, 1976; Sier et al., 2015). Apart from its undisputed biostratigraphic value for the subdivision of the Quaternary, palynology is also a *quantitative* tool for palaeoclimatic reconstructions (Kühl et al., 2007; Pidek et al., 2021; Salonen et al., 2013). Several existing techniques to deduce former temperature and precipitation on a site level, based on known climate sensitivities of plant species and associations are summarized in Chevalier et al. (2020). Furthermore, their worldwide prevalence makes pollen and spores important proxies for understanding global climate dynamics (Masson-Delmotte et al., 2013).

Both sites presented in this thesis have been sampled for palynological analysis. However, due to poor preservation, the samples from Khotylevo could not be reliably interpreted, whereas the palynological results for Lichtenberg can be found in Chapters 3 and 4 and their respective supplementary information. The samples were prepared and analysed by B. Urban at the Institute of Ecology at the Leuphana

University Lüneburg. The present author conducted sampling and shared the interpretation and discussion of the results with B. Urban.

1.5 RESEARCH OBJECTIVES

Problem statement

Using this set of methods, the overall aim of this thesis is to contribute to a better understanding of Neanderthal behavior. To facilitate that understanding, numerous case studies investigating diachronic occupational environments, manifested in palaeo-landscapes, are required. The foregoing sections, however, illustrate (i) various biases impeding this objective and (ii) a general scarcity of sites, at which the availability of reliable chronological and palaeoenvironmental data coincides. This results i.a. in (iii) many undated or unsatisfyingly dated Neanderthal open-air sites, especially in sequences or areas where stratigraphic marker horizons, such as palaeosols or tephras, are ambiguous or missing. On a methodological level, this is vastly caused by the facts, that:

1. Most open-air Neanderthal occupations may have occurred at a time-period outside of the radiocarbon dating range.
2. At many sites, state of the art luminescence dating techniques have not yet been applied.
3. Depositional environments at open-air sites may be challenging for luminescence dating, because of poor bleaching, redeposition and deformation of sediments, especially in non-aeolian settings. Thus, these sediments can hardly be unraveled on a site-level alone. However, the surrounding landscapes are often not incorporated into the research protocol, by default. This situation can affect the quality of luminescence dating and the understanding of site-formation, alike.

Approach of the research

Therefore, this thesis is aiming at the improvement of the standard research design, applied at Middle Palaeolithic open-air sites (see Figure 3), using Khotylevo I and Lichtenberg as case studies, and eventually increasing the chronostratigraphic robustness. This is trying to be achieved by:

- Extending the investigations of the sites to a landscape-level utilizing Digital Elevation Models, geophysics and all available outcrops within the closer area

and/or auxiliary sediment cores to better understand the sediment dynamics and fluxes than can be done on a site-level. This may also help to competently determine the locality of an excavation. Detailed off- and on-site macroscopic sediment descriptions, supported by on-site micromorphological and grain size analyses can further promote the comprehension of depositional environments and site-formations, but may also provide evidence as to the choice of site locations.

- Taking the obtained knowledge on depositional environments and sediment characteristics into account for luminescence dating. This encompasses: (i) a more educated identification of optimal sampling locations, (ii) taking a comparably high number of samples, (iii) using very small aliquot sizes of 0.5 mm with 10 to 100 individual grains per aliquot retrieved from the dominant grain size fraction, so as to better resolve the equivalent dose distribution within each sample (for more details and potential drawbacks, see Chapter 5.2.1), and (iv) choosing the equivalent dose with the highest likelihood to refer to the depositional process (also Chapter 5.2.1).
- Using landscape-level stratigraphic findings to better assess the position of the closest related off-site archive for palaeoecological information (esp. pollen), if on-site preservation does not allow for a direct determination. Moreover, stratigraphic relationships in the surroundings of a site may help to assign definite biostratigraphic units. For instance, the pollen zones of the late Eemian, as well as the Brörup and Odderade Interstadial have similar pollen spectra, so that disjoint samples can be difficult to classify. However, in many cases, certain options can reliably be ruled out due to the stratigraphic position of the samples (more details in Chapter 5.2.1). Furthermore, lithostratigraphic information on a landscape level can hold evidence for sediment reworking, which is relevant for palynological interpretation, but this evidence can also be provided in the opposite direction.
- Amalgamating the biostratigraphic and palaeoenvironmental data with the obtained sedimentary and chronological information, and putting the resulting framework in a wider (supra)regional chrono-/climatostratigraphic context to test for possible coincidences or discrepancies.

In turn, the obtained findings of these more detailed analyses can then be used to enhance the comprehension of the landscape-scale processes (Figure 3). The present author believes that this top-down, integrative and eventually iterative, landscape-oriented approach can result in improved chronostratigraphies, where the precision and robustness of the luminescence ages may be less affected by the error ranges of the dating method.

Chronostratigraphic robustness is considered here as the concurrence and mutual support of chronological and palaeoenvironmental data, creating an added value for both individual contributors and the overall framework. What degree of robustness and precision can be achieved, depends on respective site conditions and applicable methods. In any case, this framework is intended to offer a solid foundation for future investigations and findings at those sites.

Benefit for archaeological research

The field of Middle Palaeolithic archaeology can profit from establishing a firm chrono-, bio- and lithostratigraphic structure at and around occupational sites in multiple ways. Knowledge on the timing of occupations allows for synchronizing archaeological remains with climatic and environmental data – the latter is partly also provided by the research approach delineated above – in order to investigate possible technological and/or behavioral adaptations to changing conditions. Additionally, if robust chronostratigraphies become increasingly available in the spatial dimension, this will facilitate comparisons and correlations of occupations over longer distances. And it also enables theoretical models on migration and population geographies to be (re)formulated and tested. As a concrete application example, which is also an important subject of the thesis, the *Keilmessergruppen* shall serve here. Evidence for their occurrence is spread all across Central and Eastern Europe. Yet their temporal emergence and duration remain as unclear as the catalyst for their technology (cf. Jöris, 2006; Richter, 2016). Conceivably, this can best be resolved with a concerted synopsis of sedimentological, palaeoenvironmental and chronological methods, applied at and around the individual sites.

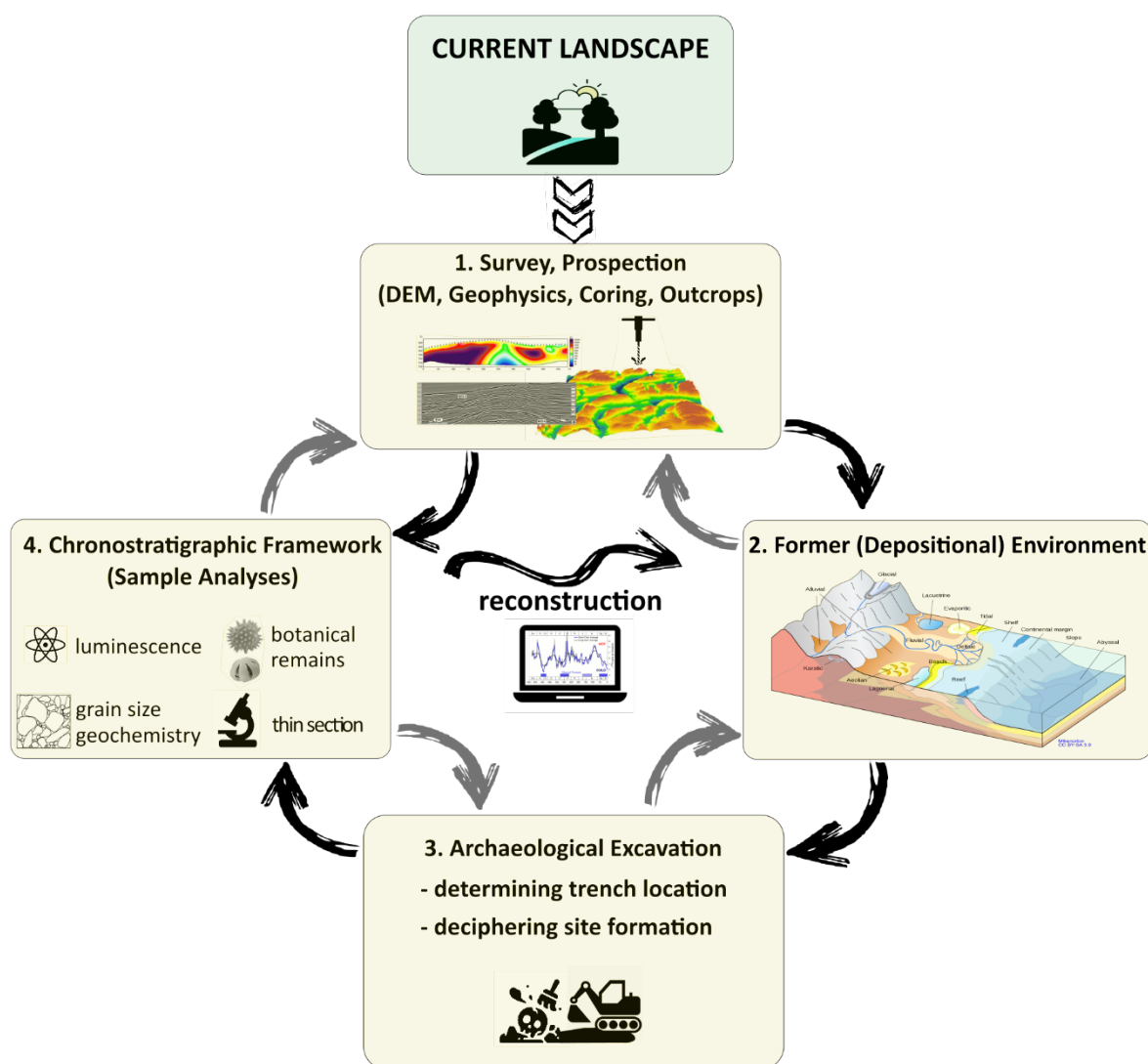


Figure 3: Stepwise and iterative, landscape-oriented research approach to increase chronostratigraphic robustness at Middle Palaeolithic open-air sites. Consecutive numbering of the working steps in the graph does not directly relate to the bullet points given in the text above.

Research questions

In the subsequent Chapters 2 to 4, the outlined approach and methods will be applied to the two Middle Palaeolithic open-air sites Khotylevo I in western Russia and Lichtenberg in northern Germany. The investigations were broadly oriented towards the following research questions (RQ):

RQ 1: *Is the inclusion of investigations within the surroundings of the sites a helpful tool to strengthen the chronostratigraphies and obtained palaeoenvironmental data of the occupational layers, and to improve the understanding of site formation processes?*

RQ 2: *Can the previous numerical dates at both sites and their correlation with MIS 3 be confirmed? Or will the results show that the occupations rather occurred at an earlier period (e.g., MIS 5), as already suggested by some authors?*

RQ 3: *Is the short or the long chronology for the Keilmessergruppen (sensu Jöris, 2004) to be favored, based on the findings of the investigations?*

RQ 4: *Can a systematic landscape-oriented and chronostratigraphic approach, even for a few consecutive years, support the discovery of new Middle Palaeolithic occupations?*

1.6 REFERENCES

- Adler, D.S., Prindiville, T.J., Conard, N.J., 2003. Patterns of spatial organization and land use during the Eemian Interglacial in the Rhineland: New data from Wallertheim, Germany. *Eurasian Prehistory* 1, 25–78.
- AG Boden, 2005. *Bodenkundliche Kartieranleitung KA5*, 5. Aufl. ed. Ad-hoc-Arbeitsgruppe Boden (German Soil Mapping Manual).
- Aitken, M.J., 1998. *An introduction to optical dating: The dating of Quaternary sediments by the use of photon-stimulated luminescence*, Oxford science publications.
[https://doi.org/10.1002/\(SICI\)1520-6548\(200001\)15:1<81::AID-GEA5>3.3.CO;2-Y](https://doi.org/10.1002/(SICI)1520-6548(200001)15:1<81::AID-GEA5>3.3.CO;2-Y)
- Aitken, M.J., Stokes, S., 1997. *Climatostratigraphy*, in: *Chronometric Dating in Archaeology*. Springer US, Boston, MA, pp. 1–30. https://doi.org/10.1007/978-1-4757-9694-0_1
- Allué, E., Mallol, C., Aldeias, V., Burguet-Coca, A., Cabanes, D., Carrancho, Á., Connolly, R., Leierer, L., Mentzer, S., Miller, C., Sandgathe, D., Stahlschmidt, M., Théry-Parisot, I., Vaquero, M., 2022. Fire among Neanderthals, in: *Updating Neanderthals*. Elsevier, pp. 227–249. <https://doi.org/10.1016/B978-0-12-821428-2.00014-7>
- Antoine, P., Coutard, S., Guerin, G., Deschodt, L., Goval, E., Locht, J.-L., Paris, C., 2016. Upper Pleistocene loess-palaeosol records from Northern France in the European context: Environmental background and dating of the Middle Palaeolithic. *Quat. Int.* 411, 4–24. <https://doi.org/10.1016/j.quaint.2015.11.036>
- Antoine, P., Goval, E., Jamet, G., Coutard, S., Moine, O., Hérissou, D., Auguste, P., Guérin, G., Lagroix, F., Schmidt, E., Robert, V., Debenham, N., Meszner, S., Bahain, J.-J., 2014. Les séquences loessiques pléistocène supérieur d'Havrincourt (Pas-de-Calais, France) : stratigraphie, paléoenvironnements, géochronologie et occupations paléolithiques. *Quaternaire* 321–368. <https://doi.org/10.4000/quaternaire.7278>
- Antoine, P., Limondin Lozouet, N., Chaussé, C., Lautridou, J.-P., Pastre, J.-F., Auguste, P., Bahain, J.-J., Falguères, C., Galeb, B., 2007. Pleistocene fluvial terraces from northern France (Seine, Yonne, Somme): synthesis, and new results from interglacial deposits. *Quat. Sci. Rev.* 26, 2701–2723. <https://doi.org/10.1016/j.quascirev.2006.01.036>
- Archer, W., 2016. *What is Still Bay ? Human behavioural variability and biogeography reflected in southern African Middle Stone Age bifacial points*. Leiden University.
- Arnold, L.J., Duval, M., Falguères, C., Bahain, J.-J., Demuro, M., 2012. Portable gamma spectrometry with cerium-doped lanthanum bromide scintillators: Suitability assessments for luminescence and electron spin resonance dating applications. *Radiat. Meas.* 47, 6–18. <https://doi.org/10.1016/j.radmeas.2011.09.001>
- Arnold, V., 1978. Neue Funde aus der Steinzeit Ditmarschens. *Dithmarschen* 3, 57–65.
- Banks, W.E., Moncel, M.-H., Raynal, J.-P., Cobos, M.E., Romero-Alvarez, D., Wouillez, M.-N., Faivre, J.-P., Gravina, B., D'Errico, F., Locht, J.-L., Santos, F., 2021. An ecological niche shift for Neanderthal populations in Western Europe 70,000 years ago. *Sci. Rep.* 11, 5346. <https://doi.org/10.1038/s41598-021-84805-6>
- Basell, L., Brown, A.G., Hosfield, R., Toms, P.S., 2011. The geoarchaeology of Palaeolithic rivers of southwest Britain. *Geol. Soc. Am. Spec. Pap.* 476, 23–36.
- Bateman, M.D., Van Huissteden, J., 1999. The timing of last-glacial periglacial and aeolian events, Twente, eastern Netherlands. *J. Quat. Sci.* 14, 277–283.

- Behre, K.-E., 1989. Biostratigraphy of the last glacial period in Europe. *Quat. Sci. Rev.* 8, 25–44. [https://doi.org/10.1016/0277-3791\(89\)90019-X](https://doi.org/10.1016/0277-3791(89)90019-X)
- Behre, K.-E., Hölzer, A., Lemdahl, G., 2005. Botanical macro-remains and insects from the Eemian and Weichselian site of Oerel (northwest Germany) and their evidence for the history of climate. *Veg. Hist. Archaeobot.* 14, 31–53. <https://doi.org/10.1007/s00334-005-0059-x>
- Behre, K.-E., van der Plicht, J., 1992. Towards an absolute chronology for the last glacial period in Europe: radiocarbon dates from Oerel, northern Germany. *Veg. Hist. Archaeobot.* 1, 111–117. <https://doi.org/10.1007/BF00206091>
- Bertran, P., Andrieux, E., Antoine, P., Coutard, S., Deschodt, L., Gardère, P., Hernandez, M., Legentil, C., Lenoble, A., Liard, M., Mercier, N., Moine, O., Sitzia, L., Van Vliet-Lanoë, B., 2014. Distribution and chronology of Pleistocene permafrost features in France: Database and first results. *Boreas* 43, 699–711. <https://doi.org/10.1111/bor.12025>
- Beschta, R.L., Ripple, W.J., 2016. Riparian vegetation recovery in Yellowstone: The first two decades after wolf reintroduction. *Biol. Conserv.* 198, 93–103. <https://doi.org/10.1016/j.biocon.2016.03.031>
- Beug, H.-J., 2004. Leitfaden der Pollenbestimmung für Mitteleuropa und angrenzende Gebiete. *Germania* 87, 542.
- Beuselinck, L., Govers, G., Poesen, J., Degraer, G., Froyen, L., 1998. Grain-size analysis by laser diffractometry: comparison with the sieve-pipette method. *CATENA* 32, 193–208. [https://doi.org/10.1016/S0341-8162\(98\)00051-4](https://doi.org/10.1016/S0341-8162(98)00051-4)
- Björck, S., Noe-Nygaard, N., Wolin, J., Houmark-Nielsen, M., Jørgen Hansen, H., Snowball, I., 2000. Eemian Lake development, hydrology and climate: a multi-stratigraphic study of the Hollerup site in Denmark. *Quat. Sci. Rev.* 19, 509–536. [https://doi.org/10.1016/S0277-3791\(99\)00025-6](https://doi.org/10.1016/S0277-3791(99)00025-6)
- Blott, S.J., Pye, K., 2001. GRADISTAT: a grain size distribution and statistics package for the analysis of unconsolidated sediments. *Earth Surf. Process. Landforms* 26, 1237–1248. <https://doi.org/10.1002/esp.261>
- Boch, R., Cheng, H., Spötl, C., Edwards, R.L., Wang, X., Häuselmann, P., 2011. NALPS: a precisely dated European climate record 120–60 ka. *Clim. Past* 7, 1247–1259. <https://doi.org/10.5194/cp-7-1247-2011>
- Bocherens, H., 2011. Diet and Ecology of Neanderthals: Implications from C and N Isotopes, in: Conard, N.J., Richter, J. (Eds.), *Neanderthal Lifeways, Subsistence and Technology*. Springer, Dordrecht, pp. 73–85. https://doi.org/10.1007/978-94-007-0415-2_8
- Bolland, A., Kern, O.A., Allstädt, F.J., Peteet, D., Koutsodendris, A., Pross, J., Heiri, O., 2021. Summer temperatures during the last glaciation (MIS 5c to MIS 3) inferred from a 50,000-year chironomid record from Füramoos, southern Germany. *Quat. Sci. Rev.* 264, 107008. <https://doi.org/10.1016/j.quascirev.2021.107008>
- Bosinski, G., 2008. Urgeschichte am Rhein, Tübingen Publications in Prehistory & Tübinger Monographien zur Urgeschichte. Kerns Verlag, Tübingen.
- Bowman, D.M.J.S., O'Brien, J.A., Goldammer, J.G., 2013. Pyrogeography and the Global Quest for Sustainable Fire Management. *Annu. Rev. Environ. Resour.* 38, 57–80. <https://doi.org/10.1146/annurev-environ-082212-134049>
- Bratlund, B., 1999. Taubach revisited. *Jahrb. des Römisch-Germanischen Zentralmuseums* 46,

- Brauer, A., Allen, J.R.M., Mingham, J., Dulski, P., Wulf, S., Huntley, B., 2007. Evidence for last interglacial chronology and environmental change from Southern Europe. *PNAS* 104, 450–455. <https://doi.org/10.1073/pnas.0603321104>
- Breest, K., 1992. Neue Einzelfunde des Alt- und Mittelpaläolithikums im Landkreis Lüchow-Dannenberg. *Die Kd. N.F.* 43, 1–23.
- Brewer, S., Guiot, J., Sánchez-Goni, M.F., Klotz, S., 2008. The climate in Europe during the Eemian: a multi-method approach using pollen data. *Quat. Sci. Rev.* 27, 2303–2315. <https://doi.org/10.1016/j.quascirev.2008.08.029>
- Bridgland, D., Westaway, R., 2008. Climatically controlled river terrace staircases: A worldwide Quaternary phenomenon. *Geomorphology* 98, 285–315. <https://doi.org/10.1016/j.geomorph.2006.12.032>
- Bridgland, D.R., Antoine, P., Limondin-Lozouet, N., Santisteban, J.I., Westaway, R., White, M.J., 2006. The Palaeolithic occupation of Europe as revealed by evidence from the rivers: data from IGCP 449. *J. Quat. Sci.* 21, 437–455. <https://doi.org/10.1002/jqs.1042>
- Brooks, J., Shaw, G., 1978. Sporopollenin: A review of its chemistry, palaeochemistry and geochemistry. *Grana* 17, 91–97. <https://doi.org/10.1080/00173137809428858>
- Busschers, F.S., Kasse, C., van Balen, R.T., Vandenberghe, J., Cohen, K.M., Weerts, H.J.T., Wallinga, J., Johns, C., Cleveringa, P., Bunnik, F.P.M., 2007. Late Pleistocene evolution of the Rhine-Meuse system in the southern North Sea basin: imprints of climate change, sea-level oscillation and glacio-isostasy. *Quat. Sci. Rev.* 26, 3216–3248. <https://doi.org/10.1016/j.quascirev.2007.07.013>
- Buylaert, J.P., Jain, M., Murray, A.S., Thomsen, K.J., Thiel, C., Sohbati, R., 2012. A robust feldspar luminescence dating method for Middle and Late Pleistocene sediments. *Boreas* 41, 435–451. <https://doi.org/10.1111/j.1502-3885.2012.00248.x>
- Canti, M.G., Meddens, F.M., 1998. Mechanical Coring as an Aid to Archaeological Projects. *J. F. Archaeol.* 25, 97–105. <https://doi.org/10.1179/jfa.1998.25.1.97>
- Caspers, G., 1997. Die eem- und weichselzeitliche Hohlform von Groß Todtshorn (Kr. Harburg; Niedersachsen) - Geologische und palynologische Untersuchungen zu Vegetation und Klimaverlauf der letzten Kaltzeit. *Schriftenr. der Dtsch. Geol. Gesellschaft* 4, 7–59.
- Caspers, G., Freund, H., 2001. Vegetation and climate in the Early- and Pleni-Weichselian in northern Central Europe. *J. Quat. Sci.* 16, 31–48. [https://doi.org/10.1002/1099-1417\(200101\)16:1<31::AID-JQS577>3.0.CO;2-3](https://doi.org/10.1002/1099-1417(200101)16:1<31::AID-JQS577>3.0.CO;2-3)
- Caspers, G., Merkt, J., Müller, H., Freund, H., 2002. The Eemian Interglaciation in Northwestern Germany. *Quat. Res.* 58, 49–52. <https://doi.org/10.1006/qres.2002.2341>
- Chevalier, M., Davis, B.A.S., Heiri, O., Seppä, H., Chase, B.M., Gajewski, K., Lacourse, T., Telford, R.J., Finsinger, W., Guiot, J., Kühl, N., Maezumi, S.Y., Tipton, J.R., Carter, V.A., Brussel, T., Phelps, L.N., Dawson, A., Zanon, M., Vallé, F., Nolan, C., Mauri, A., de Vernal, A., Izumi, K., Holmström, L., Marsicek, J., Goring, S., Sommer, P.S., Chaput, M., Kupriyanov, D., 2020. Pollen-based climate reconstruction techniques for late Quaternary studies. *Earth-Science Rev.* 210, 103384. <https://doi.org/10.1016/j.earscirev.2020.103384>
- Chu, W., Nett, J.J., 2021. The past in dust: current trends and future directions in Pleistocene

- geoarcheology of European loess. *J. Quat. Sci.* <https://doi.org/10.1002/jqs.3388>
- Chubur, A.A., 2013. Theriofauna of the paleolithic location Khotylevo 1 (Bryansk Region). *Int. J. Appl. Fundam. Res.* 3, 122–124.
- Chytrý, M., Horsák, M., Danihelka, J., Ermakov, N., German, D.A., Hájek, M., Hájková, P., Kočí, M., Kubešová, S., Lustyk, P., Nekola, J.C., Pavelková Řičánková, V., Preislerová, Z., Resl, P., Valachovič, M., 2019. A modern analogue of the Pleistocene steppe-tundra ecosystem in southern Siberia. *Boreas* 48, 36–56. <https://doi.org/10.1111/bor.12338>
- Conard, N.J., 2012. Klingentechnologie vor dem Jungpaläolithikum, in: Floss, H. (Ed.), *Steinartefakte Vom Altpaläolithikum Bis in Die Neuzeit*, Tübingen Publications in Prehistory. Kerns Verlag, Tübingen, pp. 245–266.
- Conard, N.J. (Ed.), 2001. *Settlement dynamics of the Middle Paleolithic and Middle Stone Age*. Kerns Verlag, Tübingen.
- Conard, N.J., 1992. Tönchesberg and its Position in the Paleolithic Prehistory of Northern Europe., *Monographien des RGZM*. Mainz.
- Conard, N.J., Adler, D.S., 1997. Lithic reduction and hominid behavior in the Middle Paleolithic of the Rhineland. *J. Anthropol. Res.* 53, 147–175.
- Cook, S.J., Clarke, L., Nield, J.M. (Eds.), n.d. *Geomorphological Techniques (Online Edition)*. British Society for Geomorphology, London.
- Cordier, S., Lauer, T., Harmand, D., Frechen, M., Brkojewitch, G., 2012. Fluvial response to climatic and anthropogenic forcing in the Moselle drainage basin (NE France) during historical periods: Evidence from OSL dating. *Earth Surf. Process. Landforms* 37, 1167–1175. <https://doi.org/10.1002/esp.3236>
- Culotta, E., 1999. Neanderthals Were Cannibals, Bones Show. *Science* (80-.). 286, 18–19. <https://doi.org/10.1126/science.286.5437.18b>
- Dansgaard, W., Clausen, H.B., Gundestrup, N., Hammer, C.U., Johnsen, S.F., Kristinsdottir, P.M., Reeh, N., 1982. A New Greenland Deep Ice Core. *Science* (80-.). 218, 1273–1277. <https://doi.org/10.1126/science.218.4579.1273>
- de Beaulieu, J.-L., Reille, M., 1992. The last climatic cycle at La Grande Pile (Vosges, France) a new pollen profile. *Quat. Sci. Rev.* 11, 431–438. [https://doi.org/10.1016/0277-3791\(92\)90025-4](https://doi.org/10.1016/0277-3791(92)90025-4)
- De Clercq, M., Missiaen, T., Wallinga, J., Zurita Hurtado, O., Versendaal, A., Mathys, M., De Batist, M., 2018. A well-preserved Eemian incised-valley fill in the southern North Sea Basin, Belgian Continental Shelf - Coastal Plain: Implications for northwest European landscape evolution. *Earth Surf. Process. Landforms* 43, 1913–1942. <https://doi.org/10.1002/esp.4365>
- Defleur, A.R., Desclaux, E., 2019. Impact of the last interglacial climate change on ecosystems and Neanderthals behavior at Baume Moula-Guercy, Ardèche, France. *J. Archaeol. Sci.* 104, 114–124. <https://doi.org/10.1016/j.jas.2019.01.002>
- Delpiano, D., Uthmeier, T., 2020. Techno-functional and 3D shape analysis applied for investigating the variability of backed tools in the Late Middle Paleolithic of Central Europe. *PLoS One* 15, e0236548. <https://doi.org/10.1371/journal.pone.0236548>
- Dibble, H.L., Aldeias, V., Goldberg, P., McPherron, S.P., Sandgathe, D., Steele, T.E., 2015. A critical look at evidence from La Chapelle-aux-Saints supporting an intentional

- Neandertal burial. *J. Archaeol. Sci.* 53, 649–657.
<https://doi.org/10.1016/j.jas.2014.04.019>
- Dibble, H.L., Sandgathe, D., Goldberg, P., McPherron, S., Aldeias, V., 2018. Were Western European Neandertals Able to Make Fire? *J. Paleolit. Archaeol.* 1, 54–79.
<https://doi.org/10.1007/s41982-017-0002-6>
- Dietze, E., Dietze, M., 2019. Grain-size distribution unmixing using the R package EMMAgeo. *E&G Quat. Sci. J.* 68, 29–46. <https://doi.org/10.5194/egqsj-68-29-2019>
- Dimbleby, G.W., 1961. Soil pollen analysis. *J. Soil Sci.* 12, 1–10.
<https://doi.org/10.1111/j.1365-2389.1961.tb00891.x>
- Discamps, E., Jaubert, J., Bachellerie, F., 2011. Human choices and environmental constraints: deciphering the variability of large game procurement from Mousterian to Aurignacian times (MIS 5-3) in southwestern France. *Quat. Sci. Rev.* 30, 2755–2775.
<https://doi.org/10.1016/j.quascirev.2011.06.009>
- Dutton, A., Lambeck, K., 2012. Ice Volume and Sea Level During the Last Interglacial. *Science* (80-.). 337, 216–219. <https://doi.org/10.1126/science.1205749>
- Ehlers, J., 1990. Untersuchungen zur Morphodynamik der Vereisungen Norddeutschlands unter Berücksichtigung benachbarter Gebiete. *Bremer Beiträge zur Geogr. und Raumplan.* 19, 166.
- Emiliani, C., 1955. Pleistocene Temperatures. *J. Geol.* 63, 538–578.
<https://doi.org/10.1086/626295>
- Emontspohl, A.-F., 1995. The northwest European vegetation at the beginning of the Weichselian glacial (Brørup and Odderade interstadials) – new data for northern France. *Rev. Palaeobot. Palynol.* 85, 231–242. [https://doi.org/10.1016/0034-6667\(94\)00128-7](https://doi.org/10.1016/0034-6667(94)00128-7)
- Fægri, K., Iversen, J., Kaland, P.E., Krzywinski, K., 1989. Textbook of pollen analysis, 4th ed. John Wiley & Sons Ltd., Chichester.
- Farrell, E.J., Sherman, D.J., Ellis, J.T., Li, B., 2012. Vertical distribution of grain size for wind blown sand. *Aeolian Res.* 7, 51–61. <https://doi.org/10.1016/j.aeolia.2012.03.003>
- Fergusson, L., Bangerter, P.J., 2015. Principles of environmental remediation in open and closed systems. *Int. J. Eng. Sci. Res. Technol.* 4, 1–16.
- Finlayson, C., Carrión, J.S., 2007. Rapid ecological turnover and its impact on Neanderthal and other human populations. *Trends Ecol. Evol.* 22, 213–222.
<https://doi.org/10.1016/j.tree.2007.02.001>
- Fischer, H., Wahlen, M., Smith, J., Mastroianni, D., Deck, B., 1999. Ice Core Records of Atmospheric CO₂ Around the Last Three Glacial Terminations. *Science* (80-.). 283, 1712–1714. <https://doi.org/10.1126/science.283.5408.1712>
- Flemming, B.W., 2007. The influence of grain-size analysis methods and sediment mixing on curve shapes and textural parameters: Implications for sediment trend analysis. *Sediment. Geol.* 202, 425–435. <https://doi.org/10.1016/j.sedgeo.2007.03.018>
- Folk, R.L., Ward, W.C., 1957. Brazos River bar [Texas]; a study in the significance of grain size parameters. *J. Sediment. Res.* 27, 3–26. <https://doi.org/10.1306/74D70646-2B21-11D7-8648000102C1865D>

- Fränze, O., 1988. Glaziäre, periglaziäre und marine Reliefentwicklung im nördlichen Schleswig-Holstein. *Schr. Naturwiss. Ver. Schlesw.-Holst.* 58, 1–30.
- Frew, C., 2014. Coring Methods, in: Cook, S., Clarke, L.E., Nield, J.M. (Eds.), *Geomorphological Techniques* (Online Edition). British Society for Geomorphology, London.
- Fuchs, M., Kreutzer, S., Rousseau, D.-D., Antoine, P., Hatté, C., Lacroix, F., Moine, O., Gauthier, C., Svoboda, J., Lisá, L., 2013. The loess sequence of Dolní Věstonice, Czech Republic: A new OSL-based chronology of the Last Climatic Cycle. *Boreas* 42, 664–677. <https://doi.org/10.1111/j.1502-3885.2012.00299.x>
- Gao, C., Boreham, S., 2011. Ipswichian (Eemian) floodplain deposits and terrace stratigraphy in the lower Great Ouse and Cam valleys, southern England, UK. *Boreas* 40, 303–319. <https://doi.org/10.1111/j.1502-3885.2010.00191.x>
- Garrison, E., 2016. *Techniques in Archaeological Geology, Natural Science in Archaeology*. Springer International Publishing, Cham. <https://doi.org/10.1007/978-3-319-30232-4>
- Gaudzinski, S., 1999. Middle Palaeolithic Bone Tools from the Open-Air Site Salzgitter-Lebenstedt (Germany). *J. Archaeol. Sci.* 26, 125–141. <https://doi.org/10.1006/jasc.1998.0311>
- Gavrilov, K.N., Voskresenskaya, E. V., Maschenko, E.N., Douka, K., 2015. East Gravettian Khotylevo 2 site: Stratigraphy, archaeozoology, and spatial organization of the cultural layer at the newly explored area of the site. *Quat. Int.* 359–360, 335–346. <https://doi.org/10.1016/j.quaint.2014.08.020>
- Germonpré, M., Udrescu, M., Fiers, E., 2013. The fossil mammals of Spy. *Anthropol. Præhistorica* 123, 298–327.
- Gibbard, P., Lewin, J., 2002. Climate and related controls on interglacial fluvial sedimentation in lowland Britain. *Sediment. Geol.* 151, 187–210. [https://doi.org/10.1016/S0037-0738\(01\)00253-6](https://doi.org/10.1016/S0037-0738(01)00253-6)
- Goldberg, P., Dibble, H., Berna, F., Sandgathe, D., McPherron, S.J.P., Turq, A., 2012. New evidence on Neandertal use of fire: Examples from Roc de Marsal and Pech de l’Azé IV. *Quat. Int.* 247, 325–340. <https://doi.org/10.1016/j.quaint.2010.11.015>
- Goldberg, P., Macphail, R.I., 2006. *Practical and Theoretical Geoarchaeology*. Blackwell Publishing Ltd., Malden, MA USA. <https://doi.org/10.1002/9781118688182>
- Graham, R.W., 2005. Quaternary Mammal Communities: Relevance of the Individualistic Response and Non-Analogue Faunas. *Paleontol. Soc. Pap.* 11, 141–158. <https://doi.org/10.1017/S1089332600001297>
- Grichuk, V.P., 1961. Fossil floras as a paleontological basis of Quaternary stratigraphy., in: Markov, K.K. (Ed.), *Relief and Stratigraphy of Quaternary Deposits on the North-West of Russian Plain*. USSR Academy of Sciences Press, Moscow, pp. 25–71.
- Grüger, E., 1991. Later quaternary stratigraphy in the nordic countries 150,000 - 15,000 B.P. *Striae* 34, 7–14.
- Guérin, G., Antoine, P., Schmidt, E., Gonal, E., Hérison, D., Jamet, G., Reyss, J.-L., Shao, Q., Philippe, A., Vibet, M.-A., Bahain, J.-J., 2017. Chronology of the Upper Pleistocene loess sequence of Havrincourt (France) and associated Palaeolithic occupations: A Bayesian approach from pedostratigraphy, OSL, radiocarbon, TL and ESR/U-series data. *Quat. Geochronol.* 42, 15–30. <https://doi.org/10.1016/j.quageo.2017.07.001>

- Guérin, G., Frouin, M., Talamo, S., Aldeias, V., Bruxelles, L., Chiotti, L., Dibble, H.L., Goldberg, P., Hublin, J.-J., Jain, M., Lahaye, C., Madelaine, S., Maureille, B., McPherron, S.J.P., Mercier, N., Murray, A.S., Sandgathe, D., Steele, T.E., Thomsen, K.J., Turq, A., 2015. A multi-method luminescence dating of the Palaeolithic sequence of La Ferrassie based on new excavations adjacent to the La Ferrassie 1 and 2 skeletons. *J. Archaeol. Sci.* 58, 147–166. <https://doi.org/10.1016/j.jas.2015.01.019>
- Guthrie, R.D., 2001. Origin and causes of the mammoth steppe: a story of cloud cover, woolly mammal tooth pits, buckles, and inside-out Beringia. *Quat. Sci. Rev.* 20, 549–574. [https://doi.org/10.1016/S0277-3791\(00\)00099-8](https://doi.org/10.1016/S0277-3791(00)00099-8)
- Guthrie, R.D., 1990. *Frozen fauna of the Mammoth Steppe: the story of Blue Babe*. University of Chicago Press, Chicago.
- Harrison, S.P., Bartlein, P., 2012. Records from the Past, Lessons for the Future, in: *The Future of the World's Climate*. Elsevier, pp. 403–436. <https://doi.org/10.1016/B978-0-12-386917-3.00014-2>
- Havinga, A.J., 1968. Some remarks on the interpretation of a pollen diagram of a podsol profile. *Acta Bot. Neerl.* 17, 1–4. <https://doi.org/10.1111/j.1438-8677.1968.tb00058.x>
- Helmens, K.F., 2014. The Last Interglacial–Glacial cycle (MIS 5–2) re-examined based on long proxy records from central and northern Europe. *Quat. Sci. Rev.* 86, 115–143. <https://doi.org/10.1016/j.quascirev.2013.12.012>
- Helmens, K.F., 2013. The Last Interglacial–Glacial cycle (MIS 5–2) re-examined based on long proxy records from central and northern Europe.
- Hérisson, D., Brenet, M., Cliquet, D., Moncel, M.-H., Richter, J., Scott, B., Van Baelen, A., Di Modica, K., De Loecker, D., Ashton, N., Bourguignon, L., Delagnes, A., Faivre, J.-P., Folgado-Lopez, M., Locht, J.-L., Pope, M., Raynal, J.-P., Roebroeks, W., Santagata, C., Turq, A., Van Peer, P., 2016. The emergence of the Middle Palaeolithic in north-western Europe and its southern fringes. *Quat. Int.* 411, 233–283. <https://doi.org/10.1016/j.quaint.2016.02.049>
- Hoffmann, D.L., Standish, C.D., García-Diez, M., Pettitt, P.B., Milton, J.A., Zilhão, J., Alcolea-González, J.J., Cantalejo-Duarte, P., Collado, H., de Balbín, R., Lorblanchet, M., Ramos-Muñoz, J., Weniger, G.-C., Pike, A.W.G., 2018. U-Th dating of carbonate crusts reveals Neandertal origin of Iberian cave art. *Science* (80-.). 359, 912–915. <https://doi.org/10.1126/science.aap7778>
- Höfle, H.-C., Merkt, J., Müller, H., 1985. Die Ausbreitung des Eem-Meeres in Nordwestdeutschland. *E&G Quat. Sci. J.* 35, 49–60. <https://doi.org/10.3285/eg.35.1.09>
- Hublin, J.-J., 1984. The fossil man from Salzgitter-Lebenstedt (FRG) and its place in human evolution during the Pleistocene in Europe. *Z. Morphol. Anthropol.* 75, 45–56.
- Hublin, J.-J., Roebroeks, W., 2009. Ebb and flow or regional extinctions? On the character of Neandertal occupation of northern environments. *Comptes Rendus Palevol* 8, 503–509. <https://doi.org/10.1016/j.crpv.2009.04.001>
- Hull, C.L., 1951. *Essentials of behavior*. Yale University Press.
- Jary, Z., Ciszek, D., 2013. Late Pleistocene loess–palaeosol sequences in Poland and western Ukraine. *Quat. Int.* 296, 37–50. <https://doi.org/10.1016/j.quaint.2012.07.009>
- Jöris, O., 2006. Bifacially backed knives (Keilmesser) in the central European Middle Palaeolithic, in: Goren-Inbar, N., Sharon, G. (Eds.), *Axe Age: Acheulian Tool-Making*

- from Quarry to Discard. Equinox Publishing Ltd, London, pp. 287–310.
- Jöris, O., 2004. Zur chronostratigraphischen Stellung der spätmittelpaläolithischen Keilmessergruppen: Der Versuch einer kulturgeographischen Abgrenzung einer mittelpaläolithischen Formengruppe in ihrem europäischen Kontext. Bericht RGK 84, 49–153.
- Kaspar, F., 2005. A model-data comparison of European temperatures in the Eemian interglacial. *Geophys. Res. Lett.* 32, L11703. <https://doi.org/10.1029/2005GL022456>
- Kels, H., Schirmer, W., 2011. Relation of loess units and prehistoric find density in the Garzweiler open-cast mine, Lower Rhine. *E G Quat. Sci. J.* 59, 59–65. <https://doi.org/10.3285/eg.59.1-2.05>
- Kindler, L., Smith, G.M., García Moreno, A., Gaudzinski-Windheuser, S., Pop, E., Roebroeks, W., 2020. The last interglacial (Eemian) lakeland of Neumark-Nord (Saxony-Anhalt, Germany). Sequencing Neanderthal occupations, assessing subsistence opportunities and prey selection based on estimations of ungulate carrying capacities, biomass production and energ. *RGZM-Tagungen* 37, 67–104.
- Kindler, P., Guillevic, M., Baumgartner, M., Schwander, J., Landais, A., Leuenberger, M., 2014. Temperature reconstruction from 10 to 120 kyr b2k from the NGRIP ice core. *Clim. Past* 10, 887–902. <https://doi.org/10.5194/cp-10-887-2014>
- King, E.L., Haflidason, H., Sejrup, H.P., Løvlie, R., 1998. Glacigenic debris flows on the North Sea Trough Mouth Fan during ice stream maxima. *Mar. Geol.* 152, 217–246. [https://doi.org/10.1016/S0025-3227\(98\)00072-3](https://doi.org/10.1016/S0025-3227(98)00072-3)
- Knipping, M., 2008. Early and Middle Pleistocene pollen assemblages of deep core drillings in the northern Upper Rhine Graben, Germany. *Netherlands J. Geosci. - Geol. en Mijnb.* 87, 51–65. <https://doi.org/10.1017/S0016774600024045>
- Kozowyk, P.R.B., Soressi, M., Pomstra, D., Langejans, G.H.J., 2017. Experimental methods for the Palaeolithic dry distillation of birch bark: implications for the origin and development of Neandertal adhesive technology. *Sci. Rep.* 7, 8033. <https://doi.org/10.1038/s41598-017-08106-7>
- Kühl, N., Litt, T., Schölzel, C., Hense, A., 2007. Eemian and Early Weichselian temperature and precipitation variability in northern Germany. *Quat. Sci. Rev.* 26, 3311–3317. <https://doi.org/10.1016/j.quascirev.2007.10.004>
- Kühne, O., Weber, F., Berr, K., Jenal, C. (Eds.), 2019. *Handbuch Landschaft, RaumFragen: Stadt – Region – Landschaft*. Springer Fachmedien Wiesbaden, Wiesbaden. <https://doi.org/10.1007/978-3-658-25746-0>
- Kupryjanowicz, M., Fiłoc, M., Kwiatkowski, W., 2018. Was there an abrupt cold climatic event in the middle Eemian? Pollen record from a palaeolake at the Hieronimowo site, NE Poland. *Quat. Int.* 467, 96–106. <https://doi.org/10.1016/j.quaint.2017.04.027>
- Labandeira, C.C., Kvaček, J., Mostovski, M.B., 2007. Pollination drops, pollen, and insect pollination of Mesozoic gymnosperms. *Taxon* 56, 663–695. <https://doi.org/10.2307/25065852>
- Lade, U., Hagedorn, H., 1982. Sedimente und Relief einer eiszeitlichen Hohlform bei Krempel (Elbe-Weser-Dreieck). *E&G Quat. Sci. J.* 32, 93–108. <https://doi.org/10.3285/eg.32.1.08>
- Lauer, T., Weiss, M., Bernhardt, W., Heinrich, S., Rappsilber, I., Stahlschmidt, M.C., von

- Suchodoletz, H., Wansa, S., 2020. The Middle Pleistocene fluvial sequence at Uichteritz, central Germany: Chronological framework, paleoenvironmental history and early human presence during MIS 11. *Geomorphology*.
<https://doi.org/10.1016/j.geomorph.2019.107016>
- Laurat, T., Brühl, E., 2021. Neumark-Nord 2 – A multiphase Middle Palaeolithic open-air site in the Geisel Valley (Central Germany). *Anthropologie*. 102936.
<https://doi.org/10.1016/j.anthro.2021.102936>
- Laurat, T., Brühl, E., 2006. Zum Stand der archäologischen Untersuchungen im Tagebau Neumark-Nord, Ldkr. Merseburg- Querfurt (Sachsen-Anhalt) - Vorbericht zu den Ausgrabungen 2003-2005. *Jahresschrift für mitteldeutsche Vor.* 90, 9–69.
- Leder, D., Hermann, R., Hüls, M., Russo, G., Hoelzmann, P., Nielbock, R., Böhner, U., Lehmann, J., Meier, M., Schwalb, A., Tröller-Reimer, A., Koddenberg, T., Terberger, T., 2021. A 51,000-year-old engraved bone reveals Neanderthals' capacity for symbolic behaviour. *Nat. Ecol. Evol.* 5, 1273–1282. <https://doi.org/10.1038/s41559-021-01487-z>
- Lehmkuhl, F., Zens, J., Krauß, L., Schulte, P., Kels, H., 2016. Loess-paleosol sequences at the northern European loess belt in Germany: Distribution, geomorphology and stratigraphy. *Quat. Sci. Rev.* 153, 11–30. <https://doi.org/10.1016/j.quascirev.2016.10.008>
- Lewis, S.G., Ashton, N., Jacobi, R., 2011. Testing Human Presence During the Last Interglacial (MIS 5e): A Review of the British Evidence, in: Ashton, N., Lewis, S.G., Stringer, C. (Eds.), *The Ancient Human Occupation of Britain*. pp. 125–164.
<https://doi.org/10.1016/B978-0-444-53597-9.00009-1>
- Lisiecki, L.E., Raymo, M.E., 2005. A Plio-Pleistocene stack of 57 globally distributed benthic [δ 18O records. *Paleoceanography* 20, PA1003.
<https://doi.org/10.1029/2004PA001071>
- Lisiecki, L.E., Stern, J. V., 2016. Regional and global benthic δ 18 O stacks for the last glacial cycle. *Paleoceanography* 31, 1368–1394. <https://doi.org/10.1002/2016PA003002>
- Litt, T., Weber, T., 1988. Ein eemzeitlicher Waldelefantenschlachtplatz von Gröbern, Krs. Gräfenhainichen. *Ausgrab. Funde* 33, 181–187.
- Locht, J.-L., Goval, E., Antoine, P., Coutard, S., Auguste, P., Paris, C., Hérissou, D., 2014. Palaeoenvironments and prehistoric interactions in northern France from the Eemian Interglacial to the end of the Weichselian Middle Pleniglacial, in: Foulds, W.F., Drinkall, H.C., Perri, A.R., Clinnick, D.T.G. (Eds.), *Wild Things: Recent Advances in Palaeolithic and Mesolithic Research*. Oxbow Books, pp. 70–78.
- Locht, J.-L., Hérissou, D., Goval, E., Cliquet, D., Huet, B., Coutard, S., Antoine, P., Feray, P., 2016. Timescales, space and culture during the Middle Palaeolithic in northwestern France. *Quat. Int.* 411, 129–148. <https://doi.org/10.1016/j.quaint.2015.07.053>
- Mamakowa, K., 1989. Late Middle Polish Glaciation, Eemian and Early Vistulian vegetation at Imbramowice near Wroclaw and the pollen stratigraphy of this part of the Pleistocene in Poland. *Acta Palaeobot.* 29, 11–176.
- Mania, D., 2002. Der mittelpaläolithische Lagerplatz am Ascherslebener See bei Königsau (Nordharzvorland). *Praehistoria Thuringica* 8, 16–75.
- Mania, D., Thomae, M., Litt, T., Weber, T., 1990. Neumark - Gröbern. Beiträge zur Jagd des mittelpaläolithischen Menschen. *Veröff. Landesmus. Vor. Halle* 43, 321.
- Mania, D., Toepfer, V., 1973. Königsau: Gliederung, Oekologie und Mittelpaläolithische

Funde der letzten Eiszeit. Veröffentlichungen des Landesmuseums für Vorgeschichte in Halle 26, Deutscher Verlag der Wissenschaften, Berlin.

- Marks, L., Gałazka, D., Krzysińska, J., Nita, M., Stachowicz-Rybka, R., Witkowski, A., Woronko, B., Dobosz, S., 2014. Marine transgressions during Eemian in northern Poland: A high resolution record from the type section at Cierpięta. *Quat. Int.* 328–329, 45–59. <https://doi.org/10.1016/j.quaint.2013.12.007>
- Masson-Delmotte, V., Schulz, M., Abe-Ouchi, A., Beer, J., Ganopolski, A., González Rouco, J.F., Jansen, E., Lambeck, K., Luterbacher, J., Naish, T., Osborn, T., Otto-Bliesner, B., Quinn, T., Ramesh, R., Rojas, M., Shao, X., Timmermann, A., 2013. Information from Paleoclimate Archives., in: Stocker, T.F., Qin, D., Plattner, G.-K., Tignor, M., Allen, S.K., Boschung, J., Nauels, A., Xia, Y., Bex, V., Midgley, P.M. (Eds.), *Climate Change 2013: The Physical Science Basis. Contribution of Working Group I to the Fifth Assessment Report of the Intergovernmental Panel on Climate Change*. Cambridge University Press, pp. 383–464.
- Meier-Uhlherr, R., Schulz, C., Luthardt, V., 2015. *Steckbriefe Moorsubstrate*, 2nd. ed. HNE Eberswalde, Berlin.
- Menke, B., 1992. Eeminterglaziale und nacheiszeitliche Wälder in Schleswig-Holstein. *GLASH* 1, 29–101.
- Menke, B., 1976. Neue Ergebnisse zur Stratigraphie und Landschaftsentwicklung im Jungpleistozän Westholsteins. *E&G Quat. Sci. J.* 27, 53–68. <https://doi.org/10.3285/eg.27.1.05>
- Menke, B., Tynni, R., 1984. Das Eeminterglazial und das Weichselfrühglazial von Rederstall/Dithmarschen und ihre Bedeutung für die mitteleuropäische Jungpleistozän-Gliederung. *Geol. Jahrb. A* 76, 1–120.
- Mercier, N., Valladas, H., Froget, L., Joron, J.L., Reyss, J.L., Balescu, S., Escutenaire, C., Kozłowski, J., Sitlivy, V., Sobczyk, K., Zieba, A., 2003. Luminescence dates for the palaeolithic site of Piekary IIa (Poland): Comparison between TL of burnt flints and OSL of a loess-like deposit. *Quat. Sci. Rev.* 22, 1245–1249. [https://doi.org/10.1016/S0277-3791\(03\)00025-8](https://doi.org/10.1016/S0277-3791(03)00025-8)
- Meszner, S., Faust, D., 2018. Paläoböden in den Lössgebieten Ostdeutschlands, in: *Handbuch Der Bodenkunde*. Wiley, pp. 1–20. <https://doi.org/10.1002/9783527678495.hbbk2018002>
- Meszner, S., Kreutzer, S., Fuchs, M., Faust, D., 2014. Identifying depositional and pedogenetic controls of Late Pleistocene loess-paleosol sequences (Saxony, Germany) by combined grain size and microscopic analyses. *Zeitschrift für Geomorphol. Suppl. Issues* 58, 63–90. <https://doi.org/10.1127/0372-8854/2014/S-00169>
- Miettinen, A., Head, M.J., Knudsen, K.L., 2014. Eemian sea-level highstand in the eastern Baltic Sea linked to long-duration White Sea connection. *Quat. Sci. Rev.* 86, 158–174. <https://doi.org/10.1016/j.quascirev.2013.12.009>
- Minton, E., Kahle, L., 2013. *Belief Systems, religion, and Behavioral economics*. Business Expert Press.
- Mol, J., Vandenberghe, J., Kasse, C., 2000. River response to variations of periglacial climate in mid-latitude Europe. *Geomorphology* 33, 131–148.
- Monnin, E., Indermühle, A., Dällenbach, A., Flückiger, J., Stauffer, B., Stocker, T.F., Raynaud, D.,

- D., Barnola, J.-M., 2001. Atmospheric CO₂ Concentrations over the Last Glacial Termination. *Science* (80-.). 291, 112–114. <https://doi.org/10.1126/science.291.5501.112>
- Moore, P.D., Webb, J.A., Collison, M.E., 1991. Pollen analysis. Blackwell Scientific Publications, Oxford.
- Müller, H., 1974. Pollenanalytische Untersuchungen und Jahresschichtenzählungen an der eemzeitlichen Kieselgur von Bispingen/Luhe. *Geol. Jahrb.* A21, 149–169.
- Müller, U.C., Sánchez Goñi, Maria F., 2007. Vegetation dynamics in southern Germany during marine isotope stage 5 (~ 130 to 70 kyr ago), in: Sirocko, F., Claussen, M., Sánchez Goñi, M.F., Litt, T. (Eds.), *The Climate of Past Interglacials. (Developments in Quaternary Sciences 7)*. pp. 277–287. [https://doi.org/10.1016/S1571-0866\(07\)80044-3](https://doi.org/10.1016/S1571-0866(07)80044-3)
- Murray, A.S., Thomsen, K.J., Masuda, N., Buylaert, J.P., Jain, M., 2012. Identifying well-bleached quartz using the different bleaching rates of quartz and feldspar luminescence signals. *Radiat. Meas.* 47, 688–695. <https://doi.org/10.1016/j.radmeas.2012.05.006>
- Murray, A.S., Wintle, A.G., 2003. The single aliquot regenerative dose protocol: potential for improvements in reliability. *Radiat. Meas.* 37, 377–381. [https://doi.org/10.1016/S1350-4487\(03\)00053-2](https://doi.org/10.1016/S1350-4487(03)00053-2)
- Neef, E., 1967. *Die theoretischen Grundlagen der Landschaftslehre*. Haack, Gotha/Leipzig.
- Nelson, M.S., Rittenour, T.M., 2015. Using grain-size characteristics to model soil water content: Application to dose-rate calculation for luminescence dating. *Radiat. Meas.* 81, 142–149. <https://doi.org/10.1016/j.radmeas.2015.02.016>
- Nielsen, T.K., Benito, B.M., Svenning, J.-C., Sandel, B., McKerracher, L., Riede, F., Kjærgaard, P.C., 2017. Investigating Neanderthal dispersal above 55°N in Europe during the Last Interglacial Complex. *Quat. Int.* 431, 88–103. <https://doi.org/10.1016/j.quaint.2015.10.039>
- Nielsen, T.K., Kristiansen, S.M., Riede, F., 2019. Neanderthals at the frontier? Geological potential of southwestern South Scandinavia as archive of Pleistocene human occupation. *Quat. Sci. Rev.* 221, 105870. <https://doi.org/10.1016/j.quascirev.2019.105870>
- Otcherednoi, A., Salnaya, N., Voskresenskaya, E., Vishnyatsky, L., 2014. New geoarcheological studies at the middle paleolithic sites of khotylevo i and betovo (Bryansk oblast, Russia): Some preliminary results. *Quat. Int.* 326–327, 250–260. <https://doi.org/10.1016/j.quaint.2013.11.005>
- Otto, J.-C., Prasicek, G., Blöthe, J., Schrott, L., 2018. GIS Applications in Geomorphology, in: *Comprehensive Geographic Information Systems*. Elsevier, pp. 81–111. <https://doi.org/10.1016/B978-0-12-409548-9.10029-6>
- Panin, A., Adamiec, G., Buylaert, J.-P., Matlakhova, E., Moska, P., Novenko, E., 2017. Two Late Pleistocene climate-driven incision/aggradation rhythms in the middle Dnieper River basin, west-central Russian Plain. *Quat. Sci. Rev.* 166, 266–288. <https://doi.org/10.1016/j.quascirev.2016.12.002>
- Panin, A., Borisova, O., Konstantinov, E., Belyaev, Y., Eremenko, E., Zakharov, A., Sidorchuk, A., 2020. The Late Quaternary Evolution of the Upper Reaches of Fluvial Systems in the Southern East European Plain. *Quaternary* 3, 31. <https://doi.org/10.3390/quat3040031>
- Pastors, A., 2001. *Die Mittelpaläolithische Freilandstation von Salzgitter-Lebenstedt: Genese*

der Fundstelle und Systematik der Steinbearbeitung. Archiv der Stadt Salzgitter, Salzgitter.

- Pech, G.T., Araújo, M.B., Bell, J.D., Blanchard, J., Bonebrake, T.C., Chen, I.-C., Clark, T.D., Colwell, R.K., Danielsen, F., Evengård, B., Falconi, L., Ferrier, S., Frusher, S., Garcia, R.A., Griffis, R.B., Hobday, A.J., Janion-Scheepers, C., Jarzyna, M.A., Jennings, S., Lenoir, J., Linnetved, H.I., Martin, V.Y., McCormack, P.C., McDonald, J., Mitchell, N.J., Mustonen, T., Pandolfi, J.M., Pettorelli, N., Popova, E., Robinson, S.A., Scheffers, B.R., Shaw, J.D., Sorte, C.J.B., Strugnell, J.M., Sunday, J.M., Tuanmu, M.-N., Vergés, A., Villanueva, C., Wernberg, T., Wapstra, E., Williams, S.E., 2017. Biodiversity redistribution under climate change: Impacts on ecosystems and human well-being. *Science* (80-.). 355. <https://doi.org/10.1126/science.aai9214>
- Pederzani, S., Aldeias, V., Dibble, H.L., Goldberg, P., Hublin, J.-J., Madelaine, S., McPherron, S.P., Sandgathe, D., Steele, T.E., Turq, A., Britton, K., 2021. Reconstructing Late Pleistocene paleoclimate at the scale of human behavior: an example from the Neandertal occupation of La Ferrassie (France). *Sci. Rep.* 11, 1419. <https://doi.org/10.1038/s41598-020-80777-1>
- Peeters, J., Busschers, F.S., Stouthamer, E., 2015. Fluvial evolution of the Rhine during the last interglacial-glacial cycle in the southern North Sea basin: A review and look forward. *Quat. Int.* 357, 176–188. <https://doi.org/10.1016/j.quaint.2014.03.024>
- Pereira-Pedro, A.S., Bruner, E., Gunz, P., Neubauer, S., 2020. A morphometric comparison of the parietal lobe in modern humans and Neanderthals. *J. Hum. Evol.* 142, 102770. <https://doi.org/10.1016/j.jhevol.2020.102770>
- Pfaffenberg, K., 1991. Die Vegetationsverhältnisse während und nach der Sedimentation der Fundschichten von Salzgitter-Lebenstedt, in: Busch, R., Schwabedissen, H. (Eds.), *Der Altsteinzeitliche Fundplatz Salzgitter-Lebenstedt. Teil II. Naturwissenschaftliche Untersuchungen.* Böhlau Verlag, Köln, Weimar, Wien, pp. 183–210.
- Piacente, S., 1996. Man as geomorphological agent, in: Panizza, M. (Ed.), *Environmental Geomorphology. Developments in Earth Surface Processes*, 4. Elsevier, pp. 197–214. [https://doi.org/10.1016/S0928-2025\(96\)80021-6](https://doi.org/10.1016/S0928-2025(96)80021-6)
- Pidek, I.A., Poska, A., Hrynowiecka, A., Brzozowicz, D., Żarski, M., 2021. Two pollen-based methods of Eemian climate reconstruction employed in the study of the Żabieniec-Jagodne palaeolakes in central Poland. *Quat. Int.* in press. <https://doi.org/10.1016/j.quaint.2021.09.014>
- Pop, E., 2014. Analysis of the Neumark-Nord 2/2 lithic assemblage: results and interpretations, in: Gaudzinski-Windheuser, S., Roebroeks, W. (Eds.), *Multidisciplinary Studies of the Middle Palaeolithic Record from Neumark-Nord (Germany), Veröffentlichungen Des Landesamtes Für Denkmalpflege Und Archäologie Sachsen-Anhalt – Landesmuseum Für Vorgeschichte Band 69.* Landesamt für Denkmalpflege und Archäologie Sachsen-Anhalt, Landesmuseum für Vorgeschichte, Halle(Saale), pp. 143–195.
- Pop, E., Bakels, C., 2015. Semi-open environmental conditions during phases of hominin occupation at the Eemian Interglacial basin site Neumark-Nord 2 and its wider environment. *Quat. Sci. Rev.* 117, 72–81. <https://doi.org/10.1016/j.quascirev.2015.03.020>
- Pop, E., Kuijper, W., van Hees, E., Smith, G., García-Moreno, A., Kindler, L., Gaudzinski-Windheuser, S., Roebroeks, W., 2016. Fires at Neumark-Nord 2, Germany: An analysis

- of fire proxies from a Last Interglacial Middle Palaeolithic basin site. *J. F. Archaeol.* 41, 603–617. <https://doi.org/10.1080/00934690.2016.1208518>
- Presnyakova, D., Archer, W., Braun, D.R., Flear, W., 2015. Documenting differences between early stone age flake production systems: An experimental model and archaeological verification. *PLoS One* 10, 1–26. <https://doi.org/10.1371/journal.pone.0130732>
- Preusser, F., Degering, D., Fuchs, M., Hilgers, A., Kadereit, A., Klasen, N., Krbetschek, M., Richter, D., Spencer, J.Q.G., 2008. Luminescence dating: basics, methods and applications. *E&G Quat. Sci. J.* 57, 95–149. <https://doi.org/10.3285/eg.57.1-2.5>
- Pross, J., Klotz, S., Mosbrugger, V., 2000. Reconstructing palaeotemperatures for the Early and Middle Pleistocene using the mutual climatic range method based on plant fossils. *Quat. Sci. Rev.* 19, 1785–1799. [https://doi.org/10.1016/S0277-3791\(00\)00089-5](https://doi.org/10.1016/S0277-3791(00)00089-5)
- Rapoport, A., 2008. Archaeology and Environment-Behavior Studies. *Archeol. Pap. Am. Anthropol. Assoc.* 16, 59–70. <https://doi.org/10.1525/ap3a.2006.16.1.59>
- Rasmussen, S.O., Bigler, M., Blockley, S.P., Blunier, T., Buchardt, S.L., Clausen, H.B., Cvijanovic, I., Dahl-Jensen, D., Johnsen, S.J., Fischer, H., Gkinis, V., Guillevic, M., Hoek, W.Z., Lowe, J.J., Pedro, J.B., Popp, T., Seierstad, I.K., Steffensen, J.P., Svensson, A.M., Vallelonga, P., Vinther, B.M., Walker, M.J.C., Wheatley, J.J., Winstrup, M., 2014. A stratigraphic framework for abrupt climatic changes during the Last Glacial period based on three synchronized Greenland ice-core records: refining and extending the INTIMATE event stratigraphy. *Quat. Sci. Rev.* 106, 14–28. <https://doi.org/10.1016/j.quascirev.2014.09.007>
- Reid, J.J., Rathje, W.L., Schiffer, M.B., 1974. Expanding Archaeology. *Am. Antiq.* 39, 125–126. <https://doi.org/10.2307/279227>
- Richter, D., Grün, R., Joannes-Boyau, R., Steele, T.E., Amani, F., Rué, M., Fernandes, P., Raynal, J.-P., Geraads, D., Ben-Ncer, A., Hublin, J.-J., McPherron, S.P., 2017. The age of the hominin fossils from Jebel Irhoud, Morocco, and the origins of the Middle Stone Age. *Nature* 546, 293–296. <https://doi.org/10.1038/nature22335>
- Richter, D., Krbetschek, M., 2014. Preliminary luminescence dating results for two Middle Palaeolithic occupations at Neumark-Nord 2, in: Gaudzinski-Windheuser, S., Roebroeks, W. (Eds.), *Multidisziplinäre Studien of the Middle Palaeolithic Record from Neumark-Nord (Germany)*. Volume 1. Veröffentlichungen des Landesamtes für Archäologie Sachsen-Anhalt - Landesmuseum für Vorgeschichte 69, Halle(Saale), pp. 131–136.
- Richter, D., Wagner, G.A., 2015. Chronometric Methods in Paleoanthropology, in: Henke, W., Tattersall, I. (Eds.), *Handbook of Paleoanthropology*. Springer, Berlin, Heidelberg, pp. 317–350. https://doi.org/10.1007/978-3-642-39979-4_10
- Richter, J., 2016. Leave at the height of the party: A critical review of the Middle Paleolithic in Western Central Europe from its beginnings to its rapid decline. *Quat. Int.* 411, 107–128. <https://doi.org/10.1016/j.quaint.2016.01.018>
- Richter, J., 2006. Neanderthals in their landscape., in: *Neanderthals in Europe*. pp. 51–66.
- Richter, J., 1997. Sesselfelsgrotte III. Der G-Schichten-Komplex der Sesselfelsgrotte. Zum Verständnis des Micoquien. *Quartär Bibliothek* 7, Saarbrücker Druckerei und Verlag, Saarbrücken.
- Roebroeks, W., 2014. *Terra incognita : The Palaeolithic record of northwest Europe and the*

- information potential of the southern North Sea. *Netherlands J. Geosci. - Geol. en Mijnb.* 93, 43–53. <https://doi.org/10.1017/njg.2014.1>
- Roebroeks, W., Bakels, C.C., Coward, F., Hosfield, R., Pope, M., Wenban-Smith, F., 2015. 'Forest Furniture' or 'Forest Managers'? On Neanderthal presence in Last Interglacial environments, in: *Settlement, Society and Cognition in Human Evolution*. Cambridge University Press, New York, pp. 174–188. <https://doi.org/10.1017/CBO9781139208697.011>
- Roebroeks, W., Conard, N.J., van Kolfschoten, T., Dennell, R.W., Dunnell, R.C., Gamble, C., Graves, P., Jacobs, K., Otte, M., Roe, D., Svoboda, J., Tuffreau, A., Voytek, B.A., Wenban-Smith, F., Wymer, J.J., 1992. Dense Forests, Cold Steppes, and the Palaeolithic Settlement of Northern Europe [and Comments and Replies]. *Curr. Anthropol.* 33, 551–586. <https://doi.org/10.1086/204113>
- Roebroeks, W., Soressi, M., 2016. Neandertals revised. *Proc. Natl. Acad. Sci.* 113, 6372–6379. <https://doi.org/10.1073/pnas.1521269113>
- Rolland, N., Dibble, H.L., 1990. A New Synthesis of Middle Paleolithic Variability. *Am. Antiq.* 55, 480–499.
- Roos, C.I., Bowman, D.M.J.S., Balch, J.K., Artaxo, P., Bond, W.J., Cochrane, M., D'Antonio, C.M., DeFries, R., Mack, M., Johnston, F.H., Krawchuk, M.A., Kull, C.A., Moritz, M.A., Pyne, S., Scott, A.C., Swetnam, T.W., 2014. Pyrogeography, historical ecology, and the human dimensions of fire regimes. *J. Biogeogr.* 41, 833–836. <https://doi.org/10.1111/jbi.12285>
- Russell Coope, G., 2000. The climatic significance of coleopteran assemblages from the Eemian deposits in southern England. *Netherlands J. Geosci.* 79, 257–267. <https://doi.org/10.1017/S0016774600021740>
- Salonen, J.S., Hemens, K.F., Seppä, H., Birks, H.J.B., 2013. Pollen-based palaeoclimate reconstructions over long glacial-interglacial timescales: methodological tests based on the Holocene and MIS 5d-c deposits at Sokli, northern Finland. *J. Quat. Sci.* 28, 271–282. <https://doi.org/10.1002/jqs.2611>
- Sánchez Goñi, M.F., 2020. Regional impacts of climate change and its relevance to human evolution. *Evol. Hum. Sci.* 2, 1–27. <https://doi.org/10.1017/ehs.2020.56>
- Sandgathe, D.M., Dibble, H.L., Goldberg, P., McPherron, S.P., Turq, A., Niven, L., Hodgkins, J., 2011. Timing of the appearance of habitual fire use. *Proc. Natl. Acad. Sci.* 108, E298–E298. <https://doi.org/10.1073/pnas.1106759108>
- Scherjon, F., Bakels, C., MacDonald, K., Roebroeks, W., 2015. Burning the Land. *Curr. Anthropol.* 56, 299–326. <https://doi.org/10.1086/681561>
- Schmitz, R.W., Thissen, J., 1998. Vorbericht über die Grabungen 1995–1997 in der mittelpaläolithischen B1-Schicht der Ziegeleigrube Dreesen in Rheindahlen. *Archäologisches Korrespondenzblatt* 28, 483–498.
- Schokker, J., Cleveringa, P., Murray, A.S., 2004. Palaeoenvironmental reconstruction and OSL dating of terrestrial Eemian deposits in the southeastern Netherlands. *J. Quat. Sci.* 19, 193–202. <https://doi.org/10.1002/jqs.808>
- Seierstad, I.K., Abbott, P.M., Bigler, M., Blunier, T., Bourne, A.J., Brook, E., Buchardt, S.L., Buizert, C., Clausen, H.B., Cook, E., Dahl-Jensen, D., Davies, S.M., Guillevic, M., Johnsen, S.J., Pedersen, D.S., Popp, T.J., Rasmussen, S.O., Severinghaus, J.P., Svensson,

- A., Vinther, B.M., 2014. Consistently dated records from the Greenland GRIP, GISP2 and NGRIP ice cores for the past 104 ka reveal regional millennial-scale $\delta^{18}\text{O}$ gradients with possible Heinrich event imprint. *Quat. Sci. Rev.* 106, 29–46.
<https://doi.org/10.1016/j.quascirev.2014.10.032>
- Shackleton, N.J., 1969. The last interglacial in the marine and terrestrial records. *Proc. R. Soc. London. Ser. B. Biol. Sci.* 174, 135–154. <https://doi.org/10.1098/rspb.1969.0085>
- Shackleton, N.J., 1967. Oxygen Isotope Analyses and Pleistocene Temperatures Re-assessed. *Nature* 215, 15–17. <https://doi.org/10.1038/215015a0>
- Shackleton, N.J., Chapman, M., Sánchez-Góñi, M.F., Pailler, D., Lancelot, Y., 2002. The Classic Marine Isotope Substage 5e. *Quat. Res.* 58, 14–16.
<https://doi.org/10.1006/qres.2001.2312>
- Shackleton, N.J., Sánchez-Góñi, M.F., Pailler, D., Lancelot, Y., 2003. Marine Isotope Substage 5e and the Eemian Interglacial. *Glob. Planet. Change* 36, 151–155.
[https://doi.org/10.1016/S0921-8181\(02\)00181-9](https://doi.org/10.1016/S0921-8181(02)00181-9)
- Sier, M.J., Peeters, J., Dekkers, M.J., Parés, J.M., Chang, L., Busschers, F.S., Cohen, K.M., Wallinga, J., Bunnik, F.P.M., Roebroeks, W., 2015. The Blake Event recorded near the Eemian type locality - A diachronic onset of the Eemian in Europe. *Quat. Geochronol.*
<https://doi.org/10.1016/j.quageo.2015.03.003>
- Sier, M.J., Roebroeks, W., Bakels, C.C., Dekkers, M.J., Brühl, E., De Loecker, D., Gaudzinski-Windheuser, S., Hesse, N., Jagich, A., Kindler, L., Kuijper, W.J., Laurat, T., Múcher, H.J., Penkman, K.E.H., Richter, D., van Hinsbergen, D.J.J., 2011. Direct terrestrial-marine correlation demonstrates surprisingly late onset of the last interglacial in central Europe. *Quat. Res.* 75, 213–218. <https://doi.org/10.1016/j.yqres.2010.11.003>
- Simensen, T., Halvorsen, R., Erikstad, L., 2018. Methods for landscape characterisation and mapping: A systematic review. *Land use policy* 75, 557–569.
<https://doi.org/10.1016/j.landusepol.2018.04.022>
- Soressi, M., 2005. Late Mousterian Lithic Technology. Its Implications for the Pace of the Emergence of Behavioural Modernity and the Relationship between Behavioural Modernity and Biological Modernity., in: Blackwell, L., d'Errico, F. (Eds.), *From Tools to Symbols*. University of Witwatersand Press, Johannesburg, pp. 389–417.
- Speleers, B., 2000. The relevance of the Eemian for the study of the Palaeolithic occupation of Europe. *Netherlands J. Geosci.* 79, 283–291.
<https://doi.org/10.1017/S0016774600021764>
- Stewart, J.R., 2005. The ecology and adaptation of Neanderthals during the non-analogue environment of Oxygen Isotope Stage 3. *Quat. Int.* 137, 35–46.
<https://doi.org/10.1016/j.quaint.2004.11.018>
- Strahl, J., Krbetschek, M.R., Luckert, J., Machalett, B., Meng, S., Oches, E.A., Rappsilber, I., Wansa, S., Zöller, L., 2010. Geologie, Paläontologie und Geochronologie des Eem-Beckens Neumark-Nord 2 und Vergleich mit dem Becken Neumark-Nord 1 (Geiseltal, Sachsen-Anhalt). *Eiszeitalter und Gegenwart (Quaternary Sci. Journal)* 59, 120–167.
<https://doi.org/10.3285/eg.59.1-2.09>
- Stremme, H., Felix-Henningsen, P., Weinhold, H., Christensen, S., 1982. Paläoböden in Schleswig-Holstein. *Geol. Jb. F* 14, 311–361.
- Thiel, C., Buylaert, J.P., Murray, A., Terhorst, B., Hofer, I., Tsukamoto, S., Frechen, M., 2011.

- Luminescence dating of the Stratzing loess profile (Austria) - Testing the potential of an elevated temperature post-IR IRSL protocol. *Quat. Int.* 234, 23–31.
<https://doi.org/10.1016/j.quaint.2010.05.018>
- Thieme, H., 2007. *Die Schoeninger Speere: Mensch und Jagd vor 400 000 Jahren*. Theiss, Stuttgart.
- Thieme, H., Veil, S., 1985. Neue Untersuchungen zum eemzeitlichen Elefanten-Jagdplatz Lehringen, Ldkr. Verden. *Die Kd. N.F.* 36, 11–58.
- Thrasher, I.M., Mauz, B., Chiverrell, R.C., Lang, A., 2009. Luminescence dating of glaciofluvial deposits: A review. *Earth-Science Rev.* 97, 133–146.
<https://doi.org/10.1016/j.earscirev.2009.09.001>
- Tode, A., 1982. *Der altsteinzeitliche Fundplatz Salzgitter-Lebenstedt. Teil I, archäologischer Teil*. Böhlau, Köln, Wien.
- Turner, C., 2002. Formal Status and Vegetational Development of the Eemian Interglacial in Northwestern and Southern Europe. *Quat. Res.* 58, 41–44.
<https://doi.org/10.1006/qres.2002.2365>
- Turner, C., 2000. The Eemian interglacial in the North European plain and adjacent areas. *Netherlands J. Geosci.* 79, 217–231. <https://doi.org/10.1017/S0016774600023660>
- Tzedakis, C., 2003. Timing and duration of Last Interglacial conditions in Europe: a chronicle of a changing chronology. *Quat. Sci. Rev.* 22, 763–768. [https://doi.org/10.1016/S0277-3791\(03\)00004-0](https://doi.org/10.1016/S0277-3791(03)00004-0)
- Uthmeier, T., Kels, H., Schirmer, W., Böhner, U., 2011. Neanderthals in the cold: Middle Paleolithic sites from the open-cast mine of Garzweiler, Nordrhein-Westfalen (Germany), in: Conard, N.J., Richter, J. (Eds.), *Neanderthal Lifeways, Subsistence and Technology: One Hundred Fifty Years of Neanderthal Study*. Springer, pp. 25–41.
https://doi.org/10.1007/978-94-007-0415-2_4
- Valde-Nowak, P., Łanczont, M., 2021. State-of-the-art overview of the Loess Palaeolithic of Poland. *J. Quat. Sci.* jqs.3356. <https://doi.org/10.1002/jqs.3356>
- Van Kolfschoten, T., Parfitt, S.A., Serangeli, J., Bello, S.M., 2015. Lower Paleolithic bone tools from the ‘Spear Horizon’ at Schöningen (Germany). *J. Hum. Evol.* 89, 226–263.
<https://doi.org/10.1016/j.jhevol.2015.09.012>
- Vandenberghe, J., 2015. River terraces as a response to climatic forcing: Formation processes, sedimentary characteristics and sites for human occupation. *Quat. Int.*
<https://doi.org/10.1016/j.quaint.2014.05.046>
- Vandenberghe, J., 2013a. Cryoturbation Structures, in: S.A, E. (Ed.), *The Encyclopedia of Quaternary Science*,. pp. 430–435.
- Vandenberghe, J., 2013b. Grain size of fine-grained windblown sediment: A powerful proxy for process identification. *Earth-Science Rev.* 121, 18–30.
<https://doi.org/10.1016/j.earscirev.2013.03.001>
- Vandenberghe, J., Sun, Y., Wang, X., Abels, H.A., Liu, X., 2018. Grain-size characterization of reworked fine-grained aeolian deposits. *Earth-Science Rev.* 177, 43–52.
<https://doi.org/10.1016/j.earscirev.2017.11.005>
- Veil, S., Breest, K., Höfle, H.-C., Meyer, H.-H., Plisson, H., Urban-Küttel, B., Wagner, G.A., Zöller, L., 1994. Ein mittelpaläolithischer Fundplatz aus der Weichsel-Kaltzeit bei

- Lichtenberg, Lkr. Lüchow-Dannenberg. *Germania* 72, 1–66.
- Velichko, A., Novenko, E., Pisareva, V., Zelikson, E., Boettger, T., Junge, F., 2005. Vegetation and climate changes during the Eemian interglacial in Central and Eastern Europe: comparative analysis of pollen data. *Boreas* 34, 207–219. <https://doi.org/10.1080/03009480510012890>
- Velichko, A.A., 1988. Geoecology of the Mousterian in East Europe and the adjacent areas, in: *L'Homme de Neandertal*. Liège, pp. 181–206.
- Velichko, A.A., Morozova, T.D., 2010. Basic features of late pleistocene soil formation in the east european plain and their paleogeographic interpretation. *Eurasian Soil Sci.* 43, 1535–1546. <https://doi.org/10.1134/S1064229310130120>
- Vernot, B., Zavala, E.I., Gómez-Olivencia, A., Jacobs, Z., Slon, V., Mafessoni, F., Romagné, F., Pearson, A., Petr, M., Sala, N., Pablos, A., Aranburu, A., de Castro, J.M.B., Carbonell, E., Li, B., Krajcarz, M.T., Krivoschapkin, A.I., Kolobova, K.A., Kozlikin, M.B., Shunkov, M. V., Derevianko, A.P., Viola, B., Grote, S., Essel, E., Herráez, D.L., Nagel, S., Nickel, B., Richter, J., Schmidt, A., Peter, B., Kelso, J., Roberts, R.G., Arsuaga, J.-L., Meyer, M., 2021. Unearthing Neanderthal population history using nuclear and mitochondrial DNA from cave sediments. *Science* (80-.). 372. <https://doi.org/10.1126/science.abf1667>
- Walkling, A., 1997. Käferkundliche Untersuchungen an weichselzeitlichen Ablagerungen der Bohrung Groß Todtshorn (Kr. Harburg; Niedersachsen). *Schriftenr. der Dtsch. Geol. Gesellschaft* 4, 87–102.
- Wallinga, J., 2002. Optically stimulated luminescence dating of fluvial deposits: A review. *Boreas* 31, 303–322. <https://doi.org/10.1080/030094802320942536>
- Wallinga, J., Cunningham, A.C., 2014. Luminescence Dating, Uncertainties, and Age Range, in: *Encyclopedia of Scientific Dating Methods*. Springer Netherlands, Dordrecht, pp. 1–9. https://doi.org/10.1007/978-94-007-6326-5_197-1
- Weber, T., 1990. Paläolithische Funde aus den Eemvorkommen von Rabutz, Grabschütz und Gröbern, in: Eißmann, L. (Ed.), *Die Eemwarmzeit Und Die Frühe Weichsel- Eiszeit Im Saale-Elbe-Gebiet. Geologie, Paläontologie, Palökologie, Altenburger Naturwissenschaftliche Forschungen* 5. Naturkundliches Museum Mauritium, Altenburg.
- Weber, T., Beye, U., 2015. Paläolithische „Flussfunde“ aus Mitteldeutschland. *Die Kd. N.F.* 63, 183–196.
- Weiss, M., 2020. The Lichtenberg Keilmesser - it's all about the angle. *PLoS One* 15, e0239718. <https://doi.org/10.1371/journal.pone.0239718>
- Weiss, M., 2019. Beyond the caves: stone artifact analysis of late Middle Paleolithic open-air assemblages from the European Plain. *Universiteit Leiden*.
- Weiss, M., 2015. Stone tool analysis and context of a new late Middle Paleolithic site in western central Europe - Pouch-Terrassenpfeiler, Ldkr. Anhalt-Bitterfeld, Germany. *Quartär* 62, 23–62. https://doi.org/10.7485/QU62_2
- Weiss, M., Lauer, T., Wimmer, R., Pop, C.M., 2018. The Variability of the Keilmesser-Concept: a Case Study from Central Germany. *J. Paleolit. Archaeol.* 1, 202–246. <https://doi.org/10.1007/s41982-018-0013-y>
- Wenzel, S., 2007. 12. Neanderthal presence and behaviour in central and Northwestern Europe during MIS 5e, in: Sirocko, F., Claussen, M., Sánchez-Goñi, M.F., Litt, T. (Eds.),

- The Climate of Past Interglacials. Elsevier, pp. 173–193. [https://doi.org/10.1016/S1571-0866\(07\)80037-6](https://doi.org/10.1016/S1571-0866(07)80037-6)
- Weyrich, L.S., Duchene, S., Soubrier, J., Arriola, L., Llamas, B., Breen, J., Morris, A.G., Alt, K.W., Caramelli, D., Dresely, V., Farrell, M., Farrer, A.G., Francken, M., Gully, N., Haak, W., Hardy, K., Harvati, K., Held, P., Holmes, E.C., Kaidonis, J., Lalueza-Fox, C., de la Rasilla, M., Rosas, A., Semal, P., Soltysiak, A., Townsend, G., Usai, D., Wahl, J., Huson, D.H., Dobney, K., Cooper, A., 2017. Neanderthal behaviour, diet, and disease inferred from ancient DNA in dental calculus. *Nature* 544, 357–361. <https://doi.org/10.1038/nature21674>
- Winsemann, J., Lang, J., Roskosch, J., Polom, U., Böhner, U., Brandes, C., Glotzbach, C., Frechen, M., 2015. Terrace styles and timing of terrace formation in the Weser and Leine valleys, northern Germany: Response of a fluvial system to climate change and glaciation. *Quat. Sci. Rev.* 123, 31–57. <https://doi.org/10.1016/j.quascirev.2015.06.005>
- Wintle, A.G., 1997. Luminescence dating: laboratory procedures and protocols. *Radiat. Meas.* 27, 769–817. [https://doi.org/10.1016/S1350-4487\(97\)00220-5](https://doi.org/10.1016/S1350-4487(97)00220-5)
- Wiśniewski, A., Adamiec, G., Badura, J., Bluszcz, A., Kowalska, A., Kufel-Diakowska, B., Mikolajczyk, A., Murczkiewicz, M., Musil, R., Przybylski, B., Skrzypek, G., Stefaniak, K., Zych, J., 2013. Occupation dynamics north of the Carpathians and Sudetes during the Weichselian (MIS5d-3): The Lower Silesia (SW Poland) case study. *Quat. Int.* 294, 20–40. <https://doi.org/10.1016/j.quaint.2011.09.016>
- Wiśniewski, A., Lauer, T., Chłoń, M., Pyżewicz, K., Weiss, M., Badura, J., Kalicki, T., Zarzecka-Szubińska, K., 2019. Looking for provisioning places of shaped tools of the late Neanderthals: A study of a Micoquian open-air site, Pietraszyn 49a (southwestern Poland). *Comptes Rendus Palevol* 18, 367–389. <https://doi.org/10.1016/j.crpv.2019.01.003>
- Wood, R., 2015. From revolution to convention: the past, present and future of radiocarbon dating. *J. Archaeol. Sci.* 56, 61–72. <https://doi.org/10.1016/j.jas.2015.02.019>
- Yelovicheva, Y., Sanko, A., 1999. Palynostratigraphy of the Poozerie Glaciation (Vistulian) in Belarus. *Geolocial Q.* 43, 203–212.
- Zagwijn, W., 1996. An analysis of Eemian climate in Western and Central Europe. *Quat. Sci. Rev.* 15, 451–469. [https://doi.org/10.1016/0277-3791\(96\)00011-X](https://doi.org/10.1016/0277-3791(96)00011-X)
- Zagwijn, W., 1989. Vegetation and climate during warmer intervals in the Late Pleistocene of western and central Europe. *Quat. Int.* 3–4, 57–67. [https://doi.org/10.1016/1040-6182\(89\)90074-8](https://doi.org/10.1016/1040-6182(89)90074-8)
- Zagwijn, W., 1983. Sea-level changes in The Netherlands during the Eemian. *Geol. en Mijnb.* 62, 437–450.
- Zagwijn, W., 1961. Vegetation, climate and radiocarbon datings in the Late Pleistocene of the Netherlands. Part I: Eemian and Early Weichselian. *Meded. Geol. Sticht. NS* 14, 15–45.
- Zagwijn, W., Paepe, R., 1968. Die Stratigraphie der weichselzeitlichen Ablagerungen der Niederlande und Belgiens. *E&G – Quat. Sci. J.* 19, 10–31.
- Zimov, S.A., Zimov, N.S., Tikhonov, A.N., Chapin, F.S., 2012. Mammoth steppe: a high-productivity phenomenon. *Quat. Sci. Rev.* 57, 26–45. <https://doi.org/10.1016/j.quascirev.2012.10.005>

**CHAPTER II: LUMINESCENCE CHRONOLOGY OF THE KEY-MIDDLE
PALEOLITHIC SITE OF KHOTYLEVO I (WESTERN RUSSIA) – IMPLICATIONS
FOR THE TIMING OF OCCUPATION, SITE FORMATION AND LANDSCAPE
EVOLUTION**

Published in: Quaternary Science Advances 2 (2020): 100008



Luminescence chronology of the key-Middle Paleolithic site Khotylevo I (Western Russia) - Implications for the timing of occupation, site formation and landscape evolution

M. Hein^{a,*}, M. Weiss^{a,**}, A. Otcherednoy^c, T. Lauer^{a,b}

^a Max Planck Institute for Evolutionary Anthropology, Department of Human Evolution, Leipzig, Germany

^b Leibniz Institute for Applied Geophysics, Geochronology Section, Hannover, Germany

^c Institute for the History of Material Culture, RAS, St. Petersburg, Russia

ARTICLE INFO

Keywords:

Pleistocene geochronology
Fluvial terraces
Neanderthal occupation
Periglacial environments
Middle paleolithic
Keilmesser
Paleosols
European plain

ABSTRACT

Here we present the luminescence chronology for the Middle Paleolithic open-air site of Khotylevo I, area I-6-2, in Western Russia. Even with a sizable number of such sites available on the Russian Plain, to our knowledge, no successful corresponding luminescence dating has been published before. Coupled with extensive sedimentological logs and grain-size analysis, our data is further used to infer the palaeoenvironmental conditions on site as well as the landscape-forming processes of the wider region. As the site is contained within the sediments of the 2nd fluvial terrace, our high-resolution chronostratigraphy is a valuable contribution to the understanding of this widespread phenomenon and Late Pleistocene geo-climatic events on the Russian Plain. For the formation of the 2nd terrace, a full incision/aggradation cycle was detected with a duration from MIS 5c/5b to MIS 3. Our results indicate that late Middle Paleolithic human occupation took place during the more ameliorate Early Weichselian phase of MIS 5a. Furthermore, the dates for Khotylevo I-6-2 prove the onset of the late Middle Paleolithic *Keilmessergruppen* occurred as early as MIS 5a. The archeological comparison with other numerically dated Late Middle Paleolithic assemblages across the northern central European Plain suggests a complex picture of population dynamics between MIS 5a and MIS 3.

1. Introduction

The last interglacial-glacial cycle on the European Plain has been an eventful period with respect to climatic shifts and (partially) climate-driven landscape evolution, including vegetation cover, sedimentation processes and hydrological regimes (Caspers and Freund, 2001; Christiansen, 1998; Helmens, 2014; Vandenbergh, 2015; Velichko et al., 2011). This complex of interdepending factors, in turn, was the canvas for the occupation of the Middle Paleolithic foragers, i.e. Neanderthals. Many studies have addressed their respective adaptabilities to this constantly changing environment (Gaudzinski-Windheuser et al., 2014; Gribchenko and Kurenkova, 1999; Locht et al., 2016a; Richter, 2006; Roebroeks et al., 2011; Skrzypek et al., 2011; Toepfer, 1970; Velichko, 1999, 1988). Such investigations are necessarily based on material objects, mainly lithics and skeletal remains, whether hominin or faunal, and very rarely, organic artefacts, like wooden tools or birch tar adhesives

(Gaudzinski, 1999; Hublin, 1984; Kozowyk et al., 2017; Thieme and Veil, 1985; Weiss et al., 2018). But equally important is the up-scaled view of the geographic and temporal distribution of various sites in order to try and understand occupational and migrational patterns – keeping in mind the huge bias that the established sites presumably represent a diminishingly small part of the whole record (Hublin and Roebroeks, 2009; Richter, 2016). The spatial and temporal distribution of late Neanderthal sites can help to understand human behavior within, and adaptations to, changing environmental and climatic conditions. By attributing those patterns and specific assemblages to climatic shifts, climate-driven landscape and faunal properties, it might prove possible to depict adaptive and/or evasive or simply coping-strategies of the Neanderthals. On the European Plain, where cave sites are less abundant, open-air sites assume an important role in deciphering those adaptive patterns (Weiss, 2019). The entirety of these sites can arguably be regarded as a representation of the environmental demands and habitual realities of the

* Corresponding author.

** Corresponding author.

E-mail address: michael_hein@eva.mpg.de (M. Hein).

<https://doi.org/10.1016/j.qsa.2020.100008>

Received 30 January 2020; Received in revised form 11 May 2020; Accepted 22 May 2020

Available online 30 May 2020

2666-0334/© 2020 The Author(s). Published by Elsevier Ltd. This is an open access article under the CC BY-NC-ND license (<http://creativecommons.org/licenses/by-nc-nd/4.0/>).

populations.

Necessary prerequisites for elucidating Neanderthal adaptabilities to changing environments (apart from the analyses of the finds on open-air sites) are (1) a reliable dating of those sites and (2) a way to regionally or better locally reconstruct the diachronic former states of environment, climate and landscape. Wherever bone material or other organic remains are available, ^{14}C dating is the first, obvious and right choice for chronological control, as its precision and reproducibility is unrivalled by most other methods (Wood, 2015). However, the better part of the Neanderthal overall existence has been spent well outside the range of radiocarbon, and even within the range, at its far end (ca. 50 kyrs.), the method is known to still hold some challenges (Briant and Bateman, 2009; Pigati et al., 2007).

Thus, studying suitable sediment sequences at open-air sites is an elegant way to fulfill both the dating and the paleoenvironmental requirements. Luminescence dating has been successfully applied to Lower and Middle Paleolithic sites contained within or surrounded by aeolian, fluvial and colluvial sediments (Lauer et al., 2020; Lauer and Weiss, 2018; Mercier et al., 2003; Richter and Krubetschek, 2014; Skrzypek et al., 2011; Strahl et al., 2010; Weiss, 2015; Weiss et al., 2018; Winsemann et al., 2015; Wiśniewski et al., 2019). Even though the uncertainties might sometimes impede an attribution to distinct climatic periods, the benefits of this method clearly lie in its ability to chronologically resolve records older than 50,000 years. When accompanied by thorough sedimentological logging, it can potentially account for a conceivable reworking of the find layers by cryogenic processes and periglacial mass wasting (Bateman and Van Huissteden, 1999; Döhler et al., 2018; Harrison et al., 2010; Wenban-Smith et al., 2010). Moreover, the characteristics of the sediments on site and the processes responsible for their deposition can, in many cases, be traced back to climatic and environmental driving factors that would have affected the Neanderthals' habitats accordingly.

To our knowledge though, even with a high number of Late Middle Paleolithic (LMP, Marine Isotope Stages 5d to 3) open-air sites available (Hoffecker, 1987; Matyukhin and Sapelko, 2009; Otcherednoi et al., 2014a; Velichko, 1988) on the Russian Plain, no unambiguous luminescence chronology has been presented (but see Hoffecker et al., 2019). Hence, in terms of temporal classification this area remains an "unproven domain" with enormous potential to substantially complement the pre-cognition of Neanderthal spatial behavior from Western and Central Europe (Higham et al., 2014; Locht et al., 2016a; Richter, 2016). Many of the Russian LMP sites are associated with either loess-like sediments or the deposits of the 2nd fluvial terrace (Velichko, 1988). Both of which phenomena have been extensively investigated throughout the 20th century resulting in elaborate respective stratigraphies (Matoshko et al., 2004; Panin et al., 2017; Velichko et al., 2011, 2006). Due to the relatively homogeneous nature of this macrochoric physical region (in terms of tectonics and geology) the loess and fluvial stratigraphies can seemingly be correlated over vast distances (ibid.). This allows for an easy-to-use temporal and paleoenvironmental classification of LMP open-air sites on a large proportion of the Russian Plain, while still considering potential differences in local and regional paleosol characteristics (Otcherednoi et al., 2018).

Within the time-frame of the LMP, the chronological frameworks of both the loess and the fluvial sequences to this day remain rather fragile, because they are supported by merely a handful of luminescence dates on the entire Russian Plain, represented by the works of Little et al. (2002) and Panin et al. (2017). Simple extrapolations to specific on-site environments are consequently not yet advisable. For that reason, the comparison with hemispherical climatic cycles as well as the identification of occupational patterns and any other form of Neanderthal adaptations is somewhat restrained, unless a high-resolution luminescence chronology is established directly on site.

In this study the LMP open-air site of Khotylevo I, area I-6-2, has been chosen for its geographic position and its suitable sediment archive. As one of the northernmost undisputed LMP assemblages on the European

Plain (Nielsen et al., 2015) it provides valuable insights into the extension of the Neanderthal habitat. The site preserves ~12 m of well-stratified fluvial and loess-like sediments, giving it the potential to act as a hinge between the archeological and lithostratigraphical records on the Russian Plain. The objectives of this study are to establish a robust luminescence-based chronology for the sedimentary sequence exposed at Khotylevo I-6-2 and to clarify site formation by applying sedimentological logging and granulometric analyses. In doing so we intend to (i) obtain new results for the chronology of the late Middle Paleolithic of the north central and northeastern European Plain, (ii) reconstruct Pleistocene changes in palaeoenvironment to potentially better understand the connectivity between climatic shifts and Neanderthal appearance or disappearance, and (iii) give insight on the relation of fluvial archives to better known Loess-Paleosol-Cryogenic formations. The data presented here will chronologically constrain the occupation and sedimentary units at Khotylevo I, supplementing our knowledge of the late Pleistocene stratigraphy. Analysing geological and archeological deposits in conjunction should prove to be mutually beneficial for the chronological framework of both branches of quaternary science.

2. Geological and geomorphic setting

The Middle Paleolithic site of Khotylevo I (53.3° N, 34.1° E) in Western Russia is situated near the eponymous village, ca. 20 km from Bryansk upstream the River Desna (Fig. 1). Geologically the region is characterized by sedimentary rocks from the Upper Cretaceous, where unconsolidated Cenomanian sands and marls as well as flint-bearing chalks from the Turonian predominate (Sytychkin, 1998). During the course of the Pleistocene the area witnessed a succession of alternating glacial and periglacial periods. The Desna basin was last covered by ice sheets during the Dniepr Middle Pleistocene glaciation in MIS 8 when the layout of the River Desna was set as a glacial drainage channel (Gozhik et al., 2014a; Velichko et al., 2011). Fluvio-glacial deposits of this era are found in the undulating watershed surfaces outside the river valley and consist of coarse-grained sands interlayered with bands, and clasts stemming from bedrock material (Gavrilov et al., 2015). These sediments represent the parent material for the Salyn soil formation of the Eemian (Mikulino) Interglacial (Otcherednoi and Voskresenskaya, 2009). In contrast, during the Weichselian (Valdai) glaciation between MIS 5d and 2, the region was subject to periglacial conditions interchanging with interstadials (MIS 5a, 5c and MIS 3). Several fluvial aggradation and incision phases occurred, forming the 1st and 2nd fluvial terrace, while loess accumulated in the coldest and most arid stages (especially MIS 4 and 2) (Little et al., 2002; Velichko et al., 2006). The latter cold phases were accompanied by the formation of pronounced, permafrost-induced cryogenic horizons. In contrast, pedogenic processes occurred mainly during the interstadial periods leading to intensive paleosols being frequently preserved in loess and fluvial terrace suites (Panin et al., 2018; Sycheva and Khokhlova, 2016; Velichko, 1990; Velichko et al., 2017). For many of the Weichselian processes and deposits the region constitutes the type area on the East European Plain.

The site itself is located on the raised right bank of the asymmetric Desna valley and is part of the sediment sequence that forms the 2nd fluvial terrace. Said terrace has been recognized in many fluvial catchments in Russia and the Ukraine as a morphological feature some 16–25 m above the current river courses (Grishchenko, 1976; Matoshko et al., 2004). Whether it can also be regarded as a coherent and correlatable chronostratigraphical phenomenon is difficult to assess, largely due to a shortage of numerical dates. According to Velichko (1988) it accumulated in the Early Weichselian, a notion recently supported by Panin et al. (2017). The 2nd terrace of the Desna valley has been dissected by scores of ravines, dividing the riverbank into repeating promontory-ravine successions. The trench Khotylevo I-6-2 sits directly alongside one of those ravines' outlet into the recent floodplain (Fig. 1). For the archaeologically relevant layers at the bottom, it contains a succession of slope deposits, fluvial sediments and paleosols. These are

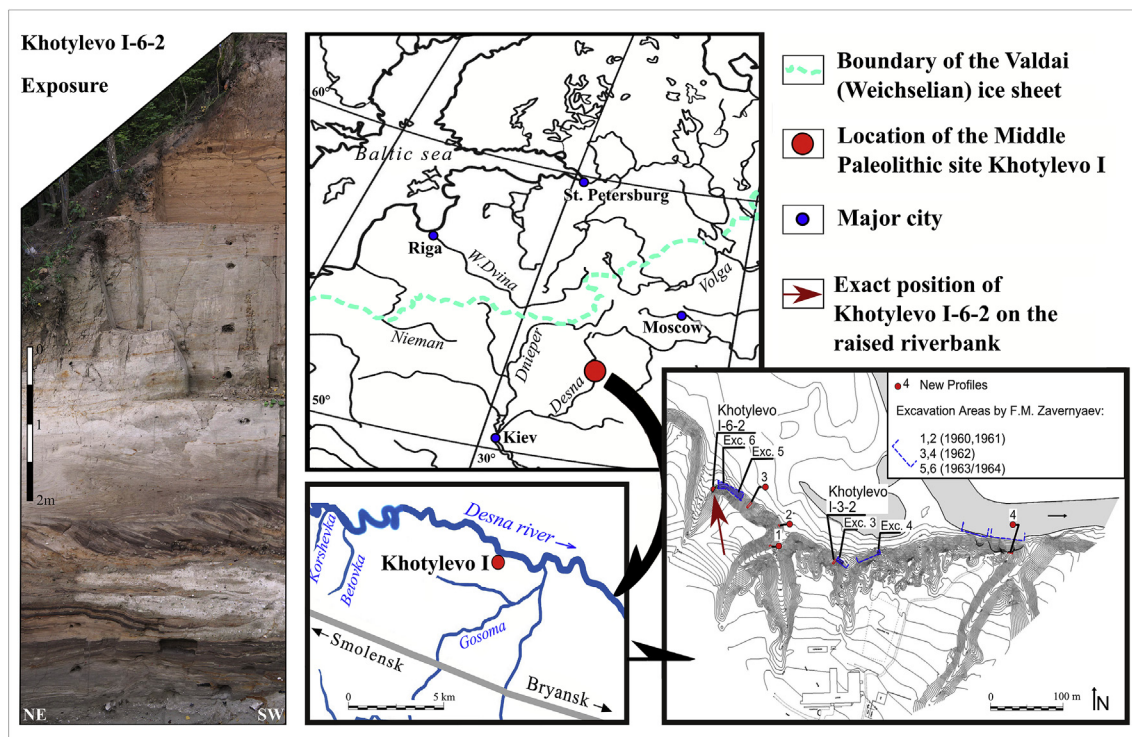


Fig. 1. Location of the site Khotylevo I, area I-6-2 with respect to the LGM ice sheet border, the other Khotylevo I trenches and the position within the river valley (adapted from Otcherednoi et al., 2014).

overlain by different alluvial sediments and topped by a cover loess. A detailed description of the exposure is given in section 4.1 of this article.

3. Materials and methods

3.1. Archeological finds

The site was found in 1958 by an archaeologist of the Bryansk Regional Museum, F.M. Zaverlyayev, who started excavations in 1960 in areas where surface finds were previously collected. His team excavated six large trenches and several test pits along the right bank of the Desna over five years (Zaverlyayev, 1978, see Fig. 1). The finds from Khotylevo I were associated with alluvial sediments. New work at the upstream sectors of the site began in 2010 and cultural remains were found in buried soils. The excavation area “Khotylevo I-6-2” is the focus of the present study.

The trench is characterized by three main find layers (Otcherednoi et al., 2014b, 2014a; Otcherednoi and Voskresenskaya, 2009; Weiss, 2019; Weiss et al., 2017): ‘Cultural Layer 1’ (CL1), ‘Cultural Layer 2’ (CL2) and ‘Cultural Layer 4’ (CL4) (Fig. 2). ‘Cultural Layer 3’ (CL3) revealed only a low number of finds (Table 1) and is not described in detail here. All occupations of Khotylevo I-6-2 can be attributed to the equivalent late Middle Paleolithic Micoquian (Bosinski, 1968, 1967), *Keilmessergruppen* (Mania, 1990; Veil et al., 1994), or the ‘Mousterian with Micoquian Option’ (Richter, 2016, 2012, 2002, 2001, 2000, 1997) of central and eastern Europe (for a discussion of the terms in relation to research history see Frick, 2020). Whereas the former terms put their emphasis on the presence of specific bifacial tools, the latter interprets Mousterian (without bifacial tools) and Micoquian (with bifacial tools) assemblages as related technocomplexes and continuous components of a single archeological entity (compare “Mousterian with bifaces”, as termed by Gladilin, 1985). The terms will be used synonymously throughout the text. All find layers of Khotylevo I-6-2 are characterized by Levallois and prepared core blank production (Table 1; Fig. 2: 1–3 & 6). The latter refers to cores with striking platform and core surface

preparation, but these do not fall into one Levallois scheme *sensu stricto*. In CL1 and CL4 also bifacial tools occur, like typical bifacial backed knives or *Keilmesser* (Fig. 2: 5 & 10) in CL4, a characteristic tool type for the late Middle Paleolithic *Keilmessergruppen* or Micoquian of central and eastern Europe. Additionally, unifacial *Keilmesser* which are part of some *Keilmessergruppen* assemblages (Weiss et al., 2018) occur as well (Fig. 2: 4 & 9) in Khotylevo I-6-2, restricting this tool concept not only to bifacial tools. Although no bifacial tools could be recovered from CL2, ten flakes resulting from bifacial production could be identified (Otcherednoi et al., 2014a; Otcherednoi and Voskresenskaya, 2019; Vishnyatsky et al., 2015; Weiss, 2019; Weiss et al., 2017) and evidence their on-site manufacture. The late Middle Paleolithic character of the stone artefacts is reinforced by the fact that the analysis of the Khotylevo I-6-2 assemblages revealed strong relationships to other late Middle Paleolithic open-air assemblages between MIS 5a and MIS 3 from the European Plain (Otcherednoi, 2010; Weiss et al., 2017), namely Pouch (Weiss, 2015) and Königsau (Mania, 2002; Mania and Toepfer, 1973), both Saxony-Anhalt/Germany, and Wrocław-Hallera Av. (Wiśniewski et al., 2013), southwestern Poland. The occurrence of high-quality flint slabs from the Cretaceous sediments directly at the site, together with the rather low frequency of tools in all layers (Table 1), as well as the potential manufacture and export of bifacial tools (CL2) point to a workshop character of the site.

3.2. Luminescence dating

3.2.1. Sampling and sample preparation

Eighteen samples were collected for luminescence dating by hammering stainless steel tubes horizontally into the freshly cleaned profile walls. For sampling positions and stratigraphy, the reader is referred to Fig. 4 and section 4.1. In order to prevent using sediment grains that might have been exposed to sunlight during sampling, the outer 2 cm were removed from both ends of the tube. These subsamples were used to estimate the burial water content. Sample preparation and equivalent dose-estimation (D_e) was conducted at the luminescence-dating laboratory of the Department of Human Evolution, Max Planck

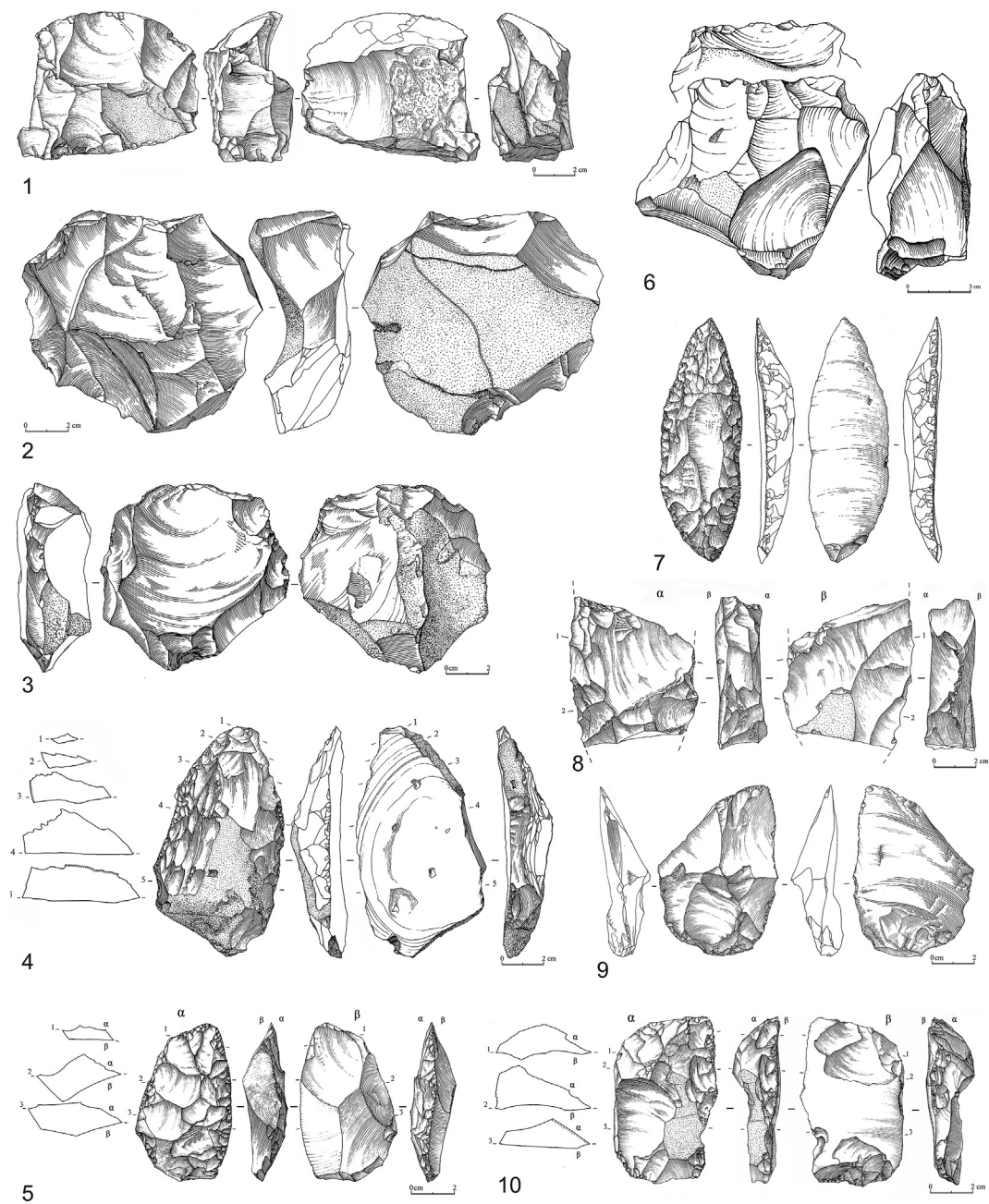


Fig. 2. Examples for artefacts from Cultural Horizon 1, 2 & 4. CL1: 1, 4, 6–8; CL2: 2; CL4: 3, 5, 9–10. 1–2: prepared cores; 3: Levallois-core (preferential), 4: unifacially surface shaped backed knife (Keilmesser-concept); 5, 10: bifacial backed knives (Keilmesser); 6: Levallois-core (preferential); 7: unifacially surface shaped point; 8: fragment of a bifacial tool; 9: retouched backed flake or simple backed knife (Keilmesser-concept). Drawings: A. Otcherednoy.

Table 1
Summary of the artefacts discovered at Khotylevo I-6-2. The result for the 2017 season of CL4 is displayed separately, as it provided the largest quantity of artefacts but is not yet fully analyzed. *Plane and prepared cores only. **Levallois centripetal only.

Cultural Layers	Cores (n*/L**)	flakes	chips	Unifacial tools	Bifacial tools	Σ
1	22/0	207	371	11	4	973
2	7/0	1074	1884	7	0	3033
3	3/0	120	191	1	0	326
4	37/3	831	2132	30	4	3388
4 (2017 season)	2446		7514	2	1	9963

Institute for Evolutionary Anthropology, Leipzig. Preparation under subdued red light comprised drying at 50 °C, sieving to obtain the desired grain-size (180–250 µm, and 4–11 µm for sample 1702), and a chemical treatment to remove carbonates and organic matter, utilizing HCl (10%) and H₂O₂ (30%) respectively. Heavy liquid separation (lithium heterotungstate) was used to separate quartz and K-feldspar from the remaining mineral matrix at densities of 2.62–2.68 g/cm³ and <2.58 g/cm³, respectively (cf. Aitken, 1998). The extracted quartz was subsequently etched with concentrated HF (40%) for 60 min to remove the naturally α-irradiated outer rind and potential feldspar contaminations (Wintle, 1997). The etched samples were re-sieved to recover the desired grain-size fraction. Laboratory measurements were made using multiple-grain aliquots by mounting grains onto stainless steel discs (24–48 aliquots) using silicone spray and a mask of 0.5 mm; each aliquot

comprised 5–10 grains (Duller, 2008). Luminescence sensitivity was tested beforehand with higher but successively decreasing aliquot sizes to ensure sufficient photon counts. Lacking adequate coarse-grained material for sample L-EVA 1702, the polymineral 4–11 μm fraction was prepared and mounted on aluminum discs (16 aliquots).

3.2.2. Dose rate determination

Additional sediment samples were collected alongside the OSL-samples for dose rate determination using high-resolution germanium gamma spectrometry. Analyses of the specific activities of the radioelements ^{238}U , ^{232}Th , ^4K and their daughter isotopes were undertaken at VKTA laboratory in Dresden (Table 2, and supplementary information). In-situ gamma spectrometry was measured using a calibrated LaBr_3 -detector (Inspector 1000) for three samples (L-EVA 1712, 1714 and 1716) to improve dose rate determinations in thin archeological layers. The saturated water content was used to approximate dose rate attenuation by moisture (Table 2). The contribution of cosmic radiation to the total dose rate was calculated based on Prescott and Hutton (1994). The internal beta dose-rate contribution for the K-feldspar samples assumed an effective potassium content of $12.5 \pm 0.5\%$ (Huntley and Baril, 1997). Radioactivity conversion factors were applied following Guérin et al. (2011). For the K-feldspar samples an a -value of 0.11 ± 0.02 was used to allow for the comparison of lower luminescence-efficient alpha particles with beta and gamma radiation (Kreutzer et al., 2014).

3.2.3. Equivalent dose estimation and testing

Equivalent doses were estimated using a Risø TL-DA-20 reader equipped with IR light-emitting diodes transmitting at 870 nm wavelength for K-feldspar measurements and blue light-emitting diodes (470 nm) for quartz. The emitted luminescence signal was detected through a D-410 filter and a Hoya U-340 filter, respectively. Artificial irradiation was delivered by a calibrated $^{90}\text{Sr}/^{90}\text{Y}$ beta source with a dose-rate of $\sim 0.23 \text{ Gy/s}$. First test-measurements on quartz using samples L-EVA 1702, 1704, 1706, 1707, 1709, 1710 and 1711 (from the upper part of the sequence) showed the natural quartz luminescence signal close to, or in saturation for the majority of the samples. The only sample that showed a natural quartz signal below $2D_0$ was sample L-Eva 1702. Thus, further measurements were undertaken solely on K-feldspars as they typically saturate at much higher doses (e.g. Buyllaert et al., 2012). To avoid the issue of anomalous fading and the potentially problematic correction involved (Huntley and Lamothe, 2001; Wintle, 1973), we used the pIRIR₂₉₀ approach as suggested by Thiel et al. (2011) and summarized in Table 3. Generally, stimulating and measuring

Table 3

Measurement steps for the pIRIR₂₉₀-approach.

Step	Treatment	Description
1	Dose	
2	Preheat (320 °C for 60s)	
3	IRSL, 100 s at 50 °C	Remove unstable signal
4	IRSL, 200 s at 290 °C	L_x
5	Test dose	
6	Cutheat (320 °C for 60s)	
7	IRSL, 100 s at 50 °C	Remove unstable signal
8	IRSL, 200 s at 290 °C	T_x
9	IRSL, 100 s at 325 °C	Hot bleach
10	Return to step 1	

feldspars at elevated temperatures after depleting the IR₅₀ signal has been shown to produce robust luminescence ages (Thomsen et al., 2008). Six samples were bleached in the solar simulator for 3 h and used for dose recovery tests with different protocols. Comparison of the residual-subtracted measured-to-given dose ratios from the different signals (pIRIR₂₂₅, pIRIR₂₉₀ and pIRIR₂₉₀ with a hotbleach), showed the most reliable results from the latter protocol (Fig. 3, see supplementary information for discrete residual doses). Thus, a 325 °C hotbleach was included at the end of each measurement cycle (Table 3, step 9). The dose response curve was built using four to five regenerative dose points following the measurement of the natural IR-signal (L_x) and fit with an exponential function. Recycling ratios were calculated by re-measuring the first low-dose point after the highest regenerative dose point and all aliquots deviating $>10\%$ were rejected. In addition, only aliquots with recuperation below 5% of the natural signal were included. To examine the stability of the pIRIR₂₉₀ signal anomalous fading was measured in 6 samples (3 aliquots each) following the procedure of Huntley and Lamothe (2001), but including a 325 °C hotbleach. All g-values obtained using the pIRIR₂₉₀ signal were substantially lower than the values from the corresponding IR₅₀ signal (Fig. 3). With the exception of samples L-EVA 1715 and 1717 all pIRIR₂₉₀ fading rates are $<2.0\%$ /decade, whereas the mean of all obtained g-values is $1.6 \pm 0.1\%$ /decade, attesting to the stability of the pIRIR₂₉₀ signal.

3.3. Grain size analysis

A portion of the material collected for luminescence dating was used for grain-size determination. Analyses were conducted at the Leibnitz Institute for Applied Geophysics, Geochronology Section using a

Table 2

Results of high resolution gamma-ray spectrometry and saturation water contents used for correction. The gamma dose rate contribution for samples L-Eva 1712, 1714 and 1716 were obtained by in-situ gamma spectrometry using a calibrated LaBr_3 detector. The alpha, beta and gamma dose rates for each sample are presented in the supplementary information.

Lab.-ID	U (ppm)	Th (ppm)	K (%)	Cosmic Dose (Gy/ka)	DR _{total} (Gy/ka)	H ₂ O (%)
1702	2.1 ± 0.4	9.6 ± 0.7	1.80 ± 0.15	0.20 ± 0.02	3.49 ± 0.22	21.5 ± 5
1703	2.1 ± 0.3	8.9 ± 0.6	1.45 ± 0.12	0.19 ± 0.02	2.81 ± 0.15	21.4 ± 5
1704	2.3 ± 0.4	7.8 ± 0.5	1.51 ± 0.12	0.18 ± 0.02	3.02 ± 0.16	12.2 ± 5
1705	1.8 ± 0.3	7.8 ± 0.5	1.10 ± 0.07	0.17 ± 0.02	2.54 ± 0.14	12.9 ± 5
1706	1.4 ± 0.2	5.7 ± 0.4	1.15 ± 0.07	0.16 ± 0.02	2.35 ± 0.14	13.3 ± 5
1707	2.0 ± 0.3	7.9 ± 0.5	1.52 ± 0.12	0.16 ± 0.02	2.84 ± 0.15	17.2 ± 5
1708	2.6 ± 0.5	9.5 ± 0.6	1.88 ± 0.14	0.15 ± 0.01	3.27 ± 0.16	19.9 ± 5
1709	1.9 ± 0.3	8.8 ± 0.6	1.73 ± 0.11	0.14 ± 0.01	3.06 ± 0.15	16.2 ± 5
1710	1.9 ± 0.5	6.6 ± 0.4	1.37 ± 0.11	0.14 ± 0.01	2.67 ± 0.16	13.5 ± 5
1711	1.6 ± 0.3	6.0 ± 0.4	1.34 ± 0.11	0.14 ± 0.01	2.56 ± 0.15	12.4 ± 5
1712	1.0 ± 0.2	4.1 ± 0.3	0.88 ± 0.07	0.13 ± 0.01	2.05 ± 0.14	12.0 ± 5
1713	1.18 ± 0.2	4.1 ± 0.3	1.10 ± 0.07	0.13 ± 0.01	2.18 ± 0.14	9.5 ± 5
1714	1.09 ± 0.2	4.9 ± 0.3	1.05 ± 0.09	0.13 ± 0.01	2.20 ± 0.15	12.1 ± 5
1715	1.43 ± 0.27	3.6 ± 0.3	1.06 ± 0.09	0.13 ± 0.01	2.15 ± 0.15	10.2 ± 5
1716	1.4 ± 0.3	5.9 ± 0.4	1.16 ± 0.07	0.12 ± 0.01	2.37 ± 0.14	12.9 ± 5
1717	0.9 ± 0.3	3.3 ± 0.3	0.83 ± 0.09	0.12 ± 0.01	1.80 ± 0.15	11.0 ± 5
1718	1.1 ± 0.3	4.7 ± 0.3	1.07 ± 0.08	0.12 ± 0.01	2.13 ± 0.14	12.6 ± 5
1719	1.5 ± 0.4	4.8 ± 0.3	0.92 ± 0.07	0.12 ± 0.01	2.08 ± 0.15	12.7 ± 5

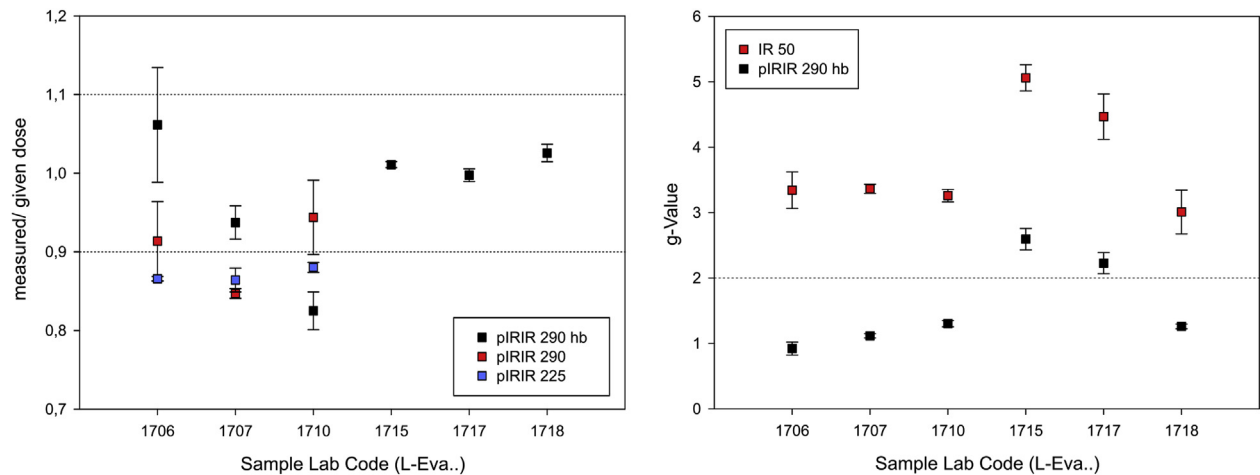


Fig. 3. Left - Comparison of dose recovery tests for the pIRIR225 and pIRIR290 (with and without a hot bleach, hb) protocols; the residual signal was subtracted from the measured dose. Right – Comparison of fading rates (g-values in %/decade) for the IR50 vs. pIRIR290 signals.

Beckman-Coulter LS 13320 PIDS laser diffractometer detecting a spectrum from 0.4 to 2000 μm . The measurement protocol was described by Machalett et al. (2008). For sample preparation, instead of ultrasonic treatment we dispersed with 1% ammonium hydroxide (NH_4OH) in overhead rotators for at least 12 h. We abstained from removing organic matter and carbonates, because organic matter apparently has a negligible effect on grain-size distribution (Beuselinck et al., 1998; Machalett

et al., 2008) and because field tests implied no significant carbonate contents in our sediments. All samples underwent a fivefold measurement, averaging the results to receive the final grain-size cluster on condition that standard deviation of all grain-size spectra remained below 5%. Sample L-EVA 1709 did not satisfy this criterion and was therefore excluded from all further interpretations.

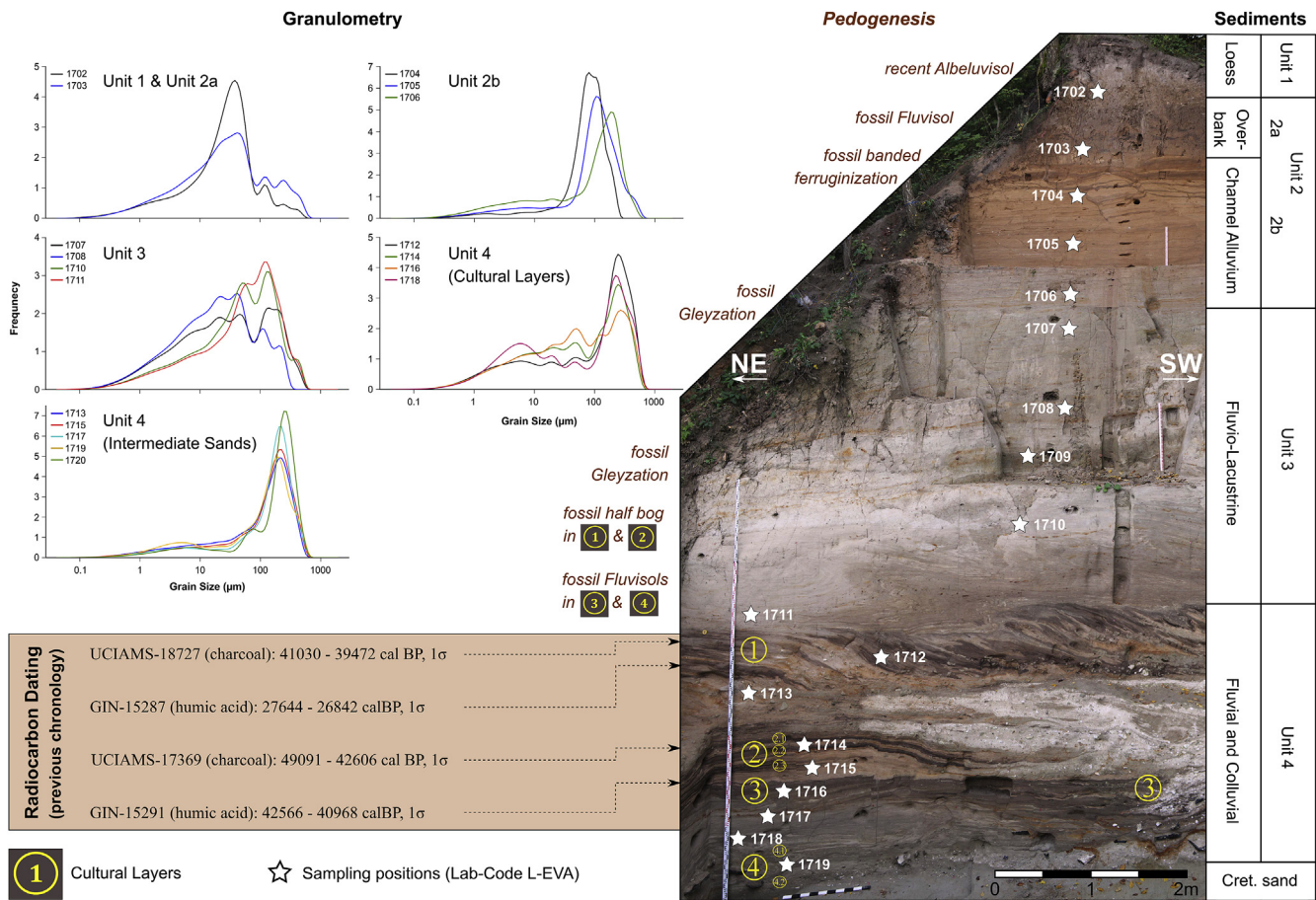


Fig. 4. Overview of the sampling positions, stratigraphy, grain-size distributions and existing ^{14}C chronology following Otcherednoi et al. (2014b); Otcherednoi and Voskresenskaya (2019) and Vishnyatsky et al. (2015).

4. Results

4.1. Site stratigraphy based on field investigations and grain-sizes

Khotylevo I-6-2 is an artificial exposure for archeological purposes. Cut into the steep river bank of the 2nd fluvial terrace, it lies directly at the conjunction with a smaller ravine ceasing at this spot and aligning with the modern floodplain. It comprises ~12 m of alluvial, colluvial and aeolian sediments, resting against the primary slope of the valley which formed earlier in the Pleistocene (Otcherednoy and Voskresenskaya, 2019). The profile was first described by E.V. Voskresenskaya (Voskresenskaya and Otcherednoy, 2010; Voskresenskaya et al., 2011; Voskresenskaya and Otcherednoy, 2012; Otcherednoi et al., 2014a). Based on field work between 2017 and 2019, the section was divided into four broad sedimentary units described from top to bottom in the following paragraphs. The results of the grain-size analysis were utilized to support attribution of the deposits to specific processes (Fig. 4).

4.1.1. Unit 1

Unit 1 consists of fine-grained loess or loess-like deposits, indicated by grain size distribution with a coherent sorting and a pronounced maximum in the coarse silt fraction (L-EVA 1702). The loess has been subjected to pedogenesis after deposition and all primary carbonates have been leached from the substrate, leading to the formation of a rather acidic Albeluvisol according to WRB (2015).

4.1.2. Unit 2a

Unit 2a is a partially laminated sandy-silty deposit (facies code *Fl* to *Fsm*, after Miall (2006)), with a distinct upper boundary and is also devoid of carbonates. Grain sizes infer the relatedness to loess, while at the same time indicating a polygenetic sedimentary process with the additional contribution of fine and middle sands (L-EVA 1703). This unit is best described as overbank fines, assuming the reworking of loess at the time of deposition. Discontinuous humic lenses with a strong blackish color and containing abundant fragments of charcoal occur in this layer, presumably derived from burning events. These overbank fines are capped by a humus-enriched soil of ca. 30 cm thickness (Fluvisol, according to WRB (2015)). A very sharp and likely erosional contact at 190 cm delimits this unit at the bottom.

Overbank sediments are deposited during or after river flooding in shallow water. Longer periods between flooding events may lead to multiphased soil formation of varying degrees within the overbank fines (Fluvisols). The deposition of fine grains is due to preferential sorting and the source material, which is often loess. As is the case in Khotylevo I-6-2, typically comparable Pleistocene overbank deposits are overlain by a younger loess in many European fluvial catchments (cf. Vandenberghe, 2015).

4.1.3. Unit 2b

This unit of ~3 m thickness consists of well-sorted light yellow to light orange fine sands. It is characterized by cm-scale horizontal beds, with individual beds sometimes showing slightly oblique lamination, and is completely devoid of gravels. Very seldom pebble-sized items occur, which are allothous clasts of the Cretaceous marls and chalks. An overall dip in any direction could not be observed. Downthrows, interpreted as unloading cracks, cut through the sequence with a displacement figure in the dm range. In the topmost 150 cm of this unit secondary ferruginous layers – Ortsands, partially consolidated as Ortstein – occur (cf. Panin et al., 2017). Their thickness gradually decreases downwards from 20 cm at the Unit 2b/2a boundary to a few mm within a meter further down. The lowermost 100 cm of the Unit possess gleyic features, in this respect pre-announcing similar conditions in Unit 3. Grain sizes of the three samples (L-EVA 1704 to 1706) display a fining-upwards trend, with a relative continuation to the top in the form of the hanging overbank fines of Unit 2a.

For this unit we allocated the facies code *Sh* (horizontally laminated

sandy fluvial sediments), as proposed by Miall (1977). However, assigning it to a specific element of the alluvial architecture proved challenging, and was not conclusive (cf. Ashworth et al., 2011; Brierley, 1989). In most periglacial rivers crudely-bedded or massive gravel layers are common (Van Huissteden et al., 2013). Horizontal lamination of sands rarely occurs and if so, the units usually have a small extent, both in the lateral and in the vertical direction (Hickin, 1993; Lynds and Hajek, 2006; Miall, 2006). This particular facies (*Sh*) is elsewhere often interpreted as a product of transitional to rapid flow regimes. High-energy, possibly shallow discharge events are held accountable. Even ephemeral, flashy sheetflood events of the “Bijou Creek-type” can lead to these plane-laminated sands (Miall, 2006). In contrast, very low flow velocities and shallow water may also result in horizontal lamination characterized by fine grading (Miall, 1977). This coincides with Vandenberghe's view (2015), whereupon the *Sh*-facies is deposited under predominantly quiet conditions towards the edges of an active channel belt.

However, in the Desna-Dniepr system horizontally laminated fine sands are very common in the alluvial suites of the 2nd terrace, whereas the coarse fraction is usually less than 1% (Matoshko et al., 2004; Panin et al., 2017). This could be explained by the low dip angle and the restricted availability of crystalline bedrock in this part of the East-European Plain, where thick Mesozoic sedimentary rocks predominate. Based on the above considerations, in conjunction with the absence of a coarse fraction in the modern channel bottom of the River Desna, we tentatively interpret Unit 2b as channel alluvium, that may have been deposited in the marginal zone of the active river.

4.1.4. Unit 3

This fine-grained, loamy unit displays definite features of gleyization throughout, in the form of reduction and lepidocrocite precipitation. Cautiously, said features can be interpreted as syngenetic (Miall, 2006). The unit is divided into two sub-units with slightly differing depositional environments. The upper ca. 200 cm (L-EVA 1707, 1708) comprise a very dense and massive loam with a noticeable clay content, a slightly raised content of organic carbon and only rare lenses of coarser sands (facies code *Fsm*, after Miall (2006, 1977)). In contrast, the lower part of the unit (L-EVA 1709 to 1711) exhibits lamination of lighter fine-sands and greyish silts with a lower clay content (facies code *Fl*). Presumably the increments represent individual flooding events. Toward the base of Unit 3, these lamellae are distorted by cryoturbation and solifluction.

Grain-size distributions reveal a polymodal distribution, with one peak in clay and silt and another peak in the fine-sand fraction, which supports the subdivision of this unit. While the upper, massive part is informed by a broader clay and silt peak, the lower part is biased toward the fine-sand fraction. As indicated by the grain-sizes, fluvial reworking of more or less contemporaneous loess deposits contributed to the sediment composition of the entire unit. This argument is further supported by the chronological position of the unit close to the time of main loess delivery (see sections 4.2. and 5.2.2).

In general, fine-grained clastics are derived from suspension load and as such cannot be deposited within active river channels. Hence, they represent low-energy (i.e. often distal) environments in floodplains, ponds or abandoned channels. In major suspension-load streams the thickness of those units can stretch up to several meters (Miall, 2006). Unit 3 was most likely deposited in the rear part of the Desna alluvium (cf. Velichko, 1988), whereas an abandoned channel fill is ruled out for the lack of peat layers, plant remains and severely clayey segments (Rust, 1972). Following Miall (1977) these sediments of Unit 3 are explained as fluvio-lacustrine or backswamp deposits (cf. Hickin, 1993). Indeed, the lower part could also be interpreted as waning flood deposits due to the lamination. It is however noteworthy, that small desiccation/frost cracks in Unit 3 only appear on the very top, indicating that up to this point in time there were no significant drying-out phases during deposition. Since the continuous gleyization supports this argument, we refute an interpretation as overbank fines in favor of fluvio-lacustrine backswamp

deposition throughout the entire Unit 3. In this milieu the binding effect of vegetation may lead to the formation of small mud laminae. Each increment represents the suspended load of one flood cycle (Rust, 1972; Miall, 2006). In the massive upper part of the Unit, the lamination may never have formed or been destroyed post-depositionally. Until further sites along the river Desna are investigated, an *anastomosing* river-type, formed by an excess of fluvially reworked loess cannot be ruled out for the formation of Unit 3. In anastomosing channels high suspension loads favor an aggradational regime and a constraint in lateral expansion (Hugget, 2011). Similar gleyic fine-grained deposits are well known to exist both in the distal part and as stable elongate islands between braided channels in anastomosed systems (Smith and Smith, 1980).

4.1.5. Unit 4

With regard to depositional regime, Unit 4 is quite diverse and additionally contains four archeological find layers (CL1 – CL4, Figs. 4 and 5). CL1 and 2 are similarly composed of thin beds of greyish-brown loams, rich in humus (L-EVA 1712 and 1714). The individual beds are interfingered with equally thin strata of fine ferruginous sands and fragments of marls and chalk. The same interbeds are found *between* CL1 and CL2. All the archeological finds are restricted to the humic beds. We argue that these humic beds are semi-terrestrial half-bog soils at the edge of the floodplain, whereas the fine-sands represent dislocated glacio-fluvial deposits being washed down the slope of the ravine. Those original deposits from the Saalian glaciation occur in abundance in the plateau positions outside the river valley (Gavrilov et al., 2015). The ravine seems to act as a conveyor of these locally-sourced sediments into the valley, as these deposits are only subordinately found at other Khotylevo I sections further afield from ravine influence (for locations see Fig. 1). CL2 comprise three sublayers interbedded with and underlain by the same dislocated glacio-fluvial ferruginous sands. In CL3 (L-EVA 1716 and 1717) there is a distinct change to gleyic, subhorizontally layered fine sands (facies codes Sh to Sm after Miall (1978)). Furthermore, the top of CL3 (L-EVA 1716) is enriched in organic carbon und thus likely

represents another short-termed Fluvisol formation. CL4 (L-EVA 1718 & 1719) is influenced by fluvial and solifluction deposits, bearing slope-adjusted tabular flints with diameters of up to 40 cm. These presumably constitute the source of raw material for stone artefact production at the site. Again, the top of this layer (L-EVA 1718) is enriched in humic material from Fluvisol formation.

The sediments of Unit 4 described above, with alternating fluvial/alluvial and slope deposits, have not all been preserved in their primary stratification. Rather, they have been partially compromised by the intrusion of an extensive lobe of Cretaceous chalks and marls, displaced either shortly after sedimentation as debris flow or solifluction bed, or post-sedimentarily as an oversaturated injection. Neither interpretation is favored at the moment as both seem to be equally reasonable explanations for the encountered sediment characteristics of Unit 4. This lobe is associated with and has been moving down the tributary ravine. It thins out within the section thereby indicating that, at the time of formation, it already reached flood plain level and did not have sufficient relief energy left for further transport. At any rate, the lobe in question causes a considerable distortion of CL1 to CL3, whereas CL4 seems to remain rather unaffected (Fig. 5):

- (1) CL1 is reversely dipped at an angle of 45° directly above the bulk of the lobe, but rapidly levels out as the lobe is thinning out in the NE part. Additionally, it is mixed with the underlying and interfingering glaciofluvial sands and clast of chalk and marl.
- (2) CL2 and 3 feature small-scale thrust faults (Fig. 5) directly underneath the lobe, probably caused by differential settlement due to its mass. Furthermore, in the southern part of the section these layers have been cut and partially reworked by the Cretaceous sediments' displacement

Below CL4 there is a sharp erosional contact and a hiatus to the underlying Cenomanian glauconite sands, containing phosphorite nodules in large quantities.

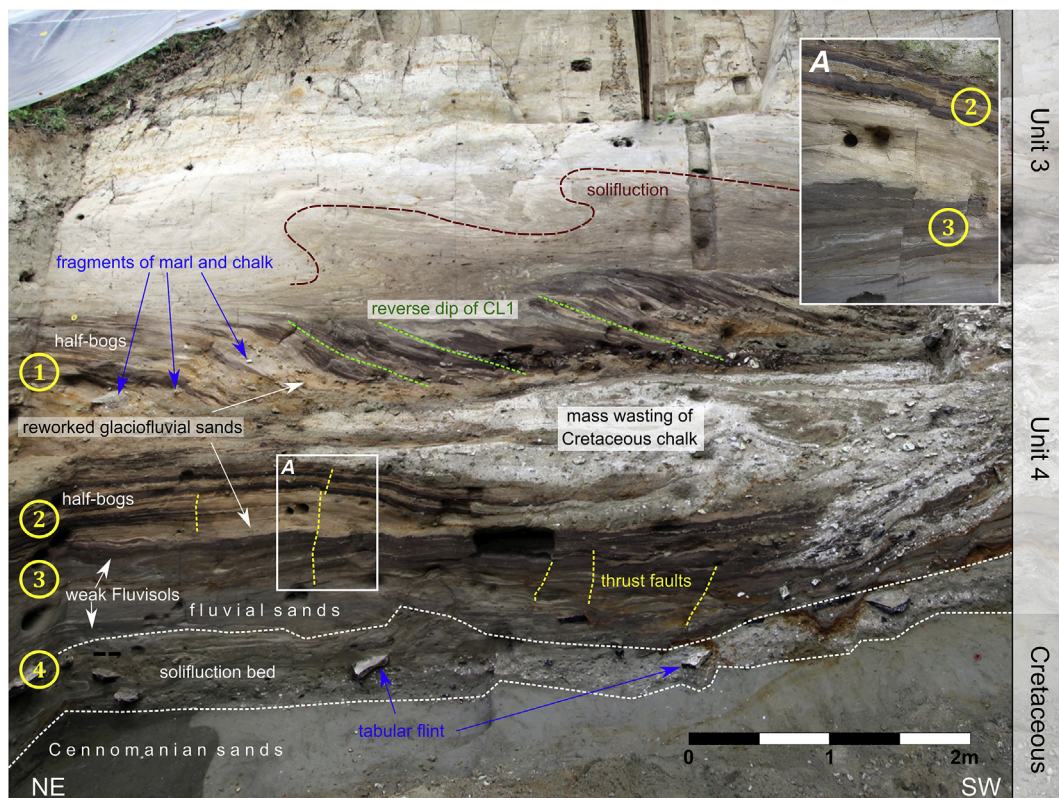


Fig. 5. Close-up view of the stratigraphy and noteworthy features of Unit 4. Details are given in section 4.1. Yellow numbering: Cultural Layers.

4.2. Luminescence dating

The obtained luminescence age-estimates of the exposed sedimentary units range from 21.1 ± 1.6 ka to 130.2 ± 11.1 ka (Table 4). Unit 4 is dated to between 77.6 ± 5.6 ka and 130.2 ± 11.1 ka, Unit 3 between 57.3 ± 4.4 ka and 69.0 ± 4.8 ka, Unit 2b is generally overestimated with an age range of 65.9 ± 6.4 ka to 76.1 ± 4.8 ka. Unit 2a yields an age of 54.1 ± 3.4 ka for the overbank deposit and the loess of Unit 1 is dated to 21.1 ± 1.6 ka. The non-fading corrected results of the feldspar pIRIR₂₉₀ dating are shown in Table 4 alongside the weighted-mean D_e-estimates. The listed one sigma standard errors do not include any systematic uncertainties, as those are not easily quantified and would have applied for all samples similarly, anyway. Using the weighted mean was deemed suitable because of the low scatter in D_e-distributions as revealed by the low overdispersion (OD) values (Table 4, Fig. 6). The reliability of these ages is discussed below in section 5.1.

5. Discussion

5.1. Luminescence ages and their robustness

5.1.1. De-distributions

Overdispersion (OD) is below 20% for most of the samples, especially in the fluvial and aeolian deposits of Unit 1 to 3 (Table 4). Furthermore, the mean OD value for the entire sample set is $19.7 \pm 0.7\%$, therefore insufficient bleaching is most likely not a serious issue (Duller, 2008). For three samples (L-EVA 1712, 1713 and 1718), OD-values are nearing or exceed 30%. Such high OD-values could result from incomplete bleaching before burial, mixing of grains after burial or small-scale differences in dose rates of same-aged grains (Jacobs and Roberts, 2007). For L-EVA 1712 and 1713 all three potential factors seem to play a role. (1) Representing reworked Saalian glaciofluvial sediments, the aliquots of L-EVA 1713 must be considered incompletely bleached as is also confirmed by the overestimated feldspar age. (2) Since CL1, where sample L-EVA 1712 was collected, is to some extent mixed with these glaciofluvial sands by the intrusion of Cretaceous sediments, the possible effect of partial bleaching on OD-values would have been imprinted upon L-EVA 1712, as well. Additionally, mixing of slope and fluvial deposits might have increased the OD. But the latter influences cannot, in fact, explain the OD spread in those two samples, as L-EVA 1715 has likewise been taken from reworked glaciofluvial sediments and much lower OD-values were obtained ($20.6 \pm 0.6\%$). For this reason, we argue (3) that small-scale differences in beta dose-rate are to be held accountable for the higher values in L-EVA 1712 and 1713 compared to 1715. The aforementioned intrusion of Cretaceous sediments into the reworked glaciofluvial sands led to

an admixture of little clasts of marls and chalk which are lacking in the otherwise similar reworked glaciofluvial sands around L-EVA 1715. The same seems to be true for L-EVA 1718, where the higher OD-values cannot easily be explained by insufficient bleaching or post-depositional mixing. Rather, here too, uncertainties in beta dose-rate might arise from the interspersed tabular flints within the sediment.

5.1.2. G-values

The g-values obtained using the pIRIR₂₉₀ signal (Fig. 3, Table 4) were generally low, apart from the samples L-EVA 1715 and 1717, whose values exceed 2%/decade. This can either be attributed to a laboratory artefact or different provenances for the respective feldspars, that may be more susceptible to fading, despite using a feldspar emission known to be characterized by a high signal stability (Buylaert et al., 2012). Fading in these two samples (L-EVA 1715 and 1717) is supported by exceptionally high g-values for the corresponding IR₅₀ measurements (Fig. 3). If these two samples are in fact prone to slight fading, their dates should be considered as minimum ages. For the overall chronological framework however, this is not a prominent issue. L-EVA 1715 stems from a proximal source, the poorly bleached reworked glaciofluvial sand, that is deemed overestimated (discussed below). And L-EVA 1717, deriving from a fluvial sand with a more distant source, is sufficiently supported by the two samples L-EVA 1718 and 1716 (immediately above and below) that show very consistent age estimates of 77.7 ± 6.4 and 77.6 ± 5.6 ka, respectively.

5.1.3. Age-depth model and reasons for age overestimations

Fig. 7 shows the pIRIR₂₉₀-ages plotted against the sampling depth. For context and orientation, a sketch of the stratigraphy is displayed and the Marine Isotope Stage-boundaries (MIS) alongside the NGRIP-record are appended. The ages are generally consistent with stratigraphic considerations. The cultural layers have fairly homogeneous ages between 77.6 ± 5.6 ka and 87.7 ± 9.0 ka. These ages fall within MIS 5a but cannot be distinguished temporally based on our chronology. For five samples an age inversion has occurred. Aforementioned processes, resulting in a high OD value might be responsible for the overestimation of sample L-EVA 1713, whereas in L-EVA 1715, and L-EVA 1704 to 1706 other factors must (additionally) be held accountable, chief among which is the uncertainty inherent in the determination of the water content. Overestimation of the burial water content would result in overestimated ages for samples L-EVA 1704 to 1706, and 1715 as well as possibly L-EVA 1713 (e.g. Nelson and Rittenour, 2015). However, this alone does not justify the entire chronological deviation as assuming a non-realistic water content of 0% still produces unsatisfactory results in terms of

Table 4

Summary of the k-feldspar pIRIR₂₉₀ dating results. The D_e-estimations are based on the weighted mean. OD: Overdispersion; No. al: Number of accepted aliquots for D_e-estimation; DR ratio: measured-to-given dose ratio from dose-recovery test.

Unit	Lab.-ID (L-EVA)	D _e (Gy), 1σ	Age (ka), 1σ	OD %	No. al	G-value (%/decade)	DR ratio pIRIR ₂₉₀ hb
1	1702	73.6 ± 3.3	21.1 ± 1.6	15.8 ± 0.7	16		
2a	1703	152.0 ± 5.2	54.1 ± 3.4	14.7 ± 0.5	21		
2b	1704	199.0 ± 6.3	65.9 ± 6.4	16.2 ± 0.5	26		
2b	1705	193.2 ± 5.4	76.1 ± 4.8	12.7 ± 0.4	24		
2b	1706	161.5 ± 5.9	68.8 ± 4.8	15.4 ± 0.5	24	0.9 ± 0.1	1.06 ± 0.07
3	1707	162.7 ± 8.8	57.3 ± 4.4	20.4 ± 0.8	19	1.1 ± 0.0	0.94 ± 0.02
3	1708	187.9 ± 5.6	57.4 ± 3.4	15.8 ± 0.5	23		
3	1709	179.9 ± 5.8	58.8 ± 3.5	14.8 ± 0.5	24		
3	1710	171.5 ± 6.6	64.3 ± 4.6	21.1 ± 0.7	22	1.3 ± 0.1	0.83 ± 0.02
3	1711	176.8 ± 6.2	69.0 ± 4.8	15.8 ± 0.5	24		
4 – CL1	1712	175.0 ± 10.7	85.4 ± 7.9	33.9 ± 1.2	20		
4	1713	254.9 ± 18.0	117.0 ± 11.3	27.9 ± 0.8	24		
4 – CL2	1714	180.1 ± 9.9	81.7 ± 7.1	21.7 ± 0.7	22		
4	1715	279.6 ± 13.9	130.2 ± 11.1	20.6 ± 0.6	24	2.6 ± 0.2	1.01 ± 0.00
4 – CL3	1716	183.6 ± 7.1	77.6 ± 5.6	17.4 ± 0.6	22		
4	1717	157.8 ± 9.8	87.7 ± 9.0	18.8 ± 0.6	23	2.2 ± 0.2	1.00 ± 0.01
4 – CL4	1718	165.2 ± 7.8	77.7 ± 6.4	29.7 ± 0.5	41	1.3 ± 0.0	1.03 ± 0.01
4 – CL4	1719	176.2 ± 9.6	84.8 ± 7.5	22.7 ± 0.7	24		

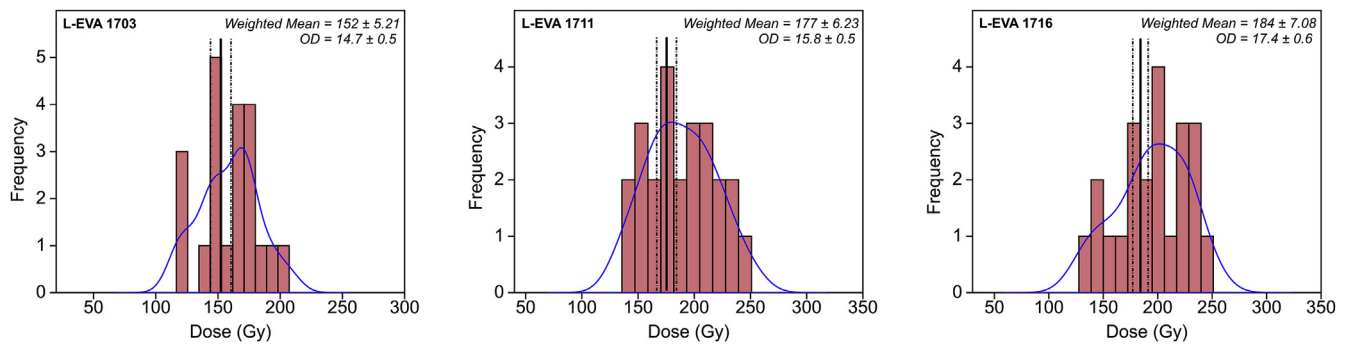


Fig. 6. De-distributions for three representative samples (black lines: weighted mean De-values with their 1σ standard error used for age calculation). Distributions for all samples can be found in the supplementary information.

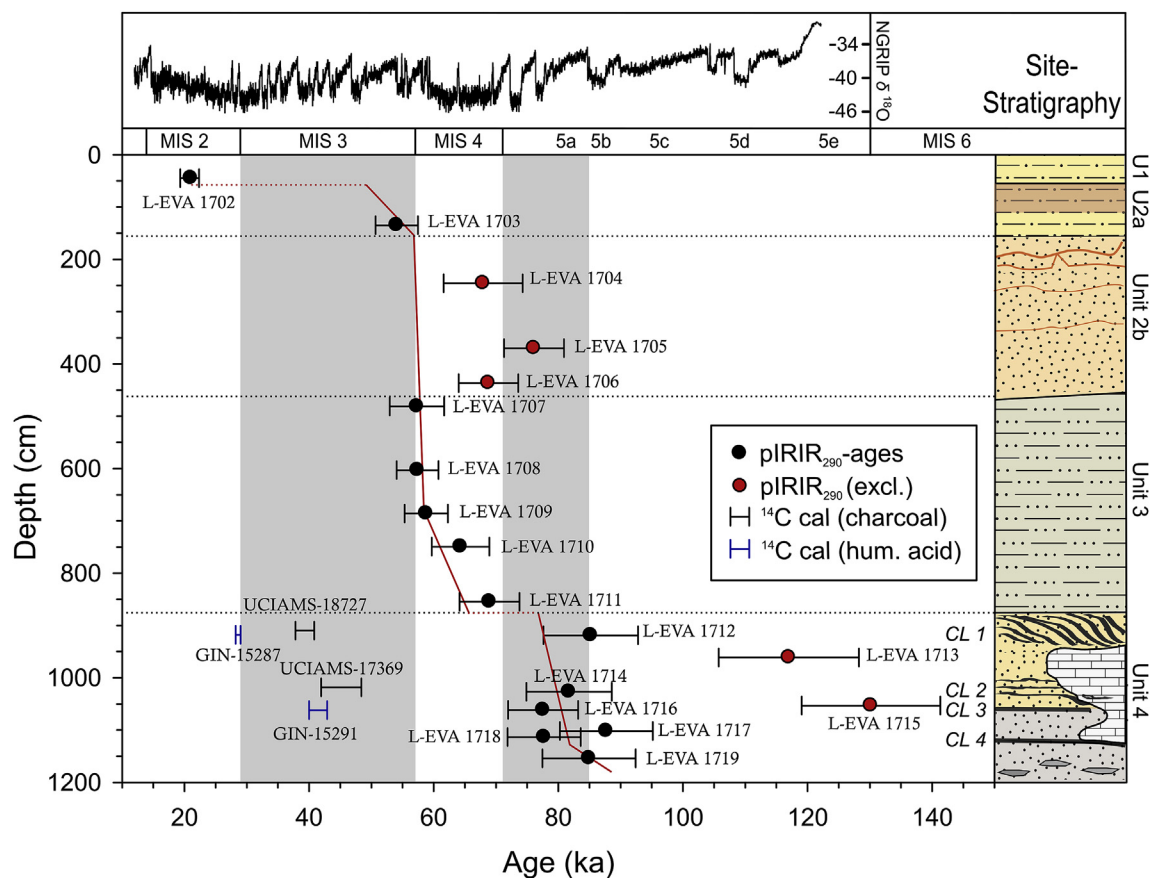


Fig. 7. Age-depth plot of all measured luminescence samples, including the former ¹⁴C chronology. The NGRIP-data has been taken from North Greenland Ice Core Project members (2004), the Marine Isotope boundaries from Lisiecki and Raymo (2005). CL1 to CL4: Cultural Layers.

alignment with the rest of the sequence. Hence, we conclude that a combination of overestimated water content and poor bleaching, which is not noticeably accounted for in the OD values, is the reason for the obtained age inversions (cf. Buylaert et al., 2009). Partial bleaching in turn could have been caused by such factors as reworking of much older material, transport distance and the mode of sediment transport. For samples L-EVA 1713 and 1715, slope sediments reworked from Saalian fluvioglacial deposits on the adjacent plateau, short transport distance conceivably hampered solar resetting. The older the original depositional ages before reworking, the more likely the luminescence signal is only partially reset during re-sedimentation. Samples L-EVA 1704 to 1706 were collected from a fluvial sediment that possibly derived from a more distal source. Mesozoic sandstones as well as (fluvio-)glacial deposits surely contributed to the sediment load. Thus sediment origin (and

inconsistent former ages and bleaching) might have played a role as well as the transportation and sedimentation process itself. It has been shown, for instance, that turbid water flow reduces the intensity of light and can lead to less complete bleaching, despite considerable transport distances (Rittenour, 2008; Wallinga, 2002). This scenario of a high-energy flow regime was previously discussed (section 4.1) for the formation of this respective sediment facies.

Excluding these five overestimated samples, a regression line was drawn in Fig. 7 through all 13 accepted ages, taking sedimentary properties into consideration and representing our most coherent proposal regarding the chronological succession of sediment delivery. The significance of this age regression for landscape-forming processes and archeological theory building is discussed in section 5.2.

5.1.4. Comparison with the previous ^{14}C chronology

In previous studies, a chronological framework for the cultural horizons of Khotylevo I-6-2 was reported based on radiocarbon dating of ABA (Acid Base Acid)-pretreated charcoals and humic acids (Otcherednoi et al., 2014b; Otcherednoi and Voskresenskaya, 2019; Vishnyatsky et al., 2015). These dates, calibrated by Weiss (2019) using OxCal 4.2 and the IntCal 13 calibration curve (Reimer et al., 2013) are presented in Figs. 4 and 7. They range from ~27 ka to 50 ka (cal BP), coinciding with MIS 3. Radiocarbon dating of Pleistocene samples is challenging in general, as low levels of modern carbon can lead to serious and systematic age underestimations towards the limit of the method. The impact of these contaminations increases with sample age (Wood, 2015). To account for that in charcoal dating, the Acid Base Oxidation/Stepped Combustion (ABOX-SC) pretreatment was introduced, which disposes of contaminants not removed by the conventional ABA pretreatment (Bird et al., 1999). Consequently, it was suggested that ABA-pretreated charcoal-samples older than 30 ka should be considered with extreme caution (cf. Briant and Bateman, 2009; Pigati et al., 2007).

With regards the humic acids, it has been shown repeatedly, that dating these compounds in buried soils and sediments may result in significant age underestimations and even random inconsistencies, because this method is particularly susceptible to contaminations (Martin and Johnson, 1995; Orlova, L.A.; Panychev, 1993; Wang et al., 1996).

Addressing the discrepancy between the ^{14}C and luminescence chronology at our section, we strongly advocate the latter to find the chronological position of the *Keilmessergruppen* in Khotylevo: Firstly, because of the mentioned methodological aspects of possible radiocarbon rejuvenation in the Weichselian Pleniglacial and early glacial and secondly for the higher number of luminescence samples spread over the whole sequence and being in accordance with stratigraphic considerations (cf. section 5.2). However, with their higher potential precision compared to luminescence dating, further application of conventional ^{14}C methods in different parts of the Khotylevo I complex is still valuable to obtain a chronology from organic remains in the upper part of the sediment suite, that is, primarily for correlation of different sections (Zaretskaya and Otcherednoi, 2019).

5.2. Implications for landscape formation and paleoenvironmental conditions

5.2.1. Timing of geomorphic processes on site

We begin by presenting the succession of geomorphic processes in

chronological order, which can be regarded as a short model on the formation of the 2nd fluvial terrace, as both a stratigraphic and a morphological entity. The mainly geomorphological information about the Weichselian terrace staircase on the East European plain has not been revised for several decades (cf. Matoshko, 2004). Despite encouraging progress brought about by recent efforts of Panin et al. (2017), there is still much uncertainty as to the timing of local geo-climatic events and their relation to global climatic variability. Our results suggest a full incision/aggradation cycle being preserved at the Khotylevo I-6-2 exposure (Fig. 8).

Unit 4: At the bottom of Unit 4 there is a long hiatus between the Weichselian sediments and the bedrock of the Cretaceous sand. The widespread MIS 5e or 5c soils and in fact any older quaternary sediments are missing. Stratigraphic evidence from the various other sections of Khotylevo I along the raised bank of the 2nd fluvial terrace (see Fig. 1 for positions), suggests that the absence of these MIS 5e and MIS 5c soils is of wider application and not just a local feature. This, in turn, requires a fluvial incision phase in the Early Weichselian, after the optimum of MIS 5c. As sediment suites of fluvial terraces are believed to correspond largely to climatic oscillations, and river incision and aggradation usually occurs at climatic transitions (Vandenberghe, 2015, 2008), we assert that this particular incision phase occurred at the 5c/5b transition. It is quite remarkable that what is expected to be a relatively minor climatic shift, seemingly induced a deeper fluvial downcutting than previous major shifts (MIS 5e/5d or MIS 6/5e) – at least in the margins of this part of the valley. A complete eradication of all pre-MIS 5b/5c sediments to bedrock level throughout the entire valley is however not to be expected, not least because of existing reports about an Eemian base of the 2nd fluvial terrace in other valleys on the Russian Plain, listed in Panin et al. (2017). Thus, for the prevailing scarcity of numerical dates, further research in the Desna river catchment is needed to corroborate our finding.

The lowermost luminescence sample in Unit 4, L-EVA 1719, yields a pIRIR₂₉₀ age that falls directly into the MIS 5a/5b boundary in the age-regression (Fig. 7). Given the dating uncertainties, the sediment could have been deposited in either of these two intervals. Since it represents a solifluction layer, permafrost has arguably played a role in its development, although not necessarily. However, the thickness (ca. 30–60 cm), combined with the sandy matrix of the deposit, implies an equal or higher freeze-thaw depth for its formation, and conditions of deep seasonal frost to warm permafrost, comparable to current subpolar mountains or mid-latitude high mountains above the tree line (Matsuoka, 2001). It is less likely that the climate and thin vegetation cover

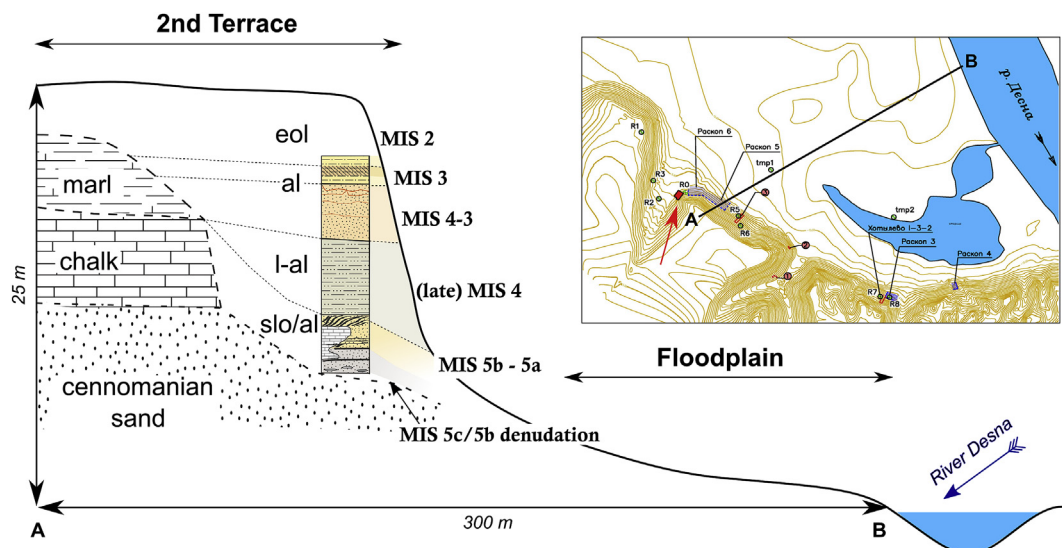


Fig. 8. Virtual cross-section of the 2nd fluvial terrace at Khotylevo I-6-2. The position of the site is shown on the topographic map by the red arrow. Orientation of the cross-section is shown on the map by line segment A-B. slo: slope/colluvial facies; l-al: fluvio-lacustrine; al: channel/overbank alluvium; eol: loess-like sediments.

requirements were met in early to mid-MIS 5a, thus we propose, solifluction occurred in MIS 5b for which matching conditions are assumed (see section 5.2.2 below). Following the age-regression line in Fig. 7, the rest of Unit 4, comprising the beginning of fluvial aggradation alternating with slope deposition and paleosols (=cultural layers), falls comfortably within MIS 5a. This complements the presence of the half-bogs and Fluvisols requiring a rather temperate climate for their formation. Based on luminescence dating however, it is not possible to distinguish the different paleosols, and hence the cultural layers, chronologically. Our interpretation of the interfingering sands of CL1 and CL2 to be local-sourced, reworked glaciofluvial sands from the Saalian glaciation is in compliance with the large age overestimations for the samples L-EVA 1713 and 1715 (117.0 ± 11.3 and 130.2 ± 11.1 ka). As indicated by the chalk-supported displaced mass in Unit 4 and solifluction structures in the lower Unit 3, slope deposition may have continued until mid-MIS 4.

Units 3 and 2: These units are considered jointly, because other than the temporal setting provided by the age regression, we do not have credible numerical dates for Unit 2b. The main fluvial aggradation phase commenced in late MIS 4 and, with a possible hiatus, resumed in the MIS 4/MIS 3 transition phase or earliest MIS 3. It started out with a low-energy and likely fluvio-lacustrine deposition in Unit 3, before the discharge changed to a high-energy flow regime for Unit 2b, reducing light-intensity during its deposition and thus *inter alia* being responsible for age overestimations. Apart from L-EVA 1710 and 1711, that are

gradually older, the larger portion of Units 3 and 2b seem to have been deposited near the MIS 4-MIS 3 transition. Alternatively, considering the desiccation/frost cracks at the boundary between these units, possibly indicating a hiatus of unknown duration, Unit 2b could have formed entirely in early MIS 3. Regardless, the sedimentation rate corresponding with the slope of the regression was potentially high during this transitional period. High vertical accretion rates of the regional rivers of that time have been highlighted by Panin et al. (2017) as well. Unit 2a in turn ties in very well with the ages of Unit 3. It is evident that in the first half of MIS 3 the deposition changed from channel alluvium to overbank fines with a likely hiatus in between, as indicated by the sharp lower boundary of Unit 2a. The potential reasons for that changeover are manifold and cannot be discussed based on our data. After deposition ceased, the overbank deposits remained a stable surface for an unknown time, enabling pedogenesis (Fluvisol formation) and likely spanning several temperature inflections within MIS 3. The timing of the follow-up incision, shaping the now observable landform of the terrace, is not accounted for in our data set, but is expected to have occurred between 45 and 35 ka (Panin et al., 2017; and discussion below).

Unit 1: Ensuing this hiatal phase, directly overlying the Fluvisol is the weathered loess with a typical LGM age of ~21 ka at the height of MIS 2 (L-EVA 1702). This loess was later subjected to decalcification and pedogenesis.

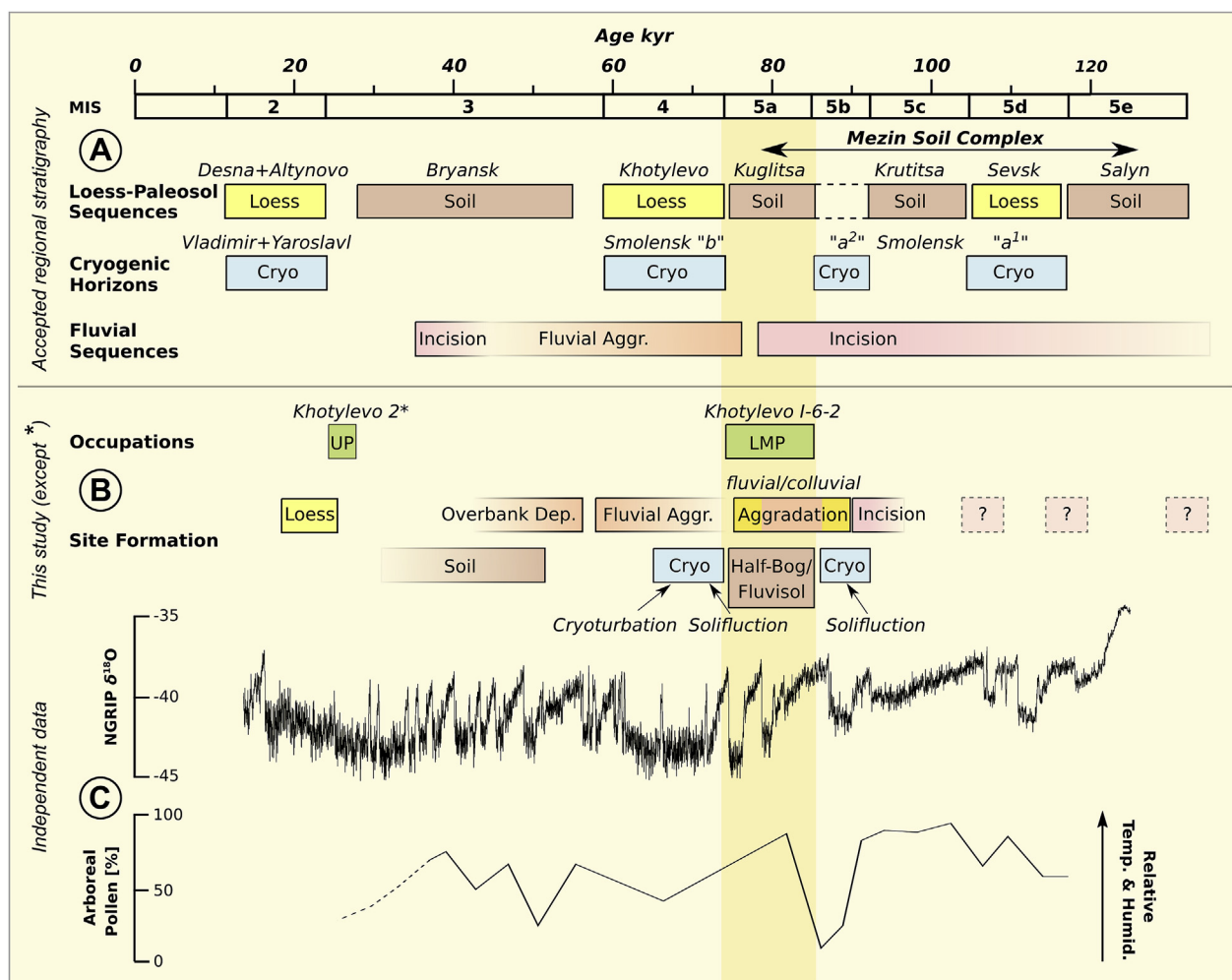


Fig. 9. (A) Accepted chronostratigraphy of the region compiled from Velichko (1990), Velichko et al. (2006, 2011, 2017) and Panin et al. (2017, 2018) compared with (B) findings of this study. Chronology for the occupation at Khotylevo 2 taken from Gavrilov et al. (2015)*. (C) NGRIP-data from North Greenland Ice Core Project members (2004), and Arboreal Pollen taken from Yelovicheva and Sanko (1999).

5.2.2. Comparison with existing chronostratigraphies and palaeoenvironmental records

In Fig. 9, we compare our chronostratigraphic findings with independent paleoclimatic data and the presently accepted stratigraphy within the observed timespan. The figure does not intend to provide detailed correlations but allows for the exploration of general patterns regarding site formation, landscape processes, occupation and climate evolution of the Late Pleistocene. Also, it does not take into account the various diachronic offsets between terrestrial sedimentation and the MIS (e.g. Kukla et al., 2002). Fig. 9A aims to give insight on the relation of fluvial archives to much better-known Loess-Paleosol-Cryogenic formations (LPC) on the Russian Plain. Significantly, the study area is the type region for several of the stratigraphic units of the LPC (Khotylevo Loess, Bryansk Soil, Desna Loess). The concept of the LPC and their relations across the Russian Plain is exceptionally well-established and incorporates regional differences (Panin et al., 2018; Velichko, 1990; Velichko et al., 2017, 2011, 2006). Considering numerical ages however, information for the time outside the radiocarbon range remains very scarce. To our knowledge, the only reliable luminescence-based geochronology has been presented by Little et al. (2002), where the period from the Eemian to the Last Glacial Maximum (LGM) is characterized by six OSL-dates. Beyond that, Gozhik et al. (2014) report a comparison of four different TL and OSL laboratories for the dating of the Maksymivka loess section in the Dniepr Lowland, based on about 20 samples each. However, the different results show very high discrepancies, rendering the overall chronology rather inconclusive. Particularly the quartz grains used for OSL-dating seem to be in saturation early on, leading to profound age underestimations. It is for this general paucity of available data that the alignment of the LPC with the hemispherical climate proxies is in fact not incorrect, but still a broad-brush rendition. This is aggravated by the fact that MIS 5a soils (Kuglitsa) have seldom been recognized in the East European Plain (Velichko et al., 2006), and so have mostly not been considered in correlation with, for example, the MIS or central European pollen zones. Sometimes a previous interstadial (Krutitsa) has been assigned to MIS 5a rather than 5c (Little et al., 2002), with contradictory statements regarding the occurrence and correlation of Kuglitsa found in the same publication (Velichko et al., 2011), adding more vagueness to the discussion.

A similar situation exists regarding the fluvial suite of the 2nd terrace. While it has been identified and elaborately described in several river systems on the East European Plain, 16–25 m above the current streams (e.g. Matoshko, 2004, with a compilation of the mostly Russian-language literature in Panin et al., 2017), until now there was only one luminescence chronology in existence (Panin et al., 2017). Conveniently, this study was conducted at the Seim River, a nearby tributary to the river Desna. It comprises three dates that delimit the formation of the 2nd terrace (included in Fig. 9). They suggest, aggradation started before 77 ka, requiring an earlier incision. Meanwhile, subsequent incision which led to the morphological landform of the 2nd terrace must have taken place between 35 and 45 ka. This is roughly in accordance with the age assumptions found in previous studies that are solely “based on climatic stratigraphy and geomorphological correlation” (ibid.), where a formation time between MIS 5d and MIS 4 is stated.

In Fig. 9B, the chronostratigraphical data acquired in our study has been compiled. Therein we argue that the fluvial incision, preceding the 2nd terrace-formation occurred probably at the MIS 5c/5b transition. While there might have been earlier incision events between this time and late MIS 6, we cannot account for these. Aggradation gathered pace in the MIS 4 and earliest MIS 3, concluded by an overbank deposit and a Fluvisol, that we suspect formed the surface for a considerable period of time. Both of these findings roughly agree with former considerations, but having a higher number of luminescence samples at our disposal, we are able to locate those events more precisely within the temporal framework.

When compared to the LPC, our data reveals striking similarities, as well. A cryogenic horizon in the form of a solifluction bed (L-EVA 1719)

is followed by various short-termed soil formations (Fluvisols and half-bogs), coinciding with the cultural layers (cf. NGRIP and arboreal pollen in Fig. 9C). The solifluction bed likely represents Smolensk a² cryogenic phase and the soils cover for the Kuglitsa phase. As mentioned, the latter is very sparsely documented in the literature, but when (at least implicitly) recognized, the paleosols are usually developed as a gleyic stratum (Velichko, 1988). The pedogenic features in Unit 4 of Khotylevo I-6-2 seem to be the semi-terrestrial, yet contemporaneous equivalents of these gleys found in loess sequences. Smolensk b cryogenic phase is asserted in our data through the solifluction and cryoturbation phenomena in lower Unit 3. The sediments of the fluvio-lacustrine Unit 3 consist largely of re-deposited loessic silts, implying that later MIS 4 was the main delivery phase for the Khotylevo loess. After all, availability of loess covers in the catchment area is imperative for its re-sedimentation. Bearing in mind the vastly impaired coupling of sediment erosion in catchments and sediment delivery in floodplains (Fryirs, 2013; first suggested by Walling, 1983), our dates for this fluvially reworked loess (MIS 4/MIS 3 transition phase) do not directly elucidate the time of primary loess deposition. Rather there is likely a temporal offset between these two respective processes. Even so, loess admixture into the fluvial suite stopped abruptly for Unit 2b. Whether this is a function of decreased loess-erodibility due to the binding effect of re-establishing vegetation after the glacial maximum, or due to a changing architecture within the fluvial system, remains a subject of future research. The Fluvisol capping the overbank fines of Unit 2a is related to the Bryansk soil in MIS 3. Indications, that MIS 3 accommodates a two-phased paleosol formation (including the ortsands in upper Unit 2b) at the Khotylevo I site will be investigated at a later time. The loess on top of the sequence (L-EVA 1702) falls within the LGM in MIS 2 and is attributed to the Desna loess phase of the western Russian stratigraphy.

5.3. Archeological implications

5.3.1. Synthesis of environmental and climatic conditions during the occupational period

It has been observed repeatedly that higher places alongside the yearly submerged floodplain, especially riverbanks and terraces, were particularly attractive to Paleolithic foragers (Vandenbergh, 2015; Velichko et al., 2009). In accordance, the occupation at Khotylevo I-6-2 has been located directly at the margin of the floodplain, with supposedly a precursor of the recent ravine granting a smooth approach from the higher banks. The solifluction bed, formed shortly before occupation set in, provides an easily-exploitable large-sized and high-quality raw material source for on-site stone tool production, supporting the workshop character of the site. At the onset of Middle Paleolithic land use, periodic to episodic shallow flooding events were likely to happen, as revealed by the fluvial sediments and weak Fluvisols in CL3 and 4. During CL2 and CL1 these events became much more sporadic. However, the half-bogs in the upper part of the archeological sequence attest to a continuously high groundwater table. Even though the paleosols indicate a phase of geomorphic stability controlled by a dense vegetation, the interfingering glaciofluvial sands, coming down the slope of the ravine point to interruptive spells within the MIS 5a, evoked by a sparser plant cover (e.g. Ballantyne, 2018). Since these spells might have been caused by climatically induced patchiness in the vegetation, it is worth considering the respective paleoclimatic proxies for that time. In the NGRIP-record, for the harsh millennial-scale oscillations within MIS 5a, such less densely vegetated spells appear plausible (Fig. 9 C), even though MIS 5a is set apart from the neighboring phases by a generally milder climate (cf. Velichko et al., 2011). A similar observation has been reported by Antoine et al. (2016) for the loess area of Northern France, where the MIS 5a paleosols indicate a pronounced alternation between phases of stabilization (pedogenesis, corresponding with Greenland Interstadials 19–21) and accelerated colluviation in between. According to the closest pollen archives for Khotylevo I in eastern Belarus, vegetation was characterized by a dense *Betula* and *Pinus* forest with the admixture of *Alnus*,

Salix and even some temperate taxa like *Quercus*, *Tilia*, *Fagus* and *Corylus* at the height of the interstadial (Yelovicheva and Sanko, 1999). Herbs and grasses were reduced to about 10%. This reveals mild, yet relatively strong continental conditions, including low precipitation values, warm growing seasons and low winter temperatures with thin snow cover (Helmens, 2013; Yelovicheva and Sanko, 1999). Although these data suggest a rather dense and therefore erosion-inhibiting plant cover in MIS 5a, we cannot exclude that drier and colder spells might have rendered the vegetation more open, making the system more prone to erosion.

A similar effect regarding erodability would have been achieved if the slope (or in fact a precursor of the ravine) was subjected to trampling by ungulates or other forms of game, accessing the valley bottom for drinking water. This would have caused compaction of the sediments and scarring of the vegetation, both triggering linear erosion. While the impact of grazing on denudation and subsequent erosion is fairly well studied, the contribution of trampling especially executed by wild ungulate herds is still only rather vaguely understood, but thought to be consequential (Heggenes et al., 2018; Moen and Danell, 2003). Previous field campaigns at Khotylevo I uncovered a reasonable number of big mammal bones, among them (odd-toed) ungulates such as horse (*Equus latipes Gromova*), bison (*Bison priscus Boj.*), red deer (*Cervulus elaphus*) and reindeer (*Rangifer tarandus L.*) (Chubur, 2013). Neither the archaeological layers nor the artefacts themselves show clear traces of animal trampling, in the form of distortions or mechanical damages. Although we are unable to definitively substantiate an animal contribution to sediment erosion in MIS 5a at Khotylevo I-6-2, we suggest this phenomenon should be given more attention in future archaeological research. Geomorphic positions, preferred as migration routes of big game might have influenced the Neanderthal choice of encampment location.

5.3.2. The age of Khotylevo I-6-2 and its influence on the chronology and population dynamics of the late Middle Paleolithic

Following the chronological and typological classification of the Keilmessergruppen proposed by Jöris (2004), the presence of prepared core blank production methods together with bifacial backed knives with convex cutting edges places the assemblages from Khotylevo I-6-2 into Keilmessergruppen Type A (KMG-A). Jöris (2004) attributes assemblages of this group chronologically to MIS 5a/early MIS 4 and geographically to the northern European lowlands. However, his chronological attribution is only tentative, as the MIS 5a/early MIS 4 ages are constructed based on stratigraphic interpretations of mainly Königsau (Mania, 2002; Mania and Toepfer, 1973), and Salzitter-Lebenstedt, Lower Saxony/Germany (Pastoors, 2009, 2001; Tode, 1982). Jöris' (2004) interpretation is in contrast to the radiocarbon ages of these sites (Hedges et al., 1998; Pastoors, 2009, 2001; Picin, 2016), which date the Neanderthal occupations to MIS 3. However, uncertainties regarding their radiocarbon dating at the limit of the ^{14}C time scale, together with the stratigraphic observations allow chronometric ages between MIS 5a and MIS 3 for these sites and the onset of the late Middle Paleolithic Keilmessergruppen. Following the initial KMG-A, KMG-B to KMG-C assemblages with differing technological assemblage characteristics are placed by Jöris between early MIS 4 and MIS 3. In general, his (Jöris, 2012, 2004) model establishes a "long chronology" for the Keilmessergruppen, with a duration from MIS 5a to MIS 3. This is in contrast to Richter (Richter, 2016, 2002), whose model of a "short chronology" places these late Middle Paleolithic groups exclusively into MIS 3. Richter's interpretation is based on the fact that in his view no Keilmessergruppen or MMO assemblage is securely dated older than MIS 3 (Richter, 2016).

With the age of the late Middle Paleolithic human occupation in Khotylevo I-6-2 we now have secure evidence for the presence of the Keilmessergruppen-makers during MIS 5a on the European Plain. Khotylevo I-6-2 adds an important data point to the growing body of radiometrically dated late Middle Paleolithic Keilmessergruppen/MMO/Micoquian sites on the European Plain from western Russia to northern Germany. The new luminescence ages support the model of a "long

chronology" from MIS 5a to MIS 3 sensu Jöris (2004) for this archaeostratigraphic unit. In other words, with the data from Khotylevo I-6-2 we can finally prove the duration of the Keilmessergruppen from MIS 5a to early MIS 3. Together with recently directly dated open-air assemblages, we see late Neanderthal presence on the northern central and eastern European Plain during the following marine isotope stages:

- 1) MIS 5a: Khotylevo I-6-2, Neumark-Nord 2/0, Saxony-Anhalt/Germany (Laurat and Brühl, 2006; Richter and Krbetschek, 2014; Strahl et al., 2010), Wrocław-Hallera Av. Lower Layer (Skrzypek et al., 2011; Wiśniewski et al., 2013)
- 2) MIS 4/3: Pietraszyn 49a, southwestern Poland (Wiśniewski et al., 2019), Lichtenberg, Lower Saxony/Germany (Veil et al., 1994)
- 3) MIS 3: Wrocław-Hallera Av. Upper Layer (Skrzypek et al., 2011; Wiśniewski et al., 2013), Pouch (Weiss, 2015; Weiss et al., 2018)

With the new data from Khotylevo I-6-2 together with the age of the additional sites mentioned here, we can draw some inferences about late Neanderthal population dynamics on the European Plain. Khotylevo I-6-2 is a striking example of Neanderthals pushing back the northern limit of their habitat up to 53.5° under continental climate conditions during MIS 5a. Interestingly, there is little evidence of doing so even from the more temperate northwestern European climate of the previous Eemian interglacial or the contemporaneous Early Weichselian (Nielsen et al., 2015). Khotylevo I-6-2, together with the other MIS 5a sites from the European Plain also mark a technological change in the Neanderthal material culture. They started to produce bifacial tools more frequently, and the assemblages show an increasing application of prepared core blank production methods. Thus, starting during MIS 5a, late Neanderthal sites are characterized by a technocomplex called the Micoquian of central and eastern Europe or Keilmessergruppen. This is substantially different from the small-tool, rather opportunistic and flake-based tool assemblages of the previous Eemian interglacial (Litt and Weber, 1988; Pop, 2014; Thieme and Veil, 1985; Weber, 1990). In other words, the MIS 5a assemblages document a change in knapping techniques and tool concepts that persisted on the European Plain until the end of the Middle Paleolithic around 40 ka, the disappearance of Neanderthals.

But the fact that Keilmessergruppen-makers or the idea of a certain knife technology "survived" the cold stadial of MIS 4 (71 ka–57 ka, Lisiecki and Raymo, 2005) on the northern European Plain, sheds new light on late Neanderthal migration patterns and existing hypotheses. The current data implies a void of Neanderthals at the northern part of the European Plain (Bobak et al., 2013), roughly above 50° N during most of the cold stadial MIS 4. Also, as of yet, the Khotylevo I-6-2 sequence yielded no late Middle Paleolithic occupation layer younger than MIS 5a. The MIS 4 cold stadial is interpreted as a bottleneck for Neanderthal populations and local extinctions (Hublin and Roebroeks, 2009; Roebroeks et al., 2011) as well as southward population movements (Jöris, 2004) are discussed. However, the presence of Neanderthals during MIS 4 cannot be excluded, yet. For example, the age of Salzitter-Lebenstedt is considered to be early MIS 4 based on stratigraphic observations (Jöris, 2004; Pastoors, 2009, 2001). Furthermore, the error ranges of the luminescence ages of some sites, like Wrocław-Hallera Av. (Bobak et al., 2013; Skrzypek et al., 2011; Wiśniewski et al., 2013) or Lichtenberg (Veil et al., 1994) also make human occupation in early and/or late MIS 4 possible. However, the absence of stone artefacts from MIS 4 in northern latitude sites like e.g., Khotylevo I-6-2 in the east or Neumark-Nord 2/0 in the west, but the presence of inventories with bifacial tools further southwest, are in favor of the movement-to-refuge-areas hypothesis. Examples are the occurrences of such assemblages during MIS 4/3 in northern France around 50° N (Locht et al., 2016b). which we interpret as possible evidence for the southward movement of Neanderthal populations from northwestern Europe. For eastern Europe, a population continuity throughout MIS 4 is suggested based on stratigraphic assumptions for regions south of the Russian Plain, specifically the Crimean Peninsula and (Trans-) Caucasia

(Velichko, 1988), but has yet to be confirmed by modern dating techniques.

Another argument for Neanderthal groups moving in and out the northern latitudes of the European Plain between MIS 5a and 3 are diachronic assemblage characteristics: contradicting some of Jöris' observations, KMG-A Keilmesser with convex cutting edges exist as well in some assemblages younger than MIS 5a, like in Pietraszyn 49 a (Wiśniewski et al., 2019), Lichtenberg (Veil et al., 1994), and Pouch (Weiss, 2015). Additionally, the latter assemblage shows that the occurrence of these Keilmesser types can be combined, like in KMG-A, with the application of Levallois and prepared core blank production methods. In other words, the MIS 3 site of Pouch shows assemblage characteristics that share similarities with MIS 5a assemblages like Khotylevo I-6-2 and, potentially, Königsau (Weiss et al., 2017). In contrast, the MIS 3 Keilmessergruppen assemblage of Wrocław-Hallera Av. Upper Layer, with more simple blank production methods, and variable bifacial tools has assemblage characteristics different from Khotylevo I-6-2 or Pouch. The presence of the latter together with KMG-A assemblages on the European Plain during MIS 3 points to a more complex picture of Neanderthal population movements between MIS 5a and MIS 3 – where southwards movements but also local extinctions and re-population of some areas seemed to interfinger with each other.

6. Conclusion

In this study we have placed particular emphasis on the intersection of natural sediment stratigraphy and the archeological find layers at Khotylevo, area I-6-2. To that end we presented a thorough sedimentological log alongside grain-size analyses and pIRIR₂₉₀ luminescence dating. The implications of the results we generated are two-fold as they yield information on both, (1) the region's fluvial and landscape evolution from the Early to the Mid-Weichselian and (2) the timing of Middle Paleolithic occupation on site.

- (1) For the high resolution of our sampling scheme we are able to report the best-dated sequence of the widely occurring 2nd river terrace, thereby adding to the understanding of the Late Pleistocene geo-climatic events on the Russian Plain. One full incision/aggradation cycle was detected, with the incision most likely taking place at the MIS 5c/5b boundary and the main aggradation phase happening in the MIS 4/MIS 3 transitional phase. When compared with the stratigraphy of loess-paleosol-cryogenic phases our chronology shows a predominant compliance. That concerns the main phases of soil formation (within the scope of our sequence) in MIS 5a and MIS 3 as well as the periods of loess deposition in MIS 2 and 4. While we can directly confirm the MIS 2 loess (Desna loess) by dating it to ~21 ka, the MIS 4 loess is represented only indirectly as redeposited silt fraction within the late MIS 4 fluvial aggradation sediments. The potential temporal offset between primary loess formation in the area and alluvial re-sedimentation in Unit 3 remains subject to later fluvio-geomorphological investigations. Future studies at the Khotylevo I sites will also address the sparse numerical information on paleoclimate and paleoenvironment in the region. Those will include a more extensive consideration of cryogenic features and paleosols using geochemical, biochemical, biological and magnetic proxies to produce more precise reconstructions of the diachronic local conditions, relevant to both archeology and geosciences.
- (2) In this paper we present the first unambiguous luminescence-based chronostratigraphy for a Late Middle Paleolithic open-air site on the Russian plain. By confidently ascribing the occupation to the rather temperate, but continental interstadial MIS 5a we gain a valuable data point for future reconstructions of Neanderthal population dynamics. Even keeping in mind the fragmented character of both preserved sites and the former land

use system(s), it is already safe to say that Neanderthals settled not only the southern mountainous areas of the East European Plain. They also penetrated the more northern lowland regions along the river valleys up to at least 53.5° N. Whether that was restricted solely to warmer periods needs further analysis. Furthermore, our sediment descriptions allow for inferences about the paleo-conditions on site (e.g. a solifluction bed being a likely raw material source, and the decreasing flooding risk of this river-side locality) during the time of (repeated) occupation in MIS 5a (section 5.3.1). Additionally, we compare our stratigraphically well-secured chronology to other numerically dated Late Middle Paleolithic assemblages across the northern central European Plain. We provide evidence for an early onset and long-term continuity, but also for complex population dynamics of the *Keilmessergruppen* or Micoquian on the European Plain, stretching from MIS 5a to MIS 3.

Declaration of competing interest

The authors declare that they have no known competing financial interests or personal relationships that could have appeared to influence the work reported in this paper.

Acknowledgements

We are grateful to Steffi Hesse, Katharina Schilling and Victoria Krippner (Max Planck Institute for Evolutionary Anthropology, Leipzig) for luminescence sample preparations and to Sonja Riemenschneider (Leibnitz Institute for Applied Geophysics, Hannover) for conducting grain size analyses. The remarks of two anonymous reviewers, as well as proofreading by Debra Colarossi substantially helped improve the manuscript. MH thanks his supervisors Jean-Jacques Hublin and Tobias Lauer. The research was funded by the Max Planck Society.

Appendix A. Supplementary data

Supplementary data to this article can be found online at <https://doi.org/10.1016/j.qsa.2020.100008>.

References

- Aitken, M.J., 1998. *An Introduction to Optical Dating: the Dating of Quaternary Sediments by the Use of Photon-Stimulated Luminescence*. Oxford University Press, New York.
- Antoine, P., Coutard, S., Guerin, G., Deschodt, L., Govaal, E., Lochet, J.-L., Paris, C., 2016. Upper Pleistocene loess-paleosol records from northern France in the European context: environmental background and dating of the middle palaeolithic. *Quat. Int.* 411, 4–24. <https://doi.org/10.1016/j.quaint.2015.11.036>.
- Ashworth, P.J., Sambrook Smith, Gregory H., Best, James L., Bridge, J.S., Lane, S.N., Lunt, I.A., Reesink, A.J.H., Simpson, C.J., Thomas, R.E., 2011. Evolution and sedimentology of a channel fill in the sandy braided South Saskatchewan River and its comparison to the deposits of an adjacent compound bar. *Sedimentology* 58, 1860–1883. <https://doi.org/10.1111/j.1365-3091.2011.01242.x>.
- Ballantyne, C.K., 2018. *Periglacial Geomorphology*. John Wiley & Sons.
- Bateman, M.D., Van Huissteden, J., 1999. The timing of last-glacial periglacial andaeolian events, Twente, eastern Netherlands. *J. Quat. Sci.* 14, 277–283.
- Beuselinck, L., Govers, G., Poesen, J., Degraer, G., Froyen, L., 1998. Grain-size analysis by laser diffractometry: comparison with the sieve-pipette method. *Catena* 32, 193–208. [https://doi.org/10.1016/S0341-8162\(98\)00051-4](https://doi.org/10.1016/S0341-8162(98)00051-4).
- Bird, M.I., Ayliffe, L.K., Fifield, L.K., Turney, C.S.M., Cresswell, R.G., Barrows, T.T., David, B., 1999. Radiocarbon dating of “old” charcoal using a wet oxidation, stepped-combustion procedure. *Radiocarbon* 41, 127–140. <https://doi.org/10.1017/S0033822200019482>.
- Bobak, D., Plonka, T., Poltowicz-Bobak, M., Wiśniewski, A., 2013. New chronological data for Weichselian sites from Poland and their implications for Palaeolithic. *Quat. Int.* 296, 23–36. <https://doi.org/10.1016/j.quaint.2012.12.001>.
- Bosinski, G., 1968. Zum Verhältnis von Jungacheuleen und Micoquian in Mitteleuropa. In: Piveteau, J. (Ed.), *La Préhistoire : Problèmes et Tendances*. Éditions du CNRS, Paris, pp. 77–86.
- Bosinski, G., 1967. *Die Mittelpaläolithischen Funde im Westlichen Mitteleuropa*. Fundamenta A/4. Böhlau-Verlag, Köln, Graz.

- Briant, R.M., Bateman, M.D., 2009. Luminescence dating indicates radiocarbon age underestimation in late Pleistocene fluvial deposits from eastern England. *J. Quat. Sci.* 24, 916–927. <https://doi.org/10.1002/jqs.1258>.
- Brierley, G.J., 1989. River planform facies models: the sedimentology of braided, wandering and meandering reaches of the Squamish River. *British Columbia. Sediment. Geol.* 61, 17–35. [https://doi.org/10.1016/0037-0738\(89\)90039-0](https://doi.org/10.1016/0037-0738(89)90039-0).
- Buylaert, J.P., Jain, M., Murray, A.S., Thomsen, K.J., Thiel, C., Sohbati, R., 2012. A robust feldspar luminescence dating method for Middle and Late Pleistocene sediments. *Boreas* 41, 435–451. <https://doi.org/10.1111/j.1502-3885.2012.00248.x>.
- Buylaert, J.P., Murray, A.S., Thomsen, K.J., Jain, M., 2009. Testing the potential of an elevated temperature IRSI signal from K-feldspar. *Radiat. Meas.* 44, 560–565. <https://doi.org/10.1016/j.radmeas.2009.02.007>.
- Caspers, G., Freund, H., 2001. Vegetation and climate in the early- and pleni-weichselian in northern central Europe. *J. Quat. Sci.* 16, 31–48. [https://doi.org/10.1002/1099-1417\(200101\)16:1<31::AID-JQS577>3.0.CO;2-3](https://doi.org/10.1002/1099-1417(200101)16:1<31::AID-JQS577>3.0.CO;2-3).
- Christiansen, H.H., 1998. Periglacial sediments in an eemian-weichselian succession at emmerlev Klev, southwestern Jutland, Denmark. *Palaeogeogr. Palaeoclimatol. Palaeoecol.* 138, 245–258. [https://doi.org/10.1016/S0031-0182\(97\)00117-X](https://doi.org/10.1016/S0031-0182(97)00117-X).
- Chubur, A.A., 2013. Theriofauna of the paleolithic location khotylevo 1 (Bryansk region). *Int. J. Appl. Fundam. Res.* 3, 122–124.
- Döhler, S., Terhorst, B., Frechen, M., Zhang, J., Damm, B., 2018. Chronostratigraphic interpretation of intermediate layer formation cycles based on OSL-dates from intercalated slope wash sediments. *Catena* 162, 278–290. <https://doi.org/10.1016/j.catena.2017.11.003>.
- Duller, G.A.T., 2008. Single-grain optical dating of Quaternary sediments: why aliquot size matters in luminescence dating. *Boreas* 37, 589–612. <https://doi.org/10.1111/j.1502-3885.2008.00051.x>.
- Frick, J.A., 2020. Reflections on the term Micoquian in Western and Central Europe. Change in criteria, changed deductions, change in meaning, and its significance for current research. *Archaeol. Anthropol. Sci.* 12, 38. <https://doi.org/10.1007/s12520-019-00967-5>.
- Fryirs, K., 2013. (Dis)Connectivity in catchment sediment cascades: a fresh look at the sediment delivery problem. *Earth Surf. Process. Landforms* 38, 30–46. <https://doi.org/10.1002/esp.3242>.
- Gaudzinski-Windheuser, S., Kindler, L., Pop, E., Roebroeks, W., Smith, G., 2014. The Eemian Interglacial lake-landscape at Neumark-Nord (Germany) and its potential for our knowledge of hominin subsistence strategies. *Quat. Int.* 331, 31–38. <https://doi.org/10.1016/j.quaint.2013.07.023>.
- Gaudzinski, S., 1999. Middle palaeolithic bone tools from the open-air site salzgitter-Lebenstedt (Germany). *J. Archaeol. Sci.* 26, 125–141. <https://doi.org/10.1006/j.jasc.1998.0311>.
- Gavrilov, K.N., Voskresenskaya, E.V., Maschenko, E.N., Douka, K., 2015. East Gravettian Khotylevo 2 site: stratigraphy, archaeozoology, and spatial organization of the cultural layer at the newly explored area of the site. *Quat. Int.* 359–360, 335–346. <https://doi.org/10.1016/j.quaint.2014.08.020>.
- Gladilin, V.N., 1985. Early palaeolithic. *Archaeology of Ukrainian SSR, Tome 1. Naukova Dumka, Kiev*, pp. 12–54 (in Russian).
- Gozhik, P., Komar, M., Lanczont, M., Fedorowicz, S., Bogucki, A., Mroczek, P., Prylypko, S., Kusiak, J., 2014a. Paleoenvironmental history of the middle Dnieper area from the Dnieper to weichselian glaciation: a case study of the Maksymivka loess profile. *Quat. Int.* (334–335), 94–111. <https://doi.org/10.1016/j.quaint.2013.11.037>.
- Gozhik, P., Komar, M., Lanczont, M., Fedorowicz, S., Bogucki, A., Mroczek, P., Prylypko, S., Kusiak, J., 2014b. Paleoenvironmental history of the middle Dnieper area from the Dnieper to weichselian glaciation: a case study of the Maksymivka loess profile. *Quat. Int.* <https://doi.org/10.1016/j.quaint.2013.11.037>.
- Gribchenko, Y., Kurenkova, E.I., 1999. Pleistocene environments and the dispersal of paleolithic groups in eastern Europe. *Anthropologie* 37, 79–87.
- Grischenko, M.N., 1976. Pleistocene and Holocene of the Upper Don Basin. *Nauk. Publ.* p. 227 pp. (in Russian).
- Guérin, G., Mercier, N., Adamiec, G., 2011. Dose-rate conversion factors: update. *Anc. TL* 29, 5–8.
- Harrison, S., Bailey, R.M., Anderson, E., Arnold, L., Douglas, T., 2010. Optical dates from British Isles 'solifluction sheets' suggests rapid landscape response to late Pleistocene climate change. *Scot. Geogr. J.* 126, 101–111. <https://doi.org/10.1080/14702541003712911>.
- Hedges, R.E.M., Pettitt, P.B., Ramsey, C.B., Klinken, G.J.V., 1998. Radiocarbon dates from the oxford AMS system: Archaeometry Datelist 25. *Archaeometry* 40, 227–239.
- Heggenes, J., Odland, A., Bjerketvedt, D.K., 2018. Are trampling effects by wild tundra reindeer understudied? *Rangifer* 38, 1–11. <https://doi.org/10.7557/2.38.1.4121>.
- Helmens, K.F., 2014. The Last Interglacial–Glacial cycle (MIS 5–2) re-examined based on long proxy records from central and northern Europe. *Quat. Sci. Rev.* 86, 115–143. <https://doi.org/10.1016/j.quascirev.2013.12.012>.
- Helmens, K.F., 2013. The Last Interglacial–Glacial Cycle (MIS 5–2) Re-examined Based on Long Proxy Records from Central and Northern Europe.
- Hickin, E.J., 1993. Fluvial facies models: a review of Canadian research. *Prog. Phys. Geogr. Earth Environ.* 17, 205–222. <https://doi.org/10.1177/030913399301700207>.
- Higham, T., Douka, K., Wood, R., Ramsey, C.B., Brock, F., Basell, L., Camps, M., Arrizabalaga, A., Baena, J., Barroso-Ruiz, C., Bergman, C., Boitard, C., Boscato, P., Caparrós, M., Conard, N.J., Drailly, C., Froment, A., Galván, B., Gambassini, P., Garcia-Moreno, A., Grimaldi, S., Haesaerts, P., Holt, B., Iriarte-Chiapusso, M.-J., Jelinek, A., Jordá Pardo, J.F., Maíllo-Fernández, J.-M., Marom, A., Maroto, J., Menéndez, M., Metz, L., Morin, E., Moroni, A., Negrino, F., Panagopoulou, E., Peresani, M., Pirson, S., de la Rasilla, M., Riel-Salvatore, J., Ronchitelli, A., Santamaria, D., Semal, P., Slimak, L., Soler, J., Soler, N., Villaluenga, A., Pinhasi, R., Jacobi, R., 2014. The timing and spatiotemporal patterning of Neanderthal disappearance. *Nature* 512, 306–309. <https://doi.org/10.1038/nature13621>.
- Hoffecker, J.F., 1987. Upper Pleistocene loess stratigraphy and paleolithic site chronology on the Russian plain. *Geoarchaeology* 2, 259–284.
- Hoffecker, J.F., Holliday, V.T., Nehoroshev, P., Vishnyatsky, L., Otcherednoy, A., Salnaya, N., Goldberg, P., Southon, J., Lehman, S.J., Cappa, P.J., Giaccio, B., Forman, S.L., Quade, J., 2019. The dating of a middle paleolithic blade industry in southern Russia and its relationship to the initial upper paleolithic. *J. Paleolit. Archaeol.* <https://doi.org/10.1007/s41982-019-00032-6>.
- Hublin, J.-J., 1984. The fossil man from Salzgitter-Lebenstedt (FRG) and its place in human evolution during the Pleistocene in Europe. *Z. Morphol. Anthropol.* 75, 45–56.
- Hublin, J.-J., Roebroeks, W., 2009. Ebb and flow or regional extinctions? On the character of Neanderthal occupation of northern environments. *Comptes Rendus Palevol* 8, 503–509. <https://doi.org/10.1016/j.crpv.2009.04.001>.
- Hugget, R.J., 2011. *Fundamentals of Geomorphology*, 3rd. ed. Routledge, New York.
- Huntley, D.J., Baril, M.R., 1997. The K content of the K-feldspars being measured in optical dating or thermoluminescence dating. *Anc. TL* 15, 11–13.
- Huntley, D.J., Lamothe, M., 2001. Ubiquity of anomalous fading in K-feldspars and the measurement and correction for it in optical dating. *Can. J. Earth Sci.* 38, 1093–1106. <https://doi.org/10.1139/cjes-38-7-1093>.
- Jacobs, Z., Roberts, R.G., 2007. Advances in optically stimulated luminescence dating of individual grains of quartz from archaeological deposits. *Evol. Anthropol. Issues News Rev.* 16, 210–223. <https://doi.org/10.1002/evan.20150>.
- Jöris, O., 2012. Keilmesser. In: Floss, H. (Ed.), *Steinartefakte Vom Altpaläolithikum Bis in Die Neuzeit*. Kerns Verlag, Tübingen, pp. 297–308.
- Jöris, O., 2004. Zur chronostratigraphischen Stellung der spätmittelpaläolithischen Keilmessergruppen: der Versuch einer kulturgeographischen Abgrenzung einer mittelpaläolithischen Formengruppe in ihrem europäischen Kontext. *Bericht RGK* 84, 49–153.
- Kozowyk, P.R.B., Soressi, M., Pomstra, D., Langejans, G.H.J., 2017. Experimental methods for the Palaeolithic dry distillation of birch bark: implications for the origin and development of Neanderthal adhesive technology. *Sci. Rep.* 7, 8033. <https://doi.org/10.1038/s41598-017-08106-7>.
- Kreutzer, S., Schmidt, C., Dewitt, R., Fuchs, M., 2014. The a-value of polymineral fine grain samples measured with the post-IR IRSI protocol. *Radiat. Meas.* 69, 18–29. <https://doi.org/10.1016/j.radmeas.2014.04.027>.
- Kukla, G.J., Bender, M.L., de Beaulieu, J.-L., Bond, G., Broecker, W.S., Cleveringa, P., Gavin, J.E., Herbert, T.D., Imbrie, J., Jouzel, J., Keigwin, L.D., Knudsen, K.-L., McManis, J.F., Merkt, J., Muhs, D.R., Müller, H., Poore, R.Z., Porter, S.C., Seret, G., Shackleton, N.J., Turner, C., Tzedakis, P.C., Winograd, I.J., 2002. Last interglacial climates. *Quat. Res.* 58, 2–13. <https://doi.org/10.1006/qres.2001.2316>.
- Lauer, T., Weiss, M., 2018. Timing of the Saalian- and Elsterian glacial cycles and the implications for Middle – Pleistocene hominin presence in central Europe. *Sci. Rep.* 1–13. <https://doi.org/10.1038/s41598-018-23541-w>.
- Lauer, T., Weiss, M., Bernhardt, W., Heinrich, S., Rappelsberger, I., Stahlschmidt, M.C., von Suchodoletz, H., Wansa, S., 2020. The Middle Pleistocene fluvial sequence at Uichteritz, central Germany: chronological framework, paleoenvironmental history and early human presence during MIS 11. *Geomorphology*. <https://doi.org/10.1016/j.geomorph.2019.107016>.
- Laurat, T., Brihl, E., 2006. Zum Stand der archäologischen Untersuchungen im Tagebau Neumark-Nord, Ldkr. Merseburg-Querfurt (Sachsen-Anhalt) - Vorbericht zu den Ausgrabungen 2003–2005. *Jahresschrift für mitteldeutsche Vor* 90, 9–69.
- Lisiecki, L.E., Raymo, M.E., 2005. A Pliocene-Pleistocene stack of 57 globally distributed benthic $\delta^{18}O$ records. *Paleoceanography* 20, 1–17. <https://doi.org/10.1029/2004PA001071>.
- Litt, T., Weber, T., 1988. Ein eemzeitlicher waldelefantenschlachtplatz von Gröbern. *Krs. Gräfenhainichen. Ausgrab. Funde* 33, 181–187.
- Little, E.C., Lian, O.B., Velichko, A.A., Morozova, T.D., Nechaev, V.P., Dlussky, K.G., Rutter, N.W., 2002. Quaternary stratigraphy and optical dating of loess from the east European Plain (Russia). *Quat. Sci. Rev.* 21, 1745–1762. [https://doi.org/10.1016/S0277-3791\(01\)00151-2](https://doi.org/10.1016/S0277-3791(01)00151-2).
- Locht, J.-L., Hérissou, D., Govaal, E., Cliquet, D., Huet, B., Coutard, S., Antoine, P., Feray, P., 2016a. Timescales, space and culture during the Middle Palaeolithic in northwestern France. *Quat. Int.* 411, 129–148. <https://doi.org/10.1016/j.quaint.2015.07.053>.
- Locht, J.-L., Hérissou, D., Govaal, E., Cliquet, D., Huet, B., Coutard, S., Antoine, P., Feray, P., 2016b. Timescales, space and culture during the Middle Palaeolithic in northwestern France. *Quat. Int.* 411, 129–148. <https://doi.org/10.1016/j.quaint.2015.07.053>.
- Lynds, R., Hajek, E., 2006. Conceptual model for predicting mudstone dimensions in sandy braided-river reservoirs. *Am. Assoc. Petrol. Geol. Bull.* 90, 1273–1288. <https://doi.org/10.1306/03080605051>.
- Machalett, B., Oches, E.A., Frechen, M., Zöller, L., Hambach, U., Mavlyanova, N.G., Marković, S.B., Endlicher, W., 2008. Aeonian dust dynamics in central Asia during the Pleistocene: driven by the long-term migration, seasonality, and permanency of the Asiatic polar front. *G-cubed* 9. <https://doi.org/10.1029/2007GC001938> n/a-n/a.
- Mania, D., 2002. Der mittelpaläolithische Lagerplatz am Ascherslebener See bei Königsau (Nordharzvorland). *Præhistoria Thuringica* 8, 16–75.
- Mania, D., 1990. Auf den Spuren des Urmenschen: Die Funde aus der Steinrinne von Bilzingsleben. *Deutscher Verlag der Wissenschaften, Berlin*.
- Mania, D., Toepfer, V., 1973. Königsau: gliederung, Oekologie und Mittelpaläolithische Funde der letzten Eiszeit. *Veröffentlichungen des Landesmuseums für Vorgeschichte in Halle* 26. *Deutscher Verlag der Wissenschaften, Berlin*.

- Martin, C.W., Johnson, W.C., 1995. Variation in radiocarbon ages of soil organic matter fractions from late quaternary buried soils. *Quat. Res.* 43, 232–237. <https://doi.org/10.1006/qres.1995.1023>.
- Matoshko, A.V., 2004. Evolution of the fluvial system of the Prypiat, Desna and Dnieper during the Late Middle - late Pleistocene [Evolution des systèmes fluviaux des rivières Prypiat, Desna et Dniepr au cours du Pléistocène moyen récent et du Pléistocène supérieur]. *Quaternaire* 15, 117–128. <https://doi.org/10.3406/quate.2004.1759>.
- Matoshko, A.V., Gozhik, P.F., Danukalova, G., 2004. Key late cenozoic fluvial archives of eastern Europe: the Dniester, Dnieper, Don and Volga. *Proc. Geol. Assoc.* 115, 141–173. [https://doi.org/10.1016/S0016-7878\(04\)80024-5](https://doi.org/10.1016/S0016-7878(04)80024-5).
- Matsuoka, N., 2001. Solifluction rates, processes and landforms: a global review. *Earth Sci. Rev.* 55, 107–134. [https://doi.org/10.1016/S0012-8252\(01\)00057-5](https://doi.org/10.1016/S0012-8252(01)00057-5).
- Matyukhin, A.E., Sapelko, T.V., 2009. Paleolithic site biryuchya balka-2: geology, chronology and paleoecology. *Archaeol. Ethnol. Anthropol. Eurasia* 37, 2–12. <https://doi.org/10.1016/j.aear.2010.02.004>.
- Mercier, N., Valladas, H., Froget, L., Joron, J.L., Reyss, J.L., Balescu, S., Escutenaire, C., Kozłowski, J., Sitaly, V., Sobczyk, K., Zieba, A., 2003. Luminescence dates for the palaeolithic site of Piekary Ila (Poland): comparison between TL of burnt flints and OSL of a loess-like deposit. *Quat. Sci. Rev.* 22, 1245–1249. [https://doi.org/10.1016/S0277-3791\(03\)00025-8](https://doi.org/10.1016/S0277-3791(03)00025-8).
- Miall, A.D., 2006. The Geology of Fluvial Deposits. Sedimentary Facies, Basin Analysis, and Petroleum Geology, fourth ed. Springer Berlin Heidelberg, Berlin, Heidelberg. <https://doi.org/10.1007/978-3-662-03237-4>.
- Miall, A.D., 1978. Lithofacies types and vertical profile models in braided river deposits: a summary. *Fluv. Sedimentol.* 5, 597–604.
- Miall, A.D., 1977. A review of the braided-river depositional environment. *Earth Sci. Rev.* 13, 1–62. [https://doi.org/10.1016/0012-8252\(77\)90055-1](https://doi.org/10.1016/0012-8252(77)90055-1).
- Moen, J., Danell, Ö., 2003. Reindeer in the Swedish mountains: an Assessment of grazing impacts. *AMBIO A J. Hum. Environ.* 32, 397–402. <https://doi.org/10.1579/0044-7447-32.6.397>.
- Nelson, M.S., Rittenour, T.M., 2015. Using grain-size characteristics to model soil water content: application to dose-rate calculation for luminescence dating. *Radiat. Meas.* 81, 142–149. <https://doi.org/10.1016/j.radmeas.2015.02.016>.
- Nielsen, T.K., Benito, B.M., Svenning, J.C., Sandel, B., McKerracher, L., Riede, F., Kjaergaard, P.C., 2015. Investigating Neanderthal dispersal above 55°N in Europe during the last interglacial complex. *Quat. Int.* 431, 88–103. <https://doi.org/10.1016/j.quaint.2015.10.039>.
- Ocherednoy, A.K., 2010. Bifacial backed knives (Keilmesser) in the middle palaeolithic of the upper Desna basin. *Strat. plus* 1, 227–233.
- Orlova, L.A., Panychev, V.A., 1993. The reliability of radiocarbon dating buried soils. *Radiocarbon* 35, 369–377.
- Ocherednoi, A., Salnaya, N., Voskresenskaya, E., Vishnyatsky, L., 2014a. New geoarchaeological studies at the middle paleolithic sites of khotylevo i and betovo (Bryansk oblast, Russia): some preliminary results. *Quat. Int.* 326–327, 250–260. <https://doi.org/10.1016/j.quaint.2013.11.005>.
- Ocherednoi, A., Vishnyatsky, L., Voskresenskaya, E., Nehoroshev, P., 2014b. News from the north-east fringe of Neanderthal Europe: recent work at khotylevo 1 (Bryansk oblast, Russia). *Antiquity* 1–3.
- Ocherednoi, A., Voskresenskaya, E., Stepanova, K., Vishnyatsky, L., Nekhoroshev, P., Larionova, A., Zaretskaya, N., Blokhin, E., Kolesnik, A., 2018. Complex geoarchaeological studies of the middle paleolithic sites in the Russian plain. *Trans. Inst. Hist. Mater. Cult. Russ. Acad. Sci.* 74–83. <https://doi.org/10.31600/2310-6557-2018-17-74-83>.
- Ocherednoi, A.K., Voskresenskaya, E.V., 2009. Stratigraphic data on middle paleolithic sites in the upper Desna basin. *Archaeol. Ethnol. Anthropol. Eurasia* 37, 28–36. <https://doi.org/10.1016/j.aear.2009.08.013>.
- Ocherednoi, A., Voskresenskaya, E.V., 2019. Khotylevo I. In: *The Cultural Geography of the Paleolithic in the East-European Plain from the Micoquian to the Epigravettian*, pp. 34–58.
- Panin, A., Adamiec, G., Buylaert, J.-P., Matlakhova, E., Moska, P., Novenko, E., 2017. Two Late Pleistocene climate-driven incision/aggradation rhythms in the middle Dnieper River basin, west-central Russian Plain. *Quat. Sci. Rev.* 166, 266–288. <https://doi.org/10.1016/j.quascirev.2016.12.002>.
- Panin, P.G., Timireva, S.N., Morozova, T.D., Kononov, Y.M., Velichko, A.A., 2018. Morphology and micromorphology of the loess-paleosol sequences in the south of the East European plain (MIS 1–MIS 17). *Catena* 168, 79–101. <https://doi.org/10.1016/j.catena.2018.01.032>.
- Pastors, A., 2009. Blades? – thanks, no interest! - Neanderthals in Salzgitter-Lebenstedt. *Quartaer* 56, 105–118.
- Pastors, A., 2001. Die Mittelpaläolithische Freilandstation von Salzgitter-Lebenstedt: Genese der Fundstelle und Systematik der Steinbearbeitung. *Archiv der Stadt Salzgitter, Salzgitter*.
- Picin, A., 2016. Short-term occupations at the lakeshore: a technological reassessment of the open-air site Königsau (Germany). *Quartaer* 63, 7–32. <https://doi.org/10.7485/QU63.1>.
- Pigati, J.S., Quade, J., Wilson, J., Jull, A.J.T., Lifton, N.A., 2007. Development of low-background vacuum extraction and graphitization systems for 14C dating of old (40–60ka) samples. *Quat. Int.* 166, 4–14. <https://doi.org/10.1016/j.quaint.2006.12.006>.
- Pop, E., 2014. Analysis of the neumark-nord 2/2 lithic assemblage: results and interpretations. In: Gaudzinski-Windheuser, S., Roebroeks, W. (Eds.), *Multidisciplinary Studies of the Middle Palaeolithic Record from Neumark-Nord (Germany)*, Veröffentlichungen Des Landesamtes Für Denkmalpflege Und Archäologie Sachsen-Anhalt – Landesmuseum Für Vorgeschichte Band 69. Landesamt für Denkmalpflege und Archäologie Sachsen-Anhalt, Landesmuseum für Vorgeschichte, pp. 143–195. Halle(Saale).
- Prescott, J.R., Hutton, J.T., 1994. Cosmic ray contributions to dose rates for luminescence and ESR dating: large depths and long-term time variations. *Radiat. Meas.* 23, 497–500. [https://doi.org/10.1016/1350-4487\(94\)90086-8](https://doi.org/10.1016/1350-4487(94)90086-8).
- Reimer, P.J., Bard, E., Bayliss, A., Beck, J.W., Blackwell, P.G., Ramsey, C.B., Buck, C.E., Cheng, H., Edwards, R.L., Friedrich, M., Grootes, P.M., Guilderson, T.P., Hafflason, H., Hajdas, I., Hatté, C., Heaton, T.J., Hoffmann, D.L., Hogg, A.G., Hughen, K.A., Kaiser, K.F., Kromer, B., Manning, S.W., Niu, M., Reimer, R.W., Richards, D.A., Scott, E.M., Southon, J.R., Staff, R.A., Turney, C.S.M., van der Plicht, J., 2013. IntCal13 and Marine13 radiocarbon age calibration curves 0–50,000 Years cal BP. *Radiocarbon* 55, 1869–1887. https://doi.org/10.2458/azu_jr.55.16947.
- Richter, D., Krbetschek, M., 2014. Preliminary luminescence dating results for two Middle Palaeolithic occupations at Neumark-Nord 2. In: Gaudzinski-Windheuser, S., Roebroeks, W. (Eds.), *Multidisciplinary Studies of the Middle Palaeolithic Record from Neumark-Nord (Germany)*. Volume 1. Veröffentlichungen des Landesamtes für Archäologie Sachsen-Anhalt - Landesmuseum für Vorgeschichte 69, pp. 131–136. Halle(Saale).
- Richter, J., 2016. Leave at the height of the party: a critical review of the Middle Paleolithic in Western Central Europe from its beginnings to its rapid decline. *Quat. Int.* 411, 107–128. <https://doi.org/10.1016/j.quaint.2016.01.018>.
- Richter, J., 2012. Moustérien und Micoquian. In: Floss, H. (Ed.), *Steinartefakte Vom Altpaläolithikum Bis In Die Neuzeit*. Kerns Verlag, Tübingen, pp. 267–272.
- Richter, J., 2006. Neanderthals in their landscape. In: Neanderthals in Europe, pp. 51–66.
- Richter, J., 2002. Die 14C-Daten aus der Sesselfelsgrötte und die Zeitstellung des Micoquien/MMO. *Germania* 80, 1–22.
- Richter, J., 2001. For lack of a wise old man? Late Neanderthal land use patterns in the Altmühl River Valley. In: Conard, N.J. (Ed.), *Settlement Dynamics of the Middle Paleolithic and Middle Stone Age*. Kerns Verlag, Tübingen, pp. 205–220.
- Richter, J., 2000. Social memory among late Neanderthals. In: Orschiedt, J., Weniger, G.-C. (Eds.), *Neanderthals and Modern Humans – Discussing the Transition*. Neanderthal Museum, Mettmann, pp. 30–41.
- Richter, J., 1997. Sesselfelsgrötte III. Der G-Schichten-Komplex der Sesselfelsgrötte. Zum Verständnis des Micoquien. *Quartär Bibliothek 7*. Saarbrücker Druckerei und Verlag, Saarbrücken.
- Rittenour, T.M., 2008. Luminescence dating of fluvial deposits: applications to geomorphic, palaeoseismic and archaeological research. *Boreas* 37, 613–635. <https://doi.org/10.1111/j.1502-3885.2008.00056.x>.
- Roebroeks, W., Hublin, J.-J., MacDonald, K., 2011. Continuities and Discontinuities in Neanderthal presence: a closer look at northwestern Europe. *Dev. Quat. Sci.* 14, 113–123. <https://doi.org/10.1016/B978-0-444-53597-9.00008-X>.
- Rust, B.R., 1972. Structure and process in a braided river. *Sedimentology* 18, 221–245. <https://doi.org/10.1111/j.1365-3091.1972.tb00013.x>.
- Skrzypek, G., Wiśniewski, A., Grierson, P.F., 2011. How cold was it for Neanderthals moving to Central Europe during warm phases of the last glaciation? *Quat. Sci. Rev.* 30, 481–487.
- Smith, D.G., Smith, N.D., 1980. Sedimentation in anastomosed river systems; examples from alluvial valleys near Banff, Alberta. *J. Sediment. Res.* 50, 157–164. <https://doi.org/10.1306/212F7991-2B24-11D7-8648000102C1865D>.
- Strahl, J., Krbetschek, M.R., Luckert, J., Machalet, B., Meng, S., Oches, E.A., Rappsilber, I., Wansa, S., Zöller, J., 2010. Geologie, Paläontologie und Geochronologie des Eem-Beckens Neumark-Nord 2 und Vergleich mit dem Becken Neumark-Nord 1 (Geiseltal, Sachsen-Anhalt). *Eiszeitalter und Gegenwart. Quaternary Sci. Journal* 59, 120–167. <https://doi.org/10.3285/eg.59.1-2.09>.
- Sycheva, S., Khokhlova, O., 2016. Genesis, 14 C age, and duration of development of the Bryansk paleosol on the Central Russian Upland based on dating of different materials. *Quat. Int.* 399, 111–121. <https://doi.org/10.1016/j.quaint.2015.08.055>.
- Sytchkin, N.I., 1998. Geological Map of Pre-quaternary Sediments of the Bryansk Region, 1:500,000 (Геологическая Карта Четвертичных Отложений Брянской Области). Ministry of Natural Resources of the Russian Federation.
- Thiel, C., Buylaert, J.P., Murray, A., Terhorst, B., Hofer, I., Tsukamoto, S., Frechen, M., 2011. Luminescence dating of the Stratzing loess profile (Austria) - testing the potential of an elevated temperature post-IR IRSI protocol. *Quat. Int.* 234, 23–31. <https://doi.org/10.1016/j.quaint.2010.05.018>.
- Thieme, H., Veil, S., 1985. Neue untersuchungen zum eemzeitlichen elefanten-Jagdplatz Lehingen. *Ldkr. Verden. Die Kd. N.F.* 36, 11–58.
- Thomsen, K.J., Murray, A.S., Jain, M., Bøtter-Jensen, L., 2008. Laboratory fading rates of various luminescence signals from feldspar-rich sediment extracts. *Radiat. Meas.* 43, 1474–1486. <https://doi.org/10.1016/j.radmeas.2008.06.002>.
- Tode, A., 1982. Der Altsteinzeitliche Fundplatz Salzgitter-Lebenstedt. Teil I, Archäologischer Teil. Böhlau, Köln, Wien.
- Toepfer, V., 1970. Stratigraphie und Ökologie des Paläolithikums. In: Richter, H., Haase, G., Lieberoth, I., Ruske, R. (Eds.), *Periglazial - Löß- Paläolithikum Im Jungpleistozän Der Deutschen Demokratischen Republik*, pp. 329–422. Leipzig/Gotha.
- Van Huissteden, K., Vandenbergh, J., Gibbard, P.L., Lewin, J., 2013. Periglacial fluvial sediments and forms. In: Elias, S.A. (Ed.), *The Encyclopedia of Quaternary Science*. Elsevier, p. 2600.
- Vandenbergh, J., 2015. River terraces as a response to climatic forcing: formation processes, sedimentary characteristics and sites for human occupation. *Quat. Int.* <https://doi.org/10.1016/j.quaint.2014.05.046>.
- Vandenbergh, J., 2008. The fluvial cycle at cold-warm-cold transitions in lowland regions: a refinement of theory. *Geomorphology*. <https://doi.org/10.1016/j.geomorph.2006.12.030>.

- Veil, S., Breest, K., Höfle, H.-C., Meyer, H.-H., Plisson, H., Urban-Küttel, B., Wagner, G.A., Zöller, L., 1994. Ein mittelpaläolithischer Fundplatz aus der Weichsel-Kaltzeit bei Lichtenberg, Lkr. Lüchow-Dannenberg. *Germania* 72, 1–66.
- Velichko, A.A., 1999. Global dispersal of hominids - a feature of their coevolution with the environment. *Anthropologie* 37, 5–18.
- Velichko, A.A., 1990. Loess-paleosol formation on the Russian plain. *Quat. Int.* 7/8, 103–114.
- Velichko, A.A., 1988. Geocology of the mousterian in east europe and the adjacent areas. In: *L'Homme de Neandertal*. Liège, pp. 181–206.
- Velichko, A.A., Borisova, O.K., Kononov, Y.M., Konstantinov, E.A., Kurbanov, R.N., Morozova, T.D., Panin, P.G., Semenov, V.V., Tesakov, A.S., Timireva, S.N., Titov, V.V., Frolov, P.D., 2017. Reconstruction of Late Pleistocene events in the periglacial area in the southern part of the East European Plain. *Dokl. Earth Sci.* 475, 895–899. <https://doi.org/10.1134/S1028334X17080098>.
- Velichko, A.A., Faustova, M.A., Pisareva, V.V., Gribchenko, Y.N., Sudakova, N.G., Lavrentiev, N.V., 2011. Glaciations of the East European Plain, pp. 337–359. <https://doi.org/10.1016/B978-0-444-53447-7.00026-X>.
- Velichko, A.A., Morozova, T.D., Nechaev, V.P., Rutter, N.W., Dlusskii, K.G., Little, E.C., Catto, N.R., Semenov, V.V., Evans, M.E., 2006. Loess/paleosol/cryogenic formation and structure near the northern limit of loess deposition, East European Plain, Russia. *Quat. Int.* 152–153, 14–30. <https://doi.org/10.1016/j.quaint.2005.12.003>.
- Velichko, A.A., Pisareva, V.V., Sedov, S.N., Sinitsyn, A.A., Timireva, S.N., 2009. Paleogeography OF KOSTENKI-14 (MARKINA GORA). *Archaeol. Ethnol. Anthropol. Eurasia* 37, 35–50. <https://doi.org/10.1016/j.aeae.2010.02.002>.
- Vishnyatsky, L., Otcherednoi, A.K., Hoffecker, J.F., Voskresenskaya, E.V., Nehoroshov, P., Pitul'ko, V.V., Holliday, V.T., 2015. The age of the Khotylevo I and Betovo sites in the light of newly obtained radiocarbon dates (preliminary report). *Trans. Inst. Hist. Mater. Cult. St. Petersburg. «DMITRY BULANIN»* 12, 9–19.
- Voskresenskaya, E.V., Otcherednoi, A.K., 2010. Chronostratigraphic position and sedimentation dynamics at the Middle Paleolithic sites of Betovo and Khotylevo "Geology, geocology, evolutionary geography", Vol. X. Herzen University Press, St. Petersburg, pp. 180–183 (in Russian).
- Voskresenskaya, E.V., Otcherednoi, A.K., 2012. New Geoarchaeological studies of the Middle Paleolithic site Khotylevo I (the Upper Desna river basin, Russia). *Geomorph. processes and Geoarchaeology* 283–286. Moscow-Smolensk.
- Voskresenskaya, E.V., Vishniyskiy, L.B., Zuzanova, I.S., Novenko, E.U., Otcherednoi, A.K., 2011. New data on the evolution and age of sediments, enclosing the cultural horizon of middle paleolithic site Khotylevo I (river Desna basin). The Quaternary in all of its variety. Basic issues, results, and major trends of further research. In: Korsakova, O.P., Kolka, V.V. (Eds.), *Proceedings of the VII All-Russian Quaternary Conference (Apatity, September 12–17, 2011)*. In 2 Volumes / Russ. Acad. Sci., Depart. of Earth Sci., Commiss. on Quaternary Period Research, Geological Institute KSC RAS, Vol. 1. Apatity, St Petersburg, pp. 116–119 (in Russian).
- Walling, D.E., 1983. The sediment delivery problem. *J. Hydrol.* 65, 209–237. [https://doi.org/10.1016/0022-1694\(83\)90217-2](https://doi.org/10.1016/0022-1694(83)90217-2).
- Wallinga, J., 2002. Optically stimulated luminescence dating of fluvial deposits: a review. *Boreas* 31, 303–322. <https://doi.org/10.1080/030094802320942536>.
- Wang, Y., Amundson, R., Trumbore, S., 1996. Radiocarbon dating of soil organic matter. *Quat. Res.* 45, 282–288. <https://doi.org/10.1006/qres.1996.0029>.
- Weber, T., 1990. Paläolithische Funde aus den Eemvorkommen von Rabutz, Grabschütz und Gröbern. In: Eißmann, L. (Ed.), *Die Eemwarmzeit Und Die Frühe Weichsel-Eiszeit Im Saale-Elbe-Gebiet*. Geologie, Paläontologie, Palökologie, Altenburger Naturwissenschaftliche Forschungen 5. Naturkundliches Museum Mauritium, Altenburg.
- Weiss, M., 2019. Beyond the Caves: Stone Artifact Analysis of Late Middle Paleolithic Open-Air Assemblages from the European Plain. Universiteit Leiden.
- Weiss, M., 2015. Stone tool analysis and context of a new late Middle Paleolithic site in western central Europe - Pouch-Terrassenpfeiler, Ldkr. Anhalt-Bitterfeld, Germany. *Quartaer* 62, 23–62. https://doi.org/10.7485/QU62_2.
- Weiss, M., Lauer, T., Wimmer, R., Pop, C.M., 2018. The variability of the Keilmesser-concept: a case study from Central Germany. *J. Paleolit. Archaeol.* 1, 202–246. <https://doi.org/10.1007/s41982-018-0013-y>.
- Weiss, M., Otcherednoi, A., Wiśniewski, A., 2017. Using multivariate techniques to assess the effects of raw material, flaking behavior and tool manufacture on assemblage variability: an example from the late Middle Paleolithic of the European Plain. *J. Archaeol. Sci.* 87, 73–94. <https://doi.org/10.1016/j.jas.2017.09.014>.
- Wenban-Smith, F.F., Bates, M.R., Schwenninger, J.-L., 2010. Early Devensian (MIS 5d-5b) occupation at Dartford, southeast England. *J. Quat. Sci.* 25, 1193–1199. <https://doi.org/10.1002/jqs.1447>.
- Winsemann, J., Lang, J., Roskosch, J., Polom, U., Böhner, U., Brandes, C., Glotzbach, C., Frechen, M., 2015. Terrace styles and timing of terrace formation in the Weser and Leine valleys, northern Germany: response of a fluvial system to climate change and glaciation. *Quat. Sci. Rev.* 123, 31–57. <https://doi.org/10.1016/j.quascirev.2015.06.005>.
- Wintle, A.G., 1997. Luminescence dating: laboratory procedures and protocols. *Radiat. Meas.* 27, 769–817. [https://doi.org/10.1016/S1350-4487\(97\)00220-5](https://doi.org/10.1016/S1350-4487(97)00220-5).
- Wintle, A.G., 1973. Anomalous fading of thermo-luminescence in mineral samples. *Nature* 245, 143–144. <https://doi.org/10.1038/245143a0>.
- Wiśniewski, A., Adamiec, G., Badura, J., Bluszcz, A., Kowalska, A., Kufel-Diakowska, B., Mikolajczyk, A., Murckiewicz, M., Musil, R., Przybylski, B., Skrzypek, G., Stefaniak, K., Zych, J., 2013. Occupation dynamics north of the Carpathians and Sudetes during the Weichselian (MIS5d-3): the lower Silesia (SW Poland) case study. *Quat. Int.* 294, 20–40. <https://doi.org/10.1016/j.quaint.2011.09.016>.
- Wiśniewski, A., Lauer, T., Chłóń, M., Pyżewicz, K., Weiss, M., Badura, J., Kalicki, T., Zarzecka-Szubińska, K., 2019. Looking for provisioning places of shaped tools of the late Neanderthals: a study of a Micoquian open-air site, Pietraszyn 49a (southwestern Poland). *Comptes Rendus Palevol* 18, 367–389. <https://doi.org/10.1016/j.crpv.2019.01.003>.
- Wood, R., 2015. From revolution to convention: the past, present and future of radiocarbon dating. *J. Archaeol. Sci.* 56, 61–72. <https://doi.org/10.1016/j.jas.2015.02.019>.
- WRB - IUSS Working Group, 2015. World Reference Base for Soil Resources 2014, Update 2015. International Soil Classification System for Naming Soils and Creating Legends for Soil Maps. World Soil Resources Reports No. 106. FAO, Rome.
- Yelovicheva, Y., Sanko, A., 1999. Palynostratigraphy of the Poozerie glaciation (Vistulian) in Belarus. *Geological Q* 43, 203–212.
- Zaretskaya, N.E., Otcherednoi, A.K., 2019. Preliminary results of the application of different dating methods to build the chronology of the monument Khotylevo I. In: *The Cultural Geography of the Palaeolithic in the East-European Plain: from the Micoquian to the Epigravettian*. Book of Abstracts. Institute of Archaeology RAS, Moscow, pp. 76–79.
- Zaveryaev, F.M., 1978. Khotylevskoe Paleoliticheskoe Mestonahozhdenie. Nauka, Leningrad.




**CHAPTER III: EEMIAN LANDSCAPE RESPONSE TO CLIMATIC SHIFTS AND
EVIDENCE FOR NORTHERLY NEANDERTHAL OCCUPATION AT A
PALAEOLAKE MARGIN IN NORTHERN GERMANY**

Published in: Earth Surf. Process. Landforms. 46 (2021): 1–18

RESEARCH ARTICLE

ESPL WILEY

Eemian landscape response to climatic shifts and evidence for northerly Neanderthal occupation at a palaeolake margin in northern Germany

Michael Hein¹  | Brigitte Urban² | David Colin Tanner³  |
 Anton Hermann Bunes³ | Mario Tucci² | Philipp Hoelzmann⁴ | Sabine Dietel⁵ |
 Marie Kaniecki¹ | Jonathan Schultz^{1,5} | Thomas Kasper⁶ |
 Hans von Suchodoletz⁷  | Antje Schwalb⁸ | Marcel Weiss^{9,1} | Tobias Lauer¹

¹Department of Human Evolution, Max Planck Institute for Evolutionary Anthropology, Leipzig, Germany

²Institute of Ecology, Leuphana University of Lüneburg, Lüneburg, Germany

³Section 1: Seismic, Gravimetry, and Magnetism, Leibniz Institute for Applied Geophysics, Hannover, Germany

⁴Institute for Geographical Sciences, Freie Universität Berlin, Berlin, Germany

⁵Institute for Geosciences and Geography, Martin Luther University Halle-Wittenberg, Halle, Germany

⁶Institute for Geography, Friedrich Schiller University Jena, Jena, Germany

⁷Department of Geography, Faculty of Physics and Geosciences, University of Leipzig, Leipzig, Germany

⁸Institute of Geosystems and Bioindication, Technical University Braunschweig, Braunschweig, Germany

⁹Institut für Ur- und Frühgeschichte, Friedrich-Alexander-Universität Erlangen-Nürnberg, Erlangen, Germany

Correspondence

Michael Hein, Department of Human Evolution, Max-Planck-Institute for Evolutionary Anthropology, Deutscher Platz 6, Leipzig, Saxony, 04103, Germany.
 Email: michael_hein@eva.mpg.de

Dr Marcel Weiss, Institut für Ur- und Frühgeschichte, Friedrich-Alexander-Universität Erlangen-Nürnberg, Kochstr. 4/18, Erlangen, Bayern, 91054, Germany.
 Email: marcel.weiss@fau.de

Funding information

Max-Planck-Gesellschaft

Abstract

The prevailing view suggests that the Eemian interglacial on the European Plain was characterized by largely negligible geomorphic activity beyond the coastal areas. However, systematic geomorphological studies are sparse. Here we present a detailed reconstruction of Eemian to Early Weichselian landscape evolution in the vicinity of a small fingerlake on the northern margin of the Salzwedel Palaeolake in Lower Saxony (Germany). We apply a combination of seismics, sediment coring, pollen analysis and luminescence dating on a complex sequence of colluvial, paludal and lacustrine sediments. Results suggest two pronounced phases of geomorphic activity, directly before the onset and at the end of the Eemian period, with an intermediate period of pronounced landscape stability. The dynamic phases were largely driven by incomplete vegetation cover, but likely accentuated by fluvial incision in the neighbouring Elbe Valley. Furthermore, we discovered Neanderthal occupation at the lake-shore during Eemian pollen zone (PZ) E IV, which is chronologically in line with other known Eemian sites of central Europe. Our highly-resolved spatio-temporal data substantially contribute to the understanding of climate-induced geomorphic processes throughout and directly after the last interglacial period. It helps unraveling the landscape dynamics between the coastal areas to the north and the loess belt to the south.

KEYWORDS

Eemian interglacial, landscape evolution, luminescence dating, Neanderthal occupation, paleolake, pollen analysis

1 | INTRODUCTION

Climate and environmental dynamics of the last interglacial, termed 'Eemian' in central and north-western Europe, have been studied more intensively on the European Plain than in any other region on Earth. This is largely due to the very frequent occurrence of Eemian geoarchives, in an area roughly equivalent to the maximum extent of the Saalian glaciation (Figure 1) (Turner, 2002; van Kolfschoten & Gibbard, 2000; Źarski et al., 2018). The vast majority of geomorphological studies focus on the loess belt (Antoine et al., 2016; Haesaerts & Mestdagh, 2000), riverine environments (Busschers et al., 2007; De Clercq et al., 2018; Gibbard & Lewin, 2002; Peeters et al., 2015), as well as the coastal areas that respond to Eemian sea level changes (Head et al., 2005; Höfle et al., 1985; Marks et al., 2014; Miettinen et al., 2014; Streif, 2004). Results of these studies suggest non-depositional, stable conditions with dominating pedogenesis during the temperate phases of the Eemian. The region in between the coasts and the loess belt, that is, the lowland landscapes remain underrepresented in this research. Nevertheless, this area hosts a multitude of mostly small isolated basins (diametres of a few decametres to some hundred metres), formed as kettle holes in the underlying Saalian till (Turner, 2000). These were formed at the end of the Saalian glaciation, when local depressions, caused by melting ice blocks (dead ice) enabled accommodation of usually lacustrine and paludal Eemian sediments. In the past decades, valuable information on the palaeoenvironmental and palaeoclimatic development of the Eemian has been retrieved from such archives (e.g., Behre et al., 2005; Björck et al., 2000; Kołaczek et al., 2016; Kupryjanowicz et al., 2018; Köhl et al., 2007; Menke & Tynni, 1984; Rother et al., 2019; Velichko et al., 2005). However, there are several disadvantages related to the small dimensions of these closed depressions, which affect the interpretation of past climate and vegetation variability, and particularly of geomorphic activity in response to environmental changes: (i) These landforms do not exclusively store information on climatic conditions, but their infills are also heavily affected by the very local hydrographic situation, likely to overprint the palaeoclimate signal (Turner, 2000;

cf. Vandenberghe & van der Plicht, 2016). (ii) Records derived from these archives are often discontinuous. This is one of the main reasons that a general agreement upon the exact timing and duration of the terrestrial Eemian is still pending (although it is generally correlated with Marine Isotope Stage [MIS] 5e) (see discussions in Brauer et al., 2007; Lisiecki & Raymo, 2005; Shackleton et al., 2002; Sier et al., 2015). (iii) Their minor extent and small-sized catchment areas do generally not allow statements about regional geomorphic landscape dynamics. Consequently, it is still not clear, how inland lowland landscapes of the European Plain responded to Eemian environmental changes.

Therefore, detailed information on the Eemian landscape dynamics in the lowlands can only be obtained by studying sedimentary basins that offer larger accommodation space compared to the small closed depressions, testifying to both, temporally and spatially varying sedimentation processes. In this study, we investigate sediments of a palaeolake margin adjacent to the Elbe ice-marginal valley to assess the Eemian landscape evolution of the northern German lowlands between the coasts in the north and the loess belt and low-mountain ranges in the south. By using a borehole transect, seismic surveys and palynology, we decipher the geomorphic, vegetation and sedimentary history of this area from the Late Saalian until the Early Weichselian period with a high spatio-temporal resolution.

2 | STUDY AREA

The study site is situated near the village of Lichtenberg in eastern Lower-Saxony, northern Germany (Figure 2). In the course of the Pleistocene, this area was formed by alternating glacial, periglacial and interglacial/interstadial conditions. Glaciers covered the area at least twice during the Elsterian glaciation (MIS 12) and three times during the Saalian glaciation (MIS 6, stages Drenthe I, Drenthe II and Warthe), depositing > 40 m of tills, glaciofluvial sands and gravels in total (Duphorn et al., 1973; Ehlers et al., 2011; Lang et al., 2018; Stephan, 2014). These glacial sediments are found in the echeloned

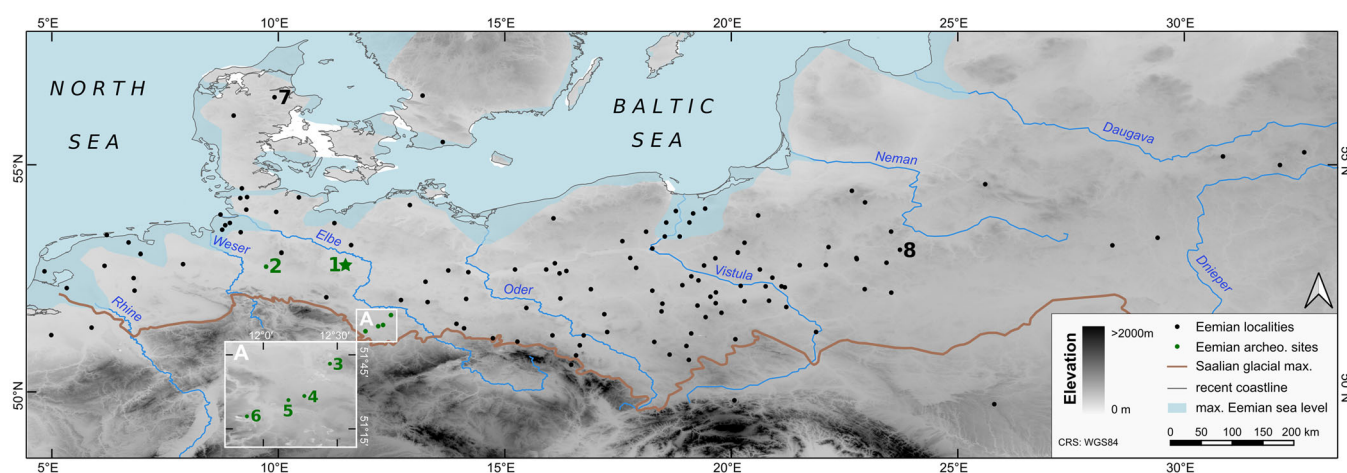


FIGURE 1 Digital elevation model (DEM) of the European Plain, showing the maximum Saalian ice margins (after Ehlers et al. [1984], Matoshko [2011] and Velichko et al. [2006]) and selected localities of Eemian deposits (compiled from Kołaczek et al. [2016], Turner [2000] and Velichko et al. [2005]). Eemian sea-level highstands after Miettinen et al. (2014). Sites mentioned in the text: 1, Lichtenberg; 2, Lehringen; 3, Gröbern; 4, Grabschütz; 5, Rabutz; 6, Neumark-Nord; 7, Hollerup; 8, Jאלówka. Localities marked in green are also archeological sites. DEM based on SRTM-data (downloaded from <https://earthexplorer.usgs.gov/>), river courses are from open streetmap data, obtained from <http://download.geofabrik.de/europe.html>

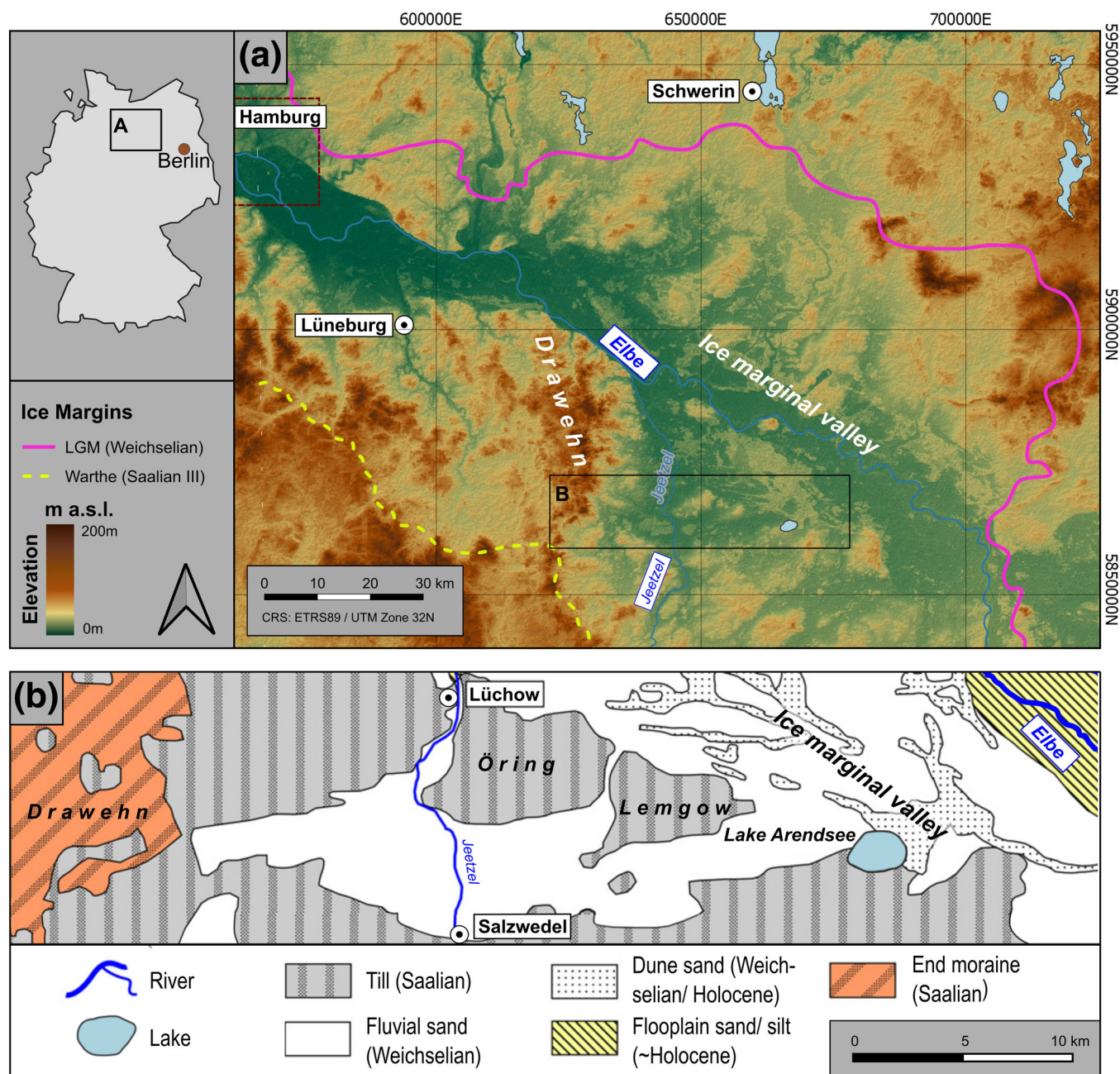


FIGURE 2 (a) Location map of the study area in northern Germany based on an SRTM-DEM (obtained from <https://earthexplorer.usgs.gov/>). Ice margins according to Ehlers and Gibbard (2004), river courses downloaded from <http://download.geofabrik.de/europe.html>. (b) Quaternary geology of the study area, modified after Turner et al. (2013)

retreatal moraine of the Drawehn (Figure 2) and as solitary inliers of morainic hills (e.g., Öring and Lemgow) within genetically-younger lowland areas (Merk, 1975; Voss, 1981). In contrast, the region and study area remained unglaciated throughout the Weichselian glaciation (MIS 4 to MIS 2), with the Last Glacial Maximum (LGM) ice margin located c. 50 km to the northeast (Figure 2a). The associated ice-marginal valley is now partly occupied by the recent River Elbe, but it covered more extensive areas (Meyer, 1983; Woldstedt, 1956), so that it delimits the Öring and Lemgow to the north (Figures 2 and 3). The Eemian course of the lower Elbe has been highly debated in the past, in particular the time at which the river occupied its current position following the Saalian glaciations (Illies, 1954; Lüttig & Meyer, 1974; Woldstedt, 1956). However, it is now widely accepted

that the ice-marginal valley formed even prior to the late Saalian Warthe Stadial and attracted the regional discharge from this time onward (Averdieck, 1976; Ehlers, 1990; Grube et al., 1976; Meyer, 1983). Significant subsidence around the Elbe tectonic lineament is thought to have been an important factor in its evolution (Brandes et al., 2019; Reicherter et al., 2005). At least since the end of the Warthe Stadial, the connection to the upper Elbe reaches in Saxony and Bohemia was established, so that a general congruence of the Eemian, the Weichselian and Holocene courses can be assumed (Ehlers, 2020).

The study site is located within the lowlands south of Öring and Lemgow, extending between Lake Arendsee and Jeetzel River (Figure 2b). Veil et al. (1994) first proposed this depression might once have contained a palaeolake (Figure 3a). This assumption was

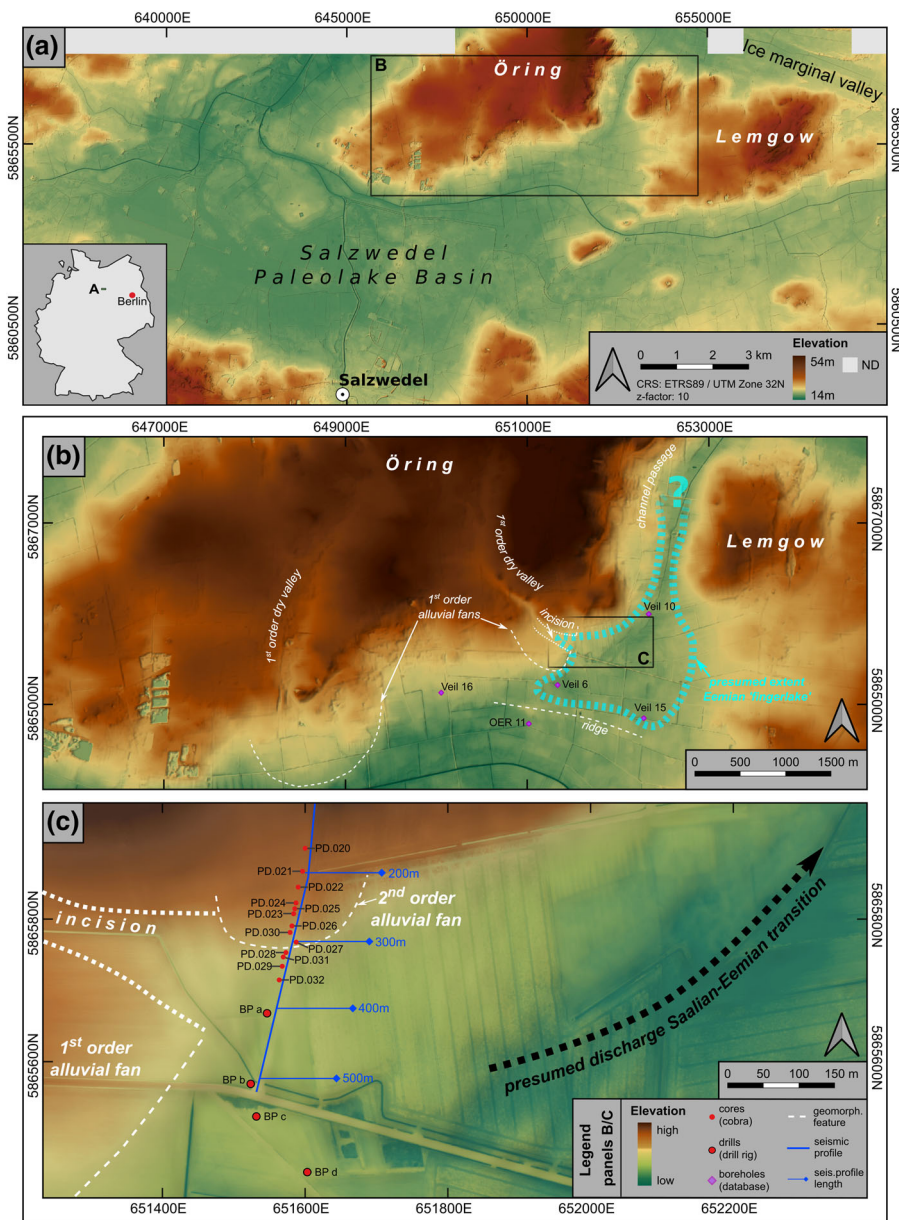


FIGURE 3 Digital elevation models (DEMs) of the study area showing geomorphic features and the positions of the seismic and borehole profiles. Descriptions in the text, Section 2 and Supporting Information Method S1. Core descriptions of previous studies found in the borehole database of Lower Saxony (<https://nibis.lbeg.de/cardomap3/>). For the geological cross-section (P1–P2) in (A), see Supporting Information Figure S1

based on the size and rhomboid shape of the basin and the fine-grained sediment infill, as documented in the borehole database of the State Office for Mining, Energy and Geology, Lower Saxony (<https://nibis.lbeg.de/cardomap3/>). Hereafter, we refer to this basin as ‘Salzwedel Palaeolake’ (named after the largest adjacent city). Moreover, Veil et al. (1994) discovered paludal and lacustrine residues at the basin margin, possibly associated with this palaeolake. By using biostratigraphic assumptions, these deposits were dated to the Eemian and the early MIS 4 (ibid.), suggesting a permanent body of water at the time of their sedimentation. Our investigations were carried out on the northern margin of Salzwedel Palaeolake, at the eastern scarp of an alluvial fan, discernible as a current geomorphic feature. In this fan, a slight elongated and west–east striking depression indicates a former incision into this landform, thereby creating a sedimentary basin, which is the subject of this study. Lengthwise, the borehole transect also cuts a smaller (second order) alluvial fan, cast into this basin. Additional information on the local geomorphological situation is given in Section 5.2 and Supporting Information Method S1.

3 | METHODS

3.1 | Fieldwork

Coring campaigns were conducted in 2019 and 2020 within the framework of an ongoing geoarchaeological research project on the Middle-Palaeolithic occupation of the Lichtenberg site (Veil et al., 1994; Weiss, 2020) and meant to provide palaeoenvironmental context for that period. Hence, fieldwork comprised also an archaeological survey. The basin infill sequence was exposed by a > 600 m long transect of 20 boreholes (16 vibrocores, down to 11 m and four rotary drills, down to 21 m), carried out perpendicular to the orientation of the basin, at carefully chosen locations (for core positions see Figures 3c and 4). The vibrocores were drilled with an *Atlas Copco Cobra* motor hammer using open probes of 1 m length and 50 to 80 mm diameter. Rotary drilling was conducted in cooperation with the State Office for Mining, Energy and Geology of Lower-Saxony (LBEG), utilizing a truck-mounted drill-rig and 3 m augers with c. 25 cm diameter. The average recovery rate for the continuous cores

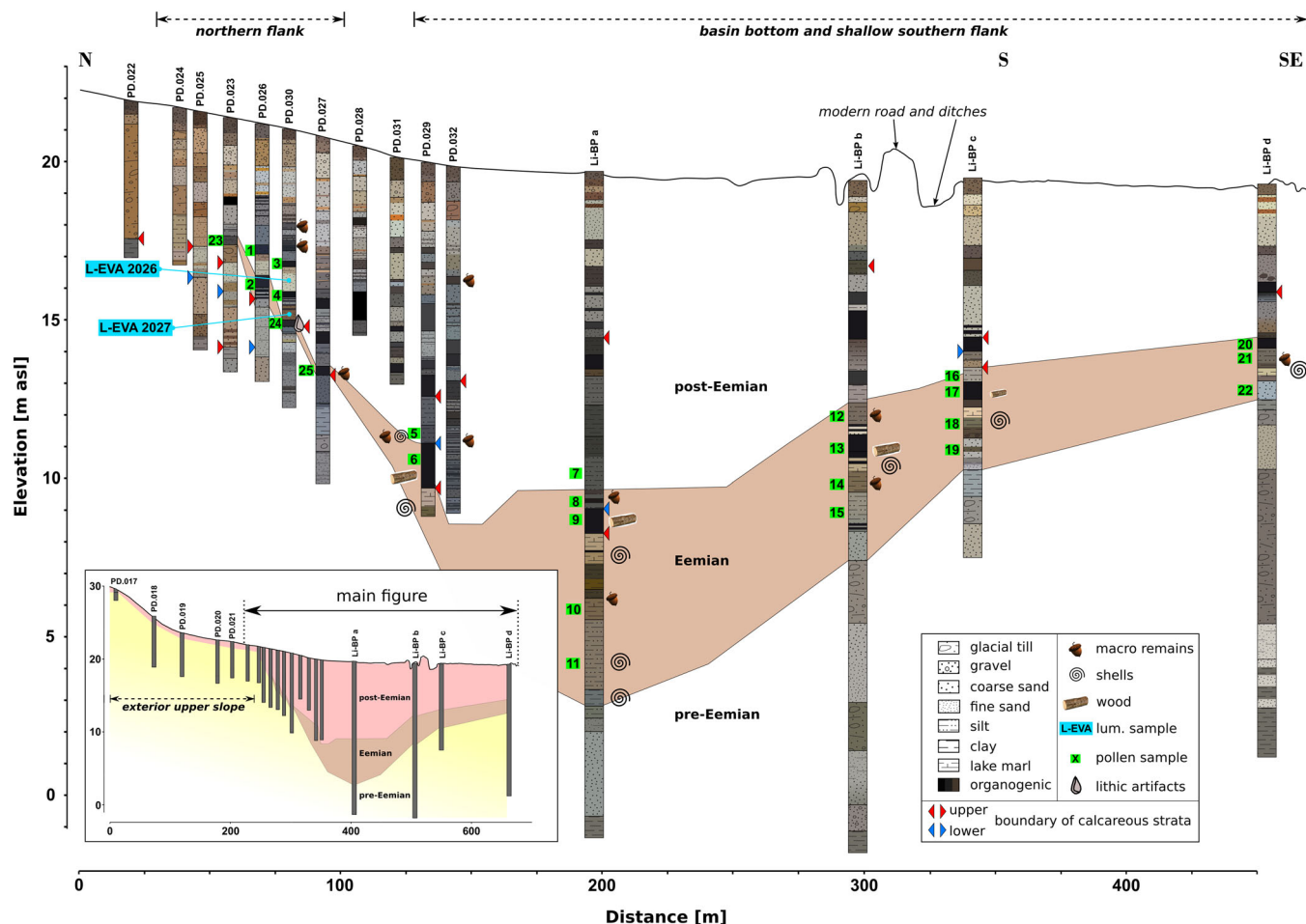


FIGURE 4 Sedimentary log of the borehole transect along with the positions of luminescence and pollen sampling (samples for organic carbon (C_{org}) and nitrogen (N) measurements taken from the pollen batch). Colouring of the cores corresponds with the MUNSELL colours, ascribed during fieldwork. Vertical exaggeration 1:12. For borehole logs of the exterior upper slope, see Supporting Information Figure S4

was always > 90%. Sediment descriptions in the field encompassed sediment boundaries, MUNSELL colours, admixtures (such as gravels, botanical macro remains, charcoal, shell fragments), grain-size compositions and carbonate contents, and followed the German soil mapping guidelines of Boden (2005). Organogenic sediments were classified according to Meier-Uhlherr et al. (2015). Subsequently, selected sediment units were sampled for luminescence dating, palynological analyses, and measurements of organic carbon and nitrogen content (Sections 3.3–3.5, Figure 4).

3.2 | S-wave seismic reflection

In alignment with the coring transect, we measured a seismic S-wave profile of 520 m length. We used a small electrodynamic vibrator (Elvis 7, Krawczyk et al., 2012) with a sweep frequency of 20 to 160 Hz. The 16 s sweep was excited perpendicular to the line direction at each shotpoint twice with opposite polarity and subtractively stacked to suppress P-wave energy. Recording was done using a landstreamer with 120 horizontally-oriented 10 Hz geophones. We worked in a symmetrical split-spread fashion by shooting 60 m to the middle of the streamer before moving it for the same distance. To maximize the seismic fold at the targeted layers we used a shotpoint spacing of 2 m, so that the corresponding common depth point (CDP)

fold was 31. Details on the processing of the seismic data are given in Supporting Information Table S1, additional methodological information is provided in Method S3.

3.3 | Palynological analysis

Twenty-five samples of characteristic lithological units/horizons were taken from nine drilled cores (PD.023, PD.026, PD.027, PD.029, PD.030, Li-BPa, Li-BPb, Li-BPc, Li-BPd) for palynological investigation and biostratigraphic determination (Figure 4). By taking bulk samples distributed across the entire borehole transect, we deliberately traded chronological resolution and unambiguity of pollen zone classification against higher spatial coverage in order to focus on the reconstruction of geomorphic dynamics. In about 10 g of wet sediment per sample, carbonates were removed first with 10% hydrochloric acid (HCl). The samples were then treated using standard methods (Faegri et al., 1989; Moore et al., 1991). The extracted residues were mounted in glycerine. Generally, one slide (24 mm × 32 mm) per sample was analysed under a transmitted light microscope for pollen and non-pollen palynomorphs at 40× magnification. Pollen and spores were identified using the atlases of Faegri et al. (1989), Moore et al. (1991) and Beug (2004), as well as the reference collections of the Palynology Laboratory of the

Institute of Ecology, Working Group Landscape Change, Leuphana University of Lüneburg, Germany.

The pollen sums, on which percentages of all taxa are based, were constructed by summing up arboreal pollen (AP), including trees and shrubs, and non-arboreal pollen (NAP), composed of terrestrial herbaceous taxa and Poaceae. In contrast, taxa from cryptogams, Ericaceae, Cyperaceae and aquatic plants were excluded from the basic sums. Pollen percentages were calculated and plotted using the software package TILIA (Grimm, 1990).

3.4 | pIRIR₂₉₀ luminescence dating

To complement the biostratigraphical age control provided by palynological analysis, we dated two samples (L-EVA 2026 and 2027) from core PD.030 using luminescence dating (see Figures 4 and 6 for sampling positions). Sample L-EVA 2027 was taken from an unstratified sand layer overlying an Eemian half-bog. A peat deposit covers this layer and is in turn overlain by a well-stratified gleyic medium sand, from which sample L-EVA 2026 was obtained. We carefully removed c. 1 cm of the outer material that was previously exposed to light and sampled 15 cm sections of the innermost sediment for luminescence (= D_e -samples) (cf., Nelson et al., 2019). The discarded outer material was added to the dose rate samples (Table S3), otherwise taken within

15 cm below and above the D_e -samples. Sample preparation and D_e -measurements on coarse-grained potassium-feldspar (125–180 μm) were conducted at the MPI-EVA, Leipzig, using the pIRIR₂₉₀ approach proposed by Thiel et al. (2011; cf., Hein et al., 2020). Detailed information on the data evaluation can be found in Method S4.

3.5 | Analyses of organic carbon and total nitrogen

To support the classification of different organogenic deposits, the contents of organic carbon (C_{org}) and total nitrogen (TN) in pollen samples 2, 6, 8, and 23–25 (Figure 4) were determined by applying the methods and equipment described in Vogel et al. (2016). The C_{org} was treated both as a discrete parameter and to calculate the molar C/N ratio, the latter used to assess the decomposition rate of organic matter in soils (e.g., Högberg et al., 2006).

4 | RESULTS AND INTERPRETATION

4.1 | Infill stratigraphy

The coring transect across the morphological depression revealed a c. 500 m wide sedimentary basin. It contains a complex succession of

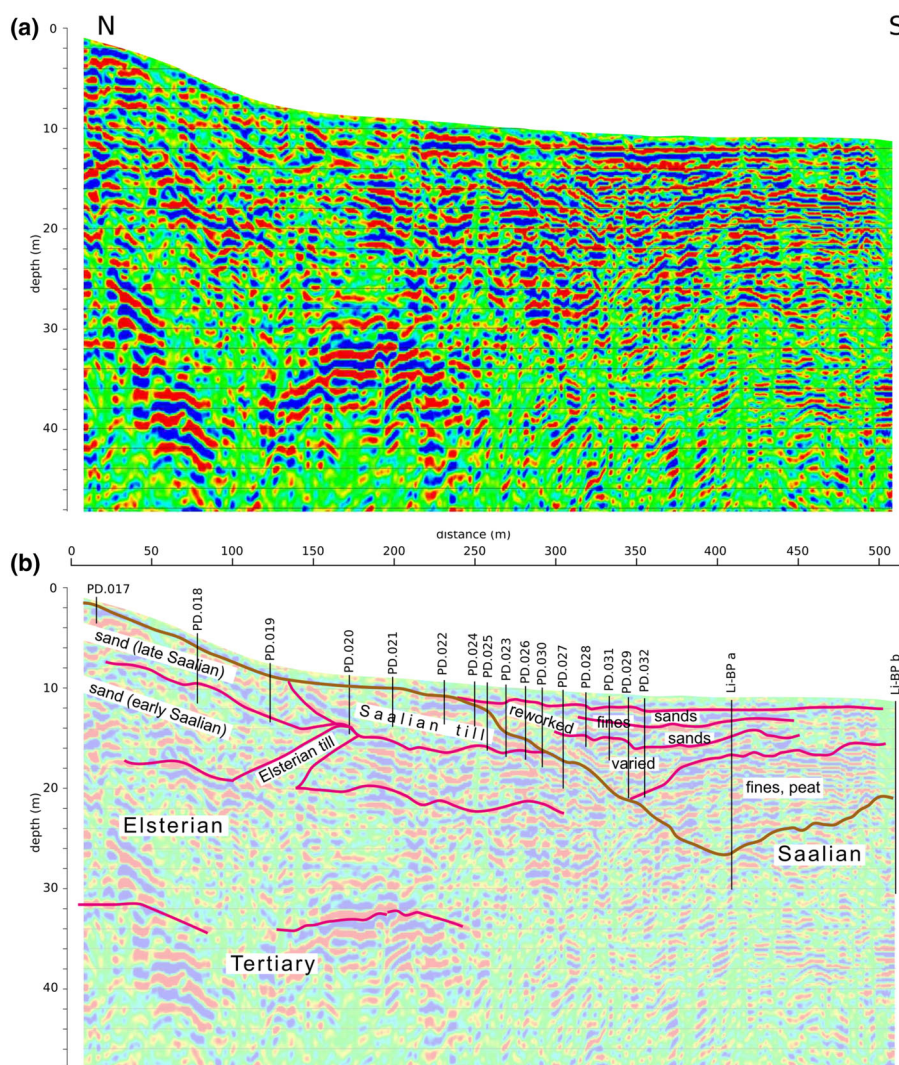


FIGURE 5 (a) S-wave seismic profile with (b) interpretations



FIGURE 6 (a) Section 450 cm to 650 cm of core PD.030 with segments chosen for luminescence samples and the stratigraphic position of the artefacts. (b) Photographs of the artefacts LIA-86 and LIA-187, obtained from this core

stacked organogenic, sandy, silty and loamy deposits, with varying hydromorphic features, and contents of organic matter and carbonates (Figure 4). For this study, we exclusively focus on the Eemian sediments; post-Eemian successions will be targeted in future studies. Our descriptions and correlations of sediment units in the field are based on three general chronological presumptions:

- The basin was created during the Saalian-Eemian transition (cf., Fränzle, 1988; Garleff & Leontaris, 1971, and Method S1).
- Organic-rich layers relate to temperate intervals (interglacials/interstadials), whereas less organic clastic deposits represent glacials and stadials.
- Following (i) and (ii), the lowermost organic-rich limnic-paludal basin infill is assumed to be of Eemian age (Veil et al., 1994).

To achieve the best spatio-temporal coverage and the utmost information for this time-period, the pollen samples were distributed across all assumed Eemian deposits along the transect (Figure 4).

The S-wave seismic profile and the borehole information complement each other well and their mutual interpretation allows sediment-body boundaries to be laterally extended (Figure 5b). According to geomorphic position, thickness and characteristics of the post-Saalian sediments, we divided the borehole transect into three different sections: (i) the exterior upper slope, located outside of the basin ('exterior'), (ii) the steep northern flank of the basin ('northern flank') and (iii) the bottom and shallow southern flank of the basin ('bottom section') (Figure 4). Next, the respective lithological and seismic properties of these three sections are presented and described.

4.1.1 | Exterior upper slope (cores PD.017 to PD.022)

The exterior part of the transect encompasses the cores PD.017 to PD.022 (Figures 4, 5b and Supporting Information Figure S4). They mainly expose Saalian glacial deposits, as also confirmed by the geological map (1:25000, number 3033 [Merkt, 1975]) and a nearby geological cross-section of the Öring (Figure S1). Between cores PD.017 and PD.019, the steeper slope corresponds with non-calcareous, well-stratified fine to coarse Saalian glaciofluvial sands. These are characterized by mildly reflective and discontinuous seismic reflectors that dip southwards in unison with the current topography (Figure 5). Southwards from core PD.019, the topography flattens out and Saalian glacial tills, partly associated with glacio-limnic clays appear. Their thickness increases to the south and reaches > 5 m in cores PD.021 and 022. Even at such depths, the tills and clays are deeply weathered and decalcified. In PD.020, at 420 cm depth, an Elsterian till was encountered, distinguished from the Saalian tills mainly by its blackish-grey colour caused by lignite-uptake of the Elsterian glaciers (cf. Voss, 1981, Figures S1 and S4). Seismic reflections suggest that it represents an intercalation rather than the surface of a continuous Elsterian sediment body (Figure 5). Other than this, the presumed top of the Elsterian is continuous and highly reflective, but the respective till quickly loses reflectivity downwards, so that its base is near transparent in the seismic data. Seismic reflectors of this sediment are generally short, less than 20 m in length. Similar to the Saalian sediments, the Elsterian material dips in accordance with the present topography. The upper Tertiary boundary is interpreted to occur below 30 m

depth, where strong reflections start. These reflectors are of long wavelength, continuous over 40–100 m and they slightly arcuate upwards. This surface can only be followed to 250 m distance in the seismic profile; it fades out directly underneath the infilled basin above (Figure 5). The glacial sediments in the exterior section are overlain by shallow (< 2 m), gravelly Weichselian slope deposits (cf., Veil et al., 1994), generated by alternating solifluction and slope wash processes. These layers continue to form the uppermost part of all the cores along the rest of the borehole transect.

4.1.2 | Northern flank (cores PD.024 to PD.027)

Both, seismic and borehole data document a basin opening up to the south, which created accommodation space to trap complex post-Saalian deposits. The base of this basin is formed by a rather steep, south-facing disconformity. In the seismic profile, this erosive surface is highly reflective itself and correlates very well with the lithology of the boreholes, showing the transition from glacial sediments to fine-grained deposits. This section includes the stretch between cores PD.024 and PD.027, while the neighbouring cores PD.028 and PD.031 are too shallow to penetrate Eemian or even Saalian glacial sediments. In cores PD.024 to PD.023, the Saalian glacial till, found in the previous exterior section still underlies the infill deposits. However, it thins out to the south until it vanishes from core PD.026 southwards, presumably due to erosion. The lowermost organic-rich layers were interpreted as Eemian and are aligned with the disconformity, and hence they dip at a sharp angle. These layers comprise 25 to 35 cm-thick, strongly organic sands (half-bog soils), and certainly developed due to water-logging or a high groundwater table. This material is devoid of carbonates, with the decalcification boundary mostly situated directly underneath (Figure 4). An exception is the loamy segment 370–400 cm in core PD.023. It is much less humic and decalcification has affected and weathered 60 cm of the underlying Saalian till, as well. This segment is thus described as a terrestrial topsoil horizon, seemingly unimpaired by hydromorphic processes during its development (see Method S5).

The assumed post-Eemian deposits show alternating sequences of peat/muds and well-bedded medium sands, which are interpreted as niveo-fluvial slope deposits (cf. Veil et al., 1994). Chaotic seismic reflections between cores PD.023 and PD.027 ('reworked' in Figure 5b) may correspond with higher-energy short-distance reworking of sediments in the middle part of these cores. The occurrence of this phenomenon is congruent with the present morphological extent of the second order alluvial fan and was therefore cautiously attributed to its formation (Figures 3b,c and S3).

4.1.3 | Bottom section (cores PD.029 to Li-BPd)

This section encompasses the flat bottom and the shallow north-facing slope of the basin. Its lower boundary shows only faint reflectivity in this part, but can still confidentially be correlated with the borehole information (Figure 5b). The lowermost fine-grained and organogenic deposits directly above the Saalian basement differ from those on the opposite flank with regards to thickness and properties, mainly due to different geomorphological and hydrological parameters

in a more aquatic setting with higher accommodation space. With a total thickness of 6 m, core Li-BPa captures the longest and most complete, supposedly Eemian sediment suite. At its base (17.3 to 15 m), a calcareous, clayey-silty sequence is found. Given the high amounts of organic matter and ubiquitous mollusk shells, these layers are classified as Eemian lacustrine sediments. The fines grade upwards into organic-enriched lake marls with intercalating detrital muds that are found between 15 and 13.4 m. Above (between 13.4 and 12.4 m), the marls appear as pure primary carbonate precipitations. These lake sediments are overlain by a 60 cm thick decalcified forest peat with large wood fragments. Upwards, the peat interfingers with calcareous silt, which eventually becomes dominant. Being in superposition of the lowest peat in the record, this silt might already mark the transition to the first Weichselian interstadial.

In cores PD.029 and Li-BPb to Li-BPd, quite similar sequences of peat and lake marls with varying thicknesses were observed across the suggested Eemian zone. However, towards the south, the basal silts known from Li-BPa are gradually substituted by sandy deposits. In addition, the peat in the southernmost core (Li-BPd) lacks wood fragments, implying a possible disparate formation process/time (see Section 5.1). Notably, most bottom deposits of this section are highly calcareous, except for the forest peat layers in cores Li-BPa and PD.029. This suggests a more acidic environment during the peat development. Within this section of the basin, the seismic data show high-amplitude reflectors up to 200 m long, where organogenic deposits alternate with silt in the lower parts and stratified sands in the upper parts of the cores. Especially in the fines and peat deposits, this alternation results in continuous, horizontal and highly reflective layers. However, north of core Li-BPa, oblique, northwards-dipping seismic phases and an area of less well-structured reflections ('varied' in Figure 5b) indicate an incision or reworking phase. This is corroborated by findings in core PD.032. Here, despite its close proximity to core PD.029, deep peat deposits are absent, even at 11 m depth. Instead, we encountered the same silty deposits that were documented above the forest peat in Li-BPa and that we interpreted as Early Weichselian. This suggests the peat had been eroded by this renewed incision.

Unfortunately, the structure below the basin is not visible in the seismic data. The boreholes, however, clearly and consistently show two Saalian calcareous glacial tills. These are detached from one another by thick bodies of glaciofluvial sands and show a basal glacio-lacustrine clay around an absolute elevation of 0 to 2 m above sea level (a.s.l.) (Figure 4, cf. Figure S1). Only at the position of core Li-BPa, these tills are missing, indicating erosion upon the formation of the basin. Nevertheless, it is apparent that the top of the upper till (visible in cores Li-BPb to Li-BPd and PD.027) created a slight depression, even before the basin formed.

4.2 | Palynology and biostratigraphy

Of the 25 analysed samples, two showed a very low pollen abundance (samples 19 and 23) and were hence rejected from interpretation. The remaining samples are presented and described in Table 1 and Figure S5. For the subdivision of the Eemian and the correlation of the pollen data, we refer to the description of Eemian pollen zones for north-western Germany by Menke and Tynni (1984) and to Behre

TABLE 1 Results of palynological analysis and geochemical proxies (C_{org} , C/N-ratio)

Sam-ple	Core	Depth (cm)	Lithology	Main pollen characteristics	Pollen zones/biostratigraphy (Menke & Tynni, 1984)	AP (%)	C_{org} (%)	C/N
23	PD.023	370–390	humic loam	pollen-sterile	–	–	0.62	8.0
1	PD.026	400–410	sandy mud	poor in pollen, only <i>Betula</i>	tentative WF II	–	1.31	18.0
2	PD.026	480–490	peat	<i>Pinus</i> 88%, <i>Betula</i> 8%	E II/(E VII)	97.0	15.6	16.1
25	PD.027	730–765	half-bog peat	<i>Quercus</i> - <i>Carpinus</i> forest to <i>Pinus</i> - <i>Picea</i> (<i>Abies</i>) forest*	EV to E VI	–	7.41	23.7
3	PD.030	510–525	mud	<i>Betula</i> , <i>Pinus</i>	tentative WF II	94.4	1.23	13.9
4	PD.030	525–540	sandy peat	50% AP, 50% NAP, heliophytes	tentative WF I	54.5	13.4	15.5
24	PD.030	620–630	half-bog peat	<i>Corylus</i> , <i>Tilia</i> , <i>Carpinus</i>	E IV to E V	97.0	4.92	25.6
5	PD.029	745–770	humic silt/silty mud	Reworked pollen, glaciolimnic genesis, similar to sample 6	indifferent, (reworked)	88.5	6.63	17.6
6	PD.029	882–1,030	forest peat	<i>Pinus</i> , <i>Picea</i> , <i>Abies</i> , <i>Carpinus</i> , <i>Alnus</i>	EV to E VI	100	29.5	21.7
7	Li-BPa	900–1,025	humic silt	reworked from preceding Eemian PZ and glaciolimnic material	deposited during E VII/WF I?	97.2	9.8	20.7
8	Li-BPa	1,060–1,100	forest peat	bad preservation (<i>Pinus</i> , <i>Betula</i> , <i>Picea</i>)	E VI (?)	96.0	19.5	24.6
9	Li-BPa	1,100–1,140	peat	<i>Pinus</i> , <i>Picea</i> , <i>Abies</i>	E VI	98.8	–	–
10	Li-BPa	1,340–1,415	lake-marl	<i>Pinus</i> , <i>Betula</i> , <i>Corylus</i> , <i>Quercus</i>	E IV	97.8	–	–
11	Li-BPa	1,500–1,625	silt, mollusks	reworked pollen, glaciolimnic genesis, similar sample 8	late Saalian/early E I?	89.9	–	–
12	Li-BPb	640–780	silt	reworked pollen from PAZ E6 and glaciolimnic input	reworked from late Eemian?	93.4	–	–
13	Li-BPb	800–850	peat	<i>Pinus</i> , <i>Picea</i> , <i>Carpinus</i> , <i>Abies</i>	E VI	97.4	–	–
14	Li-BPb	930–985	humic marl	<i>Corylus</i> peak, <i>Tilia</i> , <i>Quercus</i>	E IVb	99.7	–	–
15	Li-BPb	985–1,090	silt	<i>Corylus</i> , <i>Quercus</i> , <i>Carpinus</i> , <i>Betula</i> (50% local?), heliophytes, some reworked from glaciogenic input	tentative E IV	86.3	–	–
16	Li-BPc	600–640	silt	<i>Pinus</i> , <i>Picea</i> , <i>Abies</i>	E VI	97.5	–	–
17	Li-BPc	640–700	peat	<i>Carpinus</i> , <i>Picea</i> , <i>Corylus</i>	EV	99.2	–	–
18	Li-BPc	760–825	humic marl	<i>Carpinus</i> , <i>Corylus</i> , <i>Quercus</i> , <i>Ulmus</i> , <i>Tilia</i> , <i>Taxus</i>	EV	100	–	–
19	Li-BPc	870–900	humic sand	poor in pollen	not determined	–	–	–
20	Li-BPd	480–510	sandy peat/detritus	bad preservation, 60% <i>Pinus</i> , 27% <i>Betula</i>	E VII/(WF IIb)	90.1	–	–
21	Li-BPd	570–580	organic mud	<i>Carpinus</i> , <i>Alnus</i> , <i>Tilia</i> , <i>Picea</i> , few reworked pollen (glaciolimnic origin)	EV	96.8	–	–
22	Li-BPd	620–680	humic sand	<i>Corylus</i> peak (47%), <i>Quercus</i> , <i>Alnus</i> , <i>Taxus</i>	E IVb	96.6	–	–

AP, percentage of arboreal pollen; C_{org} , organic carbon; C/N, carbon/nitrogen ratio.

and Lade (1986). Local references are previous biostratigraphic results of an Eemian/Early Weichselian sequence from Lichtenberg (Veil et al., 1994) and yet unpublished data acquired by the authors. The amount of arboreal pollen is clearly above 85% for all samples but sample 4 (54.5%). Classification for nearly half of the samples was straightforward, based on the unambiguous taxa assemblage (samples 8–9, 13–14, 16–19, 21–22) (Table 1). The results completely confirm our sampling design and the preliminary interpretation of the deepest organogenic deposits as Eemian (see Section 4.1). However, our dispersed sampling approach in some instances made the assignment of certain palynomorph spectra to distinct pollen zones challenging, as longer sequences are lacking. In these cases, we proceeded as outlined in Method S2.

4.3 | Luminescence ages

The two pIRIR₂₉₀ ages are presented in Table 2 along with the 1σ errors and the overdispersion (OD) values. Sample L-EVA 2027 was taken from an unstratified sandy layer directly above an Eemian half-bog, and has an age of 104.6 ± 10.5 ka and an OD value of $26.6 \pm 0.8\%$. Sample L-EVA-2026 taken from a well-bedded sand at a higher stratigraphic position gave an age of 108.4 ± 17.0 ka and an OD of $33.3 \pm 1.4\%$. The D_e -estimation and the robustness of the ages are discussed in Method S4.

4.4 | Geochemical proxies

The values for C_{org} and C/N confirm the field-based sedimentological findings (Table 1). The C_{org} varies between 0.62 (sample 23) and 29.5% (sample 6), while the C/N-ratio ranges between 8.0 (sample 23) and 25.6 (sample 24). Interpretations of these values with respect to field descriptions can be found in Method S5.

4.5 | Archaeological finds

In the sandy Eemian half-bog of core PD.030 (6.20 m depth), we recovered a longitudinal broken flake of Baltic flint with characteristics of a knapped lithic artefact (LIA-86, Figure 6b). The find layer is delimited by loamy Saalian sediments below, and complex, presumably pedogenetically-altered Weichselian sands above. To validate the hypothesis of a potential Eemian find concentration, we retrieved four additional cores within a 2 m radius. In this way, we recovered another flake (LIA-187, Figure 6b) and a number of undetermined small chips and fragments. In terms of a specific Middle Palaeolithic technology, the flakes are rather undiagnostic. The limited sample size of $n = 2$ prevents any interpretation or attribution to a specific techno-complex. LIA-86 has a plain dorsal surface, and due to the

heavy dark patination, it is not clear whether this is an artificial surface resulting from a former flake removal or a natural surface. Additionally, the distal dorsal part has small recent damage from the drill. However, the right lateral edge consists of the former core edge created by earlier flake removal from the core. The striking platform is plain and not faceted. Flake LIA-187 has a natural dorsal surface, but shows an irregular retouch on the right lateral edge. The striking platform is an irregular natural surface.

Some of the smaller fragments are highly weathered due to the humic and acidic sedimentary environment, so their artificial origin is ambiguous. However, based on the occurrence of two unequivocal artefacts in juxtaposition, together with various flint fragments and chips, and the parallel presence of only a few other gravel-sized rocks, we infer a veritable occupational layer to exist in the half-bog > 6 m below the surface.

5 | DISCUSSION

5.1 | Landscape evolution model

5.1.1 | Late Saalian

The rapid disintegration of the Late Saalian Warthe stage ice-sheets at around 135 ka produced large amounts of melt-out run-off and a progressively increasing availability of free water in the hydrological cycle (Lambeck et al., 2006). In contrast to quickly rising precipitation values, vegetation developed with a certain time lag (Helmens, 2014) and was rather sparse (Menke & Tynni, 1984), leaving the surfaces prone to sediment erosion and redeposition for some time. This was amplified by sustaining (discontinuous) permafrost that hampered infiltration in favour of overland flow (Rowland et al., 2010). In the central Öring hills, the landscape dynamically responded to this impulse with linear erosion, creating the first order dry valleys that cut through Warthe stage glacial deposits, testifying to valley formation after the Warthe glacial maximum (Merk, 1975; Figure 3; Method S1). Two first order alluvial fans, associated with this linear erosion can be identified at the transition of the southern Öring and the Salzwedel Palaeolake basin (Figure 3b). The eastern fan shows deep incision oriented due east. This incision is recognized both as a slight depression in the modern topography (Figures 3c and S3) and in the sediment logs of the borehole transect, where the basal Saalian tills were eroded prior to the Eemian (Figure 4). We argue that this incision can only be explained by fluvial downcutting in the adjacent Elbe River valley, being the base level of our study area. Fluvial incision is reported for the Saalian-Eemian transition in the lower Elbe reaches (Averdieck, 1976; Ehlers, 1990; Grube et al., 1976) and for several other central European rivers, and thought to have been triggered by the spilling-over of ice-dammed lakes in the downstream areas (e.g., De Clercq et al., 2018; Winsemann et al., 2015). Downcutting in

TABLE 2 Results of pIRIR₂₉₀ dating, including D_e -values, calculated ages, the used age model, overdispersion (OD) and the number of aliquots passing the rejection criteria

Lab.-ID (L-EVA)	D_e (Gyr), 1σ	Age (ka), 1σ	Age model	OD (%)	Number of aliquots
2026	264.4 ± 36.4	108.4 ± 17.0	minimum age	33.3 ± 1.4	17
2027	295.2 ± 19.8	104.6 ± 10.5	weighted mean	26.6 ± 0.8	24

the Elbe valley would have lowered the local base level required for this incision within the alluvial fan, thus creating the shortest continuous drainage channel from the dry valley in the southern Öring to the Elbe valley by retrogressive erosion (Figures S2 and S3B). The channel passage between Öring and Lemgow that had previously formed as an Elsterian tunnel valley (Voss, 1981) would have been reactivated and overdeepened by that retrogressive (fluvial) erosion. By contrast, the western alluvial fan (Figure 3b) lacks signs of posterior erosion. Therefore, the local base level must have remained untouched during and after fan formation, which could have been caused by the longer distance to the Elbe River valley. To sum up, the studied sediment basin most likely is part of a c. 7 km long palaeovalley system that drained the southeast Öring towards the ice-marginal valley of the River Elbe (Figures 3b, S2 and S3). Based on its irregular shape and course and lacking Saalian tills at the drilling bases, possible alternative interpretations of the basin as a large Saalian kettle hole or tunnel valley are provisionally rejected (e.g., Behre & Lade, 1986; Turner, 2000).

5.1.2 | Saalian-Eemian transition to early Eemian (PZ E I and PZ E II)

Subsequently, the lower areas of the palaeovalley system, including the incised basin within the alluvial fan, partially filled up with water and accommodated an elongated fingerlake. The reason for the

topographic disconnection of the initial palaeovalley from the Elbe River valley is not yet clear, nor is the position of the blockage. We suggest that slope deposition might have obstructed the channel in the narrow passage between Öring and Lemgow. The presumed extent of the lake (size c. 1.3 km²), depicted in Figure 3(b) is based on our own data and information from the borehole database of Lower Saxony (<https://nibis.lbeg.de/cardomap3/>). At the bottom of this lake, 2 m of the first clayey and then slightly humic silty lacustrine deposits were accumulated (Figure 7a). Concomitantly, on the slope, a half-bog formed just above or even within the capillary fringe of the (ground) water table. This allows to approximate the upper and lower boundaries of the water body, that is a water depth of ~12 m for PZ E II (Figure 7a).

This pre-temperate phase at the onset of Eemian, as defined by Turner and West (1968), is characterized by an expansion of *Betula* (tree-birches) in pollen zone (PZ) E I in northern Germany. It was followed by a strong increase of *Pinus* (pine) dominating in the succeeding *Pinus-Betula* PZ E II (Menke & Tynni, 1984). In contrast to the previous Holsteinian interglacial, during this initial expansion of boreal forest, *Picea* was absent, and vegetation had not yet densely covered the immature soils. Due to the dynamic depositional and erosional processes at the onset of the Eemian in the study area, PZ E I and PZ E II are nearly missing in the transect, with the likely exceptions of samples 2 and 11 (Table 1; Figure 4). Likewise, both initial Eemian pollen zones were also missing in the

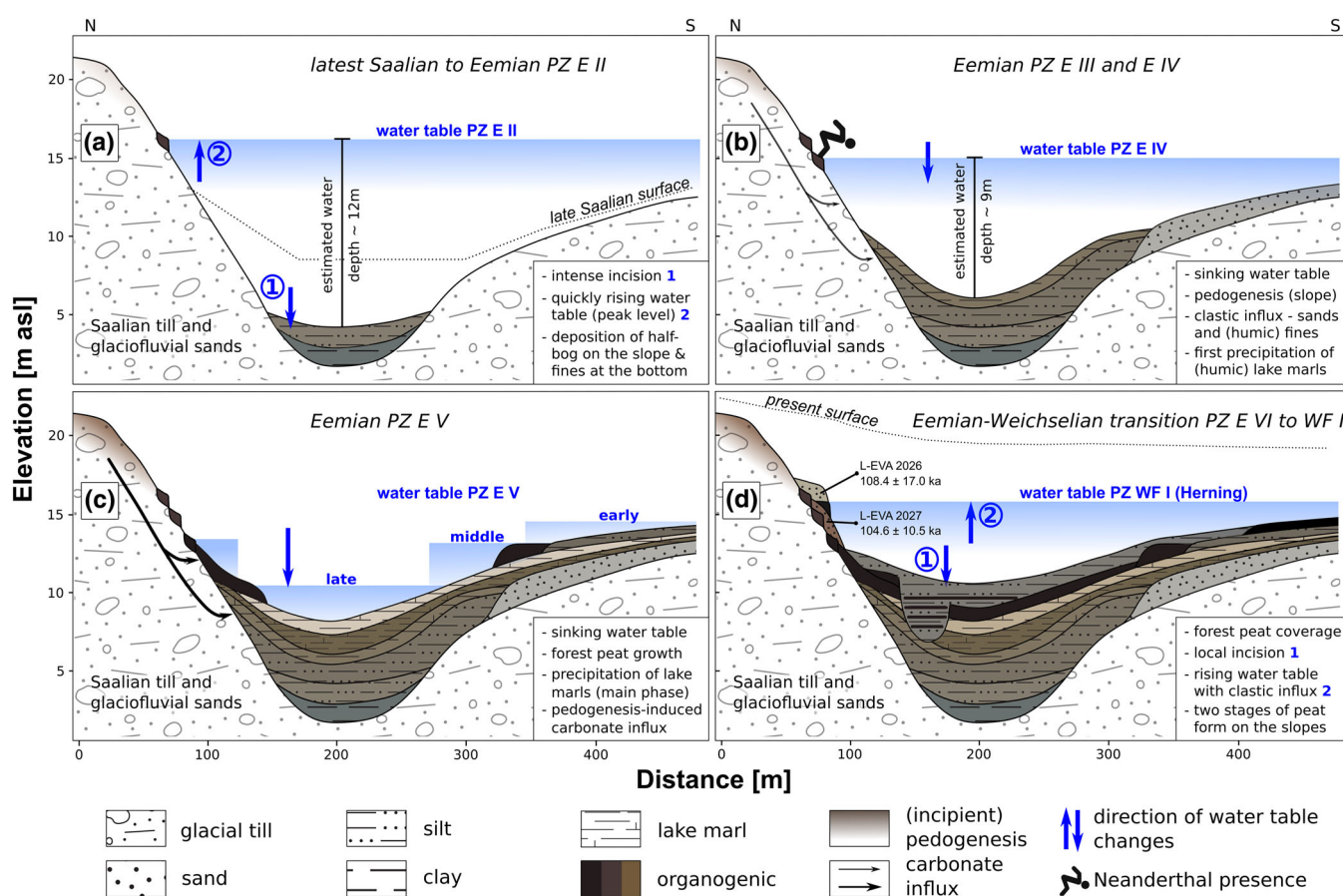


FIGURE 7 Diachronic landscape evolution model of the study area that depicts the sedimentary and hydrological changes throughout the Eemian in four phases (following the classification of the Eemian cycle by Turner and West [1968]). PZ E I to E VII – Eemian pollen zones. PZ WF I – First Weichselian Stadial (PZ after Menke and Tynni [1984])

neighbouring palynological record formerly investigated by Veil et al. (1994).

5.1.3 | Early-temperate Eemian (PZ E III and E IV)

At the lake bottom, in continuation of the previous phase, more humic silts accumulated, grading upwards into (humic) lake marls. The latter testify to increasing landscape stability with pedogenesis in the exterior section, where decalcification and weathering of the Saalian tills must have led to carbonate-rich groundwater flow that caused the lake marl precipitation within the fingerlake (Figure 7b). This relationship has been described for various sites in northern Germany in previous studies (cf., Menke, 1992). On the steeper northern flank, half-bogs formed at a lower topographic elevation than during the previous phase. This documents a decreased water table compared with PZ E II. Together with the lake bottom sediments, this marginal facies allows for the estimation of the water depth to ~9 m (Figure 7b). Furthermore, a coeval waterside Palaeolithic encampment was inferred from artefact finds within the half-bog (Section 5.3). Also during this period, the deposition of calcareous coarse sand occurred on the shallow southern slope of the fingerlake, recorded in the cores Li-BPc and Li-BPd (Figures 4 and 7b). The presence of this coarser deposit seems to indicate higher-energy sedimentation compared with the dominant lacustrine sediments of that phase. Potentially, these sediments are of fluvial, colluvial or beach deposit character. Alternatively, the coarse sands might also have been mobilized by trampling animals in search for water, scarring the vegetation on their way (Butler et al., 2018).

The first deciduous taxa to expand were *Ulmus* (elm) and *Quercus* (oak). These rapidly became dominant and were characteristic of the *Pinus-Quercetum* mixtum (PZ E III) in the lower part of the early-temperate Eemian phase (Turner, 2000). Subsequently, a strong increase of *Corylus* (hazel) marks the transition towards pollen subzone E IVa (*Quercetum*-mixtum-*Corylus*). Pollen assemblages and preservation of a few samples hampered a clear division into subzones, resulting in a general assignment of those samples to PZ E IV (Table 1). The following pollen subzone E IVb, dominated by *Corylus* with *Tilia* (lime) and *Taxus* (yew), was however identified in some samples of the transect (Table 1). The Palaeolithic artefacts (core PD.030) derive from a late phase of PZ IVb transitioning into PZ V, when *Carpinus* (hornbeam) started to expand and *Corylus* declined (Table 1). The zonal vegetation, first rich in hazel, followed by lime, oak, elm

and yew, had apparently well colonized and stabilized the terrestrial soils in the vicinity of the site. Indicators for a temporally higher groundwater level and gleyic, swampy conditions are fern spores of the polypodi family (Polypodiaceae). Frequently, also *Typha latifolia*-type (cattail) and *Sparganium*-type (bur-reed) pollen occur. These wetland/aquatic plants usually border lakes, ponds or streams. The azonal vegetation of PZ E IV in Lichtenberg is furthermore characterized by minor, yet constant occurrences of Poaceae (grasses) and terrestrial herbs. These might point to a patchily-forested site, but could also be caused by trails created by trampling animals visiting open water sources.

5.1.4 | Late-temperate Eemian (PZ E V)

This phase was characterized by its distinct landscape stability and soil formation in the exterior, induced by a dense vegetation cover (Figures 7c and 8; Table 1). Apart from a thin veil of silt that was deposited at the southern flank during the early phase, no further clastic sedimentation can be recognized in the basin over some thousand years (cf., Müller, 1974). The intensive lake marl formation at the lake bottom and the southern slope distinctly points to a period of most pronounced decalcification and pedogenesis in the exterior, causing a high carbonate influx into the lake, and to generally warmer climatic conditions enabling carbonate precipitation during summer. Eemian decalcification and weathering of Saalian tills can exceed 4 m thickness in northern Germany, and was also observed in our cores PD.022 to PD.025 (Figures 4 and S4). Thus, soil formation is assumed to have been more intense than in comparable Holocene soils on Weichselian tills (Roeschmann et al., 1982; Stremme et al., 1982; Stephan, 2014). Lake marl deposition, as an indicator of intense soil formation during PZ E V has also been recognized in other central European and south Scandinavian sites, such as Lehringen (Thieme & Veil, 1985), Gröbern (Mania et al., 1990), Hollerup (Björck et al., 2000) and the Oderbruch basin in northeast Germany (Lüthgens et al., 2011).

During PZ E V, the water table gradually decreased at the study site. This is demonstrated by a half-bog on the steep south-facing slope, and two deviating lower levels of forest peat at the channel bottom and the shallow north-facing slope, respectively (Figure 7c). The upper peat at the basin bottom and the half-bog on the northern slope are situated at almost the same elevation. Since both require

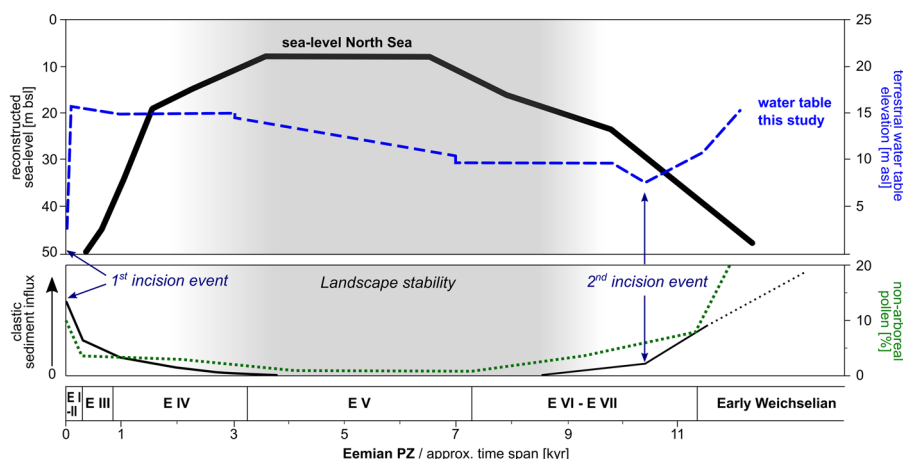


FIGURE 8 Upper panel – water table approximations of our study (blue) and Eemian North Sea-level progression (black) according to Zagwijn (1996) for comparison. Lower panel – semi-quantitative estimate of clastic influx and non-arboreal pollen through time at our study site. Horizontal scale for both panels – pollen zonation according to Menke and Tynni (1984), relative duration of the Eemian interglacial and the individual pollen zones after Müller (1974)

similar moisture conditions for their formation and half-bogs are regarded as the incipient stage of peat development, the geomorphic position plausibly determined which types of organogenic sediments were formed (cf., Göttlich, 1965). Only flat and slightly sloping areas facilitated peat growth, whereas on steeper slopes, the shallow water zone was too narrow for peat formation and half-bogs prevailed instead. Estimating the water depth is challenging for this phase, because the marginal facies as a counterpart for the subaquatic sediments at the basin bottom is lacking for the better part of this phase. However, the water depth undoubtedly decreased, likely from about 7 m in the early to about 2 m at the later phase. During this late-temperate phase, the vegetation changed from *Corylus*, *Tilia*, *Quercetum-mixtum* to *Carpinus*-dominated forests. The more articulate predominance of AP over the NAP in the pollen records points to more densely vegetated areas in comparison to previous PZ E IV (Figure 8; Table 1). In combination with the sedimentological results, increasing values of *Alnus* (alder) indicate the expansion of local fen woodland. Furthermore, a decrease of Polypodiaceae and aquatic phanerogams versus an increase of taxa of the green algae genus *Pediastrum* might point to a change in the water trophic state (Turner et al., 2014).

5.1.5 | Late Eemian and Eemian/Weichselian transition

In PZ E VI, the water depth was further reduced until it was low enough for forest peat development at the bottom of the drying-out lake (Figure 7d). Hydrochemical conditions are assumed to have been rather acidic, as is implied by the non-calcareous forest peat in cores PD.029 and Li-BPa, enveloped by highly calcareous sediments above and underneath. Strong acidification during the later Eemian has also been reported by Roeschmann et al. (1982) and Menke (1992), who ascribed this effect to the decrease of thermophilous taxa and the establishment of conifer dominance in combination with carbonate-depleted substrates. In contrast to the nearby sequence in Veil et al. (1994), the deposits of the later PZ E VI and PZ E VII reflect changes in vegetation from the *Pinus-Picea-Abies*- to the *Pinus*-zone. This phase in our record is characterized by high percentages of reworked pollen, indicating the end of the long-lasting stability phase (between PZ E IV to E VI) and a resumption of higher geomorphic activity. Accordingly, this is supported by renewed erosion at the basin bottom, evident in core PD.032 and seismic data (Figures 4, 5 and 7d and Section 4.1). Similarly to the major first erosion during the Saalian-Eemian transition, we assume fluvial incision in the neighbouring Elbe River valley that retrogressively affected the lake basin by lowering the local base level. Incision during that time is known for many European rivers (Antoine et al., 2007; De Clercq et al., 2018; Gibbard & Lewin, 2002; Winsemann et al., 2015). In Lichtenberg, the subsequent deposition of several metres of humic silts indicates a progressively rising water table that fostered peat formation at a more elevated position on the shallow southern slope. Thus, a temporary stagnation in PZ E VII is inferred (Figure 7d). The following water level rise in the transitional period to the Herning Stadial (~MIS 5d) resulted in further siltation at the bottom of the restored fingerlake and in the aggradation of sandy slope deposits on the northern flank. Eventually, at high-stand conditions, a Herning-time sandy peat

developed and interfingers with these sands (PD.030). These deposits are bracketed by luminescence ages of 105 ± 10 and 108 ± 17 ka (Section 4.3, Figures 6a and 7d). This is in agreement with the end of the Eemian interglacial, as dated by Lüthgens et al. (2011) to 108.9 ± 7.8 ka in northeast Germany. The presence of this peat points to a broader shallow-water zone on the northern flank compared to the early/mid-Eemian, when only half-bogs formed there. Unlike previously assumed by us (Section 4.1), peat growth during the Herning Stadial also means that organogenic deposits did not exclusively form during more temperate intervals. Instead, the climate throughout the Early Weichselian seems to have been warm enough to promote peat formation even during the Stadials, with the main limiting factor possibly being moisture rather than temperature at these latitudes. Similar suggestions have been made by Caspers et al. (2002) and Vandenberghe and van der Plicht (2016) for the MIS 3 in central Europe. The Herning-time sandy slope deposits on the northern flank, locally restricted to cores PD.026 and PD.030 (Figure 4, below pollen samples 1 and 3), tentatively represent an incipient stage of the formation of the second order alluvial fan (Figures 3c and S3).

5.2 | Synopsis of Eemian landscape dynamics

Three semi-quantitative proxies derived from our data give complementary information on the geomorphic activity and the hydrological development throughout the Eemian in the study area (Figure 8): Clastic sediment influx, the water table of the fingerlake (rather than its estimated depth) and the NAP. The latter have widely been used for a long time to approximate landscape openness in various studies (e.g., Faegri et al., 1989). Openness in turn, is known to be closely linked to the vulnerability of landscapes towards sediment erosion (Rohdenburg, 1970). Although the relationship between NAP and openness is complex and non-linear (e.g., Sugita et al., 1999), an NAP-based assessment of vegetation density can be reliable if additional parameters are consulted and relatively small surface areas are considered (cf., Favre et al., 2008).

In Lichtenberg, we observe a clear relationship between clastic sediment influx and NAP: Two phases of distinct geomorphic activity are indicated by higher values of both parameters. Surprisingly, even NAP amounts as low as c. 5% already correlate with considerable sediment input (Figure 8). These sediments were most likely provided by slope erosion from the shores of the fingerlake, or alternatively by deflation in its surroundings (cf., Schokker et al., 2004). The first activity phase already began in the late Saalian with the melt-out of the Warthe stage ice sheets and the dissection of the Öring by the first order dry valleys. It terminated not before Eemian PZ IV, roughly coinciding with the establishment of close deciduous woodlands (cf., Caspers et al., 2002). The second activity phase started in E PZ VI/VII and continued well into the Herning Stadial (Figure 8). Notably, both phases share common properties:

- i. They correspond to major climatic transitions at the beginning and end of the interglacial, when the sedimentary, hydrological and vegetational regimes adjusted to changing climatic conditions.

- ii. They broadly concur with local incision events, tentatively initiated by fluvial downcutting in the neighbouring Elbe River valley. Both incision events were followed by a rapid rise in lake level, possibly as a consequence of incomplete forests, leading to high effective precipitation and intensive surface run-off (cf., Behre et al., 2005; Börner et al., 2018; Fränze, 1988; Kołaczek et al., 2016; Schokker et al., 2004; but see Mirosław-Grabowska, 2009 for late Eemian desiccating basins in Poland).
- iii. The vegetation during these phases is characterized by dominant boreal woodlands. These are nowadays known to be fire regimes and to be driven largely by disturbance and selective scarring of the plant cover (cf., de Groot et al., 2013), which fosters geomorphic activity.

A prolonged period of extensive landscape stability in between these two activity phases lasted from late PZ E IV to PZ E VI, equivalent to about 6000 years (Müller, 1974). Similar observations are known from the Roer Valley Graben, the Netherlands (Schokker et al., 2004). We detected no clastic sediment deposition during that time. Instead, widespread lake marls testify to densely vegetated, stable surfaces in the area, and dominating decalcification and pedogenesis on the Saalian substrates. This agrees with the NAP that reach their lowest average values of < 2% in this part of our record. Dense vegetation however, also induces high evapotranspiration rates, accompanied by dropping (ground)water levels (Helmens, 2014; Larsen et al., 2020). Accordingly, and despite an oceanic climate at that time (Kühl et al., 2007), the water table of the fingerlake was gradually dropping during the mid-Eemian. Yet, it was still high enough to allow peat and even lake marl deposition. In contrast, at many other study sites in central Europe, lacking sedimentary remains from PZ E IV and V indicate complete desiccation (e.g., Schokker et al., 2004, and references cited therein). In Lichtenberg, the groundwater levels surpassed the surface elevation, owing to the relatively large accommodation space, provided by the initial erosion of the palaeochannel that later hosted this fingerlake.

Contrary to our findings of a stable landscape, various studies described a mid-Eemian cold episode at different sites (e.g., Field et al., 1994; Helmens et al., 2015; Seidenkrantz et al., 1995). Such a climatic deterioration would have decreased the density of forest cover and thereby have allowed erosional and associated depositional processes. This assumption cannot be confirmed by the presented Lichtenberg record (cf., Cheddadi et al., 1998; Kühl et al., 2007; Kupryjanowicz et al., 2018).

5.3 | The middle Palaeolithic finds of Lichtenberg in the context of established Eemian occupations

The archaeological finds from late PZ E IV in core PD.030 define Lichtenberg as the northernmost Eemian Palaeolithic site narrowly ahead of Lehringen, Lower Saxony (Nielsen et al., 2015; Thieme & Veil, 1985). This spatial pattern may however be biased, as most Eemian occupations are former lake sites that are currently often buried below several metres of sediments. Therefore, most sites were primarily recovered during lignite mining in central Germany (see references to the sites mentioned later). A recent geographic analysis (Nielsen et al., 2019) has shown that Neanderthals could potentially

not have reached areas much further north, since the higher Eemian sea level compared with today disconnected Jutland and southern Scandinavia from northern Germany by a marine channel (Larsen et al., 2009). Furthermore, Weichselian glaciers have likely devastated possible evidence for occupation in (southern) Scandinavia.

A cluster of Eemian archaeological sites is known from central Germany (Figure 1): Repeated Neanderthal occupations in Neumark-Nord, Saxony-Anhalt in the central German dry area are documented from PZ E III to E IVb particularly during phases of a more open environment and higher lake-levels (Pop & Bakels, 2015; Strahl et al., 2010). The sites of Rabutz/ Saxony (Toepfer, 1958), Gröbern/ Saxony-Anhalt (Litt & Weber, 1988; Mania et al., 1990) and Grabschütz/Saxony (Weber, 1990) at the margin of this dry area show occupations during PZ E IV, the IVb/V-transition and PZ E VI. Similar semi-open environments can also be expected for this region. In comparison, Lehringen (occupation in PZ E IVb) (Thieme & Veil, 1985) and Lichtenberg (PZ E IVb/V transition) are situated in northern Germany, and a more oceanic climate with a denser vegetation cover can be assumed for that time (Menke, 1992; Menke & Tynni, 1984; this study).

Interestingly, the known archaeological record of Eemian sites seems to omit (i) the main part of the Eemian temperate zone (PZ E V), and (ii) the beginning and termination of the Eemian interglacial. Pollen zone E V coincides with a distinct landscape stability (Section 5.2, Figures 7c and 8). Therefore, on the one hand, the availability of lithic raw material for tool production was rather limited, and on the other hand, sedimentation processes that could have embedded artefacts hardly existed. Furthermore, low groundwater tables during PZ E V led to the desiccation of small lake basins (see Section 5.2), reducing the attraction of otherwise potential lake occupational sites. As for the shortage of archaeological sites from the early and late Eemian, potential evidence might have been destroyed or corrupted by sediment redeposition that we reconstructed for these times. Hence, landscape dynamics could well be one explanatory factor for the lack of registered sites in certain phases of the Eemian. Based on the information presented earlier, human occupation of lakeshores in northern and central Germany seemed to be quite common during PZ E III to IV/V. Therefore, artefact finds within the corresponding sediments in Lichtenberg match the currently expected Eemian Neanderthal settlement pattern.

6 | CONCLUSIONS

This geomorphological study was carried out at a palaeolake margin on the European Plain in northern Germany, where records of landscape activity and stability beyond coastal areas and river valleys are still largely missing. Relative (biostratigraphic) chronological control of the drilled sediments was obtained by taking bulk samples for pollen analysis distributed over the whole drilling transect, instead of single core sequences. This cost and time efficient approach granted us the required spatial resolution for robust inferences about the local Eemian landscape evolution. Within this context, the inevitably lower temporal resolution of the bulk pollen samples was no major obstruction.

Our results allow to understand the interactions of sediment deposition, hydrology and vegetation density during the Eemian

interglacial in this so far largely understudied area: Two phases of geomorphic activity occurred during main climatic shifts before the onset and towards the end of the Eemian. Intensive incision during the first active phase can chronologically be restricted to the late Saalian transition towards the earliest Eemian. Incision was triggered by rapidly changing climatic conditions and a sparse vegetation cover, and was amplified by a lowered local base level due to downcutting of the River Elbe in the adjacent ice-marginal valley. The resulting deep palaeovalley system in the hinterland of the Elbe valley soon accommodated a fingerlake, whose clastic sediment infilling waned during the pre-temperate Eemian (PZ E III/IV after Menke and Tynni [1984]). Contemporaneously, the water table of the fingerlake gradually sank on account of densely vegetated slopes dominated by deciduous woodlands. These stable conditions allowed soil formation, leading to decalcification on the slopes and resulting carbonate influx into the fingerlake where the carbonate precipitated as lake marl deposits. Mid-Eemian landscape stability lasted for c. 6000 years (esp. PZ E V), while the lake successively turned into a swampy depression without drying out completely. Geomorphic activity resumed during the late, post-temperate Eemian (PZ E VI/VII), when incision into the fingerlake deposits implies a renewed fluvial downcutting of the Elbe River and a drop of local base levels. Subsequently, a quickly rising water table refilled the fingerlake and was associated with increasing clastic sediment influx into the lake basin. This second phase of geomorphic activity continued even after the end of the Eemian in the following Herning Stadial. Despite this being a case study, we assume that these activity and stability phases may also apply to comparable landscape segments during this time (cf., Fränze, 1988; Garleff & Leontaris, 1971; Schokker et al., 2004).

Future studies will complement our findings with a multi-proxy and high-resolution analysis of core Li-BPa in the centre of the lake basin (Figure 4), allowing for more detailed reconstructions of the local palaeoenvironments. Furthermore, deciphering the sedimentary history of the Elbe River is part of future endeavours in order to better understand the connection of fluvial behaviour and the geomorphic phases in the hinterland.

Mid-Eemian Neanderthal occupation was observed on the former fingerlake shoreline during a time of marginal geomorphic activity and not yet entirely closed woodlands (PZ E IVb/V). This northernmost Eemian Neanderthal presence on the European Plain is a valuable data point to reconstruct the poorly understood human-environment relationship during that time (see references earlier, cf. Nicholson, 2017). Since the overall archaeological record is still very sparse and strongly biased, additional sites need to be discovered and investigated before Eemian occupation patterns can profoundly be reconstructed and interpreted.

ACKNOWLEDGEMENTS

The authors thank the State Office for Mining, Energy and Geology of Lower-Saxony (LBEG) for use of their drilling rig, and Robert Broschinski and Thomas Jelinski for operating the machine. The authors also thank Jan Bergmann-Barrocas and Jan Bayerle who carried out the seismic survey. The authors owe their gratitude to families Dreier, Kusserow and Kohrs-Lichte for granting access to their land and to Nicolas Bourgon for supporting fieldwork and improving the manuscript. The authors thank Steffi Hesse and Victoria Krippner, who kindly conducted luminescence sample

preparation at the MPI EVA. The authors thankfully acknowledge the work done by the ESPL editors and two anonymous reviewers who helped to improve the manuscript. M.H. thanks Jean-Jacques Hublin and the Max Planck society (Max-Planck-Gesellschaft) for funding this study as part of his PhD.

CONFLICT OF INTEREST

The authors declare that they have no known competing financial interests or personal relationships that could have appeared to influence the work reported in this article.

DATA AVAILABILITY STATEMENT

The data that support the findings of this study are available from the corresponding authors upon reasonable request.

ORCID

Michael Hein  <https://orcid.org/0000-0002-5500-4020>

David Colin Tanner  <https://orcid.org/0000-0002-9488-8631>

Hans von Suchodoletz  <https://orcid.org/0000-0002-4366-9383>

REFERENCES

- Antoine, P., Coutard, S., Guerin, G., Deschodt, L., Goval, E., Loch, J.-L. & Paris, C. (2016) Upper Pleistocene loess-palaeosol records from northern France in the European context: Environmental background and dating of the Middle Palaeolithic. *Quaternary International*, 411, 4–24. Available from: <https://doi.org/10.1016/j.quaint.2015.11.036>
- Antoine, P., Limondin Lozouet, N., Chaussé, C., Lautridou, J.-P., Pestre, J.-F., Auguste, P. et al. (2007) Pleistocene fluvial terraces from northern France (Seine, Yonne, Somme): Synthesis, and new results from interglacial deposits. *Quaternary Science Reviews*, 26, 2701–2723. Available from: <https://doi.org/10.1016/j.quascirev.2006.01.036>
- Averdieck, F. R. (1976). Palynologische Untersuchungen zur Altersbestimmung und Vegetationsgeschichte des Alstertales. Mitt. Geol.-Paläont. Inst. Univ. Hamburg. Sonderband Alster: 81–89.
- Behre, K.-E., Hölzer, A. & Lemdahl, G. (2005) Botanical macro-remains and insects from the Eemian and Weichselian site of Oerel (northwest Germany) and their evidence for the history of climate. *Vegetation History and Archaeobotany*, 14, 31–53. Available from: <https://doi.org/10.1007/s00334-005-0059-x>
- Behre, K.-E. & Lade, U. (1986) Eine Folge von Eem und 4 Weichsel-Interstadialen in Oerel/Niedersachsen und ihr Vegetationsablauf. *E&G Quaternary Science Journal*, 36, 11–36. Available from: <https://doi.org/10.3285/eg.36.1.02>
- Beug, H.-J. (2004) Leitfaden der Pollenbestimmung für Mitteleuropa und angrenzende Gebiete. *Germania*, 87, 542.
- Björck, S., Noe-Nygaard, N., Wolin, J., Houmark-Nielsen, M., Jørgen Hansen, H. & Snowball, I. (2000) Eemian Lake development, hydrology and climate: a multi-stratigraphic study of the Hollerup site in Denmark. *Quaternary Science Reviews*, 19, 509–536. Available from: [https://doi.org/10.1016/S0277-3791\(99\)00025-6](https://doi.org/10.1016/S0277-3791(99)00025-6)
- Boden, A.-H.-A. (2005) Bodenkundliche Kartieranleitung. Bundesanstalt für Geowissenschaften und Rohstoffe. In: Diensten, G. (Ed.) *Zusammenarbeit mit den Staatlichen*, 5th edition. Hannover: Schweizerbart Science Publishers, pp. 141–147.
- Börner, A., Hryniewiecka, A., Stachowicz-Rybka, R., Niska, M., Moskal-del Hoyo, M., Kuznetsov, V. et al. (2018) Palaeoecological investigations and ²³⁰Th/U dating of the Eemian interglacial peat sequence from Neubrandenburg-Hinterste Mühle (Mecklenburg-Western Pomerania, NE Germany). *Quaternary International*, 467, 62–78. Available from: <https://doi.org/10.1016/j.quaint.2017.04.003>
- Brandes, C., Plenefisch, T., Tanner, D.C., Gestermann, N. & Steffen, H. (2019) Evaluation of deep crustal earthquakes in northern Germany – possible tectonic causes. *Terra Nova*, 31, 83–93. Available from: <https://doi.org/10.1111/ter.12372>

- Brauer, A., Allen, J.R.M., Mingram, J., Dulski, P., Wulf, S. & Huntley, B. (2007) Evidence for last interglacial chronology and environmental change from southern Europe. *PNAS*, 104, 450–455. Available from: <https://doi.org/10.1073/pnas.0603321104>
- Busschers, F.S., Kasse, C., van Balen, R.T., Vandenberghe, J., Cohen, K.M., Weerts, H.J.T. et al. (2007) Late Pleistocene evolution of the Rhine-Meuse system in the southern North Sea basin: Imprints of climate change, sea-level oscillation and glacio-isostasy. *Quaternary Science Reviews*, 26, 3216–3248. Available from: <https://doi.org/10.1016/j.quascirev.2007.07.013>
- Butler, D.R., Anzah, F., Goff, P.D. & Villa, J. (2018) Zoogeomorphology and resilience theory. *Geomorphology*, 305, 154–162. Available from: <https://doi.org/10.1016/j.geomorph.2017.08.036>
- Caspers, G., Merkt, J., Müller, H. & Freund, H. (2002) The Eemian Interglaciation in northwestern Germany. *Quaternary Research*, 58, 49–52. Available from: <https://doi.org/10.1006/qres.2002.2341>
- Cheddadi, R., Mamakowa, K., Guiot, J., de Beaulieu, J.-L., Reille, M., Andrieu, V. et al. (1998) Was the climate of the Eemian stable? A quantitative climate reconstruction from seven European pollen records. *Palaeogeography, Palaeoclimatology, Palaeoecology*, 143, 73–85. Available from: [https://doi.org/10.1016/S0031-0182\(98\)00067-4](https://doi.org/10.1016/S0031-0182(98)00067-4)
- De Clercq, M., Missiaen, T., Wallinga, J., Zurita Hurtado, O., Versendaal, A., Mathys, M. & De Batist, M. (2018) A well-preserved Eemian incised-valley fill in the southern North Sea Basin, Belgian Continental Shelf – Coastal Plain: Implications for northwest European landscape evolution. *Earth Surface Processes and Landforms*, 43, 1913–1942. Available from: <https://doi.org/10.1002/esp.4365>
- de Groot, W.J., Cantin, A.S., Flannigan, M.D., Soja, A.J., Gowman, L.M. & Newbery, A. (2013) A comparison of Canadian and Russian boreal forest fire regimes. *Forest Ecology and Management*, 294, 23–34. Available from: <https://doi.org/10.1016/j.foreco.2012.07.033>
- Duphorn, K., Grube, F., Meyer, K.-D., Streif, H. & Vinken, R. (1973) A. Area of Scandinavian Glaciation: 1. Pleistocene and Holocene. *E&G Quaternary Science Journal*, 23/24, 222–250. Available from: <https://doi.org/10.3285/eg.23-24.119>
- Ehlers, J. (1990) Untersuchungen zur Morphodynamik der Vereisungen Norddeutschlands unter Berücksichtigung benachbarter Gebiete. *Bremer Beiträge Zur Geographie Und Raumplanung*, 19, 166.
- Ehlers, J. (2020) *Das Eiszeitalter*. Berlin: Springer Available from: <http://link.springer.com/10.1007/978-3-662-60582-0>
- Ehlers, J. & Gibbard, P.L. (2004) Quaternary glaciations extent and chronology - Part I: Europe. *Developments in Quaternary Sciences*. Available from: [https://doi.org/10.1016/S1571-0866\(04\)80056-3](https://doi.org/10.1016/S1571-0866(04)80056-3)
- Ehlers, J., Grube, A., Stephan, H.J. & Wansa, S. (2011) Pleistocene glaciations of north Germany – new results. *Developments in Quaternary Science*, 15, 149–162. Available from: <https://doi.org/10.1016/B978-0-444-53447-7.00013-1>
- Ehlers, J., Meyer, K.-D. & Stephan, H.-J. (1984) The pre-weichselian glaciations of north-west Europe. *Quaternary Science Reviews*, 3, 1–40. Available from: [https://doi.org/10.1016/0277-3791\(84\)90003-9](https://doi.org/10.1016/0277-3791(84)90003-9)
- Fægri, K., Iversen, J., Kaland, P.E. & Krzywinski, K. (1989) *Textbook of pollen analysis*, 4th edition. Chichester: John Wiley & Sons.
- Favre, E., Escarguel, G., Suc, J.-P., Vidal, G. & Thévenod, L. (2008) A contribution to deciphering the meaning of AP/NAP with respect to vegetation cover. *Review of Palaeobotany and Palynology*, 148, 13–35. Available from: <https://doi.org/10.1016/j.revpalbo.2007.08.003>
- Field, M.H., Huntley, B. & Müller, H. (1994) Eemian climate fluctuations observed in a European pollen record. *Nature*, 371, 779–783. Available from: <https://doi.org/10.1038/371779a0>
- Fränzle, O. (1988) Glaziäre, periglaziäre und marine Reliefentwicklung im nördlichen Schleswig-Holstein. *Schriften des Naturwissenschaftlichen Vereins für Schleswig-Holstein*, 58, 1–30.
- Garleff, K. & Leontaris, S.N. (1971) Jungquartäre Taleintiefung und Flächenbildung am Wilseder Berg (Lüneburger Heide). *E&G Quaternary Science Journal*, 22, 148–155. Available from: <https://doi.org/10.3285/eg.22.1.11>
- Gibbard, P. & Lewin, J. (2002) Climate and related controls on interglacial fluvial sedimentation in lowland Britain. *Sedimentary Geology*, 151, 187–210. Available from: [https://doi.org/10.1016/S0037-0738\(01\)00253-6](https://doi.org/10.1016/S0037-0738(01)00253-6)
- Göttlich, K. (1965) Ergebnisse und Ziele bodenkundlicher Studien in Moor und Anmoor. Dargelegt an hydropedologischen Untersuchungen in Südwestdeutschland. *Arbeiten der Landwirtschaftlichen Hochschule Hohenheim*, 33, 121.
- Grimm, E. C. (1990). TILIA, TILIAGRAPH and TILIAVIEW. PC spreadsheet and graphics software for pollen data. Available from: www.geo.arizona.edu/palynology/geos581/tiliaview.html
- Grube, F., Vladi, F. & Vollmer, T. (1976). Erdgeschichtliche Entwicklung des unteren Alstertales. Mitt. Geol.-Paläont. Inst. Univ. Hamburg. Sonderband Alster: 43–56.
- Haesaerts, P. & Mestdag, H. (2000) Pedosedimentary evolution of the last interglacial and early glacial sequence in the European loess belt from Belgium to central Russia. *Netherlands Journal of Geosciences*, 79, 313–324. Available from: <https://doi.org/10.1017/S001677460002179X>
- Head, M.J., Seidenkrantz, M.-S., Janczyk-Kopikowa, Z., Marks, L. & Gibbard, P.L. (2005) Last Interglacial (Eemian) hydrographic conditions in the southeastern Baltic Sea, NE Europe, based on dinoflagellate cysts. *Quaternary International*, 130, 3–30. Available from: <https://doi.org/10.1016/j.quaint.2004.04.027>
- Hein, M., Weiss, M., Otcherednoy, A. & Lauer, T. (2020) Luminescence chronology of the key-Middle Paleolithic site Khotylevo I (western Russia) – implications for the timing of occupation, site formation and landscape evolution. *Quaternary Science Advances*, 2, 100008. Available from: <https://doi.org/10.1016/j.qsa.2020.100008>
- Helmens, K.F. (2014) The last interglacial-glacial cycle (MIS 5–2) re-examined based on long proxy records from central and northern Europe. *Quaternary Science Reviews*, 86, 115–143. Available from: <https://doi.org/10.1016/j.quascirev.2013.12.012>
- Helmens, K.F., Salonen, J.S., Pliik, A., Engels, S., Väliant, M., Kylander, M. et al. (2015) Major cooling intersecting peak Eemian interglacial warmth in northern Europe. *Quaternary Science Reviews*, 122, 293–299. Available from: <https://doi.org/10.1016/j.quascirev.2015.05.018>
- Höfle, H.-C., Merkt, J. & Müller, H. (1985) Die Ausbreitung des Eem-Meeres in Nordwestdeutschland. *E&G Quaternary Science Journal*, 35, 49–60. Available from: <https://doi.org/10.3285/eg.35.1.09>
- Högberg, M.N., Högberg, P. & Myröld, D.D. (2006) Is microbial community composition in boreal forest soils determined by pH, C-to-N ratio, the trees, or all three? *Oecologia*, 150, 590–601. Available from: <https://doi.org/10.1007/s00442-006-0562-5>
- Illies, H. (1954) Entstehung und eiszeitliche Geschichte der unteren Elbe. *Mitteilungen aus dem Geologischen Staatsinstitut in Hamburg*, 23, 42–49.
- Kolaczek, P., Niska, M., Mirosław-Grabowska, J. & Gałka, M. (2016) Periodic lake-peatland shifts under the Eemian and Early Weichselian climate changes in central Europe on the basis of multi-proxy studies. *Palaeogeography, Palaeoclimatology, Palaeoecology*, 461, 29–43. Available from: <https://doi.org/10.1016/j.palaeo.2016.08.002>
- Krawczyk, C.M., Polom, U., Trabs, S. & Dahm, T. (2012) Sinkholes in the city of Hamburg—new urban shear-wave reflection seismic system enables high-resolution imaging of subsurface structures. *Journal of Applied Geophysics*, 78, 133–143. Available from: <https://doi.org/10.1016/j.jappgeo.2011.02.003>
- Kühl, N., Litt, T., Schölzel, C. & Hense, A. (2007) Eemian and Early Weichselian temperature and precipitation variability in northern Germany. *Quaternary Science Reviews*, 26, 3311–3317. Available from: <https://doi.org/10.1016/j.quascirev.2007.10.004>
- Kupryjanowicz, M., Fiłoc, M. & Kwiatkowski, W. (2018) Was there an abrupt cold climatic event in the middle Eemian? Pollen record from a palaeolake at the Hieronimowo site, NE Poland. *Quaternary International*, 467, 96–106. Available from: <https://doi.org/10.1016/j.quaint.2017.04.027>
- Lambeck, K., Purcell, A., Funder, S., Kjaer, K.H., Larsen, E. & Møller, P. (2006) Constraints on the Late Saalian to early Middle Weichselian ice sheet of Eurasia from field data and rebound modelling. *Boreas*, 35, 539–575. Available from: <https://doi.org/10.1080/03009480600781875>

- Lang, J., Lauer, T. & Winsemann, J. (2018) New age constraints for the Saalian glaciation in northern central Europe: Implications for the extent of ice sheets and related proglacial lake systems. *Quaternary Science Reviews*, 180, 240–259. Available from: <https://doi.org/10.1016/j.quascirev.2017.11.029>
- Larsen, A., Nardin, W., Lageweg, W.I. & Bätz, N. (2020) Biogeomorphology, quo vadis? On processes, time, and space in biogeomorphology. *Earth Surface Processes and Landforms*, 46(1), 12–23. Available from: <https://doi.org/10.1002/esp.5016>
- Larsen, N.K., Knudsen, K.L., Krohn, C.F., Kronborg, C., Murray, A.S. & Nielsen, O.B. (2009) Late Quaternary ice sheet, lake and sea history of southwest Scandinavia – a synthesis. *Boreas*, 38(4), 732–761. Available from: <https://doi.org/10.1111/j.1502-3885.2009.00101.x>
- Lisiecki, L.E. & Raymo, M.E. (2005) A Plio-Pleistocene stack of 57 globally distributed benthic $\delta^{18}O$ records. *Paleoceanography*, 20(1), PA1003. Available from: <https://doi.org/10.1029/2004PA001071>
- Litt, T. & Weber, T. (1988) Ein eemzeitlicher Waldelefantenschlachtplatz von Gröbern, Krs. Gräfenhainichen. *Ausgrabungen und Funde*, 33, 181–187.
- Lüthgens, C., Böse, M., Lauer, T., Krbetschek, M., Strahl, J. & Wenske, D. (2011) Timing of the last interglacial in Northern Europe derived from Optically Stimulated Luminescence (OSL) dating of a terrestrial Saalian–Eemian–Weichselian sedimentary sequence in NE-Germany. *Quaternary International*, 241, 79–96. Available from: <https://doi.org/10.1016/j.quaint.2010.06.026>
- Lüttig, G. & Meyer, K. D. (1974). Geological history of the River Elbe, mainly of its lower course. *Annales de la Société géologique de Belgique. L'évolution quaternaire des bassins fluviaux de la Mer du Nord méridionale: 1–19.*
- Mania, D., Thomae, M., Litt, T. & Weber, T. (1990) Neumark - Gröbern. Beiträge zur Jagd des mittelpaläolithischen Menschen. *Veröffentlichungen des Landesmuseums für Vorgeschichte Halle*, 43, 321.
- Marks, L., Gałazka, D., Krzyńska, J., Nita, M., Stachowicz-Rybka, R., Witkowski, A. et al. (2014) Marine transgressions during Eemian in northern Poland: A high resolution record from the type section at Cierpięta. *Quaternary International*, 328–329, 45–59. Available from: <https://doi.org/10.1016/j.quaint.2013.12.007>
- Matoshko, A. V. (2011). Limits of the Pleistocene Glaciations in the Ukraine. In 405–418. Available from: <https://linkinghub.elsevier.com/retrieve/pii/B9780444534477000313>
- Meier-Uhlherr, R., Schulz, C. & Luthardt, V. (2015) *Steckbriefe Moorsubstrate*, 2nd. edition. Berlin: HNE Eberswalde.
- Menke, B. (1992) Eeminterglaziale und nacheiszeitliche Wälder in Schleswig-Holstein. *GLASH*, 1, 29–101.
- Menke, B. & Tynni, R. (1984) Das Eeminterglazial und das Weichselfrühglazial von Rederstaß/Dithmarschen und ihre Bedeutung für die mitteleuropäische Jungpleistozän-Gliederung. *Geologisches Jahrbuch A*, 76, 1–120.
- Merk, J. (1975) *Geologische Karte von Niedersachsen 1:25000, Blatt 3033 Woltersdorf. Energie und Geologie (LBEG)* Hannover: Landesamt für Bergbau.
- Meyer, K.D. (1983) Zur Anlage der Urstromtäler in Niedersachsen. *Zeitschrift für Geomorphologie*, 27, 147–160.
- Miettinen, A., Head, M.J. & Knudsen, K.L. (2014) Eemian sea-level highstand in the eastern Baltic Sea linked to long-duration White Sea connection. *Quaternary Science Reviews*, 86, 158–174. Available from: <https://doi.org/10.1016/j.quascirev.2013.12.009>
- Miroslaw-Grabowska, J. (2009) Evolution of palaeolake environment in Poland during the Eemian interglacial based on oxygen and carbon isotope data from lacustrine carbonates. *Quaternary International*, 207, 145–156. Available from: <https://doi.org/10.1016/j.quaint.2009.05.004>
- Moore, P.D., Webb, J.A. & Collison, M.E. (1991) *Pollen Analysis*. Oxford: Blackwell Scientific Publications.
- Müller, H. (1974) Pollenanalytische Untersuchungen und Jahresschichtenzählungen an der eemzeitlichen Kieselgur von Bispingen/Luhe. *Geologisches Jahrbuch*, A21, 149–169.
- Nelson, M., Rittenour, T. & Cornachione, H. (2019) Sampling Methods for Luminescence Dating of Subsurface Deposits from Cores. *Methods and Protocols*, 2, 88. Available from: <https://doi.org/10.3390/mps2040088>
- Nicholson, C.M. (2017) Eemian paleoclimate zones and Neanderthal landscape-use: A GIS model of settlement patterning during the last interglacial. *Quaternary International*, 438, 144–157. Available from: <https://doi.org/10.1016/j.quaint.2017.04.023>
- Nielsen, T.K., Benito, B.M., Svenning, J.C., Sandel, B., McKerracher, L., Riede, F. & Kjaergaard, P.C. (2015) Investigating Neanderthal dispersal above 55°N in Europe during the Last Interglacial Complex. *Quaternary International*, 431, 88–103. Available from: <https://doi.org/10.1016/j.quaint.2015.10.039>
- Nielsen, T.K., Kristiansen, S.M. & Riede, F. (2019) Neanderthals at the frontier? Geological potential of southwestern South Scandinavia as archive of Pleistocene human occupation. *Quaternary Science Reviews*, 221, 105870. Available from: <https://doi.org/10.1016/j.quascirev.2019.105870>
- Peeters, J., Busschers, F.S. & Stouthamer, E. (2015) Fluvial evolution of the Rhine during the last interglacial-glacial cycle in the southern North Sea basin: A review and look forward. *Quaternary International*, 357, 176–188. Available from: <https://doi.org/10.1016/j.quaint.2014.03.024>
- Pop, E. & Bakels, C. (2015) Semi-open environmental conditions during phases of hominin occupation at the Eemian interglacial basin site Neumark-Nord 2 and its wider environment. *Quaternary Science Reviews*, 117, 72–81. Available from: <https://doi.org/10.1016/j.quascirev.2015.03.020>
- Reicherter, K., Kaiser, A. & Stackedbrandt, W. (2005) The post-glacial landscape evolution of the North German Basin: Morphology, neotectonics and crustal deformation. *International Journal of Earth Sciences*, 94, 1083–1093. Available from: <https://doi.org/10.1007/s00531-005-0007-0>
- Roeschmann, G., Ehlers, J., Meyer, B., Rohdenburg, H. & Benzler, J.-H. (1982) Paläoböden in Niedersachsen, Bremen und Hamburg. *Geologisches Jahrbuch, Reihe F*, 14, 255–309.
- Rohdenburg, H. (1970) Morphodynamische Aktivitäts- und Stabilitätszeiten statt Pluvial- und Interpluvialzeiten. *E&G Quaternary Science Journal*, 21, 81–96. Available from: <https://doi.org/10.3285/eg.21.1.07>
- Rother, H., Lorenz, S., Börner, A., Kenzler, M., Siermann, N., Fülling, A. et al. (2019) The terrestrial Eemian to late Weichselian sediment record at Beckentin (NE-Germany): First results from lithostratigraphic, palynological and geochronological analyses. *Quaternary International*, 501, 90–108. Available from: <https://doi.org/10.1016/j.quaint.2017.08.009>
- Rowland, J.C., Jones, C.E., Altmann, G., Bryan, R., Crosby, B.T., Hinzman, L. D. et al. (2010) Arctic landscapes in transition: Responses to thawing permafrost. *Eos, Transactions American Geophysical Union*, 91(26), 229–230. Available from: <https://doi.org/10.1029/2010EO260001>
- Schokker, J., Cleveringa, P. & Murray, A.S. (2004) Palaeoenvironmental reconstruction and OSL dating of terrestrial Eemian deposits in the southeastern Netherlands. *Journal of Quaternary Science*, 19, 193–202. Available from: <https://doi.org/10.1002/jqs.808>
- Seidenkrantz, M.-S., Kristensen, P. & Knudsen, K.L. (1995) Marine evidence for climatic instability during the last interglacial in shelf records from northwest Europe. *Journal of Quaternary Science*, 10, 77–82. Available from: <https://doi.org/10.1002/jqs.3390100108>
- Shackleton, N.J., Chapman, M., Sánchez-Goni, M.F., Paillet, D. & Lancelot, Y. (2002) The Classic Marine Isotope Substage 5e. *Quaternary Research*, 58, 14–16. Available from: <https://doi.org/10.1006/qres.2001.2312>
- Sier, M.J., Peeters, J., Dekkers, M.J., Parés, J.M., Chang, L., Busschers, F.S. et al. (2015) The Blake Event recorded near the Eemian type locality – a diachronic onset of the Eemian in Europe. *Quaternary Geochronology*, 28, 12–28. Available from: <https://doi.org/10.1016/j.quageo.2015.03.003>
- Stephan, H.-J. (2014) Climato-stratigraphic subdivision of the Pleistocene in Schleswig-Holstein, Germany and adjoining areas: Status and problems. *E&G Quaternary Science Journal*, 63, 3–18. Available from: <https://doi.org/10.3285/eg.63.1.01>
- Strahl, J., Krbetschek, M.R., Luckert, J., Machalet, B., Meng, S., Oches, E.A. et al. (2010) Geologie, Paläontologie und Geochronologie des

- Eem-Beckens Neumark-Nord 2 und Vergleich mit dem Becken Neumark-Nord 1 (Geiseltal, Sachsen-Anhalt). *Eiszeitalter und Gegenwart (Quaternary Science Journal)*, 59, 120–167. Available from: <https://doi.org/10.3285/eg.59.1-2.09>
- Streif, H. (2004) Sedimentary record of Pleistocene and Holocene marine inundations along the North Sea coast of Lower Saxony, Germany. *Quaternary International*, 112, 3–28. Available from: [https://doi.org/10.1016/S1040-6182\(03\)00062-4](https://doi.org/10.1016/S1040-6182(03)00062-4)
- Stremme, H., Felix-Henningsen, P., Weinhold, H. & Christensen, S. (1982) Paläoböden in Schleswig-Holstein. *Geologisches Jahrbuch, Reihe F*, 14, 311–361.
- Sugita, S., Gaillard, M.-J. & Broström, A. (1999) Landscape openness and pollen records: A simulation approach. *The Holocene*, 9, 409–421. Available from: <https://doi.org/10.1191/095968399666429937>
- Thiel, C., Buylaert, J.P., Murray, A., Terhorst, B., Hofer, I., Tsukamoto, S. & Frechen, M. (2011) Luminescence dating of the Stratzing loess profile (Austria) – testing the potential of an elevated temperature post-IR IRSL protocol. *Quaternary International*, 234(1–2), 23–31. Available from: <https://doi.org/10.1016/j.quaint.2010.05.018>
- Thieme, H. & Veil, S. (1985) Neue Untersuchungen zum eemzeitlichen Elefanten-Jagdplatz Lehringen, Ldkr. *Die Kunde, Neue Folge (N.F.)*, 36, 11–58.
- Toepfer, V. (1958) Steingeräte und Palökologie der mittel- paläolithischen Fundstelle Rabutz bei Halle. *Jahresschrift für Mitteldeutsche Vorgeschichte*, 41/42, 140–179.
- Turner, C. (2000) The Eemian interglacial in the North European plain and adjacent areas. *Netherlands Journal of Geosciences*, 79, 217–231. Available from: <https://doi.org/10.1017/S0016774600023660>
- Turner, C. (2002) Formal status and vegetational development of the Eemian interglacial in northwestern and southern Europe. *Quaternary Research*, 58, 41–44. Available from: <https://doi.org/10.1006/qres.2002.2365>
- Turner, C. & West, R.G. (1968) The subdivision and zonation of interglacial periods. *E&G Quaternary Science Journal*, 19, 93–101. Available from: <https://doi.org/10.3285/eg.19.1.06>
- Turner, F., Tolsdorf, J.F., Viehberg, F., Schwalb, A., Kaiser, K., Bittmann, F. et al. (2013) Lateglacial/early Holocene fluvial reactions of the Jeetzel River (Elbe valley, northern Germany) to abrupt climatic and environmental changes. *Quaternary Science Reviews*, 60, 91–109. Available from: <https://doi.org/10.1016/j.quascirev.2012.10.037>
- Turner, T.E., Swindles, G.T. & Roucoux, K.H. (2014) Late Holocene ecohydrological and carbon dynamics of a UK raised bog: Impact of human activity and climate change. *Quaternary Science Reviews*, 84, 65–85. Available from: <https://doi.org/10.1016/j.quascirev.2013.10.030>
- van Kolfschoten, T. & Gibbard, P.L. (2000) The Eemian – local sequences, global perspectives: introduction. *Netherlands Journal of Geosciences*, 79, 129–133. Available from: <https://doi.org/10.1017/S0016774600021661>
- Vandenbergh, J. & van der Plicht, J. (2016) The age of the Hengelo interstadial revisited. *Quaternary Geochronology*, 32, 21–28. Available from: <https://doi.org/10.1016/j.quageo.2015.12.004>
- Veil, S., Breest, K., Höfle, H.-C., Meyer, H.-H., Plisson, H., Urban-Küttel, B. et al. (1994) Ein mittelpaläolithischer Fundplatz aus der Weichsel-Kaltzeit bei Lichtenberg, Lkr. *Lüchow-Dannenberg, Germania*, 72, 1–66.
- Velichko, A., Novenko, E., Pisareva, V., Zelikson, E., Boettger, T. & Junge, F. (2005) Vegetation and climate changes during the Eemian interglacial in central and eastern Europe: Comparative analysis of pollen data. *Boreas*, 34, 207–219. Available from: <https://doi.org/10.1080/03009480510012890>
- Velichko, A.A., Morozova, T.D., Nechaev, V.P., Rutter, N.W., Dlusskii, K.G., Little, E.C. et al. (2006) Loess/paleosol/cryogenic formation and structure near the northern limit of loess deposition, East European Plain, Russia. *Quaternary International*, 152–153, 14–30. Available from: <https://doi.org/10.1016/j.quaint.2005.12.003>
- Vogel, S., Märker, M., Rellini, I., Hoelzmann, P., Wulf, S., Robinson, M. et al. (2016) From a stratigraphic sequence to a landscape evolution model: Late Pleistocene and Holocene volcanism, soil formation and land use in the shade of Mount Vesuvius (Italy). *Quaternary International*, 394, 155–179. Available from: <https://doi.org/10.1016/j.quaint.2015.02.033>
- Voss, H.-H. (1981) Zur Geologie des Örings. *Veröffentlichungen der Urgeschichtlichen Sammlungen des Landesmuseums zu Hannover*, 26, 9–28.
- Weber, T. (1990) Paläolithische Funde aus den Eemvorkommen von Rabutz, Grabschütz und Gröbern. In: Eißmann, L. (Ed.) *Die Eemwärmzeit und die frühe Weichsel- Eiszeit im Saale-Elbe-Gebiet*, Geologie, Paläontologie, Palökologie. Altenburg: Naturkundliches Museum Mauritium.
- Weiss, M. (2020) The Lichtenberg Keilmesser – it's all about the angle. Peresani M (ed). *PLoS ONE*, 15, e0239718. Available from: <https://doi.org/10.1371/journal.pone.0239718>
- Winsemann, J., Lang, J., Roskosch, J., Polom, U., Böhner, U., Brandes, C. et al. (2015) Terrace styles and timing of terrace formation in the Weser and Leine valleys, northern Germany: Response of a fluvial system to climate change and glaciation. *Quaternary Science Reviews*, 123, 31–57. Available from: <https://doi.org/10.1016/j.quascirev.2015.06.005>
- Woldstedt, P. (1956) Die Geschichte des Flußnetzes in Norddeutschland und angrenzenden Gebieten. *E&G Quaternary Science Journal*, 7, 5–12. Available from: <https://doi.org/10.3285/eg.07.1.01>
- Zagwijn, W. (1996) An analysis of Eemian climate in western and central Europe. *Quaternary Science Reviews*, 15, 451–469. Available from: [https://doi.org/10.1016/0277-3791\(96\)00011-X](https://doi.org/10.1016/0277-3791(96)00011-X)
- Żarski, M., Winter, H. & Kucharska, M. (2018) Palaeoenvironmental and climate changes recorded in the lacustrine sediments of the Eemian interglacial (MIS 5e) in the Radom Plain (central Poland). *Quaternary International*, 467, 147–160. Available from: <https://doi.org/10.1016/j.quaint.2016.12.001>

SUPPORTING INFORMATION

Additional supporting information may be found in the online version of the article at the publisher's website.

How to cite this article: Hein, M., Urban, B., Tanner, D.C., Bunn, A.H., Tucci, M., Hoelzmann, P. et al. (2021) Eemian landscape response to climatic shifts and evidence for northerly Neanderthal occupation at a palaeolake margin in northern Germany. *Earth Surface Processes and Landforms*, 1–18. Available from: <https://doi.org/10.1002/esp.5219>

CHAPTER IV: NEANDERTHALS IN CHANGING ENVIRONMENTS FROM MIS 5 TO EARLY MIS 4 IN NORTHERN CENTRAL EUROPE – INTEGRATING ARCHAEOLOGICAL, (CHRONO)STRATIGRAPHIC AND PALEOENVIRONMENTAL EVIDENCE AT THE SITE OF LICHTENBERG

Published in: Quaternary Science Reviews 284 (2022): 107519



Neanderthals in changing environments from MIS 5 to early MIS 4 in northern Central Europe – Integrating archaeological, (chrono) stratigraphic and paleoenvironmental evidence at the site of Lichtenberg

Marcel Weiss ^{a, b, 1, *}, Michael Hein ^{a, 1, **}, Brigitte Urban ^c, Mareike C. Stahlschmidt ^a, Susann Heinrich ^a, Yamandu H. Hilbert ^b, Robert C. Power ^{d, a}, Hans v. Suchodoletz ^e, Thomas Terberger ^f, Utz Böhner ^f, Florian Klimscha ^g, Stephan Veil ^g, Klaus Breest ^h, Johannes Schmidt ^e, Debra Colarossi ^{i, a}, Mario Tucci ^c, Manfred Frechen ^j, David Colin Tanner ^j, Tobias Lauer ^a

^a Max Planck Institute for Evolutionary Anthropology, Leipzig, Germany

^b Institut für Ur- und Frühgeschichte, Friedrich-Alexander-Universität Erlangen-Nürnberg, Erlangen, Germany

^c Leuphana University Lüneburg, Institute of Ecology, Lüneburg, Germany

^d Institute for Pre- and Protohistoric Archaeology and Archaeology of the Roman Provinces, Ludwig Maximilian University Munich, Germany

^e Institute of Geography, Leipzig University, Leipzig, Germany

^f State Service for Cultural Heritage Lower Saxony, Hannover, Germany

^g Lower Saxony State Museum, Department for Research and Collections, Archaeology Division, Hannover, Germany

^h Volunteer Archaeologist, Berlin, Germany

ⁱ Department of Geography and Earth Sciences, Aberystwyth University, Aberystwyth, Wales, UK

^j Leibniz Institute for Applied Geophysics, Hannover, Germany

ARTICLE INFO

Article history:

Received 11 October 2021

Received in revised form

16 March 2022

Accepted 5 April 2022

Available online xxx

Handling editor: Danielle Schreve

Keywords:

Middle paleolithic

Neanderthals

Quaternary stratigraphy

Luminescence dating

Palynology

ABSTRACT

The resilience of Neanderthals towards changing climatic and environmental conditions, and especially towards severely cold climates in northern regions of central Europe, is still under debate. One way to address this is to investigate multi-layered occupation in different climatic intervals, using independently-compiled paleoenvironmental and chronological data. Unfortunately, most open-air sites on the northern European Plain lack a robust chronostratigraphy beyond the radiocarbon dating range, thereby often hampering direct links between human occupation and climate. Here we present the results of integrative research at the Middle Paleolithic open-air site of Lichtenberg, Northern Germany, comprising archaeology, luminescence dating, sedimentology, micromorphology, as well as pollen and phytolith analyses. Our findings clearly show Neanderthal presence in temperate, forested environments during the Mid-Eemian Interglacial, MIS 5e and the latest Brörup Interstadial, MIS 5c/GI 22 (Lichtenberg II). For the previously known occupation Lichtenberg I, we revise the chronology from the former early MIS 3 (57 ± 6 ka) to early MIS 4/GS 19 (71.3 ± 7.3 ka), with dominant cold steppe/tundra vegetation. The early MIS 4 occupation suggests that Neanderthals could adjust well to severely cold environments and implies recurring population in the region between MIS 5 and MIS 3. The artefact assemblages differ between the temperate and cold environment occupations regarding size, blank production, typology and tool use. We argue that this distinctness can partially be explained by different site functions and occupation duration, as well as the availability of large and high-quality flint raw material. Raw material

* Corresponding author. Max Planck Institute for Evolutionary Anthropology, Leipzig, Germany.

** Corresponding author.

E-mail addresses: marcel.weiss@fau.de (M. Weiss), michael_hein@eva.mpg.de (M. Hein).

¹ Equal contributions.

availability is in turn governed by changing vegetation cover that hindered or fostered sediment reposition as a provider of flint from the primary source of the glacial sediments nearby.

© 2022 Elsevier Ltd. All rights reserved.

1. Introduction

The “stereotype” Neanderthal is mostly perceived as a human species that lived in the cold and harsh climatic environments of the past glacial periods in Eurasia. But were Neanderthals indeed adapted to cold environments? This question has been a matter of debate in prehistory, biology and physical anthropology for a long time (e.g., Aiello and Wheeler, 2003; Churchill, 2008; Rae et al., 2011; Skrzypek et al., 2011; White and Pettitt, 2011). One way of addressing this open question is to analyze Neanderthal occupation at the northern extreme of their habitat, more precisely the northern part of Central Europe.

Currently, numerous sites suggest that Neanderthals settled in northern Central Europe during the Eemian Interglacial and during the first half of the last glacial cycle (Gaudzinski-Windheuser and Roebroeks, 2014; Hein et al., 2020; Litt and Weber, 1988; Nielsen et al., 2017; Richter, 2016; Thieme and Veil, 1985; Toepfer, 1958; Weber, 1990). However, the chronology of most late Middle Paleolithic sites is either poor and/or controversial (Jöris, 2004; Mania, 2002; Pastoors, 2001, 2009; Veil et al., 1994), and many of them are not dated at all. The majority of those sites are classified as late Middle Paleolithic by typological means only (Kegler and Fries, 2018; Richter, 2016). Due to this lack of precise site chronologies, even though we know that Neanderthals occupied the northern regions, we lack evidence of whether they stayed there only during warmer periods of the last interglacial - glacial cycle or if they also persisted through cold stadial conditions. So far, the only indication for the latter is the site of Salzgitter-Lebenstedt, Lower Saxony/Germany (Tode, 1982). At this site, the finds originate from layers containing cold climatic vegetation remains (Pastoors, 2001; Pfaffenberg, 1991; Selle, 1991), and are associated with glacial fauna. The presence of cranial and post-cranial Neanderthal remains (Hublin, 1984), clearly link Neanderthals to the accumulation of archaeological and faunal remains at the site. They hunted reindeer and manufactured bone tools from mammoth ribs (Gaudzinski, 1998, 1999). However, the dating of the site still lacks resolution. Uncertain ages at the upper limit of the ^{14}C time scale, together with contrasting stratigraphic interpretation, place the site either in the Marine Isotope Stage (MIS) 5a/4 (Jöris, 2004) or MIS 4/3 transition (Pastoors, 2001, 2009). Furthermore, the integrity of the lithic assemblage is unclear, as the artefacts were found in several geological layers (Pastoors, 2001). Evidence for occupation during warmer early last glacial interstadials only comes from two sites of the northern Central European Plain so far. The first site is Neumark-Nord 2/0 (Laurat and Brühl, 2006), Saxony-Anhalt/Germany dating to either MIS 5c or 5a (Richter and Krbetschek, 2014; Strahl et al., 2010). The second site is Königsau (Mania and Toepfer, 1973), Saxony-Anhalt/Germany. Neanderthal occupation is here associated with peat layers at a paleo-lakeshore, dating most probably to MIS 5a (Jöris, 2004; Mania, 2002; Mania and Toepfer, 1973; but see Hedges et al., 1998 for a potential MIS 3 age of the site). However, with the scarce evidence outlined above, it is currently not possible to reconstruct the timing of human presence in northern Central Europe, as well as behavioral response to short-term climatic shifts.

To address these issues, we need to contextualize the northern Neanderthal occupations using detailed paleoenvironmental

reconstructions, derived from the same chronostratigraphic frameworks as the archaeological material, preferably with a temporal resolution on the millennial scale of Greenland Interstadials (Rasmussen et al., 2014). Since the Middle Paleolithic period is mostly outside the radiocarbon range, this kind of precision is usually reserved for loess regions, where highly-resolved sediment-paleosol sequences occur (Locht et al., 2016). Beyond the loess belt, at the northern margin of the Neanderthal habitat and the European Plain, occupation is conceived to have been most particularly affected by climatic fluctuations (Depaepe et al., 2015; Hublin and Roebroeks, 2009; Roebroeks et al., 2011). Across these landscapes, however, shallow sediment deposits in unison with frequent cryoturbation features often hamper the establishment of such a precise chronostratigraphic framework (Hein et al., 2020; Wiśniewski et al., 2019). Instead, the dating resolution commonly does not exceed the much coarser scale of Marine Isotope Stages (Lisiecki and Raymo, 2005a).

Here we present new results of our recent research at the late Middle Paleolithic open-air site complex of Lichtenberg, Lower Saxony/Germany (Veil et al., 1994), which was initially discovered in 1987 and excavated until 1993 by the Niedersächsisches Landesmuseum, Hannover, Germany. Lichtenberg represents a Neanderthal site at the potential northern limit of their geographic range (Nielsen et al., 2017). The site yielded one of the most prominent late Middle Paleolithic assemblages of the northern Central European Plain, as well as a sediment sequence encompassing deposits from MIS 5e through MIS 3 (Veil et al., 1994). Neanderthal occupations at Lichtenberg were associated with a paleo-lakeshore (Hein et al., 2021). Therefore, the long-lasting highly resolved sediment sequence composed of intercalated organic and clastic sediments is an ideal location to study climatic and environmental shifts, and to investigate the Neanderthal population dynamics at the northern limit of their habitat.

Our multidisciplinary investigations combine archaeological investigations with detailed sedimentological, chronological and paleoenvironmental studies of the find-bearing and associated non-find bearing layers of the sequence. Our research focusses on the following aims: (1) Can we connect Neanderthal occupations of northern Central Europe to a chronological resolution of Greenland Interstadial-Stadial level and thus to changing climatic conditions? (2) Did Neanderthals inhabit specific environments only, or did they adapt to different environmental conditions? (3) To which extent do archaeological assemblages vary in different environments and climates? And, most importantly, (4) did Neanderthals live in northern Central Europe only during warmer, forested phases of the last glacial, or could they also cope with cold climatic conditions and open landscapes in the stadials of the Early Weichselian and the Pleniglacial?

2. Materials

2.1. Study area

Based on archaeological evidence and (paleo-)geographical considerations, the study region, here referred to as “northern Central Europe” or “northern Central European Plain”, consists mainly of the Northern German Lowlands above approximately 51°

N, as well as the northern Netherlands. Today, the latter is part of the rather maritime North-Western Europe, but due to the lower sea level during the last glacial cycle, the northern Netherlands were part of a more extensive northern Central European Plain, and thus incorporated into the study region. Northern Poland is not included here, as we currently lack Middle Paleolithic archaeological sites from the area covered by the ice shield of the last Glaciation (see e.g., Wiśniewski et al., 2013).

2.2. Geological setting

The study site is located at latitude 52°55' N in Northern Germany, eastern Lower Saxony (Fig. 1a). Throughout the Pleistocene, Scandinavian glaciers covered the region twice during the Elsterian (MIS 12) and three times during the Saalian (MIS 6) glaciation, and deposited >40 m of glacial tills and glaciofluvial sands (Ehlers et al., 2011; Lang et al., 2018). The ice-marginal valley of the River Elbe, as the major drainage channel of the region, assumed its course close to the study area, already during the late Saalian Warthe Stadial (Fig. 1) (Ehlers, 1990; Meyer, 1983). In contrast, Weichselian glaciers during MIS 4 and MIS 2 did not cross the Elbe lineament, with the margin of the furthest advance situated ca. 50 km to the NE (Duphorn et al., 1973; Ehlers, 2020) of the study area. The archaeological site is located at the southern declivity of the Öring, a confined Saalian plateau, which passes over into a major sediment basin that repeatedly hosted a lakescape since at least the Saalian-

Eemian transition (Hein et al., 2021). Therefore, in the course of the Weichselian, the depositional regime was mainly characterized by slope wash and periglacial processes (Veil et al., 1994), which were presumably interrupted by episodic lake transgressions (Hein et al., 2021).

Neanderthal occupation took place on a small alluvial fan, which likely formed between the late Eemian Interstadial and early Weichselian Pleniglacial and provided a higher and hence drier ground, in comparison to the surrounding wetlands (ibid., Fig. 1b, Supplementary Figure S49b).

2.3. Previous investigations

2.3.1. Archaeological horizon Lichtenberg I

The site Lichtenberg with its archaeological horizon Lichtenberg I (hereafter: Li-I) was discovered in 1987 by one of us (K.B.) and was subsequently excavated from 1987 to 1993 (Veil, 1995; Veil et al., 1994). The assemblage consists of about 2500 artefacts, among them 405 artefacts with recorded provenience, including 76 retouched tools (Veil et al., 1994). All artefacts are made of Baltic Flint. Most of the bifacial tools were manufactured on natural blanks, such as frost shards transported from the Saalian glacial deposits upslope and potentially directly available on the land surface (Veil et al., 1994). Cores are entirely missing in the assemblage, but faceted flake platforms may hint at the existence of Levallois blank production (Veil et al., 1994). However, faceting may

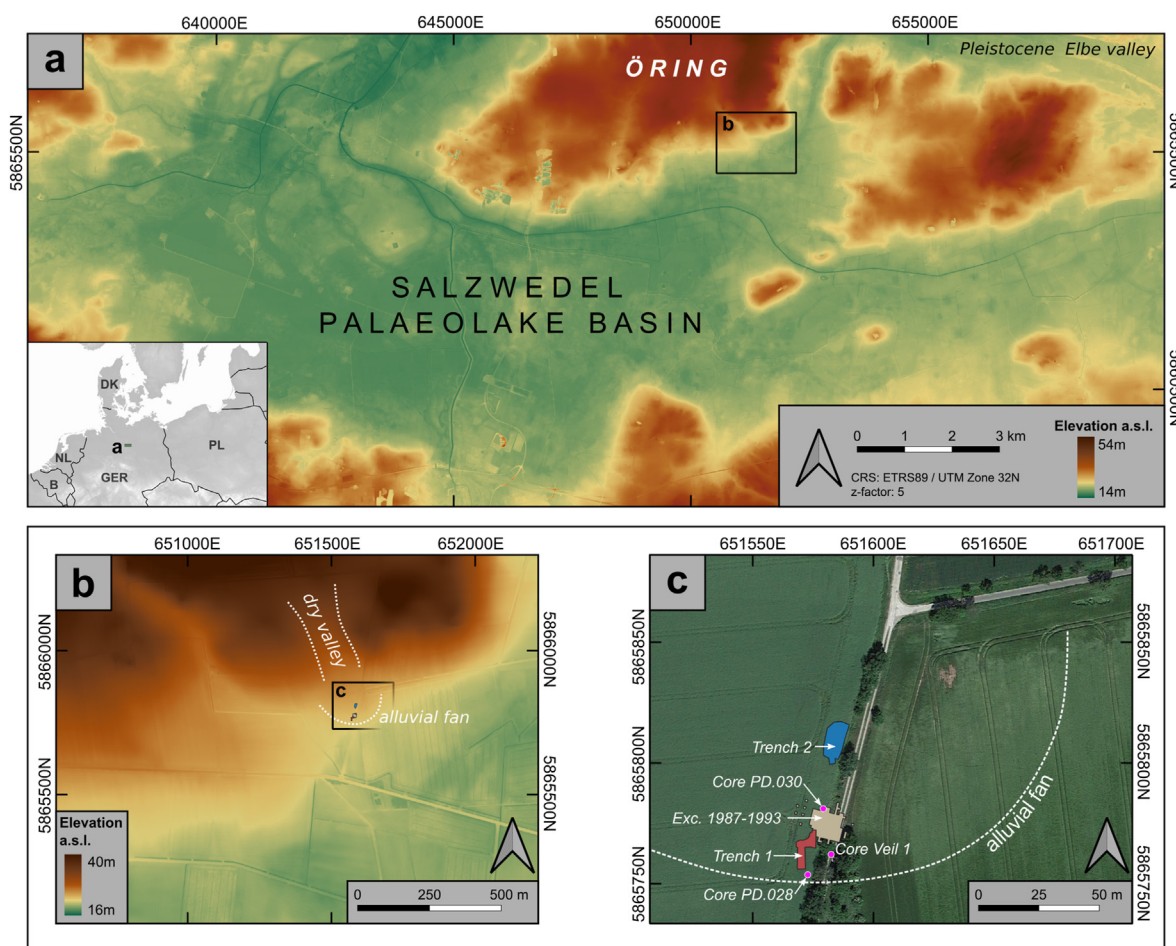


Fig. 1. Location of the study area in Northern Germany (a). The sites are situated on a small alluvial fan surrounded by lowlands (b). Panel c indicates the position of the archaeological trenches 1 and 2, the previous excavation area (1987–1993) and three sediment cores mentioned in the text (PD.028, PD.030, Veil 1). Digital elevation model (DEM 1) provided by the State Offices for Geoinformation and Land Survey in Lower Saxony and Saxony-Anhalt.

rather be the result of bifacial tool production (Veil et al., 1994; Wiśniewski et al., 2020) in this assemblage. Among the 76 tools are 19 bifacial backed knives or Keilmesser, 5 handaxes, as well as other types of bifacial tools. Keilmesser are asymmetric, mostly bifacial cutting tools with a natural and/or worked back opposite a working edge (Bosinski, 1967; Jöris, 2006, 2012; Veil et al., 1994). All of the tools have been interpreted as functionally slightly different cutting tools (Veil et al., 1994; Weiss, 2020). With a median dimension (largest width or length) of 86 mm (Supplementary Table S7) for 19 bifacial and 3 unifacial Keilmesser and one handaxe (Weiss, 2020), the tools are quite large. The assemblage is attributed to the late Middle Paleolithic Keilmessergruppen of central and eastern central Europe (Jöris, 2006, 2012; Mania, 1990; Veil et al., 1994). This represents a late Neanderthal archaeostratigraphic unit that ranges from MIS 5a to early MIS 3 (Hein et al., 2020; Jöris, 2004, 2006), and which is defined by the presence of Keilmesser. Furthermore, these assemblages are characterized by handaxes and other bifacial tools (Bosinski, 1967; Veil et al., 1994), as well as by varying blank production methods, including Levallois (Jöris, 2004; Richter, 1997). Most of the Keilmesser found in Lichtenberg I are still suitable for cutting with angles below 60° (Gladilin, 1976; Weiss, 2020), and several refits (Veil et al., 1994) evidence the production and use of the tools on the spot. This, as well as the functional uniformity point to a specialized assemblage that was produced during a short-term event, and potentially related to butchering activities, as indicated by use-wear analyses (Veil et al., 1994). The formerly-obtained thermoluminescence ages for the sediments containing the artefacts range from 66 ± 14.6 ka to 52 ± 6.8 ka (Veil et al., 1994), displaying a rather high dating uncertainty most likely resulting from the cryoturbated context in which they were found.

2.3.2. Evidence for Eemian occupation

During our coring campaign, recently published in Hein et al. (2021), we recovered a longitudinal broken flint flake (LIA-86, Supplementary Figure S13), another flint flake (LIA-187, Supplementary Figure S13), as well as a number of undetermined small chips and fragments from sandy Eemian half bog deposits of core PD.030 (6 m depth) (Fig. 1c). Some of the flint fragments are highly weathered due to the acidic, humic sedimentary environment. The two artefacts are referred to as Lichtenberg Eemian assemblage and can be attributed to Eemian pollen zone E IVb/V (Hein et al., 2021). These finds make this the northernmost Eemian site besides Lehringen, Lower Saxony/Germany (Hein et al., 2021; Nielsen et al., 2017; Thieme and Veil, 1985).

3. Methods

3.1. Fieldwork

In 2017, we localized the exact position of the 1987–1993 excavation and conducted a first attempt to locate non-cryoturbated sediments below the former trench. Then in 2019, we established geoarchaeological survey Trench 1 with a size of ca. 3 by 20 m and a depth of 2.20 m (Figs. 1c and 2a; Supplementary Figures S2 – S3). In order to better understand the stratigraphical situation of Li-I, we deliberately established Trench 1 at the southern edge of the former excavation area. Here, increasing accommodation space towards the adjacent sedimentary basin suggested less cryoturbational disturbance of the deposits. From there on, Trench 1 was extended 7 m to the south, and then, to gain a W-E profile, 7.50 m to the east and another 6 m to the south. The trench was excavated by a mechanical digger and every digger bucket was carefully searched for artefacts. If artefacts were found, the respective square meter was excavated following current standards of paleolithic excavation. We excavated the sediment by hand

according to individual layers, recorded all individual finds with a total station at a size cut-off of 1.5 cm and screened the excavated sediment with a 4 mm and a 2 mm mesh.

Furthermore, we established a north-south trending coring transect of 11 sediment cores with depths of up to 11 m. The transect started upslope, and passed through the excavation area towards the valley bottom (Hein et al., 2021). The aim was to obtain high-resolution sedimentological data about the paleolake infill. Approximately 25 m north of Trench 1, at a depth of ca. 2 m, we detected lakeshore sediments. Therefore, in this area, we established the second survey Trench 2 (Figs. 1c and 2b/c; Supplementary Figure S8), using the same geoarchaeological survey methods as described above. At the end of the field campaign 2019, we detected the Lichtenberg II (Li-II) find horizon in sandy and peaty lakeshore sediments and excavated one square meter before the season ended.

In March and June 2020, we continued fieldwork and excavated parts of the new find horizon, Li-II. The find horizon was located about 30 cm above the ground water table, necessitating the installment of a protection and water management system (Supplementary Figure S9).

All three stratigraphies presented here (Trenches 1 and 2, core PD.028, Figs. 1c and 2) were carefully described in the field, according to German soil mapping standards (AG Boden, 2005). Documented parameters included textural composition, structure, Munsell color, carbonate and gravel content, as well as hydromorphic properties. Moreover, we documented sediment structures such as bedding and cryogenic features. This allowed for the comparison and correlation of sediment units between the stratigraphies, and facilitated optimal sampling and interpretation of luminescence samples. Further stratigraphic and landscape context was provided by the remaining cores of the more extensive drilling campaign in the study area (Hein et al., 2021).

3D models and Augmented Reality 3D models of both trenches can be found under <https://marcelweiss.github.io/Lichtenberg/>.

3.2. Luminescence dating

In total, 11 samples were taken for luminescence dating, utilizing stainless steel tubes. Sampling positions are indicated in Fig. 2a/b. The material was prepared under subdued light conditions with standard methods (Aitken, 1998). As the quartz grains showed signs of early saturation (occasionally at 80–100 Gy) and inconsistent dose recovery, all measurements were conducted on coarse grain K-feldspars (125–180 μ m) using a Risø TL-DA-20 reader, equipped with IR light-emitting diodes, transmitting at 870 nm. The signal was filtered through a D-410 Chroma filter to allow detection in the blue-violet wavelength range. For sample irradiation, a calibrated $^{90}\text{Sr}/^{90}\text{Y}$ beta source was used with a dose rate of about 0.2 Gy/s. For each sample, we prepared 24 discs with very small aliquot sizes (0.5 mm) to perform multiple grain measurements applying the pIRIR₂₉₀ SAR protocol (Thiel et al., 2011) and using an a-value of 0.11 ± 0.02 (Kreutzer et al., 2014). Aliquots with a recycling ratio >10% and a recuperation >5% were excluded from age calculations. Dose rates were determined by high-resolution germanium gamma spectrometry in the VTKA laboratory Dresden (Supplementary Table S13). Further information on quality assessment and the results of dose rate determinations may be found in the Supplementary Section 6.

3.3. Palynological analysis

For biostratigraphic control and to obtain further paleoenvironmental information, we performed palynological analysis on 12 selected samples (see Fig. 2b/c, Table 1 and Supplementary

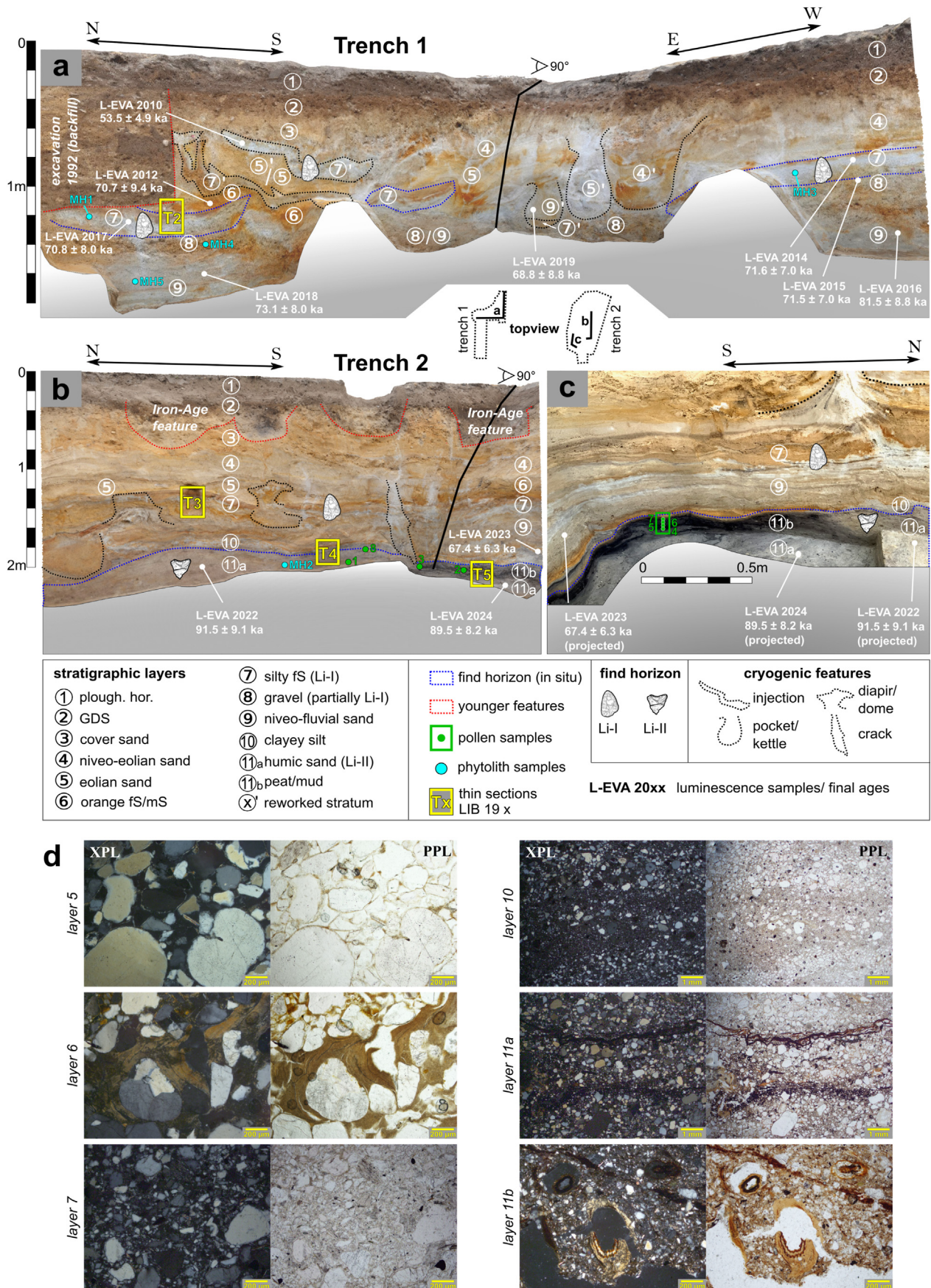


Figure S59 for sampling positions and lithological descriptions). From Trench 2, a sequence of four samples from the peaty detrital mud (samples 4 to 7; layer 11b) and supplementing bulk samples (samples 1 to 3, 8) from layers 11 (a/b/b₂) and 10 were taken. Layers 9 and 7 in Trench 1 were also sampled, but contained no pollen. Additionally, four samples (9–12) were retrieved from organogenic segments of the adjacent sediment core PD.028 (Supplementary Figure S59). All samples were treated with standard methods (Faegri et al., 1989; Moore et al., 1991), after which, pollen and spores were identified using the atlases of Faegri et al. (1989), Moore et al. (1991) and Beug (2004). Micro-charcoal particles <100 µm were counted in samples 1 to 8 and are presented alongside the pollen diagrams (Supplementary Figures S 60 and 61). The pollen sum, on which percentages of all taxa are based, is solely composed of terrestrial taxa, excluding cryptogams, Eriaceae, Cyperaceae and aquatic plants. The curve “Ericaceae indeterminate” characterizes badly preserved and therefore indeterminable Ericaceae tetrads. The arboreal pollen (AP) sum includes trees and shrubs, whereas the non-arboreal pollen (NAP) sum covers Poaceae, Cerealia-type and the group of terrestrial herbs. Pollen percentages and concentrations were calculated and displayed with the software package TILIA (Grimm, 1990). For detailed results and interpretation, see section 4.3 and Supplementary Section 7.

3.4. Phytolith analysis

To complement the palynological findings, we vertically sampled sediment from Trench 1, layer 7 (one sample each from the eastern and southern profile: samples MH1 and MH3), layer 8 (MH4) and layer 9 (MH5), and also from layer 11a in Trench 2 (sample MH2) (Fig. 2, Supplementary Table S15). Phytoliths were extracted from the sediment using a version of the Rapid Phytolith Extraction method at the Max Planck Institute for Evolutionary Anthropology (Katz et al., 2010). Phytoliths were counted on single and multi-cell counts using standard methods (Power et al., 2014). We aimed to count >200 phytoliths per sample but in some phytolith-poor samples, we could only reach 150–200. Phytolith concentrations based on the acid insoluble fraction (AIF) were also calculated to assess sediment diagenesis. Detailed sample preparation, results and interpretation can be found in Supplementary Section 8.

3.5. Micromorphology

We collected five oriented block samples for micromorphological analysis. Samples LIB 19 1 and LIB 19 2 were taken from Trench 1, samples LIB 19 3 to LIB 19 5 from Trench 2 (Fig. 2d, Supplementary Figure S50). Thin sections were prepared by G. MacLeod (University of Stirling, UK) and their analysis was performed on a petrographic microscope with a magnification of 20x to 200x using oblique incident (OIL), plane- (PPL) and cross-polarized light (XPL). Micromorphological descriptions follow established nomenclatures (Stoops, 2003; Stoops et al., 2010). Results and interpretation can be found in section 4.4 of the main text and in the Supplementary Section 5.3.

3.6. Grain size analysis

To support field descriptions and for the better assessment of sedimentary environments, we conducted grain size analysis on 28 bulk samples from most layers in both trenches (all except 1, 2, 8 and 11b) at the Leibnitz Institute for Applied Geophysics, Hannover/Germany (see Table 1 for lab codes and positions). We utilized a Beckman-Coulter LS 13320 PIDS laser diffractometer, which detects a spectrum from 0.04 to 2000 µm. We mostly followed the measurement protocol described by Machalett et al. (2008). Deviating from this, for dispersion, we treated the samples with 1% ammonium hydroxide solution (NH₄OH) and planted them in overhead rotators for >12 h. We refrained from removing organic matter and carbonates as pre-tests implied low contents, which were shown to be negligible for the grain size distribution (Beuselinck et al., 1998). All samples were subjected to a fivefold measurement and subsequently averaged, whereby sample clusters with a standard deviation > 5% were rejected.

3.7. Lithic analysis

The lithic artefacts were recorded using a detailed attribute recording system, published in detail recently (Weiss, 2015, 2019). For the aim of this study, mainly the following attributes were selected from the dataset (see Supplementary Sections 3.5–3.7): the raw material, the state of preservation, the blank type, maximum length, width, thickness, and weight. Here, the maximum dimensions were measured, whereby flake length was measured in flaking direction. The length of cores was measured in the direction of the last flake removal. The maximum length of flake tools was also measured in flaking direction, whereas the length of tools made from cores or natural blanks was measured along the technical axis (i.e., in direction of the longest working edge). Furthermore, for the flakes were recorded: the state of the platform, the exterior platform angle (EPA), the amount of worked surface on the dorsal face (i.e., flake scars), and the direction of the dorsal scars. For cores, the amount of worked (flaked) surface was recorded, as well as the number of flaking surfaces, the number of flake scars, the flaking (or striking) angle, the condition of the striking surface, and the flaking directions. Because the tools from Li-II are typologically diverse, and often combine several types on single tools together with recycling and reuse (see below), we could not always apply strict typological schemes. Where possible (e.g., notches, denticulates), types from the Bordian typology were adopted (Bordes, 1961; see also Pop, 2014 for the use of types in Eemian assemblages). Besides retouched flakes, flakes with possible macroscopic use-wear were also counted as flake tools.

The full attribute dataset is available as Supplementary Datafile (.csv).

3.8. Traceology

To provide additional data on the nature of the Neanderthal occupation at the Middle Paleolithic sites of Lichtenberg I and II, traceological analysis were conducted on a sample of 27 artefacts. Traceology (Semenov, 1964) aims to identify specific taphonomical, technological and functional traces or modifications, which allows

Fig. 2. Stratigraphic features and archaeological horizons, along with sampling positions for luminescence dating, pollen analysis and micromorphology in Trench 1 (a) and Trench 2 (b and c). GDS refers to “Geschiebedecksand” a late Weichselian solifluction layer (Table 1, Supplementary Section 5.1). (d) Microphotographs of thin sections in cross-polarized (XPL) and plane-polarized (PPL) light. Photograph of layer 5 taken from sample T3, layer 6 from T1, layer 7 from T2, layers 10 and 11a from T4 and layer 11b from T5. Layer 5 is dominantly composed of coarse sand to silty quartz grains in a massive microstructure; layer 5 shows the same composition as layer 6, but here void space is filled by clay illuviation; layer 7 shows a poor sorting for fine sand to silt sized quartz grains in a dense microstructure that presents a barrier for the clay moving down with pore water; layer 10 shows bedding of silty to coarse-sand sized quartz; layer 11a is characterized by organic-rich bands composed of amorphous staining, plant cells and tissues with rare bioturbation voids; in layer 11b organic residues increase in size as well as number and bioturbation voids are more ubiquitous.

Table 1

Sedimentary properties of the stratigraphic layers, including their interpretation (cf. [Supplementary Section 5](#)) and the sample codes for grain size analysis. Grain size samples taken layer-wise: samples 1–16 from Trench 1, samples 17 to 28 from Trench 2. The column “presence” indicates in which trench the respective layer occurs, Trench 1, Trench 2 or both (Tr1, Tr2).

Layer	Pre- sence	Thickn. (cm)	Sediment Description	Interpretation	Grain Size Sample
1	Tr1, Tr2	<40	Gravelly, slightly silty sand; very poorly sorted; humic (ca. 2%), related to layer 2	ploughing horizon formed in layer 2	–
2	Tr1, Tr2	<25	Gravelly, slightly silty sand; very poorly sorted; coincides with brunified horizon (Cambisol); unbedded; higher gravel content than in layer 3	periglacial cover bed, 'Geschiebedecksand' (GDS)	1, 17
3	Tr1, Tr2	50	Slightly gravelly and silty, poorly sorted, yellow medium sand; weakly-bedded; stoneline at its lower boundary	cover sand , solifluctive/colluvial facies	6, 18
4	Tr1, Tr2	50	Thin-bedded, wavy, moderately to poorly sorted, fine to medium sands; pale yellow; interbedded with thicker lenses of better sorted (aeolian) medium sands which are similar to layer 5	niveofluvial to niveo-aeolian facies, partially reworking layer 5 (?)	2, 19, 20,
4'	Tr1	Pocket	Original structure of layer 4 recognisable, but deformed and slightly mixed within a pocket (ca. 50 cm deep); hydromorphic overprint	cryoturbation pocket affecting layer 4	13, 15
5	Tr1, Tr2	10/30	Very loose, yellow medium sand, better sorted than surrounding layers; inclined bedding to sheet-like (unbedded)	aeolian sand (saltation)	3, 8, 11, 21
5'	Tr1 (Tr2)	Various	Similar characteristics as layer 5 but with cryogenic overprint (injections or pockets)	cryoturbation affecting layer 5	14
6	Tr1, Tr2	20	Poorly to moderately sorted, fine to medium sands, orange oxidation color; unbedded	no interpretation (may belong to adjacent layers)	22
7 Li –I	Tr1, Tr2	<15	Fine sandy very coarse silt to silty very fine sands; whitish, brown-orange ferrugination on top with drop-shaped boundary on mm to cm-scale; very poorly sorted; contains find horizon Li–I	lacustrine shoreline facies	4, 9, 23
7' Li –I (Tr2)	Tr1	10/20	Main characteristics similar to layer 7; distorted; mixing with medium sand; contains artefacts of find horizon Li–I	layer 7 injected upwards by cryoturbation	7
8	Tr1	20/40	Fine to medium gravelly, medium sands; poorly sorted; gleyic (greyish-light br.), crudely bedded, contains lithic artefacts in the upper 5 cm (lower part of find horizon Li–I)	higher-energy niveofluvial slopewash	–
9	Tr1, Tr2	40/ > 100	Thin-bedded, wavy, moderately to poorly sorted fine to medium sands; gleyic (greyish-light brown)	niveofluvial slopewash	5, 10, 12
9'	Tr1	Pocket	Gleyic, poorly sorted fine sand, characteristics of layer 9 discernible, even weak wavy bedding	cryoturbation pocket affecting layer 9	16
10	Tr2	<10	Gleyic, fine sandy to loamy silt; covers layer 11b as a thin veneer; contains very thin humic bed (drift line)	lacustrine facies , with contained drift line	26, 27, (28)
11a Li- II	Tr2	>100	Very coarse-silty fine sand, slightly humic (<0.5%); very poorly sorted; unbedded; contains find horizon Li-II and abundant small pieces of charred organic matter (both esp. in the uppermost 11 cm)	colluvial to lacustrine shoreline/ beach facies, contains drift lines	24, 25, (28)
11b	Tr2	<20	Peaty detrital mud, interfingering with layer 11a, in places overlain by thin (<1 cm) grey silt (part of layer 10?)	lake moor near the shoreline	–

us to reconstruct (i) specific technical behaviors, (ii) the post-depositional history of anthropic inclusions within sedimentary units, as well as (iii) how and for which purpose stone tools were made and used at a specific site. This is achieved by systematically scanning the edges and surfaces of stone tools under different magnifications ranging between 0.63x to 500x and plotting their location and distribution. The location and morphology of specific micro negatives, edge rounding, microscopic polish, micro scars and striations are compared to an experimental reference collection in order to establish the kinetics of stone tool use as well as the worked material ([Chan et al., 2020](#); [González-Urquijo and Ibañez-Estéves, 1994](#); [Keeley, 1980](#); [Vaughan, 1985](#)). Here, we used a Carl Zeiss Stemi 508 stereo microscope and an Olympus BXFM reflected light microscope.

4. Results

4.1. Stratigraphy

4.1.1. General stratigraphy

The sedimentary record within the Trenches 1 and 2 can be subdivided into 11 sediment layers ([Fig. 2](#), [Table 1](#)). The majority of these sediments are the product of the redeposition of Saalian glaciofluvial sands on the slope by different processes and over short distances (<100 m). These processes include solifluctive, niveofluvial, aeolian deposition. Furthermore, lacustrine deposits occur (see more detailed information in [Supplementary Sections 5.1 and 5.2](#)):

Solifluctive deposits (layers 2 and 3): Deposition and

redeposition of solifluctive sediments happens in periglacial environments under the influence of seasonally thawing permafrost ([French, 2008](#)). This usually leads to unbedded sediments. However, as solifluction can alternate with slopewash or aeolian sedimentation, internal stratification of respective layers may occur, as is the case in layer 3.

Niveofluvial deposits (layers 4, 8 and 9): Niveofluvial deposition is a slopewash triggered by annual snowmelt in sparsely-vegetated environments together with possible involvement of aeolian input ([Christiansen, 1998a](#); [Menke, 1976](#); [Zagwijn and Paepe, 1968](#)). This results in the formation of thin wavy beds of fine and middle sands, and sometimes gravel.

Aeolian deposits (layer 5): Evidence for purely aeolian sedimentation of layer 5 is provided by its mean grain size (ca. 350 µm), good sorting and inclined bedding (ca. 15°), in combination with abundant surficial impact scars and a notably loose overall structure. There are indications that this aeolian material has been transported by saltation rather than in suspension (cf. [Farrell et al., 2012](#); [Schwan, 1988](#)) (see [Supplementary Sections 5.1 and 5.2](#)).

Lacustrine deposits (layers 7, 10 and 11): In contrast to these slope and sensu stricto periglacial deposits from proximal sources, these layers are of lacustrine origin, i.e. their formation is connected to the presence of a paleolake (see directly below and [Supplementary Sections 5.1 and 5.2](#)).

Eight of the eleven layers were encountered in both trenches. Correlation was based on the agreement of macroscopic properties detected during field work, as well as micromorphological evidence and detailed evaluation of the grain size data ([Figs. 2 and 3](#), [Supplementary Sections 5.2 and 5.3](#)). The upper part of the

sequence was subjected to likely multi-phased cryoturbation in the form of different involutions, both directed upwards and downwards (Fig. 2). With amplitudes of several decimeters to nearly 1 m, these phenomena were likely produced by permafrost dynamics (cf. Vandenberghe, 2013). These features are frequent in layers 1 to 6, occasionally reaching down to layer 9, and result in a somewhat fragmentary appearance of archaeological find horizon Li-I (stratigraphic layers 7 and 8). Nevertheless, based on field observations, Li-I can predominantly be identified in an in-situ stratification. Find horizon Li-II in stratigraphic layer 11 remained entirely unaffected by those involutions.

Based on the lithological findings in Trenches 1 and 2, a schematic stratigraphy was established (see sections 5.2 and 5.3, Fig. 7), which in turn can be largely correlated with the sediment sequence of core PD.028, directly adjoining Trench 1 to the south (Figs. 1 and 2; Supplementary Figure S59). The core penetrated most layers encountered in the excavations. In addition, it exposes three organogenic segments within and below niveofluvial sands, equivalent to layer 9: A peaty mud (230–250 cm coring depth) and a strongly humiferous sand (355–390 cm coring depth) surrounded by these niveofluvial sands, and a peaty layer (465–555 cm coring depth) directly at their base. These organic-rich deposits testify to the wetlands that surrounded the former occupation site on an alluvial fan (Fig. 1, Supplementary Figure S49b) (description of core PD.028 in Supplementary Table S11).

4.1.2. Stratigraphy of the find layers Li-II and Li-I

Because of their archaeological significance, the occupational layers deserve closer consideration. Layer 11, only present in Trench 2 is a two-part formation (11a and 11b), whose members inter-finger with each other (Fig. 2c). Layer 11a (Li-II) is a slightly humic, unstratified silty fine sand, containing horizontally-oriented fragments of (charred) plant material and several thin humic drift lines, that are visible both macro- and microscopically (Supplementary Figures S52c, S59). We interpret this deposit as the beach facies of an adjoining water body (cf. Bridge and Demicco, 2008; Cohen, 2003), with the drift lines indicating fluctuations in the water-table. Layer 11b is a peaty and sandy, coarse-detrital mud with a thickness of ca. 10 cm. It grades into a humic silt (11b2) to the top and towards the intersection with layer 11a (Supplementary Figure S59). Layer 10 is a thin (<10 cm) veneer of laminated, fine-

sandy, loamy silt, that covers layer 11a. It also contains a humic drift line, and it directly emerges from the peaty detrital mud (layer 11b) and wedges out on higher ground. This layer 10 is interpreted as a lacustrine muddy shore-face deposit, caused by a rising water table (see Supplementary Section 5.1). The artefacts are scattered between a total elevation of $Z = 18.84$ m and $Z = 19.55$ m [a.s.l.] within layer 11a. This scattering is mainly caused by the inclination of the find layer towards the shore. However, based on the distribution of screen finds <1.5 cm within each quarter square, as well as the exact position of single finds >1.49 cm, we could identify a main artefact scatter in the uppermost part of layer 11a, between $Z = 19.10$ m and $Z = 19.21$ m (Supplementary Section 2.2). This distribution pattern reduces the thickness of the main find horizon to 11 cm. In addition, some artefacts were obtained from the contact zone of the top part of layer 11a and the bottom part of layer 11b (as 11b interfingers with 11a).

Find horizon Li-I (primarily in Trench 1) is mainly contained within stratigraphic layer 7 but also includes the upper part of layer 8 (Fig. 2a). It is possible that we have evidence here for succeeding occupations, which needs to be clarified by future field work. Layer 8 is a massive to crudely-bedded, niveofluvial slope wash deposit, consisting of gravelly medium sands with gleyic properties. The layer is discordantly overlain by layer 7, a thin (<10 cm) whitish, very fine-sandy silt to silty very fine sand. Our layer 7 matches the sedimentological characteristics of the main Middle Paleolithic find horizon as described in Veil et al. (1994). In the thin sections, layer 7 stands out for its remarkably low porosity and fine horizontal layering. Because of these properties comparable with layer 10, we likewise interpret layer 7 as lacustrine shoreface deposit. In Trench 2, layer 7 intertongues with the underlying slope deposits of layer 9. The single tongues of interbedded lacustrine sediments from layer 7 unify on top of layer 9 towards higher ground (Fig. 2c). This indicates alternating conditions of slope and lacustrine deposition, and testifies to their broad contemporaneity. Due to cryoturbation, layer 7 with the contained artefacts is occasionally deformed upwards in the form of diapirs or injections (then referred to as layer 7'). Based on the small number of artefacts recovered during our fieldwork (see below), we were not able to perform a statistical find distribution analysis for Li-I in our excavation. In this regard, the reader is referred to Veil et al. (1994).

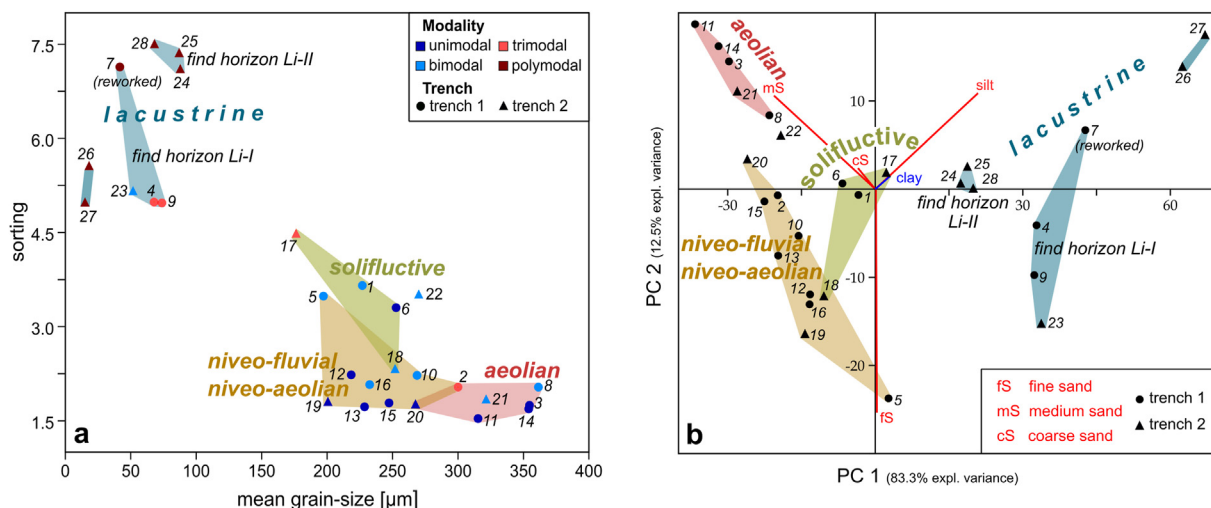


Fig. 3. Statistical analyses of grain size results. (a) Scatter plot of sorting and mean grain size. (b) Principle component analysis (PCA) with the most significant principle components (PC1 and PC2) shown. Convex hulls of sedimentary processes according to classification during field description. Stratigraphic layers related to the sample codes indicated in Table 1.

4.2. Luminescence dating

Luminescence dating yielded ages between 53.5 ± 4.9 and 91.5 ± 9.1 ka (samples L-EVA, 2010 and 2022) (Figs. 2 and 7, Table 2). The dated layers 6 to 11, including the archaeological find horizons are well aligned chronologically. For find horizon Li-I (stratigraphic layers 7 and top of layer 8), the three samples (L-EVA, 2014, 2015 and 2017) range between 70.8 ± 8.0 and 71.6 ± 7.0 ka with a mean age of 71.3 ± 7.3 ka. Find horizon Li-II (stratigraphic layer 11) gave an age between 89.5 ± 8.2 and 91.5 ± 9.1 ka and a mean age of 90.5 ± 8.7 ka (samples L-EVA, 2024 and 2022). Sample L-EVA 2010, taken in a position where find horizon Li-I was cryoturbated upwards, gave a cryoturbation age of 53.5 ± 4.9 ka. This is close to the previous TL-age of 57 ± 6 ka for this site (Veil et al., 1994). More details on data evaluation, equivalent dose (D_e) estimation and age calculation can be found in Supplementary Section 6.

4.3. Palynology

The pollen spectra and vegetation succession of sublayers 11a and 11b (incl. 11b₂) from Trench 2 (Fig. 2b and c; Supplementary Figures S60 and S61) are quite similar. They contain about 80–85% woody taxa (arboreal pollen, AP) consisting mainly of *Pinus* and *Betula* and very few *Alnus*, *Larix*, *Myrica*, *Juniperus* and *Picea*, while the NAP (non-arboreal pollen) are represented by Poaceae, Cyperaceae and heliophile herbs, which is indicative of a densely wooded boreal conifer forest. Sparsely occurring pollen of aquatic and wetland taxa like *Sparganium spec.*, respectively *Montia* indicate open water and swampy environments. In layer 10, the strong increase of Poaceae (40%), different NAP, and the drop of *Pinus* (15%) associated with *Betula* amounts of about 30%, and occurrences of the cryptogams *Ophioglossum* and *Selaginella selaginoides* are interpreted as a strong opening of the landscape towards a tundra-like vegetation. This sequence (layers 11a, 11b, 11b₂ and 10) is indicative of the late Brörup Interstadial, transitioning into the following Rederstall Stadial (Behre, 1989; Menke and Tynni, 1984; Veil et al., 1994; Supplementary Section 7).

In core PD.028, the lower peat at 465–555 cm shows distinct interstadial conditions with AP spectra characterized by *Pinus*, *Betula*, *Picea* and *Larix*, which amount to 80–90% (Supplementary Figure S62). A diverse heliophile pollen flora consisting of *Valeriana vulgaris*-type, *Matricaria*-type and *Artemisia* furthermore characterizes dry boreal forest habitats.

Both the sandy humiferous layer (355–390 cm) and the coarse detrital, peaty mud (230–250 cm) in superposition reveal pollen spectra dominated by NAP (up to 60%) with high amounts of Poaceae. The rich heliophile flora includes among others *Artemisia*, *Valeriana montana*-type, *Matricaria*-type, *Polygonum bistorta*-type,

Helianthemum oelandicum-type, *Epilobium* and *Chenopodiaceae*. Among the wooden taxa, *Betula* reaches about 30%, whereas *Pinus* values have dropped down to <15%. The spectra therefore clearly reflect a phase of rather open landscape and dry and cold conditions, also indicated by the massive occurrence of colonies of the cold-tolerant green alga *Pediastrum kawraiskyi*.

The lowermost two bulk samples are correlated with the Odderade Interstadial, WF IVb (Behre, 1989; Menke and Tynni, 1984; Veil et al., 1994; Supplementary Figure S62), whereas the uppermost samples most probably represent early phases of the Schalkholz, WP I Stadial. Pollen diagrams and detailed interpretation are presented in Supplementary Section 7 and the main palaeoenvironmental results and biostratigraphical subdivision can be found in Table 3 and Supplementary Tab. S14.

4.4. Micromorphology

The analyzed sequence is dominated by quartz sand, common clay and rare inclusions of organic material and mica. Anthropogenic remains, flint and charcoal are rare and only occur in the lithofacies associated with the archaeological layers. The microstructure and fabric, i.e., horizontal orientation of plant residues, channels filled with clay, and the good preservation of organic material indicate waterlain, potentially lacustrine environments with incipient soil formation (Bouma et al., 1990; Cohen, 2003; Taylor et al., 1998) for the lower part (layer 11a/b, 10). In contrast, for the upper part (layers 9 to 5) of the sequence the micromorphological analysis does not allow a differentiation between waterlain and aeolian deposition. Turbation features are overall rare and limited to individual layers, indicating good integrity of the archaeological assemblage. We did not, however, sample and analyze the cryoturbated parts of the sequence. The upper find horizon, Li-I, is associated with a fine and compact lithofacies (layer 7), however, the origin of this compaction was not apparent in thin section. No cementation features were observed at this scale of observations, instead the grains appear as very densely packed with very limited void space. The overlying coarse-grained layer 6 shows intense clay illuviation with the compacted, fine grained layer 7 presenting a barrier to the downward transportation of clay. This clay illuviation is not associated with further soil formation features, and it is therefore unclear whether this clay illuviation represents a soil formation process and to what former surface this process may be connected. For more details, see Supplementary Figures S 50 to S 55 and Supplementary Section 5.3.

4.5. Phytolith analysis

The ratio of grass short-to long-cells was measured to ascertain

Table 2

Results of the De-measurements along with the final pIRIR₂₉₀ luminescence ages. OD = Overdispersion value, No.al = Number of aliquots included in the age calculations. CAM = Central Age Model, MAM = Minimum Age Model, WM = Weighted Mean. ¹σb value of 0.11 was used for MAM. The choice of age model is explained in Supplementary Section 6.3

Lab.-ID (L-EVA)	Layer	D_e (Gy), 1σ	DR_{total} (Gy/ka)	Age (ka), 1σ	OD (%)	No. al.	Dose Model ¹
2010	7' – Li-I	131.9 ± 4.3	2.46 ± 0.21	53.5 ± 4.9	14.7 ± 0.4	24	MAM
2012	6	110.7 ± 4.3	1.57 ± 0.20	70.7 ± 9.4	16.0 ± 0.5	24	MAM
2014	7 – Li-I	160.8 ± 3.8	2.25 ± 0.21	71.6 ± 7.0	11.3 ± 0.4	23	MAM
2017	7 – Li-I	143.9 ± 8.2	2.03 ± 0.20	70.8 ± 8.0	21.4 ± 0.6	24	MAM
2015	8 – Li-I	174.8 ± 7.5	2.44 ± 0.21	71.5 ± 7.0	19.4 ± 0.6	24	CAM
2019	9*	112.4 ± 3.4	1.63 ± 0.20	68.8 ± 8.8	13.9 ± 0.4	24	CAM
2023	9	155.0 ± 4.8	2.30 ± 0.20	67.4 ± 6.3	14.7 ± 0.5	24	CAM
2018	9	137.3 ± 3.4	1.88 ± 0.20	73.1 ± 8.0	11.7 ± 0.4	24	CAM
2016	9	163.3 ± 5.0	2.00 ± 0.21	81.5 ± 8.8	11.8 ± 0.5	17	MAM
2022	11 – Li-II	254.7 ± 16.7	2.78 ± 0.21	91.5 ± 9.1	29.4 ± 1.0	21	CAM
2024	11 – Li-II	241.1 ± 12.7	2.69 ± 0.20	89.5 ± 8.2	20.9 ± 0.7	22	WM

Table 3

Comparison and correlation of pollen samples 1 to 8, taken from layer 11 and 10, trench 2 (2019 and 2020 excavations) and samples 9 to 12 (core PD.028). Biostratigraphic assignment follows Menke and Tynni (1984); Behre and Lade (1986). For sampling codes and positions, see Fig. 2b/c, Supplementary Figure S59. n.r. = not resolved. Correlation with Marine Isotope Stages (MIS) follows Lisiecki and Raymo (2005a) and the lithostratigraphic lexicon LITHOLEX of the German Federal Institute for Geosciences and Natural Resources, BGR (<https://litholex.bgr.de>).

Trench 2, excavation 2019		Trench 2, excavation 2020		Core PD.028		Biostratigraphy	MIS
Layer (Sample)	Vegetation	Layer (Sample)	Vegetation	Layer (Sample)	Vegetation		
n.r.	—	n.r.	—	peaty mud (12)	open landscape with dominant NAP (Poaceae and heliophile herbs), <i>Pediastrum</i>	two minor interstadial oscillations in the earliest Schalkholz (WP I)	4
n.r.	—	n.r.	—	hum. sand (11)			
n.r.	—	n.r.	—	Peat (9, 10)	dense boreal forest with <i>Pinus</i> , <i>Betula</i> , <i>Juniperus</i> and <i>Larix</i>	Late Odderade Interstadial WE IV b	5a
10 (8)	<i>Betula</i> , very few <i>Pinus</i> , Poaceae, heliophyte-rich open vegetation, micro-charcoal peak	11b (7)	<i>Betula</i> , very few <i>Pinus</i> , Poaceae, heliophyte-rich (<i>Ophioglossum</i>) open vegetation, micro-charcoal peak	n.r.	—	Early Rederstall Stadial WE III	5b
n.r.	n.r.	11b (6)	Decrease of <i>Pinus</i> , increase of <i>Betula</i> and heliophytes	n.r.	—	Transition of WE II b to WE III	5c/5b
11b ₂ (3)	Boreal forest opening up; <i>Pinus</i> , <i>Betula</i> , <i>Juniperus</i> , very few <i>Picea</i> , <i>Alnus</i> and <i>Larix</i> ;	11b (5)	Boreal forest opening up; <i>Pinus</i> , <i>Betula</i> , <i>Juniperus</i> , very few <i>Picea</i> , <i>Alnus</i> and <i>Larix</i> ;	n.r.	—	Late Brörup Interstadial WE II b	5c
11b (2)	Poaceae; <i>Selaginella selaginoides</i> , <i>Ophioglossum</i> , <i>Botrychium</i>	11b (4)	Poaceae; <i>Selaginella selaginoides</i> , <i>Ophioglossum</i> , <i>Botrychium</i>			find horizon Li-II	
11a (1)							

phytolith preservation, given that short-cells are more likely to preserve than long-cells due to their shape and higher silicification (Supplementary Table S16). Of the five analyzed samples, MH3 and MH5 (layers 7 and 9) showed lower ratios, which is suggestive of poorer preservation (Madella and Lancelotti, 2012). However, the rarity and widespread absence of dendritic long-cells indicate some taphonomic alteration in all samples. The ratio and the presence of dendritic long-cells in MH2 (layer 11a) indicates that this sample has the least taphonomic alteration. Long-cells, such as psilate and sinuate types, dominate all the assemblages, and are typical of monocot plants, particularly Poaceae. We also found many short-cells and some bulliforms, which again shows the presence of grasses as a vegetation component. Less important were phytoliths produced by eudicot shrubs and trees. These include the two main categories; wood/bark and leaves. Eudicot leaf types were found in MH4 (layer 8). Wood/bark types occur in MH2 (layer 11a) and MH3 (layer 7). In addition, sclereids deriving from sclerenchyma were found in MH3 (layer 7). Unspecific eudicot types were found in all samples, except MH5 (layer 9). This indicates the presence of a shrubby vegetation component. The relatively low total numbers in most of the samples imply a low bioproductivity with constrained growing conditions that deposited only few phytoliths. In that way, samples MH1 and MH3 to MH5 (layers 7 to 9) are very similar. In contrast, the far richer assemblage in MH2 (layer 11a) indicates warmer and wetter conditions that fostered a plant-rich environment, including grasses and woody plants (see Supplementary Tables S16, S17; Supplementary Section 8).

4.6. Grain size analysis

The 116 grain size fractions (0.04–2000 µm) for each sample were subjected to uni- and multivariate statistical analysis. Firstly, we calculated the sorting and the mean grain sizes (Blott and Pye, 2001; Folk and Ward, 1957) and displayed them as a scatter plot (Fig. 3a). Secondly, a principal component analysis (PCA) was conducted and the most significant principal components PC1 and PC2 were displayed, together accounting for 95.8% of the total data variance (Fig. 3b). In both graphs, we assigned each sample to the sedimentological process identified during field descriptions (and

micromorphological analysis, if applicable) and constructed convex hulls around all processual clusters. Both graphs differentiate well between the different classes formed during fieldwork, encompassing aeolian, niveofluvial/niveoaeolian, solifluctive and lacustrine processes. This satisfactory discrimination was unexpected, seeing that the Saalian glaciofluvial sediments as main source material for the analyzed slope deposits crop out <100 m upslope, and grain size sorting is i.a. a function of transport distance. Moreover, all classes in the graphs contain samples from Trench 1 (dots) and Trench 2 (triangles), providing further evidence that layers 3, 4, 5, 7 and 9 can be directly correlated in both trenches (Figs. 2 and 3, compare Table 1). A more detailed evaluation and interpretation of the grain size data is provided in Supplementary Section 5.2.

4.7. Archaeology

4.7.1. Lichtenberg I

During our initial survey in 2017, we found one Keilmesser (Fig. 4: 1) and one fragment of a bifacial tool (Supplementary Figure S1) in the cryoturbated layer 7' below the 1987–1993 excavation trench. In the course of our fieldwork in 2019, we excavated 17 flakes (Fig. 4: 2–7) and three cores from Trench 1. One flake was found in the cryoturbated layer 7' (Fig. 2a), 12 artefacts in layer 7 and seven artefacts in layer 8. All artefacts are made of Baltic Flint. Although being low in number and mostly typologically rather undiagnostic, finds like the Keilmesser from layer 7' as well as a relatively large flake that is potentially a product of bifacial reduction (Fig. 4: 6) helped, in addition to the sedimentological characteristics of the deposit (see section 4.1 above), to identify layer 7 as equivalent to the main find horizon of the 1987–1993 Keilmessergruppen assemblage (see Veil et al., 1994). One additional flake (Fig. 4: 8) was recovered from Layer 7 in Trench 2. This also supports an archaeological connection of the stratigraphies in Trench 1 and Trench 2.

Lichtenberg I - Traceology. Our preliminary traceological analysis (Supplementary Section 4, Supplementary Table S10) revealed neither use-wear traces on the two flakes analyzed, LIA-36 and LIA-50 (Fig. 4: 6, 7), nor on the bifacial tool fragment Li-6. For the

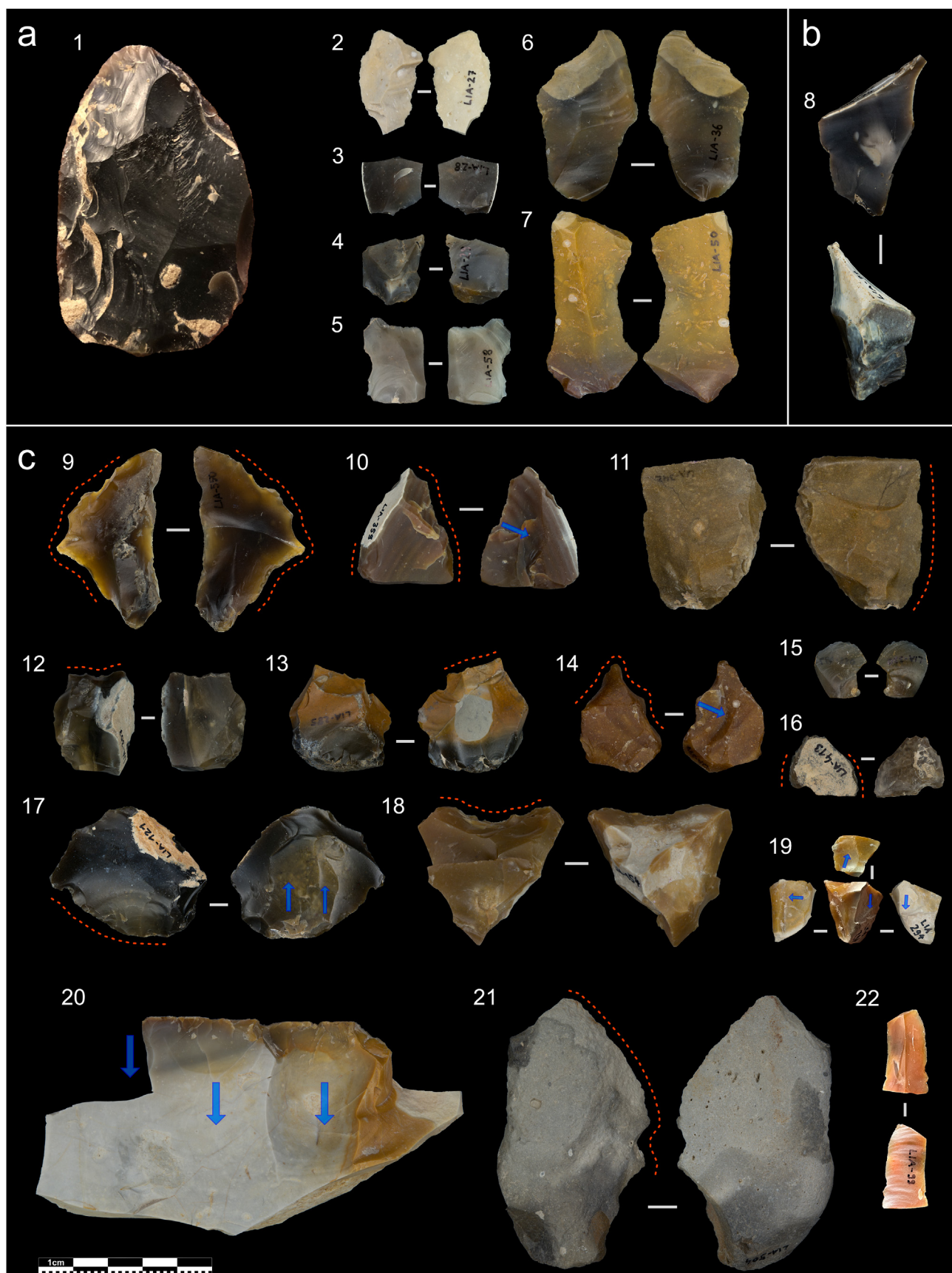


Fig. 4. Artefacts from Lichtenberg I (a), (b) and II (c) discovered in Trench 1 (a) and Trench 2 (b), (c). (a) 1 – Keilmesser (Li-7; Layer 7’); 2 – flake (LIA-27; Layer 7); 3 – proximal flake (LIA-28; Layer 7); 4 – flake (LIA-29; Layer 7); 5 – flake (LIA-58; Layer 8); 6 – flake from bifacial tool production (LIA-36; Layer 7); 7 – flake (LIA-50; Layer 8); (b) 8 – flake (LIA-74;

analyzed Keilmesser Li-7 (Fig. 4: 1; Fig. 5), however, the wear traces suggest its use as a hafted butchering knife. The tool is made of dark Baltic Flint, and shows little signs of severe post-depositional mechanical damage or chemical weathering that could have hindered the preservation of wear traces. Traces indicating the natures of the transformed material, however, are subtle and constricted to lightly developed micro polishes zones located on the distal portion of the working edge (Fig. 5a: F1). Negative edge rounding and additional polished surfaces are found further inwards on the dorsal side of the working edge (Fig. 5a: F2). Directional markers, including striations running parallel to the working edge of the tool and generally associated with lightly developed polished spots are also located on the dorsal surfaces of the working edge (Fig. 5a: F3 and F4). In combination with the micro negatives located on the ventral side of the tool (Fig. 5a: F5 and F6), a longitudinal cutting motion under the excretion of pressure is suggested, what is comparable with the interpretation of previous traceological analyses from Lichtenberg I (Veil et al., 1994). The lightly-developed polish and the presence of striations on the analyzed specimen indicates the processing of a soft organic material and occasional contact with harder organic substance. Therefore, we suggest the use as butchering knife.

The back of Keilmesser Li-7 shows a series of marked modifications and traces that are associated with intense mechanical stress (Fig. 5b). The distal portion of the back shows marked rounding and crouching that are evident by short continuous micro-negatives with step and hinge terminations (Fig. 5b: F1 and F2). Bright and semi-undulating cohesive polished areas were identified on the edges of the negatives located on the medial portion of the back, indicating the repeated contact with a hard organic substance (Fig. 5b: F3). Together, these signs may indicate the continued mechanical friction of the tool with a hard organic haft, thus possibly indicating the use of composite tools by Neanderthals at Lichtenberg. Regarding the common interpretation that Keilmesser were handheld tools (e.g., Jöris, 2006), we do not suggest that Keilmesser tools were generally hafted. However, our results make it paramount to conduct further investigations into the subject.

4.7.2. Lichtenberg II

We discovered 192 artefacts (Supplementary Table S3; Supplementary Table S9; Supplementary Datafile) in find horizon 11a (Fig. 7). 173 artefacts are preserved in a fresh condition, 7 are rolled and 12 show light edge damage (see Supplementary Datafile). The assemblage is dominated by flakes, followed by cores and flake tools. The assemblage further includes shattered pieces and core tools. We also found three manuports and one piece that was typed as 'other' which are most likely raw material imports and/or hammerstones. If we exclude manuports ($n = 3$), other ($n = 1$) and shatter ($n = 25$), the remaining assemblage of 163 artefacts consists of 51.5% flakes ($n = 84$), 30.1% tools ($n = 49$) and 18.4% cores ($n = 30$). However, the category of tools also includes cores that were later transformed into tools, so that the original share of cores was higher ($n = 42$, see Supplementary Section 3.5, 3.7). Nevertheless, the share of tools is relatively high compared to Lichtenberg I (18.8% (Veil et al., 1994)).

Lichtenberg II - Raw material. The artefacts are made

predominantly of Baltic Flint ($n = 184$; Supplementary Table S1). The raw material was of exceptionally small size, as is demonstrated by a controlled raw material sample from layer 11a that gave a median weight of 5.3 g (Supplementary Figure S33). Despite its small size, the flint was of rather good quality (Supplementary Table S2). Only one large core (Fig. 4: 20) shows internal cracks and flaws that hampered the core reduction and led to unexpected breaks of the resulting flakes. 14 (7.3%) artefacts show thermal alterations (Fig. 4: 10, 16; Supplementary Table S2), indicating the presence of artificial or natural fires at the site. Additionally to flint, six artefacts were made of quartzite (Fig. 4: 21).

Lichtenberg II - Size. The artefacts from Li-II are relatively small. Their median dimensions (either longest width or length) range between 19.48 mm for the flakes and 27.54 mm for the cores (Supplementary Table S5). Comparing the flakes from this site to 14 Central European assemblages ranging from the Eemian interglacial to early MIS 3, Li-II has the smallest artefacts (Supplementary Figure S36). Exceptional are the core LIA-335 (Fig. 4: 20), the quartzite flake LIA-513 (Supplementary Figure S41), and the quartzite flake tool LIA-504 (Fig. 4: 21). With their maximum dimensions of 114.7 mm, 106.3 mm, and 75 mm respectively, these by far exceed the median dimensions of the assemblage.

Lichtenberg II - Cores Fig. 4: 19,20; Supplementary Section 3.5). In the following analysis, we additionally included those cores that where later transformed into tools (see below). Most of the cores were only knapped up to half of their surface (72.5%, $n = 29$). Predominantly, the cores were exploited on a single (47.5%, $n = 19$) or two flaking surfaces (32.5%, $n = 13$). The angles between the striking platform and the flaking surface have a median value of 88° (min = 64° , max = 108° , sd = 8.75). 35% ($n = 14$) of the cores have only one single flake scar, but 3–5 flake scars are common as well (in total 52.5%, $n = 21$). At a significance level of $p = 0.05$, a linear model (Supplementary Figure S37) reveals a weak significant relationship between core lengths and the number of flake scars (Multiple R-squared: 0.12, Adjusted R²: 0.099, F-statistic: 5.312 on 1 and 38 DF, p-value: 0.03). This implies that larger cores have tentatively more flake scars and were thus exploited more intensively. In turn, the small raw material size tentatively led to low exploitation values on the small cores. Taking all flaking surfaces together, most cores where knapped unidirectionally (80.6%, $n = 54$). Most striking platforms consist of a natural (51.3%, $n = 20$) or plain (43.6%, $n = 17$) surface, whereas fine preparation of striking platforms does not occur in the assemblage. In conclusion, simple flaking methods dominated the blank production in Lichtenberg II. Core preparation was not common, if not entirely missing. The simple cores, sometimes just flaked once, may also be due to the small raw material size, as some nodules make only one-time flaking possible.

Lichtenberg II - Flakes (Fig. 4: 15, 22; Supplementary Section 3.6). We included 55 complete flakes into the analysis, as not all variables are preserved on flake fragments. The platform attributes reinforce the observation made on the cores that striking platform preparation (i.e., Levallois *sensu largo*) was not common, as platforms with natural (21.8%, $n = 12$) and plain surfaces (50.9%, $n = 28$) dominate the flake assemblage. Platforms that crushed during knapping also have a relatively high share of 23.6% ($n = 13$). The EPA has a median value of 85° (min = 58° , max = 109° , sd = 10.85°),

Layer 7); (c) (all Layer 11a): 9 – flake with heavy macroscopic use-wear (LIA-550); 10 – scraper with ventral surface removal and thermal alteration (LIA-359); 11 – backed knife with macroscopic use-wear (LIA-342); 12 – endscraper on thick flake (LIA-307); 13 – endscraper on thick flake (LIA-285); 14 – denticulate on thick flake with dorsal surface removal (LIA-377); 15 – small flake with fresh, sharp edged preservation (LIA-330); 16 – distal scraper fragment with thermal alteration (LIA-413); 17 – flake with macroscopic use-wear and with ventral surface removals (LIA-121); 18 – complex notch on core (LIA-154); 19 – small irregular core (LIA-294); 20 – large core on low quality raw material with internal cracks (LIA-335); 21 – flake tool with notch and sharp edge on large quartzite flake (LIA-504); 22 – medial blade fragment (LIA-99). Red dotted lines mark macroscopic working edges, blue arrows mark larger surface removals and flake removals on cores. Photos: MPI EVA. (For interpretation of the references to color in this figure legend, the reader is referred to the Web version of this article.)

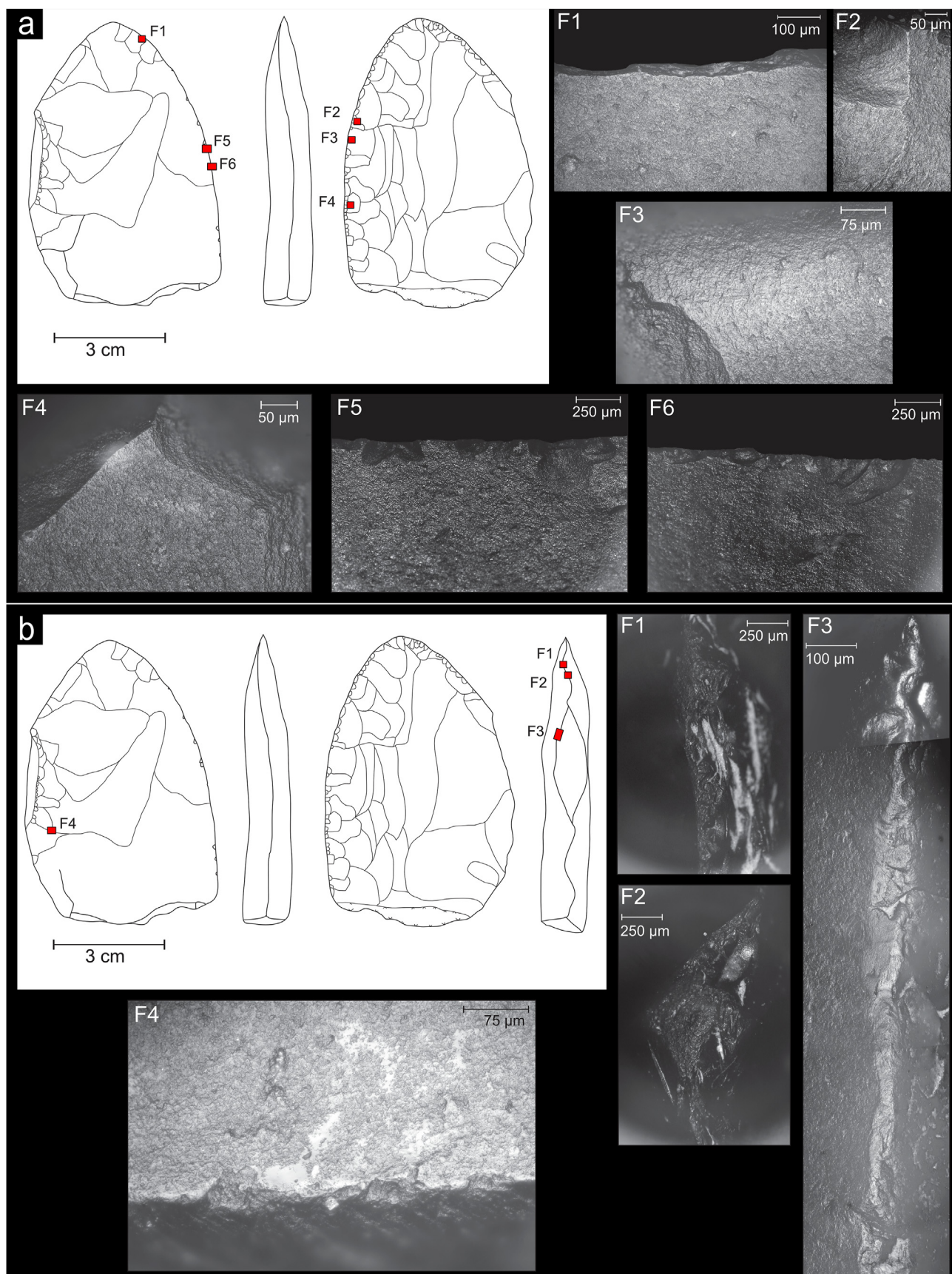


Fig. 5. Results of the traceology for the Keilmesser Li-7. (a) Use-wear traces along the working edge. F1 – taken at magnification 200x, micrograph of the light developed bright polish on the edge of the active zone of the tool; F2 – taken at magnification 200x, micrograph showing the rounded and polished edges of the negatives on the dorsal surface of the

comparable to the flaking angles observed on the cores. Most of the flakes originate from an advanced state of core reduction, as the share of fully cortical flakes is low (15.1%, $n = 8$). This may be a reasonable number, as cores naturally produce a lower share of fully cortical flakes than flakes with no or only remnants of natural surfaces. However, if we sum up all the flakes with remnants of natural surfaces on their dorsal face, we end up with 62.2%. This is more than half of the flake population and may be caused by the small size of the raw material. The observed dorsal scar directions on the flakes show the tendency that the blank production in Li-II was dominated by unidirectional flaking (51.1%, $n = 23$). This confirms the similar observation made on the cores.

Lichtenberg II - Tools (Table 4, Fig. 4: 9–14, 16–18; Supplementary Section 3.7). The tools from Lichtenberg II show a high typological diversity. They are dominated by flakes that were potentially used (Fig. 4: 9,17), tools with partial or limited edge retouch (Supplementary Figure S39) and endscrapers (Fig. 4: 12,13). They were manufactured from a diversity of blanks, such as natural pieces, cores and flakes, and are dominated by the latter (62.5%, $n = 30$). Endscrapers and endscraper combination tools were manufactured from thick blanks (Fig. 4: 12, 13; Supplementary Table S8), indicating special functional requirements. In addition, a rather steep endscraper edge can only be produced on a relatively thick blank. The high share of cores (25%, $n = 12$), as well as two shattered pieces that also served as blanks for tools, indicate the high importance of recycling within the Li-II assemblage. For example, the artefact LIA-379 was initially a core and then transformed into a hammerstone (Supplementary Figure S38). The traceology (see below) indicates that tool functions go beyond the current typological classifications and descriptions.

Lichtenberg II - Traceology (Fig. 6). The preliminary traceological analysis (Supplementary Section 4, Supplementary Table S10) of lithic material from Li-II indicates a heterogeneous pattern of activities, including the processing of soft animal materials, soft and abrasive vegetable materials and hard vegetable materials (wood). Notable are the traces located on the ventral distal working edge of artefact LIA-550 (Fig. 4: 9; Fig. 6a). They show a well-developed bright undulating polish with a high incidence of directional markers, indicating a crossed transverse motion. This bright well-developed polish likely formed by the contact with a highly abrasive and soft vegetal material, while the striations may be related to the admixture of mineral particles, possibly sand or grit, during scraping activity. The resemblance to cereal polish is remarkable (Clemente and Gibaja, 1998), indicating the working of silicate-rich grasses or sedges. The combination of percussive and pressure force was also found on the Li-II artefacts as well as the possible use of hafting technology. The latter was observed on artefact LIA-307 (Fig. 4: 12; Fig. 6b) based on the presence of G type polish (Moss, 1987; Rots, 2010) and the scarring on the dorsal surface along the edges of the central negatives. The general small-artefact characteristics of the assemblage, together with the high incidence of crushing, coupled with the high amount of force used during the different productive activities undertaken at the site, may suggest that artefact LIA-307 was not the only hafted tool. The absence of further hafting wear, however, constrains the further exploration of this possibility.

5. Discussion

5.1. Comparison with previous geochronological data

Stratigraphic layer 7 (find horizon Li-I) is locally deformed upwards by cryoturbation, especially injection, but is still associated with lithic finds there (Fig. 2). To get an impression of the timing of deformation, we dated this cryoturbated sediment with luminescence and obtained an age of 53.5 ± 4.9 ka (L-EVA, 2010; Fig. 7). This compares very well to the previous TL-age of 57 ± 6 ka for the find horizon Lichtenberg I (Veil et al., 1994). The origin of our sample from a cryoturbated context allows the following conclusions: (i) The previous age must likewise have been obtained from a cryoturbated deposit. This is supported by the fact that during the former excavation, a depth of ca. 1.2 m below surface was usually not exceeded. Our excavations revealed that in these higher stratigraphic positions only cryoturbated expressions of the find horizon occur (Fig. 2). (ii) In spite of considerable progress in luminescence dating during the last decades concerning measurement protocols and targeted signals (Buylaert et al., 2012; Murray and Wintle, 2003; Wintle and Adamiec, 2017), the similarity of the previous and newly-presented luminescence ages attest the remarkably high reliability of the former TL dates. Therefore, only lithostratigraphic challenges – i.e. the cryoturbations – apparently hindered a more accurate temporal estimation of the deposition and occupation at that time. (iii) The two dates imply a cryoturbation age that is time-equivalent to the early MIS 3. Even though permafrost – the probable driver for these deformations – was more widespread and effective in Central Europe during MIS 4 and MIS 2 (Bertran et al., 2014), it is known to have existed in MIS 3 as well (e.g. Van Huissteden et al., 2003; Van Meerbeeck et al., 2011). However, active permafrost is not a prerequisite for the partial deformation/injection of the find horizon Li-I. Instead, this can also be a function of loadcasting or cryogenic pressure during thaw degradation of the permafrost, which would be in agreement with the two independent ages suggesting a deformation during the more temperate early MIS 3 (French, 2008; Vandenberghe, 2013; Vandenberghe and Van den Broek, 1982). Nonetheless, according to our current state of knowledge, a cryoturbation age falling within the later MIS 3 or even MIS 2 cannot be completely ruled out. Therefore, a follow-up study will deal with the cryogenic capping sediments in Lichtenberg.

5.2. Comparison with global paleoclimate records

5.2.1. Find horizon Li-II

For layer Li-II, corresponding with stratigraphic layer 11a, two very similar luminescence ages from samples L-EVA 2022 and 2024 (91.5 ± 9.1 ka and 89.5 ± 8.2 ka) gave a mean age of 90.5 ± 8.7 ka. In the palynological data, we observe temperate, late interstadial conditions, characterized by an opening boreal pine-birch forest in layers 11a and the lower part of 11b, assigned to the Brörup Interstadial WE IIb (Table 3, Supplementary Section 7) (Behre et al., 2005; Behre and Lade, 1986; Menke and Tynni, 1984; Veil et al., 1994). The environment changed toward heliophyte and grass-rich, cold-stage tundra vegetation in the following Rederstall Stadial. In our sequence, this shift happens abruptly between layers 11a and 10, but gradually to the top of layer 11b. Therefore, the occupation of find horizon Li-II should have occurred during late

working edge; F3 and F4 – both taken at magnification 200x, micrographs of the striations on the interior of the dorsal side of the tools' working edge; F5 and F6 – both taken at magnification 50x, micrographs of the micro-negatives on the ventral surface of the working edge. (b) Traces on the prehensile/hafting zone of the Keilmesser Li-7. F1 and F2 – both taken at magnification 50x, crushed and abraded edges on the back of the tool; F3 – taken at magnification 200x, composed micrograph images showing the undulating bright and well interconnected polish on the edge of the negative forming the back of the Keilmesser; F4 – taken at magnification 200x, bright undulating "G" type polish on the ventral surface of the tool. Drawings and photographs: Y. H. Hilbert.

Table 4
Tool types Lichtenberg II.

tool type	number	percent	Example
backed knife	1	2%	Fig. 4: 11
Denticulate	3	6.3%	Fig. 4: 14
(partial) edge retouch	8	16.7%	Supplementary Figure S39
Endscraper	8	16.7%	Fig. 4: 12, 13
endscraper, reused as hammerstone	1	2%	—
endscraper-scraper	1	2%	—
Hammerstone	3	6.3%	Supplementary Figure S38
naturally backed knife	1	2%	Supplementary Figure S40
Notch	11	22.9%	Fig. 4: 18, 21
side scraper	2	4.2%	Fig. 4: 10, 16
flakes with possible use-wear	9	18.8%	Fig. 4: 9, 17
not identifiable	1	—	—
Total	49	100%	—

phases of the Brörup Interstadial, whereby the obtained mean age of 90.5 ± 8.7 ka represents this terminal phase (Fig. 7). Compared with global paleoclimate records, this age for the end of Brörup Interstadial corroborates the correlation with the end of MIS 5c (peak at 96 ka in Lisiecki and Raymo (2005b)) and with Greenland Interstadial (GI) 22 in the synchronized Greenland ice core records, dated to about 89 ka at its peak (Rasmussen et al., 2014). To our knowledge, for the Brörup Interstadial no direct numerical dates exist in its type region on the northern Central European Plain so far. Luminescence ages similar to ours for the end of equivalent interstadials have been obtained from loess records of Northern France at ca. 85 ka (Antoine et al., 2016) and Dolní Věstonice (CZ) at ca. 90 ka (Antoine et al., 2013; Fuchs et al., 2013). In the Alpine Foreland, the peak of the Brörup equivalent has been dated to around 96 ka (compiled by Preusser, 2004) and its end to ca. 89 ka in the highly-precise NALPS speleothem record (Boch et al., 2011). Altogether, these dates support our finding that the end of the Brörup Interstadial (mean age of 90.5 ± 8.7 ka in Lichtenberg) coincides with GI 22 and the termination of MIS 5c.

5.2.2. Find horizon Li-I

In find horizon Li-I (stratigraphic layers 7 and 8), three nearly identical luminescence ages for samples L-EVA 2014, 2015 and 2017 (71.6 ± 7.0 ka, 71.5 ± 7.0 ka and 70.8 ± 8.0 ka) gave a mean age of 71.3 ± 7.3 ka. Regarding lithostratigraphy, Li-I is under- and overlain by cold stage deposits (section 4.1, Supplementary Section 5.1), and the covering layers show clear permafrost features. This suggests a pre-pleniglacial age for Li-I (Jöris, 2004), because permafrost rarely occurred in Central Europe before MIS 4 (Bos et al., 2001; Vandenberghe and Pissart, 1993). Our chronostratigraphy implies that layer 9 (mean age of 72.5 ± 7.8 ka) is only slightly older than layers 7 and 8. Furthermore, as evidenced by the alternating deposition of layers 7 and 9 in the stratigraphy of Trench 2, these partially even occur contemporaneously (Fig. 2c). Accordingly, comparable cold-stage conditions for the formation of layers 7 to 9 are also suggested by similar phytolith results (section 4.5, Supplementary Section 8), which point to a grass-rich vegetation in these layers. However, layers 7 to 9 were pollen-sterile in the trenches, thus hindering their direct biostratigraphical assignment. In contrast, reliable information was obtained from core PD.028, directly south of Trench 1 (Figs. 1 and 7): (i) A thick peat layer directly below the niveofluvial sands of layer 9 was characterized by dense *Pinus-Betula* forest, being characteristic for the Odderade Interstadial WE IVb (Table 3, Supplementary Section 7) (Behre et al., 2005; Behre and Lade, 1986; Menke and Tynni, 1984; Veil et al., 1994). Based on the bio-/lithostratigraphy and the luminescence ages for the overlying layers 8 and 9, we correlate the Odderade peat with GI 21 (Jöris, 2004; Stephan, 2014). (ii) Unlike in the

trenches, the cold stage niveofluvial sands of layer 9 showed two interbedded organic-rich layers that were characterized by a grass- and heliophyte-rich open vegetation belonging to the early Schalkholz, WP I Stadial (Table 3, Supplementary Figure S62; Supplementary Tab. S14).

On the premise that these two organic-rich sediments represent low-magnitude climatic ameliorations (Hahne et al., 1994; Vandenberghe and van der Plicht, 2016), we cautiously regard them as minor interstadial oscillations seldomly described for Northern Germany (Supplementary Section 7). These minor oscillations following the Odderade, stratigraphically could be associated with GI 20 and 19 (Rasmussen et al., 2014), which would also agree with the mean luminescence age of layer 9 of 72.5 ± 7.8 ka (with a tendency to increase with depth, see Fig. 7). As for the find horizon Li-I, its mean luminescence age of 71.3 ± 7.3 ka and its superposition above the minor interstadial oscillations suggests correlation with Greenland Stadial (GS) 19 (Rasmussen et al., 2014).

Much like the Brörup, to our knowledge the Odderade Interstadial is mostly lacking an independent chronology in the type region of northern Central Europe, apart from previous dating attempts with ^{14}C (Behre and van der Plicht, 1992; Grootes, 1978) and unpublished luminescence ages, obtained by Thiel at the site of Osterbylund (Stephan et al., 2017). For Northern Germany, the Odderade was recently correlated with Greenland Interstadial (GI) 21 (Stephan, 2014). At a few sites (namely Keller, Schalkholz and Osterbylund), above the Odderade layer, but below the deposits of the first glacial maximum (~MIS 4), one or two weak Podzol paleosols exist, representing a slight climatic amelioration phase (Keller-Interstadial), ascribed to GI 20 and 19 (Menke, 1976; Stephan, 2014). Our chronological correlations compare very well with this northern German stratigraphy, but also with independently-dated loess and pollen/speleothem records in neighboring regions: Antoine et al. (2016) also correlated the Odderade/St. Germain II soils with GI 21 for the loess-paleosol-sequences in northern France and report this phase to end at ca. 80 ka. Above the Odderade/St. Germain II, there are two paleosols (Ognon I and II) relating to GI 20 and GI 19. The conclusion of this soil formation has been dated to ca. 71 ka (ibid.). Similarly, two paleosols in the loess-paleosol-sequence of Dolní Věstonice in the southeastern Czech Republic were dated to 73.1 ± 4.7 and 71.3 ± 4.9 ka, respectively, and were correlated with GI 20 and GI 19 (Antoine et al., 2013). Likewise, one or two minor interstadials in palynological records of South-Western Europe and southern Germany above the St. Germain II/Odderade Interstadial (e.g. Woillard, 1979) were ascribed to GI 20 and 19 (Ognon I/II and Dürnten), and the latter was dated to ca. 73 ka (Müller and Sánchez Goñi, 2007). Furthermore, in the NALPS speleothem record of the northern Alps, a minor interstadial related to GI 19 yielded an age of ca. 72 ka (Boch et al., 2011).

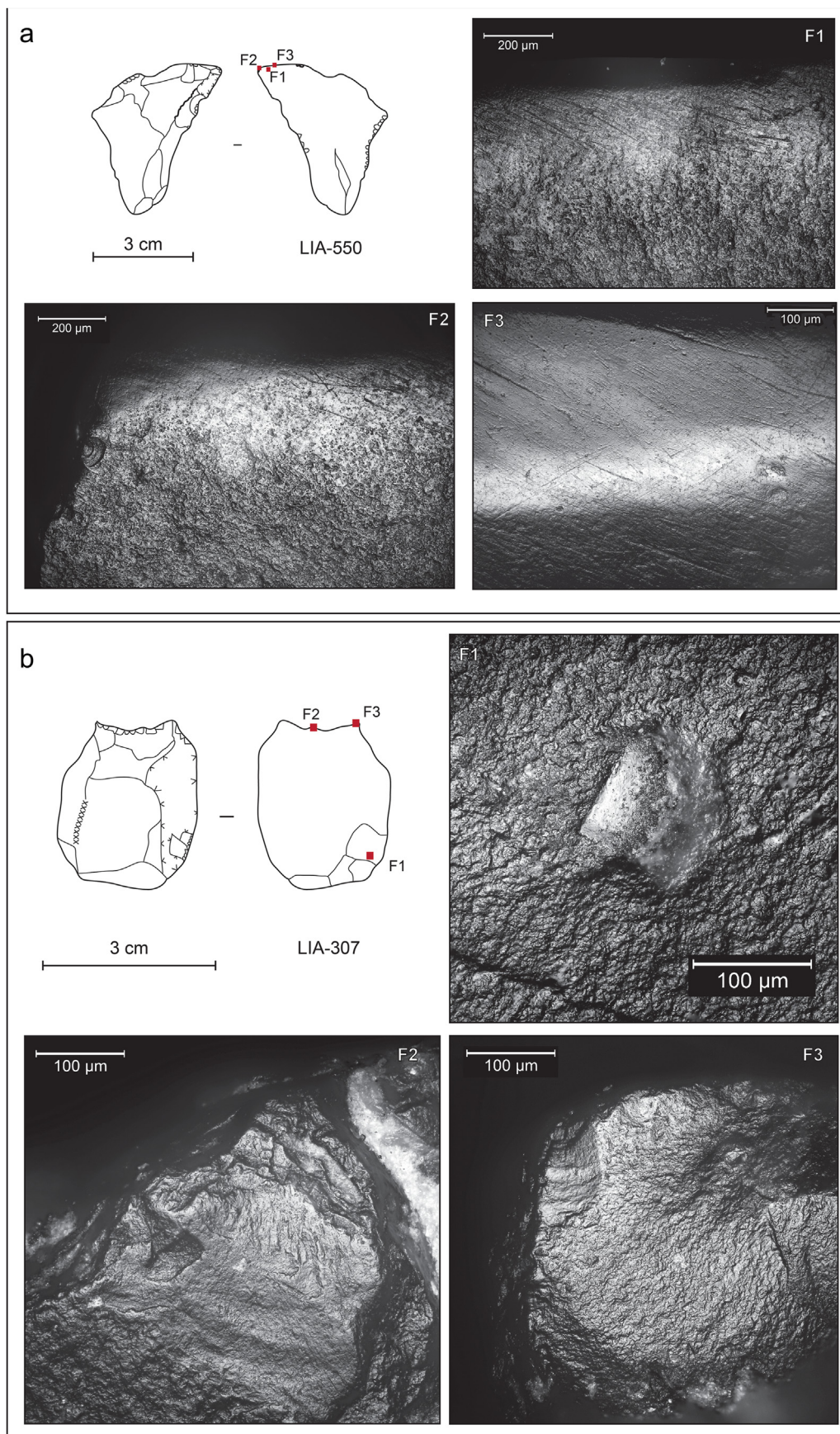


Fig. 6. Results of the traceology for the Lichtenberg II assemblage. (a) Schema of artefact LIA-550 and the location of the micrographs showing the use related polish. F1 – taken at magnification 100x, bright undulating extensive polish located on the distal portion of the working edge; F2 – taken at magnification 100x on the edge of the working surface

Although for the Lichtenberg record, numerical dating of the Odderade peat and the overlying two minor interstadials cannot be presented yet, our chronological and biostratigraphic framework suggests their close coupling to the Greenland Interstadials GI 21 to 19. Consequently, the mean age (71.3 ± 7.3 ka) of the overlying find horizon Li-I (correlated with GS 19) represents a plausible age for the inception of the MIS 4 pleniglacial. Comparing our record with the marine chronology (Lisiecki and Raymo, 2005b), we regard the Odderade peat (GI 21) and the overlying two minor interstadials (GI 20 and 19) of core PD.028 to be part of MIS 5a, whereas stratigraphic layers 8 and 7 (find horizon Li-I, GS 19) are tentatively assigned to early MIS 4. This implies that the upper boundary of the Odderade Interstadial is not congruent with the end of MIS 5a, in this region (Behre, 1989a; Jöris, 2004; Stephan, 2014).

5.3. Site formation, paleoenvironment and humans

Neanderthals occupied the northern site of Lichtenberg during the Eemian (Hein et al., 2021), the following early Weichselian Brörup Interstadial (find horizon Lichtenberg II), through to the onset of the first Weichselian glacial maximum (find horizon Lichtenberg I). In the following, we will connect our sedimentological/paleoenvironmental and archaeological results to draw inferences about past human behavior in changing environments in Lichtenberg.

5.3.1. Lichtenberg occupation during the mid-Eemian

Near the south-facing shore of a small lake, a half-bog formed just above the groundwater level during the mid-Eemian Interglacial (pollen zone E IVb/V). This was the time and position for Neanderthal occupation, as inferred from few artefact finds (2 flakes and a few small chips and fragments) within the core PD.030 (Hein et al., 2021). A densely-forested landscape was reconstructed for the area (>95% arboreal pollen), dominated by hazel (*Corylus*), alder (*Alnus*), lime (*Tilia*) and hornbeam (*Carpinus*), with the admixture of further thermophile taxa, such as elm (*Ulmus*), oak (*Quercus*) and yew (*Taxus*). Among the indicators for local swampy conditions are palynomorphs of ferns (*Polypodiaceae*), cattail (*Typha*) and bur-reed (*Sparganium*) (Behre, 1989; Menke and Tynni, 1984).

This fully-forested landscape contrasts with other contemporaneous Eemian sites from drier regions of central Germany (Gaudzinski-Windheuser and Roebroeks, 2014; Litt and Weber, 1988; Toepfer, 1958; Weber, 1990), where last interglacial Neanderthals are assumed to have lived in semi-open landscapes (Pop and Bakels, 2015). Thus, contrary to earlier hypotheses (Pop and Bakels, 2015), we suggest that the Lichtenberg-Eemian Neanderthals adapted well to wooded paleoenvironments. However, so far we have too few artefacts to draw inferences about Neanderthal behavior in Lichtenberg during the last interglacial. Therefore, future excavations are planned to reveal more about the structure and spatial pattern of the Eemian settlement at the Lichtenberg lakeshore.

5.3.2. Li-II: late Brörup Interstadial to Rederstall Stadial

During the Brörup Interstadial a beach sediment (layer 11a) was deposited at the shoreline of a small lake (ca. 1.5 km², cf. Hein et al., 2021) with fluctuating water tables. In the late interstadial the

water table was rising, as evidenced by the formation of a peaty deposit (layer 11b) partially covering the beach, but also interfingering with its deposits. Such a hydrological shift is typical for transitional phases between forested and unforested periods due to the loss of woodland and associated decreasing evapotranspiration values (Behre et al., 2005; Tucci et al., 2021). Vegetation was characterized by boreal forests, with pine (*Pinus*) and birch (*Betula*) being the main tree species (Caspers and Freund, 2001). Likewise, phytolith analysis indicates a relatively high bioproductivity (section 4.5). On the beach, local sandy to humic open stands were dominated by wet meadows, fern and heathland, and a diverse heliophytic flora. For the peaty deposit, we conclude there was a shallow water body with swampy conditions that featured rich stands of cattail (*Typha latifolia* type), reed and sedges. In this environment, the occupation of Li-II took place directly by the shoreline. Regular occurrence of macroscopic and microscopic charcoal fragments (Supplementary Sections 5.3 and 7.2) document episodic burning events, either in connection with natural wildfires or Neanderthal fire use (Dibble et al., 2018; Glückler et al., 2021; Roebroeks et al., 2015). For the site of Gröbern (Central Germany), reconstructed summer temperatures of ca. 16 °C and winter temperatures of ca. -15 °C in the late Brörup (Kühl et al., 2007) demonstrate a highly continental climate that was caused by a lower sea level at that time (Lambeck, 2004). During the late Brörup stage WE IIb transitioning into WE III, the local water table in Lichtenberg kept rising as the woodlands gradually opened up and gave way to more heliophilous plants. Wave activity on the beach reworked plant material, charcoal and also small lithic fragments, thereby creating distinct driftlines. Eventually, during Rederstall Stadial, vegetation had changed into a grass- and heliophyte-rich tundra. The former beach was largely inundated by the rising lake level due to starkly decreased evaporation values in this non-forested environment (Behre et al., 2005). Subsequently, stadial conditions are recognized in the muddy shoreface deposit of layer 10 and the uppermost part of layer 11b. Layer 10 emerges from layer 11b, that unconformably overlies layer 11a, and wedges out toward higher ground. This suggests that the top of layer 11a might have been eroded prior to being covered.

5.3.3. Li-I: Odderade Interstadial to early Schalkholz Stadial

Within our record, the Odderade Interstadial is only detected in core PD.028 on account of higher accommodation space in the basin, south of the alluvial fan (Fig. 1, Supplementary Figure S49). However, the Odderade was also represented in the previously investigated core Veil 1, only about 10 m apart from core PD.028 (Veil et al., 1994). In both parallel cores, the Odderade peat occurs at the same depth, marking the ground water/lake level of that time. Vegetation was characterized by a dry boreal pine-birch forest with admixed spruce, juniper and larch. A rich but subordinate herbal flora indicates open stands nearby. Main peat formers were likely sedges and ferns. Following the Odderade, in the earliest Schalkholz Stadial, niveofluvial slope deposition started, triggered by annual snow melt in a sparsely vegetated landscape (Christiansen, 1998a, 1998b, 1998a). The grain size data show a coarsening trend from fine-sandy, slightly silty and slightly humic deposits above the Odderade peat in core PD.028 to the fine/medium sandy sediments of layer 9 in both the core and the trenches, and finally to more gravelly layer 8. This coarsening possibly indicates a raise of base

showing the spread of the bright undulating extensive polish, note the high incidence of striations and scratches; F3 – taken at magnification 200x at the center of the maximum extension of the micro polished surface on the working edge of the tool. The spread and connectedness of the polish is very high and the surface is extremely smoothened, again the criss-cross patterned motion of tool use is particularly evident by the striations and scratches. The resemblance to cereal polish is remarkable. Worked material: soft vegetal/hard organic. (b) Schema of artefact LIA-307 and the location of the micrographs showing use and hafting related polish. F1 – flat bright polish located on the eminence of the micro topography on the ventral surface of the tool; F2 and F3 – negative edge rounding and bright undulating extensive polish on concave working surface. All micrographs taken at 200x. Worked material: hard organic/wood. Drawings and photographs: Y. H. Hilbert.

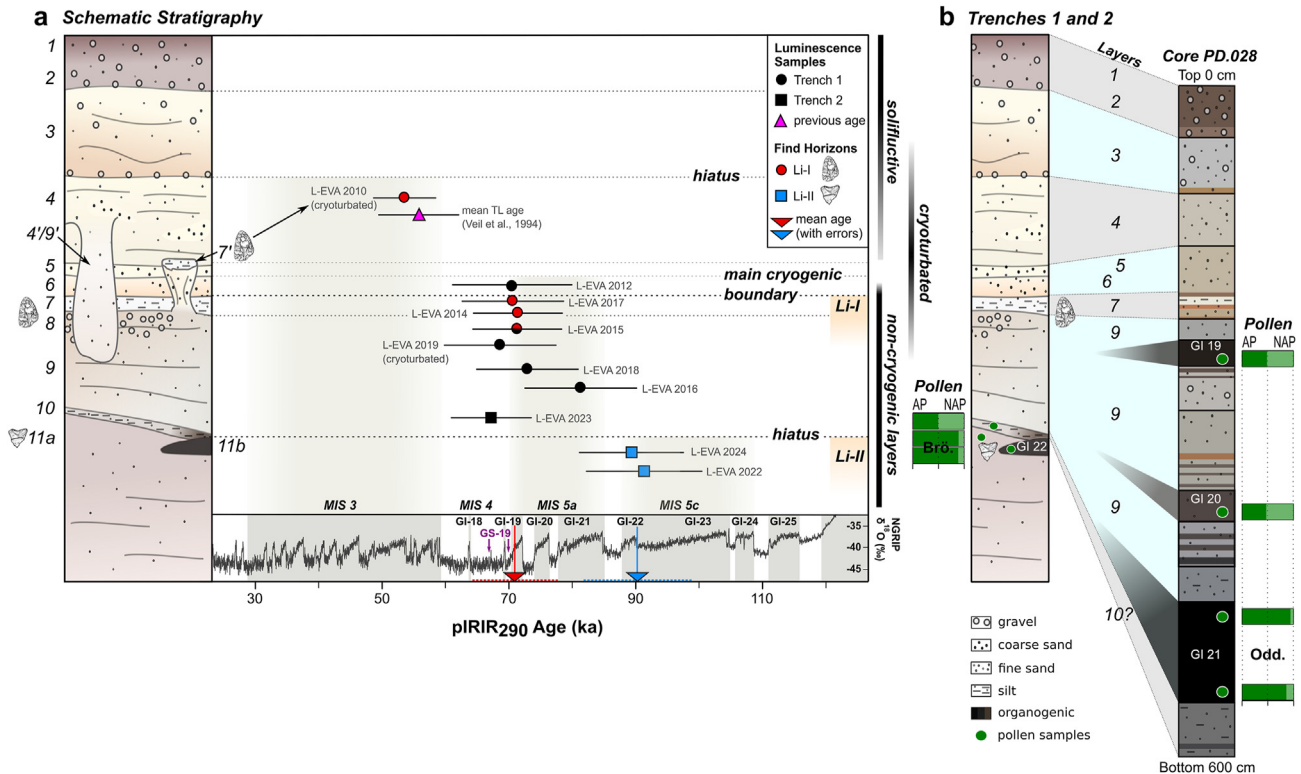


Fig. 7. (a) Schematic stratigraphic column of Trenches 1 and 2 and luminescence dating results (1σ error); position of the find horizon is highlighted and indicated by a representative artefact symbol. On the x-axis, the time line and the NGRIP $\delta^{18}\text{O}$ Greenland temperature proxy is provided (NGRIP members, 2004). (b) Correlation of the schematic stratigraphy of the trenches with sediment core PD.028 (location in Fig. 1) and simplified results of palynological analysis. AP = arboreal pollen, NAP = non-arboreal pollen.

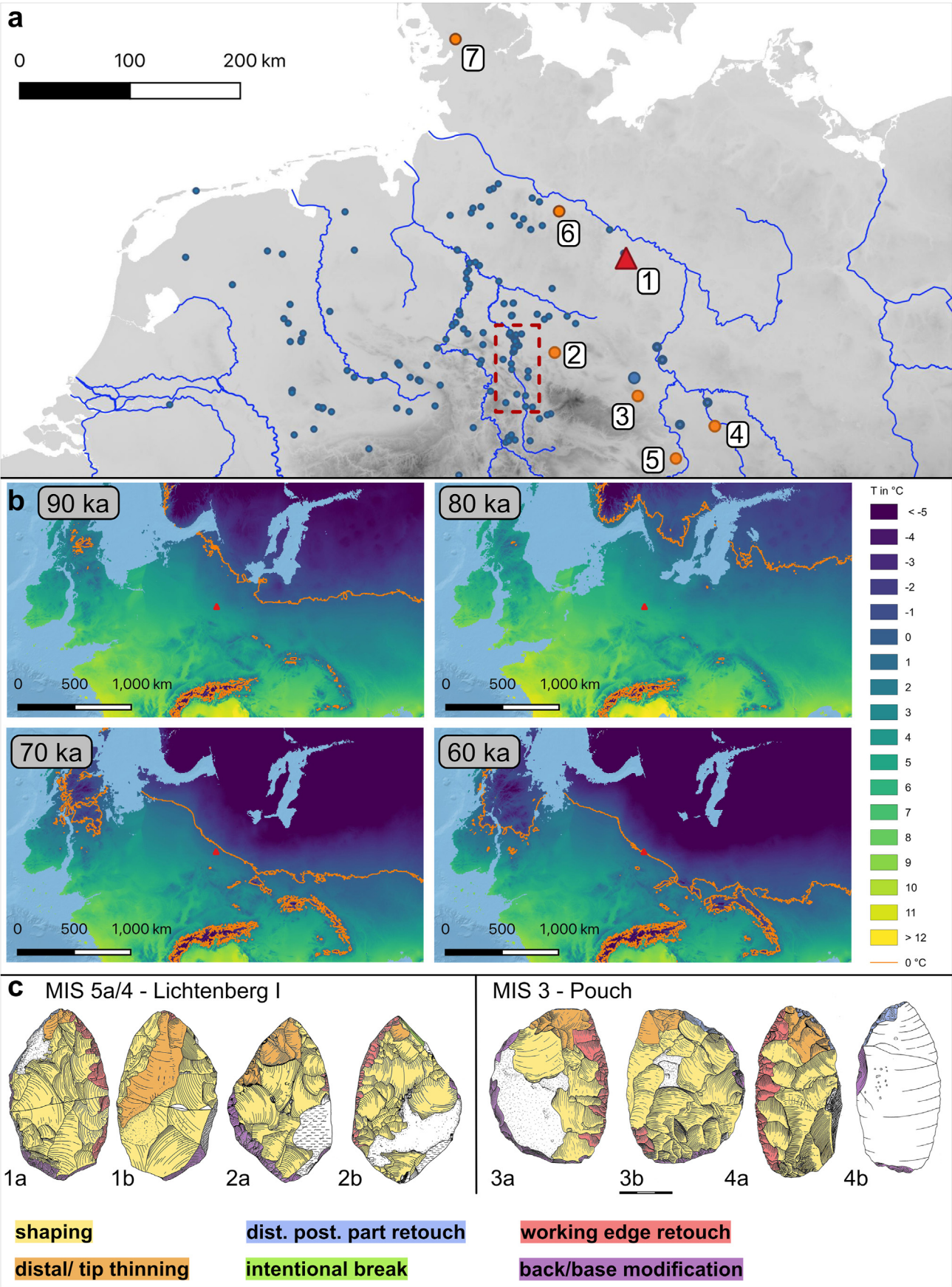
level caused by a rising lake level. In our trenches, these niveofluvial sediments (layers 9 and 8) form a relatively coherent unit, but in core PD.028 with larger accommodation space, they are interbedded with two organogenic and lacustrine deposits. These attest to a continuously rising water level, interrupted by longer spells of relative landscape stability that were induced by denser vegetation. Stability would have slowed down the lake level rise and niveofluvial slope wash alike, and allowed these lacustrine/organic-rich deposits to form. Therefore, we regard these to represent minor local interstadial oscillations (see section 5.2, Supplementary Section 7). The dominating vegetation type during both oscillations indicates an open, grass-rich habitat. Among the woody taxa, *Betula* (likely dwarf birch), juniper and heath species, such as *Calluna*, *Empetrum* and *Vaccinium* stand out. Because these minor interstadial oscillations have not yet been described for Northern Germany by palynological findings, no direct paleotemperature estimation exists. However, in the Alpine Foreland, based on a chironomid record at the site of Füramoos, summer temperatures between 9 and 11 °C were reconstructed for the two-part Dürnten Interstadial, the latter correlated with GI 19 (Bolland et al., 2021). For Northern Germany, the pleniglacial Oerel Interstadial (WP II) shows a similar pollen spectrum to those oscillations in Lichtenberg, hence, the reconstructed mean summer and winter temperatures for Oerel (9 °C and −17 °C) might be a fair approximation (Walkling, 1997). In Lichtenberg, at the culmination of lake level rise after the Odderade, large parts of the study area were inundated and an organic-free, thin, muddy shoreface sediment was deposited (layer 7). This is only missing at the higher ground in the northern part of Trench 2, which was not flooded apparently. Direct pollen information is lacking in this lacustrine deposit, but the results of phytolith analysis provide evidence that the conditions of layer 7 resembled those of the cold-stage, sparsely-vegetated

niveofluvial layers 8 and 9 (section 4.5, Supplementary Section 8). Neanderthal occupation of Li-I (layer 7 and top of layer 8) occurred after the upper minor interstadial oscillation in a severely cold environment, as is further proposed by the modelled annual mean temperature (Gamisch, 2019a, 2019b) displayed in Fig. 8b. We suggest that the occupational surface was topmost layer 8 near the lake shoreline. The artefacts must have been smoothly embedded by the muddy shoreface sediments of layer 7 during lake level rise, leaving no distinct taphonomical marks on the lithic finds.

5.3.4. Comparing Li-II to Li-I: human behavior in changing environments

The Lichtenberg find horizons represent two distinct site types, connected to different paleoenvironments and climatic conditions (Fig. 8b). Li-I and Li-II differ in raw material attributes and use, artefact size, as well as blank production, typology, and tool use.

Lichtenberg II has a high typological tool variability (Table 4, Figs. 4, Fig. 6). Edges with different functionalities on some artefacts (Supplementary Table S10) demonstrate that the tools often had several use-cycles. Further evidence for this recycling behavior comes from the cores and shattered pieces that were also recycled to tools. Traceology further suggests that the Li-II Neanderthals exploited the still richly-vegetated environment of late MIS 5c, and processed wood, plants, and other soft and hard organic material. All these assemblage characteristics indicate a longer and/or repeated stay(s) at the lakeshore with a variety of domestic activities. Under these still temperate continental conditions at the lakeshore, we see the use of small and diverse raw material, what was possibly linked with the lack of accessible natural resources. We argue that relatively stable and densely vegetated landscape surfaces inhibited sediment erosion and favored weathering, and thus reduced the availability of fresh flint from the surrounding



Saalian glacial deposits (Supplementary Section 3.4.4). Recycling and intensive tool use can also be related to this shortage of high-quality and large sized raw material. Faced with small and low-quality raw material in a forested landscape, Neanderthals at the site displayed an economic raw material management behavior. This may also explain the lack of more complex blank production techniques (e.g., Levallois, and/or discoidal methods), as the small-sized nodules in Li-II potentially did not allow for extensive core preparation (see for comparison Pop, 2014). Neanderthals mostly knapped small flint pieces a few times to obtain some larger flakes for further use, and/or to establish working edges on natural flint pieces. This behavior, as well as the small artefact size, the typological variety of tools and the recycling behavior are also known from the Eemian site of Neumark-Nord 2/2 (Pop, 2014), as well as from the subsequent MIS 5c or 5a (Richter and Krbetschek, 2014; Strahl et al., 2010) assemblage Neumark-Nord 2/0 (Laurat and Brühl, 2006, 2021). It seems that forested to semi-open landscapes (Pop and Bakels, 2015), temperate organic rich environments, as well as lakeshore areas with limited raw material availability, probably induced similar Neanderthal settlement behavior and resource management strategies on the northern European Plain between the Eemian and late MIS 5. However, besides paleoenvironmental triggers, we cannot rule out certain techno-cultural influences on the presence of typologically diverse small tool assemblages in Central Europe during the early last glacial, as these are also found in probably paleoenvironmentally slightly different, more southern regions of Central Europe. Examples are the lower layers of the Sesselfelsgrötte (Weißmüller, 1995), Bavaria/Germany, and in layer 11 of the Kůlna Cave (Moncel and Neruda, 2000; Valoch, 1988), Czech Republic. Based on these typological similarities, Li-II fits well into early last-glacial technocomplexes of Central Europe.

In contrast to Li-II, the Li-I artefacts were exclusively manufactured on large, high quality flint pieces, such as frost shards that could be recovered in this area (Veil et al., 1994). This coincides with a sparsely-vegetated landscape, fostering sediment redeposition and providing freshly eroded flint from the Saalian glacial deposits (<100 m upslope). As suggested by former use-wear and techno-functional analyses (Veil et al., 1994; Weiss, 2020), the majority of Li-I tools served mainly for cutting soft tissue, potentially meat (Veil et al., 1994). This usage of Keilmesser as cutting tools confirmed by our traceological analyses of the Keilmesser Li-7 (Fig. 4: 1). Furthermore, we recently showed (Weiss, 2020) that the Li-I Keilmesser were mostly discarded shortly before the edge angle of the working edge exceeded 60° (Gladilin, 1976), in other words, when the Keilmesser subsequently lost their functionality as cutting tools. In general, the functional focus of the Li-I tools led to a relatively low typological diversity in the presence of scrapers, bifacial scrapers, handaxes and Keilmesser. Based on the lack of cores and primary blank production in the assemblage, artefact refits that evidence on-site tool production, and the use-wear traces related to butchering activities (Veil et al., 1994), we suggest a short-term occupation event at the lakeshore with a specialized objective, i.e., a hunting/butchering stay.

Altogether, Li-I most probably represents a single, short-term event related to butchering activities in a harsh and cold environment. In contrast, Li-II is interpreted to result from repeated and probably longer stays at the lakeshore under still temperate continental climatic conditions, with a variety of activities that were carried out at this site.

5.4. Northern Neanderthals in the cold: occupations between MIS 5a and early MIS 3

From the last interglacial through to the end of MIS 5a/early MIS 4, the paleoenvironment of the European Plain gradually changed from temperate towards colder climatic conditions and open landscapes (Fig. 8b) (Caspers and Freund, 2001). The same trend is also documented in the sediment sequence of Lichtenberg (see above). Besides the subsequent replacement of the Eemian interglacial fauna by the mammoth fauna after the Eemian, we also expect to see a shift from a more local roaming behavior (Kindler et al., 2020) of the potential prey species to large herds with extended seasonal migration ranges. These changes and shifts in climate, paleoenvironment and the fauna coincided with a shift in the archaeological record of northern Central Europe. The early last-glacial small-tool assemblages such as those of Li-II gradually disappeared. On the other hand, we see that in the upper part of the lower layers in Sesselfelsgrötte or in Neumark-Nord 2/0 (Laurat and Brühl, 2006, 2021) bifacial tools, like Keilmesser start to appear in low frequencies. This transition ended during MIS 5a with the appearance of the late Middle Paleolithic Keilmessergruppen (Hein et al., 2020; Jöris, 2004; Mania, 1990) that persisted in northern and eastern Central Europe until the early MIS 3 (Fig. 8a) (Jöris, 2004; Richter, 2016; Weiss, 2015), and probably extended as far east as the Altai Mountains (Kolobova et al., 2020). Based on the short-term nature of their sites (Picin, 2016), land-use systems with scattered special task and ephemeral camps (Richter, 1997, 2016), as well as raw material transport over large distance in Central Europe (Féblot-Augustins, 1993), the Neanderthals of the Keilmessergruppen are interpreted as highly mobile groups. This is further expressed by the assumed mobile nature of the Keilmesser itself, enabling their long-term use and transport through special resharpening possibilities (Iovita, 2010; Jöris, 2004, 2012; Weiss, 2020). Our evidence for hafting the Li-I Keilmesser supports this interpretation of a tool concept with a long use-life.

As Keilmessergruppen Neanderthals of Li-I were present in the northern latitudes at the onset of the cold climatic MIS 4 (GS 19), we suggest that the increased residential and long-distance mobility inferred from the Keilmessergruppen assemblages is one aspect of Neanderthal behavioral adaptations to the cold climate and the related paleoenvironmental conditions. In contrast to this, although last interglacial Neanderthals are also interpreted as highly mobile, it was inferred from the archaeological and faunal assemblage of the Eemian site Neumark-Nord 2/0 (Kindler et al., 2020) that their mobility must have been more local instead of travelling large distances.

As mentioned above, the site Salzgitter-Lebenstedt is another

Fig. 8. Distribution of late Middle Paleolithic sites in the study area (a), mean annual temperature change between 90 ka and 60 ka (b), and Keilmesser technology (c). (a) Displayed are the late Middle Paleolithic sites documented in the database of the State Service for Cultural Heritage Lower Saxony, Hannover, Germany. Most of them are surface collections. To make sure that they date between MIS 5a and MIS 3, only collections that include Keilmesser, Handaxes, and sometimes leafpoints as late Middle Paleolithic type fossils were selected. Sites located in the rectangle were collected from a river terrace of the Leine Valley that was dated to early MIS 3 (Winsemann et al., 2015). 1–6 are sites mentioned in the text: 1 – Lichtenberg; 2 – Salzgitter-Lebenstedt; 3 – Königsau; 4 – Pouch; 5 – Neumark-Nord; 6 – Ochtmis; 7 – Drelsdorf. The map is based on SRTM data V4 (<http://srtm.csi.cgiar.org>) (Jarvis et al., 2008; Reuter et al., 2007) and was generated in QGIS v3.12. (b) Change of the mean annual temperature with focus on northern central Europe. Red triangle: Lichtenberg; orange line: 0 °C isotherm. The map was created with the oscillayers dataset (<https://doi.org/10.5061/dryad.27f8s90>) (Gamisch, 2019a, 2019b) and generated in QGIS v3.12. (c) Technological comparison of Keilmesser from the MIS 5a/4 transition (Lichtenberg) and early MIS 3 (Pouch). The Keilmesser from both sites can be classified as type Lichtenberg. They show the same shaping technology, and moreover the Keilmesser from both sites are highly comparable regarding overall morphology, working edge morphology and treatment, as well as edge angle configurations (Weiss, 2020). (For interpretation of the references to color in this figure legend, the reader is referred to the Web version of this article.)

proof of Neanderthals living under cold climatic conditions, as the find layers contain remains of a cold climatic vegetation (Pastoors, 2001; Pfaffenberg, 1991; Selle, 1991). Furthermore, that sequence shows a succession from subarctic (find horizon) to arctic conditions (silts covering the find horizon) (Pfaffenberg, 1991; Selle, 1991), comparable to the sediment sequence of Li-I. Given our paleoenvironmental results and the age of Li-I, the formerly suggested MIS 5a/4 (Jöris, 2004) age for Salzgitter-Lebenstedt seems very plausible by analogy. This implies a repeated or continuous Keilmessergruppen Neanderthal occupation of cold climatic northern latitudes with specific adaptations to these environments, like e.g., seasonal hunting of migratory game herds, such as late summer/early autumn reindeer hunting, as evidenced in Salzgitter-Lebenstedt (Gaudzinski, 1998, 1999). The latter suggests that late Neanderthals stayed at least until early autumn in northern regions of Central Europe. But even for that season, reconstructed summer temperatures of $<9-11^{\circ}\text{C}$ (Bolland et al., 2021; Walkling, 1997) for minor interstadial phases such as in Li-I or in Salzgitter-Lebenstedt (Pastoors, 2001) suggest cold summers in tundra-like landscapes, forming a challenging environment for Neanderthals. Further evidence of their successful adaptation to the cold climatic conditions of late MIS 5a, the onset of MIS 4, and early MIS 3 in northern Central Europe also comes from a large number of late Middle Paleolithic Keilmessergruppen sites and surface collections (Fig. 8a) that are aggregated along the river valleys and associated with sediments mainly dating to early MIS 3 (Mol, 1995; Weiss, 2015; Weiss et al., 2018; Winsemann et al., 2015). These assemblages, although only typologically attributed to the Keilmessergruppen, show that Lichtenberg is not the northernmost limit of the Neanderthal habitat (Nielsen et al., 2017), as late Middle Paleolithic sites, such as Ochtmissen (Thieme, 2003), Lower Saxony/Germany and Drelsdorf (Hartz et al., 2012), Schleswig-Holstein/Germany are located even further north (Fig. 8a).

Currently, we are missing direct evidence for Neanderthal occupations of northern Central Europe during the peak of MIS 4. Whereas some authors suggest that Neanderthals migrated south (Jöris, 2004) during that period, others even consider local extinctions of Neanderthal groups (Hublin and Roebroeks, 2009). However, the Keilmesser tools show technological continuity that connects MIS 5a with early MIS 3 assemblages (Fig. 8c). This is demonstrated in the assemblages of Königsau A and C (MIS 5a (Jöris, 2004; Mania, 2002; Mania and Toepfer, 1973)), Salzgitter-Lebenstedt (MIS 5a/4 or MIS 4/3 (Jöris, 2004; Pastoors, 2009, 2001)), and Pouch, Saxony-Anhalt/Germany (MIS 3 (Weiss, 2015; Weiss et al., 2018)), where the Keilmesser share the main technological and morphological features with those from Lichtenberg (Weiss, 2020) (Fig. 8c). Furthermore, some of the MIS 3 Keilmesser from the G-Complex of the Sesselfelsgrötte (Richter, 1997, 2002) also show morpho-technological similarities to those from Lichtenberg (Delpiano and Uthmeier, 2020), potentially indicating seasonal migrations to southern regions of Central Europe during the late Middle Paleolithic. Altogether, the techno-typological continuity of late Neanderthal assemblages in northern Central Europe between MIS 5a and MIS 3, as well as the successful adaptation to cold environments, favor the hypothesis of seasonal migrations during cold periods instead of local extinctions.

In summary, Li-I proves the presence of Neanderthals in the north during cold, stadial climatic conditions. This assemblage represents a short-term butchering stay associated with the central and eastern European Keilmessergruppen. We suggest that Neanderthals populated the north intensively until early MIS 3, and adapted their life ways to the regional cold climatic conditions.

6. Conclusion

- (1) In Lichtenberg, we have established a high-resolution chronological framework based on the luminescence dating results as well as sedimentological, paleoenvironmental, and archaeological analyses. This allowed us to connect the northern Neanderthal occupations to climatically different phases of the last interglacial-glacial cycle, with a chronological resolution close to the millennial scale of Greenland Interstadials/Stadials (section 5.2).
- (2) The chronostratigraphic results led to a revision of the timing for the occupation Li-I in Lichtenberg. We obtained consistent ages for this find layer with a mean of 71.3 ± 7.3 ka replacing the former mean age of 57 ± 6 ka, which was likely rejuvenated by post-depositional cryoturbation. Our new age complies with the stratigraphic and paleoenvironmental findings and is therefore considered robust and reliable.
- (3) By reporting the age for the occupation Li-II (mean of 90.5 ± 8.7 ka), we also present the first independent ages of the latest Brörup Interstadial WE IIb in its type region in northern Central Europe. The age suggests that the terminations of the continental Brörup and MIS 5c broadly coincide (section 5.1). This is valuable information for numerous paleoenvironmental and archaeological sites in the area, where the chronologies rely on biostratigraphical evidence alone.
- (4) The high-resolution chronological framework enabled us to show that Neanderthals inhabited the northern regions of central Europe during the Eemian, the early last glacial interstadials, as well as during the onset of the first glacial maximum. We conclude, they lived in changing environments: a wooded landscape during the Eemian pollen zone E IVb/V, a boreal landscape opening up during late MIS 5c and a dry tundra-like environment during earliest MIS 4.
- (5) The changing archaeological record tentatively implies resilient adaptations to changing environments. These are inferred from different raw material availabilities and resulting management strategies, as well as a high-typological tool diversity in Li-II versus specialized cutting tools and a potentially highly-mobile tool kit in Li-I. This is supported by the use-wear analysis that demonstrated a variety of tasks in Li-II in contrast to potentially specialized cutting tasks in Li-I only. Furthermore, raw material availability can also be explained by geomorphic factors. Sediment redeposition, which provided high-quality and large flint raw material from the primary source of the glacial sediments nearby was hindered in the forested intervals (Li-II and the Eemian occupation) and fostered in the much more sparsely-vegetated phases (Li-I). Future work is planned to evaluate our preliminary results.
- (6) Most importantly, we could show that Neanderthals occupied the northern regions of central Europe also during the cold phases of the last Glacial (section 5.5). Similarities in the archaeological record, especially the technological similarities of Keilmesser manufacture (see above) between Li-I and the posterior early MIS 3 sites further suggest the potential recurrence of populations in the region. That Neanderthals successfully adapted to the harsh northern climatic conditions is corroborated by the fact that early MIS 3 sites are by far the most numerous Middle Paleolithic sites in the North.

Author contributions

All authors made substantial contributions to the study and approved the final manuscript. M.H. and M.W. equally contributed to the study with respect to research design, fieldwork, data analyses, interpretation of data and the writing of the manuscript. They actively took part in the different analyses listed below and amalgamated the various data. B.U. and M.T. conducted palynological analysis; M.C.S. and S.H. conducted micromorphological analysis; Y.H.H. performed traceology on the artefacts; R.C.P. did phytolith analysis; H. v.S. co-supervised M.H.'s doctoral thesis and supported fieldwork; T.T., U.B., F.K. provided additional archaeological data of the region and supported fieldwork; S.V. and K.B. discovered and excavated the original site; J.S. supported grain size analysis; D.C. supported luminescence dating; D.C.T. and M.F. provided methodological and geological information; T.L. supervised M.H.'s doctoral thesis, contributed to the research design and supported luminescence dating. All authors contributed to the preparation of the manuscript.

Declaration of competing interest

The authors declare that they have no known competing financial interests or personal relationships that could have appeared to influence the work reported in this paper.

Acknowledgements

We would like to thank Jonathan Schultz for geodata management and cartographic support, Sonja Riemenschneider for performing grain size analysis and Steffi Hesse and Victoria Krippner for luminescence sample preparation. For assistance during field work, we are grateful to Shannon P. McPherron, Nicolas Bourgon, Sarah Pederzani, Sabine Dietel, Marie Kaniecki, Felix Riedel, Jonathan Schultz, Wiebke E. Lüdtke, Lia Berani, Floriske Meindertsma, Annika Wiebers, Detlef Trapp and Mario Pahlow. We thank Family Kusserow in Lichtenberg who granted access to their land. The authors thankfully acknowledge the work done by the QSR editors and two anonymous reviewers who helped to improve the manuscript. For financial funding we owe our gratitude to Jean-Jacques Hublin (MPI EVA) and the Max Planck Society (MPG).

Appendix A. Supplementary data

Supplementary data to this article can be found online at <https://doi.org/10.1016/j.quascirev.2022.107519>.

References

- AG Boden, 2005. *Bodenkundliche Kartieranleitung* KA5, 5. Aufl. Ed. Ad-Hoc-Arbeitsgruppe Boden.
- Aiello, L.C., Wheeler, P., 2003. Neanderthal thermoregulation and the glacial climate. In: van Andel, T.H., Davies, W. (Eds.), *Neanderthals and Modern Humans in the European Landscape during the Last Glaciation*. McDonald Institute for Archaeological Research, Cambridge, pp. 147–166.
- Aitken, M.J., 1998. *An Introduction to Optical Dating: the Dating of Quaternary Sediments by the Use of Photon-Stimulated Luminescence*. Oxford University Press, New York.
- Antoine, P., Rousseau, D.-D., Degeai, J.-P., Moine, O., Lagroix, F., Kreutzer, S., Fuchs, M., Hatté, C., Gauthier, C., Svoboda, J., Lisá, L., 2013. High-resolution record of the environmental response to climatic variations during the Last Interglacial–Glacial cycle in Central Europe: the loess-palaeosol sequence of Dolní Věstonice (Czech Republic). *Quat. Sci. Rev.* 67, 17–38. <https://doi.org/10.1016/j.quascirev.2013.01.014>.
- Antoine, P., Coutard, S., Guerin, G., Deschodt, L., Govaal, E., Locht, J.-L., Paris, C., 2016. Upper Pleistocene loess-palaeosol records from northern France in the European context: environmental background and dating of the middle palaeolithic. *Quat. Int.* 411, 4–24. <https://doi.org/10.1016/j.quaint.2015.11.036>.
- Behre, K.-E., 1989. Biostratigraphy of the last glacial period in Europe. *Quat. Sci. Rev.* 8, 25–44. [https://doi.org/10.1016/0277-3791\(89\)90019-X](https://doi.org/10.1016/0277-3791(89)90019-X).
- Behre, K.-E., Lade, U., 1986. Eine Folge von Eem und 4 Weichsel-Interstadialen in Oerel/Niedersachsen und ihr Vegetationsablauf. *Q. Sci. J.* 36, 11–36. <https://doi.org/10.3285/eg.36.1.02>.
- Behre, K.-E., van der Plicht, J., 1992. Towards an absolute chronology for the last glacial period in Europe: radiocarbon dates from Oerel, northern Germany. *Veg. Hist. Archaeobotany* 1, 111–117. <https://doi.org/10.1007/BF00206091>.
- Behre, K.-E., Hölzer, A., Lemdahl, G., 2005. Botanical macro-remains and insects from the Eemian and Weichselian site of Oerel (northwest Germany) and their evidence for the history of climate. *Veg. Hist. Archaeobotany* 14, 31–53. <https://doi.org/10.1007/s00334-005-0059-x>.
- Bertran, P., Andrieux, E., Antoine, P., Coutard, S., Deschodt, L., Gardère, P., Hernandez, M., Legentil, C., Lenoble, A., Liard, M., Mercier, N., Moine, O., Sittia, L., Van Vliet-Lanoë, B., 2014. Distribution and chronology of Pleistocene permafrost features in France: database and first results. *Boreas* 43, 699–711. <https://doi.org/10.1111/bor.12025>.
- Beug, H.-J., 2004. *Leitfaden der Pollenbestimmung für Mitteleuropa und angrenzende Gebiete*. Germania 87, 542.
- Beuselinck, L., Govers, G., Poesen, J., Degraer, G., Froyen, L., 1998. Grain-size analysis by laser diffractometry: comparison with the sieve-pipette method. *Catena* 32, 193–208. [https://doi.org/10.1016/S0341-8162\(98\)00051-4](https://doi.org/10.1016/S0341-8162(98)00051-4).
- Blott, S.J., Pye, K., 2001. GRADISTAT: a grain size distribution and statistics package for the analysis of unconsolidated sediments. *Earth Surf. Process. Landforms* 26, 1237–1248. <https://doi.org/10.1002/esp.261>.
- Boch, R., Cheng, H., Spötl, C., Edwards, R.L., Wang, X., Häuselmann, Ph., 2011. NALPS: a precisely dated European climate record 120–60 ka. *Clim. Past* 7, 1247–1259. <https://doi.org/10.5194/cp-7-1247-2011>.
- Bolland, A., Kern, O.A., Allstädt, F.J., Peteet, D., Koutsodendris, A., Pross, J., Heiri, O., 2021. Summer temperatures during the last glaciation (MIS 5c to MIS 3) inferred from a 50,000-year chironomid record from Fürmoos, southern Germany. *Quat. Sci. Rev.* 264, 107008. <https://doi.org/10.1016/j.quascirev.2021.107008>.
- Bordes, F., 1961. *Typologie du Paléolithique ancien et moyen. Mémoires de l'Institut Préhistoriques de l'Université de Bordeaux*. Delmas, Bordeaux.
- Bos, J.A.A., Bohncke, S.J.P., Kasse, C., Vandenbergh, J., 2001. Vegetation and climate during the weichselian early glacial and pleniglacial in the niederlausitz, eastern Germany? macrofossil and pollen evidence. *J. Quat. Sci.* 16, 269–289. <https://doi.org/10.1002/jqs.606>.
- Bosinski, G., 1967. *Die Mittelpaläolithischen Funde im Westlichen Mitteleuropa*. Böhlhau-Verlag, Köln, Graz. Fundamenta A/4.
- Bouma, J., Foc, C.A., Miedma, R., 1990. Micromorphology of hydromorphic soils: applications for soil genesis and land evaluation. In: Douglas, L.A. (Ed.), *Soil Micro-morphology: A Basic and Applied Science*, pp. 257–278.
- Bridge, J., Demicco, R., 2008. *Earth Surface Processes, Landforms and Sediment Deposits*. Cambridge University Press, New York.
- Buylaert, J.P., Jain, M., Murray, A.S., Thomsen, K.J., Thiel, C., Sohbati, R., 2012. A robust feldspar luminescence dating method for Middle and Late Pleistocene sediments. *Boreas* 41, 435–451. <https://doi.org/10.1111/j.1502-3885.2012.00248.x>.
- Caspers, G., Freund, H., 2001. Vegetation and climate in the early- and pleniglacial in northern central Europe. *J. Quat. Sci.* 16, 31–48. [https://doi.org/10.1002/1099-1417\(200101\)16:1<31::AID-JQS577>3.0.CO;2-3](https://doi.org/10.1002/1099-1417(200101)16:1<31::AID-JQS577>3.0.CO;2-3).
- Chan, B., Francisco Gibaja, J., García-Díaz, V., Hoggard, C.S., Mazzucco, N., Rowland, J.T., Van Gijn, A., 2020. Towards an understanding of retouch flakes: a use-wear blind test on knapped stone microdebitage. *PLoS One* 15, e0243101. <https://doi.org/10.1371/journal.pone.0243101>.
- Christiansen, H.H., 1998a. Periglacial sediments in an eemian-weichselian succession at emmerlev klev, southwestern jutland, Denmark. *Palaeogeogr. Palaeoclimatol. Palaeoecol.* 138, 245–258. [https://doi.org/10.1016/S0031-0182\(97\)00117-X](https://doi.org/10.1016/S0031-0182(97)00117-X).
- Christiansen, H.H., 1998b. Nivation forms and processes in unconsolidated sediments, NE Greenland. *Earth Surf. Process. Landforms* 23, 751–760. [https://doi.org/10.1002/\(SICI\)1096-9837\(199808\)23:8<751::AID-ESP886>3.0.CO;2-A](https://doi.org/10.1002/(SICI)1096-9837(199808)23:8<751::AID-ESP886>3.0.CO;2-A).
- Churchill, S.E., 2008. Bioenergetic perspectives on Neanderthal thermoregulatory and activity budgets. In: Harvati, K., Harrison, T. (Eds.), *Neanderthals Revisited: New Approaches and Perspectives*. Springer, pp. 113–134.
- Clemente, I., Gibaja, J.F., 1998. Working processes on cereals: an approach through microwear analysis. *J. Archaeol. Sci.* 25, 457–464. <https://doi.org/10.1006/jasc.1997.0214>.
- Cohen, A.S., 2003. *Paleolimnology: the History and Evolution of Lake Systems*. Oxford University Press.
- Delpiano, D., Uthmeier, T., 2020. Techno-functional and 3D shape analysis applied for investigating the variability of backed tools in the Late Middle Paleolithic of Central Europe. *PLoS One* 15, e0236548. <https://doi.org/10.1371/journal.pone.0236548>.
- Depaepe, P., Govaal, E., Koehler, H., Locht, J.-L., 2015. *Les plaines du Nord-Ouest : carrefour de l'Europe au Paléolithique moyen ? Société préhistorique française, Paris. Mémoires de la société préhistorique française* 59.
- Dibble, H.L., Sandgathe, D., Goldberg, P., McPherron, S., Aldeias, V., 2018. Were western European neandertals able to make fire? *J. Paleolithic Archaeol.* 1, 54–79. <https://doi.org/10.1007/s41982-017-0002-6>.
- Duphorn, K., Grube, F., Meyer, K.-D., Streif, H., Vinken, R., 1973. A. Area of scandinavian glaciation: 1. Pleistocene and holocene. *Q. Sci. J.* 23/24, 222–250. <https://doi.org/10.3285/eg.23-24.1.19>.
- Ehlers, J., 1990. *Untersuchungen zur Morphodynamik der Vereisungen Norddeutschlands unter Berücksichtigung benachbarter Gebiete*. Bremer Beiträge

- zur Geographie und Raumplanung 19, 166.
- Ehlers, J., 2020. Das Eiszeitalter. Springer Berlin Heidelberg, Berlin, Heidelberg. <https://doi.org/10.1007/978-3-662-60582-0>.
- Ehlers, J., Grube, A., Stephan, H.J., Wansa, S., 2011. Pleistocene glaciations of north Germany—new results, developments in quaternary science. <https://doi.org/10.1016/B978-0-444-53447-7.00013-1>.
- Fægri, K., Iversen, J., Kaland, P.E., Krzywinski, K., 1989. Textbook of Pollen Analysis, fourth ed. John Wiley & Sons Ltd., Chichester.
- Farrell, E.J., Sherman, D.J., Ellis, J.T., Li, B., 2012. Vertical distribution of grain size for wind blown sand. *Aeolian Res.* 7, 51–61. <https://doi.org/10.1016/j.aeolia.2012.03.003>.
- Féblot-Augustins, J., 1993. Mobility strategies in the late middle palaeolithic of central Europe and western Europe: elements of stability and variability. *J. Anthropol. Archaeol.* <https://doi.org/10.1006/jaar.1993.1007>.
- Folk, R.L., Ward, W.C., 1957. Brazos River bar [Texas]: a study in the significance of grain size parameters. *J. Sediment. Res.* 27, 3–26. <https://doi.org/10.1306/74D70646-2B21-11D7-8648000102C1865D>.
- French, H., 2008. Recent contributions to the study of past permafrost. *Permafrost. Periglac. Process.* 19, 179–194. <https://doi.org/10.1002/ppp.614>.
- Fuchs, M., Kreutzer, S., Rousseau, D.-D., Antoine, P., Hatté, C., Lagroix, F., Moine, O., Gauthier, C., Svoboda, J., Lisá, L., 2013. The loess sequence of Dolní Věstonice, Czech republic: a new OSL-based chronology of the last climatic cycle. *Boreas* 42, 664–677. <https://doi.org/10.1111/j.1502-3885.2012.00299.x>.
- Gamisch, A., 2019a. Oscillayers: A Dataset for the Study of Climatic Oscillations over Plio-Pleistocene Time Scales at High Spatial-Temporal Resolution. *Dryad*. <https://doi.org/10.5061/dryad.27f8s90>. Dataset [WWW Document].
- Gamisch, A., 2019b. Oscillayers: a dataset for the study of climatic oscillations over Plio-Pleistocene time-scales at high spatial-temporal resolution. *Global Ecol. Biogeogr.* 28, 1552–1560. <https://doi.org/10.1111/geb.12979>.
- Gaudzinski, S., 1998. Knochen und Knochengeräte der mittelpaläolithischen Fundstelle Salzgitter-Lebenstedt (Deutschland). *Jahrb. Des. Römisch-Germanischen Zentralmus. Mainz* 45, 163–220.
- Gaudzinski, S., 1999. Middle palaeolithic bone tools from the open-air site Salzgitter-lebenstedt (Germany). *J. Archaeol. Sci.* 26, 125–141. <https://doi.org/10.1006/jasc.1998.0311>.
- Gaudzinski-Windheuser, S., Roebroeks, W., 2014. Multidisciplinary Studies or the Middle Paleolithic Record from Neumark-Nord (Germany), vol. I. Beier & Beran, Halle(Saale). Veröffentlichungen des Landesamtes für Archäologie Sachsen-Anhalt 69.
- Gladilin, V.N., 1976. Problemy Rannego Paleolitha Vostochnoj Evropy. *Akademia nauk Ukrainskoi, SSR, Kiev*.
- Glückler, R., Herzschuh, U., Kruse, S., Andreev, A., Vyse, S.A., Winkler, B., Biskaborn, B.K., Pestrykova, L., Dietze, E., 2021. Wildfire history of the boreal forest of south-western Yakutia (Siberia) over the last two millennia documented by a lake-sediment charcoal record. *Biogeosciences* 18, 4185–4209. <https://doi.org/10.5194/bg-18-4185-2021>.
- González-Urquijo, J.E., Ibañez-Estévez, J.J., 1994. Metodología de análisis funcional de instrumentos tallados en sílex. *Universidad de Duesto*.
- Grimm, E.C., 1990. TILIA, TILIAGRAPH and TILIAVIEW. PC Spreadsheet and Graphics Software for Pollen Data.
- Grootes, P.M., 1978. Carbon-14 time scale extended: comparison of chronologies. *Science* 200, 11–15. <https://doi.org/10.1126/science.200.4337.11>.
- Hahne, J., Kemle, S., Merkt, J., Meyer, K.D., 1994. Eem-, weichsel- und saalezeitliche Ablagerungen der Bohrung “Quakenbrück GE 2. *Geol. Jahrb.* A134, 9–69.
- Hartz, S., Beuker, J., Niekus, M.J.L.Th., 2012. Neanderthal finds in Schleswig holstein? - middle palaeolithic flintscatters in northern Germany. In: Niekus, M.J.L.Th., Barton, R.N.E., Street, M., Terberger, T. (Eds.), *A Mind Set on Flint. Studies in Honour of Dick Stapert*, Groningen Archaeological Studies 16. Barkhuis Groningen University Library, Groningen, pp. 93–105.
- Hedges, R.E.M., Pettitt, P.B., Ramsey, C.B., Klinken, G.J.V., 1998. Radiocarbon dates from the oxford AMS system: archaeometry datelist 25. *Archaeometry* 40, 227–239.
- Hein, M., Weiss, M., Otcherednoy, A., Lauer, T., 2020. Luminescence chronology of the key-Middle Paleolithic site Khotylevo I (Western Russia) - implications for the timing of occupation, site formation and landscape evolution. *Q. Sci. Adv.* 2, 100008. <https://doi.org/10.1016/j.qsa.2020.100008>.
- Hein, M., Urban, B., Tanner, D.C., Buness, A.H., Tucci, M., Hoelzmann, P., Dietel, S., Kaniecki, M., Schultz, J., Kasper, T., Suchodoletz, H., Schwalb, A., Weiss, M., Lauer, T., 2021. Eemian landscape response to climatic shifts and evidence for northerly Neanderthal occupation at a palaeolake margin in northern Germany. *Earth Surf. Process. Landf.* 5219. <https://doi.org/10.1002/esp.5219>.
- Hublin, J.-J., 1984. The fossil man from Salzgitter-Lebenstedt (FRG) and its place in human evolution during the Pleistocene in Europe. *Z. Morphol. Anthropol.* 75, 45–56.
- Hublin, J.-J., Roebroeks, W., 2009. Ebb and flow or regional extinctions? On the character of Neanderthal occupation of northern environments. *Comptes Rendus Palevol* 8, 503–509. <https://doi.org/10.1016/j.crpv.2009.04.001>.
- Iovita, R., 2010. Comparing stone tool reshaping trajectories with the aid of elliptical Fourier analysis. In: Lycett, S.J., Chauhan, P.R. (Eds.), *New Perspectives on Old Stones. Analytical Approaches to Paleolithic Technologies*. Springer, pp. 235–253.
- Jarvis, A., Reuter, H.I., Nelson, A., Guevarra, E., 2008. Hole-filled seamless SRTM data V4. Centre for Tropical Agriculture (CIAT) [WWW Document]. URL: <http://srtm.csi.cgiar.org>.
- Joris, O., 2004. Zur chronostratigraphischen Stellung der spätmittelpaläolithischen Keilmessergruppen: der Versuch einer kulturgeographischen Abgrenzung einer mittelpaläolithischen Formengruppe in ihrem europäischen Kontext. *Bericht RGK* 84, 49–153.
- Joris, O., 2006. Bifacially backed knives (keilmesser) in the central European middle palaeolithic. In: Goren-Inbar, N., Sharon, G. (Eds.), *Axe Age: Acheulian Tool-Making from Quarry to Discard*. Equinox Publishing Ltd, London, pp. 287–310.
- Joris, O., 2012. Keilmesser. In: Floss, H. (Ed.), *Steinartefakte Vom Altpaläolithikum Bis in Die Neuzeit*. Kerns Verlag, Tübingen, pp. 297–308.
- Katz, O., Cabanes, D., Weiner, S., Maeir, A.M., Boaretto, E., Shahack-Gross, R., 2010. Rapid phytolith extraction for analysis of phytolith concentrations and assemblages during an excavation: an application at Tell es-Safi/Gath, Israel. *J. Archaeol. Sci.* 37, 1557–1563. <https://doi.org/10.1016/j.jas.2010.01.016>.
- Keeley, L.H., 1980. Experimental Determination of Stone Tool Uses: a Microwear Analysis. University of Chicago Press.
- Kegler, J.F., Fries, J.E., 2018. Neandertaler? 15m tiefer bitte! Die neandertalerzeitlichen Steinartefakte der Fundstellen Gildehaus 31 und 33 im Landkreis Grafschaft Bentheim (Niedersachsen). *Archaeol. Korresp.* 48, 455–471.
- Kindler, L., Smith, G.M., García-Moreno, A., Gaudzinski-Windheuser, S., Pop, E., Roebroeks, W., 2020. The last interglacial (Eemian) lakeland of Neumark-Nord (Saxony-Anhalt, Germany). Sequencing Neanderthal occupations, assessing subsistence opportunities and prey selection based on estimations of ungulate carrying capacities, biomass production and energ. In: García-Moreno, A., Hutson, J.M., Smith, G.M., Kindler, L., Turner, E., Villaluenga, A., Gaudzinski-Windheuser, S. (Eds.), *Human Behavioural Adaptations to Interglacial Lakeshore Environments*, RGZM - Tagungen 37. RGZM, Mainz und Heidelberg, pp. 67–104.
- Kolobova, K.A., Roberts, R.G., Chabai, V.P., Jacobs, Z., Krajcarz, M.T., Shalagina, A.V., Krivosheina, A.I., Li, B., Uthmeier, T., Markin, S.V., Morley, M.W., O’Gorman, K., Rudaya, N.A., Talamo, S., Viola, B., Derevianko, A.P., 2020. Archaeological evidence for two separate dispersals of Neanderthals into southern Siberia. *Proc. Natl. Acad. Sci. Unit. States Am.* 117, 2879–2885. <https://doi.org/10.1073/pnas.1918047117>.
- Kreutzer, S., Schmidt, C., Dewitt, R., Fuchs, M., 2014. The a-value of polymineral fine grain samples measured with the post-IR IRSF protocol. *Radiat. Meas.* 69, 18–29. <https://doi.org/10.1016/j.radmeas.2014.04.027>.
- Kühl, N., Litt, T., Schölzel, C., Hense, A., 2007. Eemian and Early Weichselian temperature and precipitation variability in northern Germany. *Quat. Sci. Rev.* 26, 3311–3317. <https://doi.org/10.1016/j.quascirev.2007.10.004>.
- Lambeck, K., 2004. Sea-level change through the last glacial cycle: geophysical, glaciological and palaeogeographic consequences. *Compt. Rendus Geosci.* 336, 677–689. <https://doi.org/10.1016/j.crte.2003.12.017>.
- Lang, J., Lauer, T., Winsemann, J., 2018. New age constraints for the Saalian glaciation in northern central Europe: implications for the extent of ice sheets and related proglacial lake systems. *Quat. Sci. Rev.* 180, 240–259. <https://doi.org/10.1016/j.quascirev.2017.11.029>.
- Laurat, T., Brühl, E., 2006. Zum Stand der archäologischen Untersuchungen im Tagebau Neumark-Nord, Ldkr. Merseburg-Querfurt (Sachsen-Anhalt) - vorbericht zu den Ausgrabungen 2003–2005. *Jahresschr. für Mitteldtsch. Vorgesch.* 90, 9–69.
- Laurat, T., Brühl, E., 2021. Neumark-nord 2 – a multiphase middle palaeolithic open-air site in the geisel valley (Central Germany). *L’Anthropologie* 102936. <https://doi.org/10.1016/j.anthro.2021.102936>.
- Lisiecki, L.E., Raymo, M.E., 2005a. A Pliocene-Pleistocene stack of 57 globally distributed benthic $\delta^{18}O$ records. *Paleoceanography* 20, 1–17. <https://doi.org/10.1029/2004PA001071>.
- Lisiecki, L.E., Raymo, M.E., 2005b. A Pliocene-Pleistocene stack of 57 globally distributed benthic $\delta^{18}O$ records. *Paleoceanography* 20, 1–17. <https://doi.org/10.1029/2004PA001071>.
- Litt, T., Weber, T., 1988. Ein eemzeitlicher waldelefantenschlachtplatz von Gröbern. *Krs. Gräfenhainichen. Ausgrabungen und Funde* 33, 181–187.
- Locht, J.-L., Hérissou, D., Govaal, E., Cliquet, D., Huet, B., Coutard, S., Antoine, P., Feray, P., 2016. Timescales, space and culture during the Middle Palaeolithic in northwestern France. *Quat. Int.* 411, 129–148. <https://doi.org/10.1016/j.quaint.2015.07.053>.
- Machalett, B., Oches, E.A., Frechen, M., Zöller, L., Hambach, U., Mavlyanova, N.G., Marković, S.B., Endlicher, W., 2008. Aeolian dust dynamics in central Asia during the Pleistocene: driven by the long-term migration, seasonality, and permanency of the Asiatic polar front. *G-cubed* 9. <https://doi.org/10.1029/2007GC001938>.
- Madella, M., Lancelotti, C., 2012. Taphonomy and phytoliths: a user manual. *Quat. Int.* 275, 76–83. <https://doi.org/10.1016/j.quaint.2011.09.008>.
- Mania, D., 1990. Auf den Spuren des Urmenschen: Die Funde aus der Steinrinne von Bilzingsleben. *Deutscher Verlag der Wissenschaften*, Berlin.
- Mania, D., 2002. Der mittelpaläolithische Lagerplatz am Ascherslebener See bei Königsau (Nordharzvorland). *Prähistoria Thuringica* 8, 16–75.
- Mania, D., Toepfer, V., 1973. Königsau: Gliederung, Ökologie und mittelpaläolithische Funde der letzten Eiszeit. *Veröffentlichungen des Landesmuseums für Vorgeschichte in Halle* 26. Deutscher Verlag der Wissenschaften, Berlin.
- Menke, B., 1976. Neue Ergebnisse zur Stratigraphie und Landschaftsentwicklung im Jungpleistozän Westholsteins. *Q. Sci. J.* 27, 53–68. <https://doi.org/10.3285/eg.27.105>.
- Menke, B., Tynni, R., 1984. Das Eeminterglazial und das Weichselfrühglazial von Jüdelstall/Dithmarschen und ihre Bedeutung für die mitteleuropäische Jungpleistozän-Gliederung. *Geologisches Jahrbuch A* 76, 1–120.
- Meyer, K.D., 1983. Zur anlage der Urstromtäler in niedersachsen. *Z. Geomorph. N.F.*

- 27, 147–160.
- Mol, J., 1995. Weichselian and Holocene river dynamics in relation to climate change on the Halle-Leipziger Tieflandsbucht (Germany). *Q. Sci. J.* 45, 32–41.
- Moncel, M.-H., Neruda, P., 2000. The Kůlna level 11: some observations on the debitage rules and aims. The originality of a Middle Palaeolithic microlithic assemblage (Kůlna Cave, Czech Republic). *Anthropologie XXXVIII*, 219–247.
- Moore, P.D., Webb, J.A., Collison, M.E., 1991. *Pollen Analysis*. Blackwell Scientific Publications, Oxford.
- Moss, E., 1987. Polish G and the question of hafting. In: *La Main et l'outil: Manches et Emmanchements Préhistoriques*. G.S. Maison de l'Orient, pp. 97–102.
- Müller, U.C., Sánchez Goñi, Maria F., 2007. Vegetation dynamics in southern Germany during marine isotope stage 5 (~ 130 to 70 kyr ago). In: Sirocko, F., Claussen, M., Sánchez Goñi, M.F., Litt, T. (Eds.), *The Climate of Past Interglacials*. (Developments in Quaternary Sciences 7), pp. 277–287. [https://doi.org/10.1016/S1571-0866\(07\)80044-3](https://doi.org/10.1016/S1571-0866(07)80044-3).
- Murray, A.S., Wintle, A.G., 2003. The single aliquot regenerative dose protocol: potential for improvements in reliability. *Radiat. Meas.* 37, 377–381. [https://doi.org/10.1016/S1350-4487\(03\)00053-2](https://doi.org/10.1016/S1350-4487(03)00053-2).
- NGRIP members, 2004. High-resolution record of Northern Hemisphere climate extending into the last interglacial period. *Nature* 431, 147–151. <https://doi.org/10.1038/nature02805>.
- Nielsen, T.K., Benito, B.M., Svenning, J.-C., Sandel, B., McKerracher, L., Riede, F., Kjærgaard, P.C., 2017. Investigating neanderthal dispersal above 55°N in Europe during the last interglacial complex. *Quat. Int.* 431, 88–103. <https://doi.org/10.1016/j.quaint.2015.10.039>.
- Pastors, A., 2001. Die Mittelpaläolithische Freilandstation von Salzgitter-Lebenstedt: Genese der Fundstelle und Systematik der Steinbearbeitung. *Archiv der Stadt Salzgitter, Salzgitter*.
- Pastors, A., 2009. Blades ? – thanks, no interest! – Neanderthals in Salzgitter-Lebenstedt. *Quartar* 56, 105–118.
- Pfaffenberg, K., 1991. Die Vegetationsverhältnisse während und nach der Sedimentation der Fundschichten von Salzgitter-Lebenstedt. In: Busch, R., Schwabedissen, H. (Eds.), *Der Altsteinzeitliche Fundplatz Salzgitter-Lebenstedt. Teil II. Naturwissenschaftliche Untersuchungen*. Böhlau Verlag, Köln, Weimar, Wien, pp. 183–210.
- Picin, A., 2016. Short-term occupations at the lakeshore: a technological reassessment of the open-air site Königsau (Germany). *Quartar* 63, 7–32. <https://doi.org/10.7485/QU63.1>.
- Pop, E., 2014. Analysis of the Neumark-Nord 2/2 lithic assemblage: results and interpretations. In: Gaudzinski-Windheuser, S., Roebroeks, W. (Eds.), *Multidisciplinary Studies of the Middle Palaeolithic Record from Neumark-Nord (Germany)*, Volume 1, Veröffentlichungen des Landesamtes für Archäologie Sachsen-Anhalt – Landesmuseum für Vorgeschichte, vol. 69, pp. 143–195. Halle(Saale).
- Pop, E., Bakels, C., 2015. Semi-open environmental conditions during phases of hominin occupation at the Eemian Interglacial basin site Neumark-Nord 2 and its wider environment. *Quat. Sci. Rev.* 117, 72–81. <https://doi.org/10.1016/j.quascirev.2015.03.020>.
- Power, R.C., Rosen, A.M., Nadel, D., 2014. The economic and ritual utilization of plants at the Raqefet Cave Natufian site: the evidence from phytoliths. *J. Anthropol. Archaeol.* 33, 49–65. <https://doi.org/10.1016/j.jaa.2013.11.002>.
- Preusser, F., 2004. Towards a chronology of the late Pleistocene in the northern alpine Foreland. *Boreas* 33, 195–210. <https://doi.org/10.1080/03009480410001271>.
- Rae, T.C., Koppe, T., Stringer, C.B., 2011. The Neanderthal face is not cold adapted. *J. Hum. Evol.* 60, 234–239. <https://doi.org/10.1016/j.jhevol.2010.10.003>.
- Rasmussen, S.O., Bigler, M., Blockley, S.P., Blunier, T., Buchardt, S.L., Clausen, H.B., Cvijanovic, I., Dahl-Jensen, D., Johnsen, S.J., Fischer, H., Gkinis, V., Guillevic, M., Hoek, W.Z., Lowe, J.J., Pedro, J.B., Popp, T., Seierstad, I.K., Steffensen, J.P., Svensson, A.M., Vallenga, P., Vinther, B.M., Walker, M.J.C., Wheatley, J.J., Winstrup, M., 2014. A stratigraphic framework for abrupt climatic changes during the Last Glacial period based on three synchronized Greenland ice-core records: refining and extending the INTIMATE event stratigraphy. *Quat. Sci. Rev.* 106, 14–28. <https://doi.org/10.1016/j.quascirev.2014.09.007>.
- Reuter, H.I., Nelson, A., Jarvis, A., 2007. An evaluation of void-filling interpolation methods for SRTM data. *Int. J. Geogr. Inf. Sci.* 21, 983–1008. <https://doi.org/10.1080/13658810601169899>.
- Richter, J., 1997. Sesselfelsgrötte III. Der G-Schichten-Komplex der Sesselfelsgrötte. Zum Verständnis des Micoquien, Quartär Bibliothek 7. Saarbrücker Druckerei und Verlag, Saarbrücken.
- Richter, J., 2002. Die 14C-Daten aus der Sesselfelsgrötte und die Zeitstellung des Micoquien/MMO. *Germania* 80, 1–22.
- Richter, J., 2016. Leave at the height of the party: a critical review of the Middle Paleolithic in Western Central Europe from its beginnings to its rapid decline. *Quat. Int.* 411, 107–128. <https://doi.org/10.1016/j.quaint.2016.01.018>.
- Richter, D., Krbetschek, M., 2014. Preliminary luminescence dating results for two Middle Palaeolithic occupations at Neumark-Nord 2. In: Gaudzinski-Windheuser, S., Roebroeks, W. (Eds.), *Multidisciplinary Studies of the Middle Palaeolithic Record from Neumark-Nord (Germany)*, Volume 1, Veröffentlichungen des Landesamtes für Archäologie Sachsen-Anhalt – Landesmuseum für Vorgeschichte, vol. 69, pp. 131–136. Halle(Saale).
- Roebroeks, W., Hublin, J.-J., MacDonald, K., 2011. Continuities and discontinuities in neanderthal presence: a closer look at northwestern Europe. In: *Developments in Quaternary Sciences*. Elsevier, pp. 113–123. <https://doi.org/10.1016/B978-0-444-53597-9.00008-X>.
- Roebroeks, W., Bakels, C.C., Coward, F., Hosfield, R., Pope, M., Wenban-Smith, F., 2015. 'Forest furniture' or 'forest managers'? On neanderthal presence in last interglacial environments. In: *Settlement, Society and Cognition in Human Evolution*. Cambridge University Press, New York, pp. 174–188. <https://doi.org/10.1017/CBO9781139208697.011>.
- Rots, V., 2010. *Prehension and Hafting Traces on Flint Tools: a Methodology*. Universitaire Press Leuven.
- Schwan, J., 1988. The structure and genesis of Weichselian to early holocene aeolian sand sheets in western Europe. *Sediment. Geol.* 55, 197–232. [https://doi.org/10.1016/0037-0738\(88\)90132-7](https://doi.org/10.1016/0037-0738(88)90132-7).
- Selle, W., 1991. Die palynologischen untersuchungen am paläolithischen fundplatz salzgitter-lebenstedt. In: Busch, R., Schwabedissen, H. (Eds.), *Der Altsteinzeitliche Fundplatz Salzgitter-Lebenstedt. Teil II. Naturwissenschaftliche Untersuchungen*. Böhlau Verlag, Köln, Weimar, Wien, pp. 149–161.
- Semenov, S.A., 1964. *Prehistoric Technology: an Experimental Study of the Oldest Tools and Artifacts from Traces of Manufacture and Wear*. Barnes and Noble.
- Skrzypek, G., Wiśniewski, A., Grieron, P.F., 2011. How cold was it for Neanderthals moving to Central Europe during warm phases of the last glaciation? *Quat. Sci. Rev.* 30, 481–487.
- Stephan, H.-J., 2014. Climato-stratigraphic subdivision of the Pleistocene in Schleswig-Holstein, Germany and adjoining areas: status and problems. *Q. Sci. J.* 63, 3–18. <https://doi.org/10.3285/eg.63.1.01>.
- Stephan, H.-J., Burbaum, B., Kenzler, M., Krienke, K., Lungershausen, U., Tummuscheit, A., Frechen, M., Thiel, C., Urban, B., Sierralta, M., 2017. Quartärgeologie und Archäologie im Norden Schleswig-Holsteins (unpublished field trip guide).
- Stoops, G., 2003. *Guidelines for Analysis and Description of Soil and Regolith Thin Sections*. Soil Science Society of America, Inc, Madison, Wisconsin, USA.
- Stoops, G., Marcelino, V., Mees, F., 2010. Interpretation of Micromorphological Features of Soils and Regoliths. <https://doi.org/10.1016/C2009-0-18081-9>.
- Strahl, J., Krbetschek, M.R., Luckert, J., Machalet, B., Meng, S., Oches, E.A., Rappsilber, I., Wansa, S., Zöller, L., 2010. Geologie, Paläontologie und Geo-chronologie des Eem-Beckens Neumark-Nord 2 und Vergleich mit dem Becken Neumark-Nord 1 (Geiseltal, Sachsen-Anhalt). *Eiszeitalt. Ggw.* 59, 120–167. <https://doi.org/10.3285/eg.59.1-2.09>.
- Taylor, G.H., Teichmüller, M., Davis, A., Diessel, C.F.K., Littke, R., Robert, P., 1998. *Organic Petrology*. Gebrüder Bornträger, Berlin Stuttgart.
- Thiel, C., Buylaert, J.P., Murray, A., Terhorst, B., Hofer, I., Tsukamoto, S., Frechen, M., 2011. Luminescence dating of the Stratzung loess profile (Austria) – testing the potential of an elevated temperature post-IR IRSL protocol. *Quat. Int.* 234, 23–31. <https://doi.org/10.1016/j.quaint.2010.05.018>.
- Thieme, H., 2003. Ochtmissen, Stadt Lüneburg – ein faustkeilreicher Fundplatz des späten Acheuleen in der Ilmenau-Niederung. In: Burdukiewicz, J.M., Justus, A., L. F. (Eds.), *Erkenntnisjäger. Kultur und Umwelt Des Frühen Menschen. Festschrift Für Dietrich Mania, Veröffentlichungen Des Landesamtes Für Denkmalpflege Und Archäologie Sachsen-Anhalt, Landesmuseum Für Vorgeschichte 57. Veröffentlichungen des Landesamtes für Denkmalpflege und Archäologie Sachsen-Anhalt, Landesmuseum für Vorgeschichte, Bd., vol. 57, pp. 593–600. Halle(Saale)*.
- Thieme, H., Veil, S., 1985. Neue untersuchungen zum eemzeitlichen elefanten-jagdplatz lehringen. *Ldkr. Verden. Die Kunde N.F.* 36, 11–58.
- Tode, A., 1982. *Der Altsteinzeitliche Fundplatz Salzgitter-Lebenstedt. Teil I, Archäologischer Teil*. Böhlau, Köln, Wien.
- Toepfer, V., 1958. Steingeräte und Paläökologie der mittel- paläolithischen Fundstelle Rabutz bei Halle. *Jahresschr. für Mitteldtsch. Vorgesch.* 41/42, 140–179.
- Tucci, M., Krah, K.J., Richter, D., van Kolfschoten, T., Álvarez, B.R., Verheijen, I., Serangeli, J., Lehmann, J., Degering, D., Schwalb, A., Urban, B., 2021. Evidence for the age and timing of environmental change associated with a Lower Palaeolithic site within the Middle Pleistocene Reinsdorf sequence of the Schöningen coal mine, Germany. *Palaeogeogr. Palaeoclimatol. Palaeoecol.* 569, 110309. <https://doi.org/10.1016/j.palaeo.2021.110309>.
- Valoch, K., 1988. *Die Erforschung der Kůlna Höhle 1961–1976*. Moravské Muzeum, Brno.
- Van Huissteden, K., Vandenberghe, J., Pollard, D., 2003. Palaeotemperature reconstructions of the European permafrost zone during marine oxygen isotope Stage 3 compared with climate model results. *J. Quat. Sci.* 18, 453–464. <https://doi.org/10.1002/jqs.766>.
- Van Meerbeeck, C.J., Renssen, H., Roche, D.M., Wohlfarth, B., Bohncke, S.J.P., Bos, J.A.A., Engels, S., Helmens, K.F., Sánchez-Goñi, M.F., Svensson, A., Vandenberghe, J., 2011. The nature of MIS 3 stadial-interstadial transitions in Europe: new insights from model–data comparisons. *Quat. Sci. Rev.* 30, 3618–3637. <https://doi.org/10.1016/j.quascirev.2011.08.002>.
- Vandenberghe, J., 2013. Cryoturbation structures. In: E. S.A. (Ed.), *The Encyclopedia of Quaternary Science*, pp. 430–435.
- Vandenberghe, J., Pissart, A., 1993. Permafrost changes in Europe during the last glacial. *Permafrost. Periglac. Process.* 4, 121–135. <https://doi.org/10.1002/ppp.3430040205>.
- Vandenberghe, J., Van den Broek, P., 1982. Weichselian Convolution Phenomena and processes in fine sediments. *Boreas* 11, 299–315. <https://doi.org/10.1111/j.1502-3885.1982.tb00539.x>.
- Vandenberghe, J., van der Plicht, J., 2016. The age of the Hengelo interstadial revisited. *Quat. Geochronol.* 32, 21–28. <https://doi.org/10.1016/j.quageo.2015.12.004>.
- Vaughan, P.C., 1985. *Use-wear Analysis of Flaked Stone Tools*. University of Arizona

- Press, Tucson.
- Veil, S., 1995. Vor 55.000 Jahren. Ein Jagdplatz früher Menschen bei Lichtenberg, Ldkr Lüchow-Dannenberg, Begleithefte zu Ausstellungen der Abteilung Urgeschichte des Niedersächsischen Landesmuseums Hannover; H.S. Isensee Verlag, Oldenburg.
- Veil, S., Breest, K., Höfle, H.-C., Meyer, H.-H., Plisson, H., Urban-Küttel, B., Wagner, G.A., Zöller, L., 1994. Ein mittelpaläolithischer Fundplatz aus der Weichsel-Kaltzeit bei Lichtenberg, Lkr. Lüchow-Dannenberg. *Germania* 72, 1–66.
- Walkling, A., 1997. Käferkundliche untersuchungen an weichselzeitlichen ablagerungen der Bohrung groß todtshorn (Kr. Harburg; niedersachsen). *Schrift. Dtsch. Geol. Ges.* 4, 87–102.
- Weber, T., 1990. Paläolithische Funde aus den Eemvorkommen von Rabutz, Grab-schütz und Gröbern. In: Eißmann, L. (Ed.), *Die Eemwarmzeit Und Die Frühe Weichsel- Eiszeit Im Saale-Elbe-Gebiet. Geologie, Paläontologie, Palökologie, Altenburger Naturwissenschaftliche Forschungen* 5. Naturkundliches Museum Mauritium, Altenburg.
- Weiss, M., 2015. Stone tool analysis and context of a new late Middle Paleolithic site in western central Europe - Pouch-Terrassenpfeiler, Ldkr. Anhalt-Bitterfeld, Germany. *Quartar* 62, 23–62. https://doi.org/10.7485/QU62_2.
- Weiss, M., 2019. *Beyond the Caves: Stone Artifact Analysis of Late Middle Paleolithic Open-Air Assemblages from the European Plain*. PhD Thesis, Universiteit Leiden.
- Weiss, M., 2020. The Lichtenberg Keilmesser - it's all about the angle. *PLoS One* 15, e0239718. <https://doi.org/10.1371/journal.pone.0239718>.
- Weiss, M., Lauer, T., Wimmer, R., Pop, C.M., 2018. The variability of the keilmesser-concept: a case study from Central Germany. *J. Paleolithic Archaeol.* 1, 202–246. <https://doi.org/10.1007/s41982-018-0013-y>.
- Weißmüller, W., 1995. Die Silexartefakte der Unteren Schichten der Sesselfelsgrötte. Ein Beitrag zum Problem des Moustérien, *Quartärbibliothek* 6. Saarbrücker Druckerei und Verlag, Saarbrücken.
- White, M.J., Pettitt, P.B., 2011. The British late middle palaeolithic: an interpretative synthesis of neanderthal occupation at the northwestern edge of the Pleistocene world. *J. World PreHistory* 24, 25–97. <https://doi.org/10.1007/s10963-011-9043-9>.
- Winsemann, J., Lang, J., Roskosch, J., Polom, U., Böhner, U., Brandes, C., Glotzbach, C., Frechen, M., 2015. Terrace styles and timing of terrace formation in the Weser and Leine valleys, northern Germany: response of a fluvial system to climate change and glaciation. *Quat. Sci. Rev.* 123, 31–57. <https://doi.org/10.1016/j.quascirev.2015.06.005>.
- Wintle, A.G., Adamiec, G., 2017. Optically stimulated luminescence signals from quartz: a review. *Radiat. Meas.* 98, 10–33. <https://doi.org/10.1016/j.radmeas.2017.02.003>.
- Wiśniewski, A., Adamiec, G., Badura, J., Bluszcz, A., Kowalska, A., Kufel-Diakowska, B., Mikołajczyk, A., Murczkiewicz, M., Musil, R., Przybylski, B., Skrzypek, G., Stefaniak, K., Zych, J., 2013. Occupation dynamics north of the carpathians and sudetes during the weichselian (MIS5d-3): the lower silesia (SW Poland) case study. *Quat. Int.* 294, 20–40. <https://doi.org/10.1016/j.quaint.2011.09.016>.
- Wiśniewski, A., Lauer, T., Chłóń, M., Pyżewicz, K., Weiss, M., Badura, J., Kalicki, T., Zarzecka-Szubińska, K., 2019. Looking for provisioning places of shaped tools of the late Neanderthals: a study of a Micoquian open-air site, Pietraszyn 49a (southwestern Poland). *Comptes Rendus Palevol* 18, 367–389. <https://doi.org/10.1016/j.crpv.2019.01.003>.
- Wiśniewski, A., Chłóń, M., Weiss, M., Pyżewicz, K., Migal, W., 2020. On making of micoquian bifacial backed tools at pietraszyn 49a, SW Poland. *J. Paleolithic Archaeol.* <https://doi.org/10.1007/s41982-020-00069-y>.
- Woillard, G., 1979. The last interglacial-glacial cycle at Grande Pile in Northeastern France. *Bulletin Société belge de Géologie* 88, 51–69.
- Zagwijn, W., Paepe, R., 1968. Die Stratigraphie der weichselzeitlichen Ablagerungen der Niederlande und Belgiens. *Q. Sci. J.* 19, 10–31.

CHAPTER V: CONCLUSION

5.1 OUTLINE OF THE THESIS CHAPTERS II TO IV

Chapter II: Luminescence chronology of the key-Middle Paleolithic site Khotylevo I (Western Russia) - Implications for the timing of occupation, site formation and landscape evolution

The Russian Plain has a rich record of open-air sites that are ascribed to the Middle Palaeolithic based on the type of lithic artifacts. Many of these sites are contained within the deposits of the 2nd fluvial terrace, which accompanies numerous Russian and Ukrainian rivers ca. 16-25 m above the current stream. The understanding of both, the Middle Palaeolithic occupations and the late Pleistocene fluvial history suffers from insufficient chronological information. For the 2nd terrace, only a handful of OSL dates exists while no open-air Neanderthal site on the Russian Plain had been dated so far. Therefore, establishing a chronology for either of these two components would be mutually beneficial for both areas of interest. The site of Khotylevo I, W-Russia (53.3° N, 34.1° E), is located at the base of the 2nd fluvial terrace fill at the River Desna. It was first discovered and excavated in the 1960s by F.M. Zavernyaev, who established several sections alongside the river (Zavernyaev, 1978). Khotylevo I attracted interest and attention in the archaeological community for its sheer size, northerly location, and its large and representative lithic artifact assemblage, associated with the Keilmessergruppen. Previous excavations in Khotylevo I were supported by stratigraphical and geological investigations by A.A. Velichko, which led to the temporal ascription of the site to the Early Valdai (Weichselian) period (Velichko, 1988). Renewed (geo)archaeological excavations were started by A.K. Otcherednoi in 2006, *inter alia* intended to refine the temporal resolution of the site (Otcherednoi and Voskresenskaya, 2009). This resulted in a revised chronology for the occupation. Newly-obtained results from radiocarbon dating and magnetostratigraphy suggested an MIS 3 age of the archaeological remains (Otcherednoi et al., 2014), which contradicts the previous stratigraphic assumption for MIS 5 made by Velichko. For that reason and for the lack of a chronostratigraphic framework for the 2nd fluvial terrace, which could potentially elucidate the “true” age of the occupation, a luminescence-based chronology became desirable. Thus, the present author and two colleagues (M. Weiß and T. Lauer) visited

Khotylevo I, section I-6-2 for the first time in 2017. The present author conducted a meticulous stratigraphic description of the whole profile and collected 17 samples for luminescence dating throughout the archaeological and the entire overlying sequence. Stratigraphic context was provided by several natural and artificial sediment exposures in the vicinity. Furthermore, on the luminescence sample material, grain sizes were determined using a laser diffractometer. Pollen samples, collected from the humic archaeological layers proved to be sterile, however.

Because of the high-resolution luminescence sampling design and the supporting stratigraphic and sedimentological information, we detected a full cycle of fluvial incision and aggradation within the 2nd fluvial terrace fills. Incision took place around the MIS 5c/5b transition in this part of the valley, evidenced by non-existent warm-stage deposits from MIS 5c and 5e. Instead, a huge hiatus to Cretaceous sediments follows below. After the incision, fluvial aggradation began slowly, so that in the distal areas of the floodplain, slope deposition and phases of humic soil formation dominated. This was the setting for the Neanderthal occupation, dated to MIS 5a. Contemporary humus accumulation implies high bioproductivity and thus a warmer interval. Availability and quality of raw material for lithic production was exceptional. It could be procured as tabular flints from slope sediments and outcrops of the primary Cretaceous deposits. Main fluvial aggradation started in MIS 4 and accelerated toward the MIS 4/3 transition. Firstly, laminated fluvio-lacustrine sediments were deposited, that are rich in reworked loess, as evidenced by their noticeable peaks or shoulders within the coarse-silt fraction of the grain size distributions (cf. Vandenberghe et al., 2018). Their deposition broadly coincides with major loess sedimentation in the region, for which Khotylevo is even the type locality (*Khotylevo loess*). Thereafter, about 3 meters of horizontally-bedded fine sands quickly aggraded around latest MIS 4. Finally, throughout MIS 3, fine-grained overbank deposition dominated, forming the uppermost part of the terrace fill. The age of an MIS 3 palaeosol (humic Fluvisol) which developed on top of these overbank fines could not be further constrained, as it is disconformably overlain by loess of the last glacial maximum. Hence, the incision/aggradation cycle of the 2nd fluvial terrace lasted from MIS 5c/b to (Mid-) MIS 3. While

the posterior incision into this terrace fill could not be accounted for, it is known to have occurred between 45 and 35 ka (Panin et al., 2017).

With this first unambiguous luminescence-based chronostratigraphy for a Middle Palaeolithic site on the Russian Plain, we can add a valuable data point for the understanding of Neanderthal population dynamics in Northern and Eastern Europe. The numerical dates as well as the stratigraphic framework without contradiction support an MIS 5a age of the occupation in Khotylevo I-6-2. This provides evidence for the early presence of the Keilmessergruppen, prior to the onset of the Weichselian Pleniglacial. Our chronology further highlights the worth of the initial stratigraphic considerations by A.A. Velichko, ascribing the occupation to the early glacial.

Chapter III: Eemian landscape response to climatic shifts and evidence for northerly Neanderthal occupation at a palaeolake margin in Northern Germany

The Eemian Interglacial is generally considered a period of stable landscapes with prevailing pedogenesis and negligible sediment (re)deposition. However, there are hardly any systematic geomorphological studies addressing this issue. Most of the palaeoenvironmental information about the terrestrial interstadial comes from small-scale palaeolake basins, formed after the Saalian ice decay in association with the glacial deposits. Owing to their small diameters and relative shallowness, these landforms are of limited value for geomorphological research. Moreover, also data on past vegetation and palaeoclimate, retrieved from such archives could be called into question because local hydrographic conditions and the general shortage of accommodation space might bias or mislead the interpretations. On the doorstep of the Middle Palaeolithic site of Lichtenberg, N-Germany, previous geological investigations yielded evidence for an Eemian to Early Weichselian palaeolake of presumably larger extent (Veil et al., 1994). Building on this, a GIS-based geomorphological survey and seismic profiling were conducted, both revealing the suitability of the study area to decipher Eemian landscape dynamics. A subsequent expansive sediment coring campaign resulted in a borehole transect ($n = 20$) that exposed a complex infill sequence of a palaeolake basin. It comprises up to 15 m thick colluvial, lacustrine and organogenic deposits, likely formed between the late Saalian and the Middle Weichselian. For this

study, we focused on the lower (i.e. Eemian) part of these infill deposits and applied palynological analysis on bulk samples ($n = 25$), dispersed across the transect, and luminescence dating on two samples in one core (PD.030). Regrettably, datable and well-bleached clastic sediments were scarce within the deeper segments of the transect. But since the subdivision of the Eemian is hinged on pollen zones anyway, numerical dates were not of primary importance for the actual research question. Our results further the understanding of interactions between sedimentation, hydrology and vegetation density in the Eemian Interglacial, since we obtained information on sediment dynamics and relative lake levels alike: Two pronounced phases of geomorphic activity have occurred at the beginning and toward the end of the Eemian in times of reduced vegetation cover, with a prolonged period of landscape stability in between. The intense incision of the first active phase can be restricted to the Saalian/Eemian transition and is likely linked to fluvial downcutting in the neighboring Elbe River valley. It formed a side valley, which hosted an elongated lake in due course. At first, clastic sedimentation was high but it decreased gradually towards the Mid-Eemian, parallel to the establishment of dense forests. From then on, stabilized slopes and temperate climate promoted soil formation in the exterior of the basin and also hindered surface flow into the lake. In combination with the higher evapotranspiration rates of the forests, this lack of influx led to a progressively sinking water table until the end of the Eemian. It also led to the total absence of clastic sedimentation within the lake basin for a period of ca. 6,000 years in the Mid-Eemian. Instead, organogenic deposits and lake marls can be found, the latter indicative of intense soil formation and decalcification of the Saalian sediments in the exterior. This must have led to subterranean carbonate influx and its precipitation at the lake bottom. At an early stage of this stability phase, we discovered a few diagnostic Middle Palaeolithic artifacts in repeated corings. They indicate a Neanderthal occupation on a semi-terrestrial (half-bog) soil at the lakeshore during Mid-Eemian pollen zone E IVb/V. In later phases of the Eemian, the lake had been reduced to a swampy depression, without drying out completely, and acidic forest peat covered the bottom of the basin. Geomorphic activity soon resumed with an incision into the basin infill deposits, implying renewed fluvial downcutting in the adjacent Elbe River valley, which also affected this distal side valley. The subsequent rise of the water table refilled the lake nearly to its initial extent and was associated with

increasing clastic sedimentation, coinciding with sparser forest cover. This late Eemian geomorphic activity phase lasted well into the following first Early Weichselian stadial (Herning Stadial).

Our highly-resolved spatio-temporal data can substantially contribute to the comprehension of climate-induced geomorphic processes throughout the Eemian and the earliest Weichselian. It elucidates Eemian landscape dynamics on the European Plain between the loess belt to the south and coastal areas to the north. Neanderthal presence in the fully-forested optimum of the interglacial makes Lichtenberg the northernmost Eemian Middle Palaeolithic site in Europe, closely ahead of Lehringen (Thieme and Veil, 1985). At the time of writing the article of Chapter 3, the present author had no knowledge of Eemian artifact finds in a sandpit near the neighboring Woltersdorf (Breest, 1992, see 1.3.3), which outranks Lichtenberg by about 3 km in terms of northernness.

Chapter IV: Neanderthal presence in changing environments from MIS 5 to early MIS 4 at the northern limit of their habitat in Central Europe – Integrating archeological, (chrono)stratigraphic and paleoenvironmental results at the site of Lichtenberg

The site of Lichtenberg, N-Germany, has been discovered by K. Breest in 1987, whereupon several years of excavation have been carried out by S. Veil (Breest and Leunig, 1989; Veil et al., 1994). Similar to the case of Khotylevo I, the northerly location of Lichtenberg (52°55' N) and the impressive artifact assemblage (ca. 4,000 pieces) led to special recognition of this site within the Palaeolithic scientific community (Jöris, 2006). And equally similar to the case of Khotylevo I, the Lichtenberg assemblage is attributed to the Keilmessergruppen of Central and eastern Central Europe. The occupation deposit had been dated with thermoluminescence to a mean age of 57 ± 6 ka, with the individual dates ranging from 66 ± 14.6 ka to 52 ± 6.8 ka (Veil et al., 1994). Based on this mean age, Lichtenberg is mainly considered an early MIS 3 site, however, this view is not uncontested. In particular, Jöris (2004) holds the opinion that the occupation must have occurred before the first glacial maximum (~MIS 4). This is justified by the fact, that the integrity of the find layers is disturbed by post-depositional cryoturbation, likely to have happened in MIS 4. In agreement with this alternative view,

the present author and colleague M. Weiß located the previous excavation area and revisited the site in 2017, 2019 and 2020 in order to re-date the sequence. Targeted excavations took place in the latter two years. Cryoturbation disturbances of the find layer have largely been avoided by excavating at the southern fringe of the former area. It was known from the accompanying coring campaign (Chapter 3), that sediment overburden thickens toward the adjacent palaeolake basin, rendering post-depositional distortion of the find-bearing sediments by cryoturbation less likely. That way, the find layer could mostly be identified in original stratification and three luminescence samples yielded absolutely consistent ages with a range from 70.8 ± 8.0 ka to 71.6 ± 7.0 ka and a mean age of 71.3 ± 7.3 ka. In a sediment core, retrieved directly next to the excavation, a humic sand with pollen preservation was detected a few centimeters underneath the deposit of the find layer and could be correlated with Greenland Interstadial GI-19 (ca. 71 ka) (Rasmussen et al., 2014). This is the first evidence of this minor interstadial at the transition from the Weichselian Early- to Pleniglacial on the European Plain. Not only does its presence firmly support the numerical dates obtained by luminescence, but it also proves that Neanderthals could cope with severely cold environments because the vegetation of GI-19 was characterized by an open tundra steppe. The occupation of the previously known site Lichtenberg I (Li-I) could therefore only have taken place in Greenland Stadial GS-19, whereas the former age of 57 ± 6 ka likely corresponds to the timing of cryoturbation.

During the coring campaign, another unknown occupation has been discovered in a stratigraphic position between Li-I and the Eemian artifacts (reported in Chapter 3). It was partly excavated and has been named Li-II. Its assemblage differs from Li-I in terms of smaller tool size, lower raw material quality, and a higher typological tool diversity. The artifacts are contained within shoreline deposits of the palaeolake, which clearly can be related to the late Brörup Interstadial in the palynological analysis. Two luminescence samples returned nearly congruent ages of 90.5 ± 8.7 ka (range from 89.5 ± 8.2 to 91.5 ± 9.1). Therefore, in unison of these two methods the occupation is correlated with the forested interval of GI-22 and late MIS 5c. By extension, it could be shown for the first time in the type area that the terminations of the terrestrial Brörup Interstadial and MIS 5c coincide.

This chronostratigraphic framework allows for the inspection of palaeoenvironments and palaeoclimates in their possible effect on migration and tool production. Neanderthals seem to have been well-adapted to interglacial (Eemian) and forested interstadial (Brörup) conditions but similarly coped with cold environments at the transition of the Early- and Pleniglacial at exactly the same location. Differences between the tools of Li-I and Li-II are partly explainable by the availability of raw material, only provided by Saalian glacial sediments in the region. In relatively stable landscapes during the Eemian and the Brörup, dense forest covers concealed surface objects and also impeded sediment erosion. By contrast, unstable landscapes at the brink of the Pleniglacial promoted the exposure and redeposition of Saalian deposits and the contained flint nodules. Our data set adds a whole new occupation (Li-II) to the spacious map of Early Weichselian sites and provides further evidence, that the Keilmessergruppen had already settled the European Plain prior to the first glacial maximum (Li-I) (cf. Chapter 2).

5.2 DISCUSSION

5.2.1 Evaluation of the chronological and biostratigraphic data

A chronostratigraphic resolution at the level of Marine Isotope Stages (Lisiecki and Stern, 2016) is arguably often insufficient to relate Middle Palaeolithic occupations to distinct climatic and environmental phases and to compare spatially-detached occupations. Rather, in order to unlock a higher synthetic-interpretative potential of the various findings made in the course of excavations, a correlation with Greenland Interstadials and Stadials (Rasmussen et al., 2014) is desirable. In case of the occupations in Lichtenberg, the opportunity arose to succeed in this attempt, despite a challenging depositional setting at the immediate sites. Beneficial factors were the good pollen preservation in certain strata and the remarkably well-resolved sediment basin which is adjacent to and partly overlapping with the position of the sites (see Chapter 3). For a better transparency, the high temporal resolution presented for the Lichtenberg find layers Li-I and Li-II in Chapter 4 shall be critically reviewed in terms of the methodological precision and the applied approach.

Chronostratigraphy

Since the advent of the SAR protocol (Murray and Roberts, 1998; Murray and Wintle, 2000) and the later introduction of novel procedures for feldspar measurements (Buylaert et al., 2012; Thiel et al., 2011), luminescence ages for Pleistocene sediments have become significantly more reliable, reproducible, and less prone to be affected by anomalous fading. But still, internal measurement errors, disparate luminescence characteristics, and uncertainties in water content estimation and dose rate determinations regularly add up to overall error ranges of about $\pm 10\%$, but at least 5% of the obtained ages, even in well-bleached and favorable deposits (Mahan et al., 2022). In these latter settings, the choice of statistical model for equivalent dose (D_e) estimation arguably does not have a decisive influence on the resulting ages (cf. Galbraith and Roberts, 2012). However, in less advantageous depositional environments, characterized by insufficient and partial bleaching, the accurate (1) selection of the sampling position and (2) D_e -estimation is of the utmost importance in the present author's opinion to produce robust ages (cf. Mahan et al., 2022). Possibly, misjudgments in these aspects can cause deviations from the "true" depositional age of much higher magnitude than the errors and uncertainties mentioned above. Therefore, these two factors and how they were handled for the research in Lichtenberg will be explained in more detail here:

(1) Periglacial hillslope deposits are among the most challenging sediments for luminescence dating due to unclear exposure to light prior to burial and possible post-depositional mixing (Bateman, 2019). Thus, only limited research has been done on these features (Bateman, 2008; Christiansen, 1998; Hülle et al., 2009), and an independent age or biostratigraphic control is to be recommended. In archaeological sequences, cryoturbated sediments are generally best avoided for luminescence dating, as they are likely to produce inconsistent ages that fall somewhere between the deposition and involution events. From the previous excavation in Lichtenberg it was known, that the find layer was (i) intensively disturbed by cryoturbation, and that it (ii) dipped steeper than the terrain surface in a north-south section through the excavation (Veil et al., 1994), implying increasing accommodation space due south. The latter could be con-

firmed during our sediment coring campaign as reported in Chapter 3. This necessarily results in a thickening sediment overburden of this find layer so that (possibly multi-phased) cryoturbation would be less likely to have affected this layer in the respective permafrost phases. For that very reason, we established our re-excavation (Trench 1) at the southern margin of the former investigation area and exceeded the depth of the previous excavation by about 1 m. In effect, we were able to detect the find layer in original stratification and could sample it in a non-cryoturbated position. The present author argues that the avoidance of this major sampling error has led to more consistent ages, as is illustrated by the comparison of the newly-obtained and previous dates (section 5.1 in Chapter 4).

(2) For the research presented here, each luminescence sample was subdivided into 24 subsamples/replicates (aliquots) on which the measurements were carried out. Deliberately, a very small aliquot size was chosen (0.5 mm diameter) corresponding to a number of ~ 10 to 20 individual grains per aliquot. As a result, the statistical variation is higher when compared to measurements using bigger aliquot sizes of 1, 2 or 5 mm (Duller, 2008). However, it has been shown in detail, that these ‘ultra small’ aliquots substantially help identify different age components in poorly-bleached sediments and especially periglacial environments (e.g. Bateman, 2019; Olley et al., 1999; Tooth et al., 2007). That way, individual modes that would otherwise fall prey to averaging effects in bigger aliquots can better be detected within the age frequency distribution. Therefore, an advantage of this higher spread and resolution in the data is a likely better-informed D_e -estimation to use for age calculations. For identifying the appropriate D_e -estimates that correspond with the targeted bleaching event, a number of statistical models are available e.g., the *Central Age Model* (CAM) and the *Minimum Age Model* (MAM) (Galbraith et al., 1999). The choice of model is a scientific decision made by the researchers and specific to each individual sample. It is mainly governed by the sedimentary context and stratigraphic considerations (Galbraith et al., 2005; Galbraith and Roberts, 2012; Mahan et al., 2022). Previous attempts to formalize a universal protocol for the choice of age model based on statistic criteria (e.g. Bailey and Arnold, 2006; Rowan et al., 2012) have been discarded within the luminescence dating commu-

nity more recently (e.g. Mahan et al., 2022). In well-bleached deposits, resulting in almost normal D_e -distributions, the CAM is usually thought to be the best means of estimating the equivalent dose (Galbraith and Roberts, 2012; Mahan et al., 2022). By contrast, heterogeneous or poor bleaching can lead to skewed, non-normal or multi-modal D_e -distributions that may be better accounted for when applying the MAM (Bateman, 2019; Galbraith et al., 1999). The MAM assumes a sub-population of well-bleached grains and thus targets the lower values within the D_e -frequency distribution. Notes on the correct application of the MAM can be found in Chamberlain et al. (2018) and Galbraith and Roberts (2012).

Apart from a comprehensive understanding of the depositional environment and the application of suitable statistical models, an adequate visualization of the D_e -distribution is indispensable for the straightforward inspection and interpretation of the measured values (see overview of various plot types in Galbraith and Roberts, 2012). Because of the challenging sedimentary history at the site of Lichtenberg, the present author has chosen Abanico Plots (Dietze et al., 2016; Kreutzer et al., 2020) to display the data presented in Chapter 4. These graphs merge the benefits of a radial plot - a widely-used but not very intuitive technique to illustrate replicate D_e -values - with those of a kernel density estimation (KDE). Thus, they provide a way to explore the distribution in a less biased way than in a histogram (by means of the KDE part), while presenting the individual standard errors for each measured value at the same time in the radial plot part (Dietze et al., 2016).

An example of how Abanico Plots can contribute to a parsimonious D_e -estimation and thereby help justify the choice of age model is given in Figure 4, using luminescence data of the Lichtenberg find layers (Chapter 4). After plotting the data, a particular age model was chosen if it reflected the most informative D_e -population in terms of (i) sediment formation, (ii) data precision (in the radial plot part), and (iii) data representation (in both parts of the plot). For find layer Li-I (stratigraphic layer 7), the interpretation as a shallow lacustrine deposit implies an incomplete and partial bleaching of the feldspar grains, making the MAM the likely adequate option. The two samples taken <10m apart in the very same layer (L-EVA 2014 and 2017) display surprising differences in their distributions, demonstrating the spatially heterogeneous nature of

the sedimentation process. L-EVA 2014 shows a unimodal distribution with comparably low variability, whereas the D_e -values in L-EVA 2017 are bimodally distributed and exhibit a much higher variability (Figure 4). However, when applying the MAM, in both cases the final D_e -estimates concur with a distinct mode in the distribution and high data precision. Eventually, for both samples very similar ages were obtained (71.6 ± 7.0 and 70.8 ± 8.0 ka, respectively). This reproducibility suggests a functional analytical chain (cf. Bateman, 2019; Mahan et al., 2022).

Similarly, for find layer Li-II (stratigraphic layer 11a) the D_e -distributions of the two samples L-EVA 2022 and 2024, taken <5 m apart, differ concerning modality and variability (Figure 4). The sediment of this layer was interpreted as a beach sand, and thus, a better bleaching is to be expected, because the grains would have been repeatedly reworked on the beach face by wave action and movement. Therefore, the CAM is likely the best way to approach the D_e -estimation. This holds true for sample L-EVA 2022, where a broad and smooth unimodal curve describes the D_e -distribution of the replicates and the CAM estimate is close to the mode of this distribution. Conversely, the distribution of individual values in sample L-EVA 2024 is discontinuous and can be described as bi- to polymodal. The use of the CAM would likely lead to an age overestimation, because the position of the CAM estimate – indicated as grey bar and line in Figure 4 – does not reflect a distinct population. Therefore, the *Weighted Mean* was chosen for final D_e -estimation, as its result is congruent with the first mode of the distribution and data precision is sufficiently high. Again, very comparable ages for these two samples (91.5 ± 9.1 and 89.5 ± 8.2 ka), despite the application of disparate age models, imply an adequate reproducibility and support this analytical chain.

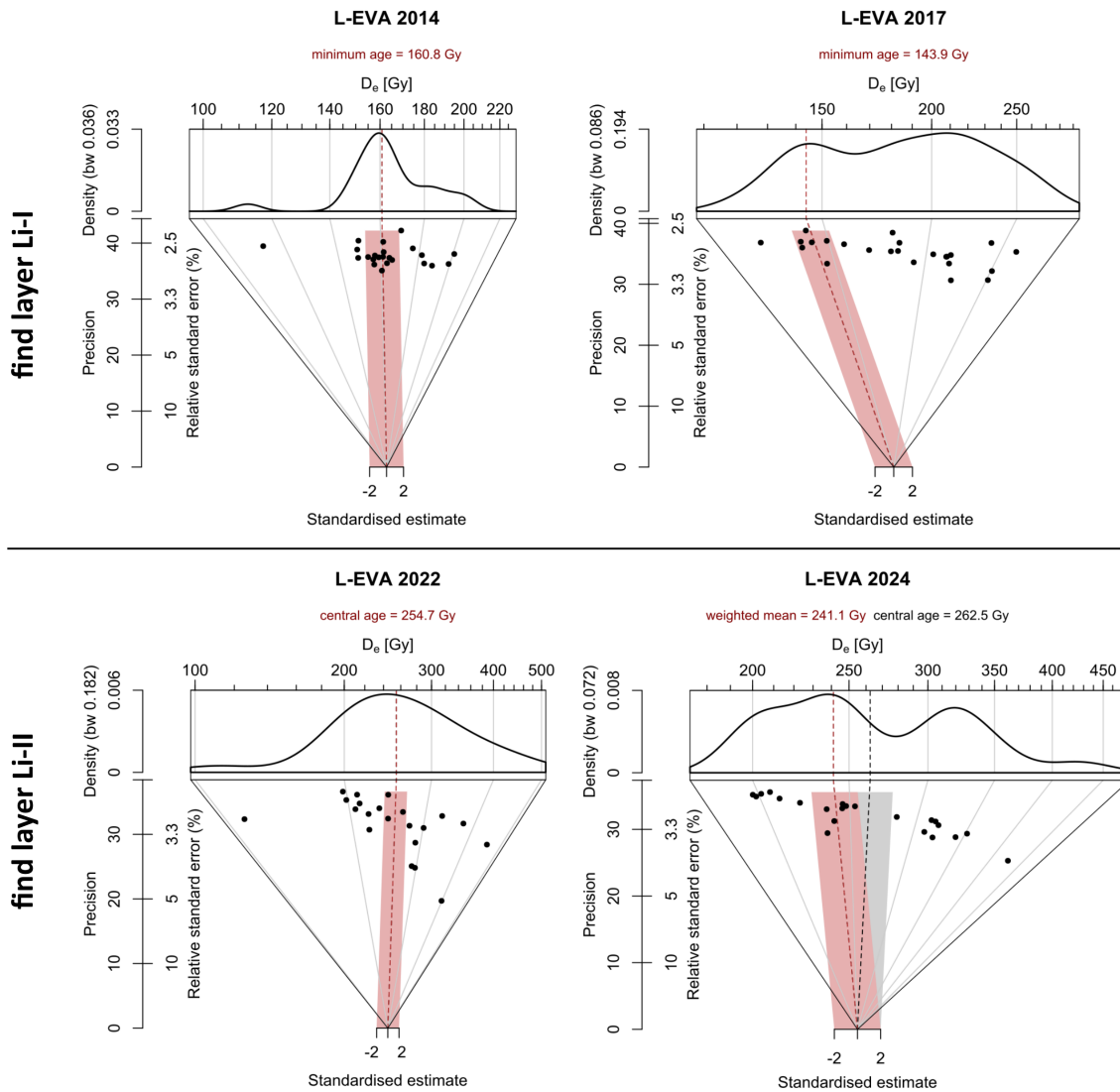


Figure 4: Abanico Plots of the D_e -distributions for the two samples each, taken from the find layers Li-I and Li-II in Lichtenberg. Red bars and red dotted lines indicate the resulting position of the equivalent dose (D_e) estimated with the selected age model. The age models were chosen to correspond with a distinct and sedimentologically most informative mode within the distributions (see text). For both find layers, two different samples returned nearly congruent ages using this approach. For comparison, in the plot of L-EVA 2024 the position of the CAM (not used for age calculation) is additionally displayed with a grey bar and line. The CAM does not represent a population within the data in that case and was therefore discarded in favor of the *Weighted Mean*.

Biostratigraphy

In suitable deposits, ancient pollen can preserve over long periods of time and are considered a key tool for the biostratigraphic subdivision of the Quaternary in general, but also of the later Pleistocene in particular (Sanchez Goñi, 2022; Stojakowits and Mayr, 2022). When analyzing coherent sedimentary sequences, the established local to supraregional palynostratigraphic frameworks facilitate a mostly unequivocal assignment of local pollen spectra and pollen assemblage zones to distinct biostratigraphic

units within the last interglacial-glacial cycle in Northern Germany (Behre and Lade, 1986; Caspers et al., 2002; Caspers and Freund, 2001; Menke and Tynni, 1984). Contrastingly, the sampling design for palynological analysis presented here pursued two slightly deviating approaches.

(1) For the research presented in Chapter 3, we took bulk samples distributed across the entire borehole transect. They were collected from organogenic units at the bottom of the palaeochannel infill and were presumed to have formed during the Eemian. This approach may introduce a certain ambiguity in pollen zone classification, because of quite similar pollen spectra from the early/late Eemian and the Brörup Interstadial, that may be difficult to distinguish in individual samples (Caspers et al., 2002; Caspers and Freund, 2001). This uncertainty could largely be resolved by taking into account (i) local references of coherent Eemian/Early Weichselian sequences from the immediate study site, both unpublished and published (Veil et al., 1994), and (ii) stratigraphic considerations, i.e., the directionality of respective depositional units and their relationship to one another. By using this cost- and time-efficient sampling approach, we gained a much higher spatial coverage of biostratigraphic information, enabling us to focus on the reconstruction of geomorphic dynamics and landscape evolution throughout the Eemian. The plausibility and connectivity of the results seem to confirm that such a design can generally produce a viable outcome, despite some undeniable drawbacks.

(2) For the research presented in Chapter 4, we could make use of a pollen-bearing organogenic deposit in Trench 2, layer 11b, which we sampled as a four-part sequence. Additionally, we took three bulk samples from the find layer Li-II (stratigraphic layer 11a) and the overlying stratigraphic layer 10. The four-part sequence in itself is indicative of the late Brörup Interstadial and the transition to the following Rederstall Stadial. The bulk samples from the find layer Li-II – and thereby the occupation – can clearly be connected with the late Brörup within this sequence. Again, excellent local reference is available through the pollen sequence described in Veil et al. (1994), situated merely 40 m apart. Furthermore, litho- and biostratigraphic control is provided by the findings presented in Chapter 3, where for instance a half-bog soil c. 130 cm directly underneath layer 11 has been described as Eemian formation.

Since there is no pollen preservation in the deposits exposed within Trench 1, we sampled three organogenic beds in the core PD.028 right at the southern margin of the trench. The lowermost bed is a peat and is represented by two pollen samples that place it into the Odderade Interstadial. Stratigraphic considerations derived from the borehole transect in Chapter 3/Figure 4 concur with this interpretation, as the Brörup and the Eemian can be expected to lie much further down the profile. Moreover, the upper boundary of this Odderade peat in PD.028 is at 16 m a.s.l. nearly congruent with the top of the Odderade in core Veil 1 (Veil et al., 1994), positioned ~10 m away in a matching geomorphological position (Chapter 4, Figure 1c).

Considering the described stratigraphic control and the fact that the palynologist who analyzed the reference sequence in Veil et al. (1994), namely B. Urban, was also responsible for the biostratigraphic assignments in Chapter 3 and 4, the present author is confident, that the pollen-based interpretations presented in these chapters are in line with the best scientific practice, despite a comparably low sampling resolution.

Integration of chronological and (bio)stratigraphical data

The combination of the litho-, chrono- and biostratigraphic findings reveals a good accordance of the respective data and thus justifies the attempt to assign certain deposits to climatostratigraphic phases. This shall briefly be exemplified for the find layers Li-II and Li-I in Lichtenberg (Chapter 4) in the following paragraphs.

Li-II - Palynological information places Li-II into the late Brörup Interstadial. Warm-stage conditions are corroborated by:

- the sediment characteristics (e.g. considerable to very high total organic carbon content, charcoal fragments, plant residues in thin sections, no discernible cryogenic features)
- the presence of rich and temperate phytolith assemblages
- archaeological evidence (raw material, size/type/use of tools, traceology)

The mean luminescence age of two very similar dates is 90.5 ± 8.7 ka. This mean age is time-equivalent to the terminal phase of MIS 5c (Lisiecki and Stern, 2016) and to the terminal phase of the warm stage represented in the Greenland ice core record by the

Greenland Interstadials GI-23 and GI-22 (Rasmussen et al., 2014). And it coincides chronologically with the on-site finding of sediment deposition in the late Brörup Interstadial, with the Brörup usually being equated to MIS 5c in Northern Germany and neighboring regions (e.g. Antoine et al., 2016; Boch et al., 2011; Bolland et al., 2021; Litt et al., 2007). Hence, within the nearly identical temporal references of the Marine Isotope Stages and Greenland Interstadials, the late Brörup Interstadial would equal GI-22 and the terminal MIS 5c. Furthermore, within the luminescence dating uncertainty of ± 8.7 ka for Li-II, apart from the late Brörup, no other interstadial termination seems to occur in the North Atlantic records (Chapter 4, Figure 7). This integrative consideration of the available data supports the tentative correlation of find layer Li-II with Greenland Interstadial GI-22 and the termination of MIS 5c.

Li-I – This find layer itself and in fact, the entire excavation of Trench 1 does not yield any pollen-bearing deposits. The basal peat in the sediment core PD.028 at the southern boundary of this trench is assigned to the Odderade Interstadial (section Biostratigraphy above). It is succeeded by two humic deposits separated by niveofluvial sands. The humic deposits display cold-stage pollen spectra and are interpreted as minor interstadial formations occurring after the Odderade. Two climatic oscillations following the Odderade are well documented for many regions in Central and Western Europe and correlated to the Greenland Interstadials GI-20 and -19 (Antoine et al., 2016; Boch et al., 2011; Bolland et al., 2021; Müller and Sánchez Goñi, 2007; Woillard, 1979). The latter are positioned at c. 75 and 71 ka in the Greenland ice core record (Rasmussen et al., 2014). In direct superposition of these two minor interstadials in core PD.028, lies sediment layer 7 that contains the find layer Li-I in Trench 1. The mean age of Li-I with 71.3 ± 7.3 ka, calculated from three nearly congruent individual dates, is in accordance with the classification of the two minor interstadials below as GI-19 and GI-20. According to stratigraphic relationships, the sediment characteristics, the lacking organic compounds and the grass-dominated vegetation as implied from phytolith analysis, Li-I was deposited shortly after GI-19 under stadial conditions. Hence, we assign this find layer to Greenland Stadial GS-19. At both ends of the error range (71.3 ± 7.3 ka) no plausible alternative position seems to exist. At its upper end, an age of 78.6 ka would interfere with the termination of Odderade and the two minor

interstadials GI-20 and -19. All of which, Li-I (layer 7) is clearly overlying in core PD.028. At the lower end of the luminescence error range, GS-19 (c. 64 - 70.5 ka) is entirely covered by the 7.3 ka error margin (Chapter 4, Figure 7). An even younger date for Li-I is equally unlikely, as Li-I is overlain by deposits with clear cryogenic features, which can be expected to have formed under stadial conditions in MIS 4. For these reasons, correlating Li-I with GS-19 is the most parsimonious and credible assumption.

Currently, sediment cores Li-BPa, PD.031 and PD.028 (for positions, see Chapter 3, Figure 4) are subjected to detailed and high-resolution analysis using a multi-proxy approach including sedimentology, biostratigraphy, dating and geo-biochemistry. The incoming results so far fully support the preliminary allocations described above.

5.2.2 Stratigraphic implications of the results

Establishing firm and highly-resolved chronostratigraphies was the overall objective of the present thesis. It is a prerequisite for synchronizing behavioral traits with distinct climatic and environmental phases in order to explore possible connections (cf. Pederzani et al., 2021). Encouragingly, this is more and more being achieved for cave and loess sites of the latest Middle Palaeolithic (MP), the Upper Palaeolithic (UP) and the MP/UP transition (Fewlass et al., 2020, 2019; Fuchs et al., 2013; Guérin et al., 2017). It is mainly facilitated by the high precision of radiocarbon dating, often in combination with luminescence-based chronologies and well-stratified sediment sequences. By contrast, numerical dates in general and especially accurate chronostratigraphic data are still sparse for Eemian to early Pleniglacial sites. This is particularly true for open-air sites beyond the loess belt, where mostly shallow slope deposits dominate. Additionally they were often subjected to polycyclic cryoturbation, rendering these deposits challenging for luminescence dating (Bateman, 2008; Fuchs and Lang, 2009; Veit et al., 2017; Waroszewski et al., 2020). While fluvial deposits are much better-suited for luminescence chronologies (Cunningham and Wallinga, 2012), the sequences often lack the required resolution and present artifacts are frequently in secondary (i.e. re-worked) positions (Bridgland et al., 2006; Vandenberghe, 2015; Winsemann et al., 2015), which in turn complicates precise chronostratigraphic allocation of the finds.

As expected, our own chronostratigraphic investigations for Khotylevo I and Lichtenberg show varying precision, owing to different site conditions and available auxiliary information (Chapter 1.5). Whereas occupations of Li-I and Li-II in Lichtenberg could be resolved at the scale level of Greenland Stadials and Interstadials, the Eemian occupation was only biostratigraphically assigned to a distinct Eemian pollen zone (E IVb/V). The two respective luminescence dates of the overlying deposits (108.4 ± 17.0 ka and 104.6 ± 10.5 ka) have to be regarded as minimum ages for the Eemian termination. Outside of the radiocarbon range, this exceptional chronostratigraphic resolution and robustness for Li-I and Li-II has otherwise only been achieved for occupations within loess-palaeosol-sequences, so far (Locht et al., 2016). In the former riverine landscape of Khotylevo I, interfingering low-energy deposition of slope and fluvial deposits in the rear part of the floodplain resulted in a well-resolved sediment sequence for the time of occupation. However, such a close-meshed framework as in Lichtenberg could not be fully achieved, and the age estimates, although very consistent, remain on the scale of Marine Isotope Stages. On the one hand, this is due to missing biostratigraphic information for the non-pollen bearing deposits. On the other hand, the setting is even more demanding for luminescence dating, because of mixing with poorly bleached Saalian sediments and the ubiquitous clasts of Cretaceous marl and chalk, leading to small-scale dose rate variations within the sequence (e.g. Jacobs and Roberts, 2007). Still, apart from this relatively lower dating precision, the chronostratigraphy does not lack robustness, as the correlation with regional loess stratigraphy permits a confident and unambiguous assignment of the occupation to MIS 5a. Thus, a firm chronostratigraphic foundation has been established at both sites, allowing for future correlations, archaeological inferences and the purposeful application of additional methods.

At both sites, this framework already led to the discovery of – or helped contextualize – hitherto unknown occupations (research question **RQ 4**): In Lichtenberg, the coring campaign directly resulted in the detections of the Mid-Eemian (PZ E IVb/V) and late Brörup occupations. By reporting the first independent numerical dates for the latest Brörup Interstadial WE IIb (mean of 90.5 ± 8.7 ka) in its type region on the NW European Plain, we advocate the broad coincidence of the Brörup Interstadial and MIS 5c

in their terminal phases (research question **RQ 1**). This is fundamental information for several archaeological (and palaeoenvironmental) sites in the wider area, at which the chronologies only rely on biostratigraphical evidence, e.g. the Middle Palaeolithic occupation in Schalkholz, N-Germany (Arnold, 1978; Menke, 1980; Nielsen et al., 2017). Our research approach in Lichtenberg further provided the first evidence of climatic fluctuations at the MIS 5a/4 transition after the Odderade Interstadial (research question **RQ 1**), which had already been demonstrated for southern Germany, Switzerland and France (Boch et al., 2011; Müller and Sánchez Goñi, 2007; Woillard, 1979). They are equally traceable in the North Atlantic palaeoclimate records as high-amplitude oscillations (Lisiecki and Stern, 2016; Rasmussen et al., 2014) and the loess sequences of northern France (Antoine et al., 2016), where they are associated with numerous Middle Palaeolithic sites (Locht et al., 2016). The two detected minor interstadials of that stratigraphic position in Lichtenberg (GI-20 and GI-19, cf. Rasmussen et al., 2014) display pollen spectra similar to the Oerel and Glinde Interstadials, usually correlated with early MIS 3 based on older protocols of radiocarbon dating (Behre and van der Plicht, 1992). If it can be substantiated that the chronology of Oerel and Glinde needs to be revised, and they are in fact attributable to GI-20 and GI-19, this would have far-reaching archaeological implications, as many Neanderthal sites are linked with these presumed MIS 3 interstadials (cf. Jöris, 2004).

In Khotylevo I, thanks to the chronostratigraphic framework, artifact finds within similar sequences and at the same stratigraphic level, can now be easily and reliably assigned to a distinct period in neighboring sections along the riverbank (research question **RQ 1**). Additionally, because all overlying deposits have been included in the framework, a newly-found artifact scatter at a higher level can confidently (but preliminarily) be constrained to the latest MIS 4 already (Otcherednoi et al., in prep.) (research question **RQ 4**). The knowledge on the temporal setting of fluvial aggradation and incision events forming the widespread 2nd fluvial terrace on the Russian Plain, has substantially been improved. With this understanding, also a chronological background for more remote palaeoenvironmental and archaeological findings, and their correlation over large distances is provided (Bridgland et al., 2006; Matoshko et al., 2004; Panin et al., 2017; Vandenberghe, 2015).

In conclusion, an optimistic answer can be given to the research question **RQ 4**, raised in Chapter 1.5: A systematic landscape-oriented and chronostratigraphic approach, even for a few consecutive years, can indeed support the discovery of new Middle Palaeolithic sites, but also the contextualizing of existing ones.

5.2.3 Implications for late Pleistocene Neanderthal population dynamics

The timing and duration of *Keilmessergruppen* assemblages found in Central and Eastern Europe have been widely discussed. Ambiguous and contrasting evidence of stratigraphical considerations and radiocarbon dating existed so far. This made both, the restriction of the *Keilmessergruppen* to the first half of MIS 3 or their earlier emergence in MIS 5a and subsequent persistence until MIS 3 seem possible (Jöris, 2012, 2004; Richter, 2016, 2002). Among such sites with chronologically inconclusive data were Lichtenberg (Veil et al., 1994), Salzgitter-Lebenstedt (Pastoors, 2009; Tode, 1982), Königsau (Mania, 2002; Mania and Toepfer, 1973) and also Khotylevo I (Otcherednoi et al., 2014; Velichko, 1988; Weiss, 2019). The ages presented in this thesis place the *Keilmesser* occupations of Khotylevo I and Lichtenberg I into MIS 5a and MIS 5a/4, respectively, rather than MIS 3, as previously assumed (research question **RQ 2**). Therefore, these new ages provide substantial evidence for an early appearance, i.e. a “long chronology” of the *Keilmessergruppen*, *sensu* Jöris (2004) (research question **RQ 3**). The emergence coincides with increasingly destabilizing landscapes granting access to larger-sized and high-quality raw material through sediment erosion (Chapter 4). It further coincides with gradual climatic deterioration and the completed dominance of cold-adapted fauna (cf. Chapter 1.3). Hence, it seems likely, that this environmental and climatic constellation has co-determined technological development. A long chronology of the *Keilmessergruppen* from MIS 5a to MIS 3, moreover, implies the survival of the *Keilmesser* concept or its general idea throughout the first glacial maximum (~MIS 4). For the latter period, virtually no unequivocal Neanderthal presence was demonstrated above ca. 50° N, so far (Chapter 1.3.3, cf. Bobak et al., 2013). It could be argued, that such a long-term “collective memory” of tool technology would best be preserved if Neanderthal response to glacial conditions was not local extinction, but rather a southward movement to more habitable refuges (cf. Hublin and Roebroeks,

2009). The appearance of resembling bifacial tool types in northern France (around 50° N) during the MIS 5a/4 transition, and at least their ephemeral re-appearance during GI-18 (ca. 64 ka) in Mid-MIS 4 (Antoine et al., 2014; Guérin et al., 2017; Loch et al., 2016) seem to rather support the migration theorem. In any case, Neanderthal occupation Li-I in Lichtenberg (GS-19) – right *after* a minor interstadial, which was characterized by open tundra-steppe – displays their ability to cope with severely cold environments. Therefore, colonization even throughout MIS 4 should not entirely be precluded (cf. Uthmeier et al., 2011).

But on the other hand, Neanderthals were equally capable to adapt to densely-forested environments. In Lichtenberg, the Eemian and Brörup artifacts are characterized by small, variable and simple tools, made from small-size and low-quality raw material. In these properties they resemble each other and also the assemblages from other occupations in forested MIS 5 environments of the wider area, e.g. Neumark Nord 2/2 (Pop, 2014) and 2/0 (Laurat and Brühl, 2021). Prevailing conditions can be described as temperate with a warm-adapted fauna and (relatively) stable surfaces covered by dense forests and undergrowth, which made raw material procurement difficult (e.g. Loch et al., 2014). Just as discussed above for the *Keilmessergruppen*, palaeoenvironments seem to have co-determined the lithic tool technology. Arguably, its variation in parallel with changing conditions can be regarded as a testimony to Neanderthal adaptive capacities. By contrast, the very low number of existing sites from the Eemian and the Brörup has motivated the theory that dense forests were rather unfavorable for Middle Palaeolithic sustenance (Defleur and Desclaux, 2019; Hublin and Roebroeks, 2009; Richter, 2016; Wenzel, 2007). However, our ‘accidental’ discovery of an Eemian and a Brörup occupation in Lichtenberg during a single coring campaign suggests that taphonomic and research biases are mainly to be blamed for this shortage instead of forested conditions (cf. Nielsen et al., 2017). Considering the Eemian finds in the nearby Woltersdorf (Breest, 1992), there are now three MIS 5 occupations in forest environments within a radius of 3 km near Lichtenberg.

As Chapter 3 clearly illustrates, a severe erosional phase occurred in the late Eemian and the early Herning Stadial, while other active phases within the Early Weichselian are implicitly linked to all the subsequent climatic transitions, when landscapes

needed to readjust toward a new equilibrium (Fränzle, 1988; Lade and Hagedorn, 1982; Schokker et al., 2004). Even though this statement suffers from a low research intensity, the general trend can be transferred to river and loess plains, as well (Antoine et al., 2016; Vandenberghe, 2008). Leaving out these loess landscapes as special aggradation areas, chances are high that erosion toward a cold interval eradicated most of the sediments, soils and archaeological remains, which were formed in the warmer interval before. Only favorable geomorphological situations and landforms reliably preserve Eemian and Early Weichselian natural or archaeological deposits. They comprise especially lake basins but also toe-slopes, dry valleys and distal parts of floodplains. This gives rise to the identification of promising positions with the geomorphological and stratigraphic potential to host unknown sites (cf. Nielsen et al., 2019). But it may also serve as a reminder, that the established occupations of that time could represent a distorted picture which only pretends (i) particularly low population densities (cf. Richter, 2006) and (ii) topographic depressions as the major Neanderthal habitats on the European Plain. While there might eventually be some truth to both assumptions, scientific reasoning demands to only accept the paucity of evidence, if the evidence of paucity is given. In that case, this must involve pursuing predictive modeling approaches for potential archives of Neanderthal occupation, which are firmly based on geomorphological considerations and chronostratigraphic “ground-truthing”.

In summary, the presented results and discussions within this thesis document both the potential and the need for integrated archaeological and palaeoenvironmental research, which is jointly coordinated from an early stage of project planning (cf. Garrison, 2016; Goldberg and Macphail, 2006).

5.3 OUTLOOK

The encouraging results and their various implications are merely the basis for ongoing and future studies that the present author and colleagues are conducting in Lichtenberg, Khotylevo and beyond. In fact, too many aspects are worth taking a closer look at to be mentioned here. In the following, the current palaeoenvironmental research, which aims to make use of the outstanding sediment archives of these two sites, will briefly be outlined.

Khotylevo I:

The MIS 5a and MIS 3 palaeosols at this site have only preliminarily been described so far (Chapter 2), which is why current and future research focuses on their characteristics. Especially, the MIS 3 palaeosols differ from the Western and Central European ones in terms of resolution, typology and the higher intensity of soil formation (cf. Meszner and Faust, 2018; Sauer et al., 2016; Terhorst et al., 2015). Therefore, disparate, and possibly more temperate conditions are to be assumed by comparison, which could have repercussions on the MIS 3 population dynamics and the MP-UP transition on the Eastern European Plain (cf. Hoffecker et al., 2019; Sedov et al., 2010). Detailed sedimentological, micromorphological, magnetic and geochemical analyses coupled with luminescence dating will try to shed new light on this.

Most of the large-scale natural and artificial exposures along the Desna riverbank display nearly congruent stratigraphies, so that only select positions have to be luminescence-dated to confirm the newly-established chronology. However, in one section ("*Крючка/Kryutchka*" = "*the hook*") at the current cut bank, higher-energy deposition of seemingly MIS 5 and MIS 4 fluvial sediments took place (cf. Zavernyaev, 1978). Therefore, the chronostratigraphic analysis of the *Крючка* exposure can yield information on fluvial dynamics and on site selection of the Neanderthal occupations, which may well be transferable to other rivers or at least different segments of the catchment (cf. Panin et al., 2017).

Lichtenberg:

Just like for Khoylevo I, the palaeosols in Lichtenberg deserve closer attention. A first fossil soil is directly associated with the occupation of Li-II (ca. 90 ka) and is characterized by the accumulation of organic matter under semi-terrestrial conditions. At the immediate shoreface of the palaeolake, this half-bog soil and parts of the artifact-bearing underlying beach sand have been eroded. For that reason, investigating the soil properties and distribution can be informative of the environmental conditions during occupation, the extent of the site and the archaeostratigraphic integrity. A second incipient palaeosol formation seems to have affected the sediments containing the occupation Li-I (ca. 71 ka). From preliminary descriptions, a non-analog and possibly multi-phased soil development is assumed, resulting in a Podsol-Gley soil type. Its chronostratigraphic position suggests, soil formation likely took place in MIS 4 and/or the MIS 5a to MIS 4 transition (GI-18 and/or GI-19.1 according to Rasmussen et al., 2014). This palaeosol can provide an assessment, whether or not brief spells of habitable conditions existed in the period between 70 ka and 60 ka, which would in principle have allowed the ephemeral use of sites in the region. A similar set of methods as used for the palaeosols in Khotylevo will also be applied to the pedogenic phenomena in Lichtenberg, including sedimentology, micromorphology, geochemistry, magnetic susceptibility, luminescence dating, and also palynological and phytolith analyses.

Three sediment cores (Li-BPa, PD.032 and PD.028, see Fig. 4 of Chapter 3) are being subjected to high-resolution multi-proxy analysis. We make use of a multitude of luminescence samples ($n \sim 50$), palynology, sedimentology, geochemistry, magnetic susceptibility, malacology as well as the analysis of chironomidae and various biochemical markers. Climatic conditions will be reconstructed from chironomids, biomarkers and pollen, i.e. in three different and parallel ways, which will be compared and jointly interpreted. Integrating all findings, Lichtenberg has the potential to become one of the standard profiles for vegetation, landscape and climate development on the western European Plain from the late Saalian to the Mid-Weichselian. In that capacity, valuable background information is provided for the occupations in Lichtenberg and the wider area. Furthermore, parallel investigations of an infilled late Saalian dead-ice kettle-hole (ca. 2 km away from the site) will help to disentangle the influences of climate

and landform geometry of the archive on the reconstruction of former conditions. One of the numerous sub-aspects is the more detailed investigation of the humic sands correlated with GI-20 and GI-19 (Chapter 4). As these late MIS 5a climate variations have been detected for the first time on the European Plain, palynological analysis in 1 cm resolution is being conducted. This will facilitate a climatic reconstruction of these intervals and the inspection of their comparability or even congruence with the presumed MIS 3 interstadials Oerel and Glinde (Jöris, 2004). A last sub-aspect of the core analysis mentioned here is the identification of wildfire cyclicity and its major determinants using micro-charcoal counting, indicator floral taxa and the application of novel pyrogenic biomarkers (de Groot et al., 2013; Dietze et al., 2020; Pop et al., 2016). Once this natural baseline is established, a potential Neanderthal contribution to fire history can be explored for phases in which known occupation and above-expected pyrogenic activity coincide (Dibble et al., 2018; Roebroeks et al., 2015; Scherjon et al., 2015). Due to the investigated three sediment cores from the archaeological sites to the deepest part of the palaeolake basin, the range of a possible human impact could also be accounted for (cf. Bos and Janssen, 1996).

Lastly, because the need for understanding MIS 5 geomorphic dynamics has repeatedly been addressed in the foregoing chapters, research at an additional location is referenced here. In Zeuchfeld, Central Germany, a deep sand pit exposes the infill of a dry valley covering the late Saalian to the Late Weichselian. What makes Zeuchfeld special is that it is not a loess-palaeosol-sequence, but a sequence of alternating and well-preserved *colluvial* deposits and palaeosols. They create a high-resolution record of geomorphic stability and activity phases, which is being deciphered with the palaeopedological methods listed above for Khotylevo I and Lichtenberg I/II. The results, together with all the findings from Lichtenberg, will be used to propose a long-overdue comprehensive model of diachronic landscape dynamics in Central Europe from late MIS 6 to MIS 3/2 (cf. Lade and Hagedorn, 1982).

5.4 REFERENCES

- Antoine, P., Coutard, S., Guerin, G., Deschodt, L., Goval, E., Loch, J.-L., Paris, C., 2016. Upper Pleistocene loess-palaeosol records from Northern France in the European context: Environmental background and dating of the Middle Palaeolithic. *Quat. Int.* 411, 4–24. <https://doi.org/10.1016/j.quaint.2015.11.036>
- Antoine, P., Goval, E., Jamet, G., Coutard, S., Moine, O., Hérissou, D., Auguste, P., Guérin, G., Lagroix, F., Schmidt, E., Robert, V., Debenham, N., Meszner, S., Bahain, J.-J., 2014. Les séquences loessiques pléistocène supérieur d'Havrincourt (Pas-de-Calais, France) : stratigraphie, paléoenvironnements, géochronologie et occupations paléolithiques. *Quaternaire* 321–368. <https://doi.org/10.4000/quaternaire.7278>
- Arnold, V., 1978. Neue Funde aus der Steinzeit Dithmarschens. *Dithmarschen* 3, 57–65.
- Bailey, R.M., Arnold, L.J., 2006. Statistical modelling of single grain quartz De distributions and an assessment of procedures for estimating burial dose. *Quat. Sci. Rev.* 25, 2475–2502. <https://doi.org/10.1016/j.quascirev.2005.09.012>
- Bateman, M.D., 2019. Applications in glacial and periglacial environments, in: Bateman, M.D. (Ed.), *Handbook of Luminescence Dating*. Whittles Publishing, pp. 191–221.
- Bateman, M.D., 2008. Luminescence dating of periglacial sediments and structures. *Boreas* 37, 574–588. <https://doi.org/10.1111/j.1502-3885.2008.00050.x>
- Behre, K.-E., Lade, U., 1986. Eine Folge von Eem und 4 Weichsel-Interstadialen in Oerel/Niedersachsen und ihr Vegetationsablauf. *E&G Quat. Sci. J.* 36, 11–36. <https://doi.org/10.3285/eg.36.1.02>
- Behre, K.-E., van der Plicht, J., 1992. Towards an absolute chronology for the last glacial period in Europe: radiocarbon dates from Oerel, northern Germany. *Veg. Hist. Archaeobot.* 1, 111–117. <https://doi.org/10.1007/BF00206091>
- Bobak, D., Plonka, T., Poltowicz-Bobak, M., Wiśniewski, A., 2013. New chronological data for Weichselian sites from Poland and their implications for Palaeolithic. *Quat. Int.* 296, 23–36. <https://doi.org/10.1016/j.quaint.2012.12.001>
- Boch, R., Cheng, H., Spötl, C., Edwards, R.L., Wang, X., Häuselmann, P., 2011. NALPS: a precisely dated European climate record 120–60 ka. *Clim. Past* 7, 1247–1259. <https://doi.org/10.5194/cp-7-1247-2011>
- Bolland, A., Kern, O.A., Allstädt, F.J., Peteet, D., Koutsodendris, A., Pross, J., Heiri, O., 2021. Summer temperatures during the last glaciation (MIS 5c to MIS 3) inferred from a 50,000-year chironomid record from Fürmoos, southern Germany. *Quat. Sci. Rev.* 264, 107008. <https://doi.org/10.1016/j.quascirev.2021.107008>
- Bos, J.A.A., Janssen, C.R., 1996. Local Impact of Palaeolithic Man on the Environment During the End of the Last Glacial in the Netherlands. *J. Archaeol. Sci.* 23, 731–739. <https://doi.org/10.1006/jasc.1996.0069>
- Breest, K., 1992. Neue Einzelfunde des Alt- und Mittelpaläolithikums im Landkreis Lüchow-Dannenberg. *Die Kd. N.F.* 43, 1–23.
- Bridgland, D.R., Antoine, P., Limondin-Lozouet, N., Santisteban, J.I., Westaway, R., White, M.J., 2006. The Palaeolithic occupation of Europe as revealed by evidence from the rivers: data from IGCP 449. *J. Quat. Sci.* 21, 437–455. <https://doi.org/10.1002/jqs.1042>

- Buylaert, J.P., Jain, M., Murray, A.S., Thomsen, K.J., Thiel, C., Sohbati, R., 2012. A robust feldspar luminescence dating method for Middle and Late Pleistocene sediments. *Boreas* 41, 435–451. <https://doi.org/10.1111/j.1502-3885.2012.00248.x>
- Caspers, G., Freund, H., 2001. Vegetation and climate in the Early- and Pleniglacial in northern Central Europe. *J. Quat. Sci.* 16, 31–48. [https://doi.org/10.1002/1099-1417\(200101\)16:1<31::AID-JQS577>3.0.CO;2-3](https://doi.org/10.1002/1099-1417(200101)16:1<31::AID-JQS577>3.0.CO;2-3)
- Caspers, G., Merkt, J., Müller, H., Freund, H., 2002. The Eemian Interglaciation in Northwestern Germany. *Quat. Res.* 58, 49–52. <https://doi.org/10.1006/qres.2002.2341>
- Chamberlain, E.L., Wallinga, J., Shen, Z., 2018. Luminescence age modeling of variably-bleached sediment: Model selection and input. *Radiat. Meas.* 120, 221–227. <https://doi.org/10.1016/j.radmeas.2018.06.007>
- Christiansen, H.H., 1998. Periglacial sediments in an Eemian-Weichselian succession at Emmerlev Klev, southwestern Jutland, Denmark. *Palaeogeogr. Palaeoclimatol. Palaeoecol.* 138, 245–258. [https://doi.org/10.1016/S0031-0182\(97\)00117-X](https://doi.org/10.1016/S0031-0182(97)00117-X)
- Cunningham, A.C., Wallinga, J., 2012. Realizing the potential of fluvial archives using robust OSL chronologies. *Quat. Geochronol.* 12, 98–106. <https://doi.org/10.1016/j.quageo.2012.05.007>
- de Groot, W.J., Cantin, A.S., Flannigan, M.D., Soja, A.J., Gowman, L.M., Newbery, A., 2013. A comparison of Canadian and Russian boreal forest fire regimes. *For. Ecol. Manage.* 294, 23–34. <https://doi.org/10.1016/j.foreco.2012.07.033>
- Defleur, A.R., Desclaux, E., 2019. Impact of the last interglacial climate change on ecosystems and Neanderthals behavior at Baume Moula-Guercy, Ardèche, France. *J. Archaeol. Sci.* 104, 114–124. <https://doi.org/10.1016/j.jas.2019.01.002>
- Dibble, H.L., Sandgathe, D., Goldberg, P., McPherron, S., Aldeias, V., 2018. Were Western European Neandertals Able to Make Fire? *J. Paleolit. Archaeol.* 1, 54–79. <https://doi.org/10.1007/s41982-017-0002-6>
- Dietze, E., Mangelsdorf, K., Andreev, A., Karger, C., Schreuder, L.T., Hopmans, E.C., Rach, O., Sachse, D., Wennrich, V., Herzsuh, U., 2020. Relationships between low-temperature fires, climate and vegetation during three late glacials and interglacials of the last 430 kyr in northeastern Siberia reconstructed from monosaccharide anhydrides in Lake El'gygytyn sediments. *Clim. Past* 16, 799–818. <https://doi.org/10.5194/cp-16-799-2020>
- Dietze, M., Kreutzer, S., Burow, C., Fuchs, M.C., Fischer, M., Schmidt, C., 2016. The abanico plot: Visualising chronometric data with individual standard errors. *Quat. Geochronol.* 31, 12–18. <https://doi.org/10.1016/j.quageo.2015.09.003>
- Duller, G.A.T., 2008. Single-grain optical dating of Quaternary sediments: why aliquot size matters in luminescence dating. *Boreas* 37, 589–612. <https://doi.org/10.1111/j.1502-3885.2008.00051.x>
- Fewlass, H., Talamo, S., Kromer, B., Bard, E., Tuna, T., Fagault, Y., Sponheimer, M., Ryder, C., Hublin, J.-J., Perri, A., Sázlová, S., Svoboda, J., 2019. Direct radiocarbon dates of mid Upper Palaeolithic human remains from Dolní Věstonice II and Pavlov I, Czech Republic. *J. Archaeol. Sci. Reports* 27, 102000. <https://doi.org/10.1016/j.jasrep.2019.102000>
- Fewlass, H., Talamo, S., Wacker, L., Kromer, B., Tuna, T., Fagault, Y., Bard, E., McPherron,

- S.P., Aldeias, V., Maria, R., Martisius, N.L., Paskulin, L., Rezek, Z., Sinet-Mathiot, V., Sirakova, S., Smith, G.M., Spasov, R., Welker, F., Sirakov, N., Tsanova, T., Hublin, J.-J., 2020. A 14C chronology for the Middle to Upper Palaeolithic transition at Bacho Kiro Cave, Bulgaria. *Nat. Ecol. Evol.* 4, 794–801. <https://doi.org/10.1038/s41559-020-1136-3>
- Fränzle, O., 1988. Glaziäre, periglaziäre und marine Reliefentwicklung im nördlichen Schleswig-Holstein. *Schr. Naturwiss. Ver. Schlesw.-Holst.* 58, 1–30.
- Fuchs, M., Kreutzer, S., Rousseau, D.-D., Antoine, P., Hatté, C., Lagroix, F., Moine, O., Gauthier, C., Svoboda, J., Lisá, L., 2013. The loess sequence of Dolní Věstonice, Czech Republic: A new OSL-based chronology of the Last Climatic Cycle. *Boreas* 42, 664–677. <https://doi.org/10.1111/j.1502-3885.2012.00299.x>
- Fuchs, M., Lang, A., 2009. Luminescence dating of hillslope deposits – A review. *Geomorphology* 109, 17–26. <https://doi.org/10.1016/j.geomorph.2008.08.025>
- Galbraith, R.F., Roberts, R.G., 2012. Statistical aspects of equivalent dose and error calculation and display in OSL dating: An overview and some recommendations. *Quat. Geochronol.* 11, 1–27. <https://doi.org/10.1016/j.quageo.2012.04.020>
- Galbraith, R.F., Roberts, R.G., Laslett, G.M., Yoshida, H., Olley, J.M., 1999. Optical dating of single and multiple grains of quartz from Jinmium Rock Shelter, northern Australia: Part I, Experimental design and statistical models. *Archaeometry* 41, 339–364. <https://doi.org/10.1111/j.1475-4754.1999.tb00987.x>
- Galbraith, R.F., Roberts, R.G., Yoshida, H., 2005. Error variation in OSL palaeodose estimates from single aliquots of quartz: a factorial experiment. *Radiat. Meas.* 39, 289–307. <https://doi.org/10.1016/j.radmeas.2004.03.023>
- Garrison, E., 2016. *Techniques in Archaeological Geology, Natural Science in Archaeology.* Springer International Publishing, Cham. <https://doi.org/10.1007/978-3-319-30232-4>
- Goldberg, P., Macphail, R.I., 2006. *Practical and Theoretical Geoarchaeology.* Blackwell Publishing Ltd., Malden, MA USA. <https://doi.org/10.1002/9781118688182>
- Guérin, G., Antoine, P., Schmidt, E., Goval, E., Hérissou, D., Jamet, G., Reyss, J.-L., Shao, Q., Philippe, A., Vibet, M.-A., Bahain, J.-J., 2017. Chronology of the Upper Pleistocene loess sequence of Havrincourt (France) and associated Palaeolithic occupations: A Bayesian approach from pedostratigraphy, OSL, radiocarbon, TL and ESR/U-series data. *Quat. Geochronol.* 42, 15–30. <https://doi.org/10.1016/j.quageo.2017.07.001>
- Hoffecker, J.F., Holliday, V.T., Nehoroshev, P., Vishnyatsky, L., Otcherednoy, A., Salnaya, N., Goldberg, P., Southon, J., Lehman, S.J., Cappa, P.J., Giaccio, B., Forman, S.L., Quade, J., 2019. The Dating of a Middle Paleolithic Blade Industry in Southern Russia and Its Relationship to the Initial Upper Paleolithic. *J. Paleolit. Archaeol.* <https://doi.org/10.1007/s41982-019-00032-6>
- Hublin, J.-J., Roebroeks, W., 2009. Ebb and flow or regional extinctions? On the character of Neandertal occupation of northern environments. *Comptes Rendus Palevol* 8, 503–509. <https://doi.org/10.1016/j.crpv.2009.04.001>
- Hülle, D., Hilgers, A., Kühn, P., Radtke, U., 2009. The potential of optically stimulated luminescence for dating periglacial slope deposits – A case study from the Taunus area, Germany. *Geomorphology* 109, 66–78. <https://doi.org/10.1016/j.geomorph.2008.08.021>
- Jacobs, Z., Roberts, R.G., 2007. Advances in optically stimulated luminescence dating of

- individual grains of quartz from archeological deposits. *Evol. Anthropol. Issues, News, Rev.* 16, 210–223. <https://doi.org/10.1002/evan.20150>
- Jöris, O., 2012. Keilmesser, in: Floss, H. (Ed.), *Steinartefakte Vom Altpaläolithikum Bis in Die Neuzeit*. Kerns Verlag, Tübingen, pp. 297–308.
- Jöris, O., 2004. Zur chronostratigraphischen Stellung der spätmittelpaläolithischen Keilmessergruppen: Der Versuch einer kulturgeographischen Abgrenzung einer mittelpaläolithischen Formengruppe in ihrem europäischen Kontext. *Bericht RGK* 84, 49–153.
- Kreutzer, S., Burow, C., Dietze, M., Fuchs, M.C., Schmidt, C., Fischer, M., Friedrich, J., 2020. *Luminescence: Comprehensive Luminescence Dating Data Analysis*. R package version 0.9.7. <https://CRAN.R-project.org/package=Luminescence>.
- Lade, U., Hagedorn, H., 1982. Sedimente und Relief einer eiszeitlichen Hohlform bei Krempel (Elbe-Weser-Dreieck). *E&G Quat. Sci. J.* 32, 93–108. <https://doi.org/10.3285/eg.32.1.08>
- Laurat, T., Brühl, E., 2021. Neumark-Nord 2 – A multiphase Middle Palaeolithic open-air site in the Geisel Valley (Central Germany). *Anthropologie*. 102936. <https://doi.org/10.1016/j.anthro.2021.102936>
- Lisiecki, L.E., Stern, J. V., 2016. Regional and global benthic δ 18 O stacks for the last glacial cycle. *Paleoceanography* 31, 1368–1394. <https://doi.org/10.1002/2016PA003002>
- Litt, T., Behre, K.-E., Mexer, K.-D., Stephan, H.-J., Wansa, S., Litt, T.; Behre, K.-E.; Meyer, K.-D.; Stephan, H.-J.; Wansa, S., 2007. Stratigraphische Begriffe für das Quartär des norddeutschen Vereisungsgebietes. *Eiszeitalter und Gegenwart* 56, 7–65.
- Locht, J.-L., Goval, E., Antoine, P., Coutard, S., Auguste, P., Paris, C., Hérissou, D., 2014. Palaeoenvironments and prehistoric interactions in northern France from the Eemian Interglacial to the end of the Weichselian Middle Pleniglacial, in: Foulds, W.F., Drinkall, H.C., Perri, A.R., Clinnick, D.T.G. (Eds.), *Wild Things: Recent Advances in Palaeolithic and Mesolithic Research*. Oxbow Books, pp. 70–78.
- Locht, J.-L., Hérissou, D., Goval, E., Cliquet, D., Huet, B., Coutard, S., Antoine, P., Feray, P., 2016. Timescales, space and culture during the Middle Palaeolithic in northwestern France. *Quat. Int.* 411, 129–148. <https://doi.org/10.1016/j.quaint.2015.07.053>
- Mahan, S.A., Rittenour, T.M., Nelson, M.S., Atae, N., Brown, N., DeWitt, R., Durcan, J., Evans, M., Feathers, J., Frouin, M., Guérin, G., Heydari, M., Huot, S., Jain, M., Keen-Zebert, A., Li, B., López, G.I., Neudorf, C., Porat, N., Rodrigues, K., Sawakuchi, A.O., Spencer, J.Q.G., Thomsen, K., 2022. Guide for interpreting and reporting luminescence dating results. *GSA Bull.* <https://doi.org/10.1130/B36404.1>
- Mania, D., 2002. Der mittelpaläolithische Lagerplatz am Ascherslebener See bei Königsau (Nordharzvorland). *Praehistoria Thuringica* 8, 16–75.
- Mania, D., Toepfer, V., 1973. Königsau: Gliederung, Oekologie und Mittelpaläolithische Funde der letzten Eiszeit. *Veröffentlichungen des Landesmuseums für Vorgeschichte in Halle* 26, Deutscher Verlag der Wissenschaften, Berlin.
- Matoshko, A. V., Gozhik, P.F., Danukalova, G., 2004. Key Late Cenozoic fluvial archives of eastern Europe: the Dniester, Dnieper, Don and Volga. *Proc. Geol. Assoc.* 115, 141–173. [https://doi.org/10.1016/S0016-7878\(04\)80024-5](https://doi.org/10.1016/S0016-7878(04)80024-5)
- Menke, B., 1980. Schalkholz. Quartär-Exkursionen/Quaternary Excursions in Schleswig-

- Holstein, 70–74.
- Menke, B., Tynni, R., 1984. Das Eeminterglazial und das Weichselfrühglazial von Rederstall/Dithmarschen und ihre Bedeutung für die mitteleuropäische Jungpleistozän-Gliederung. *Geol. Jahrb. A* 76, 1–120.
- Meszner, S., Faust, D., 2018. Paläoböden in den Lössgebieten Ostdeutschlands, in: *Handbuch Der Bodenkunde*. Wiley, pp. 1–20.
<https://doi.org/10.1002/9783527678495.hbbk2018002>
- Müller, U.C., Sánchez Goñi, Maria F., 2007. Vegetation dynamics in southern Germany during marine isotope stage 5 (~ 130 to 70 kyr ago), in: Sirocko, F., Claussen, M., Sánchez Goñi, M.F., Litt, T. (Eds.), *The Climate of Past Interglacials*. (Developments in Quaternary Sciences 7). pp. 277–287. [https://doi.org/10.1016/S1571-0866\(07\)80044-3](https://doi.org/10.1016/S1571-0866(07)80044-3)
- Murray, A.S., Roberts, R.G., 1998. Measurement of the equivalent dose in quartz using a regenerative-dose single-aliquot protocol. *Radiat. Meas.* 29, 503–515.
[https://doi.org/10.1016/S1350-4487\(98\)00044-4](https://doi.org/10.1016/S1350-4487(98)00044-4)
- Murray, A.S., Wintle, A.G., 2000. Luminescence dating of quartz using an improved single-aliquot regenerative-dose protocol. *Radiat. Meas.* 32, 57–73.
[https://doi.org/10.1016/S1350-4487\(99\)00253-X](https://doi.org/10.1016/S1350-4487(99)00253-X)
- Nielsen, T.K., Benito, B.M., Svenning, J.-C., Sandel, B., McKerracher, L., Riede, F., Kjærgaard, P.C., 2017. Investigating Neanderthal dispersal above 55°N in Europe during the Last Interglacial Complex. *Quat. Int.* 431, 88–103.
<https://doi.org/10.1016/j.quaint.2015.10.039>
- Nielsen, T.K., Kristiansen, S.M., Riede, F., 2019. Neanderthals at the frontier? Geological potential of southwestern South Scandinavia as archive of Pleistocene human occupation. *Quat. Sci. Rev.* 221, 105870.
<https://doi.org/10.1016/j.quascirev.2019.105870>
- Olley, J., Caitcheon, G., Roberts, R., 1999. The origin of dose distributions in fluvial sediments, and the prospect of dating single grains from fluvial deposits using optically stimulated luminescence. *Radiat. Meas.* 30, 207–217. [https://doi.org/10.1016/S1350-4487\(99\)00040-2](https://doi.org/10.1016/S1350-4487(99)00040-2)
- Otcherednoi, A., Salnaya, N., Voskresenskaya, E., Vishnyatsky, L., 2014. New geoarcheological studies at the middle paleolithic sites of khotylevo i and betovo (Bryansk oblast, Russia): Some preliminary results. *Quat. Int.* 326–327, 250–260.
<https://doi.org/10.1016/j.quaint.2013.11.005>
- Panin, A., Adamiec, G., Buylaert, J.-P., Matlakhova, E., Moska, P., Novenko, E., 2017. Two Late Pleistocene climate-driven incision/aggradation rhythms in the middle Dnieper River basin, west-central Russian Plain. *Quat. Sci. Rev.* 166, 266–288.
<https://doi.org/10.1016/j.quascirev.2016.12.002>
- Pastors, A., 2009. Blades ? – Thanks, no interest! - Neanderthals in Salzgitter-Lebenstedt. *Quartaer* 56, 105–118.
- Pederzani, S., Aldeias, V., Dibble, H.L., Goldberg, P., Hublin, J.-J., Madelaine, S., McPherron, S.P., Sandgathe, D., Steele, T.E., Turq, A., Britton, K., 2021. Reconstructing Late Pleistocene paleoclimate at the scale of human behavior: an example from the Neandertal occupation of La Ferrassie (France). *Sci. Rep.* 11, 1419.
<https://doi.org/10.1038/s41598-020-80777-1>

- Pop, E., 2014. Analysis of the neumark-nord 2/2 lithic assemblage: results and interpretations, in: Gaudzinski-Windheuser, S., Roebroeks, W. (Eds.), *Multidisciplinary Studies of the Middle Palaeolithic Record from Neumark-Nord (Germany)*, Veröffentlichungen Des Landesamtes Für Denkmalpflege Und Archäologie Sachsen-Anhalt – Landesmuseum Für Vorgeschichte Band 69. Landesamt für Denkmalpflege und Archäologie Sachsen-Anhalt, Landesmuseum für Vorgeschichte, Halle(Saale), pp. 143–195.
- Pop, E., Kuijper, W., van Hees, E., Smith, G., García-Moreno, A., Kindler, L., Gaudzinski-Windheuser, S., Roebroeks, W., 2016. Fires at Neumark-Nord 2, Germany: An analysis of fire proxies from a Last Interglacial Middle Palaeolithic basin site. *J. F. Archaeol.* 41, 603–617. <https://doi.org/10.1080/00934690.2016.1208518>
- Rasmussen, O., Bigler, M., Blockley, S.P., Blunier, T., Buchardt, S.L., Clausen, H.B., Cvijanovic, I., Dahl-Jensen, D., Johnsen, S.J., Fischer, H., Gkinis, V., Guillevic, M., Hoek, W.Z., Lowe, J.J., Pedro, J.B., Popp, T., Seierstad, I.K., Steffensen, J.P., Svensson, A.M., Vallelonga, P., Vinther, B.M., Walker, M.J.C., Wheatley, J.J., Winstrup, M., 2014. A stratigraphic framework for abrupt climatic changes during the Last Glacial period based on three synchronized Greenland ice-core records: refining and extending the INTIMATE event stratigraphy. *Quat. Sci. Rev.* 106, 14–28. <https://doi.org/10.1016/j.quascirev.2014.09.007>
- Richter, J., 2016. Leave at the height of the party: A critical review of the Middle Paleolithic in Western Central Europe from its beginnings to its rapid decline. *Quat. Int.* 411, 107–128. <https://doi.org/10.1016/j.quaint.2016.01.018>
- Richter, J., 2006. Neanderthals in their landscape., in: *Neanderthals in Europe*. pp. 51–66.
- Richter, J., 2002. Die 14C-Daten aus der Sesselfelsgrötte und die Zeitstellung des Micoquien/MMO. *Germania* 80, 1–22.
- Roebroeks, W., Bakels, C.C., Coward, F., Hosfield, R., Pope, M., Wenban-Smith, F., 2015. ‘Forest Furniture’ or ‘Forest Managers’? On Neanderthal presence in Last Interglacial environments, in: *Settlement, Society and Cognition in Human Evolution*. Cambridge University Press, New York, pp. 174–188. <https://doi.org/10.1017/CBO9781139208697.011>
- Rowan, A. V., Roberts, H.M., Jones, M.A., Duller, G.A.T., Covey-Crump, S.J., Brocklehurst, S.H., 2012. Optically stimulated luminescence dating of glaciofluvial sediments on the Canterbury Plains, South Island, New Zealand. *Quat. Geochronol.* 8, 10–22. <https://doi.org/10.1016/j.quageo.2011.11.013>
- Sanchez Goñi, M.F., 2022. Pollen: A Key Tool for Understanding Climate, Vegetation, and Human Evolution. https://doi.org/10.1007/124_2022_63
- Sauer, D., Kadereit, A., Kühn, P., Kösel, M., Miller, C.E., Shinonaga, T., Kreutzer, S., Herrmann, L., Fleck, W., Starkovich, B.M., Stahr, K., 2016. The loess-palaeosol sequence of Datthausen, SW Germany: Characteristics, chronology, and implications for the use of the Lohne Soil as a marker soil. *CATENA* 146, 10–29. <https://doi.org/10.1016/j.catena.2016.06.024>
- Scherjon, F., Bakels, C., MacDonald, K., Roebroeks, W., 2015. Burning the Land. *Curr. Anthropol.* 56, 299–326. <https://doi.org/10.1086/681561>
- Schokker, J., Cleveringa, P., Murray, A.S., 2004. Palaeoenvironmental reconstruction and OSL dating of terrestrial Eemian deposits in the southeastern Netherlands. *J. Quat. Sci.* 19,

- 193–202. <https://doi.org/10.1002/jqs.808>
- Sedov, S.N., Khokhlova, O.S., Sinitsyn, A.A., Korkka, M.A., Rusakov, A. V., Ortega, B., Solleiro, E., Rozanova, M.S., Kuznetsova, A.M., Kazdym, A.A., 2010. Late pleistocene paleosol sequences as an instrument for the local paleographic reconstruction of the Kostenki 14 key section (Voronezh oblast) as an example. *Eurasian Soil Sci.* 43, 876–892. <https://doi.org/10.1134/S1064229310080053>
- Stojakowits, P., Mayr, C., 2022. Quaternary Palynostratigraphy of Germany with special emphasis on the Late Pleistocene, in: *Stratigraphy & Timescales*, 7. pp. 81–136. <https://doi.org/10.1016/bs.sats.2022.09.001>
- Terhorst, B., Sedov, S., Sprafke, T., Peticzka, R., Meyer-Heintze, S., Kühn, P., Solleiro Rebolledo, E., 2015. Austrian MIS 3/2 loess–palaeosol records – Key sites along a west-east transect. *Palaeogeogr. Palaeoclimatol. Palaeoecol.* 418, 43–56. <https://doi.org/10.1016/j.palaeo.2014.10.020>
- Thiel, C., Buylaert, J.P., Murray, A., Terhorst, B., Hofer, I., Tsukamoto, S., Frechen, M., 2011. Luminescence dating of the Stratzing loess profile (Austria) - Testing the potential of an elevated temperature post-IR IRSL protocol. *Quat. Int.* 234, 23–31. <https://doi.org/10.1016/j.quaint.2010.05.018>
- Tode, A., 1982. Der altsteinzeitliche Fundplatz Salzgitter-Lebenstedt. Teil I, archäologischer Teil. Böhlau, Köln, Wien.
- Tooth, S., Rodnight, H., Duller, G.A.T., McCarthy, T.S., Marren, P.M., Brandt, D., 2007. Chronology and controls of avulsion along a mixed bedrock-alluvial river. *Geol. Soc. Am. Bull.* 119, 452–461. <https://doi.org/10.1130/B26032.1>
- Uthmeier, T., Kels, H., Schirmer, W., Böhner, U., 2011. Neanderthals in the cold: Middle Paleolithic sites from the open-cast mine of Garzweiler, Nordrhein-Westfalen (Germany), in: Conard, N.J., Richter, J. (Eds.), *Neanderthal Lifeways, Subsistence and Technology: One Hundred Fifty Years of Neanderthal Study*. Springer, pp. 25–41. https://doi.org/10.1007/978-94-007-0415-2_4
- Vandenberghe, J., 2015. River terraces as a response to climatic forcing: Formation processes, sedimentary characteristics and sites for human occupation. *Quat. Int.* <https://doi.org/10.1016/j.quaint.2014.05.046>
- Vandenberghe, J., 2008. The fluvial cycle at cold-warm-cold transitions in lowland regions: A refinement of theory. *Geomorphology*. <https://doi.org/10.1016/j.geomorph.2006.12.030>
- Veil, S., Breest, K., Höfle, H.-C., Meyer, H.-H., Plisson, H., Urban-Küttel, B., Wagner, G.A., Zöller, L., 1994. Ein mittelpaläolithischer Fundplatz aus der Weichsel-Kaltzeit bei Lichtenberg, Lkr. Lüchow-Dannenberg. *Germania* 72, 1–66.
- Veit, H., Trauerstein, M., Preusser, F., Messmer, T., Gnägi, C., Zech, R., Wüthrich, L., 2017. Late Glacial/Early Holocene slope deposits on the Swiss Plateau: Genesis and palaeo-environment. *CATENA* 158, 102–112. <https://doi.org/10.1016/j.catena.2017.06.012>
- Velichko, A.A., 1988. Geoecology of the Mousterian in East Europe and the adjacent areas, in: *L'Homme de Neandertal*. Liège, pp. 181–206.
- Waroszewski, J., Sprafke, T., Kabala, C., Muszyńska, E., Kot, A., Tsukamoto, S., Frechen, M., 2020. Chronostratigraphy of silt-dominated Pleistocene periglacial slope deposits on Mt. Ślęza (SW, Poland): Palaeoenvironmental and pedogenic significance. *CATENA* 190,

104549. <https://doi.org/10.1016/j.catena.2020.104549>

Weiss, M., 2019. Beyond the caves: stone artifact analysis of late Middle Paleolithic open-air assemblages from the European Plain. Universiteit Leiden.

Wenzel, S., 2007. 12. Neanderthal presence and behaviour in central and Northwestern Europe during MIS 5e, in: Sirocko, F., Claussen, M., Sánchez-Goni, M.F., Litt, T. (Eds.), *The Climate of Past Interglacials*. Elsevier, pp. 173–193. [https://doi.org/10.1016/S1571-0866\(07\)80037-6](https://doi.org/10.1016/S1571-0866(07)80037-6)

Winsemann, J., Lang, J., Roskosch, J., Polom, U., Böhner, U., Brandes, C., Glotzbach, C., Frechen, M., 2015. Terrace styles and timing of terrace formation in the Weser and Leine valleys, northern Germany: Response of a fluvial system to climate change and glaciation. *Quat. Sci. Rev.* 123, 31–57. <https://doi.org/10.1016/j.quascirev.2015.06.005>

Woillard, G., 1979. The last interglacial-glacial cycle at Grande Pile in Northeastern France. *Bull. Société belge Géologie* 88, 51–69.

Zavernyaev, F.M., 1978. *Khotylevskoe paleoliticheskoe mestonahozhdenie*. Nauka, Leningrad.

APPENDIX I: SUPPLEMENTARY INFORMATION FOR CHAPTER II

Luminescence chronology of the key-Middle Paleolithic site Khotylevo I (Western Russia) - Implications for the timing of occupation, site formation and landscape evolution

Supplementary Information

Tab. 1: Contributions of alpha, beta and gamma dose rates to the total dose rate of each sample. In-situ gamma spectrometry was used for samples L-EVA 1712, L-EVA 1714 and L-EVA 1716 (shown in bold).

Lab.-ID (L-EVA)	Alpha DR (mGy/a)	Beta DR (mGy/a)	Gamma DR (mGy/a)	Cosmic DR (mGy/a)	Total DR (mGy/a)
1702	0.86 ± 0.15	1.55 ± 0.13	0.88 ± 0.09	0.20 ± 0.02	3.49 ± 0.22
1703	0.10 ± 0.05	1.74 ± 0.18	0.79 ± 0.05	0.19 ± 0.02	2.81 ± 0.15
1704	0.10 ± 0.06	1.90 ± 0.20	0.84 ± 0.06	0.18 ± 0.02	3.02 ± 0.16
1705	0.09 ± 0.06	1.57 ± 0.17	0.71 ± 0.06	0.17 ± 0.02	2.54 ± 0.14
1706	0.07 ± 0.05	1.52 ± 0.16	0.60 ± 0.05	0.16 ± 0.02	2.35 ± 0.14
1707	0.09 ± 0.05	1.81 ± 0.19	0.78 ± 0.06	0.16 ± 0.02	2.84 ± 0.15
1708	0.11 ± 0.05	2.07 ± 0.20	0.94 ± 0.06	0.15 ± 0.01	3.27 ± 0.16
1709	0.10 ± 0.05	1.96 ± 0.18	0.86 ± 0.06	0.14 ± 0.01	3.06 ± 0.15
1710	0.08 ± 0.05	1.73 ± 0.19	0.72 ± 0.06	0.14 ± 0.01	2.67 ± 0.16
1711	0.08 ± 0.06	1.68 ± 0.19	0.67 ± 0.06	0.14 ± 0.01	2.56 ± 0.15
1712	0.05 ± 0.05	1.29 ± 0.16	0.58 ± 0.06	0.13 ± 0.01	2.05 ± 0.14
1713	0.06 ± 0.06	1.48 ± 0.17	0.52 ± 0.05	0.13 ± 0.01	2.18 ± 0.14
1714	0.06 ± 0.05	1.42 ± 0.17	0.60 ± 0.06	0.13 ± 0.01	2.20 ± 0.15
1715	0.06 ± 0.06	1.46 ± 0.18	0.51 ± 0.06	0.13 ± 0.01	2.15 ± 0.15
1716	0.07 ± 0.05	1.54 ± 0.17	0.64 ± 0.06	0.12 ± 0.01	2.37 ± 0.14
1717	0.04 ± 0.06	1.24 ± 0.18	0.39 ± 0.06	0.12 ± 0.01	1.80 ± 0.15
1718	0.06 ± 0.05	1.43 ± 0.17	0.52 ± 0.05	0.12 ± 0.01	2.13 ± 0.14
1719	0.06 ± 0.05	1.37 ± 0.17	0.52 ± 0.06	0.12 ± 0.01	2.08 ± 0.15

Tab. 2: Residual doses (RD) of the three different protocols measured after 3 hours of solar bleaching.

Sample (L-EVA)	<i>pIRIR</i> ₂₂₅ RD (Gy)	<i>pIRIR</i> ₂₉₀ RD (Gy)	<i>pIRIR</i> ₂₉₀ (hb) RD (Gy)	
	1706	1706	1706	1715
	8.20	26.65	21.75	21.61
	8.12	26.36	22.11	33.67
	9.77	30.40	27.20	30.42
				33.64
Sample (L-EVA)	1707	1707	1707	1717
	3.31	16.59	14.81	17.76
	3.02	17.70	29.83	21.58
	6.27		23.41	17.94
				19.58
Sample (L-EVA)	1710	1710	1710	1718
	2.11	1.81	14.00	19.33
	3.50	5.62	32.93	19.95
	10.32		34.61	21.76
				27.52

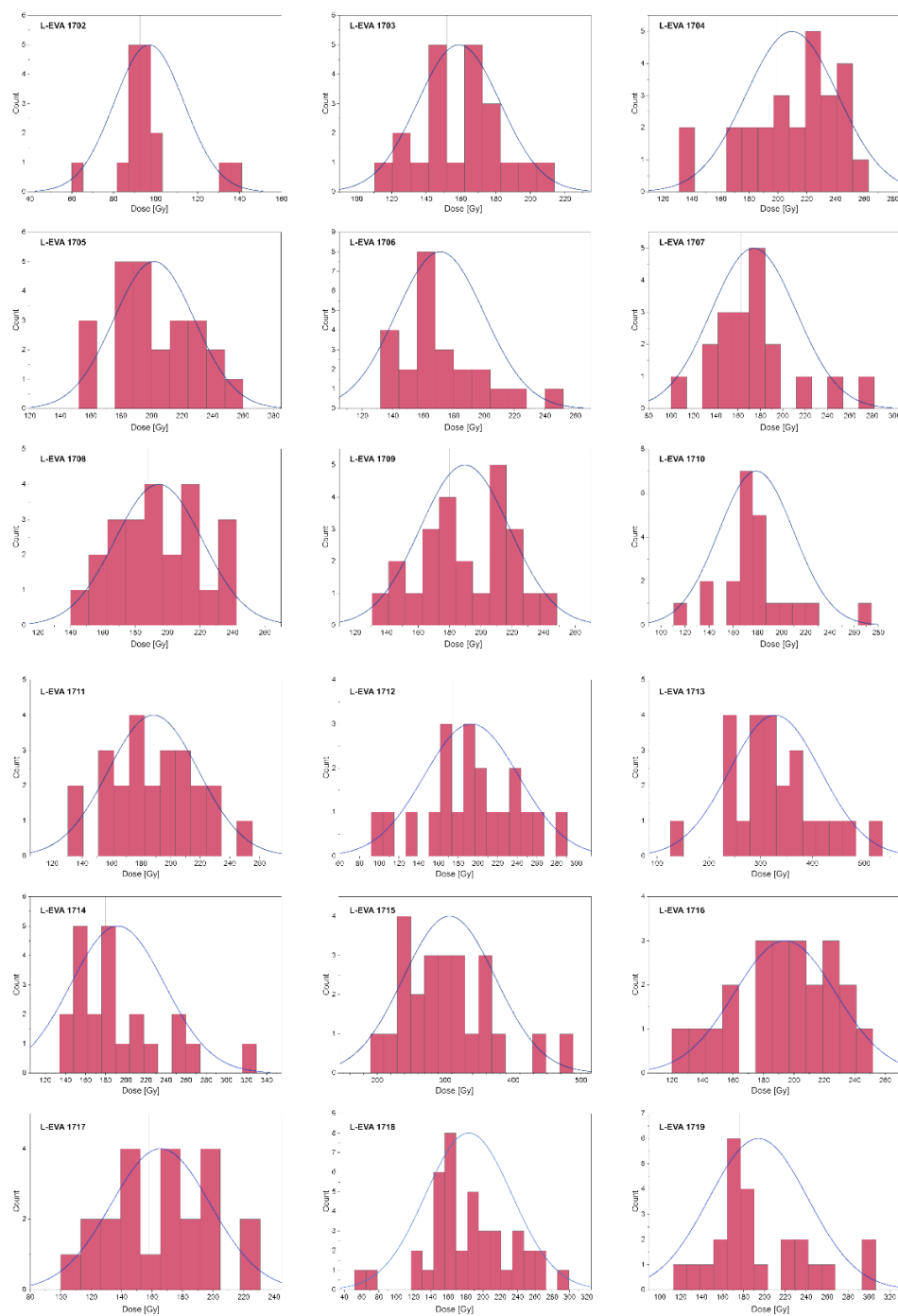


Fig. 1: De-distributions of all measured samples. The vertical reference line represents the weighted-mean estimate, and the blue curve displays an ideal normal distribution.

APPENDIX II: SUPPLEMENTARY INFORMATION FOR CHAPTER III

Eemian landscape response to climatic shifts and evidence for northerly Neanderthal occupation at a palaeolake margin in Northern Germany

Michael Hein, Brigitte Urban, David Colin Tanner, Anton Hermann Buness, Mario Tucci, Philipp Hoelzmann, Sabine Dietel, Marie Kaniecki, Jonathan Schultz, Thomas Kasper, Hans von Suchodoletz, Antje Schwalb, Marcel Weiss, Tobias Lauer

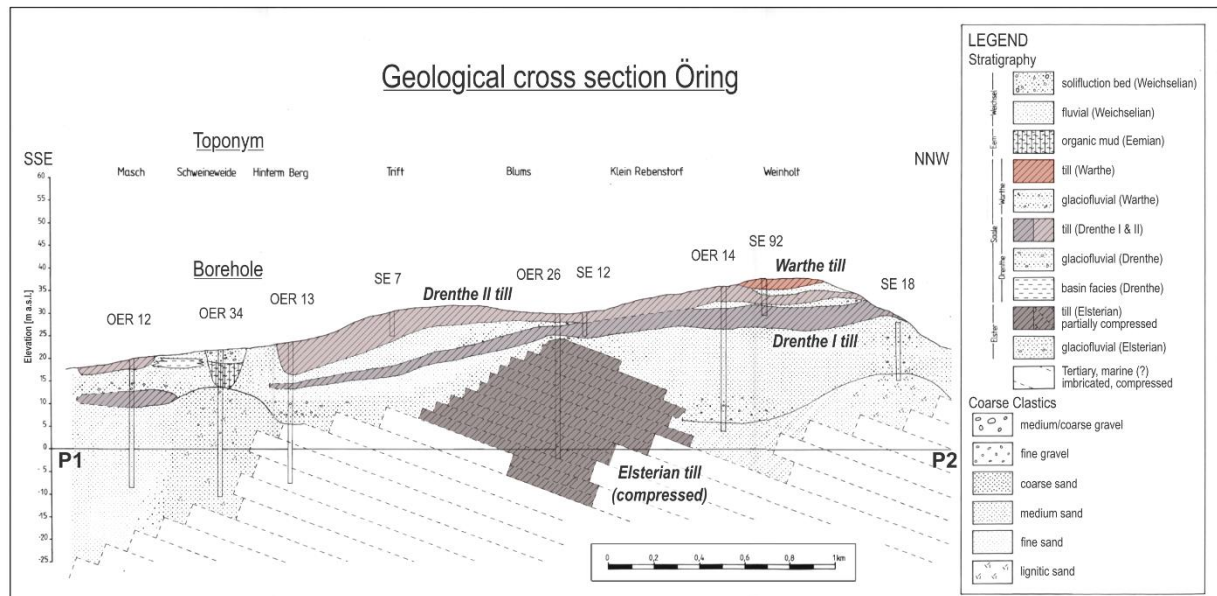
Published in ESPL (DOI: [10.1002/esp.5219](https://doi.org/10.1002/esp.5219))

Supplementary information

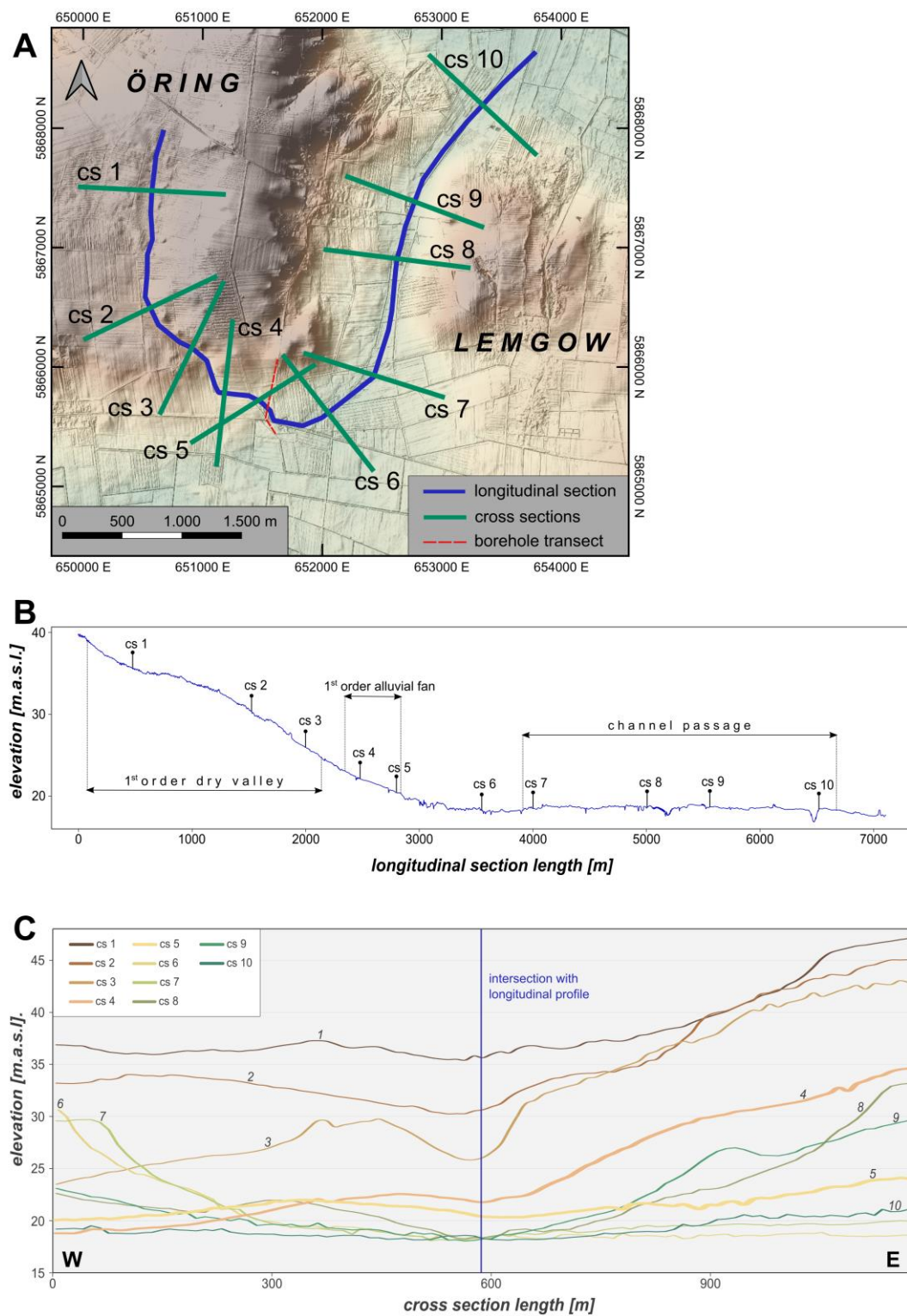
1. Geomorphological situation revealed by DEM analysis

Prior to fieldwork, we carried out a simple GIS-based exploration of the study area so that we could integrate stratigraphic findings into a landscape context and assess the validity of the investigated archive. We used QGIS (version 3.15) and digital elevation models (DEM) with 1 m spatial resolution (State Offices for Geoinformation and Land Survey in Lower Saxony and Saxony-Anhalt). Furthermore, digitized geological maps (1:25.000) were part of our GIS database (Merk, 1975; Schwalb, 1987), acquired from the State Office for Mining, Energy and Geology, Lower Saxony and the State Office for Geology and Mining, Saxony-Anhalt. We used the data to identify landforms such as depressions, channels and periglacial features, and to distinguish those from the Saalian glacial landforms by means of stratigraphic relationship. The southern slope of the morainic remnant of the Öring is dissected by at least two larger valleys with lengths >2000 m, and corresponding alluvial fans formed at their mouths (referred to here as 1st order alluvial fans, Suppl. Fig. 3; Fig. 3B/C, main article). According to Fränze (1988; cf. Garleff and Leontaris, 1971; Schokker et al., 2004), these erosional and depositional features developed during the late Saalian – early Eemian transition. Because the 1st order dry valleys dissect the Warthe glacial deposits from the latest Saalian, the Saalian-Eemian transition can safely be assumed for their formation, as well (Suppl. Fig. 1; Fig. 3B, main article). Our study site is located near the easternmost of these Öring alluvial fans, in proximity to a channel passage between Öring and Lemgow (Fig. 3, Suppl. Figs. 2 and 3). This channel passage is assumed to have its origins in a precursive Elsterian tunnel valley (Voss, 1981), and to have facilitated hydrological exchange ever since with the adjacent ice-marginal valley of the River Elbe. After the formation of the eastern fan, a subsequent incision created a roughly

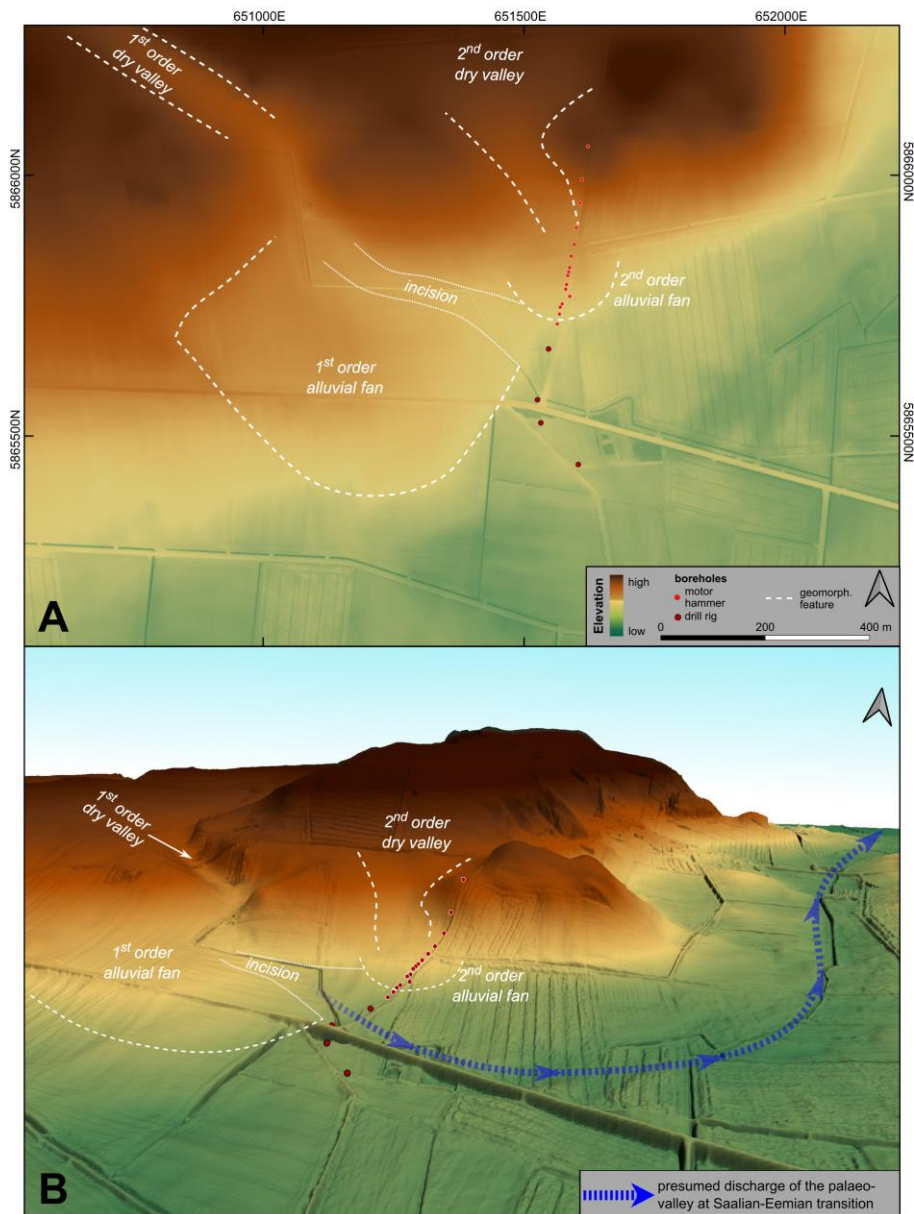
W-E striking depression within this fan (Suppl. Fig. 3), which is physically linked with this channel passage between Öring and Lemgow. In Suppl. Fig. 2 we geometrically explore the whole palaeovalley system, including the 1st order dry valley in the SE Öring, the incised depression within the 1st order alluvial fan and the channel passage (between Öring and Lemgow) by means of longitudinal and cross sections. It shows the high likeliness of a discharge from the SE Öring on the shortest course towards the adjacent ice-marginal valley (cf. Suppl. Fig. 3). Later on, a smaller dry valley from the north aggraded a smaller fan within this preceding incised depression of the eastern 1st order alluvial fan (Suppl. Fig. 3), which had turned into a part of a fingerlake in the meantime. Stratigraphic superposition requires that these smaller features developed after the incision within the 1st order fan. Hence, we refer to the smaller landforms as 2nd order dry valley and alluvial fan. The location of our borehole transect and seismic profile was chosen to cut the 2nd order fan lengthwise and the incised depression within the 1st order fan crosswise (Fig. 3C). South of our study site a WNW – ESE striking and ca. 2 km long distinct ridge rises ~1.5 m above the surroundings, detaching our study site from the centre of the basin. This ridge has likely acted as a hydrographic divide in former times, as it does today (see Fig. 3B). Even well into the 20th century, the basin was periodically submerged with seepage waters during flooding of the Elbe valley, until the expansion of the drainage network in the 1960s artificially lowered the groundwater level (pers. comm. with residents). Thus, it is safe to assume that the basin repeatedly accommodated a water body whenever favourable hydrographic conditions existed. There is little other information about the formation of the basin itself that concerns the geological evolution, and the different stages and chronology of the lake development.



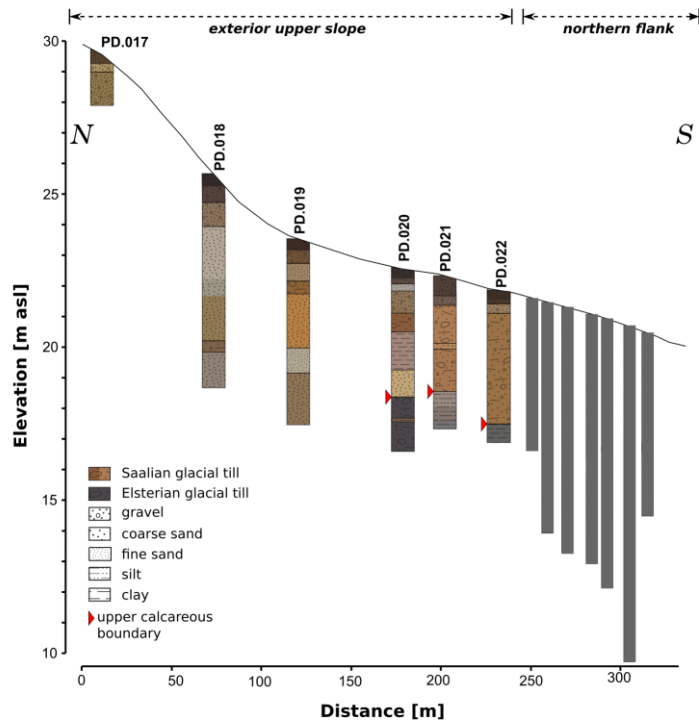
Suppl. Fig. 1: Geological cross-section of the Öring (modified after Schwalb, 1987) showing the stratigraphic relations of the occurring glacial tills. Note the deformed Elsterian till in core OER 26 (about 7 m depth), which we encountered in our core PD.020 as well. P1 and P2 refer to the position of the cross-section that is indicated in main Fig. 3A.



Suppl. Fig. 2: Positions of the longitudinal and cross-sections for morphometrical assessment of the presumed palaeovalley system at the Saalian-Eemian transition (for spatial context see Fig. 3, main article). B Exaggerated slope of the palaeovalley system along the longitudinal section. Intersection with the cross-sections and the main geomorphological units are indicated. C Morphometry and elevation of the cross-sections.



Suppl. Fig. 3: Main geomorphological features around the presented borehole transect in a 2d (A) and 3d-view with a 20x exaggeration (B). For spatial context see Fig. 3, main article. Presumed discharge direction of the palaeovalley at the Saalian-Eemian transition is derived from Suppl. Fig. 2.



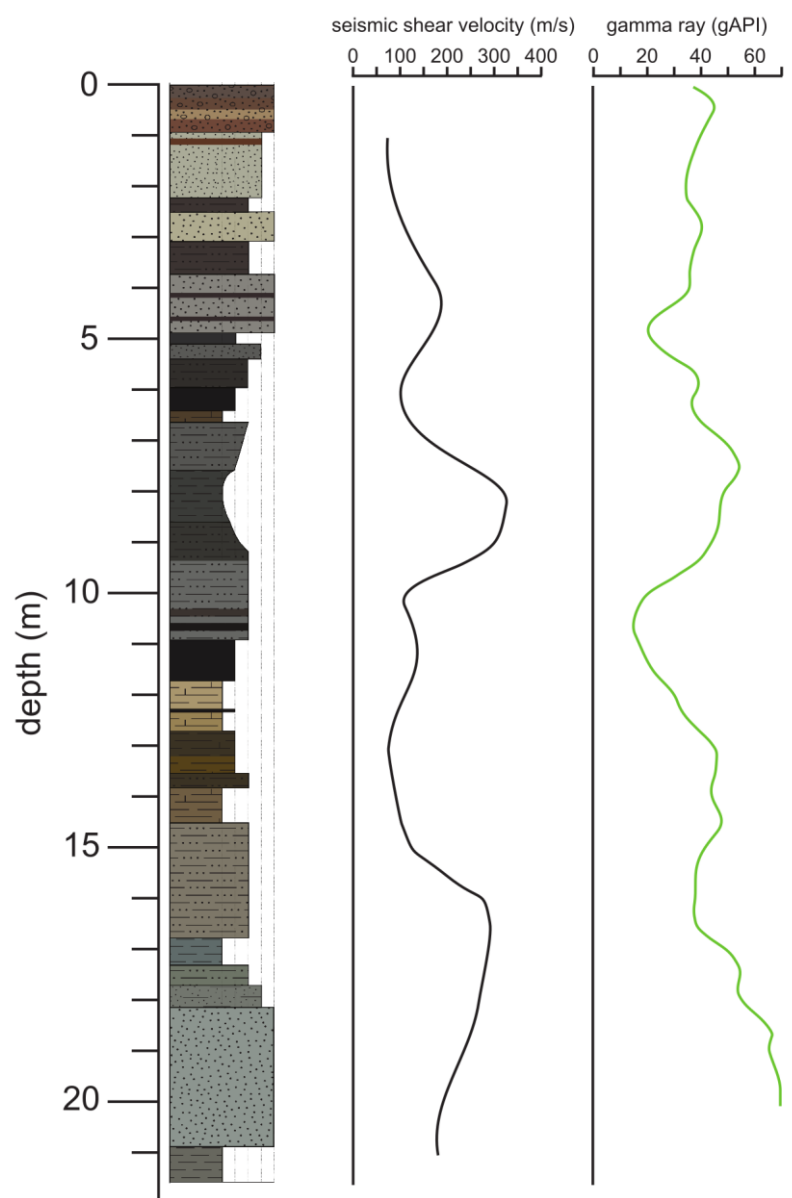
Suppl. Fig. 4: Sedimentary log of the exterior part of the borehole transect. For position, see Figs. 3 and 4 of the main article. Descriptions in section 4.1, main article.

2. Criteria for the assignment of distinct pollen zones

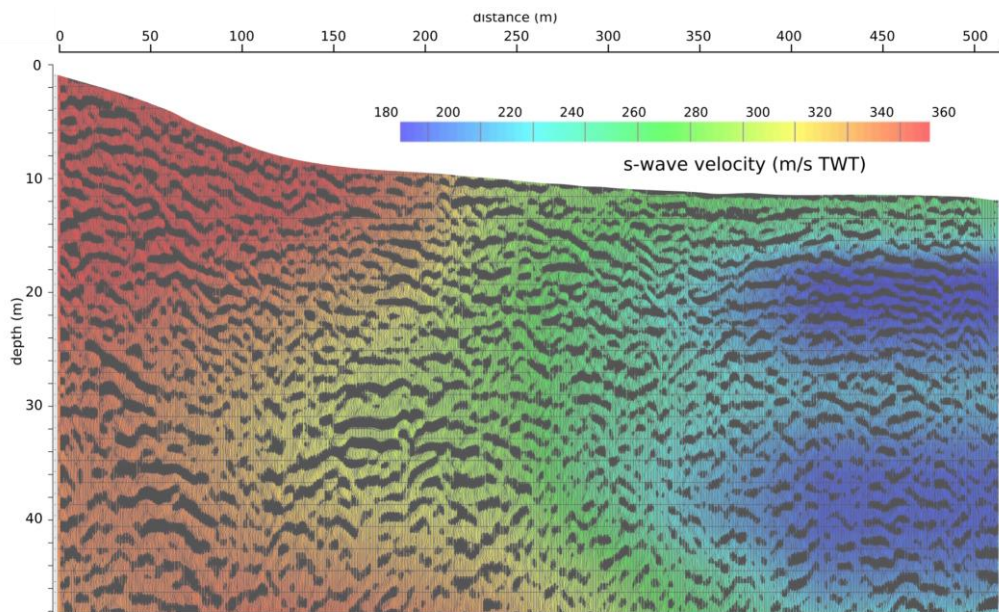
When working on single bulk samples, assemblages characteristic of certain pollen zones (e.g. E II, E VII, WF II) are at times hardly distinguishable from one another. In these cases we took stratigraphic considerations into account and tentatively assigned the (two) most likely pollen zones. Examples are samples 1, 2, 3, 7 and 20. Especially in the early and late Eemian periods, the amount of reworked pollen is partially quite high, obscuring the in-situ proportion and making attribution to a pollen zone difficult (samples 5, 7, 11, 12, 15, 21). When parts of an undisturbed underlying assemblage are found in the redepositional zone, they indicate the maximum stratigraphic age. In the same manner, the overlying in-situ assemblages constrain the minimum stratigraphic age. If no postdating sample was available, we could only narrow down deposition to a transitional period (samples 7, 12). Only in one case, we refrained from assigning a pollen zone, because redeposition could have occurred between PZ E V/VI and WF I (sample 5). Due to a gradually-sinking water table, the pollen-bearing organogenic deposits on the slopes fell dry at some point and formed the surface for an uncertain time. In this way, the dominating part of the pollen spectrum would be from the time of sediment formation, with a later overprint of continuing pollen deposition. As this is not easily detected in bulk samples, we sometimes assigned two equitable, neighboring pollen zones (samples 24 and 25).

3. Additional seismic information

A special difficulty of the S-wave seismic measurements is the velocity distribution in the very shallow region. The profile was measured on concrete slabs, and the high velocity of concrete and the compacted material below influenced the stacking velocities. The raw records show strong signals with velocities of $\sim 4000 \text{ m s}^{-1}$ that correspond to P-waves, and $\sim 1000 \text{ m s}^{-1}$ that most probably correspond to flexural waves in the slabs. This energy was attenuated first by amplitude scaling with t^2 up to 150 ms and second by a tight mute after normal move-out (Suppl. Tab. 1). Nevertheless, the high velocities of the consolidated material influence the stacking velocities that decrease strongly in the upper tens of milliseconds. This becomes particularly more obvious in the southern part of the profile, where peat layers also reduce the seismic velocities. To check the velocities derived by seismic processing (and therefore the processing itself), we conducted a S-wave VSP (vertical seismic profile) in the 22 m-deep Li-BPa borehole, as well as a gamma ray borehole survey (for position see Figs. 3 and 4, main article; Suppl. Fig 6). The distance to the seismic line is 13 m. We used the same source as used for the survey and a three-component borehole geophone that was lowered successively by 1 m to record two shots of opposite polarity. The results (Suppl. Fig. 6) show S-wave velocities between very low values of 70 m s^{-1} up to 330 m s^{-1} , where an upper zone of low velocities reaches down to 7 m and another one exists between 10 and 16 m. They positively correlate well with the gamma-ray log; i.e. low velocity values correspond to low gamma-ray values (Suppl. Fig 6). These values represent peat and fines (Fig. 5B, main article). The velocities in the VSP survey reach lower values than those derived from stacking velocities; this can be attributed to the much lower resolution of the stacking velocities. Seismic S-wave velocity shows lateral variations (compare Fig. 5B, main article and Suppl. Fig. 7) from higher values in the Saalian and Tertiary sediments with over 300 m s^{-1} TWT to very low values ($170\text{--}230 \text{ m s}^{-1}$ TWT) in the youngest sediments, especially the peat layers. These extremely low velocities testify to the unconsolidated nature of these sediments and support our stratigraphic interpretations.



Suppl. Fig. 6: Borehole geophysics from borehole Li-BPa. First column, borehole with lithological column. Colours see Figure 4, main article. Second column, S-wave velocity derived from a Vertical Seismic Profiling (VSP). Third column, gamma ray log.



Suppl. Fig. 7: S-wave velocity of the seismic profile.

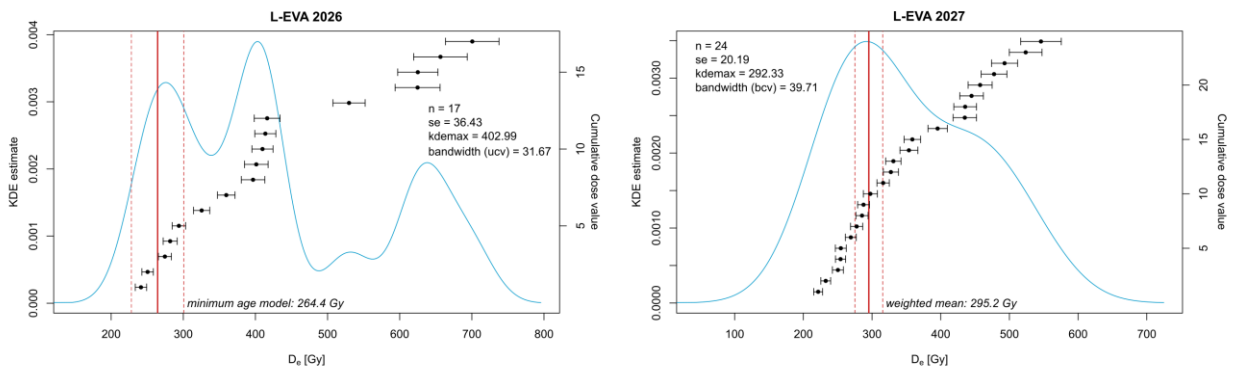
1	Correlation using recorded sweep
2	Vertical stack
3	Elevation static
4	Bad trace editing
5	True amplitude recovery (T^{**2})
6	AGC (150 ms)
7	Spectral whitening (20-160 Hz)
8	Time variant bandpass filter (60-160 Hz, 40-160 Hz)
9	Interactive velocity analysis
10	Normal moveout correction (100 % stretch mute)
11	Top mute of refracted and oscillating events
12	CDP stack (α trimmed mean, 20% excluded)
13	Tau-P filter (± 0.5 ms/trace)
14	Time-depth conversion (smoothed velocities)
15	Correction to final datum

Suppl. Tab. 1: Seismic processing stages.

4. Luminescence data evaluation

We utilized coarse-grained (125-180 μm) potassium-feldspar on account of its higher saturation values compared with quartz (Lauer et al., 2017) and the pIRIR290 protocol (Suppl. Tab. 2) (Thiel et al., 2011), as it is characterized by only negligible anomalous fading (Buylaert et al., 2012). First performance tests included dose recovery (residual-subtracted measured/given dose of 0.95) and anomalous fading (two samples below 1.6%/decade) on the samples L-EVA 1859 and 1862. These were taken from a neighbouring core with a very comparable sedimentology and expected time horizon. The ages of L-EVA 1859 and 1862 will be reported in a follow-up publication. For De-measurements, we mounted twenty-four small-sized aliquots (0.5 mm) per sample onto stainless steel discs, using with silicone spray. We measured on a Risø TL-DA-20 reader with an internal calibrated $^{90}\text{Sr}/^{90}\text{Y}$ beta source ($\sim 0.22 \text{ Gy s}^{-1}$) and IR light-emitting diodes (870 nm). The applied pIRIR290 protocol is summarized in Suppl. Tab. 2. Aliquots with a recycling ratio $>10\%$ and a recuperation $>5\%$ were excluded from further calculations. The equivalent doses for age calculations were established using kernel density estimates (KDE) by choosing the age model closest to the most meaningful KDE peak in terms of sedimentology and stratigraphy (Suppl. Fig. 7) (Galbraith and Roberts, 2012). Dose rates were determined with high-resolution germanium gamma spectrometry at the VTKA laboratory Dresden (Suppl. Tab. 3). Contributions of cosmic radiation and internal beta dose-rate were accounted for by following Prescott and Hutton (1994) and Huntley and Baril (1997), whereas alpha particle efficiency was approximated with an a -value of 0.11 (Kreutzer et al., 2014). In spite of comparable bandwidths selected for both luminescence samples in the KDE plots (31.67 for L-EVA 2026 and 39.71 for L-EVA 2027), their distributions differ substantially. L-EVA 2026 features multiple De-populations, presumable due to short-distance reworking of Saalian glaciofluvial sands with only partial bleaching during the process. Since the overlying stratum in core PD.030 is an undisturbed peat, we do not expect post-depositional mixing by cryo- or bioturbation. We consequently opted for the minimum age model after Galbraith et al. (1999), using the *r.luminescence* package (Burow, 2020), with the default settings and a σ_b -value of 0.1, which assumes 10% hypothetical overdispersion in an ideally bleached sample (Galbraith and Roberts, 2012). This model and the obtained De-value (264.4 Gy) best reflect the youngest population within our De-spectrum (Tab. 2, Suppl. Fig. 8). Sample L-EVA 2027 shows a more coherent and single-mode De-distribution, although a small shoulder in the KDE curve around 470 Gy indicates a distinct older population. For age

calculations, we chose the weighted mean (De-value of 295.2 Gy), which is nearly coincident with the main mode of the distribution. The ages (108.4 ± 17.0 ka for L-EVA 2026 and 104.6 ± 10.5 ka for L-EVA 2027) imply early Weichselian deposition and are therefore in compliance with the stratigraphy of the samples above the mid-Eemian stratum (cf. section 4.1, main article). They are also in excellent agreement with the end of the Eemian interglacial, as dated by Lüthgens et al. (2011) to 108.9 ± 7.8 ka in NE Germany. As we do not know how much time passed at our site before clastic sedimentation commenced after the Eemian, our ages primarily help constrain the chronology of the peat deposit between the sampling positions of L-Eva 2026 and L-EVA 2027, determined to be of Herning Stadial age (Tab. 1, sample 4, main article) (Menke and Tynni, 1984). The high OD-values ($33.3 \pm 1.4\%$ for L-EVA 2026 and $26.6 \pm 0.8\%$ for L-EVA 2027) could result from post-depositional mixing, incomplete bleaching and small-scale dose-rate differences (Jacobs and Roberts, 2007). We exclude post-depositional mixing because of seemingly intact overlying organogenic sediments in both cases. Incomplete bleaching could be an issue because of short transport distances of the grains on the slope. Dose rate variations are just as likely, keeping in mind that we took the samples from relatively broad (15 cm) segments of the cores.



Suppl. Fig. 8: D_e -distribution of the measured luminescence samples, plotted as Kernel Density Estimates (KDE). The KDE modes helped to choose the appropriate age models.

Step	Treatment
1	Dose
2	Preheat (320°C for 60s)
3	IRSL, 100s at 50°C
4	IRSL, 200s at 290°C → L _x
5	Test dose
6	Preheat (320°C for 60s)
7	IRSL, 100s at 50°C
8	IRSL, 200s at 290°C → T _x
9	IRSL, 100s at 325°C → hot bleach
10	Return to step 1

Suppl. Tab. 2: Measurement steps of the pIRIR₂₉₀ protocol.

Lab.-ID	Area (Core)	U (ppm)	Th (ppm)	K (%)	Cosmic Dose (Gy/ka)	DR _{total} (Gy/ka)	H ₂ O (%)
L-EVA							
2026	1 (PD.030)	1.6 ± 0.2	4.2 ± 0.3	1.4 ± 0.1	0.12 ± 0.01	2.44 ± 0.20	14.2 ± 10
2027	1 (PD.030)	4.7 ± 0.5	4.1 ± 0.3	1.1 ± 0.1	0.11 ± 0.01	2.82 ± 0.21	14.8 ± 10

Suppl. Tab. 3: Results of high-resolution gamma spectrometry and utilized water contents for luminescence measurements.

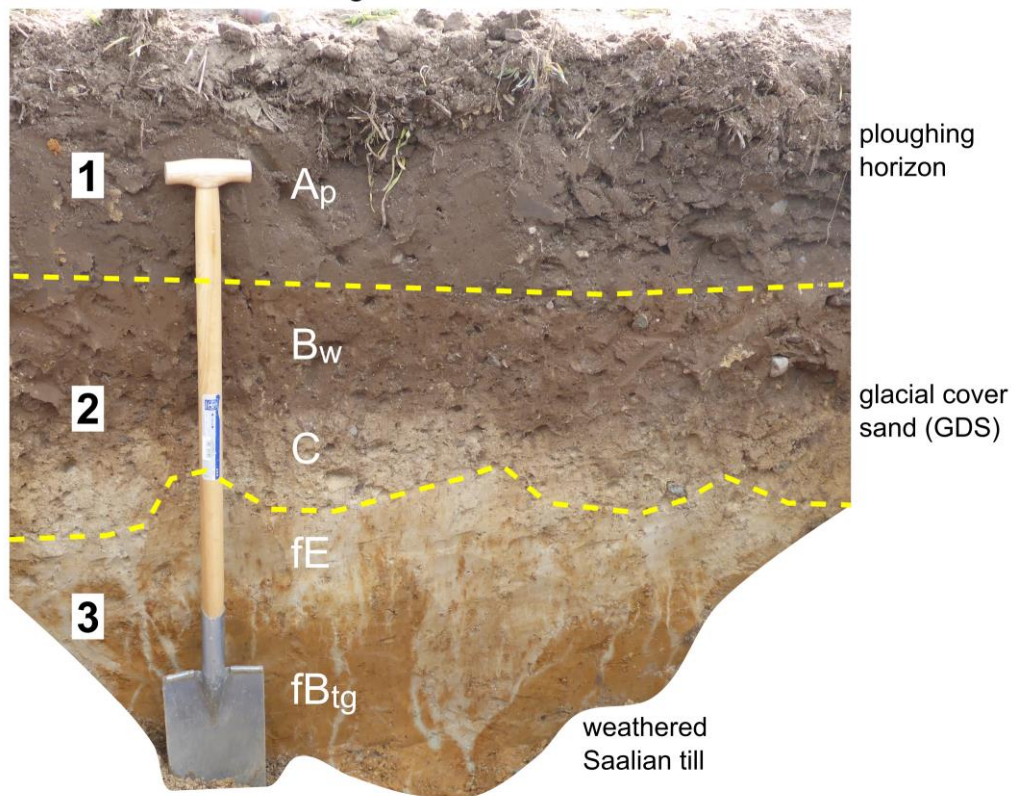
5. Interpretation of the geochemical values

Sample number 23 was taken from a terrestrial, non-hydromorphic soil. It shows low Corg contents (0.62%) and a very narrow C/N ratio of 8.0, in the typical range for present Central European forest soils with mull humus (Ad-hoc-Arbeitsgruppe Boden, 2005). These values suggest good soil aeration that promotes decomposition of organic material and lowering of the C/N ratio. This also explains the poor pollen preservation in this soil, rendering the pollen sample indeterminable (Tab. 1, main article). Samples 2, 24 and 25, which stem from semi-terrestrial half-bogs on the south-facing slope of the channel, feature medium Corg values (4.9 to 15.6%) and wider C/N ratios (16.1 to 25.6), indicating that decomposition of organic material was impaired and its accumulation was favoured by moistening. Again, these values are characteristic for half-bogs ('Anmoor' in German), according to AG Boden (2005). Finally, the samples from the forest peat at the bottom part of the channel reveal equally wide C/N ratios (21.7 and 24.6), but even higher Corg contents of 19.5 and 29.5%, pointing to a mesotrophic peat accumulation (Meier-Uhlherr et al., 2015). The Corg and C/N values successfully distinguish the humus-enriched layers and horizons along the Eemian zone of the transect and further justify its meaningful subdivision into a northern flank and a bottom part.

6. Eemian soil formation on Saalian glacial substrates

Generally, Eemian soils on Saalian glacial materials are known to form thick, orange-brown Bt-horizons with illuviated sesquioxides and clay, and their decalcification/weathering zone can exceed 4 m thickness in northern Germany. Thus, soil formation is assumed to have been more intense than in comparable Holocene soils on Weichselian tills. Additionally, the distinctive red colouring and less hydromorphic features in the soils suggest warmer and drier climate throughout their formation, as compared to the present interglacial (Roeschmann et al., 1982; Stephan, 2014; Stremme et al., 1982). At the position of core PD.021 we dug a prospection pit, exposing a pebbly and partly brunified Weichselian cover sand (Geschiebedecksand [GDS] in German) and the Eemian soil formed in a Saalian till (Suppl. Fig. 9). The upper part of the till has albic properties, being depleted in iron oxides and clay minerals (WRB, 2015). Along cracks and tongues, this albic fossil E horizon has started to consume the Btg horizon below. The Btg horizon is rich in clay and shows incipient stagnic properties. Overall, the decalcification depth of the Saalian till amounts to about 4 m (cf. cores PD.022 to 025; Suppl. Fig. 9; Fig. 4 in the main article). In terms of weathering intensity and depth, the findings confirm the statements on soil formation and stable surfaces in section 5.1 (main article). They also match the general properties known for such soils (see above). However, a possible weak Holocene continuation of pedogenesis cannot be reliably distinguished from that of the Eemian in this test pit (cf. Roeschmann et al., 1982).

Cambisol over albic, stagnic Endoluvisol



Suppl. Fig. 9: Soil exposure at the position of PD.022 (see Fig. 4, main article), showing weathered Saalian till caused mainly by Eemian pedogenesis. The length of the spade is about 110 cm.

APPENDIX III: SUPPLEMENTARY INFORMATION FOR CHAPTER IV

Supplementary Information S1 – Sections 1 to 4

Archaeology and Artefact Analyses

Neanderthals in changing environments from MIS 5 to early MIS 4 in northern Central Europe – Integrating archaeological, (chrono)stratigraphic and paleoenvironmental evidence at the site of Lichtenberg

Marcel Weiss^{*1,2}, Michael Hein^{*1}, Brigitte Urban³, Mareike C. Stahlschmidt¹, Susann Heinrich¹, Yamandu H. Hilbert², Robert C. Power^{4,1}, Hans v. Suchodoletz⁵, Thomas Terberger⁶, Utz Böhner⁶, Florian Klimscha⁷, Stephan Veil⁷, Klaus Breest⁸, Johannes Schmidt⁵, Debra Colarossi^{9,1}, Mario Tucci³, Manfred Frechen¹⁰, David Colin Tanner¹⁰ & Tobias Lauer¹

¹Max Planck Institute for Evolutionary Anthropology, Leipzig, Germany

²Institut für Ur- und Frühgeschichte, Friedrich-Alexander-Universität Erlangen-Nürnberg, Erlangen, Germany

³Leuphana University Lüneburg, Institute of Ecology, Lüneburg, Germany

⁴Institute for Pre- and Protohistoric Archaeology and Archaeology of the Roman Provinces, Ludwig Maximilian University Munich, Germany

⁵Institute of Geography, Leipzig University, Leipzig, Germany

⁶State Service for Cultural Heritage Lower Saxony, Hannover, Germany

⁷Lower Saxony State Museum, Department for Research and Collections, Archaeology Division, Hannover, Germany

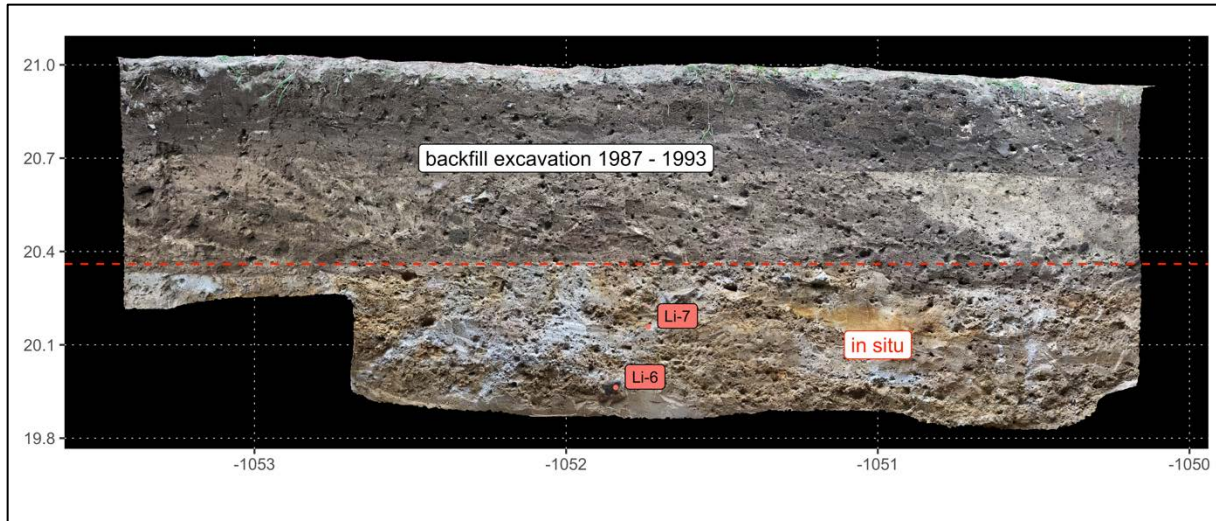
⁸Volunteer archaeologist, Berlin, Germany

⁹Department of Geography and Earth Sciences, Aberystwyth University, Aberystwyth, Wales, UK

¹⁰Leibniz Institute for Applied Geophysics, Stilleweg 2, Hannover, Germany

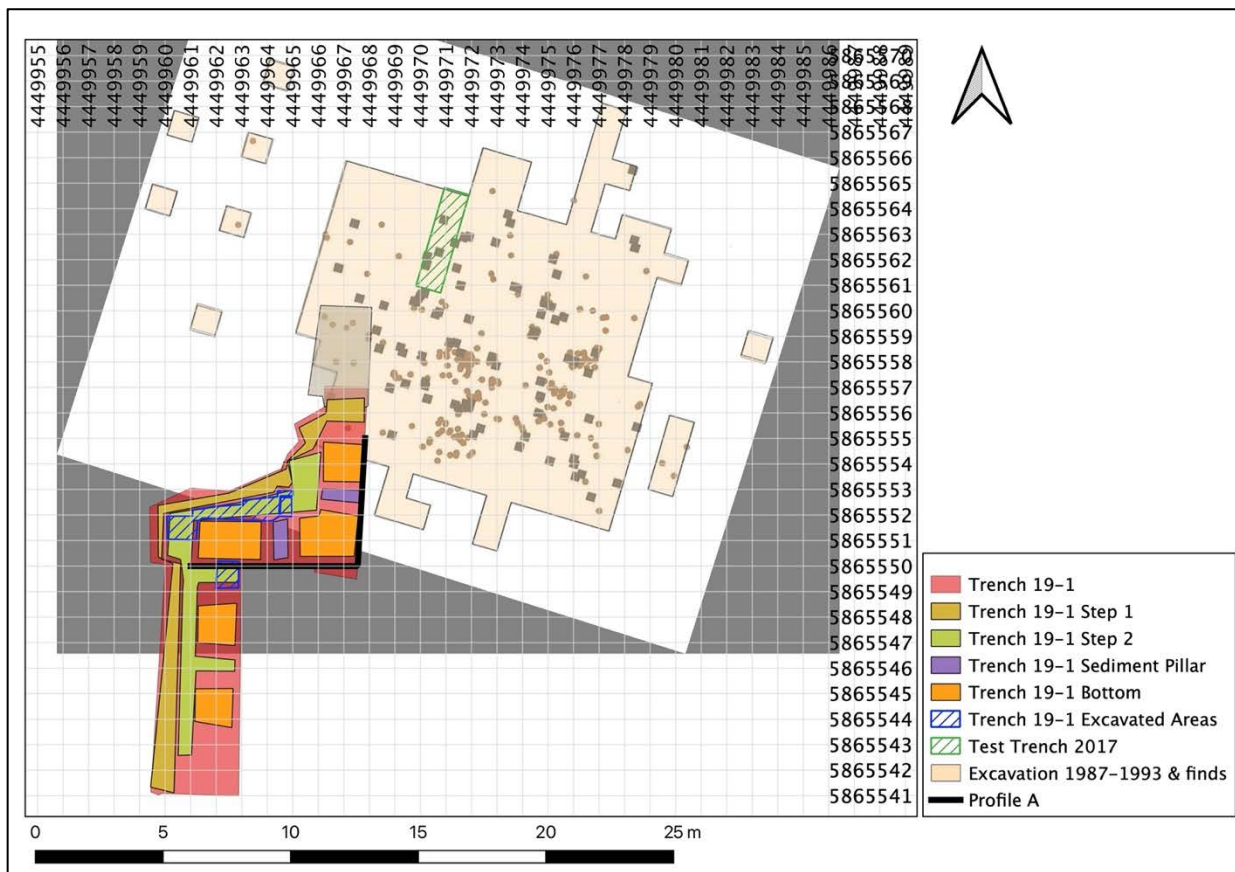
Section 1: Excavation Lichtenberg I and II

Lichtenberg I: 2017

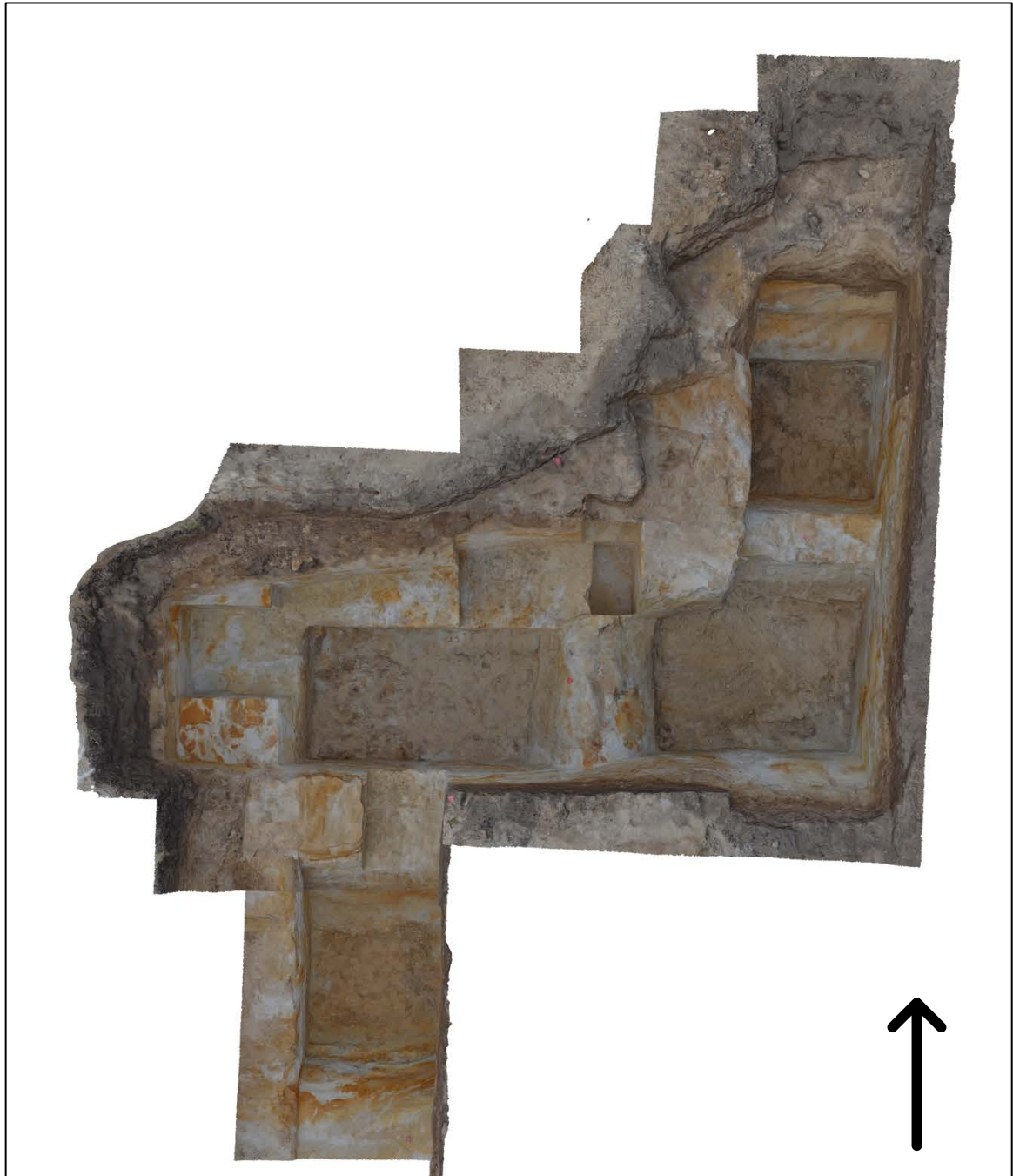


Supplementary Figure S1. Test trench 2017, East profile. Li-7: Keilmesser from Layer 7', Li-6: fragment of a bifacial tool from Layer 7'. Orthophoto created with Agisoft Metashape.

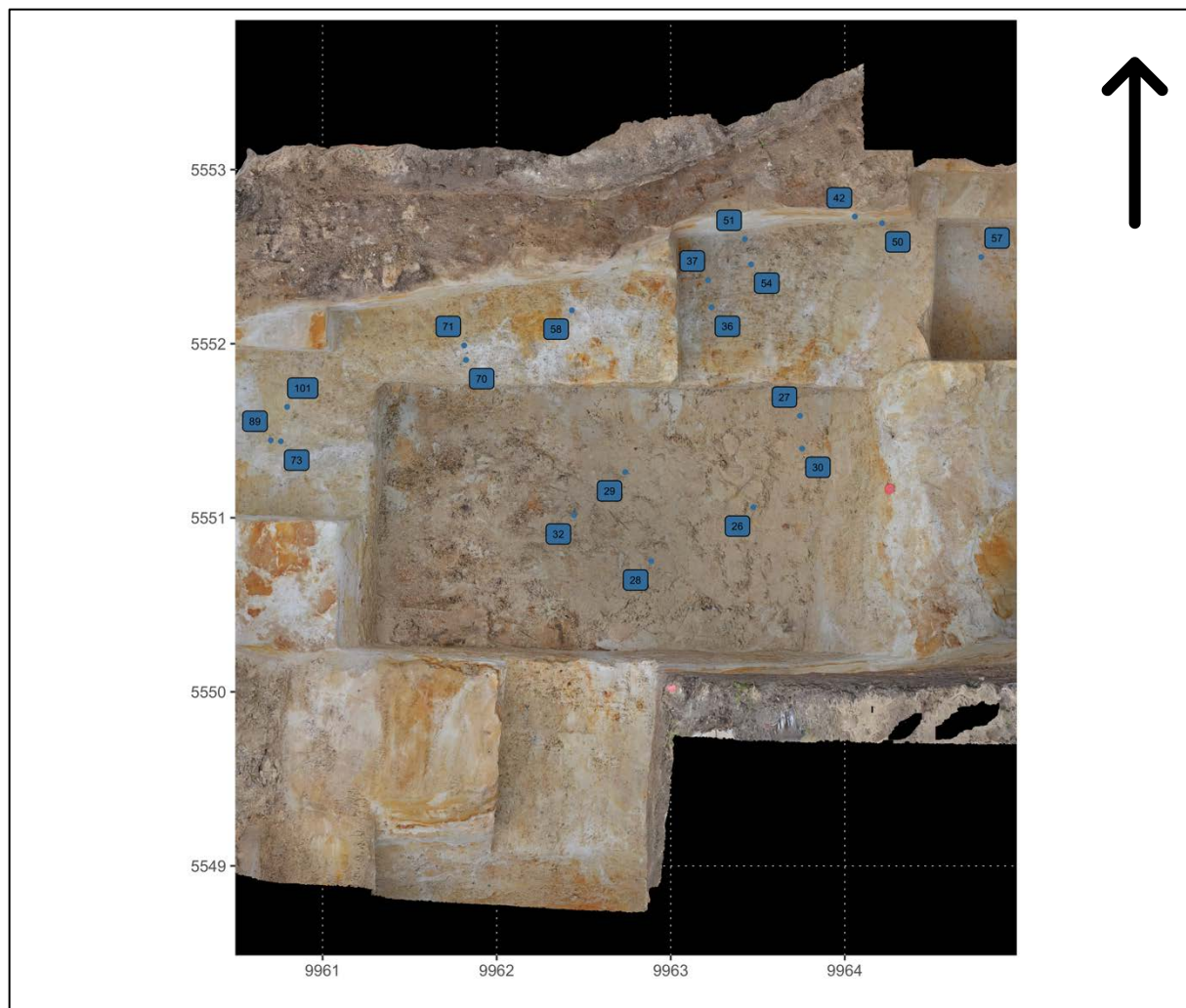
Lichtenberg I: 2019



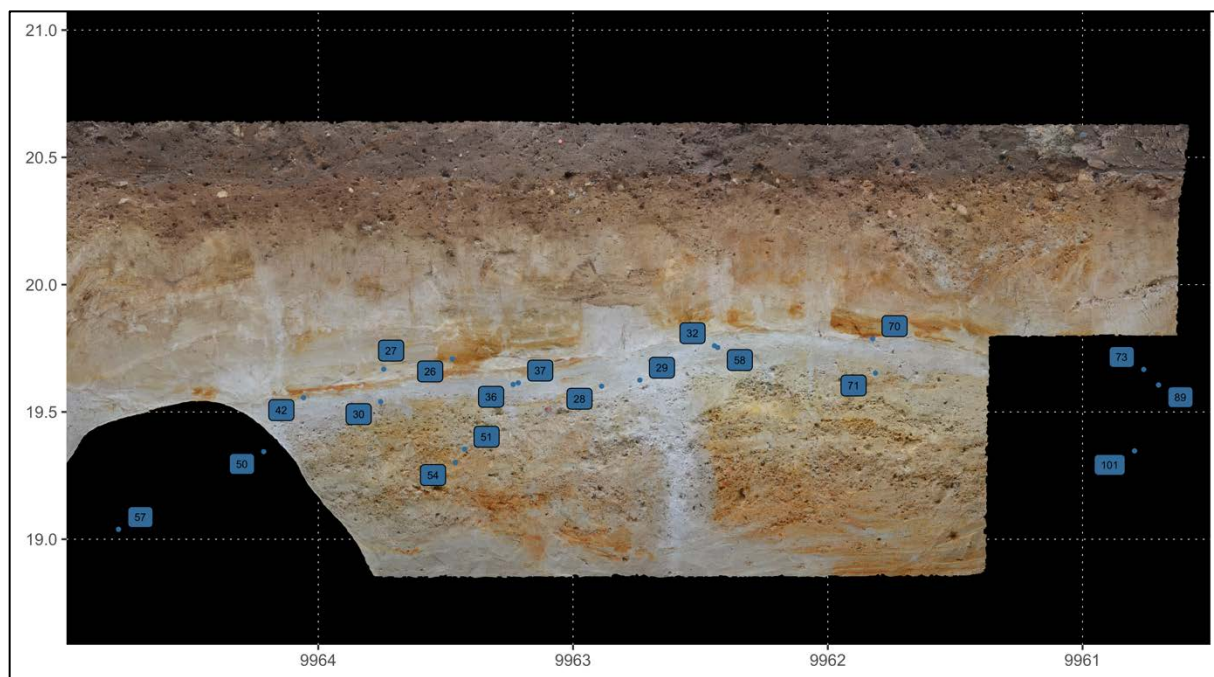
Supplementary Figure S2. Excavation plan Lichtenberg I. Plan created with QGIS 3.12.3.



Supplementary Figure S3. Ortho view Trench I. 3D model created with Agisoft Metashape.



Supplementary Figure S4. Orthographic view of the excavated area and find numbers of artefacts $\geq 15\text{mm}$. Orthophoto created with Agisoft Metashape.



Supplementary Figure S5. Trench 1, South profile with plotted artefacts $\geq 15\text{mm}$, Layer 7 and Layer 8. Orthophoto created with Agisoft Metashape.

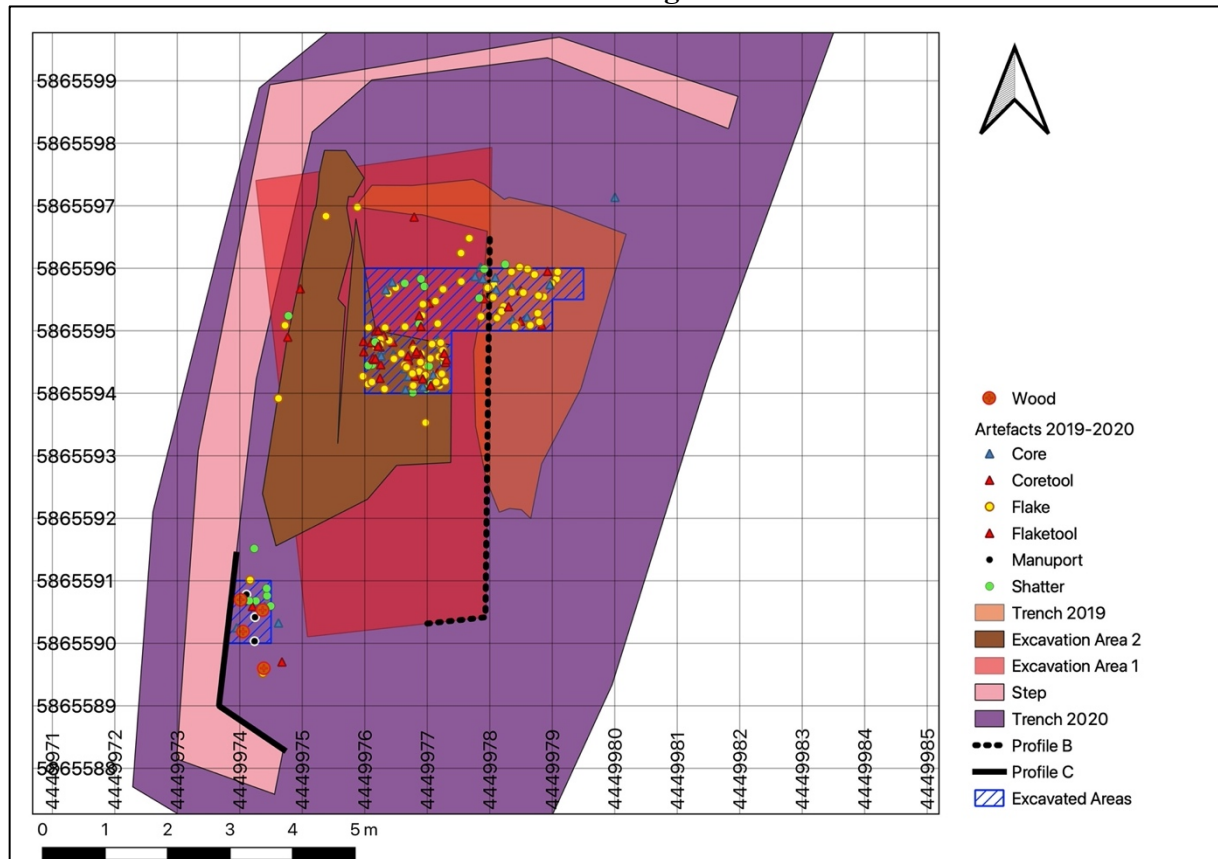


Supplementary Figure S6. Flake LIA-36 in situ in Layer 7 (formerly: Layer package 2).
Photo: M. Weiss.



Supplementary Figure S7. Flake LIA-50 (N) and undiagnostic flint fragment (E) in situ in Layer 8 (formerly: Layer package 2). Photo: M. Weiss.

Lichtenberg II





Supplementary Figure S10. Endscraper LIA-285 in situ in Layer 11a. Photo: M. Weiss.

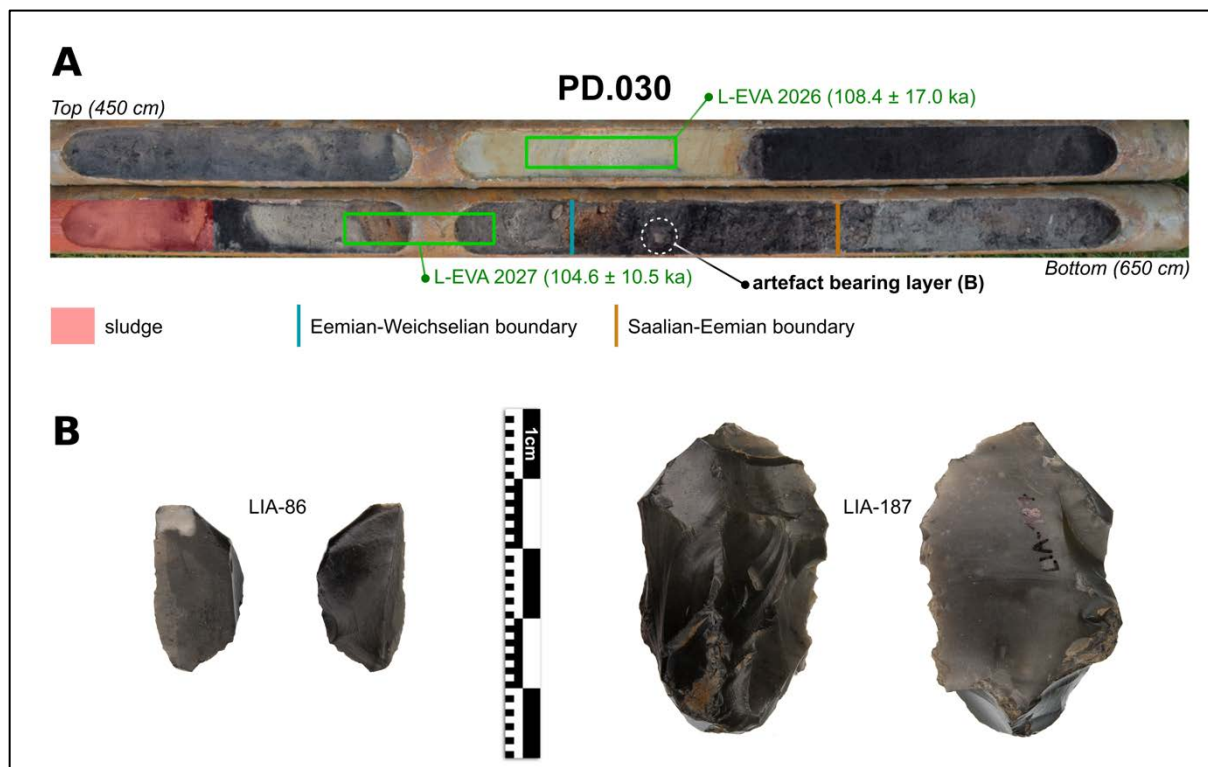


Supplementary Figure S11. Core LIA-335 in situ in Layer 11a. Photo: M. Weiss.



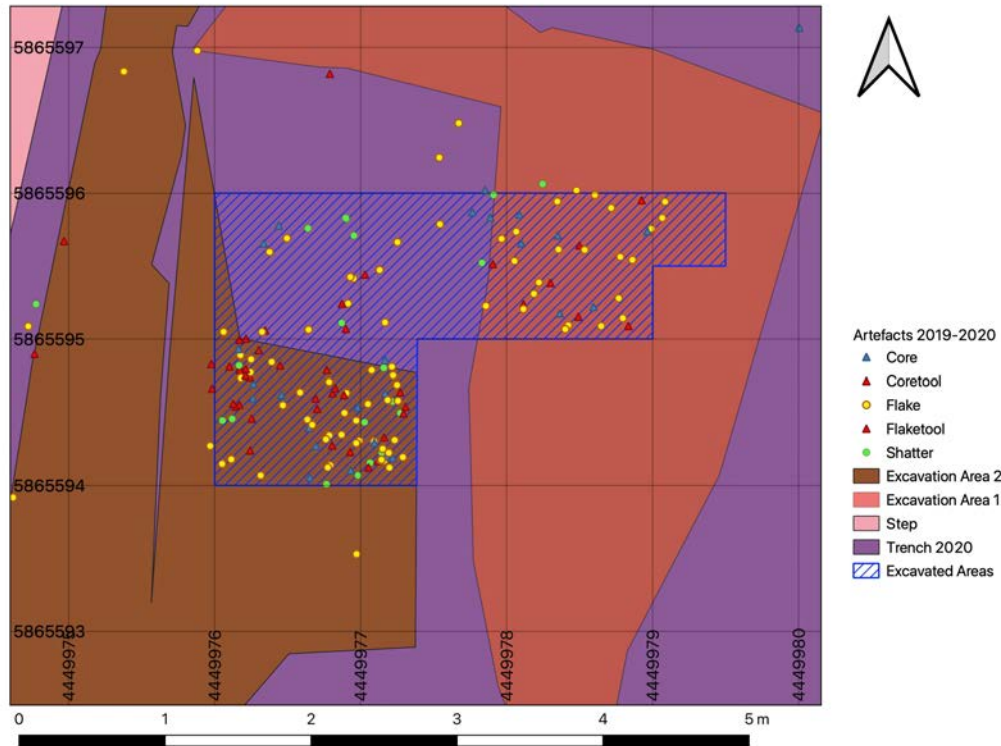
Supplementary Figure S12. Tool LIA-478 in situ in Layer 11a, with a charcoal concentration in the East. Photo: M. Weiss.

Lichtenberg III



Supplementary Figure S13. A: Core PD.030 with the position of the Eemian artefacts. B: Flakes LIA-86 and LIA-187 from the Eemian Layer. Photos: M. Weiss.

Section 2: Analysis of the find horizon Lichtenberg II



Supplementary Figure S14. Plan of the excavation and position of the excavated squares. Finds outside the excavated squares were made during the preparation of the excavation and the West-profile. Plotted are alle artefacts $\geq 15\text{mm}$. In the following analysis, squares are named based on the last 4 digits of the coordinates. Plan created with QGIS 3.12.3

Preface

In the following, we present our analysis of the find horizon (humic sand) from the squares excavated in 2020. The squares are named based on the last 4 digits of the coordinates. The goal of the analysis is to evaluate whether there exists a single, or more than one find horizon within the humic sand. Small lithics <1.5 cm are prone to dislocation by post depositional processes (animal trampling, cryoturbation, sediment movements). Therefore, the small lithics between 4 mm and 1.49 cm from the screen were counted from each excavated bucket from each quarter square. This resulted in several plots presented in the first section.

Additionally, the position of the lithics >1.49 cm was added to the individual plots. This is to see if accumulations of small and large finds are distributed similarly. A further analysis of the depths follows in Section 2.2.

Further, the thickness of the datapoints in the diagrams displays the gravel content of each bucket. In Section 2.3, we analyze the relationship between small lithics and gravel content further. This is to evaluate whether gravels and small lithics are affected equally by post depositional processes. In the reverse that means, if the depths of the small lithic counts show no clear find horizon but they correlate with gravel content, post depositional disturbances of the find horizon are probable.

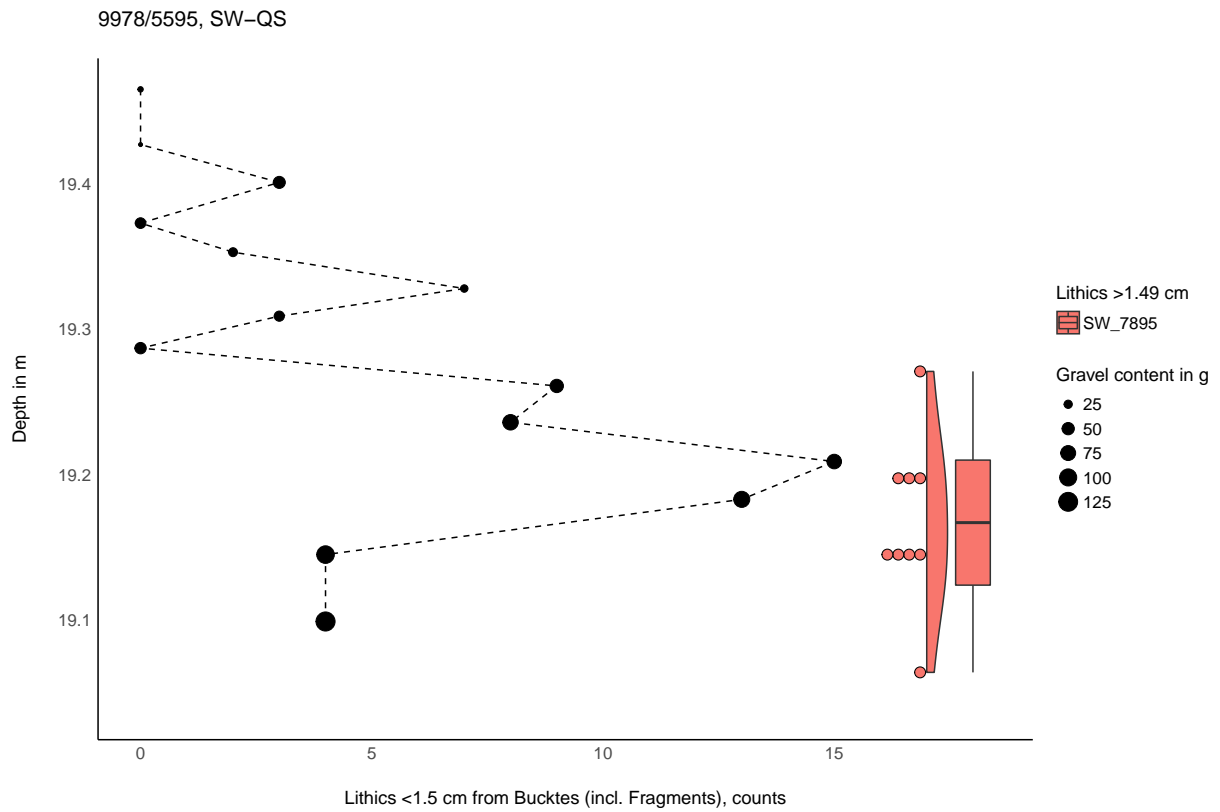
An interesting feature of the Li-II assemblage is that lithics are relatively small (see further Supplementary Section 3.4). Cores from small nodules already hint that this may be due to small raw material available at the site. Therefore, we checked raw material size sampled from the excavation area in relation to artefact size in Section 2.4.

This section was written in RMarkdown.

2.1. The lithics <1.5 cm of the individual quarter squares

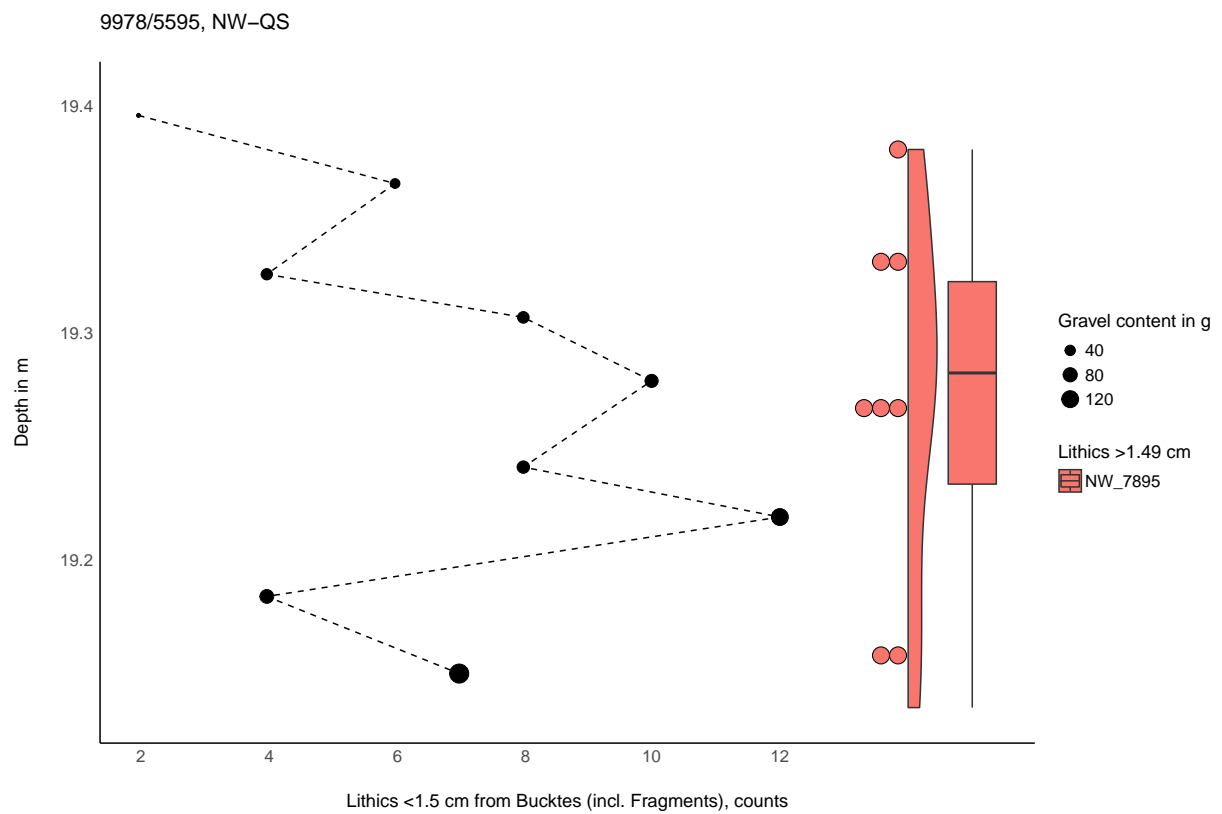
2.1.1 square 9978/5595

2.1.1.1 9978/5595 Southwest-Quarter Square



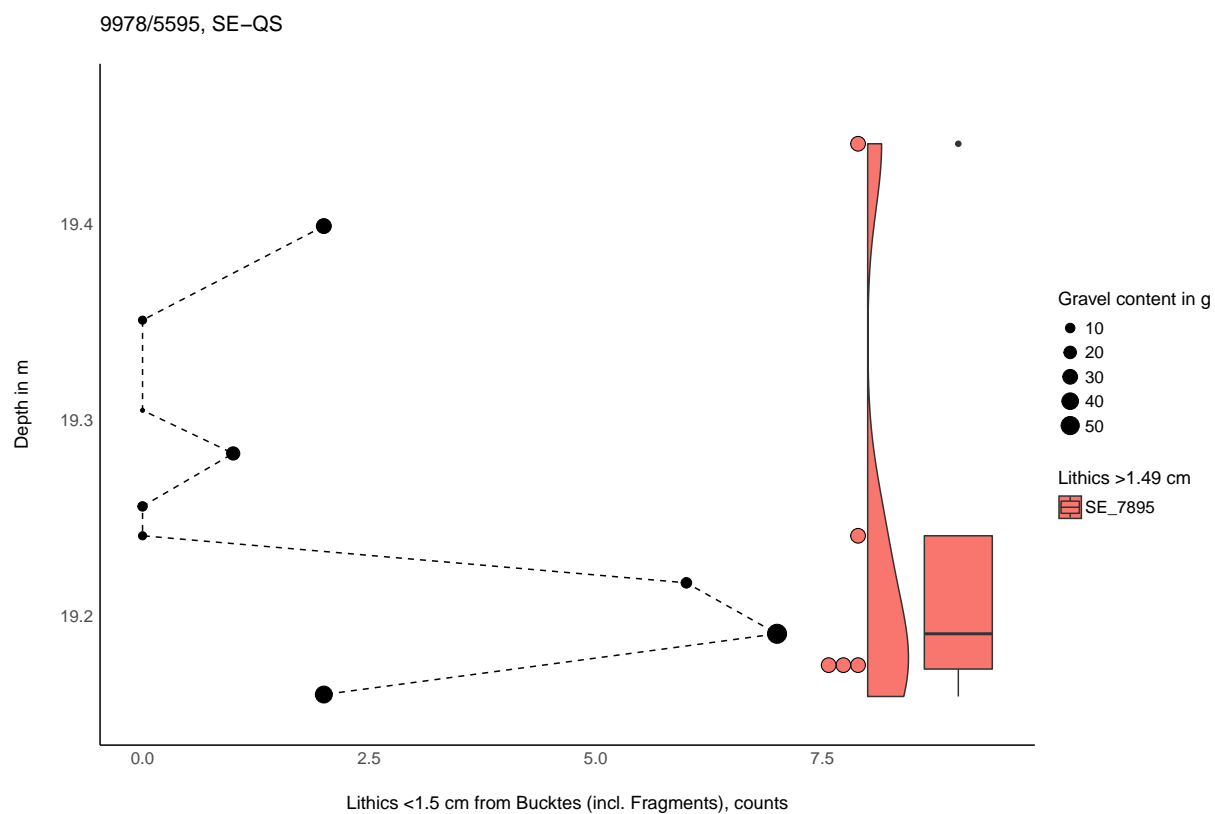
Supplementary Figure S15.

2.1.1.2 9978/5595 North-West Quarter Square



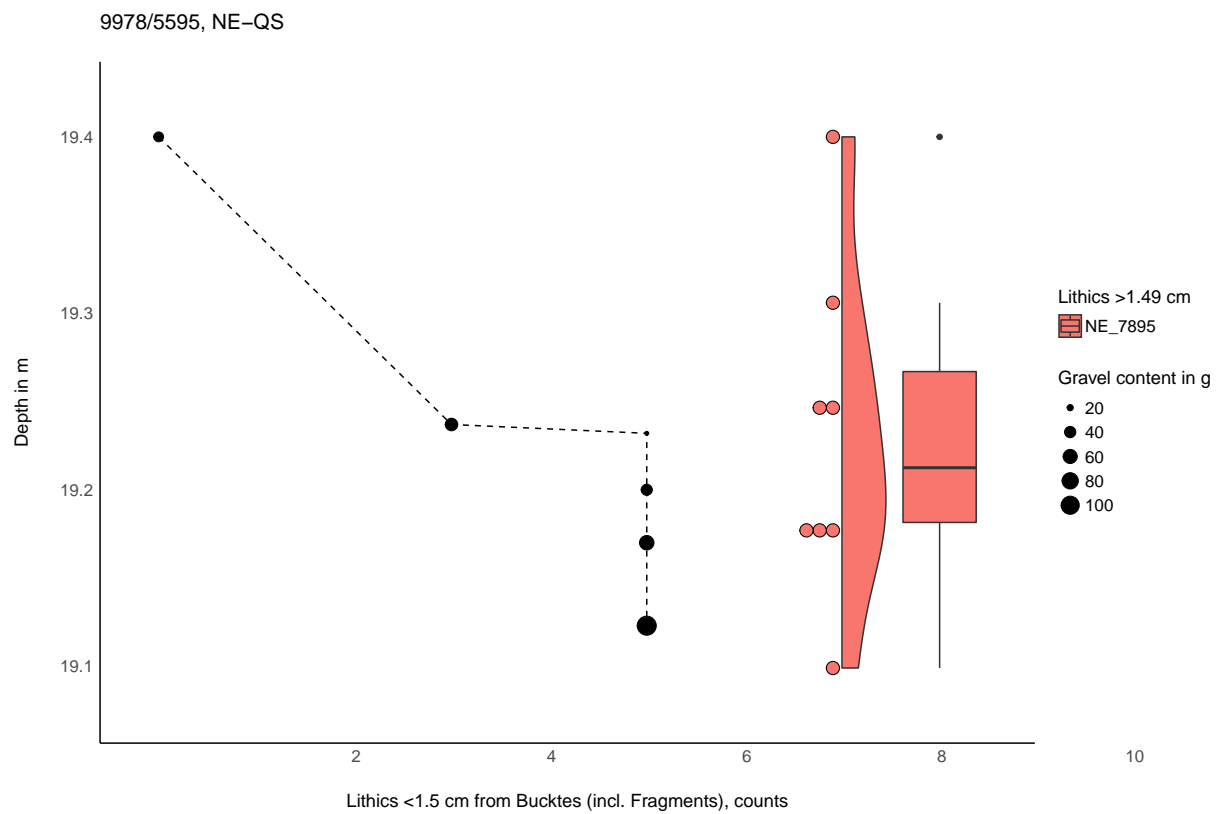
Supplementary Figure S16.

2.1.1.3 9978/5595 Southeast-Quarter Square



Supplementary Figure S17.

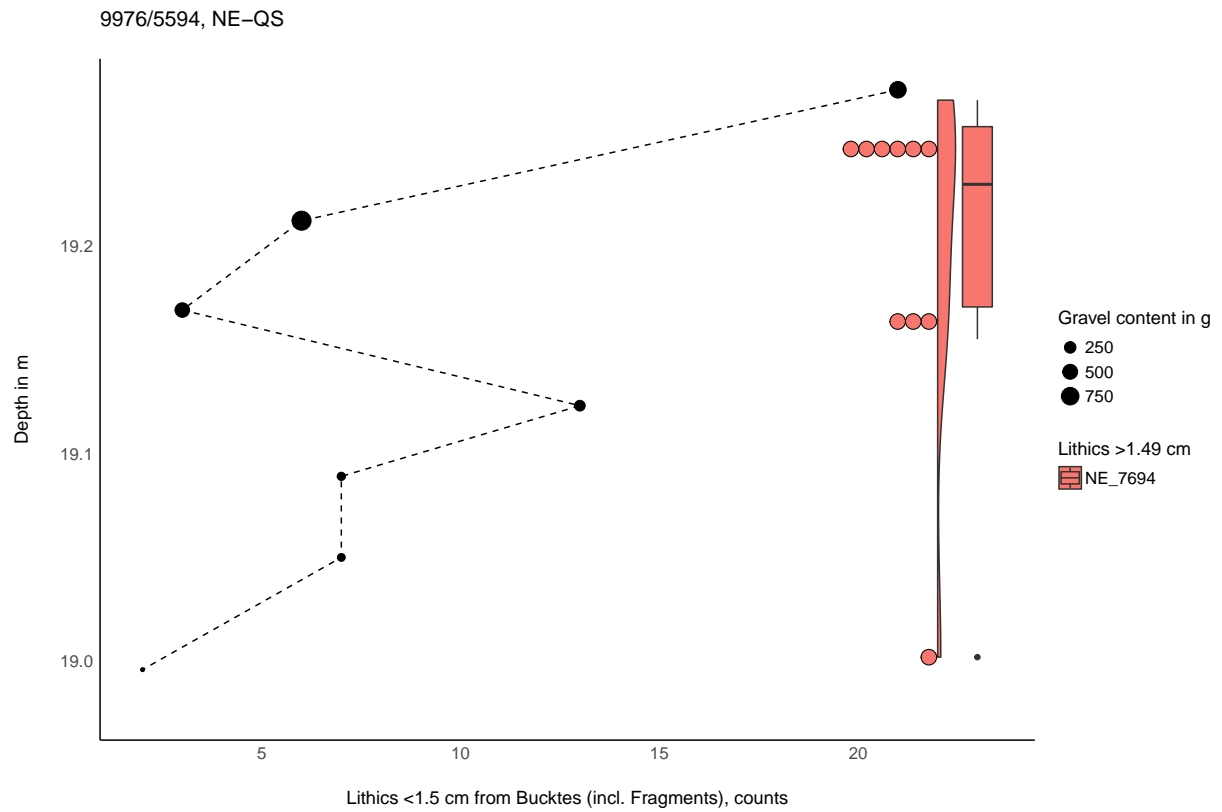
2.1.1.4 9978/5595 North-East Quarter Square



Supplementary Figure S18.

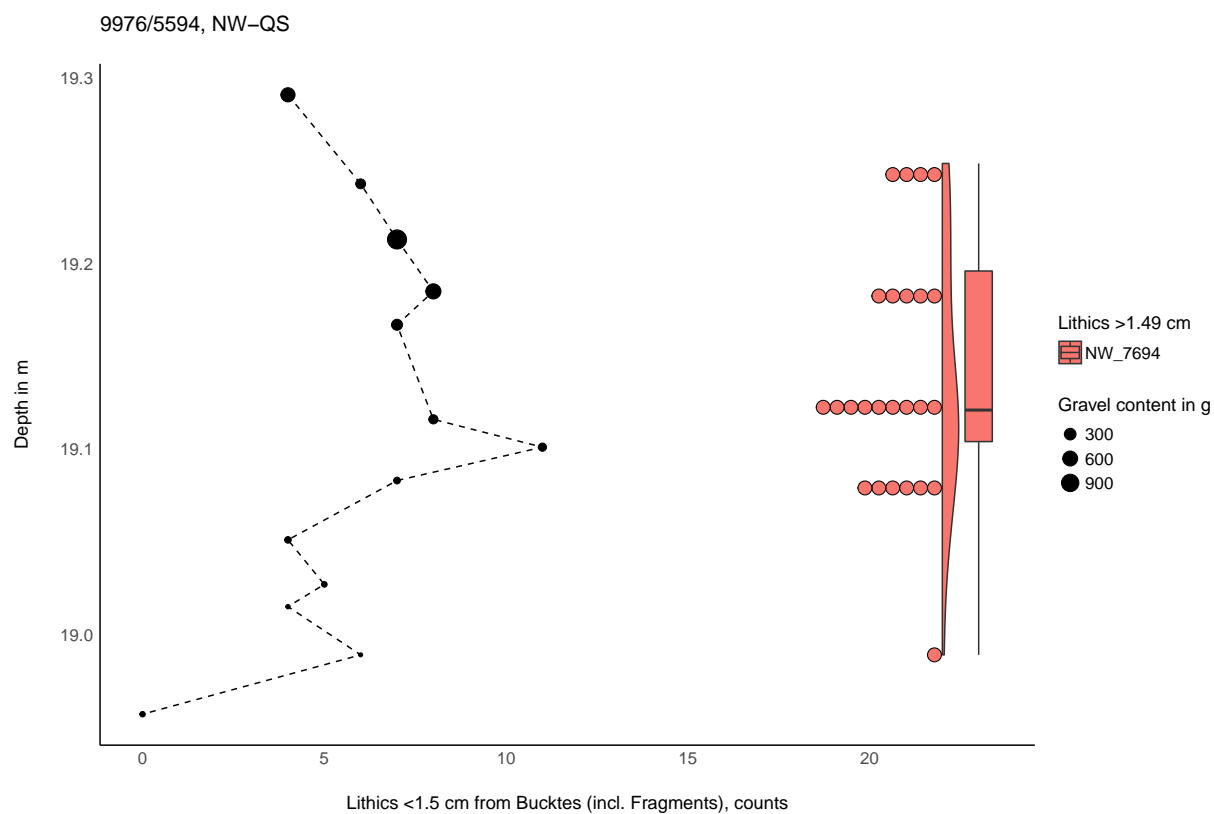
2.1.2 Square 9976/5594

2.1.2.1 9976/5594 North-East-Quarter Square - Top removed by excavator



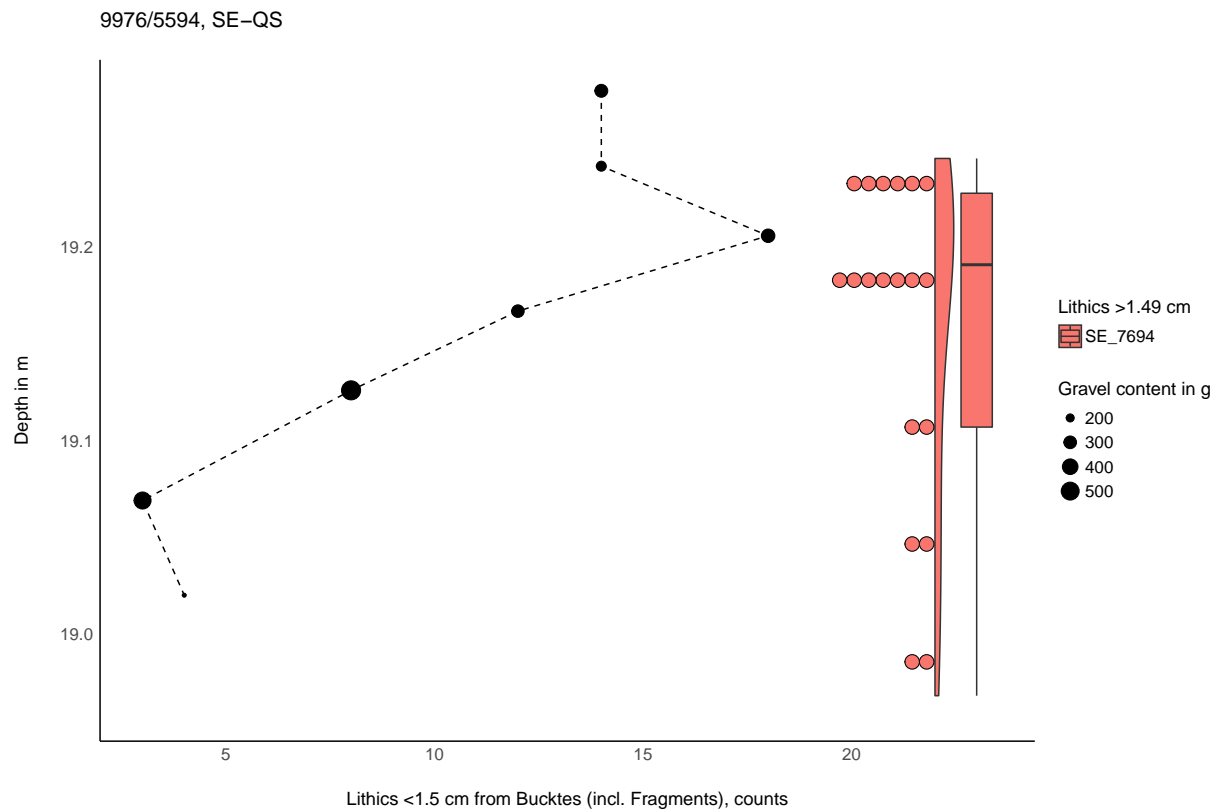
Supplementary Figure S19.

2.1.2.2 9976/5594 North-West-Quarter Square - Top removed by excavator



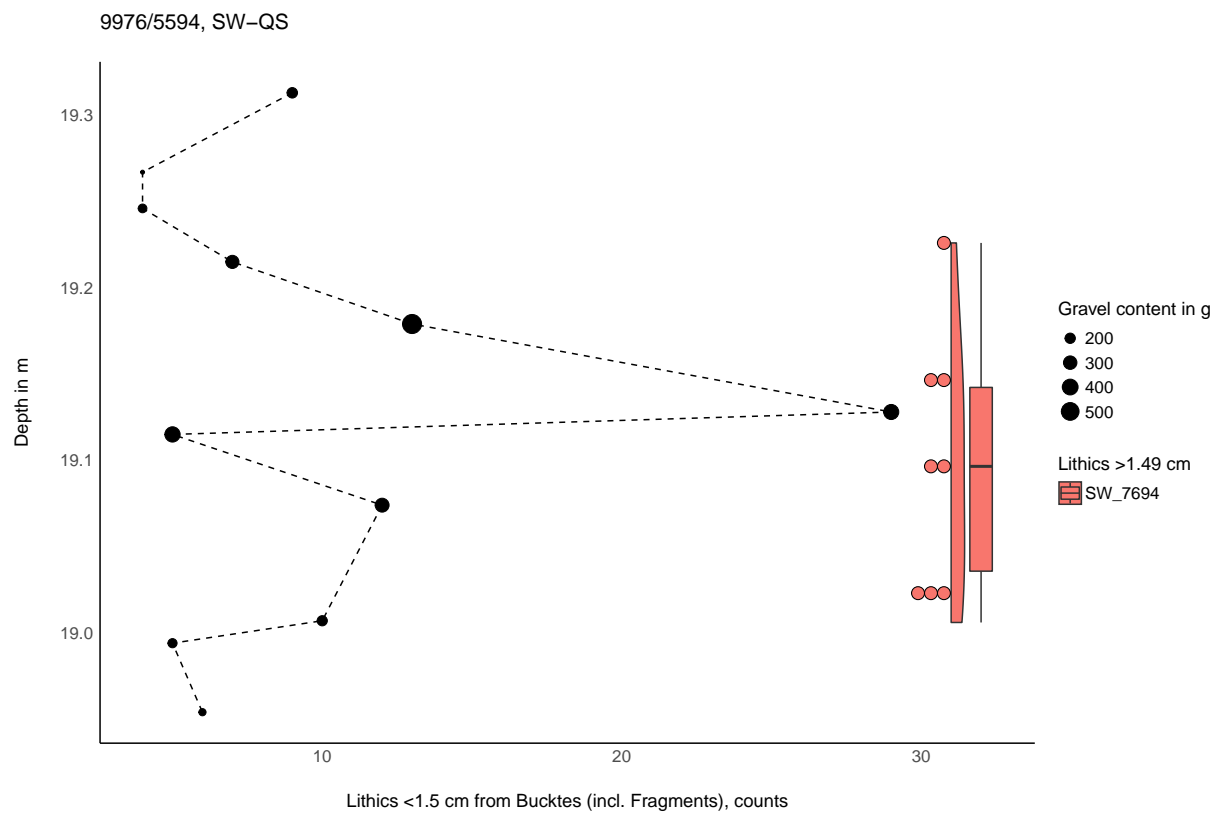
Supplementary Figure S20.

2.1.2.3 9976/5594 South-East-Quarter Square - Top removed by excavator



Supplementary Figure S21.

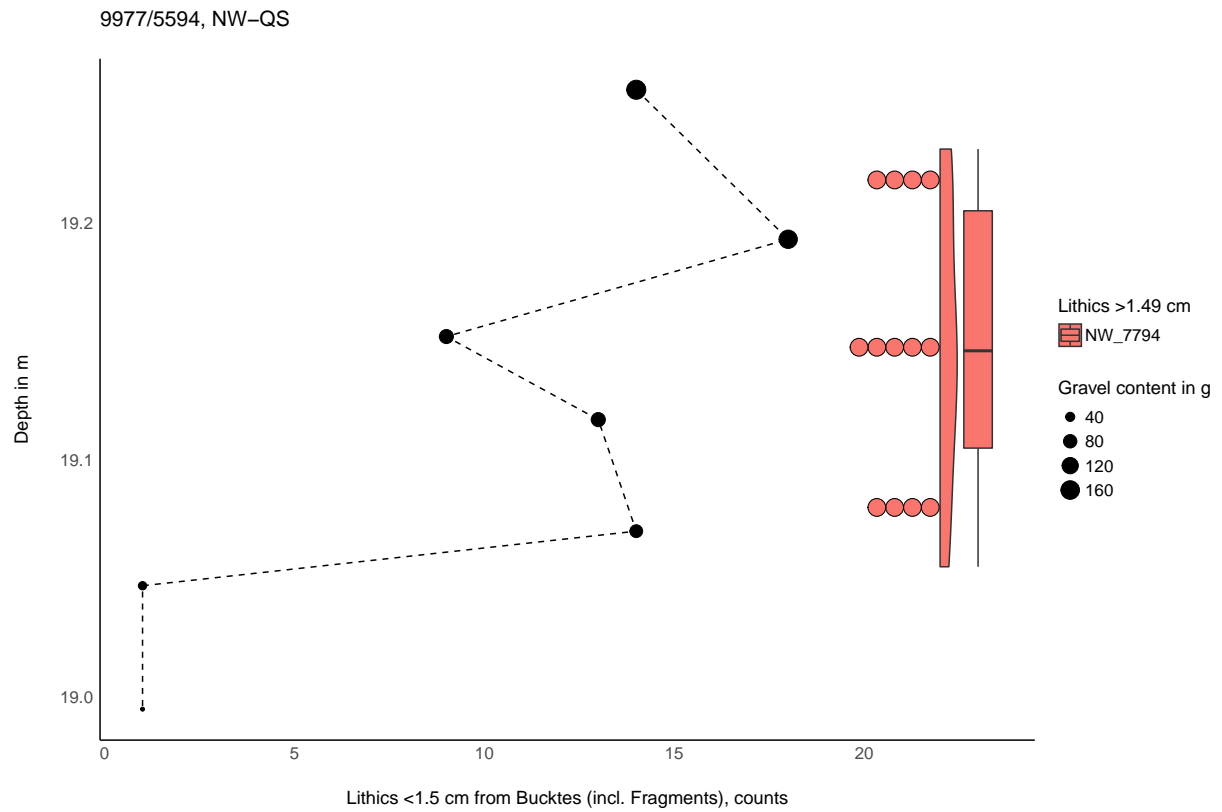
2.1.2.4 9976/5594 South-West-Quarter Square - Top removed by excavator



Supplementary Figure S22.

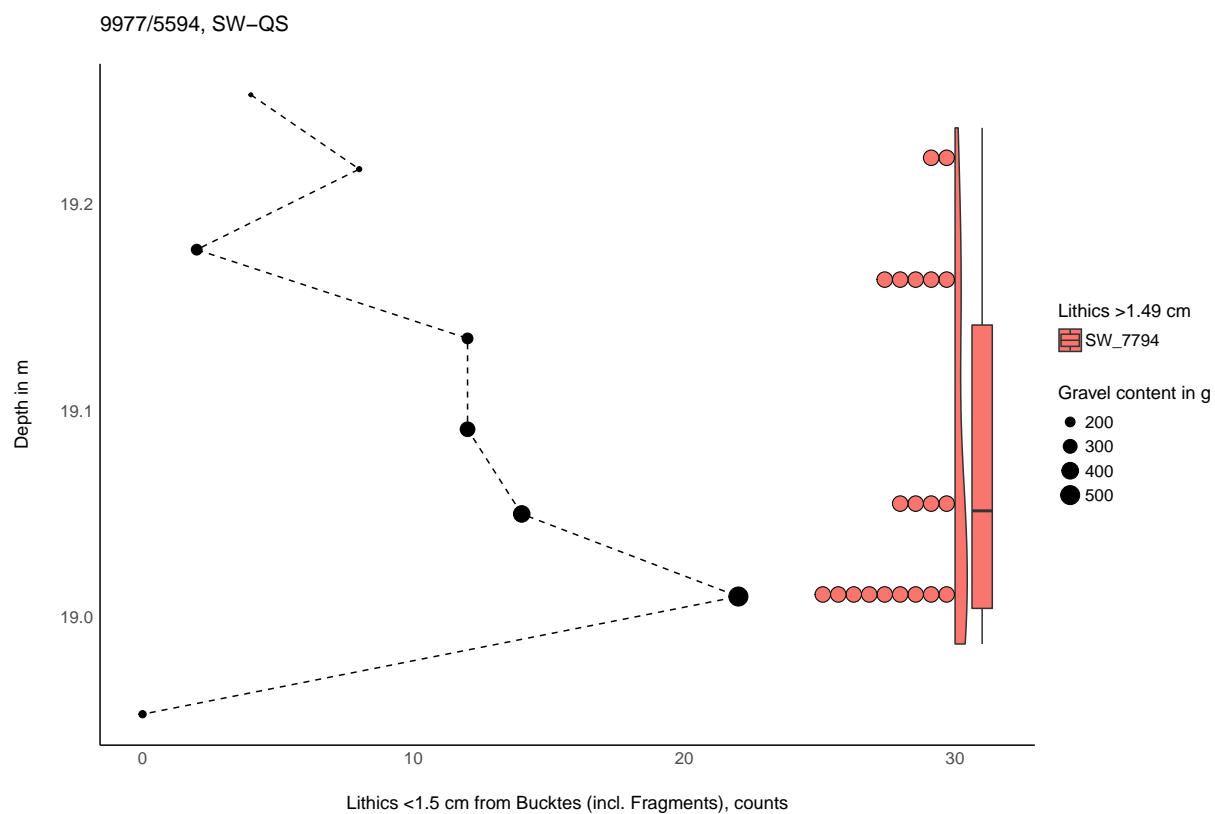
2.1.3 Square 9977/5594

2.1.3.1 9977/5594 North-West-Quarter Square - Top removed by excavator



Supplementary Figure S23.

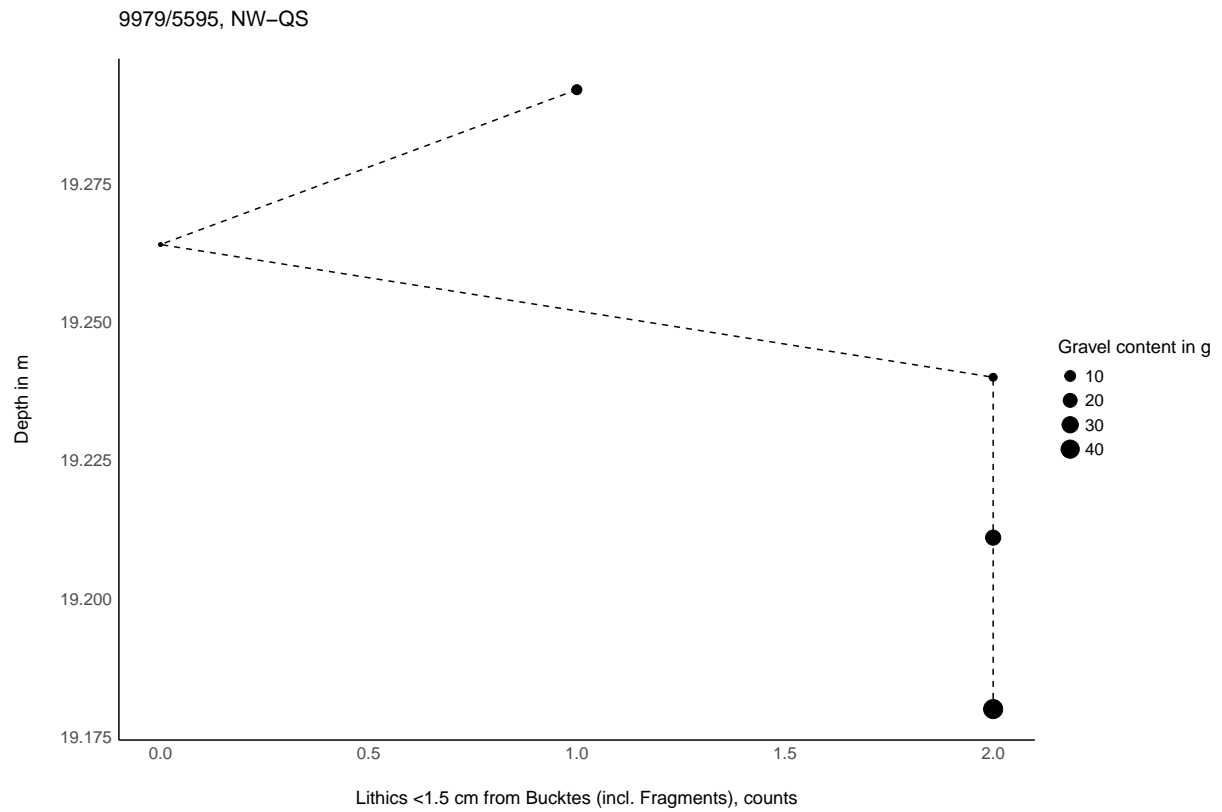
2.1.3.2 9977/5594 South-West-Quarter Square - Top removed by excavator



Supplementary Figure S24.

2.1.4 Square 9979/5595

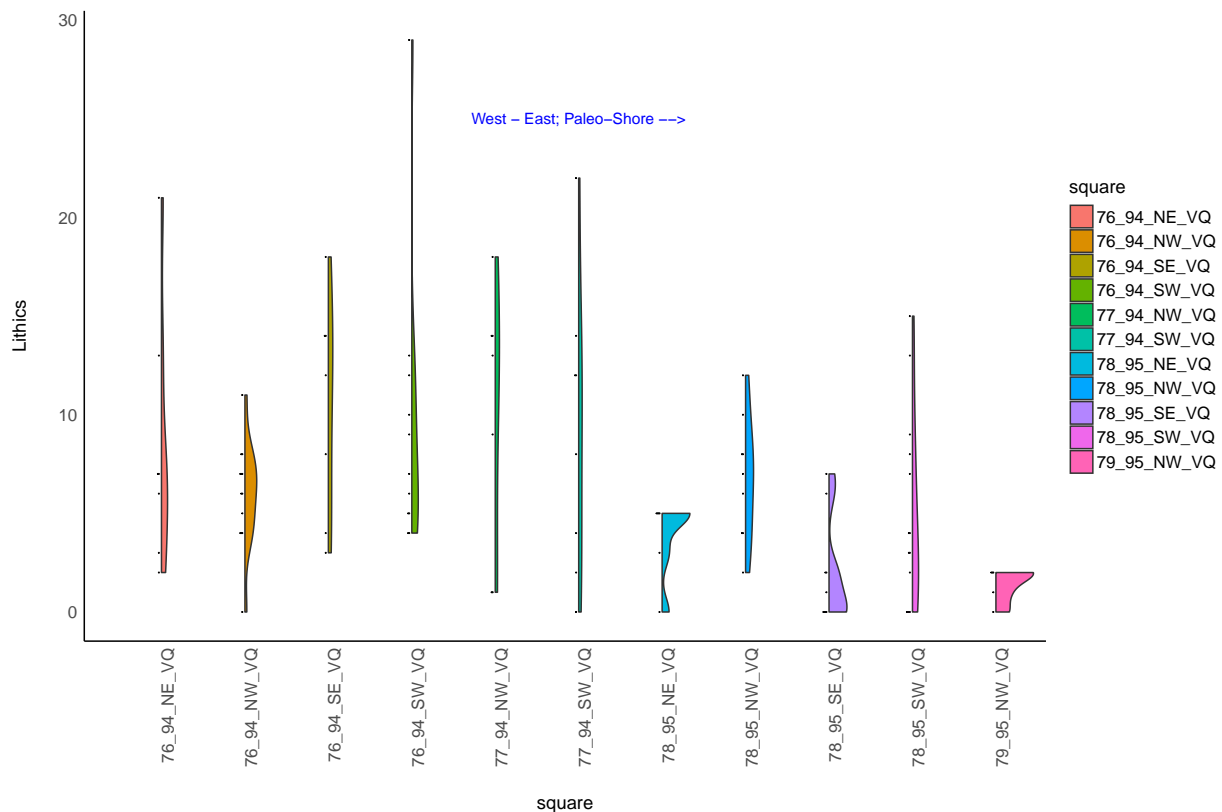
2.1.4.1 9979/5595 North-West Quarter Square



Supplementary Figure S25.

2.1.5 Lithic counts <1.5 cm from all squares

To summarize, the small lithics from all squares are plotted below (Figure S26). The diagram indicates that the lithic counts decrease towards the suspected paleoshore in the East. This may be due to human behavior and the spatial distribution of the artefacts at the site. On the other hand, this could be an artefact of the excavation circumstances, as we had to stop at a specific depth due to the ground water table. It may be that the artefact concentrations of the find horizon dipped down towards the paleoshore, but we could not reach them. We will check this in a future campaign when the ground water table is lower.



Supplementary Figure S26.

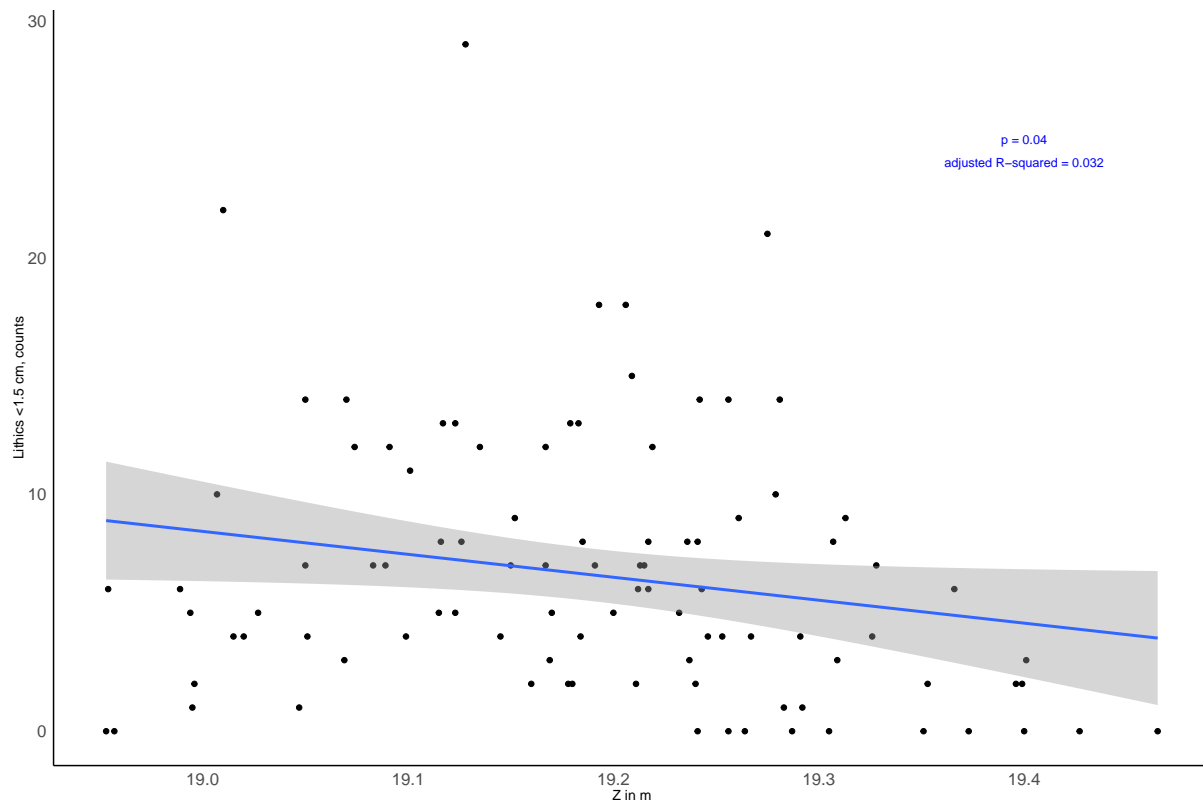
2.2 Further inspection of lithics and depth

2.2.1 The relationship between artefact <1.5 cm counts and Z

The results of a linear model reveal a relationship between small lithic counts and depth:

```
##
## Call:
## lm(formula = All_Buckets$Lithics ~ All_Buckets$Z)
##
## Residuals:
##   Min    1Q  Median    3Q   Max
## -8.893 -3.986 -1.390  2.675 21.803
##
## Coefficients:
```

```
##           Estimate Std. Error t value Pr(>|t|)
## (Intercept)  192.469    91.220   2.110  0.0375 *
## All_Buckets$Z -9.686     4.754  -2.038  0.0444 *
## ---
## Signif. codes:  0 '***' 0.001 '**' 0.01 '*' 0.05 '.' 0.1 ' ' 1
##
## Residual standard error: 5.466 on 94 degrees of freedom
## Multiple R-squared:  0.0423, Adjusted R-squared:  0.03211
## F-statistic: 4.152 on 1 and 94 DF, p-value: 0.0444
```



Supplementary Figure S27. The relationship between small artefact <1.5 cm counts and depth.

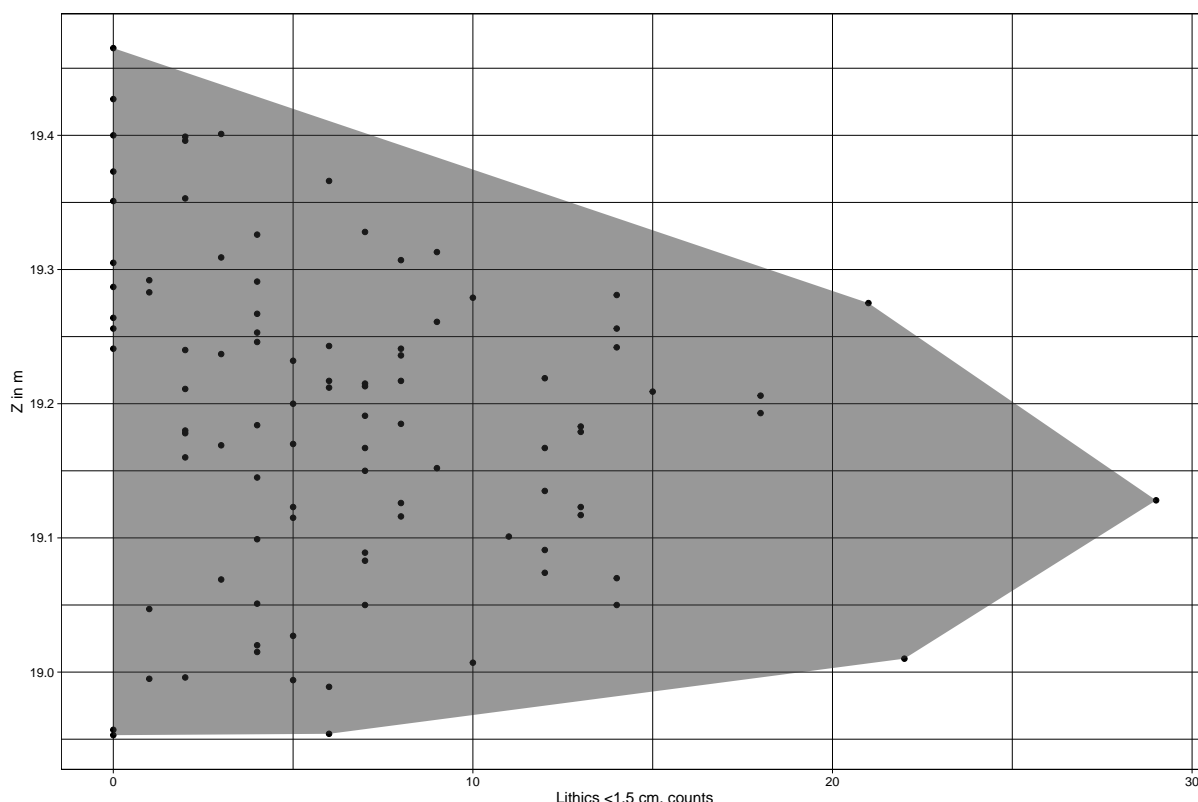
The plot of the linear model in Figure S27 shows that there is a significant relationship (at a p-value of 0.05) between the small find counts and depth.

This result is further reinforced by the following plot (Figure S28) of the small lithic counts from all quarter squares and depth. Here, a convex hull illustrates the distribution range.

The results indicate that there is a find horizon within the humic sand around a depth of $Z = 19.2$ m. However, the small artefacts scatter within the entire range. This may be due to small lithics being more prone to dislocation within the sediment than the larger artefacts. Therefore, we need to look again at the distribution of artefacts >1.49 cm within the humic sand:

2.2.2 Artefacts >1.49 cm and depth

From the plots above (Figures S15-S25) we gain the impression that the large finds are also distributed somewhat randomly within the humic sand. Therefore, let's plot all the large finds



Supplementary Figure S28. Small artefact <1.5 cm counts and depth.

together (We included the artefacts found in the test excavation 2019 and the lithics from the 2020 campaign.), illustrated in Figure S29.

Comparable to the results for the small lithics, the plot in Figure S29 shows that most artefacts >1.49 cm are concentrated between $Z = 19.09$ m and $Z = 19.24$ m. Let's take a closer look at the distribution:

```
##  Min. 1st Qu.  Median  Mean 3rd Qu.  Max.
## 18.84 19.09 19.17 19.17 19.24 19.55
```

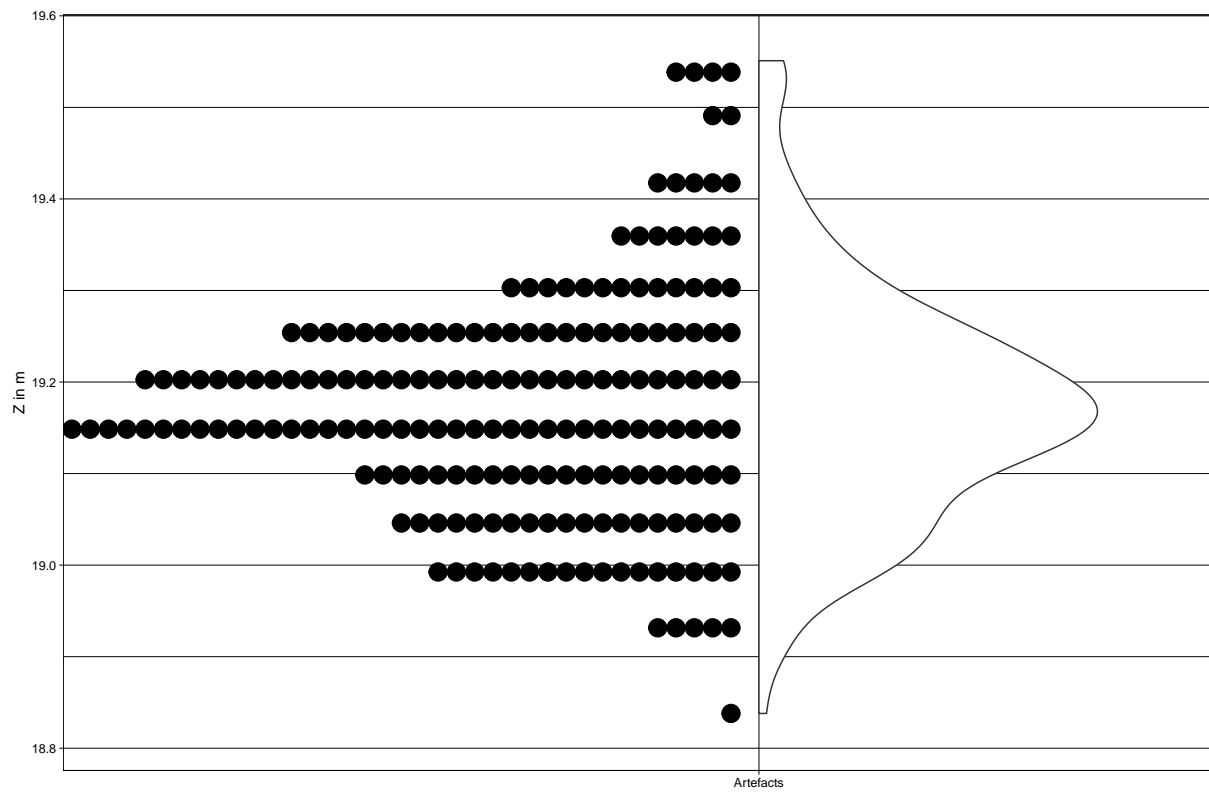
With this result, we can infer the existence of a concentrated find horizon that ranges within 15 cm.

2.2.3 The the depth distribution of artefacts >1.49 cm weight

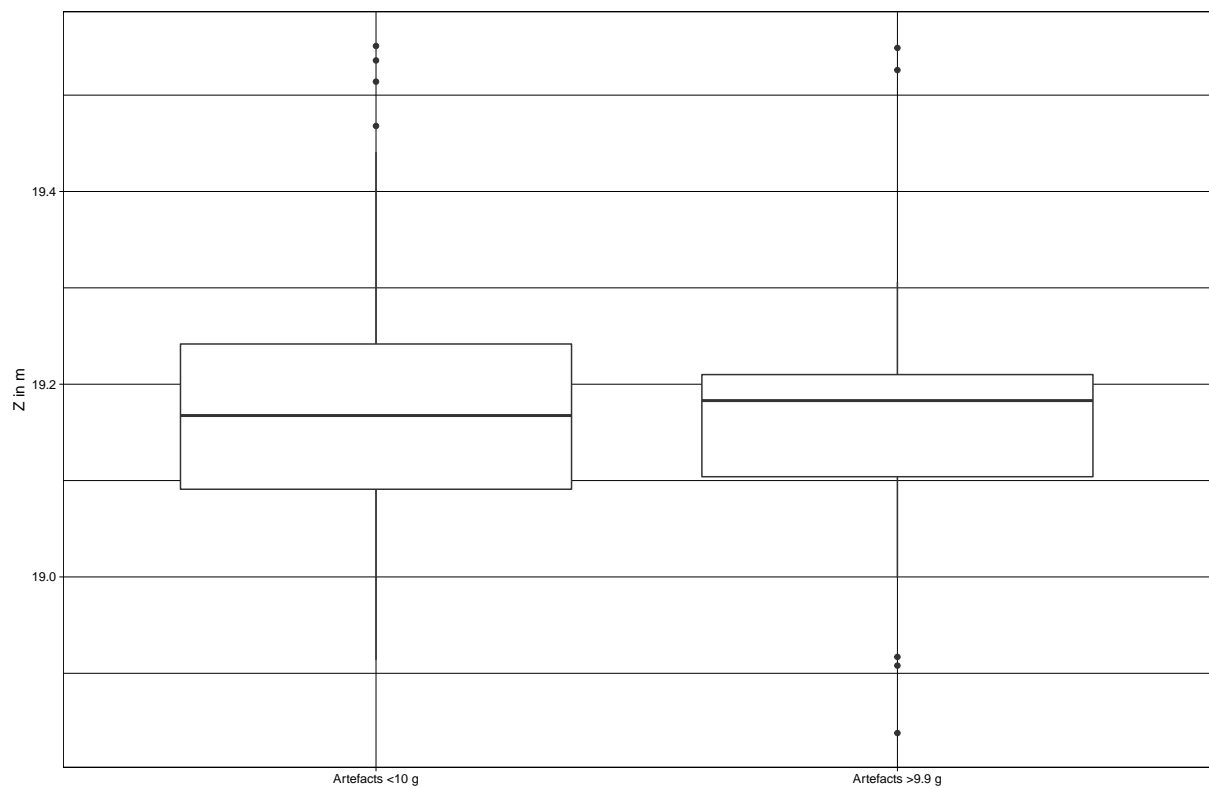
With the assumption that lighter artefacts are more prone to dislocation within the sandy sediment, the distribution of the heavier pieces could help to narrow down the range of the main find horizon. Therefore, we analyze in the following the depth distribution of artefacts regarding their weight. Therefore, we divided the artefacts in heavy lithics (>9.9 g) and light lithics (>10 g). We included the artefacts found in the test excavation 2019 and the lithics from the 2020 campaign.

As illustrated by the plot (Figure S30), the light artefacts are distributed as follows:

```
##  Min. 1st Qu.  Median  Mean 3rd Qu.  Max.
## 18.91 19.09 19.17 19.17 19.24 19.55
```



Supplementary Figure S29. Large artefacts >1.49 cm and depth



Supplementary Figure S30. Large Artefacts divided into light artefacts <10 g and heavier artefacts >9.9 g, and depth.

The heavier artefacts show a more narrow distribution between the 1st and the 3rd quartile:

```
##  Min. 1st Qu. Median  Mean 3rd Qu.  Max.
## 18.84 19.10 19.18 19.16 19.21 19.55
```

These results let us slightly narrow down the main find horizon based on the heavier artefacts between $Z = 19.10$ m and $Z = 19.21$ m, indicating a thickness of 11 cm.

2.3 The relationship between gravel and lithic <1.5 cm counts

To analyze whether small lithics and the gravel content within the humic sand may be affected by similar post-depositional processes, we take a look at the linear relationship of gravel content in g of each bucket and the respective small lithic counts.

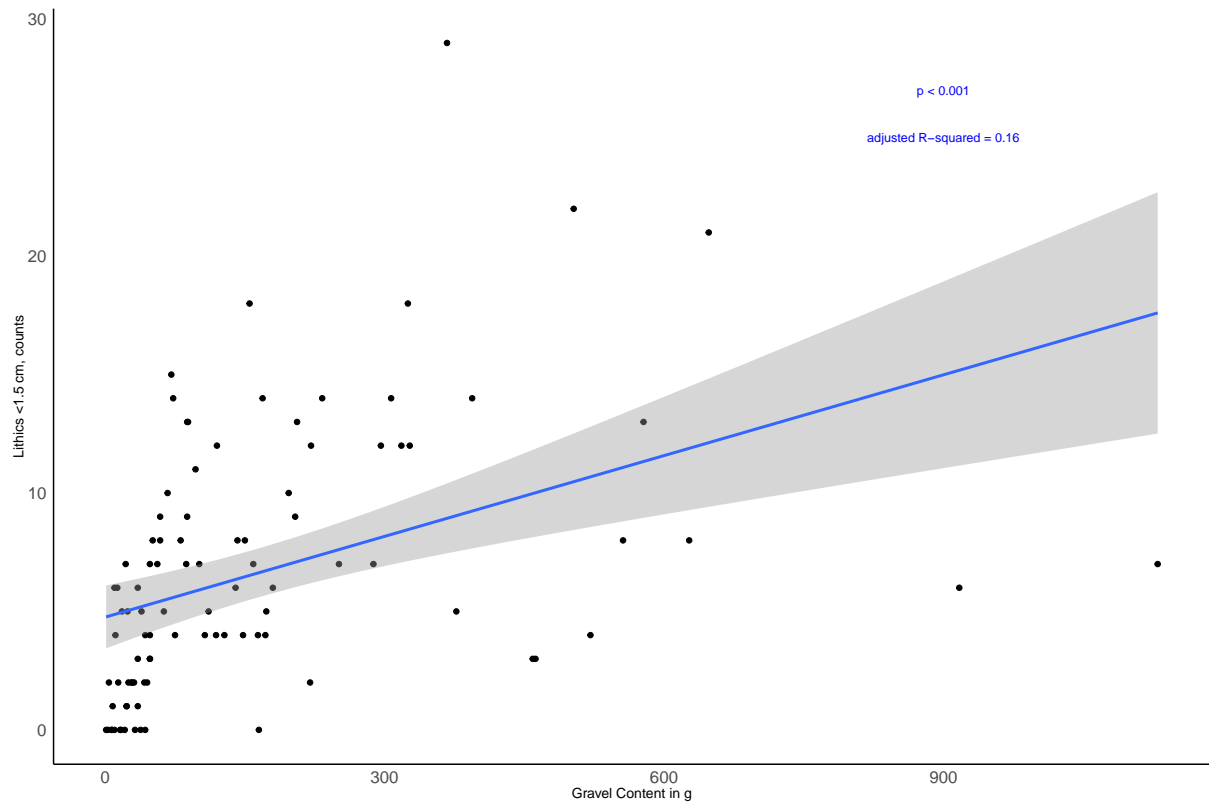
The linear model of the relationship between small lithic counts and gravel content reveals a significant result:

```
##
## Call:
## lm(formula = All_Buckets$Lithics ~ All_Buckets$Gravel)
##
## Residuals:
##  Min      1Q  Median      3Q      Max
## -10.6045 -3.4153 -0.9523  2.7464 20.0691
##
## Coefficients:
##              Estimate Std. Error t value Pr(>|t|)
## (Intercept)    4.758911   0.669042   7.113 2.21e-10 ***
## All_Buckets$Gravel 0.011368   0.002597   4.378 3.10e-05 ***
## ---
## Signif. codes:  0 '***' 0.001 '**' 0.01 '*' 0.05 '.' 0.1 ' ' 1
##
## Residual standard error: 5.091 on 94 degrees of freedom
## Multiple R-squared:  0.1694, Adjusted R-squared:  0.1605
## F-statistic: 19.17 on 1 and 94 DF, p-value: 3.105e-05
```

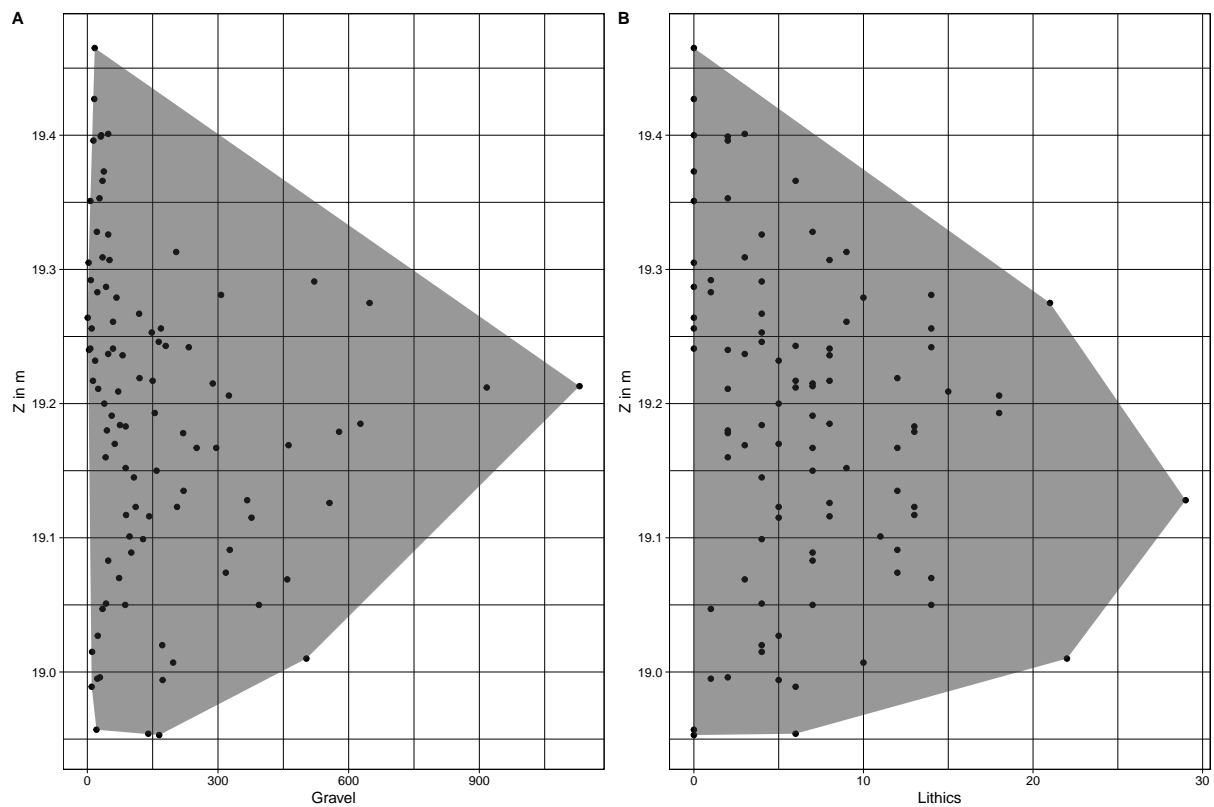
The plot in Figure S31 illustrates further that at a p-value of 0.05, there exists a linear relationship between the gravel content of the find horizon and the small finds. This indicates that small gravels and artefacts may have been affected by the same post-depositional processes.

But how is the data actually distributed? Let's take a look at another diagram (Figure S32).

The graphs in Figure S32 show the distribution of the gravel content and the lithic counts in relation to depth. The polygons highlight the maximum values. The plot shows that the maximum lithic values in relation to depth do not necessarily correlate 1:1 with the maximum gravel values. This indicates also a certain initial independence (before potential disturbances) of lithic accumulation by humans and natural gravel content. The three maximum values for small lithic counts match the 1st to 3rd quartiles ($Z = 19.1$ m to $Z = 19.21$ m, see above) for the Z values of the large finds. This lets us infer the original find horizon within this depth range.



Supplementary Figure S31. The relationship between small lithic <1.5 cm counts and gravel content.



Supplementary Figure S32. The distribution of the gravel content and the lithic counts <1.5 cm in relation to depth.

Conclusion of Section 2.2 and Section 2.3

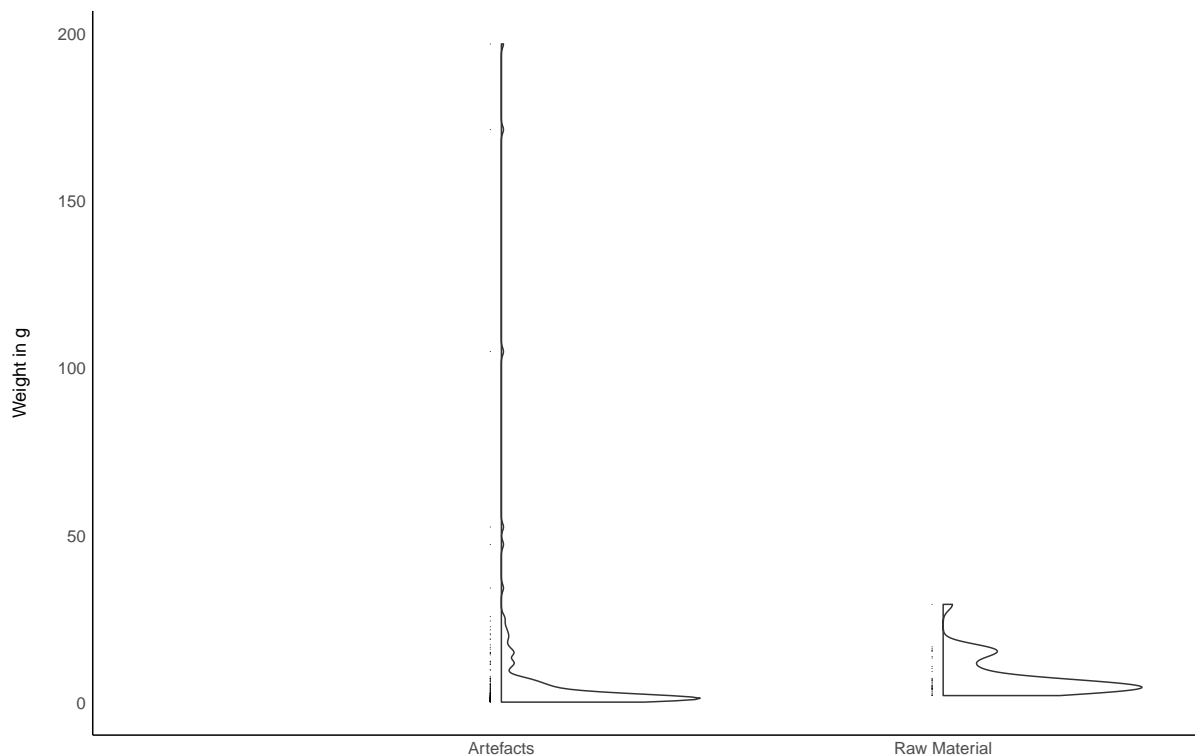
We can conclude that there exists a denser concentration of small and large artefacts between a depth of 19.10 m and $Z = 19.21$ m. However, the finds also scatter within the entire excavated depth and some post depositional dislocation needs to be taken into account. Further evidence for these processes comes from the gravel content of the sediment. A correlation of small finds and gravel content in relation to depth indicates that the objects were affected by similar post depositional processes within the humic sand. Nevertheless, the highest gravel contents and lithic counts do not correlate 1:1 with each other, indicating the remnants of original find distributions within the sediment.

2.4 Raw material size and Artefact size

An interesting feature of the Lichtenberg II assemblage is the small artefact size. To see if this corresponds to the local raw material, we did the following: We sampled quarter squares with high gravel content, the North-West quarter square 9976/5594, as well as the North-West quarter square 9977/5594 for baltic flint gravels and recorded the specimens. The aim was to evaluate raw material size of Baltic Flint that naturally occurs within the find horizon. We included the flint artefacts found in the test excavation 2019 and the lithics (flint) from the 2020 campaign.

Comparison of weight

Weight is used here as an estimation of artefact and raw material size.



Supplementary Figure S33. The comparison of artefact and raw material weight.

The plot in Figure S33 illustrates that the ranges of raw material and artefact weight (i.e. size) largely overlap. We can infer that part of the archaeological assemblage was manufactured on

the small raw material found at the site. Thereby, the artefacts reveal a smaller median weight value:

[1] 2.2

than the raw material:

[1] 5.3

This is logical, as the assemblage consists of knapped cores (reduced nodules) and light flakes and tools.

But the assemblage includes also some larger artefacts, e.g., a large quartzite flake (not included in the plot) or a flint core. This indicates that humans were able to access and collect larger raw material from the surrounding landscape which they transported to the site.

Section 3: Artefacts Lichtenberg I and Lichtenberg II

In the following analysis we focus mainly on the artifacts from Lichtenberg II, as the material from Lichtenberg I was already published elsewhere (Veil et al., 1994; Weiss, 2020).

This section was written in Rmarkdown.

3.1 Rawmaterial Lichtenberg II

Table S1 shows that we have a raw material diversity in Lichtenberg II, relative to Lichtenberg I where all artifacts were made of Baltic Flint (Veil et al., 1994).

Although being small, the quality of the raw material was good, as most artifacts show no special raw material features (Table S2).

3.2 Classification Lichtenberg II

Table S3 shows the classification of the n=192 Lichtenberg II artefacts. The assemblage is dominated by flakes, followed by cores and flake tools. The latter two have the same numbers. The assemblage consists further of shattered pieces and coretools. We also found 3 manuports and one piece typed as 'other' which are most likely raw material imports and/or hammerstones. If we exclude manuports, other and shatter, the assemblage of 163 artefacts consist of 51.5% flakes, 30.1% tools and 18.4% cores. This is a relatively high share of tools compared to Lichtenberg I (18.8% (Veil et al., 1994)).

3.3 Classification Lichtenberg I

During our fieldwork in 2019, we recovered the small number of 20 artefacts from the find horizon of Lichtenberg I, summarized in Table S4. The assemblage consists mainly of flakes, one of which is potentially the product of bifacial production (see main text). The low number of artifacts is explained by the fact that the main find concentration has already been excavated

Supplementary Table S1. Rawmaterial Lichtenberg II. Included are also manuports and a potential hammer stone (category: 'other')

Raw Material	n
FLINT	184
IronConc	1
Porphyry	1
Quartzite	5
Quartzite(?)	1

Supplementary Table S2. Rawmaterial characteristics Lichtenberg II

Raw Material Characteristics	n
BRYOZOANS	9
EXTENSIVE FROSTCRACK	1
FOSSIL	1
GRANULAR	14
INTRUSIONS_ FLAWS	23
NONE	130
THERMAL_ FRACTURES	14

Supplementary Table S3. Classification Lichtenberg II

Classification	n
CORE	30
CORETOOL	18
FLAKE	84
FLAKETOOL	31
MANUPORT	3
OTHER	1
SHATTER	25

before (Veil et al., 1994). Additionally, we recovered one Keilmesser and one tool fragment in the find horizon below the 1987-1993 excavation during our initial sondage in 2017 (Table S4).

3.4 Size

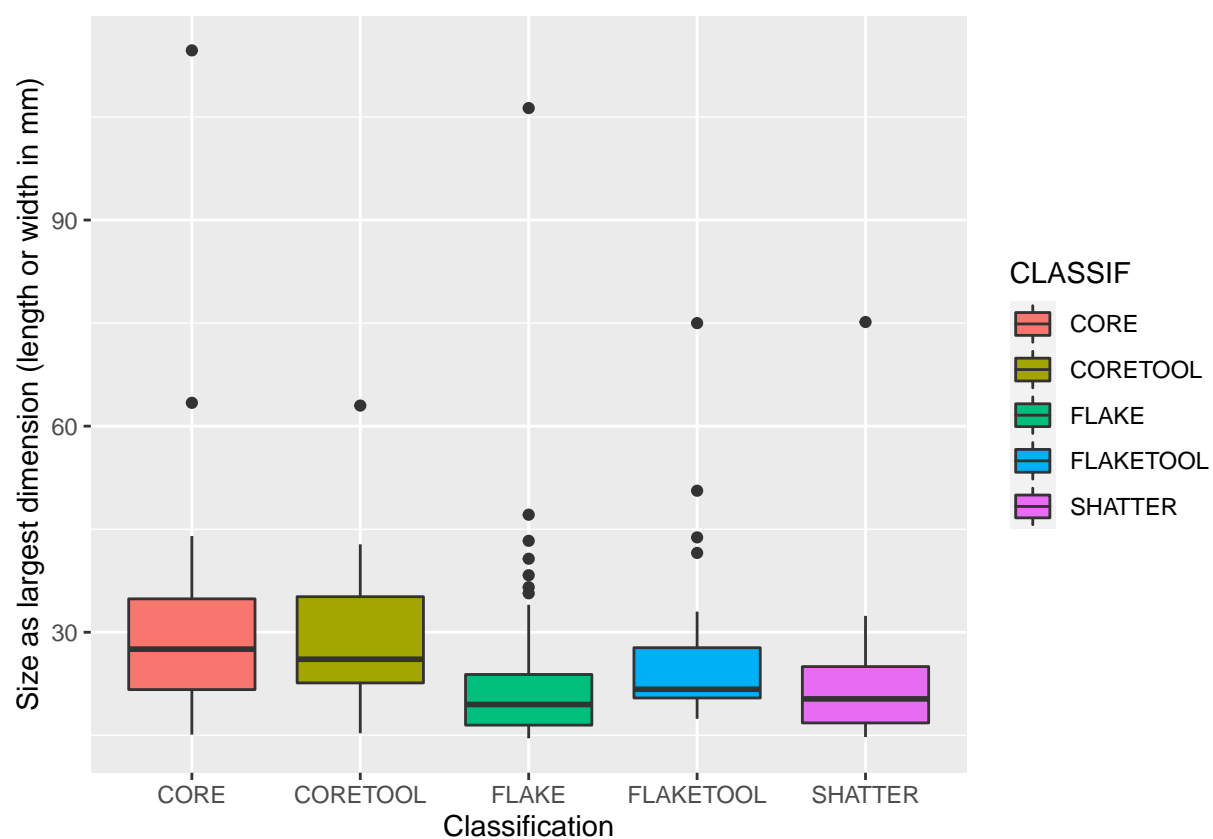
During our excavation of Lichtenberg II, we already recognized the small size of the artefacts. Therefore, we set the usual 2 cm size cut-off for single recorded artefacts to 1.5 cm. In the following, we first present the size of artefacts from Lichtenberg II and I (2019) and compare Lichtenbverg II in the next steps to a sample from Lichtenberg I (1987-1993), as well as diachronically to other Central European assemblages.

3.4.1 Lichtenberg II

Cores and coretools show a similar range of size, potentially directly dependent of the small sized raw material (see SI 3 - Analysis of the find horizon Lichtenberg II). Secondary and subsequent products within the operational chain, i.e. flakes, flakertools and shattered pieces are smaller than the latter two. The median dimensions are all below 3 cm, as presented in Table S5.

Supplementary Table S4. Classification Lichtenberg I

Classification	n
CORE	3
FLAKE	17
TOOL	2



Supplementary Figure S34. Artefact size Lichtenberg II.

Supplementary Table S5. Artefact Size Lichtenberg II

CLASSIF	n	Median_Dimension
CORE	30	27.54
CORETOOL	18	26.07
FLAKE	84	19.48
FLAKETOOL	31	21.70
SHATTER	25	20.30

Supplementary Table S6. Artefact Size Lichtenberg I - new excavation

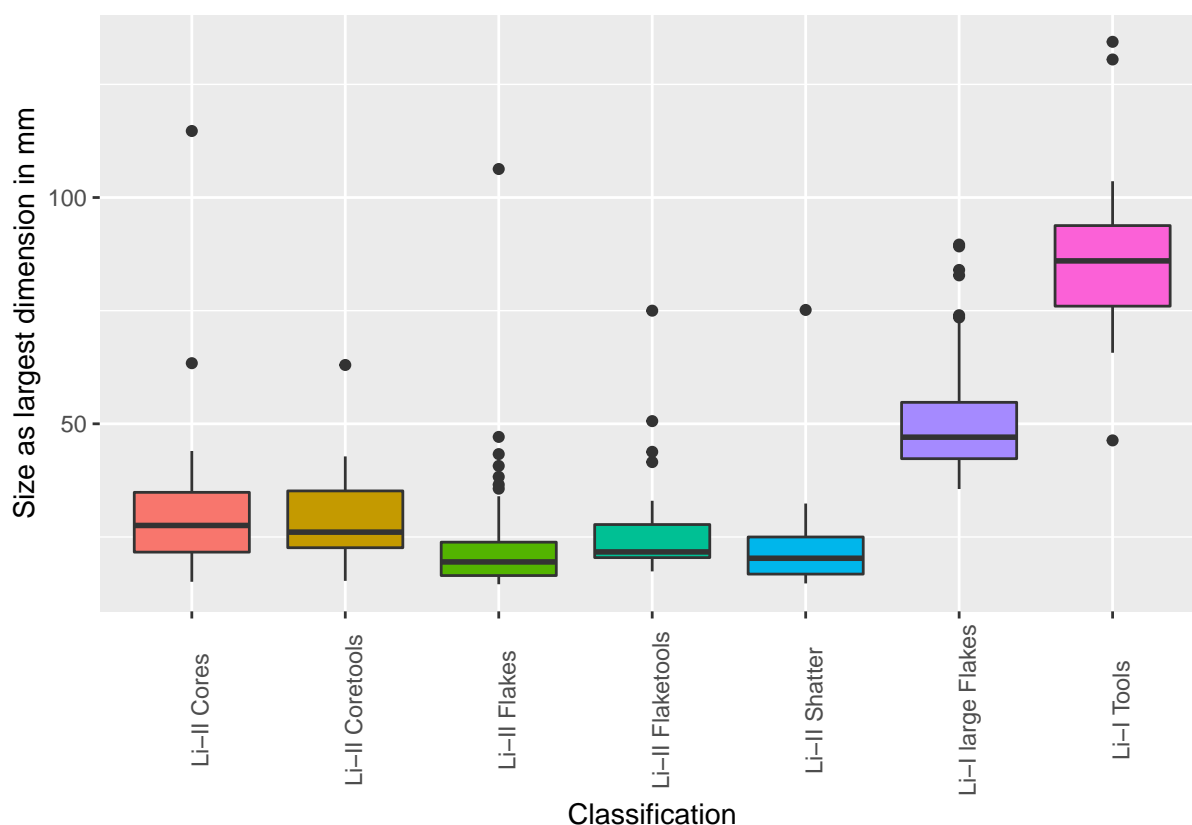
CLASSIFICATION	n	Median_Dimension
CORE	3	33.2
FLAKE	17	19.8

3.4.2 Lichtenberg I

During our fieldwork in 2019, we discovered 20 cores and flakes (Table S4). This is a too small number for a reliable estimation of artefact size. The median size data is presented in Table S6, but will not be used for further comparison (see below).

3.4.3 Size comparison of Lichtenberg I and II

As stated above, we cannot use the Lichtenberg I (2019) artefacts for a reliable comparison of size. To illustrate the size differences between Lichtenberg I and II, we use a dataset of recently published Lichtenberg I Keilmesser (and one handaxe (Weiss, 2020)) instead. Additionally, we use the data of 88 large flakes from the 1987-1993 excavation to demonstrate the maximum possible size difference for the flakes and in consequence for the raw material.



Supplementary Figure S35. Artifact size Lichtenberg I and I.

The plot in Fig. S35 demonstrates the artefact size difference of the Lichtenberg I and II assemblages. The mean values for the median size values of the Lichtenberg I flakes and tools are displayed in Table S7. Although we did not include the data for small flakes (between 1.5 cm and 3 cm) from Lichtenberg I, the large flakes exceed by far the main flake size distribution of Lichtenberg II. The large tools from Lichtenberg II demonstrate even more drastic the

Supplementary Table S7. Artefact size Lichtenberg I (large flakes only), 1983-1993 excavation

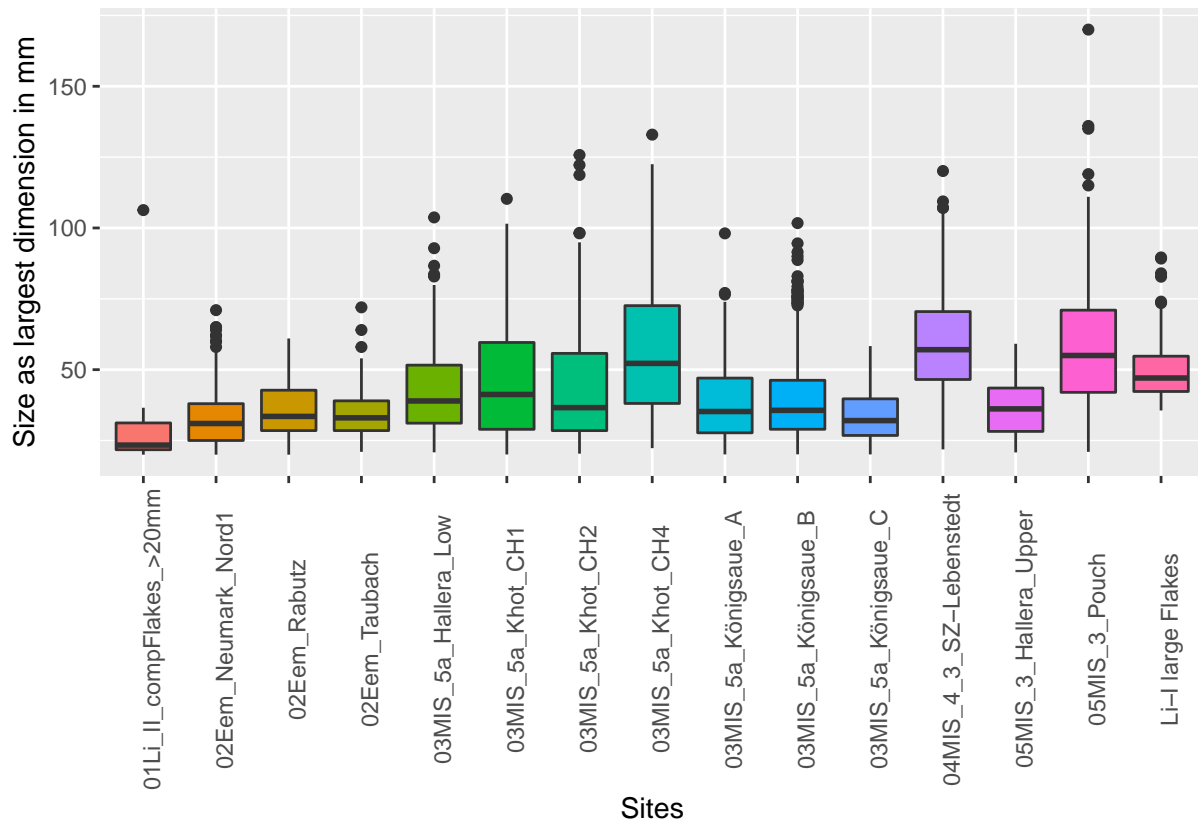
Classification	n	Median_Dimension
FLAKE	88	47.05
Tool_Li_I	23	86.00

differences in artefact (and -in the end- raw material) size between Lichtenberg I and II.

3.4.4 Diachronic size comparison of Lichtenberg II and other Central European assemblages between MIS 5e and MIS 3

To analyze if Lichtenberg II can in fact be characterized as a small artefact assemblage, we compared the size of flakes to other Central to Eastern Central European sites. The data was mainly collected by one of us (MW) and was previously published in Weiss et al. 2017 (Weiss et al., 2017) and in Weiss & Weber 2019 (Weiss and Weber, 2019). As for the other assemblages only complete artefacts >1.99 cm were measured, we adjusted the flake data from Lichtenberg accordingly. We incorporated the following assemblages from the Eemian: Taubach, Thuringia/Germany (Bratlund, 1999), Neumark-Nord, Saxony-Anhalt/Germany (Gaudzinski-Windheuser and Roebroeks, 2014) and Rabutz, Saxony/Germany (Toepfer, 1958). From MIS 5a, we included: Königsau, Saxony-Anhalt/Germany (Mania and Toepfer, 1973), Khotylevo I, Russian Federation (Hein et al., 2020), and Wrocław-Hallera-Avenue Lower Find layer, Poland (Wiśniewski et al., 2013). Salzgitter-Lebenstedt, Lower-Saxony /Germany (Pastoors, 2001; Tode, 1982) dates either to the MIS 5a/ MIS 4 transition or to early MIS 3. From the latter time period, we included: Pouch, Saxony-Anhalt/Germany (Weiss, 2015), and the Upper Find layer of Wrocław-Hallera-Avenue, Poland (Wiśniewski et al., 2013).

The plot in Figure S36 shows that Lichtenberg II has the smallest flakes of all assemblages, followed by the Eemian sites. There is a general trend that flakes get larger during MIS 5a and early MIS 3. That smaller artefact assemblages in the latter two time periods are raw material related, was recently shown in a study by Weiss et al. (Weiss et al., 2017): in Königsau, it seems that nodules were pre-shaped at the raw material outcrop and the then smaller initial cores were transported to the lake site. Second, in Wrocław-Hallera-Avenue, only small sized nodules occur naturally (Weiss et al., 2017; Wiśniewski et al., 2013). Generally, we can tentatively infer that during periods with high plantcover (Eemian, Brörup) raw material was rather small sized, and good quality raw material may have been harder to access than in time periods with less plant cover (MIS 3, MIS 5a/ MIS 4 transition). During the latter, large sized raw material was accessible in erosional channels or braided river valleys, like, e.g., in Pouch (Weiss, 2015).



Supplementary Figure S36. Flake size comparison between Lichtenberg II and other central European assemblages, dating between MIS 5e and MIS 3.

3.5 Lichtenberg II: Cores

The main attributes of the cores are listed in the following. Included are also cores that were transformed into tools in a subsequent step. “NA” values are excluded.

- Amount of secondary (worked) surface on the cores:
 - “10-30%”: n=14, 35%
 - “40-60%”: n=15, 37.5%
 - “70-90%”: n=9, 22.5%
 - “100%”: n=2, 5%
- Number of flaking surfaces:
 - “0”: n=1, 2.5%
 - “1”: n=19, 47.5%
 - “2”: n=13, 32.5%
 - “3”: n=6, 15%
 - “4”: n=1, 2.5%

- Number of flake scars:
 - “1”: n=14, 35%
 - “2”: n=3, 7.5%
 - “3”: n=6, 15%
 - “4”: n=8, 20%
 - “5”: n=7, 17.5%
 - “6”: n=1, 2.5%
 - “7”: n=1, 2.5%

- Flaking directions (all flaking surfaces):
 - “Unidirectional”: n=54, 80.6%
 - “Unidirectional and Lateral”: n=4, 6%
 - “Bidirectional”: n=7, 10.4%
 - “Concentric”: n=2, 3%

- State of the striking platform:
 - “Primary (i.e. natural) Surface”: n=20, 51.3%
 - “Plain”: n=17, 43.6%
 - “Coarse prepared (~2 large scars)”: n=2, 5.1%

- Exploitation:
 - “Tested Nodule”: n=20, 50%
 - “Flaking Core”: n=9, 22.5%
 - “Exhausted Core”: n=11, 27.5%

Summarizing the data provided above, we can say that most cores:

1. are knapped on half of their entire surface
2. have one or two flaking surfaces
3. have mainly only a single flake scar, but 3 to 5 flake scars are also common
4. are knapped unidirectionally
5. have natural or plain striking surfaces (no facetting!)
6. are either flaked a single time or exhausted

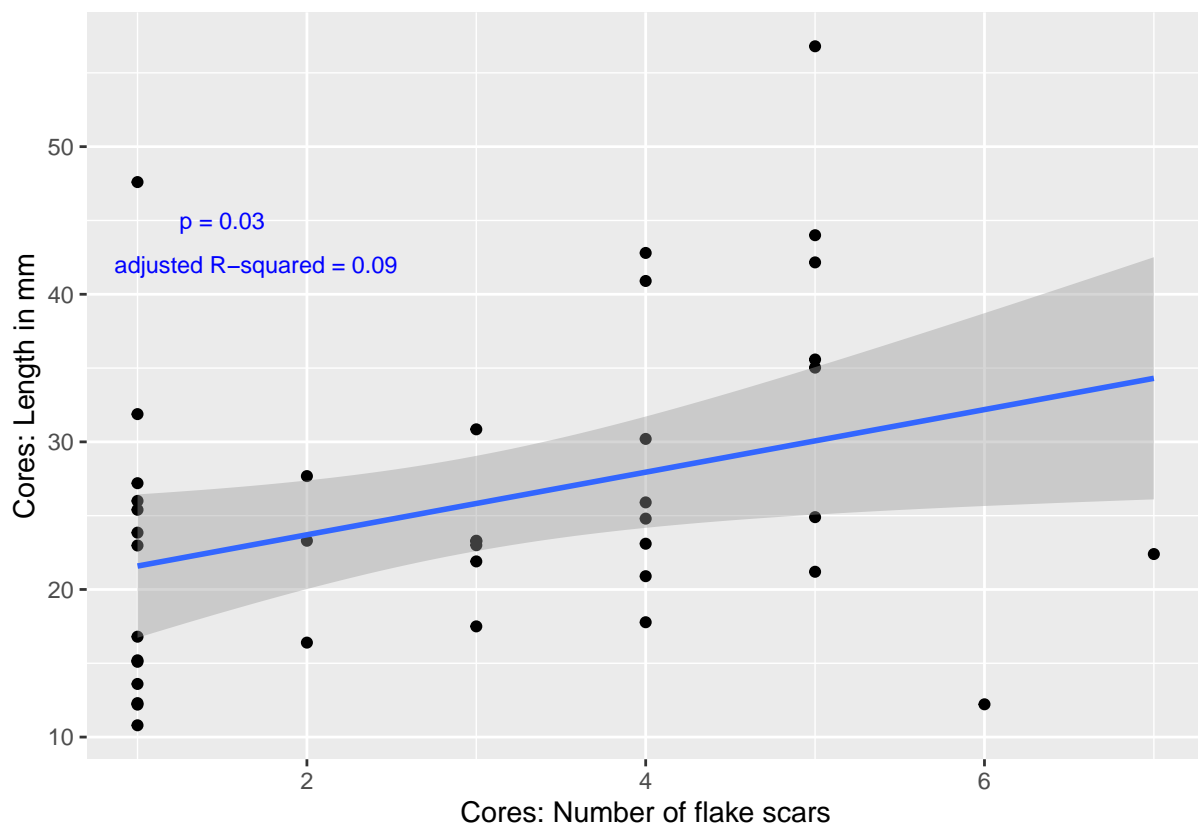
This leads to the conclusion that simple flaking methods dominate the blank production in Lichtenberg II. Core preparation is not common, if not entirely missing. The simple and sometimes just once knapped cores may also be due to the small raw material size, as some nodules make only one-time flaking possible. This is confirmed by the model illustrated below, showing that core length and the number of flake scars are significantly related (at a significance level of 0.05).

```
##
```

```
## Call:
```

```
## lm(formula = Core$LENGTH ~ Core$FLAKE_SCARS)
```

```
##
## Residuals:
##   Min     1Q   Median     3Q      Max
## -19.966  -7.111  -2.541   4.979  26.734
##
## Coefficients:
##              Estimate Std. Error t value Pr(>|t|)
## (Intercept)    19.4647    3.1466   6.186 3.16e-07 ***
## Core$FLAKE_SCARS 2.1203    0.9199   2.305 0.0267 *
## ---
## Signif. codes:  0 '***' 0.001 '**' 0.01 '*' 0.05 '.' 0.1 ' ' 1
##
## Residual standard error: 10.07 on 38 degrees of freedom
## (2 observations deleted due to missingness)
## Multiple R-squared:  0.1227, Adjusted R-squared:  0.09956
## F-statistic: 5.312 on 1 and 38 DF, p-value: 0.02673
```



Supplementary Figure S37. The relationship between core length and flake scars.

3.6 Lichtenberg II: Flakes

The main attributes of the flakes are listed in the following. Included are n=55 complete flakes. “NA” values are excluded.

- State of the platform:
 - “Crushed”: n=13, 23.6%
 - “Primary Surface”: n=12, 21.8%
 - “Plain-NA” (natural or worked surface): n=10, 18.2%
 - “Plain-100%”: n=18, 32.7%
 - “Scars-100%”: n=1, 1.8%
 - “Removed”: n=1, 1.8%

“Plain-100%” refers to platforms with one or two large negatives. “Scars-100%” refers to platforms that were prepared with 3 or more flake scars.

- Share of secondary (worked or artificial) surface on the dorsal face:
 - “0%” (natural surface): n=8, 15.1%
 - “10-30%”: n=9, 17%
 - “40-60%”: n=5, 9.4%
 - “70-90%”: n=11, 20.7%
 - “100%”: n=20, 37.7%
- Directions of the dorsal scars:
 - “Aligned” (i.e. same direction as ventral): n=23, 51.1%
 - “Lateral”: n=9, 20%
 - “Opposed” (i.e., opposed to ventral): n=3, 6.7%
 - “Aligned and Lateral”: n=5, 11.1%
 - “Bidirectional”: n=3, 6.7%
 - “Bilateral”: n=2, 4.4%
 - “Concentric”: n=0, 0%

The platform attributes reinforce the observation made on the cores that striking platform preparation (i.e. Levallois sensu largo) was not common. Most of the flakes stem from an advanced state of core reduction, the share of fully cortical flakes is lower. This might be a reasonable distribution, as cores naturally produce a lower share of fully cortical flakes compared flakes with no or only remnants of natural surfaces. However, if we sum up all the flakes with remnants of natural surface on their dorsal face, we end up with 62.2% (compared to ~37.7% of non-cortical flakes). This is more than half of the flake population and may have its reason in the small size of the raw material. The observed dorsal scar directions on the flakes show the same trend as the flaking directions on the cores: the blank production in Lichtenberg II is dominated by unidirectional flaking.

3.7 Lichtenberg II: Tools

The tools can be subdivided into 30 flakertools and 18 coretools.

- The tools where manufactured on diverse blank types:

Supplementary Table S8. Tool type size Lichtenberg II

TOOL_TYPE	n	Median_Length	Median_Width	Median_Thickness
BACKED_KNIFE	1	41.55	34.59	12.96
DENTICULATE	3	25.46	16.55	5.50
EDGE_RETOUCH	8	15.30	20.16	6.45
ENDSCRAPER	8	22.96	23.28	11.45
ENDSCRAPER_HAMMER	1	23.30	18.70	13.40
ENDSCRAPER_SCRAPER	1	14.30	27.90	16.40
HAMMERSTONE	3	40.90	26.80	19.20
NATBACK	1	21.90	14.80	13.00
NOTCH	11	24.80	19.50	11.60
POSS_USE	9	20.90	19.90	8.80
SCRAPER	2	24.85	23.65	7.50
NA	1	21.14	12.65	2.91

- “Natural Piece”: n=2, 4.2%
 - “Flake”: n=30, 62.5%
 - “Core”: n=12, 25%
 - “Shatter”: n=4, 8.3%
- The typological classifications are presented in the following in alphabetical order:
 - “Backed Knife”: n=1, 2%
 - “Denticulate”: n=3, 6.3%
 - “Edge Retouch” (limited retouch, not scraper-like): n=8, 16.7%
 - “Endscraper”: n=8; 16.7%
 - “Endscraper, reused as hammerstone”: n=1, 2%
 - “Endscraper-Scraper”: n=1, 2%
 - “Hammerstone”: n=3, 6.3%
 - “Naturally Backed Knife”: n=1, 2%
 - “Notch”: n=11, 22.9%
 - “Scraper”: n=2, 4.2%
 - “Use-wear”: n=9, 18.8%

The tools from Lichtenberg II are dominated by flakes with use-wear, simple edge retouch and endscrapers. They were manufacture on a diversity of blanks, dominated by flakes. Endscrapers and endscraper combination tools were manufactured on thick blanks (Supplementary Table S8), indicating special functional requirements. Also, the rather steep endscraper edge can only be produced on a relatively thick blank. The high share of cores and shattered pieces that also served as blanks for tools indicate that recycling played an important role in the Lichtenberg II assemblage. For example, the artefact LIA-379 was initially a core and then reused as hammerstone (Supplementary Figure S38).



Supplementary Figure S38. Artefact LIA-379. Initially, it was a core. The battering marks (red circle) show that the core was recycled as hammerstone.



Supplementary Figure S39. Flake with edge retouch LIA-536 and edge retouched former core LIA-416.



Supplementary Figure S40. Naturally backed knife LIA-538. The blank was either a core or a natural piece that was shaped with a view strikes (blue arrows).



Supplementary Figure S41. Large quartzite flake LIA-513.

Supplementary Table S9. Selected attributes for Lichtenberg II

INVENTARNUMBER	RAWMAT	PRESERVATION	BLANK	CLASSIF	LENGTH	WIDTH	THICK	WEIGHT	PLATFORM	DORSALSCARS	DORSALDIRECT	TOOL_TYPE	AMOUNT_RETICORE	FLAKE_SUR	FLAKE_SCARS	CONDITION_STRIKE	FLAKING_DIR_A_B_C_D
LIA-097	FLINT	COMPLETE	FLAKE	FLAKE	16.56	28.62	4.71	2.15	CRUSHED	100%	BIDIRECTIONAL	NA	NA	NA	NA	NA	NA-NA-NA-NA
LIA-098	FLINT	COMPLETE	FLAKE	FLAKE	22.48	12.82	6.13	1.40	CRUSHED	100%	BIDIRECTIONAL	NA	NA	NA	NA	NA	NA-NA-NA-NA
LIA-099	FLINT	MEDIAL	FLAKE	FLAKE	24.79	13.29	3.95	1.40	NA	100%	ALIGNED_LATERAL	NA	NA	NA	NA	NA	NA-NA-NA-NA
LIA-103	FLINT	COMPLETE	CORE	CORETOOL	22.82	26.14	7.55	5.70	NA	NA	NA	ENDSCRAPER	NA	NA	NA	NA	NA-NA-NA-NA
LIA-105	FLINT	DISTAL	FLAKE	FLAKE	15.97	21.16	5.27	1.60	NA	NA	NA	NA	NA	NA	NA	NA	NA-NA-NA-NA
LIA-129	FLINT	COMPLETE	FLAKE	FLAKE	32.91	12.84	4.10	2.35	PRIMARY_SURFACE-0%	70-90%	ALIGNED	NA	NA	NA	NA	NA	NA-NA-NA-NA
LIA-121	FLINT	COMPLETE	FLAKE	FLAKE/TOOL	37.10	43.81	9.90	14.90	REMOVED	70-90%	ALIGNED	POSS USE	NA	NA	NA	NA	NA-NA-NA-NA
LIA-127	FLINT	PROXIMAL	FLAKE	FLAKE	16.34	15.86	3.42	0.75	CRUSHED	NA	NA	NA	NA	NA	NA	NA	NA-NA-NA-NA
LIA-128	FLINT	COMPLETE	FLAKE	FLAKE	17.88	23.23	7.79	4.40	PLAIN-100%	100%	ALIGNED	NA	NA	NA	NA	NA	NA-NA-NA-NA
LIA-129	FLINT	DISTAL	FLAKE	FLAKE	12.25	15.88	4.10	0.75	NA	NA	NA	NA	NA	NA	NA	NA	NA-NA-NA-NA
LIA-132	FLINT	COMPLETE	FLAKE	FLAKE	15.63	24.79	6.03	1.80	PLAIN-NA	100%	LATERAL	NA	NA	NA	NA	NA	NA-NA-NA-NA
LIA-133	FLINT	COMPLETE	NATURAL_PIECE	CORE	31.88	23.35	14.65	7.30	NA	NA	NA	NA	40-60%	1	1	PRIMARY_SURFACE	UNIDIRECTIONAL-NA-NA-NA
LIA-140	FLINT	COMPLETE	FLAKE	SHATTER	17.99	11.58	6.64	1.45	NA	NA	NA	NA	NA	NA	NA	NA	NA-NA-NA-NA
LIA-143	FLINT	COMPLETE	FLAKE	SHATTER	19.71	20.30	6.95	2.75	NA	NA	NA	NA	NA	NA	NA	NA	NA-NA-NA-NA
LIA-146	FLINT	COMPLETE	FLAKE	FLAKE	10.42	15.57	2.52	0.40	PLAIN-NA	100%	ALIGNED	NA	NA	NA	NA	NA	NA-NA-NA-NA
LIA-147	FLINT	SHATTERED	NA	FLAKE/TOOL	21.14	12.45	2.91	1.00	NA	NA	NA	NA	NA	NA	NA	NA	NA-NA-NA-NA
LIA-150	FLINT	COMPLETE	FLAKE	FLAKE	21.58	10.55	6.96	1.60	PRIMARY_SURFACE-0%	10-30%	ALIGNED	NA	NA	NA	NA	NA	NA-NA-NA-NA
LIA-152	FLINT	COMPLETE	FLAKE	SHATTER	53.79	75.16	12.95	47.40	NA	NA	NA	NA	NA	NA	NA	NA	NA-NA-NA-NA
LIA-154	FLINT	COMPLETE	CORE	CORETOOL	42.16	40.70	24.15	24.55	NA	NA	NA	NOTCH	70-90%	1	5	PLAIN	UNI_LAT-NA-NA-NA
LIA-156	FLINT	COMPLETE	CORE	CORETOOL	23.85	31.05	18.70	14.40	NA	NA	NA	ENDSCRAPER	70-90%	1	1	PLAIN	UNIDIRECTIONAL-NA-NA-NA
LIA-158	FLINT	COMPLETE	NATURAL_PIECE	CORE	22.98	38.87	11.87	1.60	NA	NA	NA	NA	40-60%	1	1	PLAIN	UNIDIRECTIONAL-NA-NA-NA
LIA-159	FLINT	COMPLETE	FLAKE	FLAKE	31.80	36.56	5.33	5.50	PLAIN-NA	0%	NA	NA	NA	NA	NA	NA	NA-NA-NA-NA
LIA-165	FLINT	COMPLETE	FLAKE	SHATTER	32.39	10.72	7.80	2.05	NA	NA	NA	NA	NA	NA	NA	NA	NA-NA-NA-NA
LIA-166	FLINT	COMPLETE	FLAKE	SHATTER	13.95	14.74	3.95	0.80	NA	NA	NA	NA	NA	NA	NA	NA	NA-NA-NA-NA
LIA-190	FLINT	COMPLETE	NATURAL_PIECE	CORE	35.63	27.49	32.14	25.85	NA	NA	NA	NA	70-90%	2	5	COARSE_PREPARED	UNIDIRECTIONAL-UNIDIRECTIONAL-NA-NA
LIA-191	FLINT	COMPLETE	NATURAL_PIECE	CORE	32.27	30.78	13.95	7.20	NA	NA	NA	NA	10-30%	0	3	PRIMARY_SURFACE	NA-NA-NA-NA
LIA-192	FLINT	LONGIT_BROKEN	FLAKE	FLAKE	17.54	13.51	3.60	0.85	NA	NA	NA	NA	NA	NA	NA	NA	NA-NA-NA-NA
LIA-199	FLINT	COMPLETE	FLAKE	FLAKE	8.01	17.97	2.73	0.55	CRUSHED	100%	ALIGNED	NA	NA	NA	NA	NA	NA-NA-NA-NA
LIA-216	FLINT	DISTAL	FLAKE	FLAKE	47.11	30.32	10.07	17.40	NA	NA	NA	NA	NA	NA	NA	NA	NA-NA-NA-NA
LIA-219	FLINT	COMPLETE	FLAKE	FLAKE	25.94	23.10	10.32	5.10	PRIMARY_SURFACE-0%	0%	NA	NA	NA	NA	NA	NA	NA-NA-NA-NA
LIA-220	FLINT	SHATTERED	FLAKE	FLAKE	12.79	14.56	2.99	0.60	NA	NA	NA	NA	NA	NA	NA	NA	NA-NA-NA-NA
LIA-223	FLINT	LONGIT_BROKEN	NATURAL_PIECE	CORE	32.63	13.31	6.72	2.95	NA	NA	NA	NA	NA	NA	NA	NA	NA-NA-NA-NA
LIA-240	FLINT	COMPLETE	FLAKE	FLAKE	35.67	17.76	12.03	7.25	PLAIN-100%	10-30%	LATERAL	NA	NA	NA	NA	NA	NA-NA-NA-NA
LIA-242	FLINT	COMPLETE	FLAKE	FLAKE	11.40	18.04	3.42	0.65	PLAIN-100%	10-30%	OPPOSED	NA	NA	NA	NA	NA	NA-NA-NA-NA
LIA-244	FLINT	COMPLETE	FLAKE	FLAKE/TOOL	25.46	16.55	4.92	2.45	REMOVED	100%	ALIGNED_LATERAL	DENTICULATE	NA	NA	NA	NA	NA-NA-NA-NA
LIA-245	Quartzite	COMPLETE	CORREL	CORE	27.68	30.99	17.95	8.75	NA	NA	NA	NA	40-60%	NA	2	PLAIN	UNI_LAT-NA-NA-NA
LIA-251	FLINT	COMPLETE	FLAKE	FLAKE	15.62	5.98	2.07	0.35	CRUSHED	0%	ALIGNED	NA	NA	NA	NA	NA	NA-NA-NA-NA
LIA-253	FLINT	COMPLETE	FLAKE	FLAKE/TOOL	23.85	8.71	6.20	1.45	REMOVED	0%	NA	POSS USE	NA	NA	NA	NA	NA-NA-NA-NA
LIA-263	FLINT	COMPLETE	NATURAL_PIECE	CORE	17.78	11.28	18.36	3.00	NA	NA	NA	NA	40-60%	2	4	PRIMARY_SURFACE	UNIDIRECTIONAL-UNIDIRECTIONAL-NA-NA
LIA-265	FLINT	COMPLETE	FLAKE	FLAKE	19.47	17.66	6.10	2.30	PLAIN-NA	0%	NA	NA	NA	NA	NA	NA	NA-NA-NA-NA
LIA-271	FLINT	MEDIAL	FLAKE	FLAKE	27.70	29.06	8.00	6.75	NA	NA	NA	NA	NA	NA	NA	NA	NA-NA-NA-NA
LIA-279	FLINT	COMPLETE	FLAKE	FLAKE	15.40	12.49	3.69	0.75	PLAIN-NA	10-30%	ALIGNED	NA	NA	NA	NA	NA	NA-NA-NA-NA
LIA-285	FLINT	COMPLETE	FLAKE	FLAKE/TOOL	30.37	28.65	15.84	15.05	PRIMARY_SURFACE-0%	10-30%	BIDIRECTIONAL	ENDSCRAPER	NA	NA	NA	NA	NA-NA-NA-NA
LIA-286	FLINT	COMPLETE	FLAKE	FLAKE	19.80	16.96	7.44	2.15	PLAIN-100%	100%	BIDIRECTIONAL	NA	NA	NA	NA	NA	NA-NA-NA-NA
LIA-287	FLINT	COMPLETE	FLAKE	FLAKE	16.63	19.84	3.66	1.40	PRIMARY_SURFACE-0%	100%	LATERAL	NA	NA	NA	NA	NA	NA-NA-NA-NA
LIA-290	Quartzite	DISTAL	FLAKE	FLAKE	26.40	30.99	8.79	3.75	NA	NA	NA	NA	NA	NA	NA	NA	NA-NA-NA-NA
LIA-294	FLINT	COMPLETE	NATURAL_PIECE	CORE	12.22	16.40	11.75	2.10	NA	NA	NA	NA	70-90%	3	4	COARSE_PREPARED	UNIDIRECTIONAL-UNIDIRECTIONAL-UNIDIRECTIONAL-NA
LIA-299	FLINT	COMPLETE	NATURAL_PIECE	CORE	35.58	40.57	21.87	22.80	NA	NA	NA	NA	40-60%	2	5	PRIMARY_SURFACE	BIDIRECTIONAL-UNIDIRECTIONAL-NA-NA
LIA-301	FLINT	COMPLETE	FLAKE	FLAKE	18.60	17.99	5.00	1.40	PLAIN-100%	100%	BILATERAL	NA	NA	NA	NA	NA	NA-NA-NA-NA
LIA-303	FLINT	COMPLETE	FLAKE	FLAKE/TOOL	11.61	19.61	4.58	1.25	REMOVED	100%	BILATERAL	EDGE_RETTOUCH	NA	NA	NA	NA	NA-NA-NA-NA
LIA-307	FLINT	COMPLETE	FLAKE	FLAKE/TOOL	27.60	23.06	16.96	11.70	REMOVED	40-60%	ALIGNED	ENDSCRAPER	NA	NA	NA	NA	NA-NA-NA-NA
LIA-308	FLINT	LONGIT_BROKEN	FLAKE	FLAKE	17.50	8.71	3.87	0.75	NA	NA	NA	NA	NA	NA	NA	NA	NA-NA-NA-NA
LIA-314	FLINT	SHATTERED	FLAKE	SHATTER	21.70	11.10	8.03	1.85	NA	NA	NA	NA	NA	NA	NA	NA	NA-NA-NA-NA
LIA-315	FLINT	COMPLETE	FLAKE	FLAKE	20.16	16.41	5.67	1.65	PLAIN-100%	100%	OPPOSED	NA	NA	NA	NA	NA	NA-NA-NA-NA
LIA-316	FLINT	SHATTERED	CORE	SHATTER	21.36	16.48	10.17	3.75	NA	NA	NA	NA	NA	NA	NA	NA	NA-NA-NA-NA
LIA-317	FLINT	COMPLETE	FLAKE	FLAKE	31.27	19.28	9.13	4.95	PLAIN-100%	100%	ALIGNED	NA	NA	NA	NA	NA	NA-NA-NA-NA
LIA-318	FLINT	COMPLETE	FLAKE	FLAKE/TOOL	21.55	13.01	7.17	2.20	REMOVED	NA	NA	EDGE_RETTOUCH	NA	NA	NA	NA	NA-NA-NA-NA
LIA-321	FLINT	COMPLETE	FLAKE	FLAKE	16.43	23.54	8.48	3.30	SCARS-100%	10-30%	ALIGNED	NA	NA	NA	NA	NA	NA-NA-NA-NA
LIA-322	FLINT	COMPLETE	FLAKE	FLAKE	15.18	19.04	4.12	0.90	CRUSHED	70-90%	ALIGNED	NA	NA	NA	NA	NA	NA-NA-NA-NA
LIA-326	FLINT	COMPLETE	FLAKE	FLAKE	16.00	9.57	3.59	0.50	PLAIN-100%	70-90%	ALIGNED_LATERAL	NA	NA	NA	NA	NA	NA-NA-NA-NA
LIA-329	FLINT	COMPLETE	FLAKE	FLAKE	15.31	17.51	5.30	1.45	PLAIN-NA	NA	NA	NA	NA	NA	NA	NA	NA-NA-NA-NA
LIA-330	FLINT	COMPLETE	FLAKE	FLAKE	16.40	14.86	3.54	0.50	PLAIN-100%	100%	ALIGNED	NA	NA	NA	NA	NA	NA-NA-NA-NA
LIA-331	FLINT	COMPLETE	FLAKE	FLAKE	16.43	22.27	6.25	2.75	PRIMARY_SURFACE-0%	100%	ALIGNED_LATERAL	NA	NA	NA	NA	NA	NA-NA-NA-NA
LIA-332	FLINT	DISTAL	FLAKE	FLAKE	4.92	21.70	4.89	0.60	NA	NA	NA	NA	NA	NA	NA	NA	NA-NA-NA-NA
LIA-335	FLINT	COMPLETE	NATURAL_PIECE	CORE	56.80	114.70	34.80	196.90	NA	NA	NA	NA	70-90%	3	5	PRIMARY_SURFACE	UNIDIRECTIONAL-UNIDIRECTIONAL-UNIDIRECTIONAL-NA
LIA-336	FLINT	COMPLETE	FLAKE	FLAKE	21.76	32.73	15.41	5.50	PRIMARY_SURFACE-0%	NA	NA	NA	NA	NA	NA	NA	NA-NA-NA-NA
LIA-342	FLINT	COMPLETE	FLAKE	FLAKE/TOOL	41.35	34.59	12.96	16.10	REMOVED	100%	ALIGNED_LATERAL	BACKED_KNIFE	NA	NA	NA	NA	NA-NA-NA-NA
LIA-346	FLINT	DISTAL	FLAKE	FLAKE	36.37	43.31	9.59	14.80	NA	NA	NA	NA	NA	NA	NA	NA	NA-NA-NA-NA
LIA-349	FLINT	COMPLETE	NATURAL_PIECE	CORE	30.85	34.35	33.33	21.90	NA	NA	NA	NA	70-90%	3	3	PRIMARY_SURFACE	UNIDIRECTIONAL-UNIDIRECTIONAL-UNIDIRECTIONAL-NA
LIA-350	FLINT	DISTAL	FLAKE	FLAKE/TOOL	9.48	20.57	5.75	0.85	NA	NA	NA	ENDSCRAPER	NA	NA	NA	NA	NA-NA-NA-NA
LIA-356	FLINT	COMPLETE	FLAKE	FLAKE	23.20	15.10	6.90	2.25	CRUSHED	70-90%	ALIGNED	NA	NA	NA	NA	NA	NA-NA-NA-NA
LIA-359	FLINT	COMPLETE	FLAKE	FLAKE/TOOL	33.00	27.00	10.20	8.00	REMOVED	70-90%	ALIGNED	SCRAPER	NA	NA	NA	NA	NA-NA-NA-NA
LIA-360	FLINT	COMPLETE	FLAKE	FLAKE	21.90	12.50	7.60	1.80	PLAIN-NA	0%	NA	NA	NA	NA	NA	NA	NA-NA-NA-NA
LIA-361	FLINT	DISTAL	FLAKE	FLAKE	38.30	19.40	12.00	7.25	NA	NA	NA	NA	NA	NA	NA	NA	NA-NA-NA-NA
LIA-362	FLINT	SHATTERED	FLAKE	SHATTER	16.40	13.90	8.00	1.45	NA	NA	NA	NA	NA	NA	NA	NA	NA-NA-NA-NA
LIA-364	FLINT	SHATTERED	FLAKE	SHATTER	25.30	12.10	7.00	2.85	NA	NA	NA	NA	NA	NA	NA	NA	NA-NA-NA-NA
LIA-367	FLINT	COMPLETE	NATURAL_PIECE	CORE	12.30	16.30	19.90	3.15	NA	NA	NA	NA	10-30%	1	1	PRIMARY_SURFACE	UNIDIRECTIONAL-NA-NA-NA
LIA-368	FLINT	DISTAL	FLAKE	FLAKE	40.70	36.50	29.10	20.70	NA	NA	NA	NA	NA	NA	NA	NA	NA-NA-NA-NA
LIA-370	FLINT	SHATTERED	FLAKE	SHATTER	26.30	13.20	9.50	1.80	NA	NA	NA	NA	NA	NA	NA	NA	NA-NA-NA-NA

Supplementary Table S9. Selected attributes for Lichtenberg II (*continued*)

INVENTARNUMBER	RAWMAT	PRESERVATION	BLANK	CLASSIF	LENGTH	WIDTH	THICK	WEIGHT	PLATFORM	DORSALSCARS	DORSALDIRECT	TOOL_TYPE	AMOUNT_RETICORE	FLAKE_SUR	FLAKE_SCARS	CONDITION_STRIKE	FLAKING_DIR_A_B_C_D	
LJA-372	FLINT	COMPLETE	NATURAL_PIECE	CORE	17.50	27.90	16.00	9.90	NA	NA	NA	NA	10-30%	2	3	PLAIN	UNIDIRECTIONAL-BIDIRECTIONAL-NA-NA	
LJA-373	FLINT	COMPLETE	NATURAL_PIECE	CORE	25.90	13.60	8.50	2.75	NA	NA	NA	NA	70-90%	2	4	PLAIN	UNIDIRECTIONAL-UNIDIRECTIONAL-NA-NA	
LJA-375	FLINT	COMPLETE	FLAKE	CORE	16.40	24.00	13.50	4.75	NA	NA	NA	NA	40-60%	1	2	PLAIN	UNIDIRECTIONAL-NA-NA-NA	
LJA-376	FLINT	DISTAL	FLAKE	FLAKE	18.10	6.50	3.60	0.50	NA	NA	NA	NA	NA	NA	NA	NA	NA-NA-NA-NA	
LJA-377	FLINT	COMPLETE	FLAKE	FLAKE/TOOL	31.20	22.50	8.40	6.50	PLAIN-100%	NA	NA	NA	DENTICULATE	NA	NA	NA	NA-NA-NA-NA	
LJA-378	FLINT	COMPLETE	NATURAL_PIECE	CORE	23.30	40.10	18.60	15.20	NA	NA	NA	NA	40-60%	2	3	PRIMARY_SURFACE	UNIDIRECTIONAL-UNIDIRECTIONAL-NA-NA	
LJA-379	FLINT	COMPLETE	CORE	CORE/TOOL	40.90	24.40	18.30	12.55	NA	NA	NA	NA	HAMMERSTONE	40-60%	2	4	PRIMARY_SURFACE	UNIDIRECTIONAL-UNIDIRECTIONAL-NA-NA
LJA-380	FLINT	COMPLETE	FLAKE	FLAKE	19.50	15.80	6.60	1.40	PLAIN-100%	70-90%	ALIGNED	NA	NA	NA	NA	NA	NA-NA-NA-NA	
LJA-381	FLINT	COMPLETE	FLAKE	1 FLAKE	20.00	18.60	8.40	1.90	REMOVED	70-90%	LATERAL	NA	NA	NA	NA	NA	NA-NA-NA-NA	
LJA-383	FLINT	COMPLETE	FLAKE	FLAKE/TOOL	17.40	14.30	8.80	1.85	REMOVED	NA	NA	POSS_USE	NA	NA	NA	NA	NA-NA-NA-NA	
LJA-384	FLINT	COMPLETE	FLAKE	FLAKE	16.40	16.41	5.00	1.30	CRUSHED	100%	OPPOSED	NA	NA	NA	NA	NA	NA-NA-NA-NA	
LJA-387	FLINT	COMPLETE	CORE	CORE/TOOL	23.10	23.50	14.50	7.50	NA	NA	NA	ENDSCRAPER	40-60%	2	4	PLAIN	BIDIRECTIONAL-UNI_LAT-NA-NA	
LJA-388	FLINT	SHATTERED	FLAKE	SHATTER	17.10	8.50	4.80	0.65	NA	NA	NA	NA	NA	NA	NA	NA	NA-NA-NA-NA	
LJA-390	FLINT	COMPLETE	NATURAL_PIECE	CORE	21.20	14.90	12.40	4.20	NA	NA	NA	NA	100%	4	5	PLAIN	UNIDIRECTIONAL-UNIDIRECTIONAL-UNIDIRECTIONAL-UNIDIRECTIONAL	
LJA-392	FLINT	COMPLETE	FLAKE	FLAKE	8.30	15.80	4.70	0.55	PLAIN-100%	70-90%	ALIGNED	NA	NA	NA	NA	NA	NA-NA-NA-NA	
LJA-396	FLINT	DISTAL	FLAKE	FLAKE	15.70	14.40	4.20	0.85	NA	NA	NA	NA	NA	NA	NA	NA	NA-NA-NA-NA	
LJA-397	FLINT	COMPLETE	CORE	CORE/TOOL	23.30	18.70	13.40	5.60	NA	NA	NA	ENDSCRAPER_HAMMER	40-60%	2	2	PLAIN	UNIDIRECTIONAL-UNIDIRECTIONAL-NA-NA	
LJA-398	FLINT	COMPLETE	FLAKE	FLAKE/TOOL	14.30	27.90	16.40	7.45	REMOVED	100%	NA	ENDSCRAPER_SCRAPER	NA	NA	NA	NA	NA-NA-NA-NA	
LJA-399	FLINT	COMPLETE	NATURAL_PIECE	CORE	22.40	29.10	18.10	5.55	NA	NA	NA	NA	70-90%	3	7	PLAIN	CONCENTRIC-UNIDIRECTIONAL-BIDIRECTIONAL-NA	
LJA-400	FLINT	PROXIMAL	FLAKE	FLAKE	15.60	16.40	3.40	0.70	NA	NA	NA	NA	NA	NA	NA	NA	NA-NA-NA-NA	
LJA-401	FLINT	COMPLETE	FLAKE	FLAKE	21.70	8.30	4.70	0.70	PLAIN-100%	0%	NA	NA	NA	NA	NA	NA	NA-NA-NA-NA	
LJA-405	FLINT	COMPLETE	FLAKE	FLAKE/TOOL	21.00	12.40	8.40	2.30	REMOVED	70-90%	NA	ENDSCRAPER	NA	NA	NA	NA	NA-NA-NA-NA	
LJA-406	FLINT	COMPLETE	FLAKE	FLAKE/TOOL	8.10	17.60	3.60	0.55	CRUSHED	NA	NA	EDGE_RETIC/TOUCH	NA	NA	NA	NA	NA-NA-NA-NA	
LJA-413	FLINT	DISTAL	FLAKE	FLAKE	16.70	20.30	4.80	1.80	NA	NA	NA	SCRAPER	NA	NA	NA	NA	NA-NA-NA-NA	
LJA-416	FLINT	COMPLETE	CORE	CORE/TOOL	26.00	20.70	13.20	5.25	NA	NA	NA	EDGE_RETIC/TOUCH	10-30%	1	1	PLAIN	UNIDIRECTIONAL-NA-NA-NA	
LJA-419	FLINT	COMPLETE	NATURAL_PIECE	CORE	23.00	13.70	10.60	3.95	NA	NA	NA	NA	10-30%	2	3	PRIMARY_SURFACE	UNIDIRECTIONAL-UNI_LAT-NA-NA	
LJA-421	FLINT	COMPLETE	FLAKE	FLAKE	16.60	14.30	4.20	1.00	CRUSHED	0%	NA	NA	NA	NA	NA	NA	NA-NA-NA-NA	
LJA-422	FLINT	COMPLETE	NATURAL_PIECE	CORE	15.10	13.40	7.80	1.25	NA	NA	NA	NA	10-30%	1	1	PRIMARY_SURFACE	UNIDIRECTIONAL-NA-NA-NA	
LJA-427	FLINT	COMPLETE	FLAKE	FLAKE	17.90	17.30	5.00	1.65	PLAIN-100%	100%	ALIGNED	NA	NA	NA	NA	NA	NA-NA-NA-NA	
LJA-428	FLINT	COMPLETE	FLAKE	FLAKE/TOOL	21.70	11.10	5.50	0.95	CRUSHED	100%	OPPOSED	DENTICULATE	NA	NA	NA	NA	NA-NA-NA-NA	
LJA-429	FLINT	COMPLETE	FLAKE	FLAKE	16.50	15.00	4.30	1.05	CRUSHED	10-30%	ALIGNED	NA	NA	NA	NA	NA	NA-NA-NA-NA	
LJA-432	FLINT	COMPLETE	FLAKE	FLAKE	11.70	22.90	4.60	1.10	CRUSHED	0%	NA	NA	NA	NA	NA	NA	NA-NA-NA-NA	
LJA-433	FLINT	COMPLETE	NATURAL_PIECE	CORE	44.00	33.40	14.90	19.10	NA	NA	NA	NA	40-60%	1	5	PRIMARY_SURFACE	BIDIRECTIONAL-NA-NA-NA	
LJA-434	FLINT	PROXIMAL	FLAKE	FLAKE	16.30	17.70	6.30	2.45	NA	NA	NA	NA	NA	NA	NA	NA	NA-NA-NA-NA	
LJA-436	FLINT	COMPLETE	FLAKE	FLAKE	31.00	27.90	17.20	12.40	PLAIN-100%	70-90%	ALIGNED	NA	NA	NA	NA	NA	NA-NA-NA-NA	
LJA-437	FLINT	SHATTERED	FLAKE	SHATTER	20.60	14.40	8.50	2.50	NA	NA	NA	NA	NA	NA	NA	NA	NA-NA-NA-NA	
LJA-439	FLINT	SHATTERED	CORE	SHATTER	15.60	8.70	4.70	0.90	NA	NA	NA	NA	NA	NA	NA	NA	NA-NA-NA-NA	
LJA-440	FLINT	COMPLETE	FLAKE	FLAKE/TOOL	20.70	11.20	7.50	1.50	REMOVED	40-60%	ALIGNED	NOTCH	NA	NA	NA	NA	NA-NA-NA-NA	
LJA-441	FLINT	SHATTERED	FLAKE	SHATTER	18.10	14.00	3.00	0.70	NA	NA	NA	NA	NA	NA	NA	NA	NA-NA-NA-NA	
LJA-442	FLINT	COMPLETE	FLAKE	FLAKE	15.00	6.60	3.10	0.40	PLAIN-100%	100%	ALIGNED	NA	NA	NA	NA	NA	NA-NA-NA-NA	
LJA-446	FLINT	COMPLETE	NATURAL_PIECE	CORE	12.20	18.00	8.80	1.80	NA	NA	NA	NA	10-30%	1	1	PRIMARY_SURFACE	UNIDIRECTIONAL-NA-NA-NA	
LJA-447	FLINT	COMPLETE	FLAKE	FLAKE	14.50	19.30	14.00	3.90	PRIMARY_SURFACE-0%	40-60%	BILATERAL	NA	NA	NA	NA	NA	NA-NA-NA-NA	
LJA-448	FLINT	SHATTERED	SHATTER	SHATTER	25.00	19.60	12.70	4.80	NA	NA	NA	NA	NA	NA	NA	NA	NA-NA-NA-NA	
LJA-449	FLINT	COMPLETE	FLAKE	FLAKE	15.00	7.60	4.50	0.50	PLAIN-100%	100%	ALIGNED_LATERAL	NA	NA	NA	NA	NA	NA-NA-NA-NA	
LJA-450	FLINT	MIDIAL	FLAKE	FLAKE	18.30	16.50	3.20	1.55	NA	NA	NA	NA	NA	NA	NA	NA	NA-NA-NA-NA	
LJA-451	FLINT	COMPLETE	NATURAL_PIECE	CORE	25.40	21.00	30.00	105.00	NA	NA	NA	NA	10-30%	NA	1	PRIMARY_SURFACE	UNIDIRECTIONAL-NA-NA-NA	
LJA-453	FLINT	MIDIAL	FLAKE	FLAKE	15.20	15.70	2.80	0.75	NA	NA	NA	NA	NA	NA	NA	NA	NA-NA-NA-NA	
LJA-454	FLINT	COMPLETE	FLAKE	FLAKE	17.10	6.30	4.10	0.45	PLAIN-NA	40-60%	LATERAL	NA	NA	NA	NA	NA	NA-NA-NA-NA	
LJA-455	FLINT	COMPLETE	FLAKE	FLAKE	15.40	17.80	4.10	1.35	CRUSHED	70-90%	ALIGNED	NA	NA	NA	NA	NA	NA-NA-NA-NA	
LJA-456	FLINT	DISTAL	FLAKE	FLAKE	15.00	10.90	4.40	0.90	NA	NA	NA	NA	NA	NA	NA	NA	NA-NA-NA-NA	
LJA-457	FLINT	COMPLETE	SHATTER	CORE/TOOL	18.30	12.20	8.50	2.15	NA	NA	NA	NOTCH	NA	NA	NA	NA	NA-NA-NA-NA	
LJA-458	FLINT	COMPLETE	FLAKE	FLAKE/TOOL	17.30	19.90	7.20	2.20	REMOVED	10-30%	LATERAL	POSS_USE	NA	NA	NA	NA	NA-NA-NA-NA	
LJA-461	FLINT	COMPLETE	FLAKE	FLAKE/TOOL	22.20	24.30	13.20	6.90	REMOVED	70-90%	CONCENTRIC	POSS_USE	NA	NA	NA	NA	NA-NA-NA-NA	
LJA-462	FLINT	COMPLETE	NATURAL_PIECE	CORE	16.80	37.20	17.20	11.50	NA	NA	NA	NA	10-30%	1	1	PRIMARY_SURFACE	UNIDIRECTIONAL-NA-NA-NA	
LJA-463	FLINT	COMPLETE	NATURAL_PIECE	CORE/TOOL	28.80	24.10	6.30	6.00	NA	NA	NA	NOTCH	NA	NA	NA	NA	NA-NA-NA-NA	
LJA-464	FLINT	COMPLETE	FLAKE	FLAKE/TOOL	15.90	23.90	11.40	4.40	REMOVED	100%	ALIGNED_LATERAL	POSS_USE	NA	NA	NA	NA	NA-NA-NA-NA	
LJA-465	FLINT	PROXIMAL	FLAKE	FLAKE	22.40	17.40	9.50	3.20	NA	NA	NA	NA	NA	NA	NA	NA	NA-NA-NA-NA	
LJA-467	FLINT	COMPLETE	FLAKE	FLAKE/TOOL	18.70	16.10	8.50	2.80	PRIMARY_SURFACE-0%	10-30%	LATERAL	NOTCH	NA	NA	NA	NA	NA-NA-NA-NA	
LJA-468	Quartzite(?)	COMPLETE	COBBLE	OTHER	34.00	25.10	26.50	26.60	NA	NA	NA	HAMMERSTONE	NA	NA	NA	NA	NA-NA-NA-NA	
LJA-469	FLINT	COMPLETE	FLAKE	FLAKE/TOOL	20.70	11.60	6.80	1.15	NA	70-90%	BILATERAL	POSS_USE	NA	NA	NA	NA	NA-NA-NA-NA	
LJA-470	FLINT	COMPLETE	CORE	CORE/TOOL	27.20	31.50	20.90	12.25	NA	NA	NA	NOTCH	10-30%	1	1	PRIMARY_SURFACE	UNIDIRECTIONAL-NA-NA-NA	
LJA-471	FLINT	COMPLETE	NATURAL_PIECE	CORE	15.20	13.70	7.70	1.35	NA	NA	NA	NA	40-60%	1	1	PRIMARY_SURFACE	UNIDIRECTIONAL-NA-NA-NA	
LJA-472	FLINT	DISTAL	FLAKE	FLAKE	15.80	9.90	3.20	0.55	NA	NA	NA	NA	NA	NA	NA	NA	NA-NA-NA-NA	
LJA-473	FLINT	COMPLETE	CORE	CORE/TOOL	24.80	19.00	14.50	5.40	NA	NA	NA	NOTCH	70-90%	3	4	PLAIN	UNIDIRECTIONAL-UNIDIRECTIONAL-UNIDIRECTIONAL-NA	
LJA-474	FLINT	COMPLETE	FLAKE	FLAKE	20.00	17.20	6.80	2.70	PRIMARY_SURFACE-0%	70-90%	ALIGNED	NA	NA	NA	NA	NA	NA-NA-NA-NA	
LJA-475	FLINT	COMPLETE	FLAKE	1 FLAKE	15.70	21.70	5.90	1.80	NA	100%	LATERAL	EDGE_RETIC/TOUCH	NA	NA	NA	NA	NA-NA-NA-NA	
LJA-476	FLINT	MIDIAL	FLAKE	FLAKE	15.30	14.50	3.10	1.00	NA	NA	NA	NA	NA	NA	NA	NA	NA-NA-NA-NA	
LJA-478	FLINT	COMPLETE	SHATTER	CORE/TOOL	22.40	13.70	12.00	3.15	NA	NA	NA	NOTCH	NA	NA	NA	NA	NA-NA-NA-NA	
LJA-479	FLINT	COMPLETE	FLAKE	FLAKE/TOOL	17.80	13.80	5.00	1.40	REMOVED	100%	LATERAL	EDGE_RETIC/TOUCH	NA	NA	NA	NA	NA-NA-NA-NA	
LJA-481	FLINT	COMPLETE	FLAKE	FLAKE	20.30	8.70	5.40	1.40	CRUSHED	40-60%	ALIGNED	NA	NA	NA	NA	NA	NA-NA-NA-NA	
LJA-482	FLINT	COMPLETE	CORE	CORE/TOOL	20.90	18.50	8.00	2.75	NA	NA	NA	POSS_USE	40-60%	1	4	PLAIN	CONCENTRIC-NA-NA-NA	
LJA-483	FLINT																	

Supplementary Table S9. Selected attributes for Lichtenberg II (*continued*)

INVENTARNUMBER	RAWMAT	PRESERVATION	BLANK	CLASSIF	LENGTH	WIDTH	THICK	WEIGHT	PLATFORM	DORSALSCARS	DORSALDIRECT	TOOL_TYPE	AMOUNT_RETCORE	FLAKE_SUR	FLAKE_SCARS	CONDITION_STRIKE	FLAKING_DIR_A_B_C_D
LIA-503	FLINT	SHATTERED	CORE	SHATTER	16.40	9.60	8.40	0.70	NA	NA	NA	NA	NA	NA	NA	NA	NA-NA-NA-NA
LIA-504	Quartzite	COMPLETE	FLAKE	FLAKEITOO	75.00	41.50	11.60	41.00	PRIMARY_SURFACE-0%	0%	NA	NOTCH	NA	NA	NA	NA	NA-NA-NA-NA
LIA-505	FLINT	DISTAL	FLAKE	FLAKE	31.90	23.70	8.30	5.90	NA	NA	NA	NA	NA	NA	NA	NA	NA-NA-NA-NA
LIA-506	FLINT	DISTAL	FLAKE	FLAKE	20.70	12.20	6.10	3.70	NA	NA	NA	NA	NA	NA	NA	NA	NA-NA-NA-NA
LIA-508	FLINT	COMPLETE	CORE	CORETOOL	42.80	33.10	33.20	52.60	NA	NA	NA	HAMMERSTONE	10-30%	2	4	NA	BIDIRECTIONAL-UNIDIRECTIONAL-NA-NA
LIA-511	FLINT	SHATTERED	FLAKE	SHATTER	22.60	10.60	5.20	1.10	NA	NA	NA	NA	NA	NA	NA	NA	NA-NA-NA-NA
LIA-513	Quartzite	COMPLETE	FLAKE	FLAKE	53.70	106.30	25.00	90.60	PRIMARY_SURFACE-0%	40-60%	LATERAL	NA	NA	NA	NA	NA	NA-NA-NA-NA
LIA-514	IronCone	COMPLETE	COBBLE	MANUPORT	80.20	54.80	41.00	255.40	NA	NA	NA	NA	NA	NA	NA	NA	NA-NA-NA-NA
LIA-515	FLINT	COMPLETE	SHATTER	CORETOOL	13.50	15.30	6.90	1.25	NA	NA	NA	ENDSCRAPER	NA	NA	NA	NA	NA-NA-NA-NA
LIA-516	FLINT	PROXIMAL	FLAKE	FLAKE	17.70	22.10	7.10	3.45	NA	NA	NA	NA	NA	NA	NA	NA	NA-NA-NA-NA
LIA-517	FLINT	COMPLETE	FLAKE	FLAKE	29.20	13.60	8.80	2.55	PLAIN-100%	100%	LATERAL	NA	NA	NA	NA	NA	NA-NA-NA-NA
LIA-518	FLINT	COMPLETE	NATURAL_PIECE	CORE	47.60	63.40	60.10	171.30	NA	NA	NA	NA	10-30%	1	1	PRIMARY_SURFACE	UNIDIRECTIONAL-NA-NA-NA
LIA-521	FLINT	COMPLETE	FLAKE	FLAKE	18.00	12.70	22.10	4.80	PRIMARY_SURFACE-0%	0%	NA	NA	NA	NA	NA	NA	NA-NA-NA-NA
LIA-522	FLINT	COMPLETE	NATURAL_PIECE	CORE	24.90	12.00	12.40	4.45	NA	NA	NA	NA	100%	2	5	PLAIN	UNIDIRECTIONAL-UNIDIRECTIONAL-NA-NA
LIA-524	FLINT	COMPLETE	FLAKE	FLAKE	34.00	33.10	9.50	6.45	PLAIN-NA	100%	ALIGNED_LATERAL	NA	NA	1	NA	NA	NA-NA-NA-NA
LIA-526	FLINT	COMPLETE	NATURAL_PIECE	CORE	13.60	27.40	34.40	19.15	NA	NA	NA	NA	10-30%	1	1	PRIMARY_SURFACE	UNIDIRECTIONAL-NA-NA-NA
LIA-527	FLINT	PROXIMAL	FLAKE	FLAKE	10.40	18.00	4.50	1.20	NA	NA	NA	NA	NA	NA	NA	NA	NA-NA-NA-NA
LIA-528	FLINT	COMPLETE	FLAKE	FLAKE	16.10	12.70	2.60	0.30	PLAIN-NA	100%	ALIGNED	NA	NA	NA	NA	NA	NA-NA-NA-NA
LIA-529	FLINT	SHATTERED	CORE	SHATTER	16.00	12.00	7.40	1.15	NA	NA	NA	NA	NA	NA	NA	NA	NA-NA-NA-NA
LIA-532	FLINT	COMPLETE	SHATTER	CORETOOL	63.00	31.00	22.80	34.40	NA	NA	NA	NOTCH	NA	NA	NA	NA	NA-NA-NA-NA
LIA-536	FLINT	COMPLETE	FLAKE	FLAKEITOO	14.90	26.00	11.80	3.55	PRIMARY_SURFACE-0%	NA	NA	EDGE_RETTOUCH	NA	NA	NA	NA	NA-NA-NA-NA
LIA-537	FLINT	COMPLETE	FLAKE	FLAKE	16.60	19.20	5.70	1.95	PRIMARY_SURFACE-0%	40-60%	ALIGNED_LATERAL	NA	NA	NA	NA	NA	NA-NA-NA-NA
LIA-538	FLINT	COMPLETE	CORE	CORETOOL	21.90	14.80	13.00	3.20	NA	NA	NA	NATBACK	40-60%	2	3	PLAIN	UNIDIRECTIONAL-BIDIRECTIONAL-NA-NA
LIA-541	FLINT	COMPLETE	FLAKE	FLAKE	11.50	21.50	7.00	1.65	PRIMARY_SURFACE-0%	10-30%	LATERAL	NA	NA	NA	NA	NA	NA-NA-NA-NA
LIA-543	Quartzite	SHATTERED	SHATTER	SHATTER	20.30	12.00	7.70	1.55	NA	NA	NA	NA	NA	NA	NA	NA	NA-NA-NA-NA
LIA-545	FLINT	SHATTERED	FLAKE	SHATTER	29.60	26.00	6.60	4.00	NA	NA	NA	NA	NA	NA	NA	NA	NA-NA-NA-NA
LIA-548	FLINT	COMPLETE	FLAKE	FLAKE	12.80	15.80	3.50	0.80	CRUSHED	10-30%	LATERAL	NA	NA	NA	NA	NA	NA-NA-NA-NA
LIA-549	FLINT	SHATTERED	SHATTER	SHATTER	16.80	8.00	7.20	0.55	NA	NA	NA	NA	NA	NA	NA	NA	NA-NA-NA-NA
LIA-550	FLINT	COMPLETE	FLAKE	FLAKEITOO	50.60	27.70	9.70	11.65	CRUSHED	10-30%	ALIGNED	POSS_USE	NA	NA	NA	NA	NA-NA-NA-NA
LIA-554	FLINT	SHATTERED	CORE	SHATTER	17.80	10.90	7.80	1.10	NA	NA	NA	NA	NA	NA	NA	NA	NA-NA-NA-NA
LIA-556	Porphyry	COMPLETE	COBBLE	MANUPORT	55.00	51.60	42.50	167.85	NA	NA	NA	NA	NA	NA	NA	NA	NA-NA-NA-NA
LIA-557	FLINT	COMPLETE	FLAKE	FLAKEITOO	12.70	24.40	7.00	2.15	REMOVED	0%	NA	EDGE_RETTOUCH	NA	NA	NA	NA	NA-NA-NA-NA
LIA-558	FLINT	DISTAL	FLAKE	FLAKE	16.50	8.30	2.60	0.50	NA	NA	NA	NA	NA	NA	NA	NA	NA-NA-NA-NA
LIA-559	FLINT	COMPLETE	NATURAL_PIECE	CORETOOL	36.40	26.80	19.20	16.70	NA	NA	NA	HAMMERSTONE	NA	NA	NA	NA	NA-NA-NA-NA

References

- Bratlund, B., 1999. Taubach revisited. *Jahrbuch des Römisch-Germanischen Zentralmuseums* 46, 61–114.
- Gaudzinski-Windheuser, S., Roebroeks, W., 2014. Multidisciplinary studies of the Middle Paleolithic record from Neumark-Nord (Germany). Volume I, *Veröffentlichungen des Landesamtes für Archäologie Sachsen-Anhalt* 69. Beier & Beran, Halle(Saale).
- Hein, M., Weiss, M., Otcherednoy, A., Lauer, T., 2020. Luminescence chronology of the key-Middle Paleolithic site Khotylevo I (Western Russia) - Implications for the timing of occupation, site formation and landscape evolution. *Quaternary Science Advances* 2, 100008. <https://doi.org/10.1016/j.qsa.2020.100008>
- Mania, D., Toepfer, V., 1973. Königsau: Gliederung, Ökologie und mittelpaläolithische Funde der letzten Eiszeit. *Veröffentlichungen des Landesmuseums für Vorgeschichte in Halle* 26, Deutscher Verlag der Wissenschaften, Berlin.
- Pastors, A., 2001. Die Mittelpaläolithische Freilandstation von Salzgitter-Lebenstedt: Genese der Fundstelle und Systematik der Steinbearbeitung. *Archiv der Stadt Salzgitter, Salzgitter*.
- Tode, A., 1982. Der altsteinzeitliche Fundplatz Salzgitter-Lebenstedt. Teil I, archäologischer Teil. Böhlau, Köln, Wien.
- Toepfer, V., 1958. Steingeräte und Palökologie der mittel- paläolithischen Fundstelle Rabutz bei Halle. *Jahresschrift für mitteldeutsche Vorgeschichte* 41/42, 140–179.
- Veil, S., Breest, K., Höfle, H.-C., Meyer, H.-H., Plisson, H., Urban-Küttel, B., Wagner, G.A., Zöller, L., 1994. Ein mittelpaläolithischer Fundplatz aus der Weichsel-Kaltzeit bei Lichtenberg, Lkr. Lüchow-Dannenberg. *Germania* 72, 1–66.
- Weiss, M., 2020. The Lichtenberg Keilmesser - it's all about the angle. *PLOS ONE* 15, e0239718. <https://doi.org/10.1371/journal.pone.0239718>
- Weiss, M., 2015. Stone tool analysis and context of a new late Middle Paleolithic site in western central Europe - Pouch-Terrassenpfeiler, Ldkr. Anhalt-Bitterfeld, Germany. *Quartär* 62, 23–62. https://doi.org/10.7485/QU62_2
- Weiss, M., Otcherednoy, A., Wiśniewski, A., 2017. Using multivariate techniques to assess the effects of raw material, flaking behavior and tool manufacture on assemblage variability: An example from the late Middle Paleolithic of the European Plain. *Journal of Archaeological Science* 87, 73–94. <https://doi.org/10.1016/j.jas.2017.09.014>
- Weiss, M., Weber, T., 2019. Das Mittelpaläolithikum in Mitteldeutschland – Auswertung und Interpretation von Abschlaginventaren anhand multivariater Analysemethoden, in: Baales, M., Pasda, C. (Eds.), *All Der Holden Hügel Ist Keiner Mir Fremd - Festschrift Zum 65. Geburtstag von Claus-Joachim Kind*, Universitätsforschungen Zur Prähistorischen Archäologie [Upa]. Habelt, Bonn.
- Wiśniewski, A., Adamiec, G., Badura, J., Bluszcz, A., Kowalska, A., Kufel-Diakowska, B., Mikolajczyk, A., Murczkiewicz, M., Musil, R., Przybylski, B., Skrzypek, G., Stefaniak, K., Zych, J., 2013. Occupation dynamics north of the Carpathians and Sudetes during the Weichselian (MIS5d-3): The Lower Silesia (SW Poland) case study. *Quaternary International* 294, 20–40. <https://doi.org/10.1016/j.quaint.2011.09.016>

Section 4: Lichtenberg I and II Traceology

In order to provide additional data on the nature of the human occupation at the Middle Paleolithic site of Lichtenberg I and II, traceological analysis were conducted on a sample of 27 artefacts. The traceological method (Semenov, 1964) aims at identifying specific taphonomical, technological and functional traces or modifications, which allows us to reconstruct specific technical behaviours, the post-depositional history of anthropic inclusions within sedimentary units as well as how and to what end stone tools were made and used at a specific site. This is achieved by systematically scanning the edges and surfaces of stone tools under different magnifications ranging between 0.63 X to 500x and plotting their location and distribution. The location and morphology of specific micro negatives, edge rounding, microscopic polish, micro scars and striations are compared to an experimental reference collection in order to establish the kinetics of stone tool use as well as the material transformed (Chan et al., 2020; González-Urquijo and Ibañez-Estéves, 1994; Keeley, 1980; Vaughan, 1985). For this study a Carl Zeiss Stemi 508 stereo microscope and an Olympus reflected light microscope have been used.

The majority of the analyzed artefacts have been made on flint and show a light developed soil polish, which presents itself as an ephemeral bright sheen that covers the entire surface of the artefacts and impedes the secure identification of the materials transformed. Out of the 27 lithics eight have suffered less from taphonomic processes making the identification of both motion and material transformed possible, while on six only the motion and location of working edges could be detected (Table S10). Artefacts from Lichtenberg I and II have been analyzed. The Lichtenberg I sample was composed of one Keilmesser, two flakes and one fragmented tool with bifacial shaping. Due to taphonomical constraints, the tool fragment and the flakes presented no discernible traces of use. The Keilmesser, on the other hand, presented traces resulting from longitudinal (cutting) motions. The Lichtenberg II tools were used with different modalities of force, including pressure and percussion. Tools used with the application of pressure have been wielded in longitudinal, transverse and drilling motions (Figure S42).

Table S10. Summary of the traceological analysis. Li-6, Li-7, LIA-36, and LIA-50 are from Lichtenberg I, the other artefacts come belong to Lichtenberg II.

#	Blank	Use	Force	Motion	Striations	Working Edges	Material Worked
Li-6	Fractured bifacial tool	No	-	-	-	1	-
Li-7	Keilmesser	Yes	Pressure	Longitudinal	Y	1	Soft Organic
LIA-36	BTF	No	-	-	-	-	-
LIA-50	Flake	No	-	-	-	-	-
LIA-99	Flake,	No	-	-	-	-	-
LIA-103	Flake/Spal	Probably,	Pressure/ Percussive	Drilling	-	2	Hard Organic
LIA-120	Flake	No	-	-	-	-	-
LIA-121	Flake	Yes	Pressure/ Percussive	Transverse/ Longitudinal	Y	2	Hard Organic
LIA-128	Flake	Probably,	Pressure/ Percussive	Transverse	No	1	-
LIA-133	Ckunk	Yes	Pressure	Drilling	No	1	Hard Organic
LIA-147	Flake	No	-	-	-	1	-
LIA-152	Flake/Spal	?	Pressure	-	-	1	-
LIA-154	Core/Chunk	Yes	Pressure	Transverse	Y	1	Hard Organic
LIA-216	Flake/Spall	Yes	Pressure	Longitudinal / Transverse	Y	2	Soft Organic/ Hard Organic
LIA-285	Chunk	Probably	Percussive	-	-	1	-
LIA-307	Flake	Yes	Pressure	Transverse	Y	1	Hard Organic/Wood
LIA-327	Flake	No	-	-	-	1	-
LIA-330	Flake	No	-	-	-	-	-
LIA-342	Flake	Probably	Pressure/ Percussive	Longitudinal / Transverse	-	2	-
LIA-359	Flake	Yes	Pressure	Transverse	Y	1	Soft Vegetal/ Hard Organic

LIA-377	Core/Chunk	No	Percussive	-	-	-	-
LIA-379	Chunk	?	Percussive	-	-	-	-
LIA-398	Flake/Spal	Probably,	Pressure	Transverse	-	1	Hard Organic
LIA-478	Chunk	No	-	-	-	-	-
LIA-504	Flake/Spall	No	-	-	-	1	-
LIA-538	Flake/Spal	Probably	Pressure	Transverse	-	1	-
LIA-550	Flake	Yes	Pressure	Transverse	Y	2	Soft Vegetal / Hard Organic

Artefact LIA-550 (Figure S43), a flake made on dark translucent flint, shows two working edges, one on the distal termination, which ends on a hinge fracture, and one on the lateral edge of the tool; both have been used in transverse motions. The traces located on the distal working edge show a well-developed bright undulating polish with a high incidence of directional markers indicating a crossed transverse motion. This bright well-developed polish likely formed from the contact with a highly abrasive and soft vegetal material while the striations may be related to the admixture of mineral particles, possibly sand or grit during the scraping activity. The working edge was re-sharpened leaving only a small part of the original traces preserved.

Artefact LIA-307 shows a small concave truncation placed on the distal portion of a dark translucent thick flake, which was intentionally thinned along the proximal ventral surface (Figure S44). The working edge shows intense rounding from use indicative for the processing of a hard organic material. Well-developed bright polish on both extremities of the working edge, associated with the rounding may indicate the working of wood. The edges of the negatives on the dorsal surface of the tool shows signs of crushing while “G” type polish (Moss, 1987; Rots, 2010) spots on the ventral surface may indicate that the artefacts was hafted.

The processing of soft animal material has been attested at artefact LIA-216, which is an elongated flake with parallel sides that shows two working edges, one on the acute lateral edge and one on the steeper distal portion (Figure S45). Along the edge a patterned distribution of micro negatives on both dorsal and ventral faces, coupled with micro stria indicate a longitudinal and transverse motions. Light developed undulating mate micro polish and circular micro pits indicate a soft, but abrasive organic material; in combination with punctuated bright flat polish areas, which hint at the repeated contact with a harder material may indicate a possible use of this tool as a meat knife or butchering tool.

Artefact LIA-359 shows a concave working edge with a steep cortical back. The high incidence of micro negatives with step fracture and hinge fracture terminations in combination with the punctuated crushed appearance of the working edge may be a result of combination of both the application of pressure and percussive motions during use activities. Different traces including bright undulating micro polish observed on the distal portion of the dorsal working edge, flat bright spots and scars as well as an extensive bright flat micro polish surface with striations on the ventral surface have been observed (Figure S46). The processing of both hard, possibly wood, and soft abrasive vegetable material is suggested for this tool.

The analyzed Keilmesser (LI-7) presents a symmetrical outline and well-defined techno functional elements including a working edge, a transformative part and a prehensile/hafting zone. The continuous and symmetric convex working surface shows signs of repeated re-sharpening on the dorsal face, evident by the continuous retouch, which is absent on the ventral surface save for a series of larger negatives on the distal end of the working edge. A considerable amount of effort was placed in thinning the prehensile/hafting zone or back of the tool. The tool is made on dark Baltic flint and shows little signs of severe post-depositional modification, i.e. mechanical damage or chemical weathering furthering the preservation of wear traces. Traces indicating the natures of the transformed material, however, are subtle being constricted to lightly developed micro polishes zones located on the distal portion of the working edge (Figure S47 F1). Negative edge rounding and additional polished surfaces are found further inwards on the dorsal side of the working edge. Directional markers, including striations running parallel to the working edge of the tool and generally associated with lightly developed polished spots are also located on the dorsal surfaces of the working edge. In combination with the micro negatives located on the ventral side of the tool a longitudinal cutting motion under the excretion of pressure is suggested for the tool comparable with the interpretation offered by previous traceological analysis from Lichtenberg (Veil et al., 1994). The light developed polish and the presence of striations on the analyzed specimen indicates the processing of a soft organic material and occasional contact with harder organic substance; a use as butchering knife is therefore suggested.

The back of the analyzed Keilmesser shows a series of marked modifications and traces associated with intense mechanical stress. The distal portion of the back shows marked rounding and crouching evident by short continuous micro-negatives with step and hinge terminations (Figure S48 F1 and F2). Bright and semi undulating cohesive polished areas have been identified on the edges of the negatives located on the medial portion of the back indicating the repeated contact with a hard organic

substance. Together these signs may indicate the continued mechanical friction of the tool with a hard organic haft, thus possibly indicating the use of composite tools by Neanderthals at the site. Which is not to say that Keilmesser tools in general were hafted, a sample of one hardly establishes a pattern making it paramount to conduct further investigations into the subject.

In summary the preliminary traceological analysis of the Lichtenberg II lithic material indicates a heterogeneous pattern of activities including the processing of soft animal materials, soft and abrasive vegetable materials and hard vegetable materials (wood). The combination of percussive and pressure force has been noted as well as the possible use of hafting technology. The latter has been observed on artefact LIA-307 based on the presence of G type polish and the scarring on the dorsal surface along the edges of the central negatives. The diminutive characteristics of the assemblage in general, the high incidence of crushing coupled with the high amount of force used during the different productive activities undertaken at the site may suggest that artefact LIA-307 was not the only hafted tool. The absence of further hafting wear, however, constrains the further exploration of this possibility. In respect to the traceological analysis of the sample from the Keilmesser horizon from Lichtenberg I, a use of the analyzed specimen as a hafted butchering knife is suggested due to the wear traces identified. It cannot be stressed enough, however, that additional specimens need to be analyzed in order to fully understand the function of the Neanderthal occupation in order to add information to the already existing traceological investigation (Veil et al., 1994). While the analyzed lithic assemblage from Lichtenberg II is yet too small to properly address site function the preliminary analysis supports the interpretation of the site as being more than a raw material extraction and tool production station and likely the accumulation of the lithics reflects a diversified spectrum of tasks and productive activities undertaken by Neanderthals at a lakeshore environment.

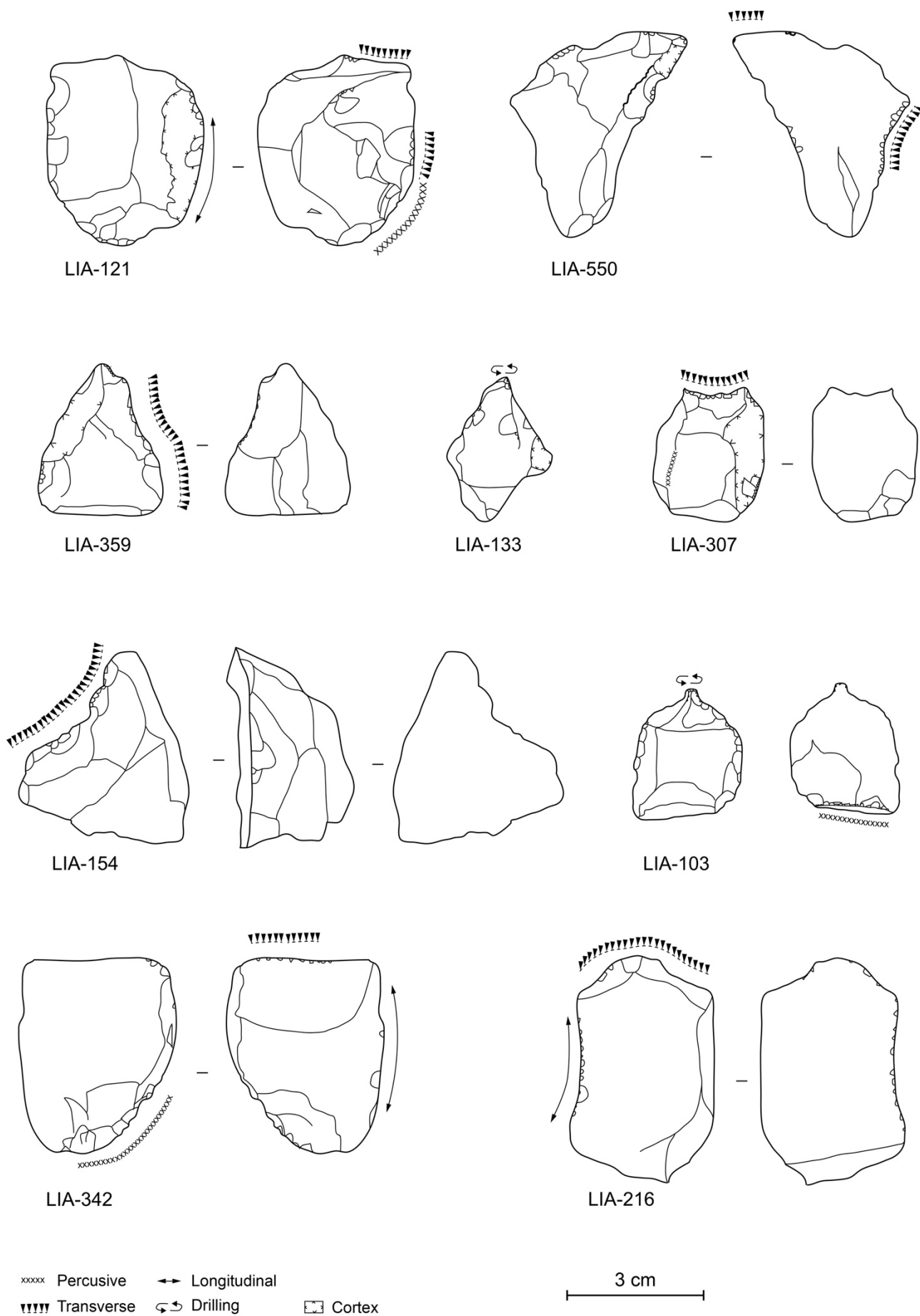


Figure S42. Schematic drawings of the tools with definite and probable use traces showing the location of working edges, the type of force used and use motions.

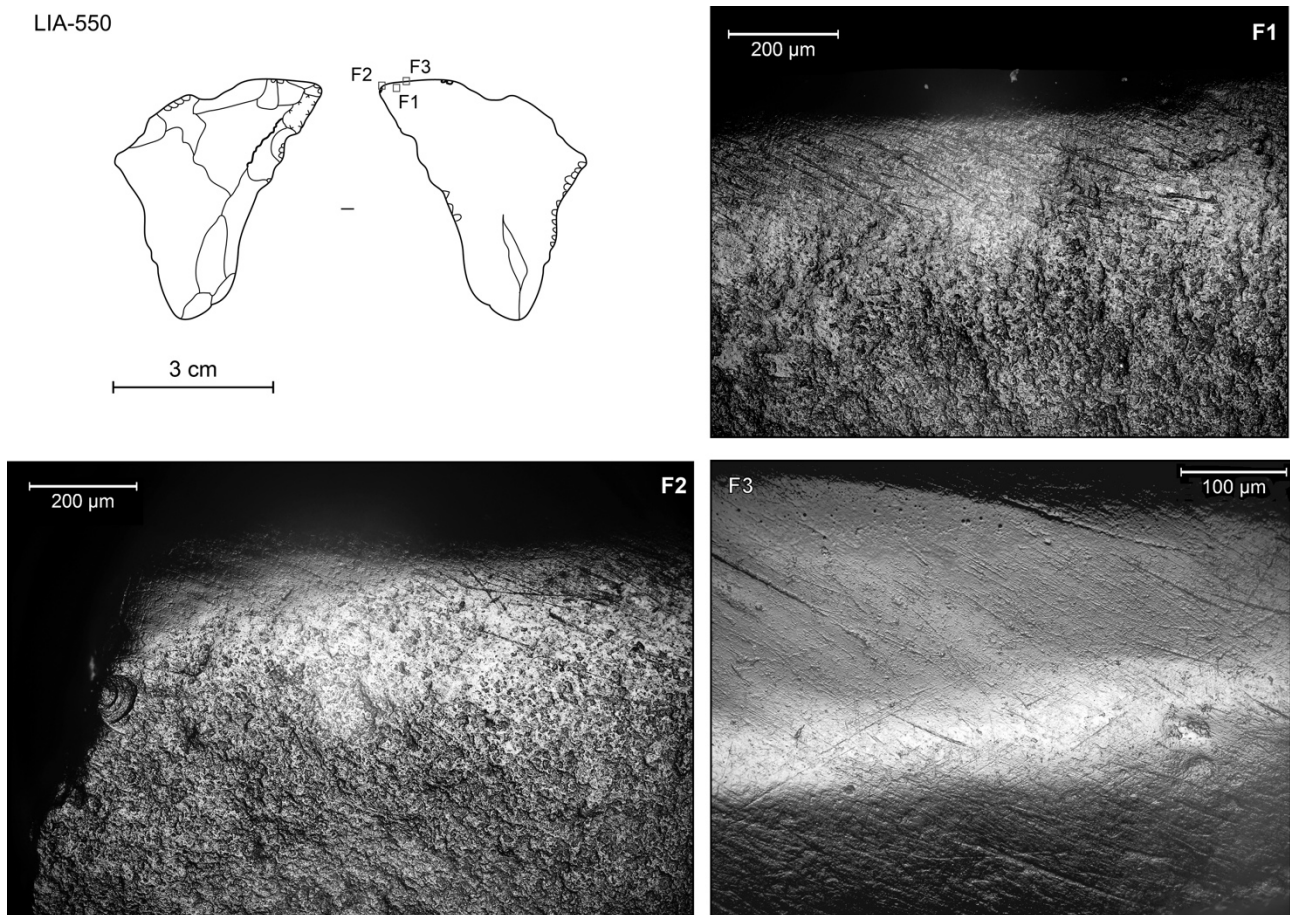


Figure S43. Schema of artefact LIA-550 and the location of the micrographs showing the use related polish. F1 – taken at magnification 100 x bright undulating extensive polish located on the distal portion of the working edge; F2 – taken at magnification 100x on the edge of the working surface showing the spread of the bright undulating extensive polish, note the high incidence of striations and scratches; F3 – taken at magnification 200x at the center of the maximum extension of the micro polished surface on the working edge of the tool. The spread and connectedness of the polish is very high and the surface is extremely smoothed, again the criss-cross patterned motion of tool use is particularly evident by the striations and scratches. The resemblance to cereal polish (Clemente and Gibaja, 1998) is remarkable.

LIA-307

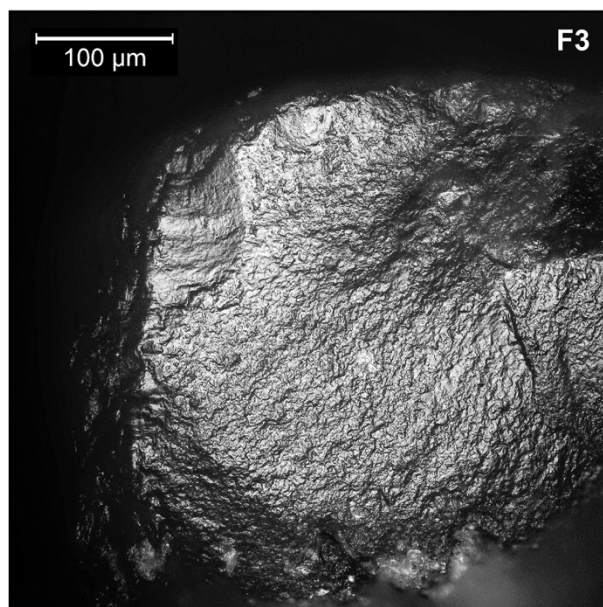
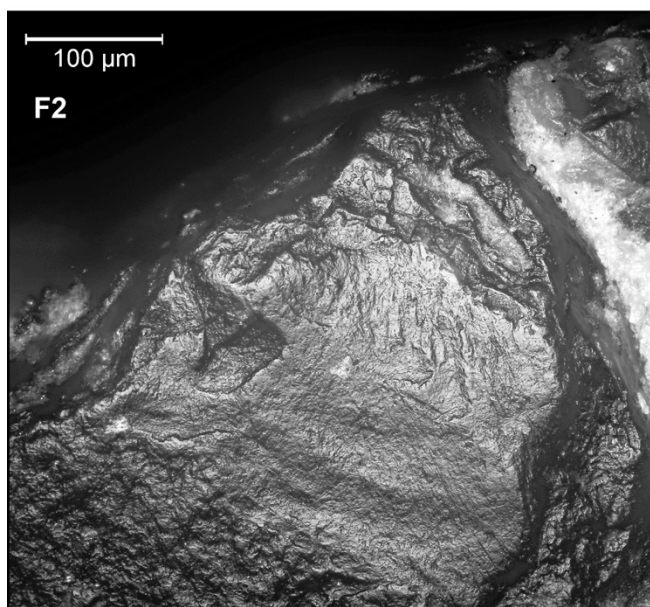
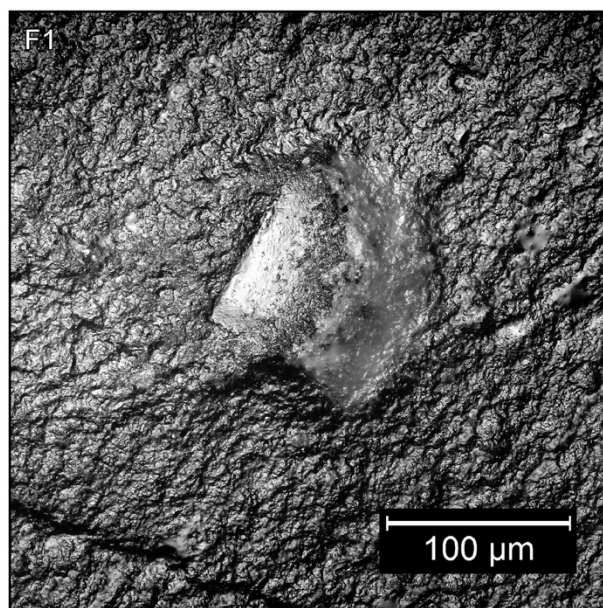
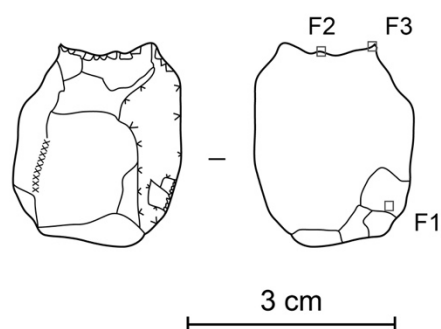


Figure S44. Schema of artefact LIA-307 and the location of the micrographs showing use and hafting related polish. F1 – flat bright polish located on the eminence of the micro topography on the ventral surface of the tool; F2 and F3 – negative edge rounding and bright undulating extensive polish on concave working surface. All micrographs taken at magnification 200x.

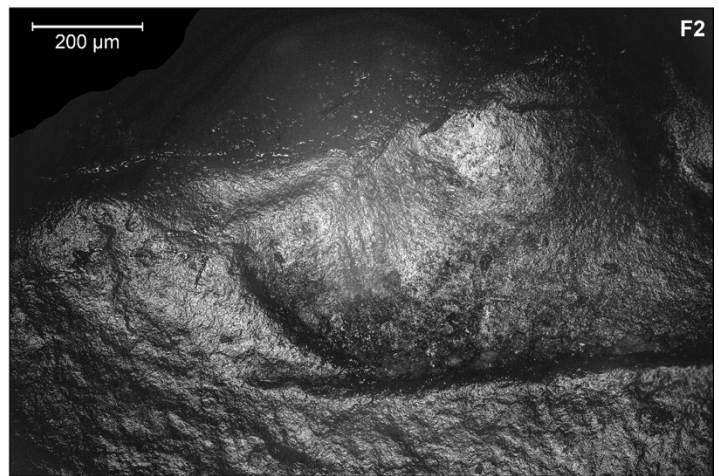
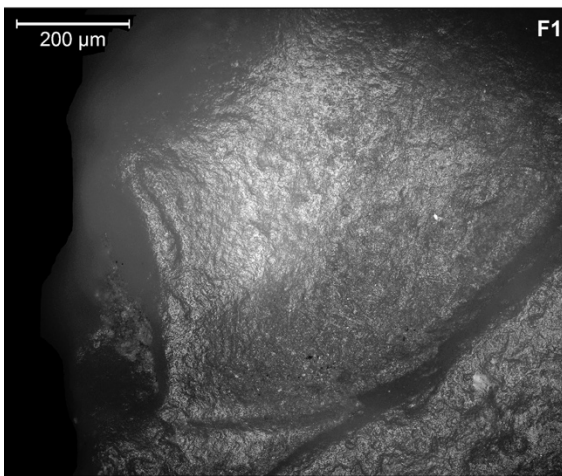
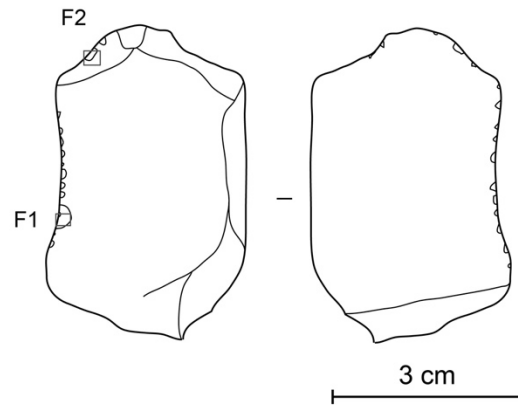


Figure S45 Schema of artefact LIA-216. F1 – micrograph of the polish showing the orientation and motion of tools use, note the micro pits and the undulating character of the micro polish; F2 – micrograph showing the rounded edges of the micro negatives and the lightly developed micro polish with parallel striations oriented perpendicularly to the working edge. All micrographs taken at 200x.

LIA-359

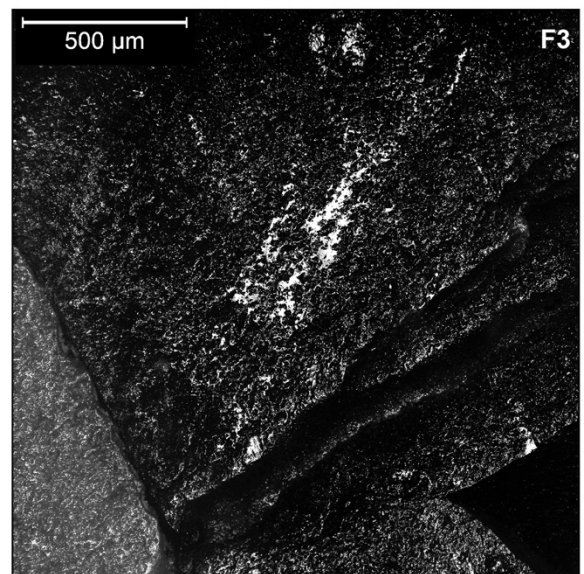
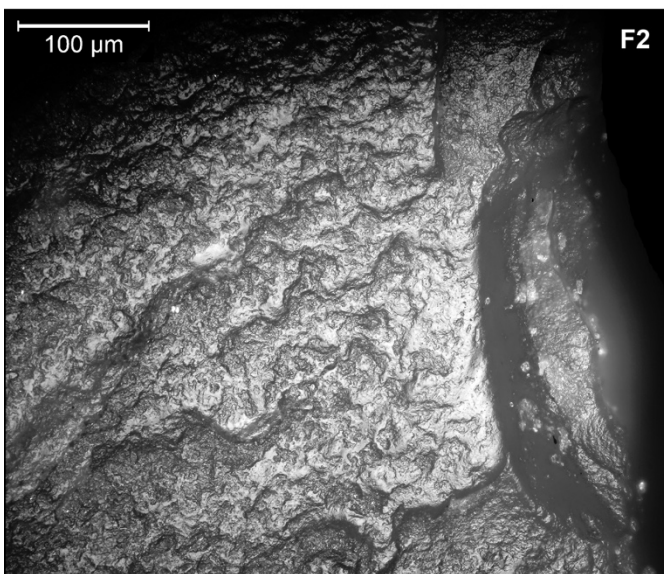
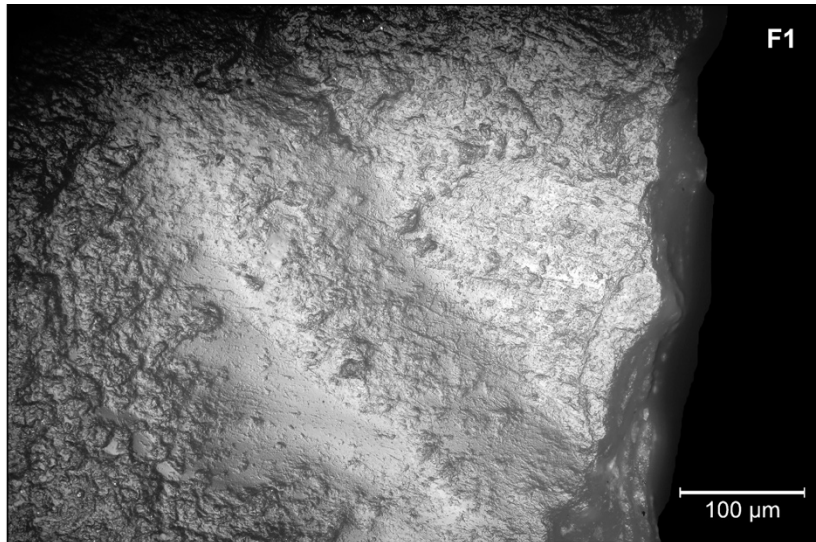
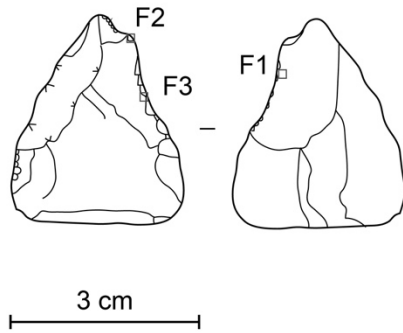


Figure S46. Schema of artefact LIA-359. F1 – micrograph showing the well-developed and interconnected bright undulating micro polish, micrograph at 200x; F2 – Micrograph showing the rounded edges of the negatives and the well interconnected undulating polish on the eminences of the micro topography of the stone tool edge, micrograph at 200x; F3 – bright and flat polish at magnification 50x.

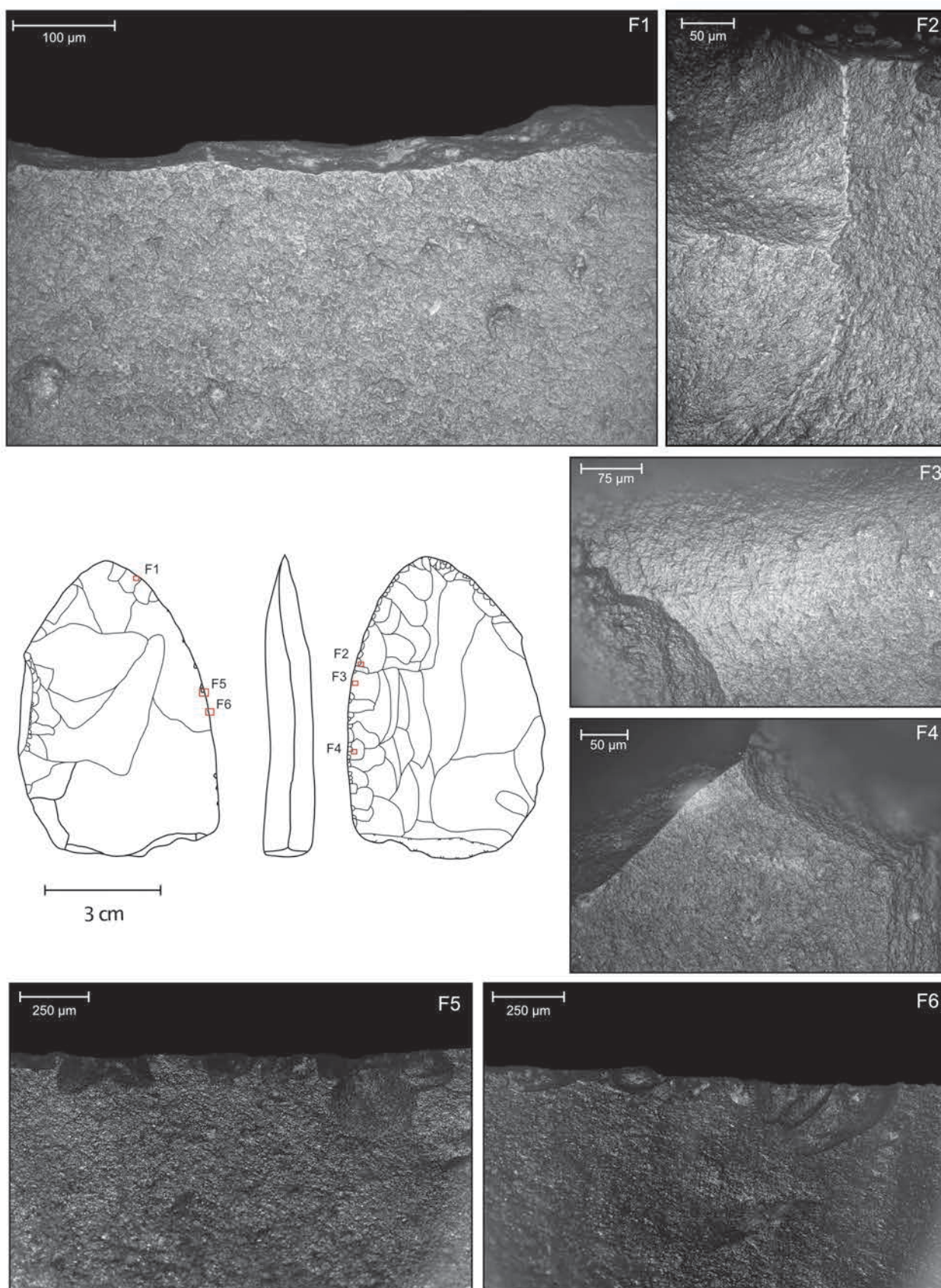


Figure S47. Keilmesser Li-7 from Lichtenberg. F1 – micrograph of the light developed bright polish on the edge of the active zone of the tool; F2 – micrograph showing the rounded and polished edges of the negatives on the dorsal surface of the working edge; F3 and F4 – micrographs of the striations on the interior of the dorsal side of the tools' working edge; F5 and F6 – micrographs of the micro-negatives on the ventral surface of the working edge.

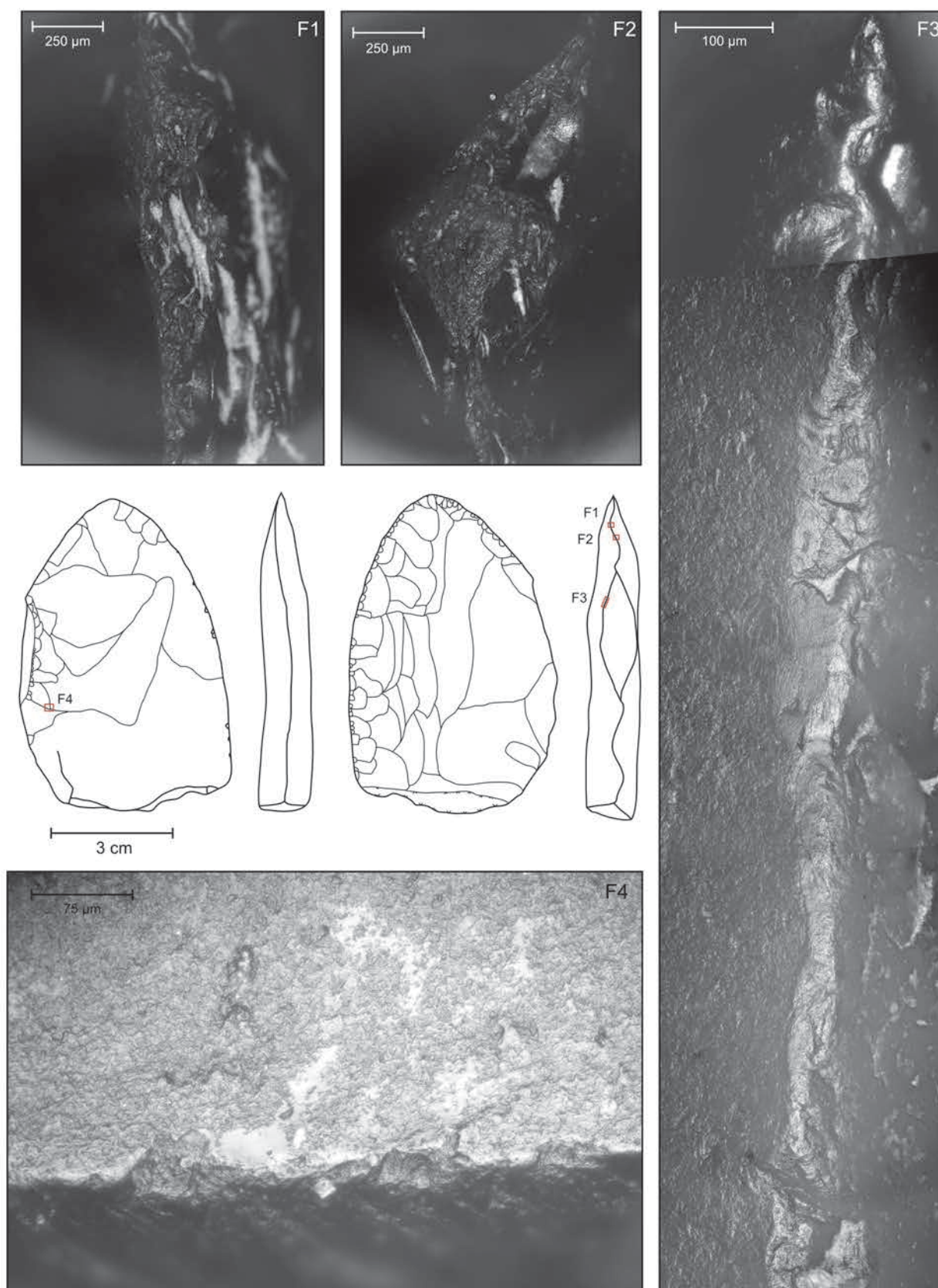


Figure S48. Traces on the prehensile/hafting zone of the Keilmesser Li-7. F1 and F2 – crushed and abraded edges on the back of the tool; F3 – composed micrograph images showing the undulating bright and well interconnected polish on the edge of the negative forming the back of the Keilmesser; F4 – bright undulating “G” type polish on the ventral surface of the tool.

References

- Chan, B., Francisco Gibaja, J., García-Díaz, V., Hoggard, C.S., Mazzucco, N., Rowland, J.T., Van Gijn, A., 2020. Towards an understanding of retouch flakes: A use-wear blind test on knapped stone microdebitage. *PLoS One* 15, e0243101. <https://doi.org/10.1371/journal.pone.0243101>
- Clemente, I., Gibaja, J.F., 1998. Working Processes on Cereals: An Approach Through Microwear Analysis. *J. Archaeol. Sci.* 25, 457–464. <https://doi.org/10.1006/jasc.1997.0214>
- González-Urquijo, J.E., Ibañez-Estéves, J.J., 1994. Metodología de análisis funcional de instrumentos tallados en sílex. Universidad de Duesto.
- Keeley, L.H., 1980. Experimental Determination of Stone Tool Uses: a Microwear Analysis. University of Chicago Press.
- Moss, E., 1987. Polish G and the question of hafting, in: *La Main et l'outil: Manches et Emmanchements Préhistoriques*. G.S. Maison de l'Orient, pp. 97–102.
- Rots, V., 2010. Prehension and hafting traces on flint tools: a methodology. Universitaire Press Leuven.
- Semenov, S.A., 1964. Prehistoric Technology: an Experimental Study of the Oldest Tools and Artifacts from Traces of Manufacture and Wear. Barnes and Noble.
- Vaughan, P.C., 1985. Use-wear analysis of flaked stone tools. University of Arizona Press Tucson.
- Veil, S., Breest, K., Höfle, H.-C., Meyer, H.-H., Plisson, H., Urban-Küttel, B., Wagner, G.A., Zöller, L., 1994. Ein mittelpaläolithischer Fundplatz aus der Weichsel-Kaltzeit bei Lichtenberg, Lkr. Lüchow-Dannenberg. *Germania* 72, 1–66.

Supplementary Information S2 – Sections 5 to 8 Geo-Biosciences

Neanderthals in changing environments from MIS 5 to early MIS 4 in northern Central Europe – Integrating archaeological, (chrono)stratigraphic and paleoenvironmental evidence at the site of Lichtenberg

Marcel Weiss^{*1,2}, Michael Hein^{*1}, Brigitte Urban³, Mareike C. Stahlschmidt¹, Susann Heinrich¹, Yamandu H. Hilbert², Robert C. Power^{4,1}, Hans v. Suchodoletz⁵, Thomas Terberger⁶, Utz Böhner⁶, Florian Klimscha⁷, Stephan Veil⁷, Klaus Breest⁸, Johannes Schmidt⁵, Debra Colarossi^{9,1}, Mario Tucci³, Manfred Frechen¹⁰, David Colin Tanner¹⁰ & Tobias Lauer¹

¹Max Planck Institute for Evolutionary Anthropology, Leipzig, Germany

²Institut für Ur- und Frühgeschichte, Friedrich-Alexander-Universität Erlangen-Nürnberg, Erlangen, Germany

³Leuphana University Lüneburg, Institute of Ecology, Lüneburg, Germany

⁴Institute for Pre- and Protohistoric Archaeology and Archaeology of the Roman Provinces, Ludwig Maximilian University Munich, Germany

⁵Institute of Geography, Leipzig University, Leipzig, Germany

⁶State Service for Cultural Heritage Lower Saxony, Hannover, Germany

⁷Lower Saxony State Museum, Department for Research and Collections, Archaeology Division, Hannover, Germany

⁸Volunteer archaeologist, Berlin, Germany

⁹Department of Geography and Earth Sciences, Aberystwyth University, Aberystwyth, Wales, UK

¹⁰Leibniz Institute for Applied Geophysics, Stilleweg 2, Hannover, Germany

Section 5: Stratigraphic framework

5.1 Field descriptions and interpretation

Layer 1 is a ploughing horizon, developed in layer 2 and the humic topsoil that formed in layer 2 during the Holocene.

Layer 2 consists of gravelly, slightly silty and loamy sand, which is very poorly sorted and unbedded, i.e. massive. Its vertical extent coincides with a distinctly brunified Bw-horizon of a Cambisol. In some places, there is an accumulation of coarser gravel (stoneline) at its lower boundary. However, more often, a gravel concentration is found in the central parts of the layer. These characteristics are typical for a phenomenon called ‘Geschiebedecksand’ (GDS, periglacial cover sand), which is ubiquitously observed in the northern German lowlands. Its genesis is still a matter of debate, but there is general agreement, that different periglacial processes contributed, most importantly solifluction with a varying aeolian influx. The GDS is thought to have formed as a cold stage deposit during the late or latest Weichselian in MIS 2 (Altermann et al., 2008; Grimm, 1973; cf. Semmel and Terhorst, 2010).

Layer 3 is characterized by slightly gravelly and silty, poorly sorted, yellow medium sand. The structure varies between a well-bedded planar to trough-like lamination and entirely structureless segments. The layer is interveined by thin gravel beds/stonelines, the most pronounced situated at the lower boundary, where occasional wind-faceted pebbles occur. These stonelines are very common in periglacial deposits of northern Central Europe and are usually interpreted as erosional residues or deflation beds (Van Huissteden et al., 2000; Zagwijn and Paepe, 1968). Accordingly, an alternation of solifluction, slopewash and likely aeolian influence needs to be assumed for the formation of layer 3 (cf. Fränkle, 1988; Richter et al., 1970). In that regard, it is related to layer 2 above, which is confirmed by grain size analysis (Fig. 3, main text, Supplementary Section 5.2). Contrary to layer 2, evidence for pedogenesis is missing. Frost features (involutions and cracks) can be observed in layer 3, but it is unclear, whether they developed in conjunction with MIS 4 or MIS 2 permafrost processes.

Layer 4 contains finely laminated, wavy plane-bedded, pale yellow, moderately to poorly sorted, fine to medium sands, which are interbedded with thicker lenses of better sorted medium sands, similar to those of layer 5. Occasionally, the mm to cm thick laminae of layer 4 are interspersed with organic matter (plant fibers), that might be redeposited residues from an upslope interglacial or interstadial. Genetically, this sediment is interpreted as a niveofluvial to niveoaeolian deposit, triggered by annual snowmelt and associated slopewash in loosely

vegetated conditions. The lenses of better sorted sands (cm to dm scale) are either produced by erosional redeposition of aeolian sands (e.g. from layer 5) on the slope or by contemporaneous aeolian saltation processes, alternating with the slopewash (Christiansen, 1998a; Christiansen, 1998c; Van Huissteden et al., 2000). Niveofluvial and niveoaeolian deposition is known to have been one of the most important geomorphic processes in the former periglacial areas of northern Central Europe (see references for layer 8/9). Post-depositionally, layer 4 has experienced a cryogenic overprint in the form of involutions, updoming and frost-cracking. In such clear ex-situ positions, the layer is referred to as 4'.

Layer 5 comprises very loose, yellow medium sands that are better sorted than in the surrounding layers. In Trench 2, they are sheet-like (ca. 10 cm thickness) and sometimes display an inclined, fine bedding (dip angle of ca. 15°), possibly indicating foreset-lamination. However, in Trench 1, they are predominantly structureless, macroscopically massive and frequently subjected to former cryoturbation, in that case referred to as layer 5'. The interpretation of layer 5 as an aeolian sand, transported and deposited by saltation rather than in suspension is supported by micromorphology and grain size analysis (cf. reference given there). Thin aeolian sand sheets with limited lateral extent and well-sorted medium sands are commonly found in periglacial Weichselian sequences of Central and Western Europe (Schwan, 1988; cf. Vandenberghe, 1992).

Layer 6 is characterized by unbedded, poorly to moderately sorted, fine to medium sands with an orange oxidation color. The latter is likely due to lepidocrocite dominance, inferred from the high chroma values in the Munsell colors (between 6 and 8). Lepidocrocite is formed in redoximorphic environments by episodic water logging and might be related to permafrost processes but also fluctuating groundwater levels (Cornell and Schwertmann, 2003). Layer 6 cannot be assigned to any depositional process with confidence, so far. This is mainly because of its low extent in the sequences, rendering it impossible to distinguish between original properties and posterior alterations by cryogenesis or hydromorphic conditions. Furthermore, because of the patchy occurrence and undiagnostic features in the field, only one grain size sample has been taken and analyzed from layer 6 (sample 22, Fig. 3, main text). A ferruginated zone on top of layer 7 (see there) might actually be a pedogenic feature of layer 6. This hypothesis is strengthened by a three-part banded occurrence of this ferrugination in the northern section of Trench 1 (Supplementary Figure S 50), where the individual members are separated by medium sands seemingly belonging to layer 6. Additional exposures within the excavation area in Lichtenberg might help to resolve this ambiguity in the future.

Layer 7 is a thin bed (< 15 cm) of whitish, very poorly sorted fine sandy silt to silty very fine sand that appears to be massive in macroscopic examination (but weakly bedded in thin sections; Supplementary Figure S 53, Supplementary Section 5.3). Notably, it has a very brittle and dense structure, therefore it is not easily deformable but all the more easy to recognize even in cryoturbated segments that occur as injections and diapiric structures (layer 7'). At the study site, this deposit covers extensive areas as a thin veneer with distinct upper and lower boundaries. Given that the site is situated alongside an Eemian to Weichselian palaeolake (Hein et al., 2021), we interpret this layer as a lacustrine, muddy shoreface deposit, which is typical for small lakes with very narrow coastal belts. According to Cohen (2003, cf. Bridge and Demicco, 2008) this facies frequently shows very thin laminar beds but is often massive due to bioturbation or rapid deposition. In Trench 2 (Fig. 2c, main text), layer 7 is intertonguing and alternating with the underlying slope deposits of layer 9. A bit further upslope the individual filamentary members of layer 7 first unify in a single layer and then wedge out shortly afterwards. Throughout the sequence, at the upper boundary of layer 7, a brown-orange ferrugination can be observed, seemingly formed in overlying medium sands (layer 6?) that became cemented by the process. The Munsell color implies that ferrihydrite might be the dominant iron oxide here (Cornell and Schwertmann, 2003). This ferruginated zone encroaches into the whitish silty deposit of layer 7 along a drop-shaped boundary, resembling a micro-drop soil on a mm to cm-scale. While a pedogenic influence cannot be ruled out (Supplementary Section 5.3), the origin of this overlying iron-cemented medium sand is not clear therefore the stratigraphic and chronological relationship of a possible soil formation with layer 7 is uncertain. This question will be the topic of a follow-up publication. Both the in situ layer 7 and the cryoturbated expression 7' accommodate Middle Palaeolithic artefacts and comprise the main part of the archaeological find horizon Li-I.

Layer 8 consists of fine to medium gravelly, medium sands that are poorly sorted, crudely to non-bedded and possess a greyish to light brown color with redoximorphic features. This deposit is only present in Trench 1 and its upper 5 to 10 cm contain lithic artefacts as part of the archaeological find horizon Li-I. Interpretation will be undertaken together with layer 9.

Layer 9 is a thick deposit (40 cm to >1 m) of finely laminated, wavy plane-bedded and moderately to poorly sorted fine to mediums sands with greyish to light brown color. In some places, it is streaked with horizontal or mottled iron oxide accumulation. In Trench 2 (western section) the layer is interbedded with the lacustrine sediments from layer 7 (see there), in the eastern section it is heavily distorted by cryogenic processes (cryoturbation/solifluction). In Trench 1 (southern section) it is contained within a cryoturbation pocket. We refer to these

reworked segments as layer 9' (Fig. 2, main text). The thin, wavy lamination and the granulometric properties (Supplementary Section 5.2) clearly lead to an interpretation as niveofluvial slopewash sediment, whose deposition was induced by annual snowmelt (Christiansen, 1998b). Layer 8 was likely formed by the same process, only that higher-energy slopewash also transported pebble-sized grains. This points to comparatively more intense melting, which often results in a massive, unbedded structure (cf. Christiansen, 1998c). Niveofluvial processes played a major role in the erosion and re-shaping of periglacial landscapes during the Weichselian in Central and Western Europe (Lade and Hagedorn, 1982; Menke, 1976; Zagwijn and Paepe, 1968).

Layer 10 is a very thin veneer (<10 cm) of fine-sandy to loamy silt with gleyic properties and a very slight organic carbon (C_{org}) content. Appearing massive in the field, the layer shows clear bedding structures in thin sections (Supplementary Section 5.3, Supplementary Figure S 52). It possesses particularly distinct upper and lower boundaries. Only present in Trench 2, layer 10 emerges from layer 11b and covers extensive parts of layer 11a, but wedges out towards higher ground in the northern half of Trench 2 (cf. Fig. 2 main text). The layer discontinuously contains very thin humic veins of a few mm thickness. Contrary to the overlying sediments, layer 10 has not been affected by cryoturbation in the observed exposure. In terms of thickness, structure and texture, it shows a strong resemblance to layer 7. Therefore, just like the latter, layer 10 is interpreted as a muddy, lacustrine shoreline or shoreface sediment, deposited within the narrow coastal zone of a small lake (Bridge and Demicco, 2008; Cohen, 2003). The humic vein is taken to represent a drift line (cf. Supplementary Figure S 52), formed by wave activity that reworked organic compounds (possibly from layer 11b) in the intertidal zone of the lake.

Layer 11 only occurs in Trench 2, does not display apparent cryogenic deformations and has a bipartite nature (11a and 11b). Both members incorporate lithic artefacts of the archaeological find horizon Li-II, with the highest find densities existing in the uppermost 11 cm of 11a. *Layer 11a* consists of a slightly humic, very silty, very poorly sorted fine sand, that appears massive in the upper ~40 cm, but gradually changes to a crude, weakly inclined (consequent) bedding and a notable redoxidomorphic mottling underneath. The archaeologically relevant upper part also contains high abundancies of charred organic matter. Additionally, in the uppermost 10 cm on the slope near the contact with layer 11b, various, stacked humic veins occur (Supplementary Figure S 59). In the northern part of Trench 2, where layer 10 is wedging out (see there), a ca. 10 cm thick half-bog horizon developed within and on top of layer 11a. The presence of this half-bog and layer 10 seems to be mutually exclusive, which might point towards an erosive contact between both layers. This palaeosol will be the subject of a follow-up publication. *Layer*

11b is a peaty, detrital and sandy mud, that becomes more silty and fine-detrital towards the north in Trench 2 (layer 11b₂) (Supplementary Figure S 59). Generally, layer 11b is directly overlain by layer 9. However, in some places very shallow kettles on the surface of layer 11b (due to slight subsidence) accommodate a thin (<1 cm) grey silt, that might correlate with layer 10. While in the eastern section of Trench 2 the stratigraphic relationship between layers 11a and 11b remains rather ambiguous (possibly due to erosion or settlement/slippage of neighboring deposits – see below), it can be clarified in the western section (Fig. 3b/c, main text, Supplementary Figure S 59a/b). A branch of 11b₂ is horizontally extending to the north and turns into a highly humic sand, which clearly interfingers with layer 11a. Consequently, the two sub-layers can be regarded as stratigraphically contemporaneous, even though layer 11a started forming shortly before 11b, because it not only interfingers with, but also underlies the latter. In small closed-basin lakes, sediments of the actual lake and the coastal plain are hardly distinguishable, because of usually significant water table fluctuations that alternately expose or inundate certain deposits. We understand layer 11 in its entirety to comprise different coastal-lacustrine environments (cf. Bridge and Demicco, 2008; Cohen, 2003; Mania and Toepfer, 1973). Layer 11a as a beach face deposit, situated next to the shoreline represented by layer 11b. Beach deposits are often lakeward-dipping, but can be massive around small lakes due to low wave energy or bioturbation. The vertical and lateral extent of the beach deposit is shown in Supplementary Figure S 49a. It possesses a constant thickness of just under 1 m and can be traced along a section of ca. 30 m in the accompanying coring transect (Hein et al., 2021). These dimensions and the silty, fine sandy texture are typical for small-lake beach faces (see references above). In Trench 2, the stacked humic veins in the uppermost part of the downslope segment in layer 11a represent drift lines (compare layer 10), formed by wind driven waves that ran on the beach, depositing organic compounds and redistributing beach sands. From the stacked, multi-generation nature of these drift lines, a prograding lake with a rising water table can be inferred. This also caused the deposition of the peaty layer 11b (which partially overlies layer 11a) in shallow waters near/at the shore. Beyond that, the lateral contact zone between the more aquatic 11b and the beach deposit of 11a seems to be complex and variable, with very small-scale differences. Whereas in the western section of Trench 2, this contact shows an interfingering of both deposits, the situation in the eastern section resembles that of a minor wave-cut niche (Supplementary Figure S 59).

The lithostratigraphy of core PD.028 (for position see Fig.1, main text) is presented in Supplementary Table S 11.

5.2 Grain sizes analysis

Scatter plot (Fig. 3a, main text)

The aeolian sands, found in layer 5, were initially thus described for their remarkably loose sedimentary structure and the microscopic impact scars on the individual grains (see Supplementary Section 5.1). This group shows the best sorting (median of 1.7) and the highest mean grain size (median of 354.0 μm), which is in line with typical values for saltated sand both in wind tunnel experiments and field-based investigations (Cheng et al., 2015; Farrell et al., 2012; cf. Schwan, 1988). The niveofluvial (layer 9) and niveofluvial to niveoaeolian (layer 4) sands were treated as a coherent group statistically, because the processes are genetically related and difficult to distinguish in the palaeorecord (see Supplementary Section 5.1 above). Niveofluvial and niveoaeolian sands are common phenomena in Weichselian slope deposits of northern Central Europe (e.g. Zagwijn and Paepe, 1968) and usually consist of thin-bedded fine to medium sands. In our data, the typical grain size is reproduced (median of 227.6 μm). The depositional process results in a slightly poorer sorting, compared with the aeolian sands (median of 2.2). The niveofluvial to niveoaeolian layer 4 contains lenses (up to 10 cm thick, up to 15 cm long) of coarser sand that seem to derive from the aeolian layer 5 below. Samples 2 and 20 were taken from these lenses and confirm that relatedness by their position at the intersection of both grain size clusters (compare Fig. 3b, main text). The solifluctive layers 2 and 3 feature the highest gravel contents by far and thus the statistical data are somewhat distorted by excluding this fraction from the analysis, which is also the reason for the relatively low mean grain sizes (median of 227.0 μm). Nevertheless, the poorer sorting (median of 3.4) still separates this group from the aforementioned. The overlap of sample 18 with the niveofluvial/-aeolian deposits is likely caused by solifluction alternating with slopewash deposition for layer 3 (see Supplementary Section 5.1, compare Fig. 3b, main text). The lacustrine deposits are set apart by their very poor sorting and lowest mean grain sizes and can be subdivided according to their position within the coastal zone (Supplementary Section 5.1). Samples 24, 25 and 28 (layer 11b, find horizon Li-II) belong to the beach face deposit, with a mean grain size of 80.7 μm (median of the three samples) and a sorting of 7.3 (median of the three samples). The remaining two lacustrine clusters represent thin, muddy shoreface deposits from layers 7 (find horizon Li-I) and 10 with median values for the mean grain sizes of 58.8 μm and 16.5 μm , respectively. Both show similarly poor sorting of 5.6 and 5.2.

Principal Component Analysis (PCA) (Fig. 3b, main text)

Whereas for the scatter plot only two descriptive parameters were taken into account, the PCA is based on all 116 dimensions of the grain size fractions. Between them, PC1 and PC2 explain 95.8 % of total variance of the data set. The associated biplots display the relative influences of the categorical grain size fractions clay, silt, fine/medium/coarse sand on the analysis of the data. The results strongly resemble those of the scatter plot and the same clusters, based on field descriptions can plausibly be formed. The biplots reveal, that the aeolian, niveofluvial-/aeolian and solifluctive deposits are distinguished by their contents of the different sand fractions, while the position of the lacustrine members within the data matrix is mainly determined by their relative silt and also fine sand contents.

5.3. Micromorphology

We here report on the micromorphological analyses of five block samples from the 2019 excavation Trenches 1 and 2 at Lichtenberg (for sample locations see Fig. 2, main text and Supplementary Figure S 50). Sampling concentrated on the two archaeological find layers, Li-I and Li-II, and associated, under- and overlying lithofacies. From the bottom up, the analyzed sequence contains (field interpretations in brackets): layer 11b (peaty mud), layer 11a (humic sand) and archaeological layer Li-II at its top, layer 10 (clayey silt), layer 9 (niveo-fluvial sands) as well as layer 7 (silty fine sand) containing archaeological layer Li-I and the overlying layer 6 (orange fine to medium sand). In the following we describe and interpret each layer and note where differences exist between thin sections of the same layer.

The lower sequence contains layers 11a, 11b, 10, 9 as well as archaeological find horizon Li-II and is present in two thin sections from Trench 2 (Fig. 2, main text and Supplementary Figures S 51, 52). The two thin sections reflect lateral variability in the sequence here, layer 9 is only present in LIB 19 5 (SI fig. 2), while layer 11b and 10 are only preserved in LIB 19 4 (Supplementary Figure S 52). Starting from the bottom, layer 11a is mainly composed of (sub)rounded, generally unsorted silt to coarse sand sized quartz grains (Supplementary Figure S 51f, g), but some lenses with coarser grains were observed as well and a slight coarsening upwards. The next common component are plant residues in the form of amorphous organic staining to plant tissues and organs (Supplementary Figure S 51d, e). Elongated plant tissue have a tendency for horizontal alignment (Supplementary Figure S 51c) indicating a waterlain nature (Taylor et al., 1998). This is in accordance with the macroscopic interpretation of this phenomenon as a drift line at the shoreface of a small lake (section 4.1, main text and Supplementary Section 5.1). Few mica, flint, charcoal (Supplementary Figure S 52f) and

unidentified heavy minerals are also present. Void space is mainly limited to simple packing voids, but a few channels are present as well, which are often filled with clay (Supplementary Figure S 52e, g), supporting periods of surface stabilization with vegetation growth and incipient soil formation (Bouma et al., 1990). Fine material is sparse and composed of brown to grey (only in LIB 19 4) clay, which is arranged in porphyric or a weakly developed chitonic and gefuric related distribution. In thin section LIB 19 5, layer 11a is overlain by layer 11b, a peaty deposit, with a clear, but gradual conformable contact. The two layers show only limited compositional or structural differences. In layer 11b, the occurrence of a possible krotovina feature indicates more intense bioturbation here. The main difference between these two layers, however, is an increase in the number and size of organic residues in layer 11b compared to layer 11a, which may reflect a greater proximity to the shore or lower energy setting for layer 11b compared to layer 11a (Dobrowolski et al., 2001). At the same time layer 11b shows internal stratification (Supplementary Figure S 51c), in the upper part, organic residues are dominantly composed of cells and tissue residues (Supplementary Figure S 51b), while in the lower part larger tissues to organs (Supplementary Figure S 51d, e) were deposited, reflecting an upward increase in energy or greater transport distance of the organic material with increasing distance to the shore (Cohen, 2003; Taylor et al., 1998). Overall layer 11 shows characteristics of a shore environment with repeated flooding events and periods of surface stabilization, potentially the eulittoral zone of a lake (Bouma et al., 1990).

In thin section, the contact between layer 11 and the overlying layer 9 and 10 respectively is clear with the two overlaying layers showing slight compositional and structural differences. In thin section LIB 19 4, layer 10 is characterized by bedded sands and silt (Supplementary Figure S 52a-c). At the top of this thin section a red orange layer is present (Supplementary Figure S 52a, c), where the same depositional bedding structure is present but overprinted by post-depositional iron oxidation. The contact with the red orange layer is sharp and potentially presents an former groundwater line (Fedoroff et al., 2010). The main components in layer 10 are medium to coarse or fine to medium sand sized quartz grains, while mica, plant residues and heavy minerals are rare. Void space dominantly consists of simple packing voids with few chambers and fissures, which are filled with dusty and limpid clay coatings. Clay is arranged in a porphyric to chitonic and gefuric related distribution. Thin sections LIB 19 5 preserved the contact between layer 11b and 9 (Supplementary Figure S 51a) but only a limited exposure of layer 9 (Supplementary Figure S 51c), which shows a slightly different expression from layer 10. Layer 9 is moderately sorted for medium sand sized quartz grains. Rare components – mica, plant residues, heavy minerals – are the same, but organic-rich soil aggregates and charcoal

present additional, rare components here. A further difference, but of minor magnitude only, is the more common and thicker occurrence of clay coatings here (SI fig. 2a).

The upper sequence contains layers 5, 6, 7, archaeological find horizon Li-I and is present in three thin sections, two from Trench 1 (LIB 19 1 and 2, Fig. 2 in the main text and Supplementary Figure S 54, 55) and one from Trench 2 (LIB 19 3, Fig. 2 in the main text and Supplementary Figure S 53). Starting from the bottom, layer 7 containing the find horizon Li-I shows the same expression in all three thin sections. This layer is composed of weakly bedded (sub)rounded quartz grains, which are silt to sand sized, but the layer is poorly sorted for silt and fine sand (Supplementary Figures S 53f, g; 54e, f; 55f, g). Other components include mica and clay, which are both rare. The microstructure is very compact, grain supported and only simple packing voids were observed. A great degree of compaction is a unique characteristic of this layer and it resembles a fragipan but for the lack of pedofeatures. The contact with the overlying layer 6 is clear and characterized by an increase in sand sized quartz and clay here (Supplementary Figures S 53c-e; 54c, d; 55c, f, g). Grains in layer 6 are dominantly composed of (sub)rounded silty to coarse sand sized quartz grains (Supplementary Figures S 53d, e; 54a, b; 55d, e), but silt sized grains are rare. However, in thin section LIB 19 3 this increase in grain size and the contact zone extends over almost 1 cm and is also characterized by amorphous organic staining (SI fig. 4c, e), reflecting local variability. Further variation is visible in the interstitial clay component. Clay is arranged in a geyuric related distribution and as clay illuviation, most expressed in LIB 19 2 (Supplementary Figure S 54a, b), while in LIB 19 1 the upper part of this layer shows only thinly expressed clay coatings (Supplementary Figure S 55a-c). There are also color changes in the clay. In LIB 19 3, the clay is generally brown reddish, resulting from iron staining (Supplementary Figure S 53b, d). In LIB 19 1 and 2 the color changes from grey over dark or black to reddish brown (Supplementary Figures S 54b; 55d, e). This pattern may indicate spatial variation in water saturation (Fedoroff et al., 2010). Otherwise, layer 6 shows a dense, massive microstructure with simple packing voids and is grain supported. The contact with the overlying layer 5 is clear and conformable in LIB 19 2 (SI fig. 6), but gradual in LIB 19 3 (SI fig. 4c). The structure and composition of layer 5 is similar to layer 6, and the main difference is the thinner and more scarce nature of clay coatings here, but again LIB 19 3 shows a slightly different expression with thicker clay coatings (Supplementary Figure S 53a, b) compared to LIB 19 2. Furthermore, LIB 19 3 shows weak bedding.

Section 6: Robustness of luminescence ages

6.1 Testing and choice of measurement protocol

On three samples (L-EVA 2013, 2016 and 2021) from the two trenches, we performed a dose recovery and an anomalous fading test using three aliquots each. After bleaching in the solar simulator for 3 h, the dose recovery test was conducted with three different protocols for potassium feldspar: pIRIR₂₂₅, pIRIR₂₉₀ and pIRIR₂₉₀ with a hotbleach. For further measurements and age calculations, we opted for the pIRIR₂₉₀ hotbleach protocol (summarized in Supplementary Table S 12), as it produced the most reliable residual-subtracted measured-to-given dose ratios (0.98, Supplementary Figure S 56). This approach has been shown to produce robust luminescence ages and to be less prone to anomalous fading (Thiel et al., 2011; Thomsen et al., 2008). We measured the signal stability following Huntley and Lamothe (2001) and obtained a mean g-value of 2.2%/decade (Supplementary Figure S 56). Hence, the ages were not fading corrected so as to avoid age overestimations (cf. Arnold et al., 2015; Buylaert et al., 2012). Even though L-EVA 2013 and 2021 were later excluded from the scope of this publication, their measured to given dose rates and g-values are fully representative for the measured samples described in the main text. The ages of L-EVA 2013 and 2021 will be reported in a forthcoming publication.

6.2. Dose rate determination

The results of the high-resolution germanium gamma spectrometry are presented in Supplementary Table S 13. To calculate the total dose rates, the contribution of cosmic radiation was accounted for based on Prescott and Hutton (1994). For the internal beta dose rate contribution we assumed an effective potassium content of 12.5 ± 0.5 % (Huntley and Baril, 1997), furthermore, we applied radioactivity conversion factors suggested by Guérin et al. (2011). An a-value of 0.11 ± 0.02 was used to approximate alpha particle efficiency (Kreutzer et al., 2014).

6.3 D_e-estimation

After measuring the independent equivalent dose (D_e) estimates for each sample, we used Abanico plots for exploration and visualization of the data (Supplementary Figures S 57, 58). Abanico plots combine the benefits of radial plots, suitable for depicting the precision of individual D_e-values, with kernel density estimates (KDE), which more comprehensively show

D_e frequency distributions (Dietze et al., 2016). This amalgamation allows for an enhanced identification of patterns within the individual D_e -estimates (Galbraith and Roberts, 2012). An adequate inspection of the distributions, however, requires a sufficiently small bandwidth (bw) for the univariate KDE part of the plot, preventing over-smoothing of the curve and associated loss of data variability (ibid.). Therefore we chose the bw to achieve an accordance between the radial plot and KDE representation of the data and based on the bw-selectors “bw.ucv” and “bw.nrd0” as implemented in the *r.luminescence* package (Kreutzer et al., 2020). The choice of dose model for the final D_e -estimation ensued according to the most meaningful cluster and peak in the Abanico plot with respect to the depositional process and characteristics of the sediment (Tab. 1, main text). As a tendency, samples from the niveofluvial layers 8 and 9 and the beach sand (layer 11) were mostly subjected to the central age model (CAM), whereas the aquatic deposits of layer 7 were treated with the minimum age model (MAM), using a σ_b -value of 0.11 (e.g. Cunningham and Wallinga, 2012). In one instance, for sample L-EVA 2024, with a complicated depositional history of short-distance reworking on the slope and suspected posterior bioturbation by trampling, we opted for the weighted mean, because no other age model was in better compliance with the distribution.

Sample L-EVA 2010 was taken from a stratigraphic position where the archaeological find horizon Li-I is injected upwards through cryoturbation. The obtained age of 53.5 ± 4.9 ka (applying MAM) does not refer to the deposition of the sediment, but to the cryoturbation incident, whereas the main mode of this sample’s KDE curve (159.1 Gy) results in an age of 64.6 ± 5.8 ka and thus better corresponds with the in situ samples from the same layer (L-EVA 2014, 2015 and 2018; 70.8 ± 8.0 to 71.6 ± 7.0 ka). However, the cryoturbation age of L-EVA 2010 (53.5 ± 4.9 ka) is in line with the date of 57 ± 6 ka that was previously presented for the same find horizon in Lichtenberg (Veil et al., 1994). Hence, there is evidence to suggest, that unmixing distinct age populations (original deposition and cryoturbation event) in very small (0.5 mm) multiple grain aliquots is to some extent possible, if the genuine age of the initial deposition is known from independent samples. For the previous chronology, an in situ representation of the find horizon was not available, because the depth of the non-cryoturbated layers had not been reached during the preceding excavation (cf. Fig. 2a, main text). So while the actual former age appears to be comparably accurate, its stratigraphic and archaeological interpretation needs to be updated in view of our data.

Section 7: Palynology

7.1 Detailed sample preparation

All samples were treated by standard methods (Faegri et al., 1989; Moore et al., 1991). About 5 g of sediment were prepared per sample, including dispersion with 10% KOH, flotation using sodium polytungstate hydrate ($3 \text{ Na}_2\text{WO}_4 \cdot 9 \text{ WO}_3 \cdot \text{H}_2\text{O}$) and acetolysis to dissolve cellulose. Residues were embedded in glycerine and up to three slides (24 x 32 mm) per sample were analysed under a transmitted light microscope for pollen and non-pollen palynomorphs at 40x magnification. Pollen and spores were identified using the atlases of Faegri and Iversen (1989), Moore et al. (1991) and Beug (2004). Micro-charcoal particles smaller than 100 μm were counted in samples of Trench 2 of the excavations (2019 and 2020) and are presented by a curve for each 24x32 mm slide in the pollen diagrams.

7.2 Results and Interpretation

7.2.1 Bulk samples 1, 2, 3 and 8 (excavation 2019, Trench 2)

Results

The pollen and spore content of the four analysed samples is low but sufficient for statistical evaluation, although pollen preservation is partially poor. For sampling positions, see Fig. 2 main text, Supplementary Figure S 59. The three lowermost samples of layers 11a, 11 b and 11 b₂ (samples 1 to 3) are rather similar concerning their AP and NAP assemblages. They are characterized by high values of *Pinus* (60%) and *Betula* (20%) and some *Salix*, whereas Poaceae amount to 10% and total NAP to 15% (Supplementary Figure S 60). Very few *Picea* pollen occur (samples 2, 3) and single grains of the thermophile trees (*Quercus* and *Carpinus*), most probably reworked from subjacent Eemian layers. Additionally, *Alnus*, *Larix*, *Myrica* and *Juniperus* occur in layer 11 b₂ (sample 3). The pollen spectra of all four samples are furthermore characterized by the occurrence of cryptogam spores (*Ophioglossum*, *Botrychium* and *Selaginella selaginoides*) and by low amounts of Cyperaceae and Ericaceae (mean about 5%) in layer 11b₂ (sample 3). Very few pollen of aquatic taxa such as *Potamogeton*, *Sparganium* type, *Typha latifolia* type and of wetland plants like *Montia* and taxa representing the *Ranunculus acris* pollen type (including for example *R. acris*, *R. aquatilis*, *R. sceleratus*) have been found. Remains of a coenobium of the green algae *Pediastrum* spec. occur. *Sphagnum* peaks in sample 2, layer 11b (30%), but is present in all four samples.

Particular differences between the pollen assemblage of the topmost sample 8 (drift line within layer 10) and those of the underlying layers are a strong decrease of *Pinus* (15%) and increase

of Poaceae up to 40% and of total NAP to about 50%, whereas the *Betula* curve has slightly increased (>20%). The micro-charcoal particle counts increase from bottom (sample 1, layer 11a) to top (sample 8, layer 10 [drift line]) from 6 to 260) (Supplementary Figure S 60).

Discussion

From the palynological record, a shallow water body and a swampy environment can be concluded for the lowermost three layers (11a, 11b and 11b₂). This is indicated by the occurrence of the aquatic, wetland and boggy, peat-forming taxa *Pediastrum*, *Ranunculus cf. sceleratus*, *Typha spec.*, *Sparganium spec.*, *Montia*, Polypodiaceae, *Sphagnum*, Ericaceae, *Myrica* and *Juniperus*. Behre et al. (2005) describe macro remains of *Ranunculus sceleratus* for the Brörup and Glinde interstadials. The presence of the Ophioglossaceae ferns *Ophioglossum spec.* and *Botrychium cf. lunaria* points to sandy, humic open stands, as for example meadows or heathland. The arctic-alpine, as well light-demanding *Selaginella selaginoides* found in layer 11 b₂, known from Late Glacial plant communities, has probably occupied peat bogs or other open moist stands, like meadows. *Selaginella selaginoides* macro-remains are recorded from the Early-Weichselian Rederstall Stadial and Pleni-Weichselian Glinde Interstadial (Behre et al., 2005), pointing to opening-up of the landscape and most probably to a temperature drop. The azonal vegetation observed in samples 1, 2, 3 and 8 records a gradual change in vegetation and climate from the (late) Brörup Interstadial to the Rederstall Stadial. From an open boreal pine-birch forest (layer 11a and 11b) with a relatively rich undergrowth of mosses and grasses in association with wetter and dryer heliophyte (*Larix*) and grass rich stands, it likely shifted to slightly lighter and cooler conditions towards the end of the interstadial (layer 11b₂). Finally, the uppermost layer 10 indicates the development of a grass rich open, *Betula* dominated Steppe-Tundra, caused by a strong climatic decline in the following Rederstall Stadial.

7.2.2 Trench 2, excavation 2020 (samples 4 to 7)

Results

High resolution analyses of 4 samples (4 to 7) from the ca. 8 cm thick, peaty and sandy detrital mud (layer 11b), shows a medium to poor pollen preservation. The directly overlying thin silt (part of layer 10?) (Fig. 2c, main text) has been sterile on the other hand (Supplementary Figure S 59).

The bottom sample 4 (0-2 cm) of layer 11b has a similar pollen assemblage as layers 11a, 11b and 11 b₂ in the bulk samples 1 to 3 (Supplementary Figures S 59a,b; 61.). *Pinus* is the predominant woody taxon (60%), followed by *Betula* (20%). *Salix*, *Juniperus*, *Larix*, *Alnus*, *Picea* and *Myrica* occur with values between <1-2%. NAP are mainly composed of Poaceae

(10%), Rosaceae, Caryophyllaceae, *Artemisia* and Asteraceae and reach 15% in total. The sum of Ericaceae amounts to 6%; Sphagnum is present with 11% and Polypodiaceae with 4%. Only single grains of *Typha latifolia* type and *Sparganium* type were found. Micro-charcoal counts amount to 280 particles. The subsequent sample 5 (2-4 cm) shows a slight increase of *Betula* (31%) and *Myrica* (2%) and of NAP (19%), mainly composed of *Artemisia*, Asteraceae and Rosaceae. Few pollen of Chenopodiaceae occur in this depth and in the overlying sample 6 (4-6 cm). Amounts of Poaceae and of *Pinus* have decreased down to 7.5% and to 45.5% respectively. Pollen of *Polygonum bistorta* type (syn. *Bistorta officinalis*) appear for the first time. Among the aquatic taxa, *Myriophyllum spicatum* is recorded by a single grain, whereas the amount of *Typha latifolia* type has increased. Micro-charcoal particles amount to 828 counts.

In sample 6 (4-6 cm) *Pinus* has dropped further down to 37%, whereas *Betula* stays around 30% and *Salix* increases up to 5%. *Juniperus* slightly increases (2%) while *Myrica* values stay constant at around 2%; NAP amount to 23%. A slight increase of total Ericaceae is observed. Among the terrestrial herbs, *Artemisia*, Cichoriaceae and *Polygonum cf. bistorta* (synonym *Bistorta officinalis*) are prominent. The Poaceae curve increases again up to 12%. One coenobium of *Pediastrum boryanum* and one pollen of *Myriophyllum spicatum* were identified among the aquatic taxa. Micro-charcoal counts further increase up to 900 particles.

The uppermost sample 7 (at 6-8 cm) is characterized by the intersection of the *Betula* and *Pinus* curves particularly. *Betula* increases up to 42%, whereas *Pinus* drops down to 28%. A further increase of heliophytes as for example of Caryophyllaceae, Rosaceae and Asteraceae as well as of *Sphagnum* is observed. Among the aquatic taxa *Typha latifolia* type is present, albeit with very low amounts. Several spores of *Ophioglossum* occur in this layer. The micro-charcoal counts slightly decrease down to 720 particles.

Discussion

As stated earlier, the pollen assemblage of the lowermost sample 4 (0-2 cm) of layer 11b (Supplementary Figure S 61.), shows great similarities regarding vegetation and environmental conditions with those of the three bulk samples 1,2 and 3 from layers 11a, 11b, and 11b₂ (Tab. 3, main text; Supplementary Figure S 60). They are therefore considered to be of the same depositional age. Samples 5 (2-4 cm) and 6 (4-6 cm) on the other hand reflect the slow transition from boreal woodlands into the open, grass- and heliophyte-rich steppe-tundra-like vegetation. This shift seems to be fully completed in sample 7 (6-8 cm) and also in sample 8, which already belongs to layer 10. That means that the top of layer 11b and layer 10 have to be regarded as

coeval formations. Micro-charcoal counts are highest in the uppermost samples 7 and 8 pointing to burning. It remains unclear, however, whether these were natural fire events or related to human activity.

In comparison with the former Eemian/Early Weichselian pollen profile of Lichtenberg (Veil et al., 1994) (Supplementary Table S 14) and other northern German Early Weichselian key profiles (Behre et al., 2005; Behre and Lade, 1986; Caspers, 1997; Caspers and Freund, 2001; Hahne et al., 1994; Menke and Tynni, 1984), the obtained pollen spectra might be either correlated with the transition of the Brörup Interstadial into the Rederstall Stadial or the Odderade Interstadial into the Schalkholz Stadial, respectively. The main distinction between these two transitional phases is the differing amounts of the Poaceae and total NAP. Because of the relatively low amounts of Poaceae and total NAP in our record, and taking into account the known occurrence of the heliophytic *Selaginella selaginoides* already in the Rederstall Stadial (Behre et al., 2005), we assign the samples 1 to 8 from Trench 2 to late Brörup (WE II b) transitioning into the Rederstall Stadial (WE III) (Tab. 3, main text; Supplementary Table S 14). This is in good accordance with the established lithostratigraphy and the geochronological time scale for Trench 2 (see section 5.2, main text; Supplementary Section 5.1).

7.2.3 Bulk samples of core PD.028 (9 to 12)

Results

The two lowermost bulk samples (10 and 9) of core PD.028 (530-555 cm and 465-530 cm) (Supplementary Figure S 59c and Supplementary Table S 11 for sediment description) show relatively similar pollen spectra, characterized by high *Pinus* values between 60 and 70%, whereas *Betula* amounts to 16% in both samples. Values of *Salix* are between 0.8% and about 3%. *Picea*, *Juniperus* and *Larix* occur with amounts below 1%. Pollen of heliophytic genus such as *Valeriana vulgaris*-type, *Matricaria*-type, *Artemisia*, Asteraceae and Chenopodiaceae occur. A decrease of the Poaceae from bottom (11%) to top (3%) can be observed. NAP are between 6% and 17%. A spore of cf. *Botrychium lunaria* and a few *Sphagnum* spores were found in the upper sample (9; 530-465 cm) (Supplementary Figure S 62).

The two overlying samples 11 and 12 (355-375 cm and 230-250 cm) of core PD.028 are also very similar in their qualitative and quantitative pollen composition. They are showing very high amounts of NAP (between 50 and 60%), mainly composed of Poaceae (ca. 35%). The very rich heliophytic flora includes *Artemisia*, *Valeriana montana*-type, *Matricaria*-type, *Polygonum bistorta*-type, *Helianthemum oelandicum*-type, Rosaceae, Apiaceae, Brassicaceae, Asteraceae, Chenopodiaceae and *Epilobium*. Among the arboreal pollen, *Betula* is predominant (ca. 30%), whereas *Pinus* values are between 11 and 15%. Ericaceae indeterminate, *Calluna*,

Empetrum and *Vaccinium*-type have unambiguously increased. Characteristic for both samples are highly abundant cell colonies of the green algae *Pediastrum* (Supplementary Figure S 62). Due to preservation only two species could be determined, namely *P. boryanum* and cf. *P. kawraiskyi*, the majority of colonies is listed as *Pediastrum* indeterminate.

Discussion

Both lowermost samples (9 and 10) reflect a boreal *Pinus-Betula* forest with some *Picea*, *Juniperus*, *Larix* and a relatively diverse but not predominant heliophytic herbal flora, indicating open stands. The occurrence of *Botrychium cf. lunaria* in sample 10 points to sandy and humic open areas in the closer vicinity.

The samples 11 and 12 on the other hand reflect an open landscape with grasses and heliophytic herbs predominating. Among the wooden taxa only *Betula*, most probably *Betula nana* and very few *Salix* and *Juniperus* are part of the zonal vegetation of this severe cold phase. We assume *Pinus* pollen to be the result of long-distance transport. The occurrence of extremely large numbers of *Pediastrum* colonies points to wet local conditions. Among the *Pediastrum* species recorded, *P. kawraiskyi* is the most cold tolerant (Turner et al., 2014) with Holocene occurrences in Arctic and Antarctic environments (Komárek and Jankovská, 2001). The increase of moisture and a rise of water tables is typical for transitional phases between forested and nonforested phases due to the loss of woodland (Behre et al., 2005).

The core Veil 1 (Veil et al., 1994) taken a few meters apart from core PD.028 with a quite similar lithology (Fig. 1, main text; Supplementary Table S 11) provides a sound basis for correlation. Based on this continuous record and further data obtained by the authors, the two lowermost bulk samples of core PD.028 (samples 9 and 10) are correlated to late phases of the Odderade Interstadial (WE IVb). Regarding the two uppermost samples (11 and 12), on the premise that organic-rich deposits mostly refer to relatively temperate conditions (Hahne et al., 1994; cf. Vandenberghe and van der Plicht, 2016), we interpret these two layers to have formed during individual minor interstadials, not yet described for Northern Germany. Their position on top of the Odderade, but below the clearly cryogenic deposits, induces their ascription to early phases of the Schalkholz Stadial (WP I) (Tab. 3, main text) (cf. Antoine et al., 2016; Müller and Sánchez Goñi, 2007). This correlation is furthermore mainly based on the occurrence of high NAP, particularly Poaceae values in pollen records of the Schalkholz Stadial (Caspers and Freund, 2001; Hahne et al., 1994; Veil et al., 1994), which are not documented from the previous stadials Herning (WF I) and Rederstall (WF III). Due to sampling manner

and low number of samples, the correlation and denomination remains preliminary. A future publication will provide more detail and resolution.

Section 8: Phytolith analysis

Detailed Sample preparation

Phytolith extraction according to the Rapid Phytolith Extraction method (Katz et al., 2010) required sieving the dry samples to remove particles larger than 0.5 mm. We then weighed between 30- 50 mg of sieved sediment from each sample and recorded the weight. Due to the low organic content in the samples hydrogen peroxide or dry ashing was not required. We added this to a 0.5 ml centrifuge tube and removed carbonates minerals and bones in the sediment with the addition of 50 µl of 6 N HCl with a mechanical pipette (Eppendorf Research Plus). Each tube was gently agitated to ensure the HCl fully saturated the sample. After bubbling ceased and no carbonates remained, after approximately about 30 minutes, we added 450 µl 2.4 g/ml sodium polytungstate solution (SPT, $\text{Na}_6 (\text{H}_2\text{W}_{12}\text{O}_{40}) \cdot \text{H}_2\text{O}$). The samples were then agitated for 1 minute, and then sonicated (Elma E-One) for ten minutes and then centrifuged for 10 min at 5000 rpm (Eppendorf Centrifuge 5424). The phytolith-rich supernatant was transferred to a new 0.5 ml centrifuge tube and agitated for 1 minute. An aliquot of 50 µl was then pipetted onto a slide and covered with a 24 mm x 24 mm coverslip. Phytoliths were counted at 200 -400x magnification (0.95) using a field count method with a transmitted light microscope (Axio scope A1, Zeiss).

For calculating phytolith concentrations, 100 mg of dry sediment was weighed and then heated in crucibles at 500 °C for 5 min in a muffle oven to remove organic material. After cooling, we transferred the sample to 2 ml Eppendorf tubes, and then added 100 µl of 1 N HCl. The samples were then centrifuged at 6000 rpm for 5 minutes. The supernatant was discarded, and the samples were washed twice. The samples were then dried over a few days and then weighed in the Eppendorf tubes.

Additional discussion

Quantifications of the phytolith assemblage established that the concentrations of phytoliths per gram of sediment and per gram of acid-insoluble sediment are mainly similar between different samples. Similarity indicates that intra samples comparison is not distorted by large amounts of

carbonates or organic material in particular samples that would misleadingly inflate phytoliths per gram of sediment (Karkanis et al., 2000). The phytolith assemblages exhibit low densities (< 70,000 phytoliths/gram, see Supplementary Tables S15, S16, S17) and have large amounts of weathered and indeterminate phytoliths. The assemblages are nearly entirely composed of single-cell morphologies. The most common morphotypes were derived from monocot plants, including parallelepiped elongate thin psilates, parallelepiped elongate thin sinuates, rondels and indeterminate short-cells. These types are either diagnostic of grasses or occur in grasses. Phytoliths diagnostic of non-grass type monocots such as sedges or reedmaces were not evident. Although highly rare, a small number of multi-cell forms occurred including parallelepiped elongate thin psilates. Phytoliths associated with eudicots were found in all samples. These included leaf types such as eudicot-type hairs, hair bases, jigsaws, tracheids (cylindric sulcates), and multi-cell polyhedral. Unfortunately diagnostic types of specific genera were absent. Wood/bark types include spheroid, discoid and ellipsoid types were much rare, but this reflects the small numbers produced by these plants. Phytolith associated with burning with color or melting damage was not evident. Monoaxon sponge spicules were found in MH3 and MH5. Diatoms were present in one sample but were too damaged to identify beyond showing a pennate form (MH4). Occasional starches were observed in some samples but they were attributed to contamination and not counted.

The nature of the assemblage suggests it is probable that some morphologies such as dendritics, sedge cones, and plates may be disproportionately damaged and lost from the assemblage due to taphonomic processes. These patterns and the limited sample size prevent detailed vegetation reconstruction on-site. For example, the assemblages are too limited to apply bulliform cell, anatomical-based aridity or forest cover indexes. However, they do provide a broad environmental picture and this overall picture is consistent with sedimentation processes at open-air sites (Wroth et al., 2019). Although several samples are relatively similar, phytolith variation does show diachronic patterning in plant assemblages. For example, the earliest sample from layer 7 had low numbers (~8,000 phytoliths/g), both in terms of phytoliths of 1 g of sediment and phytoliths in 1 g of AIF, there are much higher numbers associated with the browner-colored layer 11a (<60,000 phytoliths/g). Later layers (layer 8 and 9) were more similar to layer 7. This indicates that layer 11a was formed during distinct, warmer and more plant rich conditions.

References

- Altermann, M., Jäger, K.-D., Kopp, D., Kowalkowski, A., Kühn, D., Schwanecke, W., 2008. Zur Kennzeichnung und Gliederung von periglaziär bedingten Differenzierungen in der Pedosphäre - On characteristics and subdivision of pedospheric differentiations due to previous periglacial conditions. *Waldökologie, Landschaftsforsch. und Naturschutz* 6, 5-42 (German with english abstract and captions).
- Antoine, P., Coutard, S., Guerin, G., Deschodt, L., Goval, E., Loch, J.-L., Paris, C., 2016. Upper Pleistocene loess-palaeosol records from Northern France in the European context: Environmental background and dating of the Middle Palaeolithic. *Quat. Int.* 411, 4–24. <https://doi.org/10.1016/j.quaint.2015.11.036>
- Arnold, L.J., Demuro, M., Parés, J.M., Pérez-González, A., Arsuaga, J.L., Bermúdez de Castro, J.M., Carbonell, E., 2015. Evaluating the suitability of extended-range luminescence dating techniques over early and Middle Pleistocene timescales: Published datasets and case studies from Atapuerca, Spain. *Quat. Int.* 389, 167–190. <https://doi.org/10.1016/j.quaint.2014.08.010>
- Behre, K.-E., Hölzer, A., Lemdahl, G., 2005. Botanical macro-remains and insects from the Eemian and Weichselian site of Oerel (northwest Germany) and their evidence for the history of climate. *Veg. Hist. Archaeobot.* 14, 31–53. <https://doi.org/10.1007/s00334-005-0059-x>
- Behre, K.-E., Lade, U., 1986. Eine Folge von Eem und 4 Weichsel-Interstadialen in Oerel/Niedersachsen und ihr Vegetationsablauf. *E&G Quat. Sci. J.* 36, 11–36. <https://doi.org/10.3285/eg.36.1.02>
- Beug, H.-J., 2004. Leitfaden der Pollenbestimmung für Mitteleuropa und angrenzende Gebiete. *Germania* 87, 542.
- Bouma, J., Foc, C.A., Miedma, R., 1990. Micromorphology of Hydromorphic Soils: Applications for Soil Genesis and Land Evaluation, in: Douglas, L.A. (Ed.), *Soil Micro-Morphology: A Basic and Applied Science*. pp. 257–278.
- Bridge, J., Demicco, R., 2008. *Earth Surface Processes, Landforms and Sediment Deposits*. Cambridge University Press, New York.
- Buylaert, J.P., Jain, M., Murray, A.S., Thomsen, K.J., Thiel, C., Sohbati, R., 2012. A robust feldspar luminescence dating method for Middle and Late Pleistocene sediments. *Boreas*

- 41, 435–451. <https://doi.org/10.1111/j.1502-3885.2012.00248.x>
- Caspers, G., 1997. Die eem- und weichselzeitliche Hohlform von Groß Todtshorn (Kr. Harburg; Niedersachsen) - Geologische und palynologische Untersuchungen zu Vegetation und Klimaverlauf der letzten Kaltzeit. *Schriftenr. der Dtsch. Geol. Gesellschaft* 4, 7–59.
- Caspers, G., Freund, H., 2001. Vegetation and climate in the Early- and Pleni-Weichselian in northern Central Europe. *J. Quat. Sci.* 16, 31–48. [https://doi.org/10.1002/1099-1417\(200101\)16:1<31::AID-JQS577>3.0.CO;2-3](https://doi.org/10.1002/1099-1417(200101)16:1<31::AID-JQS577>3.0.CO;2-3)
- Cheng, H., He, J., Zou, X., Li, J., Liu, C., Liu, B., Zhang, C., Wu, Y., Kang, L., 2015. Characteristics of particle size for creeping and saltating sand grains in aeolian transport. *Sedimentology* 62, 1497–1511. <https://doi.org/10.1111/sed.12191>
- Christiansen, Hanne Hvidtfeldt, 1998a. Periglacial sediments in an Eemian-Weichselian succession at Emmerlev Klev, southwestern Jutland, Denmark. *Palaeogeogr. Palaeoclimatol. Palaeoecol.* 138, 245–258. [https://doi.org/10.1016/S0031-0182\(97\)00117-X](https://doi.org/10.1016/S0031-0182(97)00117-X)
- Christiansen, Hanne H., 1998. ‘Little Ice Age’ nivation activity in northeast Greenland. *The Holocene* 8, 719–728. <https://doi.org/10.1191/095968398666994797>
- Christiansen, Hanne Hvidtfeldt, 1998b. Nivation forms and processes in unconsolidated sediments, NE Greenland. *Earth Surf. Process. Landforms* 23, 751–760. [https://doi.org/10.1002/\(SICI\)1096-9837\(199808\)23:8<751::AID-ESP886>3.0.CO;2-A](https://doi.org/10.1002/(SICI)1096-9837(199808)23:8<751::AID-ESP886>3.0.CO;2-A)
- Cohen, A.S., 2003. *Paleolimnology: the history and evolution of lake systems*. Oxford University Press.
- Cornell, R.M., Schwertmann, U., 2003. *The Iron Oxides*, 2nd ed. WILEY-VCH, Weinheim. <https://doi.org/10.1002/3527602097>
- Cunningham, A.C., Wallinga, J., 2012. Realizing the potential of fluvial archives using robust OSL chronologies. *Quat. Geochronol.* 12, 98–106. <https://doi.org/10.1016/j.quageo.2012.05.007>
- Dietze, M., Kreutzer, S., Burow, C., Fuchs, M.C., Fischer, M., Schmidt, C., 2016. The abanico plot: Visualising chronometric data with individual standard errors. *Quat. Geochronol.* 31, 12–18. <https://doi.org/10.1016/j.quageo.2015.09.003>

- Dobrowolski, R., Bałaga, K., Bogucki, A., Fedorowicz, S., Melke, J., Pazdur, A., Zubovič, S., 2001. Chronostratigraphy of the okunin and Czerepacha Lake-mire geosystems (Volhynia polesiye, NW Ukraine) during the Late Glacial and Holocene. *Geochronometria* 20, 107–115.
- Faegri, K., Iversen, J., Kaland, P.E., Krzywinski, K., 1989. Textbook of pollen analysis, 4th ed. John Wiley & Sons Ltd., Chichester.
- Farrell, E.J., Sherman, D.J., Ellis, J.T., Li, B., 2012. Vertical distribution of grain size for wind blown sand. *Aeolian Res.* 7, 51–61. <https://doi.org/10.1016/j.aeolia.2012.03.003>
- Fedoroff, N., Courty, M.-A., Guo, Z., 2010. Palaeosoils and Relict Soils, in: Stoops, G., Marcelino, V., Mees, F. (Eds.), *Interpretation of Micromorphological Features of Soils and Regoliths*. Elsevier, pp. 623–662. <https://doi.org/10.1016/B978-0-444-53156-8.00027-1>
- Fränzle, O., 1988. Glaziäre, periglaziäre und marine Reliefentwicklung im nördlichen Schleswig-Holstein. *Schr. Naturwiss. Ver. Schlesw.-Holst.* 58, 1–30.
- Galbraith, R.F., Roberts, R.G., 2012. Statistical aspects of equivalent dose and error calculation and display in OSL dating: An overview and some recommendations. *Quat. Geochronol.* 11, 1–27. <https://doi.org/10.1016/j.quageo.2012.04.020>
- Grimmel, E., 1973. Bemerkungen zum Geschiebedecksand. *E&G – Quat. Sci. JournalG Quat. Sci. J.* 23/24, 16–25. <https://doi.org/10.3285/eg.23-24.1.02>
- Guérin, G., Mercier, N., Adamiec, G., 2011. Dose-rate conversion factors: update. *Anc. TL* 29, 5–8.
- Hahne, J., Kemle, S., Merkt, J., Meyer, K.D., 1994. Eem-, weichsel- und saalezeitliche Ablagerungen der Bohrung “Quakenbrück GE 2.” *Geol. Jahrb.* A134, 9–69.
- Hein, M., Urban, B., Tanner, D.C., Buness, A.H., Tucci, M., Hoelzmann, P., Dietel, S., Kaniecki, M., Schultz, J., Kasper, T., Suchodoletz, H., Schwalb, A., Weiss, M., Lauer, T., 2021. Eemian landscape response to climatic shifts and evidence for northerly Neanderthal occupation at a palaeolake margin in Northern Germany. *Earth Surf. Process. Landforms* esp.5219. <https://doi.org/10.1002/esp.5219>
- Huntley, D.J.; Baril, M.R., 1997. The K content of the K-feldspars being measured in optical dating or thermoluminescence dating. *Anc. TL* 15, 11–13.

- Huntley, D.J., Lamothe, M., 2001. Ubiquity of anomalous fading in K-feldspars and the measurement and correction for it in optical dating. *Can. J. Earth Sci.* 38, 1093–1106. <https://doi.org/10.1139/cjes-38-7-1093>
- Karkanas, P., Bar-Yosef, O., Goldberg, P., Weiner, S., 2000. Diagenesis in Prehistoric Caves: the Use of Minerals that Form In Situ to Assess the Completeness of the Archaeological Record. *J. Archaeol. Sci.* 27, 915–929. <https://doi.org/10.1006/jasc.1999.0506>
- Komárek, J., Jankovská, V., 2001. Review of the Green Algal Genus *Pediastrum*; Implication for Pollenanalytical Research. *Bibl. Phycol.* 108, 1–127.
- Kreutzer, S., Burow, S., Dietze, M., Fuchs, M.C., Schmidt, C., Fischer, M., Friedrich, J., 2020. Luminescence: Comprehensive Luminescence Dating Data Analysis.
- Kreutzer, S., Schmidt, C., Dewitt, R., Fuchs, M., 2014. The a-value of polymineral fine grain samples measured with the post-IR IRSL protocol. *Radiat. Meas.* 69, 18–29. <https://doi.org/10.1016/j.radmeas.2014.04.027>
- Lade, U., Hagedorn, H., 1982. Sedimente und Relief einer eiszeitlichen Hohlform bei Krempel (Elbe-Weser-Dreieck). *E&G Quat. Sci. J.* 32, 93–108. <https://doi.org/10.3285/eg.32.1.08>
- Mania, D., Toepfer, V., 1973. Königsau: Gliederung, Oekologie und Mittelpaläolithische Funde der letzten Eiszeit. Veröffentlichungen des Landesmuseums für Vorgeschichte in Halle 26, Deutscher Verlag der Wissenschaften, Berlin.
- Menke, B., 1976. Neue Ergebnisse zur Stratigraphie und Landschaftsentwicklung im Jungpleistozän Westholsteins. *E&G Quat. Sci. J.* 27, 53–68. <https://doi.org/10.3285/eg.27.1.05>
- Menke, B., Tynni, R., 1984. Das Eeminterglazial und das Weichselfrühglazial von Rederstall/Dithmarschen und ihre Bedeutung für die mitteleuropäische Jungpleistozän-Gliederung. *Geol. Jahrb. A* 76, 1–120.
- Moore, P.D., Webb, J.A., Collison, M.E., 1991. Pollen analysis. Blackwell Scientific Publications, Oxford.
- Müller, U.C., Sánchez Goñi, M.F., 2007. Vegetation dynamics in southern Germany during marine isotope stage 5 (~ 130 to 70 kyr ago), in: Sirocko, F., Claussen, M., Sánchez Goñi, M.F., Litt, T. (Eds.), *The Climate of Past Interglacials*. (Developments in

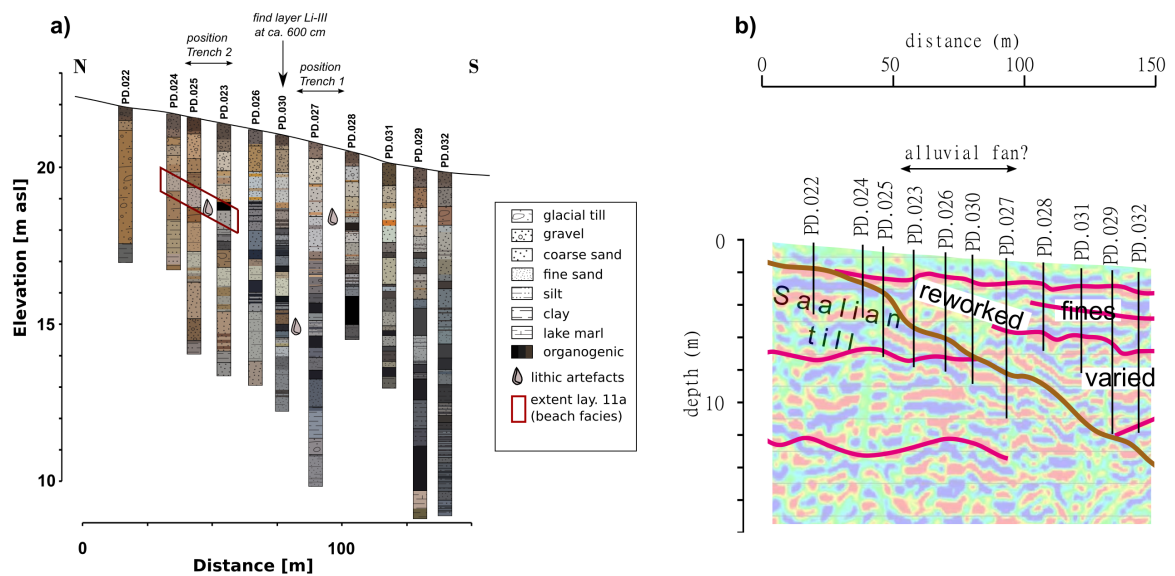
- Quaternary Sciences 7). pp. 277–287. [https://doi.org/10.1016/S1571-0866\(07\)80044-3](https://doi.org/10.1016/S1571-0866(07)80044-3)
- Prescott, J.R., Hutton, J.T., 1994. Cosmic ray contributions to dose rates for luminescence and ESR dating: Large depths and long-term time variations. *Radiat. Meas.* 23, 497–500. [https://doi.org/10.1016/1350-4487\(94\)90086-8](https://doi.org/10.1016/1350-4487(94)90086-8)
- Richter, H., Haase, G., Lieberoth, I., 1970. Periglazial-Löß-Paläolithikum im Jungpleistozän der Deutschen Demokratischen Republik (Petermanns Geogr. Mitt. Ergänzungsheft Nr. 274). VEB Hermann Haack, Gotha.
- Schwan, J., 1988. The structure and genesis of Weichselian to early hologene aeolian sand sheets in western Europe. *Sediment. Geol.* 55, 197–232. [https://doi.org/10.1016/0037-0738\(88\)90132-7](https://doi.org/10.1016/0037-0738(88)90132-7)
- Semmel, A., Terhorst, B., 2010. The concept of the Pleistocene periglacial cover beds in central Europe: A review. *Quat. Int.* 222, 120–128. <https://doi.org/10.1016/j.quaint.2010.03.010>
- Taylor, G.H., Teichmüller, M., Davis, A., Diessel, C.F.K., Littke, R., Robert, P., 1998. *Organic Petrology*. Gebrüder Bornträger, Berlin Stuttgart.
- Thiel, C., Buylaert, J.P., Murray, A., Terhorst, B., Hofer, I., Tsukamoto, S., Frechen, M., 2011. Luminescence dating of the Stratzing loess profile (Austria) - Testing the potential of an elevated temperature post-IR IRSL protocol. *Quat. Int.* 234, 23–31. <https://doi.org/10.1016/j.quaint.2010.05.018>
- Thomsen, K.J., Murray, A.S., Jain, M., Bøtter-Jensen, L., 2008. Laboratory fading rates of various luminescence signals from feldspar-rich sediment extracts. *Radiat. Meas.* 43, 1474–1486. <https://doi.org/10.1016/j.radmeas.2008.06.002>
- Turner, F., Pott, R., Schwarz, A., Schwalb, A., 2014. Response of Pediastrum in German floodplain lakes to Late Glacial climate changes. *J. Paleolimnol.* 52, 293–310. <https://doi.org/10.1007/s10933-014-9794-2>
- Van Huissteden, J. (Ko., Vandenberghe, J., Van der Hammen, T., Laan, W., 2000. Fluvial and aeolian interaction under permafrost conditions: Weichselian Late Pleniglacial, Twente, eastern Netherlands. *CATENA* 40, 307–321. [https://doi.org/10.1016/S0341-8162\(00\)00085-0](https://doi.org/10.1016/S0341-8162(00)00085-0)
- Vandenberghe, J., 1992. Periglacial phenomena and pleistocene environmental conditions in

- the Netherlands—An overview. *Permafr. Periglac. Process.* 3, 363–374.
<https://doi.org/10.1002/ppp.3430030410>
- Vandenberghe, J., van der Plicht, J., 2016. The age of the Hengelo interstadial revisited. *Quat. Geochronol.* 32, 21–28. <https://doi.org/10.1016/j.quageo.2015.12.004>
- Veil, S., Breest, K., Höfle, H.-C., Meyer, H.-H., Plisson, H., Urban-Küttel, B., Wagner, G.A., Zöller, L., 1994. Ein mittelpaläolithischer Fundplatz aus der Weichsel-Kaltzeit bei Lichtenberg, Lkr. Lüchow-Dannenberg. *Germania* 72, 1–66.
- Wroth, K., Cabanes, D., Marston, J.M., Aldeias, V., Sandgathe, D., Turq, A., Goldberg, P., Dibble, H.L., 2019. Neanderthal plant use and pyrotechnology: phytolith analysis from Roc de Marsal, France. *Archaeol. Anthropol. Sci.* 11, 4325–4346.
<https://doi.org/10.1007/s12520-019-00793-9>
- Zagwijn, W., Paepe, R., 1968. Die Stratigraphie der weichselzeitlichen Ablagerungen der Niederlande und Belgiens. *E&G – Quat. Sci. J.* 19, 10–31.

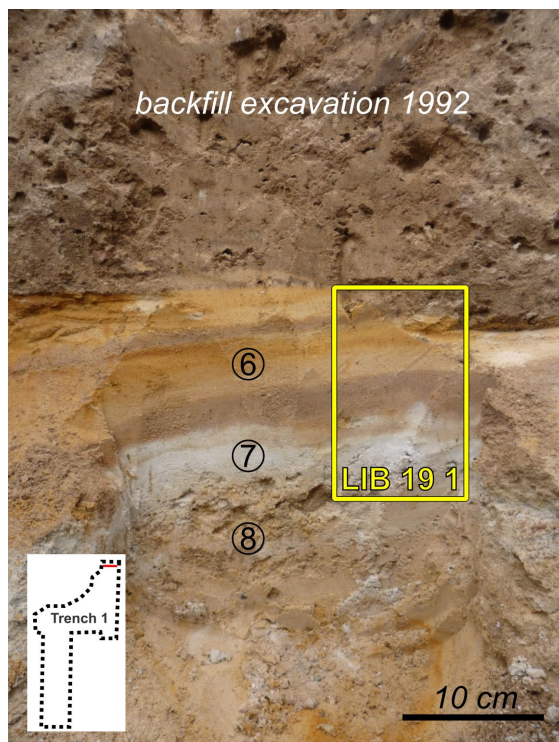
Figures and Tables

Supplementary Table S 11. Stratigraphic description of core PD.028 and correlation with the stratigraphic layers of Trench 1 and 2. For a picture of the core, see Supplementary Figure S 59.

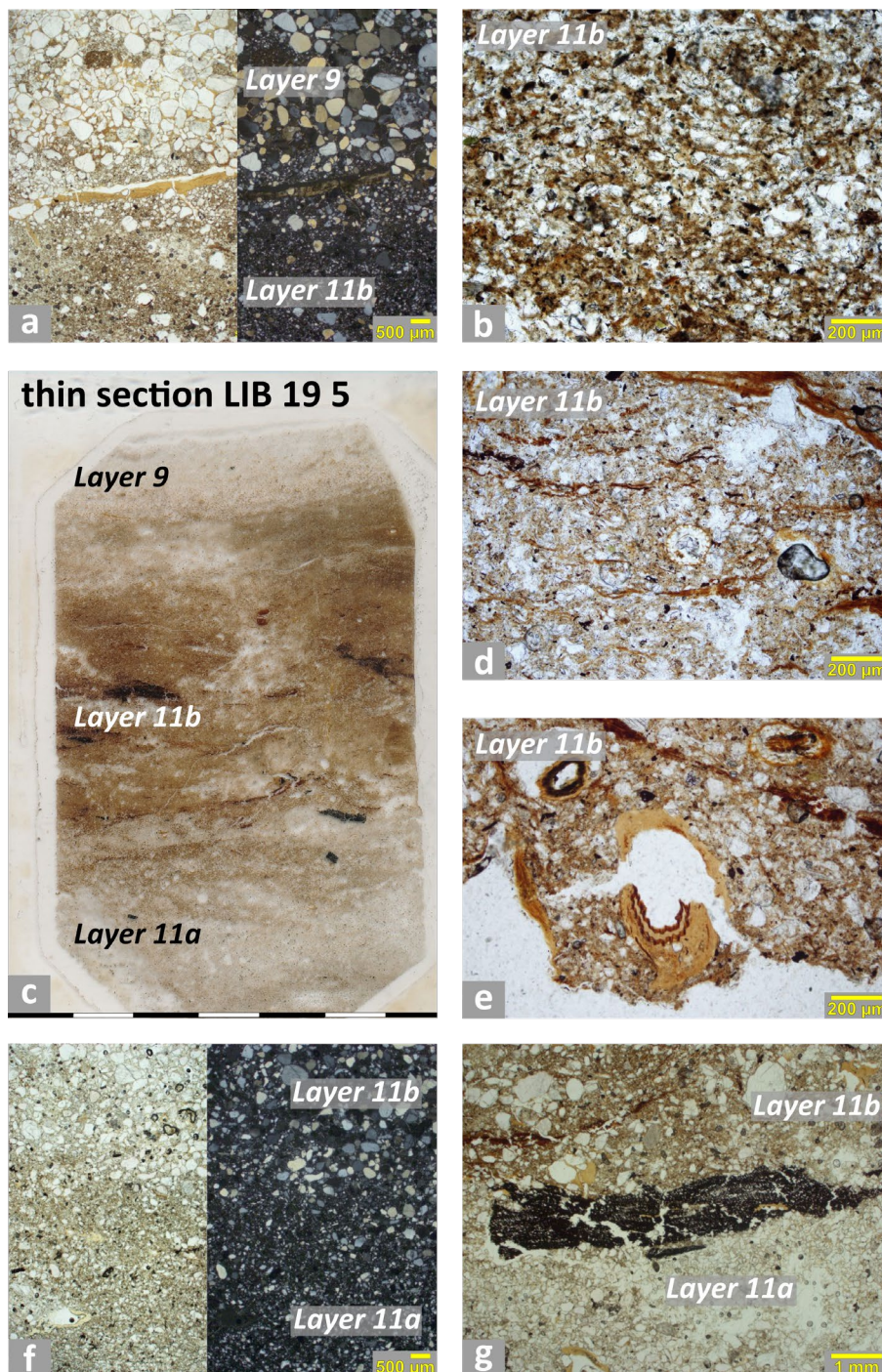
Depth [cm]	Properties	Layer	CO ₃	Munsell-Colour
0-30	Ploughing horizon, medium humic, silty medium to coarse sand, 10% gravel content	1	-	10YR 3/4
30-50	Bw-horizon, glacial cover sand (<i>Geschiebedecksand</i>), loamy medium sand, 10% gravel content, unbedded	2	-	10YR 5/7
50-120	crudely to unbedded silt and fine to coarse sand, varying gravel contents (10 to 50%), varying hydromorphic features	7', 3	-	10YR 8/2 - 10YR 5/7
120-175	Alternating well to crudely bedded medium sand, gravel content <1%	4, 5	-	10YR 7/5
175-200	Precipitation of ferrihydrite in unbedded yellowish medium sand and precipitation of lepidocrocite in thin (5cm) whitish (5Y 7/2) fine-sandy silt (multi-phased soil formation?), gravel content <1%	6, 7	-	10YR 4/4 - 2.5YR 6/4 - 10YR 5/8
200-215	Bore detritus	-	-	-
215-230	Wavy, thin-bedded, slightly silty fine to medium sand, <1% gravel	9	-	7/5GY
230-250	Peaty mud, 20% medium to coarse sand, no plant remains, lower boundary humic sand alternating with subjacent stratum	9	-	2.5Y 2.5/1- 2.5Y 3/2
250-325	Weak wavy thin bedded coarsening-up sequence of fine sands to gravelly (5%) medium sands	9	-	5Y 7/1 - 5Y 7/3
325-355	Same as above, alternating with thin, redeposited humic beds, lepidocrocite precipitation on top, bore detritus between 300 and 310 cm	9	-	2.5YR 3/2- 2.5YR 7/8
355-390	Strongly humiferous fine to medium sand, humic content gradually decreasing to the bottom	9	-	2.5 YR 3/2
390-465	Medium to fine sands, interbedded with thin humic layers, grading into very slightly humic, silty fine sands, bore detritus between 400 and 425 cm	9	-	2.5YR 6/2- 5/5BG
465-555	Peat, upper part (ca. 465-530 cm): weakly decomposed, plant remains; lower part (530-555 cm): strongly decomposed, no plant remains, gradual lower boundary; between 500 and 510 cm bore detritus or intercalation of overlying stratum	9(?)	-	2.5Y 3/2- 2.5Y 2.5/1
555-600	Well-bedded, very silty fine to medium sands, slightly to medium humic	10(?)	-	5Y 4/1



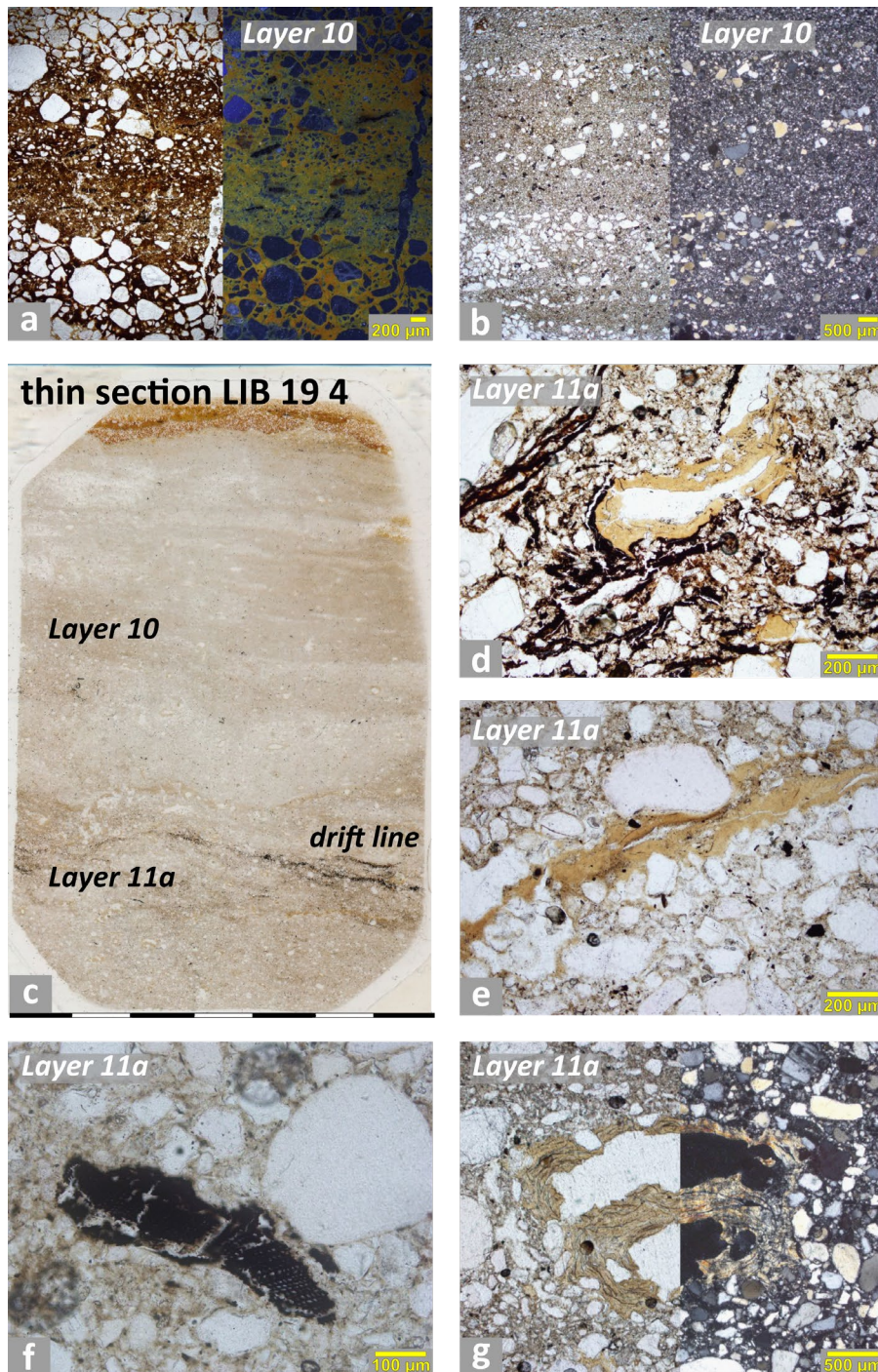
Supplementary Figure S 49. a) Section of the coring transect (Hein et al., 2021) with the position of the find layers Li-I to Li-III indicated by artefact symbols and arrows. The extent of the beach sand (layer 11a) is highlighted with a red box. b) Section of the seismic profile (Hein et al., 2021) with interpretation. The segment between core PD.025 (in the north) and PD.028 (in the south) is poorly stratified, classified as “reworked” and interpreted to represent a small alluvial fan, hosting the occupational sites.



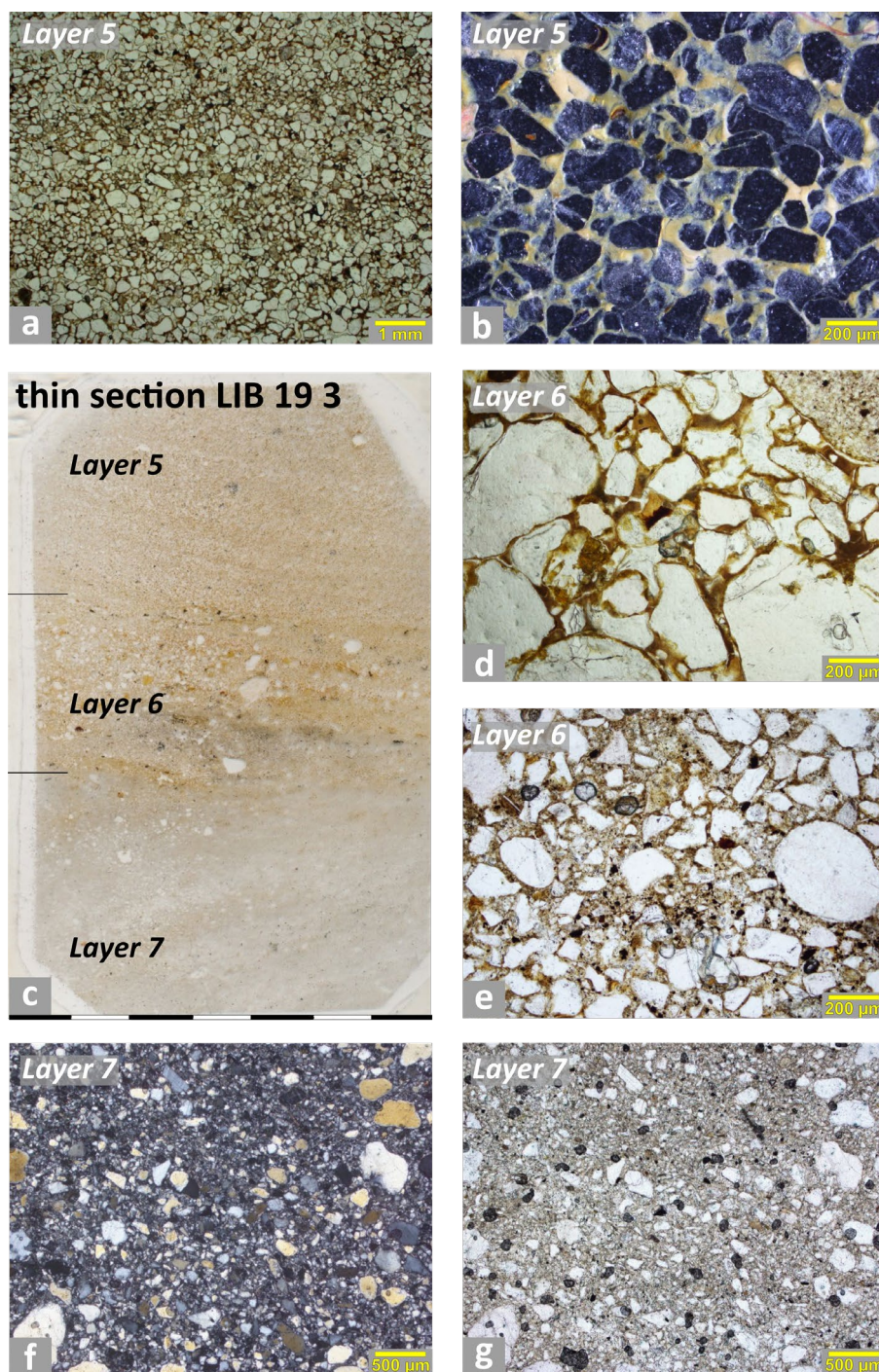
Supplementary Figure S 50. Location of the block sample, from which LIB 19 1 was produced at the northern profile of Trench 1 (indicated by red line in the insert). This block sample captures the contact of layer 6 and 7 as well as the overlying refill from the 1992 excavation of the site.



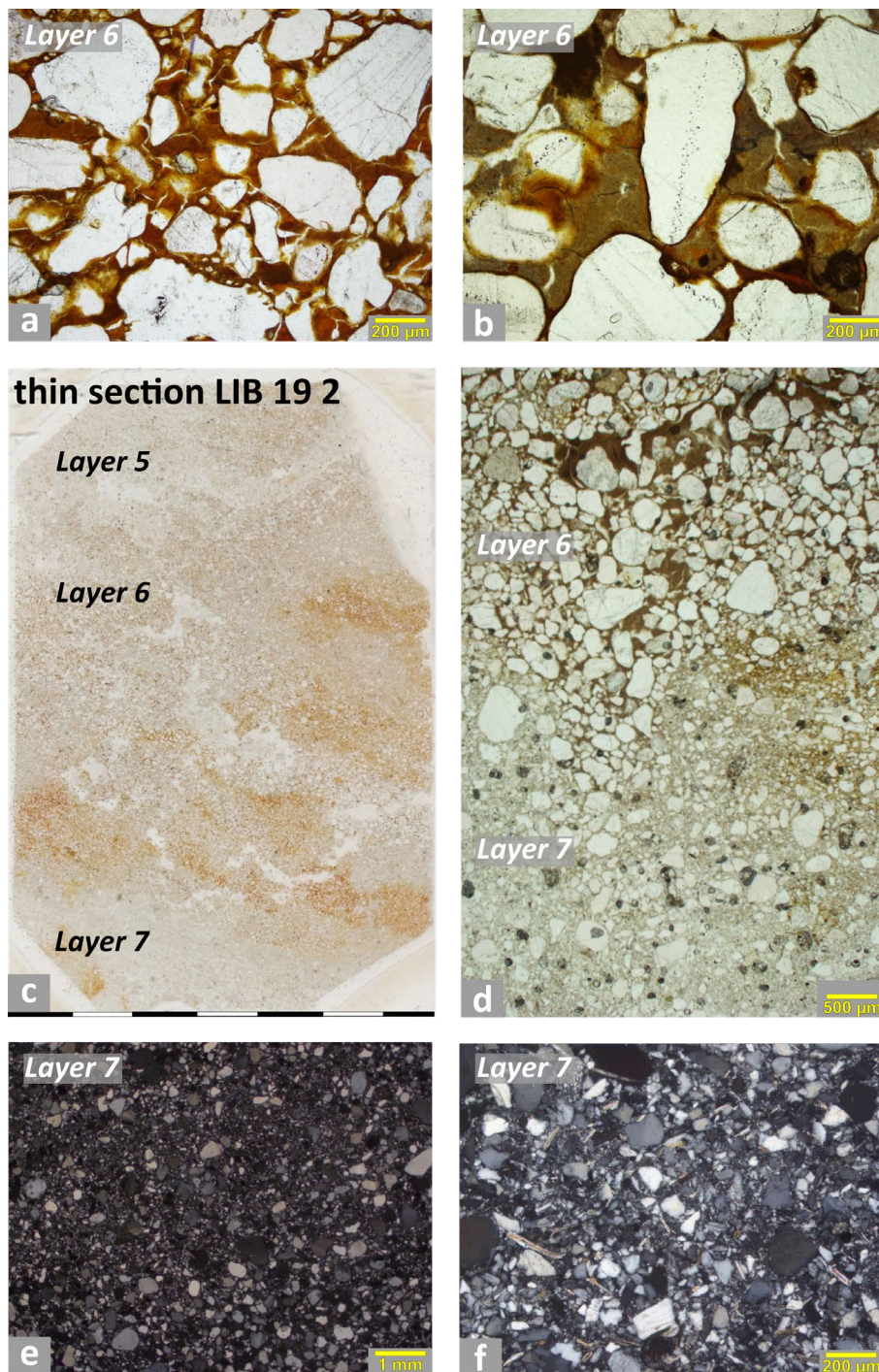
Supplementary Figure S 51. Thin section and microphotographs of sample LIB 19 5 containing layer 11a (humic sand), overlain by 11b (peat/mud) and layer 9 (Niveo-fluvial sand). (a) Contact of layer 11b with layer 9, showing a difference in grain size and organic content. Note also the clay infilling of a channel here. PPL (left) and XPL (right), scale 500 µm. (b) The upper part of layer 11b is dominated by fine, detrital organics. PPL, 200 µm. (c) Scan of thin section LIB 19 5 showing a clear contact between layers 10, 11a and 11b. Note also the upper, more greyish part in layer 11b. Scale in cm. (d) The central part of layer 11b is organic-rich and elongated plant tissues are aligned horizontally. PPL, 200 µm. (e) Plant residue, roots and clay illuviation in layer 11b. PPL, 200 µm. (f) Contact between layers 11a and 11b showing different grain size, the upper layer 11b is coarser grained than the lower layer 11a. PPL (left) and XPL (right), scale 500 µm. (g) A charcoal fragment at the contact of layer 11b with 11a. Note also the increase in organic content in layer 11b compared to layer 11a. PPL, scale 1 mm.



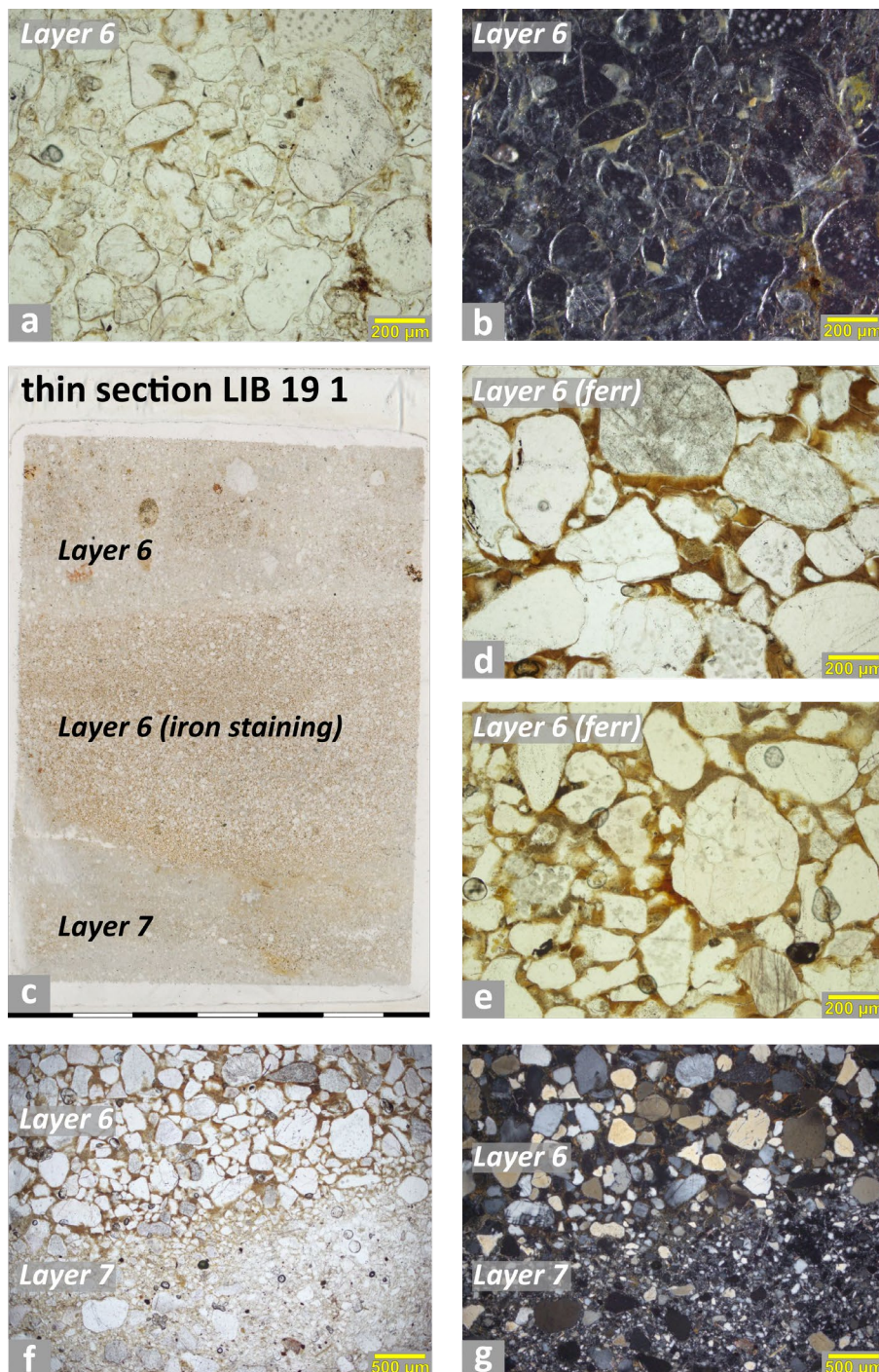
Supplementary Figure S 52. Thin section and microphotographs of sample LIB 19 4 containing layer 11a (humic sand) with find horizon Li-II on top and overlain by layer 10 (clayey silt). (a) The top of layer 10 is here overprinted with iron. PPL (left) and OIL (right), scale 200μm. (b) Layer 10 shows graded bedding. PPL (left) and XPL (right), scale 500 μm. (c) Thin section scan of LIB 19 4 showing humic bands in layer 11a and a gradual contact with layer 10. Scale in cm (d) Layer 11a is enriched in organic materials that are often humified. Note also the yellow clay coating in a void at the center of the photo. PPL scale, 200 μm. (e) A channel refilled with clay in layer 11a. PPL, 200 μm. (f) A charcoal fragment in layer 11a. PPL, 100 μm. (g) Clay illuviation in layer 11a often has a weathered/degraded appearance. PPL (left) and XPL (right), 200 μm.



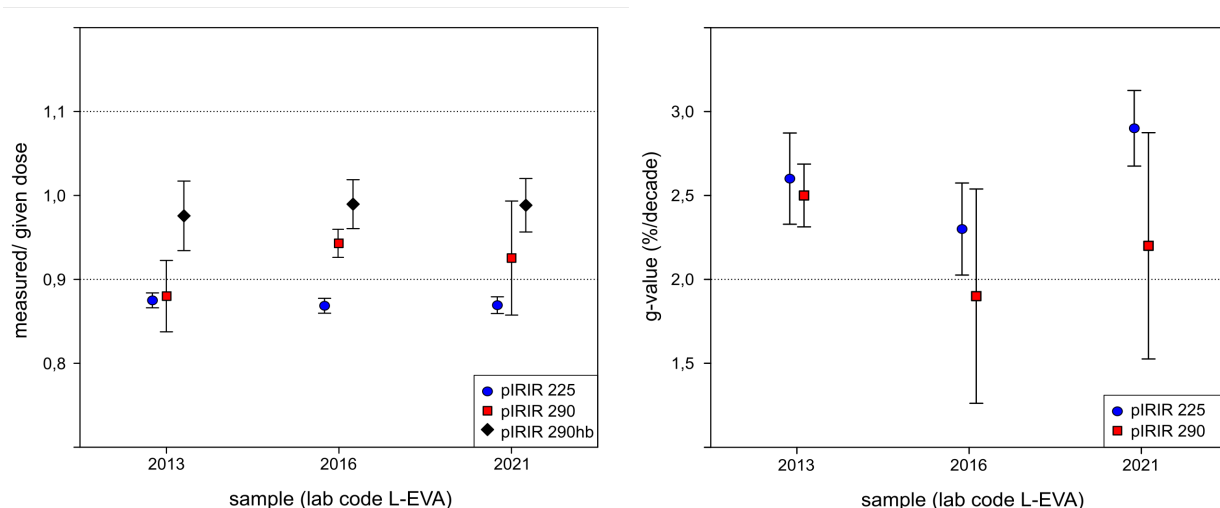
Supplementary Figure S 53. Thin section and microphotographs of sample LIB 19 3 containing the find horizon Li-I in layer 7 (silty fS) and the overlying layer 6 (orange fS) and layer 5 (eolian sand). (a) Layer 5 is mainly composed of silt to coarse sand sized, rounded quartz grains, but it is also poorly sorted for medium sized sand and also expresses weak bedding. PPL, Scale 1 mm. (b) The packing voids are filled with clay illuviation, which shows weak iron and organic staining. OIL, 200 μm . (c) Thin section showing the clear contact of layer 7 with layer 6, but a gradual contact of layer 6 with layer 5. Note also that layer 6 is here composed of two subunits showing different color expressions, more greyish in the lower opposed to orange in the upper part. Scale in cm. (d) Iron stained clay illuviation in layer 6, similar as in the other thin sections of this layer, but also similar to the overlying layer 5. PPL, scale 200 μm . (e) The lower subunit of layer 6 is enriched in amorphous organic fine material, explaining the color difference between the two subunits. (f & g). Layer 7 has a typical expression here with densely packed silt to coarse sand sized quartz and a poor sorting for fine sized material. XPL (f) and PPL (g), scale 500 μm .



Supplementary Figure S 54. Thin section and microphotographs of sample LIB 19 2 containing the find horizon Li-I in layer 7 (silty fS) as well as overlying layer 6 (orange fS) and layer 5 (eolian sand). (a) Iron stained clay coatings and infillings in layer 6. PPL, 200 μm. (b) Here, the clay coatings are only locally iron stained (red) and are otherwise greyish-yellowish or show black amorphous staining. PPL, 200 μm. (c) This local variation in iron staining of the clay coatings is resulting in a mottled appearance of layer 6 in thin section. Note also the clear contact with the underlying layer 7. Scale in cm. (d) The contact between layer 6 and 7 is characterized by a change in grain size, layer 6 is coarser grained than layer 7. PPL, 500 μm. (e & f) Layer 6 at different magnifications (scale 1 mm in e and 200 μm in f) showing a very dense microstructure with a poor sorting for silt and fine sand. Note also the presence of mica. Both XPL.



Supplementary Figure S 55. Thin section and microphotographs of sample LIB 19 1 containing the find horizon Li-I in layer 7 (silty fS) and the overlying layer 6 (orange fS). (a) Layer 5 is mainly composed of silty to coarse sand sized quartz grains with simple packing voids. PPL, scale 200 μm. (b) Fine material in the layer 5 consists of iron stained fine organics and clay OIL, 200 μm. (c) Thin section LIB 19 1 showing clear contact between the three layers and color differences. Scale in cm. (d) The darker color in the orange sand results from iron stained clay coatings. Note the similarity in grain size between layers 5 and 6. PPL 200 μm. (e) There is variability in the clay coatings with some exhibiting a lighter, more greyish color. PPL, 200 μm. (f & g) Clear contact between layers 6 and 7 (F in PPL, G in XPL). Note the clear difference in grain size, the underlying layer 7 is sorted for silt and fine sand, while coarse grains are rare. Layer 7 also lacks the clay coatings characteristic of layer 6. Layer 7 is very dense and shows limited void space in the form of simple packing voids.



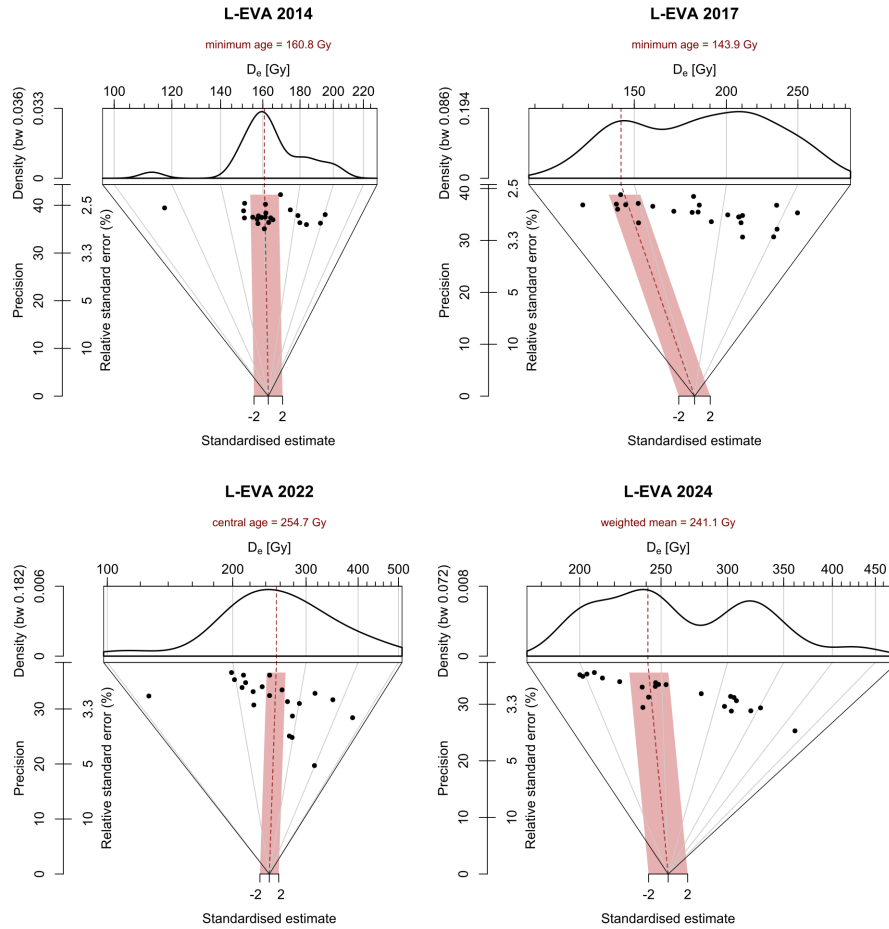
Supplementary Figure S 56. Results of the dose recovery (left) and anomalous fading (right) experiments using different elevated temperatures for the feldspar SAR protocol. For dose recovery testing, the residual signal was subtracted from the measured dose. For the chosen signal pIRIR₂₉₀ (with hotbleach, which is not relevant for the fading test), the mean measured-to-given dose ratio was 0.98 and the mean g-value was 2.2 %/decade.

Supplementary Table S 12. Measurement steps of the applied pIRIR₂₉₀ protocol

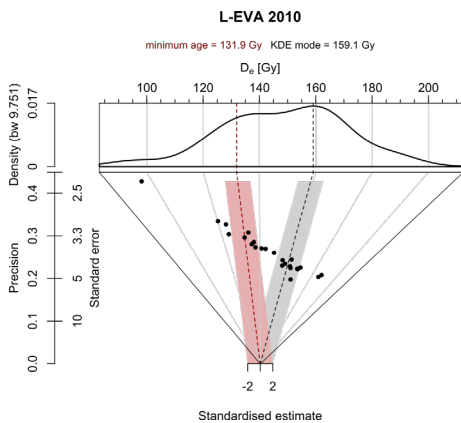
Step	Treatment
1	Dose
2	Preheat (320°C for 60s)
3	IRSL, 100s at 50°C
4	IRSL, 200s at 290°C → L _x
5	Test dose
6	Preheat (320°C for 60s)
7	IRSL, 100s at 50°C
8	IRSL, 200s at 290°C → T _x
9	IRSL, 100s at 325°C → hot bleach
10	Return to step 1

Supplementary Table S 13. Results of the high-resolution germanium gamma spectrometry, cosmic and total dose rates as well as water contents used for correction

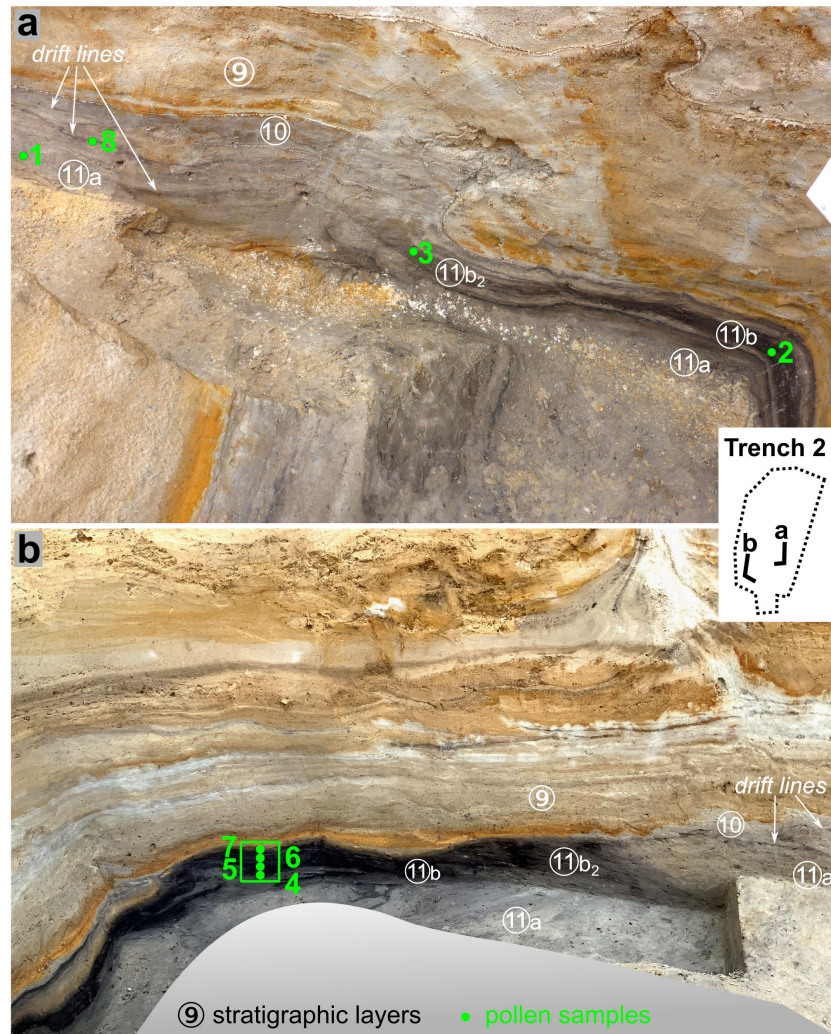
Lab.-ID (L-EVA)	U (ppm)	Th (ppm)	K (%)	Cosmic Dose (Gy/ka)	DR _{total} (Gy/ka)	H ₂ O (%)
2010	1.49 ± 0.23	4.90 ± 0.40	1.24 ± 0.10	0.19 ± 0.02	2.46 ± 0.21	11.92 ± 10
2012	0.50 ± 0.10	1.80 ± 0.10	0.73 ± 0.08	0.18 ± 0.02	1.57 ± 0.20	12.90 ± 10
2014	1.50 ± 0.20	4.00 ± 0.30	1.06 ± 0.11	0.18 ± 0.02	2.25 ± 0.21	11.36 ± 10
2015	1.47 ± 0.20	4.10 ± 0.30	1.26 ± 0.10	0.18 ± 0.02	2.44 ± 0.21	10.19 ± 10
2016	1.28 ± 0.22	2.55 ± 0.18	0.98 ± 0.10	0.17 ± 0.02	2.00 ± 0.21	12.56 ± 10
2017	0.97 ± 0.17	3.57 ± 0.24	1.01 ± 0.07	0.18 ± 0.02	2.03 ± 0.20	13.25 ± 10
2018	1.06 ± 0.19	3.00 ± 0.20	0.85 ± 0.06	0.16 ± 0.02	1.88 ± 0.20	11.94 ± 10
2019	0.73 ± 0.18	1.68 ± 0.13	0.74 ± 0.08	0.18 ± 0.02	1.63 ± 0.20	11.77 ± 10
2022	3.90 ± 0.40	4.90 ± 0.30	1.11 ± 0.08	0.16 ± 0.02	2.78 ± 0.21	13.59 ± 10
2023	1.79 ± 0.24	4.60 ± 0.30	1.09 ± 0.11	0.16 ± 0.02	2.30 ± 0.20	14.77 ± 10
2024	3.50 ± 0.40	5.10 ± 0.30	1.17 ± 0.07	0.15 ± 0.02	2.69 ± 0.20	11.46 ± 10



Supplementary Figure S 57. D_e -distributions of selected samples using Abanico plots. L-EVA 2014 and 2017 represent find horizon Li-I (stratigraphic layer 7); L-EVA 2022 and 2024 were taken from find-layer Li-II (stratigraphic layer 11a). Compare final ages in Tab. 2 main text.



Supplementary Figure S 58. Abanico plot of the D_e -distribution of L-EVA 2010 (cryoturbated find horizon Li-I, stratigraphic layer 7'). The final D_e -estimation (applying the MAM) is indicated in red and equates a cryoturbational age of 53.5 ± 4.9 ka. For comparison, the main mode of the Kernel Density Estimation (KDE) is presented (grey bar and black dashed line). It relates to a distinct cluster in the radial plot and corresponds with a calculated age of 64.6 ± 5.8 ka, which is closer to the depositional age of this layer (see section 5.1, main text).

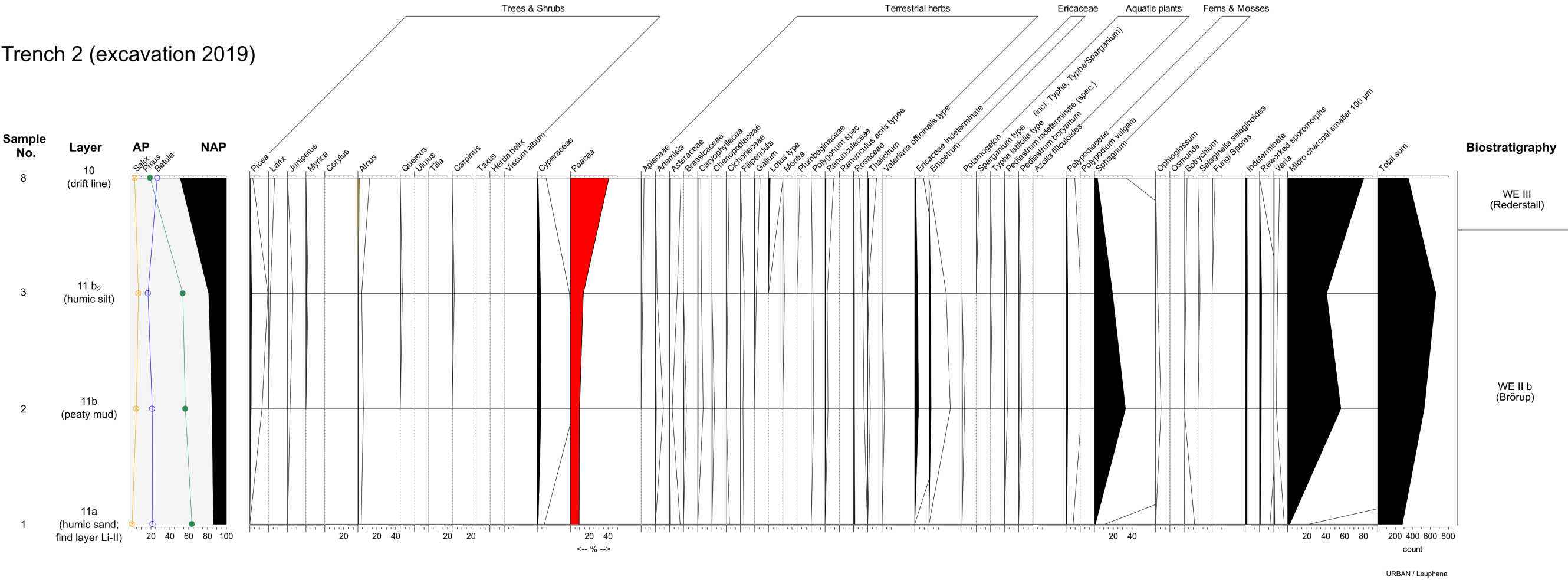


Supplementary Figure S 59. Detailed pollen sampling positions and sample codes in Trench 2 (a, b) and core PD.028 (c). Sample 8 taken from the drift line within layer 10. Lithological descriptions can be found in Supplementary Section 5.1 and Supplementary Table S 11.

Supplementary Table S 14. Summary of palynological results compared to core Veil 1 (Veil et al., 1994, Fig. 1 in the main text) and biostratigraphic subdivision. NAP = non-arboreal-pollen (terrestrial herbs and grasses); E = Eemian (pollen zone in brackets); WE = Early Weichselian, WP = Weichselian Pleniglacial.+

Lichtenberg core Veil 1 (Veil et al., 1994)		Lichtenberg excavations trench2 (2019 and 2020)	Lichtenberg core PD.028	Biostratigraphy (Menke and Tynni, 1984; Behre and Lade, 1986)
Pollen/Vegetation	LPAZ	Layer and Pollen/vegetation	Depth [m] Pollen/vegetation	
NAP, strong increase of Poaceae	Li 9		3.75m - 3.55m, 2.5m - 2.3m NAP, very strong rise of Poaceae Steppe-Tundra vegetation	Schalkholz (WP I)
<i>Pinus-Picea (Larix)</i> , Sphagnum	Li 8		4.65m – 5.3m, 5.55m - 5.3m <i>Pinus-Betula-Picea (Larix)</i> boreal coniferous forest	(WE IV b) Odderade
<i>Betula-Salix-Pinus</i> , Cyperaceae	Li 7			(WE IV a)
NAP dominance, Sphagnum, Ericaceae	Li 6	transition 11 to 10 NAP dominance, <i>Betula</i> , Poaceae, open Tundra-like vegetation		Rederstall (WE III)
<i>Pinus-Betula-Picea (Larix, Alnus)</i>	Li 5	11a, 11b, 11b₂ <i>Pinus-Betula</i> , very few <i>Picea (Alnus, Larix)</i> Boreal coniferous forest (opening up)		(WE II b) Brörup
<i>Betula-Pinus</i> (strong decrease of NAP)	Li 4			(WE II a)
NAP dominance (Poaceae, Artemisia)	Li 3			Herning (WE I)
<i>Pinus-Picea-Alnus</i>	Li 2			(E VI (/VII))
<i>Carpinus-Alnus-Quercetum mixtum-Corylus (Picea)</i>	Li 1			Eemian (E V)

Trench 2 (excavation 2019)



Supplementary Figure S 60. Pollen diagram of bulk samples 1, 2, 3 and 8 (Trench 2, excavation Lichtenberg 2019). Layers from bottom to top: 11a, 11b, 11b2, 10. Biostratigraphic assignment on the right

Trench 2 (excavation 2020)

Sample No. 7, 6, 5, 4

Layer 11b (6-8 cm), 11b (4-6 cm), 11b (2-4 cm), 11b (0-2 cm)

AP Salix, Pinus, Betula, NAP

Trees & Shrubs Larix, Juniperus, Myrica, Alnus

Terrestrial herbs Cyperaceae, Poaceae, Apiaceae, Artemisia, Asteraceae, Caryophyllaceae, Chenopodiaceae, Cichoriaceae, Galium, Polygonum spec., Polygonum bistorta type, Rosaceae, Valeriana officinalis type, Ericaceae indeterminate, Calluna, Empetrum, Vaccinium type (incl. Erica)

Ericaceae Myrica spicata, Sparganium type (incl. Typha, Typha/Sparganium), Pedicularis type, Pedicularis duplex, Pedicularis boryanum

Aquatic plants Equisetum, Polypodiaceae, Spaghnum, Ophioglossum

Ferns & Mosses Botrychium, Fungi Spores, Indeterminate, Reworked palynomorphs, Microcharcoal smaller 100 µm

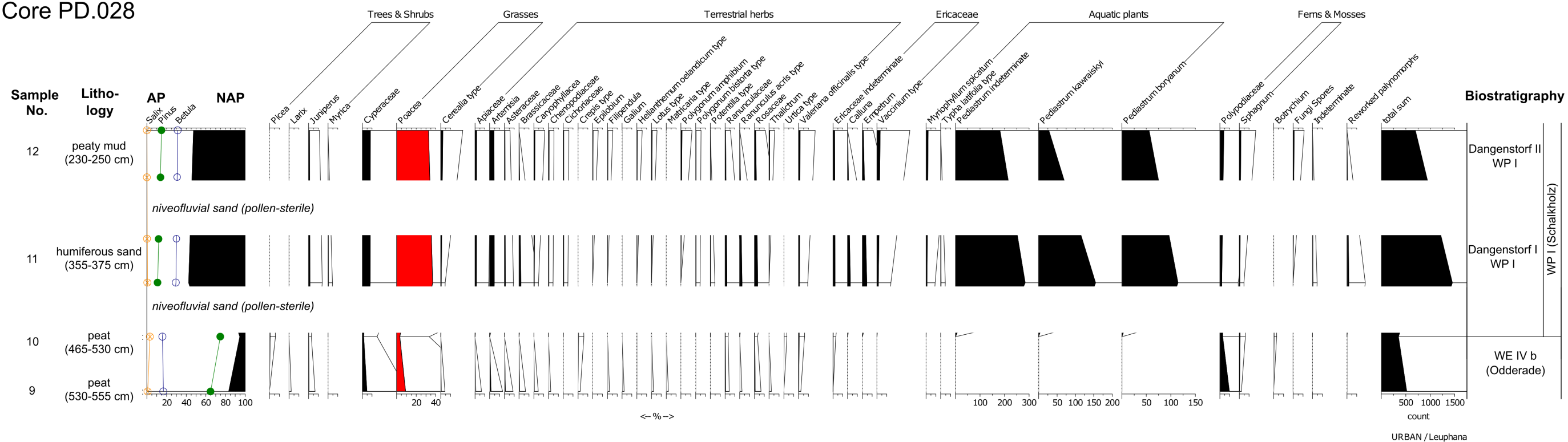
Total sum

Biostratigraphy WE III (Rederstall), WE II b (Brörup)

URBAN / Leuphana

Supplementary Figure S 61. Pollen diagram of bulk samples 4 to 7 (0-8 cm) from layer 11b (Trench 2, excavation Lichtenberg 2020), documenting the gradual transition from Brörup Interstadial to Rederstall Stadial.

Core PD.028



Supplementary Figure S 62. Pollen diagram of bulk samples 9 to 12 from core PD.028.

Supplementary Table S 15. Phytolith sample information by layer.

Sample	Phytoliths in 1 g of sediment	Phytoliths in 1 g of sediment count	Layer	Area designation	Collector	Year collected
MH1	7,636	213	layer 7	Trench 1 East	MH	2019
MH2	62,740	306	layer 11a	Trench 2	MH	2019
MH3	18,379	271	layer 7	Trench 1 South	MH	2019
MH4	6,980	156	layer 8	Trench	MH	2019
MH5	5,556	150	layer 9	Trench	MH	2019

Supplementary Table S 16. The number of multi-cell phytoliths and other biogenic silica particles per gram of dry sediment and summary information. For the summary, grey histogram bars show the row-wise (sample-wise) proportion of values related to the highest value in a row (invariably sample MH2).

Sample:	MH1	MH2	MH3	MH4	MH5
MULTI-CELL	n/g	n/g	n/g	n/g	n/g
Leaf/Stem:		205	272	97	
Polyhedral honeycomb:				45	0
Indeterminate:			68	0	38
Monoaxon spicule			68		31
Pennate diatom				45	
Grass stem	2,310	13,942	2,723	1,126	457
Grass floral	0	615	0	0	0
Grass	5,775	34,856	8,849	3,107	2,093
Monocots	5,775	35,061	8,849	3,107	2,055
Eudicots	1,091	3,896	1,429	270	266
Panicoid	0	820	0	0	0
Festucoid	1,348	8,201	1,702	676	457
Total long cell	36	72	40	26	12
Total short cell	41	77	71	30	35
Long cell/short cell index	36:41	72:77	40:71	13:15	12:35
Multi-cell/Single cell	0.00	0.00	0.00	0.00	0.00
Total identifiable	7,636	44,902	11,640	4,008	2,770
Total no. phytoliths	13,604	62,740	18,379	6,980	5,670
Total fields on slide	9,062	2,261	7,776	15,052	17,221

Supplementary Table S 17. The number of single-cell phytoliths per gram of dry sediment.

Sample:	MH1	MH2	MH3	MH4	MH5
Parallelepiped elongate thin psilate:	1,733	9,432	2,451	901	419
Parallelepiped elongate thin sinuate:	193	2,460	136	45	0
Parallelepiped thin echinate:	0	410	0	0	0
Parallelepiped elongate thin indurmin:	0	205	0	45	
Parallelepiped elongate thin wavy:		410	0	90	
Cylindroid psilate:	385	1,640	136	90	38
Parallelepiped elongate thin dendriform:	0	205	0		
Trichome:	578	2,665	749	495	266
Unspecific hair:	0	205	0		
Prickle:	0	0	68		
Bulliform:	321	615	408	45	38
Bulliform fan:	0	205	0		
Oval:	0	410	68	45	
Short cell rondel:	898	5,536	817	360	152
Short cell square trapezoid:	193	410	340	45	114
Short cell smooth trapezoid:	193	0	0	0	38
Short cell sinuate trapezoid:		0	0	0	38
Short cell oblong trapezoid:	64	2,255	545	270	152
Short cell reniform:		205	68		
Short cell truncated tip bilobate:		820			
Indeterm shortcell:	1,219	6,561	3,063	676	837
Elongate trapezoid:		410	0		
Rugulose Spheroid:	64	0	0		
Spheroid smooth:		205	68		
Stellate-like spheroid:		0	0	45	
Platey:	257	1,640	68	90	0
Elongate:	128	2,050	545	405	228
Trapezoid:		205	0		
Oblong thick:		0	68		
Parallelepiped thin:		615	68		38
Block:		0	0		
Thick block:	385	1,435	749	45	38
Thin block:	128	410	204	45	266
Eudicot stoma:	0	205			
Parallelepiped thick elongate:	0	0		45	
Parallelepiped sinuathick elongate:			68		
Parallelepiped thick elongate scalloped:	64	0	136		
Sulcate:	64	0			
Sclereids:	0	0	204		
Polyhedron:	128	0	68	90	
Jigsaw type:	64	205			
Parallelepiped curved:	0	205			
Epidermal anticlinal pinus possible:	64				
Irregular:	513	2,665	476	90	76
Indeterminate:	5,968	17,838	6,807	3,017	2,930
Highly eroded count:	1,218	4,101	1,361		304

SUMMARY

The research presented in this thesis is aimed at the establishment of robust chronostratigraphic frameworks for Late Pleistocene Neanderthal open-air sites on the European Plain. It is argued that a firm chronological and stratigraphic foundation is the prerequisite for understanding Neanderthal behavior and its potential synchronization with environmental or climatic events. Only that way, behavioral traits can be inspected in terms of adaption to certain developments and changes. This is trying to be illustrated by conducting case studies at Khotylevo I, Western Russia and Lichtenberg, Northern Germany at opposite ends of the European Plain. Very deliberately, the surroundings of these sites were included in the consideration. They can provide insightful background information, which help to better decipher site formation processes and may also elucidate Neanderthal habitat preferences. The two study sites share many similarities, concerning their northern location, their Keilmesser-dominated artifact assemblage, and the stratigraphic potential of their embedding sediment sequences. While for both sites, previous chronological data supported their assignment to MIS 3, the characteristics of their deposits also made an earlier occupation in MIS 5a seem possible. This ambiguity was to be resolved using geomorphological surveys, pIRIR₂₉₀ luminescence dating (ca. 30 samples) and sediment analyses, the latter also including palynology for additional environmental context. The chronostratigraphic results led to a revision of the timing for the occupations at the two sites: In Khotylevo I it happened during MIS 5a and in Lichtenberg at the MIS 5a/4 transition. The new ages are consistent with the stratigraphic and palaeoenvironmental findings and are therefore considered robust and reliable. They provide evidence for an emergence of the Keilmessergruppen before the onset of the Pleniglacial/ MIS 4, which had been a matter of debate so far. The MIS 5a/4 occupation in Lichtenberg further demonstrates Neanderthal capability to cope with severely cold conditions that could be reconstructed for that phase.

The landscape-oriented approach of the investigations directly resulted in the discovery of two unknown occupations in Lichtenberg. The first one could be allocated to the Mid-Eemian Interglacial (PZ E IVb/V), the second one was dated and palynologically assigned to the late Brörup Interstadial (ca. 90 ka, PZ WE IIb). Since

the artifacts from these two fully-forested intervals differ from the later Keilmesser-dominated artifact assemblages considering shape, size and tool variability, it is proposed that changing environments co-determined the lithic technology.

Chronostratigraphic achievements also include the first comprehensive chronology of the widespread 2nd fluvial terrace (MIS 5b to MIS 3) on the Russian Plain, a first numerical age for the termination of Brörup Interstadial (ca. 90 ka) in the type region, and the first detection of climatic fluctuations during the MIS 5a/4 transition on the European Plain (correlated with Greenland Interstadials GI-20 and GI-19). These findings will help to better contextualize contemporaneous archaeological sites in the wider region.

SAMENVATTING

Het onderzoek van dit proefschrift is gericht op het opzetten van robuuste chronostratigrafische kaders voor laat-Pleistocene Neanderthaler-openluchtsites op de Europese Laagvlakte. Er wordt beargumenteerd dat een stevige chronologische en stratigrafische basis een belangrijke voorwaarde is om het gedrag van Neanderthalers, en de mogelijke synchronisatie ervan met omgevings- of klimatologische gebeurtenissen, te begrijpen. Alleen zo kan worden gecontroleerd of bepaalde gedragskenmerken kunnen gecorreleerd worden met bepaalde ontwikkelingen en veranderingen. Er werd getracht dit te illustreren door casestudies uit te voeren in Khotylevo I, West-Rusland en Lichtenberg, Noord-Duitsland, aan weerszijden van de Europese Laagvlakte. De omgevingsfactoren van deze sites werden bewust mee geïntegreerd in dit onderzoek aangezien ze belangrijke achtergrondinformatie bieden die kunnen helpen bij het ontcijferen van zowel de processen verantwoordelijk voor de formatie van een site en habitatvoorkeuren van Neanderthalers. De twee onderzoekslocaties hebben veel overeenkomsten, wat betreft hun noordelijke locatie, hun door Keilmesser gedomineerde lithische ensembles en het stratigrafische potentieel van de sedimentsequenties. Terwijl voor beide sites eerdere chronologische gegevens hun toewijzing aan MIS 3 ondersteunden, leken stratigrafische ook een occupatie in MIS 5a mogelijk te maken. Deze dubbelzinnigheid moest worden opgelost met behulp van geomorfologisch onderzoek, luminescentiedatering en sedimentanalyses, inclusief palynologie. De resultaten van dit chronostratigrafische onderzoek leidden tot een herziening van de timing van de occupatie op de twee locaties: in Khotylevo I gebeurde het tijdens MIS 5a en in Lichtenberg bij de overgang van MIS 5a naar MIS 4. Deze nieuwe tijdsaanwijzingen zijn in lijn met de stratigrafische en paleomilieubevindingen en worden daarom als robuust en betrouwbaar beschouwd. Ze leveren bewijs voor het ontstaan van de Keilmessergruppen vóór het begin van het Pleniglaciaal/MIS 4, waarover tot dusver gediscussieerd was. De MIS 5a/4-occupatie in Lichtenberg toont verder aan dat Neanderthalers in staat waren om om te gaan met de extreem koude omstandigheden die voor deze fase kunnen gereconstrueerd worden.

De landschapsgerichte aanpak van dit onderzoek heeft verder geleid tot de ontdekking van twee onbekende fases van occupatie in Lichtenberg. De eerste kon worden toegewezen aan het Midden-Eemiaan Interglaciaal (PZ E IVb/V), de tweede kon worden gedateerd en palynologisch toegewezen aan het late Brörup-interstadiaal (ca. 90 ka, PZ WE IIb). Aangezien de artefacten van deze twee fases met dichte bebossing verschillen van de Keilmessergruppen wat betreft artefactvorm, grootte en lithische variabiliteit, wordt gesuggereerd dat besloten kan worden dat veranderende omgevingsfactoren de aard van de lithische technologie meebepaalden.

Chronostratigrafische verwezenlijkingen van dit onderzoek omvatten ook nog de eerste uitgebreide chronologie van het wijdverbreide tweede rivierterras op de Russische vlakte, een eerste numerieke leeftijd voor de beëindiging van Brörup-interstadiaal (ca. 90 ka) in het typegebied, en de eerste ontdekking van klimaatschommelingen tijdens de MIS 5a/4 overgang op de Europese vlakte (gecorrleerd met Groenland-interstadialen GI-20 en GI-19). Deze bevindingen zullen een belangrijke rol spelen om andere archeologische vindplaatsen van deze tijdsperiode in de wijdere regio beter te contextualiseren.

ACKNOWLEDGEMENTS

I want to thank my supervisors Dr. Tobias Lauer, Prof. Jean-Jacques Hublin and Dr. habil. Hans von Suchodoletz for support and guidance. And for realizing, that my mode of operation necessitates both, a high degree of freedom and a gentle nudge once in a while. I am grateful to Steffi Hesse, Katharina Schilling and Victoria Krippner (all MPI EVA) and Sonja Riemenschneider (LIAG Hannover) for sample preparation and technical analyses, but especially for their otherworldly expertise and patience.

It is not a secret that implementing and conducting a PhD project vitally depends on a huge variety of people who make it colorful, durable, worthwhile, challenging, informative, feasible, amusing and finishable. Among those people are colleagues, loving friends and family, collaborators, office mates and coffee buddies, mentors and distractors, short-term close acquaintances as well as long-term allies. All these roles constantly change and evolve - and most people take on several at once. Without mentioning you by name here, you may feel directly addressed. Rest assured that you have my deepest gratitude and earned a special place in my heart.

CURRICULUM VITAE

The author of this dissertation, Michael Hein, was born in Sebnitz, Germany, on the 25th of March 1982. He completed his B.Sc. in Geography in 2010 and his M.Sc. in Physical Geography in 2013, both at the University of Leipzig, graduating with a first class degree. During his studies, he developed a proclivity for the interface of Geography and Archaeology. Michael did an internship and worked as a student helper at the State Heritage Office in Saxony. Both his Bachelor's and Master's theses had geoarchaeological topics. Between 2014 and 2017, Michael worked for the University of Jena, Department of Archaeology in different capacities, as associate researcher or self-employed geoscientific consultant. In parallel, from 2016 to 2017 he did a Federal Voluntary Service at the regional environmental NGO "Ökolöwe – Umweltbund Leipzig", where he was the head of environmental education. In 2017, Michael started his doctoral research under the supervision of Prof. Jean-Jacques Hublin, Dr. Tobias Lauer and Dr. Hans von Suchodoletz in the Department of Human Evolution at the Max Planck Institute for Evolutionary Anthropology in Leipzig, Germany. He conducted his research in close collaboration with Palaeolithic archaeologist Dr. Marcel Weiss, together with whom, Michael initialized and conducted a fieldwork project at the Middle Palaeolithic site of Lichtenberg. After he presented his work at various international and national conferences, and published his research in international peer-reviewed journals, he submitted his doctoral dissertation to the University of Leiden in the Netherlands in 2021.

